Constraining diagenetic timings, processes and reservoir quality in igneous-affected basins

SAMANTHA JEAN CLARK

Constraining diagenetic timings, processes and reservoir quality in igneous-affected basins

Samantha Jean Clark

A thesis submitted to Durham University in fulfilment of the requirements for the degree of Doctor of Philosophy

Department of Earth Sciences, Durham University

May 2014

Abstract

As the demand for hydrocarbons increases, more complex, non-conventional plays have been targeted in volcanic margin settings. Consequently, it is important to understand the role igneous rocks have in affecting hydrocarbon systems. This is particularly relevant to the Rosebank Field, offshore UK Continental Shelf, North Atlantic. The field was discovered in 2004 with the 213/27-1z well and encountered Palaeogene volcanic rocks interbedded with siliciclastic and volcaniclastic rocks, representing a brand new play type. Three appraisal wells were drilled and encountered good quality light oil (37° API) with drill steam tests achieving ~ 6000 STB per day (Duncan et al., 2009). Initially four companies had a stake in the field; Chevron (40%), Statoil (30%), OMV (20%) and Dong (10%) however in 2011, OMV bought out Statoil leaving them with a 50% stake. Chevron remain the operators.

The importance of volcaniclastic sediments within these sequences has previously been overlooked and so a better understanding of how these rocks behave during burial is essential. This research quantitatively characterises and assesses the reservoir potential of a range of volcaniclastic and siliciclastic sedimentary rocks within such basins.

The Rosebank Field comprises a range of volcaniclastic lithic arenites and lava flows interbedded with sublithic arenites and quartz arenites. However samples could only be taken from limited the limited cores. This made interpreting 3D architecture difficult and therefore it was decided that a onshore analogue was require. The Staffa Formation of the Palaeogene Mull Lava Field, NW Scotland, provides an excellent analogue to the Rosebank Field within the Faroe-Shetland Basin. It comprises basaltic lava flows interbedded with a variety of volcaniclastic and sedimentary rocks. A range of rock types occur within the Staffa Formation, including vent-proximal pyroclastic rocks, such as massive scoria rich tuffs to re-worked volcaniclastic lithic arenites to vent-distal facies where the siliciclastic component begins to dominate, such as quartz arenites. The Staffa Formation has therefore, been compared and contrasted to the Rosebank rocks to better understand composition, burial history and reservoir potential.

Detailed characterisation of the volcaniclastic rocks has been undertaken using a variety of analytical techniques (optical microscopy, SEM and XRD), and demonstrates that volcanic material in potential reservoir rocks may significantly reduce their

reservoir quality. Proximal pyroclastic rocks, which can have reasonably good porosity and permeability at the surface, degrade to non-reservoir values at shallow depths (<1km), as reactive volcanic components alter to both grain-coating and pore-filling clays during diagenesis. This process dominates diagenesis meaning that it only requires small proportions of volcanic material to be incorporated within a sediment to destroy its porosity. In some cases, alteration is so severe that the original rock textures and clast outlines are lost, making the rock difficult to identify. Several generations of pore-filling and grain-coating clays, formed from the alteration of volcanic glass, including gel and fibrous palagonite, Fe-smectite and chlorite, have been identified in the volcaniclastic rocks samples from both the Rosebank core and the Staffa Formation.

The nature of the volcanic material plays an important role in a rock's ability to retain reservoir quality. Factors such as the composition, shape and grain size of volcanic clasts in these rocks affect how the sediment behaved during diagenesis. Spatter bombs and scoria, for example, react differently clasts derived from lava. Labile volcanic ash shards that underwent minimal surface reworking altered to fibrous clay, and were then flattened and moulded around framework grains during diagenesis and burial. This reduced the local porosity and permeability in the rocks. Clay alteration of weathered basaltic clasts resulted in the development of pseudomorph grains that preserved the original grain structure and had only a minimal effect on surrounding pore throats. Clay formation in these rocks was extremely heterogeneous and highly dependent on the immediate grain-scale mineralogy. Clay phases developed during early diagenetic stages blocked or altered later fluid pathways, which led to an extremely patchy diagenetic mineralogy. Rocks inferred to be located at more distal locations from the vent have higher proportions of siliciclastic components and somewhat simpler paragenetic sequences that are characterised by carbonate and silicic cements and minimal authigenic clays. Oxygen and hydrogen isotopic data provide constraints on pore water chemistry and temperatures during diagenesis.

Together, these data have been used to determine the diagenetic histories of the Rosebank Field and Staffa Formation, and enabled the development of a conceptual model to determine the threshold at which volcaniclastic rocks are no longer viable as petroleum reservoir rocks. The model shows that volcaniclastic rocks containing more than 10% volcanic clasts are likely to have very poor reservoir quality at depth. However, this is dependent on a number of factors such as clast size, clast type,

depositional setting, sorting, pore water composition and timing. These data will be of use in the assessment of potential plays in volcanic rifted margins worldwide.

TABLE OF CONTENTS

CHAPTER 5: PETROGRAPHIC AND SEM CHARACTERISATION OF VOLCANICLASTIC ROCKS

CHAPTER 8: CONCLUSIONS

LIST OF FIGURES

CHAPTER 1

CHAPTER 2

CHAPTER 3

CHAPTER 4

CHAPTER 5

CHAPTER 6

CHAPTER 7

LIST OF TABLES

CHAPTER 2

CHAPTER 3

CHAPTER 4

CHAPTER 6

LIST OF ABBREVIATIONS

BGS	British Geological Society
BPIP	British-Irish Palaeogene Igneous Province
C	Conglomerate
cL	Clastogenic lava
Co	Coal
D	Dolerite
EDAX	Energy Dispersive X-ray Analysis
fC	Flint dominated conglomerate
FIB-TEM	Focused Ion Beam - Transmission Electron Microscopy
FMI	Formation Micro Imager
FSB	Faroe–Shetland Basin
FSSC	Faroe-Shetland Sill Complex
GS	Genetic Sequence
ICDD	International Centre for Diffraction Data
ISAAC	Imaging Spectroscopy and Analysis Centre
KCF	Kimmeridge Clay Formation
L	Basalt lava
M	Organic rich Mudstone
mcvBr	Massive clast-supported volcaniclastic breccia
mmvBr	Massive matrix-supported volcaniclastic breccia
mscBr	Massive scoria-rich breccia
mscT	Massive scoria-rich tuff
NAIP	North Atlantic Igneous Province
NTG	Net to Gross
OBS	Ocean Bottom Seismic
ODP	Ocean Drilling Program
P	Peperite
ppl	Plane polarised light
Q	Quartz arenite
QXRD	Quantitative X-ray Diffraction
scvBr	Scoria-rich volcaniclastic breccia
SEM	Scanning Electron Microscopy
slA	Sublithic arenite
SMsT	Staffa Magma sub-Type
SSSI	Sites of Special Scientific Interest
STB	Stock Tank Barrel
SUERC	Scottish University Environment Research Council
T	Basaltic tuff
TOC	Total Organic Content
vlA	Volcaniclastic lithic arenite
vlW	Volcaniclastic lithic wacke
vS	Volcaniclastic siltstone
xpl	Cross polarised light
XRD	X-ray Diffraction

DECLARATION

No part of this thesis has previously been submitted for a degree at this or any other university. The work described in this thesis is entirely that of the author, except where a specific reference is made to previously published or unpublished work.

Samantha Jean Clark
Durham University
Department of Earth Sciences
May 2014

Acknowledgements

The supervisors:

Jon Gluyas: Thank you for your help and support, and for giving me the confidence and self-belief to see this through to completion.

Richard Brown: As the last one of your "adopted" students, I thank you for your guidance throughout this project. I am sorry you had to battle the Samish during editing. Oh, and I will never be able to eat Juicy Fruit again without thinking of your "excellent" impression!

David Brown: The only member of my original supervisory team to make it through to the end! I can't thank you enough for your help and support not just through the last 4 years, but throughout all of my earth science career so far!

Chris Greenwell: Thank you for all your clay and XRD related knowledge.

The supporting company:

I thank Chevron for funding this research, providing data and giving me the opportunity to do an internship. Thank you to my supervisor Steve Garrett, all the Rosebank team (past and present), Elaine Campbell and all the Value Creation team for their support.

The field support:

In addition to the supervisors, I would like to thank Brian Bell, for his thoughts both in and out of the field. I would also like to thank Louise McCann, Alistair Clark and Cat Hirst for their support as field assistants.

The lab support:

I would like to thank the following people for lab support:

Adrian Boyce, Terry Donnelly, Alison MacDonald and everyone at SUERC for the support during the isotopic study.

Steve Hillier for his help with my XRD lab work and for the opportunity to carry out QXRD in his lab.

Peter Chung (SEM), John Gilleece (thin sections) and all the Glasgow University staff for their ongoing support over the years.

Leon Bowen (SEM); Gary Oswald and Jack Rowbotham (XRD); Dave Sales (thin sections) and Alan Carr and Eddie Dempsey (optical microscopy) at Durham University for their technical support.

I would also like to thank C21 Data Services (support during core viewings), Core laboratories (core sampling and thin section production) and Kate Dobson (word and formatting help).

Other people who provided expertises:

I would like to thank the following people for meaningful project discussions:

Henry Emeleus (Mull, mineralogy and diagenesis), Colin Macpherson and Max Coleman (isotope work), João Trabucho-Alexandre (clay minerals, XRD and general sedimentology), Stuart Jones (sedimentology) and Martin Lee (flint).

I acknowledge Dougal Jerram for setting up the original project, the internship and for giving me the opportunity to study at Durham. Thank you for providing many "character building moments". You may be glad to learn my character is now much more complete.

The groups

I would like to thank everyone involved in the following groups; VMRC, CeREES and the CDT for all the useful discussions over the last 4 years.

The flatties and the housies

Thank you to: Nina, Erik, Addy, Lindsey, Colin, Alison, Katie and Michael for putting up with my mess and all the panicking! Thank you for all your support and the laughs along the way!

The friends

Thank you to:

Durham PhDs (past and present) of which there are too many to name individually.

Kirstie, Tim, Clay, Bansri, Pete, Heather, Charlotte, Joanne, BJ, Ben, Amy and Siân for all their helpful project related discussions.

The old Greg gang: Louise, Ross, Susie, Stew and Nicki, without your ongoing support I would have never made it this far! The old Glasgae guys and girls, the Straiton Ninjas and the Carrick gang. You know who you all are. Thank you!

All of the Ustinov Woman's Football team. Fran, sorry I just couldn't type it, guess I owe you a quid? And to my favourite Kiwi (Wanda), thanks for all the advice and for introducing me to the most marvellous cake in the world!

The besties

Laura “smors” Corrigan and Mel “smell” Gallagher. Thank you for believing in me, making me smile when I was sad, fending off the NEDs, playing our guitars like we’re from Mars and generally being the bestest friends a girl could ask for!

Alison “Oh, gosh” Auld. Thank you for all your negative cutting over the past few months. Sorry I have been in “ahhh I have to write” mode since, well...forever! Here’s to many more (maybe less controversial) piñata parties and to a few less “oh we appear to be having a fire” moments.

Cat “catster” Hirst. Thank you for all of those “Stop panicking!” moments, for all the times you brought me emergency sweets and Irn Bru, for all the times you drove me home late at night, for all those times you made me my tea, for all the times you sang “my face is leaking”, for all those times you translated the Samish and for all those times you were just there when I needed someone to be. You are the best.

The negative cutters:

Thank you for cutting the negativity. Sarah Cameron, James Bell and Jessica Bell (the ultimate negative cutters!!!), Alison, Andy, Ben, Bob, the Browns, Cathy, Claire, David, Debbie, Di, the Dunlops, Doreen, Emma, Fran, Hannah, Helen, the Hirsts, Iza, Jude, Kate, Katie D, Katie S, Karen, Kristie, Loraine, Matt, Michael, Mossy, Murray, Nick, Phil, Rachael B, Rachael Syco, Siân, Suzie, Wanda and Zak.

The family:

Dad, Grandma, Guy, Robbie, Karen and David. Thank you for believing in me and supporting me throughout the PhD. You are the best family I could ask for. I can’t wait to spend more time with you now this thesis is submitted. I love you.

Ok, just one more!

Finally, I would like to thank the “Database”. I hope it works one more time. Then maybe I will pass it on.

DEDICATION

In memory of my mum

Gillian Clark

Love you forever.

1 Introduction

1.1 Research Rationale

As conventional hydrocarbon reserves decline, the oil industry has been forced to find alternative hydrocarbon resources in more unconventional settings such as crystalline basements and volcanic terrains, off West Greenland, offshore Faroe Islands and offshore Namibia. Until recently, volcanic-dominated sequences have been disregarded as containing potentially significant hydrocarbon reservoirs (Remy, 1994) due to:

Difficulties with seismic imaging

The crystalline nature and irregular morphology of extrusive igneous bodies (e.g. basaltic lava flows) result in significant scattering of seismic wave energy and attenuation of higher frequency seismic waves (Hardwick et al., 2012). The resolution of sub-basalt imaging is poor and this leads to large errors in interpretation (Maresh et al., 2006; Nelson et al., 2009; Shaw et al., 2008; Wright, 2013). Intrusive dykes are often not visible on seismic profiles due to their sub-vertical angles. However, recent improvements in seismic interpretation techniques has resulted in better imaging and has allowed sub-basalt plays to be explored (Ziolkowski et al., 2001; Gallagher and Dromgoole, 2007; Spitzer and White, 2005; Petersen et al., 2012).

Complexities of volcanic facies architecture

The facies architecture within basaltic-dominated sequences was until recently, poorly understood. Recent work by Jerram, (2002), Passey and Bell, (2007) and Watton et al, (2013; 2014) have provided insights into volcanic facies architecture however it is difficult to identify individual flow units using geochemistry leading to significant uncertainties surrounding correlations between units encountered in well logs. How volcanic rocks interact on entry into sedimentary basins is also poorly understood.

Poor characterisation of non-marine basaltic volcaniclastic rock diagenesis

Much of the previous work has focused on the diagnosis of marine volcaniclastic rocks at hydrothermal vents and during seafloor spreading. The non-marine diagenesis of basaltic volcaniclastic and pyroclastic rocks is not as well characterised within the literature. This thesis will focus on non-marine diagenesis as the bulk of Rosebank and Staffa Formation rocks are from a non-marine environment. The relationship between the diagenetic paragensis and reservoir qualities, such as porosity and permeability is also poorly quantified. Nomenclature of volcanic rocks often varies from author to author, spawning a wide variety of classification schemes (e.g. Fisher, 1961; Cas and Wright, 1987; McPhie et al., 1993; White and Houghton, 2006), none of which have been adopted as standard. Figure 1.1 shows a simple flow chart that attempts to help users correctly classify rocks (White and Houghton, 2006). However, there are a number of problems with this approach. Firstly, the term primary volcaniclastic itself is a genetic term that may not always be suitable, due to difficulties in determining fragmentation, transportation and deposition. Reworked volcaniclastic material could be classified as primary, epiclasts or as sedimentary clasts. Difficulties also arise when determining if a clast is primary or has been reworked. Hyaloclastites for example contain fragmented clasts that are primary in origin. This thesis used indicators such as sedimentary structures, proportion of quartz and clast roundedness as indicators to wither a rock was primary or reworked. The proportion of volcanic material required in order for a rock to be classified as volcaniclastic is also debated. The Integrated Ocean Drilling Program (Shipboard Scientific Party, 2002) defines the amount at 60% volcanic clasts before the rock is classified volcaniclastic, whereas the BGS (Gillespie and Styles, 1999) define the threshold as 10% volcanic clasts. However, both these definitions may lead to over or under classification of many volcaniclastic rocks. Within this thesis, the BGS definition will be used and the term volcaniclastic will refer to rock within a volcanic terrain that contains >10% volcanic clasts. Historic connotations between the term "volcaniclastic" and poor reservoir quality within hydrocarbon companies has led to the more conservative BGS scheme to be adopted within this thesis.

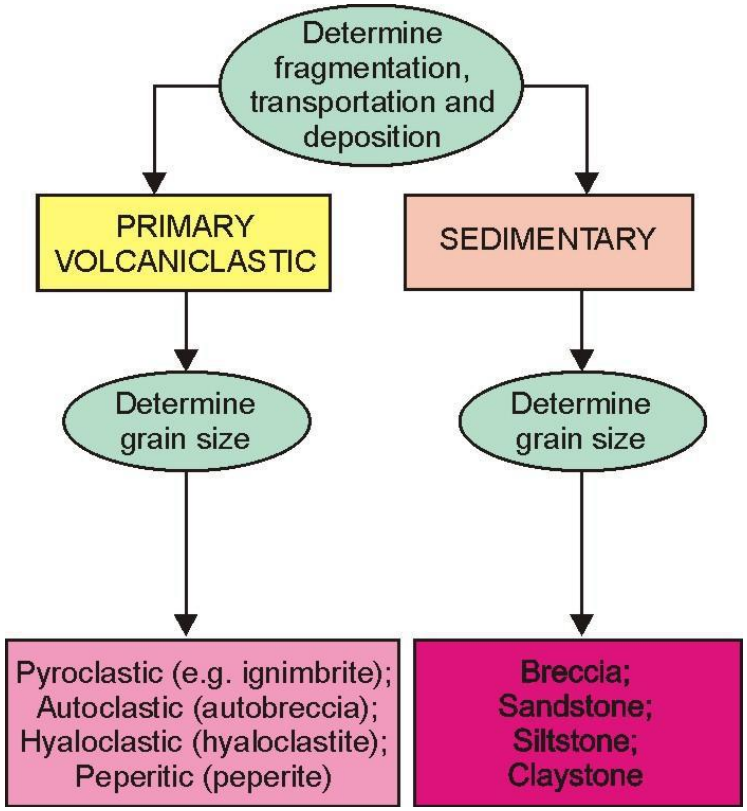

Figure 1.1: Classification scheme by White and Houghton, (2006). The classification is over simplified as they argue reworked volcanic (e.g. non primary) volcaniclastic rocks are classified as "ordinary" sedimentary rocks. This is something that forms an important constituent of volcaniclastic terrains.

Diagenetic effects of volcanic material

The diagenetic effect of volcanic clasts on host sedimentary rocks within sedimentary basins is poorly understood. Much of the research on volcaniclastic diagenesis focuses on silicic rocks (Hay, 1978; Lijima, 1978; Utada, 1991; Kawano and Tomita, 1997), whereas the majority of work on basaltic rocks focuses on sea floor and marine settings (Bonatti, 1965; Furnes, 1975; Hein and Scholl, 1978; Honnorez, 1978; Lijima, 1978; after Brey and Schmincke, 1980; Viereck et al., 1982; Fisher and Schmincke, 1984; Zhou and Fyfe, 1989; Gislason and Oelkers, 2003; Walton and Schiffman, 2003). Volcaniclastic sandstones are highly susceptible to diagenesis due to the instability of volcanic fragments (e.g. volcanic glass) at the Earth's surface (Pettijohn et al., 1987). The diagenetic history of volcaniclastic sandstone is controlled by a number of inter-related factors (Remy, 1994); including depositional environment, detrital mineralogy, grain size, pore-water chemistry, temperature, pressure, and burial history (Hay, 1966, 1978; Surdam and Boles, 1979 and Chan, 1985). Volcaniclastic rocks are mineralogically heterogeneous compared to aeolian sandstones, which are almost entirely composed of quartz (SiO_2) and is therefore, chemically inert. Some authors

have linked the diagenetic paragenesis of volcanic rocks to reservoir quality. Figure 1.2 shows how a complex number of phases can lead to the destruction and creation of porosity (Mathisen and McPherson, 1991).

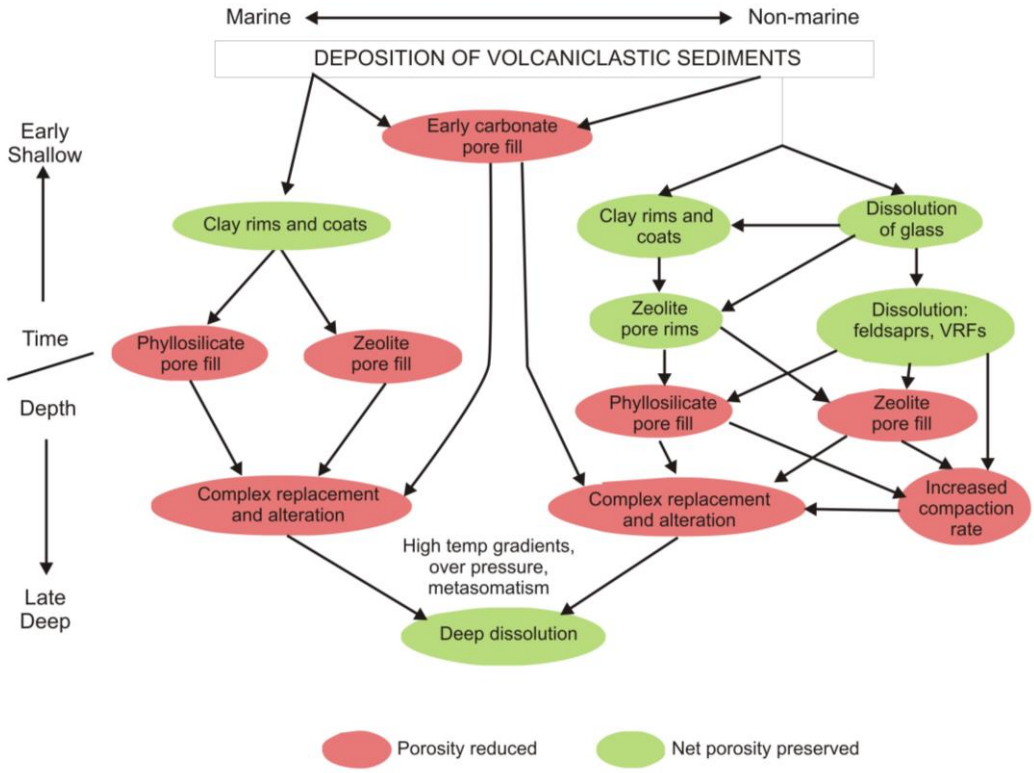

Figure 1.2: Flow chart showing the complex paragenesis that leads to the destruction and creation of porosity within volcaniclastic rocks. (Edited from: Mathisen and McPherson, 1991).

Volcanic diagenesis can be linked to changes in porosity. Remy (1994) demonstrated how reactive volcanic grains behave plastically under compaction and can eliminate porosity. Several other authors have linked the alteration of basaltic glass to pore-filling palagonite and other mixed-layer clay minerals that greatly reduce porosity and permeability (Pittman, 1979; Tang et al., 1994; Stroncik and Schmincke, 2001 and Burley and Worden, 2003). As the degradation of volcanic components happens at relatively shallow depths, any clay produced may shield framework grains from fluid flow and halt further diagenetic reactions during deeper burial. Dobson et al., (2003) studied photomicrographs of cored volcaniclastic sandstones taken from Yellowstone National Park. Silicification of these sandstones had resulted in a porosity reduction of 50%, and a decrease in permeability of nearly two orders of magnitude. Stewart and McCulloch, (1977) demonstrated that zeolites (in particular laumontite) can be produced during burial of volcaniclastic sandstones, thus reducing primary porosity.

The above evidence suggests that volcanic material within any given reservoir should render that reservoir unproductive. However, the presence of volcanic material within reservoir sands does not always produce a poor quality reservoir.

Direct effects of igneous bodies on sedimentary basins

The thermal, mechanical and chemical effects of an igneous body on reservoir rocks is poorly constrained. Intrusions may act as barriers to fluid migration, resulting in the compartmentalisation of reservoir units (Schutter, 2003). Conversely, they can provide fluid pathways that focus diagenetic fluid flow, or even oil migration within the reservoir (Rohrman, 2007; Cukur et al., 2010; Schofield et al., 2012). Contact metamorphic effects, including calcite cementation and metasomatic clay formation, can reduce porosity around intrusions (Girard et al., 1989; Merino et al., 1997; Doyle, 2001; Mckinley, 2001; Iima and De Ros, 2002; Bernet and Gaupp 2005). Direct diagenetic effects on sandstone reservoir rocks are also seen underlying ponded lava flows (Jerram, and Stollhofen, 2002; Grove, 2013).

Volcaniclastic reservoirs

Seemann and Scherer, (1984) and Mathisen and McPherson, (1991) reviewed the hydrocarbon potential of volcaniclastic reservoirs across the world and found a number of viable reservoirs within volcanic terrains. High quality hydrocarbon reservoirs within volcanic settings have subsequently been reported in Australia (Hawlader, 1990), Georgia (Vernik, 1990), East Java, Indonesia (Willumsen and Schiller, 1994), Brazil (dos Anjos et al., 2000), Turkey (Büyükutku, 2006), Pakistan (Berger et al., 2009), Central Mexico (Lendhart and Gotz, 2011), Argentina (Sruoga et al., 2004; Sruoga and Rubinstein, 2007), and more recently in China (Wu et al., 2006; Zou et al., 2008; Zou et al., 2012). Many of these studies link diagenetic paragenesis within volcanic rocks to porosity and permeability; however, most of these studies lack quantification and are concentrated on site specific processes.

1.2 Research Aims and Objectives

Recent exploration within the Faroe-Shetland Basin (Figure 1.3) has highlighted the need to understand and quantify the diagenetic history of volcanic rocks. The Rosebank Field is approximately 20 km long by 5 km wide and sits on the Corona Ridge, ~125 km northwest of Shetland and close to the boundary between the UK and Faroese Territorial waters. The Rosebank Field was discovered during the drilling of the 213/27-1z well by the Rosebank Partnership (Chevron 40% and operator, Statoil 30%, OMV 20% and DONG 10%) in 2004. The well encountered a series of petroleum-bearing siliciclastic rocks (quartz arenites) with high porosity and permeability that are interbedded with volcanic rocks (basaltic lava flows) with poor reservoir qualities. However, lateral heterogeneity also exists along strike within each of the sedimentary interbedded units, with volcaniciclastic rocks at one end of the reservoir and siliciclastic rocks at the other. This vast contrast in reservoir quality highlights the need to understand how volcanic material reacts during burial. Rosebank lies north east of the Cambo discovery which comprises of a similar intra basaltic play (Quinn et al., 2011; Fielding et al., 2014).

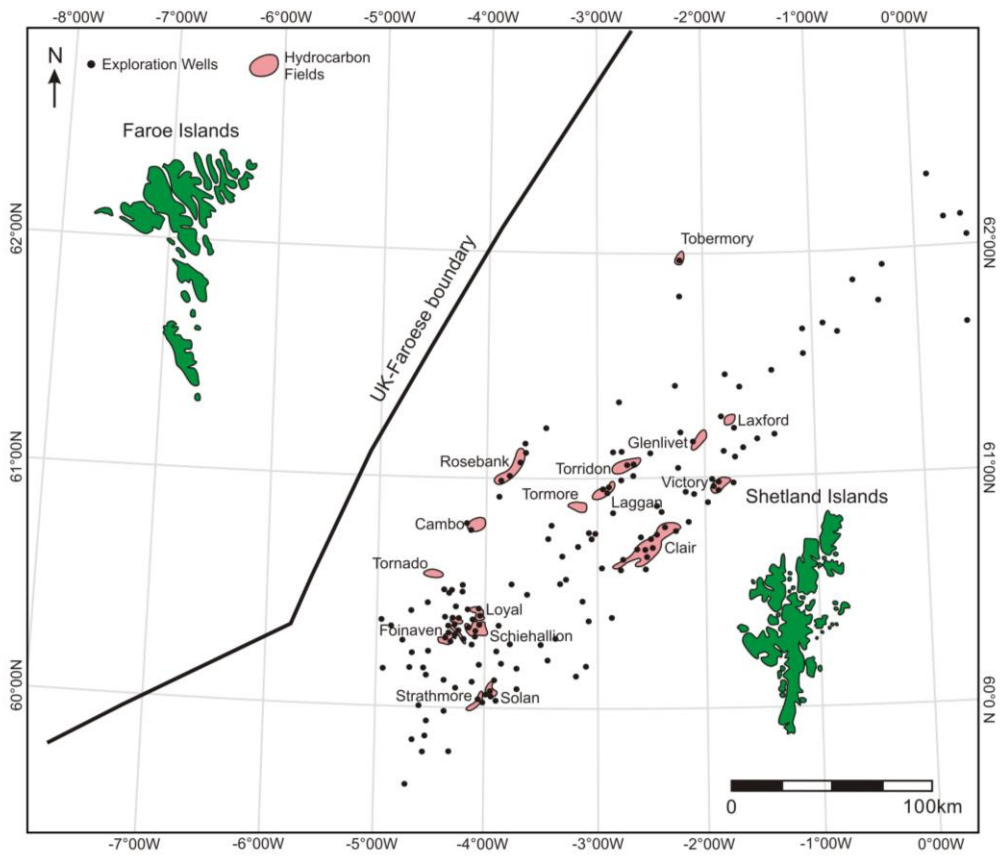

Figure 1.3: Location map showing the Rosebank Field and other hydrocarbon fields in the Faroe-Shetland Basin. Edited from: Wright (2013).

The primary aim of this thesis is to characterise and quantitatively assess the reservoir potential of volcaniclastic rocks and compare them to the siliciclastic sandstone reservoir rocks. This has been achieved by quantifying the proportion of contaminant volcanic material within a sample, and investigating variations in diagenetic history and developing a conceptual model to determine the threshold at which volcaniclastic sands are no longer viable reservoir rocks (i.e., the minimum % of volcanic clast inclusions needed to occlude porosity). The local diagenetic effects of lava flows on adjacent siliciclastic and volcaniclastic rocks (e.g., are there changes in porosity, alteration towards the contacts, and the nature of magma-sediment contacts). From these data facies models are developed using onshore analogues (Staffa Formation, Mull, NW Scotland) in order to inform depositional models for offshore plays. These data will be useful in the assessment of potential plays in rifted volcanic margins. The onshore analogue used is the Staffa Formation which crops out in the southwest of Mull. The Staffa Formation was chosen as an analogue as it is composed of similar rocks to those found in the Roseabk Field. It comprises an ~275 m thick sequence of basaltic lava

flows interbedded with subordinate volcaniclastic and sedimentary rocks. The Staffa Formation is also logistically easier to access than other analogues such as Greenland.

A number of key questions were identified by the Rosebank Development Team at Chevron and will be addressed within this thesis. These questions include:

- How do basaltic volcanic clasts react to burial? What physical and chemical changes do basaltic volcanic clasts in clastic rocks undergo during diagenesis? What factors control the diagenetic history (e.g. particle size, clast type, abundance)? In addition, what effect does this have on reservoir quality (e.g., porosity and permeability).
- Does the distance from volcanic source have an impact on subsequent reservoir quality?
- How much volcaniclastic material do you need before reservoir quality is degraded?
- What are the diagenetic effects of lava flows at sediment/lava interfaces?
- What is the paragenetic sequence of the Rosebank Field and Staffa Formation, and can this be linked to basin wide evolution?
- Is the Staffa Formation a viable onshore analogue?

The key objectives of the thesis are to:

- describe and classify the reservoir intervals and their diagenetic evolution in both the Rosebank Field and Staffa Formation.
- determine the how rock composition affected the diagenetic history of the Rosebank and Staffa Formation rocks.
- determine the diagenetic history and the evolution of reservoir quality of the reservoir rocks in the Rosebank Field.
- elucidate the diagenetic effects caused by lava flows and igneous intrusions on adjacent reservoir rocks.
- use analogue outcrop data from the Staffa Formation to inform our understanding geological history of the Rosebank Field.

1.3 Thesis Outline

Chapter 2 – Methods

Chapter 2 describes and discusses the methodology used throughout the thesis. It details how data and samples were collected from the Rosebank drill core and from the field. It then describes the analytical methods used (including (1) petrographical analysis using polished blocks, thin sections, manual point counting and image analysis, (2) scanning electron microscopy (SEM), (3) Energy Dispersive X-ray Analysis (EDAX) and element mapping (4) bulk, clay separate and quantitative X-ray diffraction (QXRD) and (5) hydrogen and oxygen isotopic analysis.

Chapter 3 – Geology of the Rosebank Field

Chapter 3 introduces the geology of the Faroe-Shetland Basin and Rosebank Field. The stratigraphy and paleogeography of the field are briefly discussed and then each chronostratigraphical unit is described in detail. Lithofacies are described and interpreted and the nature of contacts between lava flows and sedimentary rocks are detailed.

Chapter 4 - Sedimentation of vent-proximal pyroclastic and volcaniclastic deposits: Staffa Formation, Mull

Chapter 4 describes the geology of the onshore analogue of the Rosebank Field: the Staffa Formation, Isle of Mull. An introduction to the British-Irish Palaeogene Igneous Province (BPIP) is provided before introducing the basic geology of the Staffa Formation, and discussing its suitability as an onshore analogue. Nineteen lithofacies identified within the Staffa Formation rocks are described and interpreted in detail. Samples were collected from five localities, which are described and interpreted in detail, building on previous work by Williamson and Bell (2012). Models of formation are then presented for each location, highlighting the importance of understanding depositional relationships. A comparison between the onshore and offshore rocks is

then made. Igneous – sedimentary contacts within the Staffa Formation are described and interpreted and are compared to examples in the Rosebank cores.

Chapter 5- Petrographic and SEM characterisation of volcaniclastic rocks

This chapter provides a detailed petrographical analysis of the different lithofacies of the Staffa Formation and Rosebank Field. The main rock forming minerals are identified, together with diagenetic phases, and alteration textures described and discussed. Optical properties of the igneous – sedimentary contacts are described. The chapter also focuses on understanding how alteration of key phases has led to the reduction or preservation of porosity. The diagenetic paragenesis is explored using results from SEM, EDAX and element mapping analysis.

Chapter 6 - Quantification of diagenetic phases in volcaniclastic rocks and their role in hydrocarbon reservoir quality

Quantification of the diagenetic phases within the samples are presented within this chapter. Firstly, bulk XRD results are used to identify the main rock-forming minerals. These results proved inconclusive so clay orientated XRD was undertaken. QXRD was undertaken on a small sample set to allow relationships between phases to be determined.

The relationship between diagenetic phases and porosity was determined using point counting data. The relationship between volcanic content and permeability is also briefly examined using data provided from Chevron. The direct effects of an igneous – sedimentary contact on porosity and permeability are then considered. Finally isotopic data are presented and discussed for selected samples.

Chapter 7 - The diagenetic evolution of onshore Staffa Formation rocks and offshore Rosebank rocks

This chapter interprets the diagenetic histories of the two case studies and compares them to the regional diagenesis. A conceptual model for predicting the diagenetic evolution of volcanic rocks is presented and discussed.

Chapter 8 – Conclusions

A synopsis of the thesis is provided and draws together the main conclusions from each of the proceeding chapters.

2 Methods

In order to address the aims and objectives of the project a wide range of analytical and field techniques were undertaken. This chapter discusses each of the field and analytical methods in turn. A list of samples for both on and offshore locations is provided in the appendix (Sample List). A glossary of terms used throughout this thesis can also be found within the appendix.

2.1 Fieldwork

The Staffa Formation on the south west of Mull was selected as the location for field work for a number of reasons:

- The Staffa Formation is part of the British and Irish, Igneous Palaeocene Provenance and was deposited at a broadly similar time to rocks within the Rosebank prospect.
- The Staffa Formation is composed of a series of interbedded lavas and sedimentary rocks similar to those found in Rosebank. These units can be traced laterally for 10–100 of metres. This allows field relationships to be determined both vertically and laterally, something that is difficult to do offshore.

During each field session a series of common field techniques were undertaken at the following locations (Figure 2.1; Table 2.1):

Field location	**Grid Reference**
Ardtun	NM 3772 2480
Biod Buidhe	NM 4518 1926
Carraig Mhor	NM 5565 2118
MacCulloch's Tree	NM 4024 2783
Malcolm's Point – Carsaig Bay	NM 4906 1853 - NM 5019 1881
The isle of Staffa	NM 3230 3510
The Ladder	NM 4025 2780

Table 2.1 Field locations

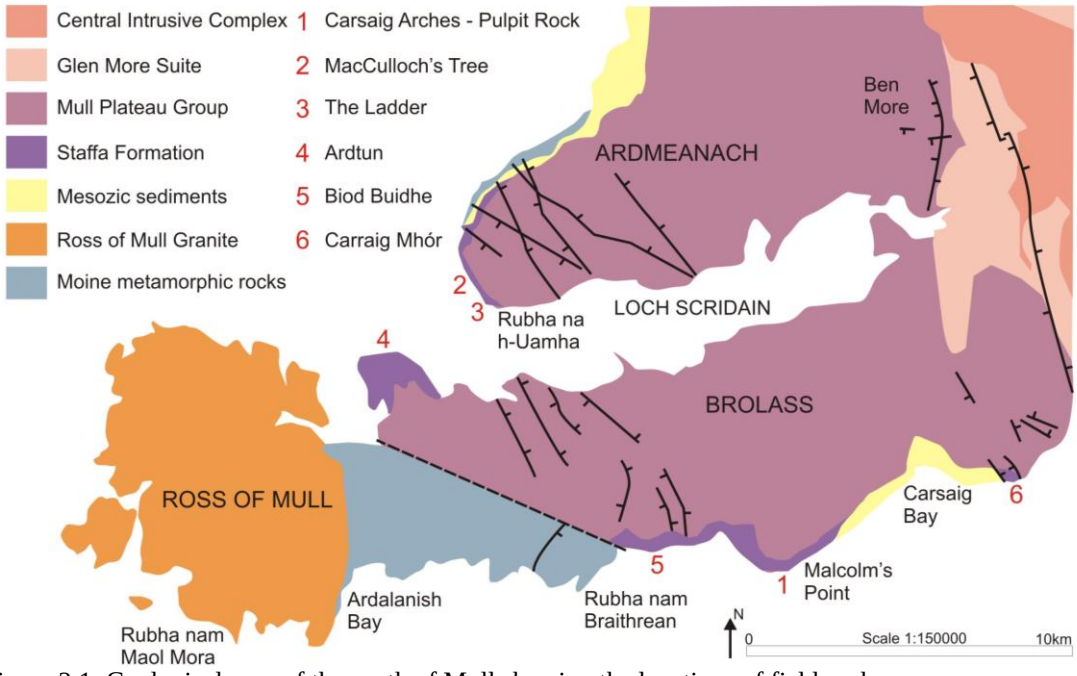

Figure 2.1: Geological map of the south of Mull showing the locations of fieldwork.

Detailed measured stratigraphic sections through sedimentary rocks sections were made at 26 locations (Ardtun, MacCulloch's Tree and Malcolm's Point–Carsaig Bay, see Figure 2.2). Rocks were logged at a centimetre scale.

Field sketches were made at all locations. Sketches allowed 3D facies relationships to be better determined. All notable outcrops were photographed at a number of scales. Several photographs were then used for image analysis.

A total of 60 rock samples were taken from all five main field sites. Rock samples were taken from a full range of lithofacies from primary pyroclastic fall deposits through to siliciclastic sandstones and conglomerates. A suite of samples of sedimentary rocks close to lava flow contacts were also collected. Some rocks could not be sampled due to poor lithification. Ardtun, MacCulloch's Tree and Malcolm's Point are sites of special scientific interest (SSSI) and samples were taken from loose blocks that could be traced to their original location.

Basic clast analysis was undertaken on conglomerates at Ardtun and Malcolm's Point – Carsaig Bay and on primary pyroclastic deposits at MacCulloch's Tree and Malcolm's Point. One metre by one metre areas where marked off using masking tape. Clast lithology, size, morphology and orientation were recorded.

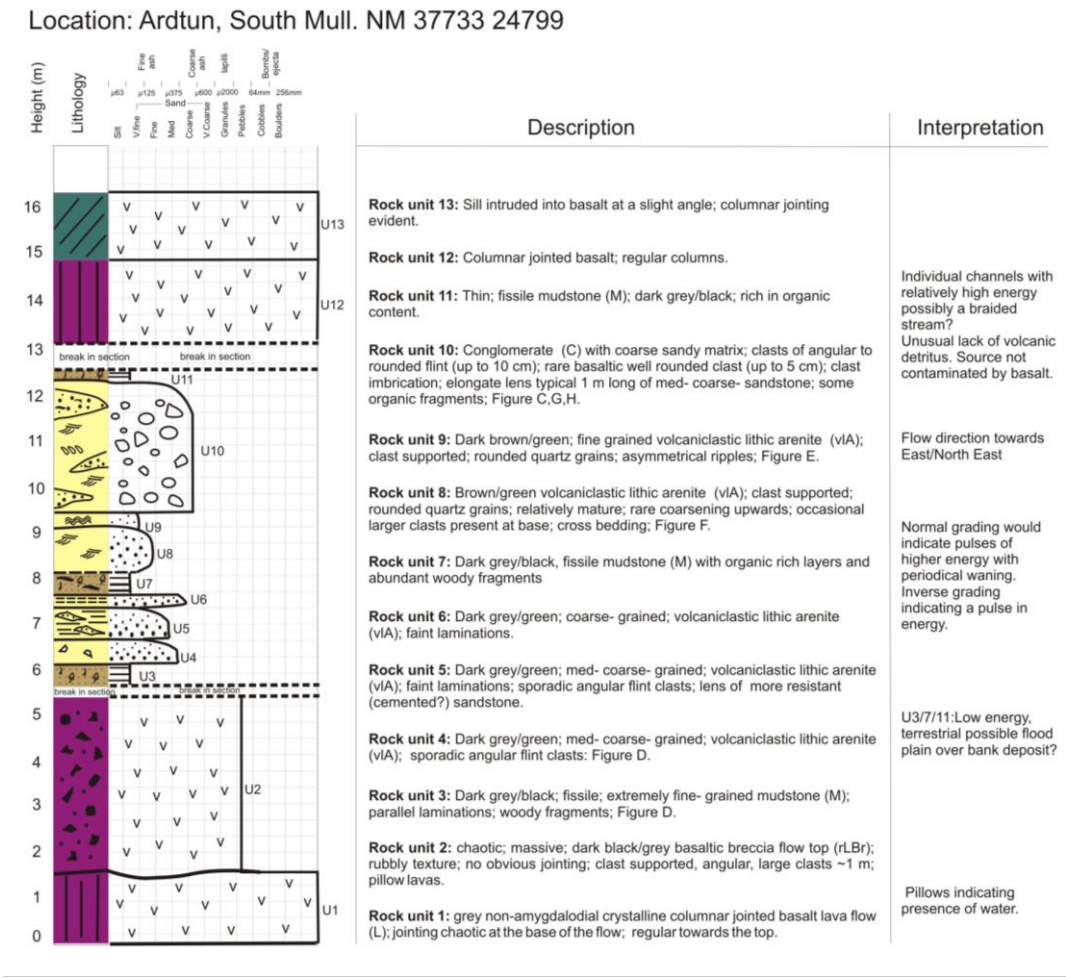

Figure 2.2: Example of a graphic log taken at Ardtun, South of Mull.

2.2 Rosebank Field

2.2.1 Core Logging

The Rosebank core was viewed at the C21 Core Store, Aberdeen (Table 2.2).

Well Name	Core Number	Depth range (m)
213/26-1	3	2872.4 – 2888.6
205/1-1	1	2926.4 – 2938.6
213/27-2	1	2872.7 – 2877.9
213/27-2	2	2934.0 – 2961.1

Table 2.2: Core numbers and depths. Relative well locations can be found in Section 3.4.2, Figure 3.14.

The wells in Table 2.2, were logged in detail, photographed and areas of interest where marked out for sampling (Figure 2.3).

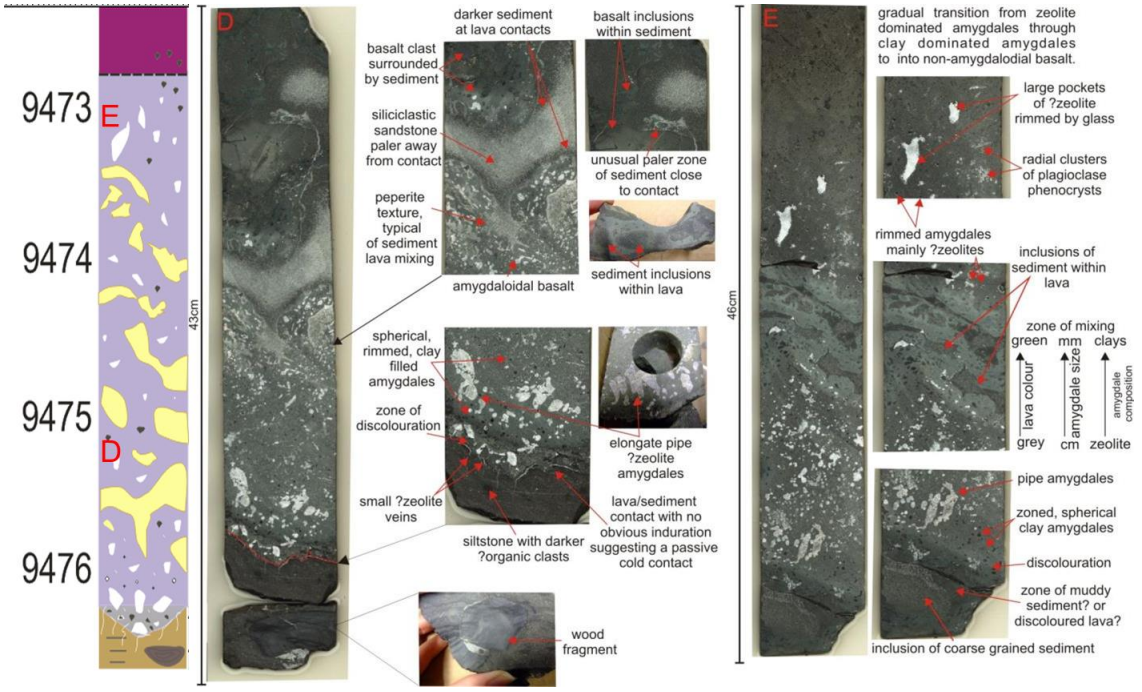

Figure 2.3: Example of a log and notes taken from Rosebank core.

2.2.2 Core Sampling

Core boxes were sent to Core Laboratories in Aberdeen for sample extraction. The majority of the samples were from lava-sedimentary rock boundaries. Four samples were taken from silliclastic sandstones 10 were taken from adjacent lava flows and volcaniclastic units, at varying distances (max 20cm due to limitations in the core) from the contacts. A total of 40 samples were successfully cut from the core

A second sampling visit identified 20 volcaniclastic rocks. Due to the high value of the core plugs, only 1-2 cm of each plug could be taken as a sample, but this proved sufficient quantities for analysis.

2.3 Optical Analysis

2.3.1 Polished Slabs

A number of larger (30 cm x15 cm) samples were taken from pyroclastic units at MacCulloch's Tree and Malcolm's Point. These samples were cut and polished by John Gilleece at the University of Glasgow. The slabs were examined using a hand lens and a binocular microscope. On wet polished surfaces, mineralogy and textures can be better resolved.

2.3.2 Thin Sections

Thirty-eight standard size 30 µm polished thin sections and 2 large format 30 µm polished thin sections were made from a range of representative lithofacies from the Mull samples. All sections were stained blue for porosity using blue epoxy resin.
Thin sections were made in a series of batches (Table 2.3):

Batch Number	Made by
1,2,3	Dave Sales, Durham University
4	Birmingham University as facilities at Durham were temporally unavailable

Table 2.3: Thin section batch

Forty large format 30 µm polished thin sections were made from the Rosebank core samples. These thin sections were made by Core Laboratories (Canada). The large format allowed sedimentary rock-lava contacts to be examined. The thin sections were blue stained to highlight porosity.

2.3.3 Thin section scans

Thin sections were scanned using two different methods. Standard size slides were scanned using a Minolta DiMAGE Scan Elite II film scanner. Large format sections were scanned using a flat bed scanner in refractive light mode. A number of different scan modes and thin section positions were tested in order to gain the best quality image. It was found that rock down at 2.5X magnification and at a resolution of 3200 dpi provided the clearest images within a reasonable time limit. While the film scanner produced the best results, the mechanical set-up limited the size of thin sections that could be scanned.

2.3.4 Petrology

All thin sections were examined using a polarising microscope. Thin sections were characterised according to grain size, texture, sorting, mineralogy and alteration. A

paragenetic sequence was then established for each thin section by examining spatial and cross-cutting relationships of alteration of mineral phases. Samples were classified based on volcanic clast content and primary volcanic textures. In some cases alteration was so extreme that identification of phases proved difficult. Analysis using the SEM was therefore required to refine the mineralogy and paragenesis of each sample. Thin section maps highlighted key features and photomicrographs at a variety of scales.

2.4 Modal analysis

2.4.1 Manual analysis

Point counting was undertaken on all thin sections manually using an ID818 Stepping Stage and Petroglite Point Counting Software. Several vertical and horizontal transects were made across each section to gain representative results. Thin sections were analysed for 500 counts using a step size of 2 mm. This had a number of inherent problems: 1) heterogeneity between and within each thin section lead to problems setting a consistent step size, without over-estimating the proportion of larger grains; 2) difficulties in distinguishing the mineral phases, especially in sections of strongly altered rock. The latter reduced the accuracy of the point counting data. Some of the most altered thin sections were re-counted after SEM analysis to refine the point counting data set.

2.4.2 Image analysis

Typical siliciclastic thin sections scans were analysed using JPOR software in Image J using the method described in Grove and Jerram (2011) to estimate porosity. The method was adapted to a range of volcaniclastic thin sections by making custom pallets. The pallets threshold colours to highlight percentages of components such as quartz, feldspar, and volcanic lithoclasts. However, difficulties in thresholding occurred, because many authigenic clay phases are similar shades of brown. A more detailed custom pallet improved the thresholding results but made the process very time consuming, so the decision was taken not to analyse every sample in this way. Although the results from the JPOR method incurred smaller total errors and are more accurate, they were still in error of manual point counting methods.

Groups of mineral phases with similar hue (such as quartz and feldspar) were created and thresholding was applied. The resultant black and white image was converted into a binary image in Image J. This was opened in image tool and the "count black and white pixels" action was performed. This is a faster method than JPOR and allows a greater number of thin sections to be analysed. Although the results are less accurate because they do not take into account areas of shadow on mineral grains, they were still within error of the JPOR results.

2.5 Scanning Electron Microscope (SEM)

The scanning electron microscope was used to examine samples at extremely high magnifications (up to 30000x) and determine authigenic mineral structures, grain boundaries, grain coating and pore-filling material and is very useful in understanding the diagenetic history of rock samples.

The SEM uses a high power electron gun to emit a beam of electrons through two or more electromagnetic lenses targeted at the sample surface. These electrons interact with the sample in three ways: (1) secondary electrons (SE) are emitted when the electron beam causes loosely bound electrons in the sample surface to become excited and ejected. The collection of secondary electrons provides topographic information about the sample surface. (2) Backscattered electrons (BSE) are primary beam electrons that are scattered from within the sample. The amount of these electrons detected is related to the atomic number of the phase in which they have interacted. Therefore BSE gives you information on chemical composition. (3) X-rays are produced when the electron beam excites an electron in an inner shell causing it to move to an outer shell. When a high energy outer electron then moves back to replace the inner electron an X-ray is emitted. The process is dependent on atomic number and the collected X-rays (EDAX) give information on the chemical composition of the target.

2.5.1 Sample Preparation

Thin sections and rock chips were coated in ~20 nm thick layer of carbon using a carbon coater. One batch of samples was coated by Peter Chung at Glasgow University; all others were coated at Durham University. Sections containing organic matter were prone to charging during SEM analysis—these were coated in a thicker layer (~30 nm) of carbon. Core Laboratory thin sections were prepared using an oil-based grinding method. As a result these samples charged significantly during analysis and had to be cleaned and re-ground before analysis.

2.5.2 Analysis

A Hitachi SU-70 Scanning Electron Microscope at Durham University and a Carl Zeiss Sigma Variable Pressure Analytical Scanning Electron Microscope at the Imaging Spectroscopy and Analysis Centre (ISAAC), Glasgow University, were used to analyse the samples (Figure 2.4). The secondary electron mode was used to study sample morphology. Relationships between mineral phases, such as clay grain coats could be established using this method, which helped to unravel the sample paragenesis. This mode also helped to refine the mineralogy by examining clay morphologies when used in conjunction with the SEM Petrology Atlas, Welton (1984). The backscattered electron mode was used to obtain compositional data, which proved most useful when examining the complex diagenetic histories within the samples. Areas that could not be resolved optically were refined by studying compositional differences. Phase relationships that were undetectable petrographically could be resolved under the SEM. Areas of interest were photographed using the inbuilt camera systems within the SEMs.

Figure 2.4: Hitachi SU-70 Scanning Electron Microscope, Durham University.

2.5.3 Energy-dispersive X-ray Spectroscopy (EDX)

Compositional data were collected using an Oxford Instruments EDX system and then processed using INCA software. Data were collected in order to identify mineral phases and this was particularly useful in identifying extremely altered volcanic grains and authigenic clays.

2.5.4 Element Mapping

Highly complex areas of the thin sections where the paragenetic sequence was difficult to resolve were chosen for element mapping. These areas were pre-programmed into the SEM along with the time and scan rate. The SEM was then left running the scan overnight (8–12 hours) to collect spatial element data. These maps proved a useful tool in understanding complex areas at a range of magnifications (Figure 2.5). For example, the detail highlighted in these maps allowed original grain boundaries of extremely

altered feldspar grains to be resolved. The maps also helped show alteration rims on volcanic grains that are not initially obvious in backscatter images due to components being similar shades of grey.

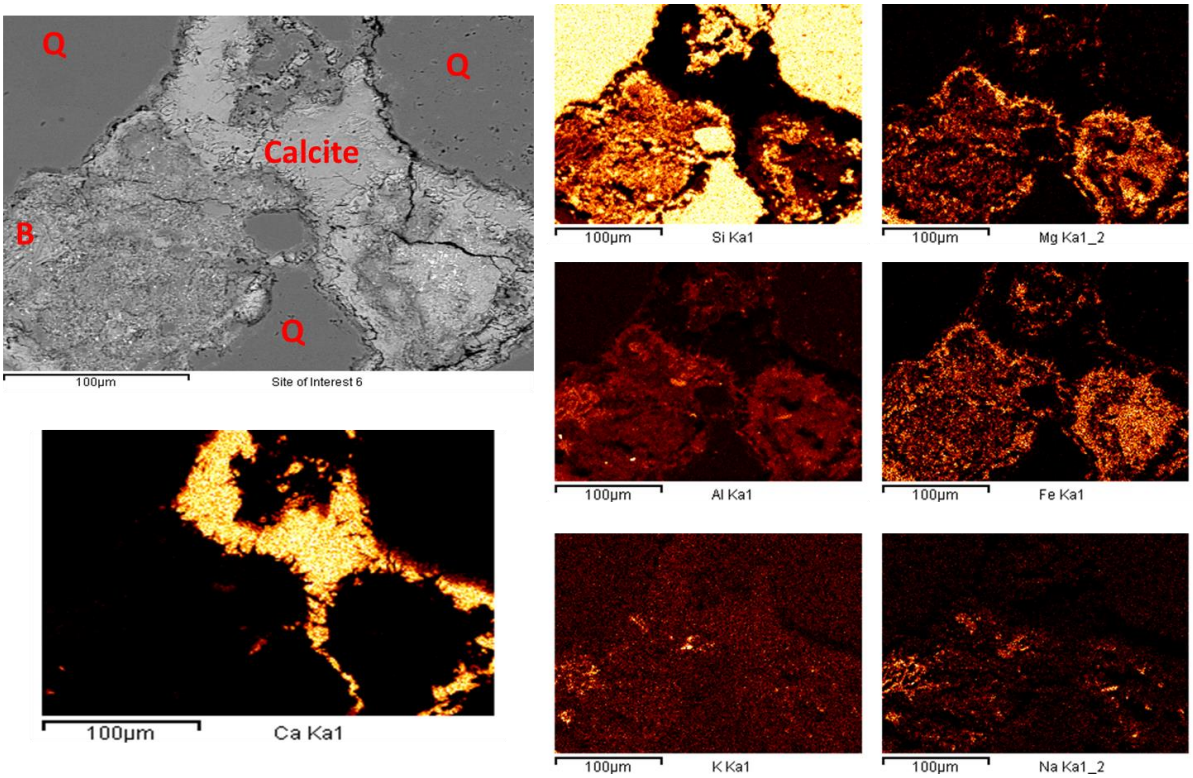

Figure 2.5: Example of element mapping on the SEM. The top left image shows a BSE SEM image. Q- Quartz, B- Basalt clast. All other images are element maps of this image. From these maps grain boundaries and complex interactions between phases can be resolved.

2.6 X-ray Diffraction (XRD)

X-ray diffraction can be used to identify mineral phases within a sample. X-rays diffract off the atomic structure of atoms in set patterns as determined by Bragg's Law:

$2d\sin\theta = n\lambda.$

Where d is the spacing between diffracting planes, θ is the incident angle, n is an integer and λ is the wavelength of the beam. These patterns (reflections) are unique to a mineral phase and therefore, if the intensities of the reflections can be measured then the mineral phase can be identified. The XRD technique was first developed in 1912 by von Laue.

Rather than out-source XRD analysis on the samples it was decided that an attempt be made to carry out the analysis in house despite expertise being limited and use the process as a training exercise. Much useful advice was gained from converse with Dr Steve Hillier, an expert on clay XRD from the Hutton Institute in Aberdeen.

2.6.1 Bulk XRD

2.6.1.1 Sample preparation

Bulk XRD was undertaken on a number of samples to identify mineral phases. Rock samples were crushed gently by hand using an agate mortar and pestle. Care was taken not to shear or over-grind the samples in order to preserve the clay particles. Larger blocks that were too hard to be manually crushed were first broken into smaller pieces using a weighted press. It is noted that other methods such as freeze drying produce better results, but due to time constraints within the project it was decided that hand grinding was the optimal method. To minimise contamination all equipment was cleaned between samples.

2.6.1.2 Sample packing

Two methods of bulk analysis were undertaken. The smear method involves a glass slide (already inserted in the sample holder) smeared with a small amount of Vaseline. The sample powders were then sieved through a 250 mesh sieve in an attempt to remove larger particles. A thin layer of sample was then sieved onto the Vaseline. Care was taken to cover the whole slide with an even thickness of sample. Excess sample was wiped from the edges and the sample holder was tapped to remove loose powder. The sample was then analysed as described below. Results from this method had extremely large background levels that obscured several peaks. This could be explained by the large amount of amorphous volcanic glass in some samples combined with the effects seen from the Vaseline. As the sample is sieved onto the glass, grains will preferentially orientate as they fall. This can lead to a bias within the sample. Hillier (1999; 2002) has patented a spray drier that will spray the sample onto the holder and eliminate the preferential orientation (discussed in the QXRD section). Future studies and any follow up work carried out follow this method.

The second method of bulk XRD analysis was to use a random orientation packing method. Samples were crushed to a powder following the technique above and then packed into a well within a Perspex holder. The surface was roughened using the sharp edge of a spatula helping to minimise the effects of packing.

2.6.1.3 Bulk XRD analysis

Samples were analysed in a Bruker D8 Advance Diffractometer (CuKα radiation) counting from 5 to 90° 2θ with a 0.02° 2θ steps at 0.85s per step. Results were analysed by fitting whole patterns to standard patterns within the International Centre for Diffraction Data (ICDD) powder diffraction data base using Bruker Diffrac Plus EVA™ software. Patterns were also matched in EXCEL to standard D spacing from literature.

2.6.1.4 Confidence in XRD data

Several checks were made to improve the confidence in the XRD data obtained at Durham. Firstly, the Reynolds Cup, XRD competition 2012 was entered as a check on the quality of the methods. Three unknown samples were analysed for bulk XRD at Durham and the results showed that the majority of the main mineral phases and clays were correctly identified, however many of the minor phases, such as pyrite and magnetite had been missed. This was due to a large number of background counts, thought to come from a combination of interference from the sample holder, poor beam alignment and having samples that were preferentially aligned rather than being randomly orientated.

As the minor phases may be important when considering the diagenetic history of the samples it was decided to analyse a number of samples at the Hutton Institute in Aberdeen. Several representative samples were prepared following the method discussed in the QXRD section below. The results showed a lower background with better resolution of peaks. For future analysis I recommend the reader follows this method for clearer XRD results.

2.6.2 Clay orientated XRD

Due to the extremely heterogeneous nature of the volcaniclastic samples the results from both bulk techniques proved difficult to interpret. The sheer number of mineral phases meant multiple overlapping peaks and the large proportion of amorphous glass in some samples lead to a large background signal. Most samples showed a distinctive "bump" at low 2 theta angles indicating the presence of clays, however these could not be resolved and the a decision was taken to undertake clay orientated XRD.

2.6.2.1 Sample preparation

Sample preparation for XRD is dependent on a number of factors and can be approached in several different ways. The method outlined in Moore and Reynolds, Jr (1997) was adapted following advice from Joao Trabucho-Alexandre (pers. Comm.).

Rock samples (approx. 2 cm^3) were gently disaggregated with mortar and pestle as described above and efforts were made to avoid hitting or shearing of the sample, which can damage clay structures. Many authors advise against milling the sample as they say friction and heat caused in the milling process can also affect clay structures. The sample was then sieved to remove larger fragments.

Organic matter can cause noise within the results and was removed. This involved leaving the sample in a solution of 6% hydrogen peroxide (20 ml for each gram of sediment) for two days. The samples were heated to 70ºC to remove the remaining organic matter and then dried at 50ºC.

Removal of carbonate material was achieved using the method in Moore and Reynolds, Jr (1997). The sample powder was reacted in ≤ 3 molar acetic acid until it stopped effervescing. It was important to continually monitor the samples to insure that the acid would not start to react with the clay minerals within the sample. The samples were then washed by centrifuging with demineralised water to remove the left-over acid.

Enough sample powder to cover the conical end of a centrifuge tube (below the 5ml line) was placed in a standard 50 ml centrifuge vial. Five millilitres of peptisation liquid (Hydrated Sodium Pyrophosphate) was then added and the sample was mixed by vigorous shaking. Initial samples were prepared using 20 ml of peptisation solution as in Trabucho-Alexandre (2007), however higher concentrations of solution proved

difficult to wash out. Initially it was unclear of the exact effects the peptisation solution would have on future isotopic work and therefore the amount was reduced to 5ml. At 5ml the powder appeared to adequately defloculate. Some repeat samples were prepared without using a peptisation solution to act as a control for later isotopic studies. These samples had significantly lower clay yields than those where peptisation solution had been added highlighting the need for a defloculant. Centrifuge vials were then filled with deionised water and were shaken well. Vials were centrifuged at 750 rpm for 3 minutes before checking that all larger fragments had sunk to the bottom, if not the vials were re-centrifuged. This could be achieved faster by replacing centrifuging in an ultra centrifuge at 20000 rpm for 3 minutes. According to Moore and Reynolds, Jr (1997), the supernatant contained particles below 2μm (defined as the clay fraction) and so was decanted off into another centrifuge vial. This was then topped up with more deionised water and centrifuged at 3300 rpm for 30 minutes. While this new supernatant can be coloured it must not be cloudy: where it was cloudy the centrifuge step was repeated. The supernatant now contains particles less than 0.2 μm, while the pellet contains grains between 2 μm and 0.2 μm—therefore the supernatant was removed (Table 2.4). These steps were repeated to concentrate as large a clay fraction as possible. Samples must be thoroughly washed by toping up the vial with deionised water and centrifuging at 3300 rpm for 30mins. The water was decanted off and a few ml of new deionised water was added to the pellet. The amount of water added depends on the amount of pellet in the vial; a "gloopy" consistency was desired.

A small amount of the clay solution was pipetted onto half a standard glass slide. A sediment concentration of 60 mg of clay per millilitre of liquid was desired (Figure 2.6). The glass slides were designed to fit into custom-made Perspex XRD holders (Figure 2.7). Glass slides were chosen as the desired substrate because they can cope with heating treatments. Custom-made aluminium holders were also made and although cheaper, they contributed to a large background signal during analysis.

In order to distinguish between clays heating and glycol treatments were performed on the samples (Figure 2.8)

Particle diameter (µm)	sp. g. mineral	Centrifuge speed (RPM)	time (min)
5	2.65	300	3.3
2	2.65	750	3.3
0.2	2.50	2400	35.4

Table 2.4: Settling times for sedimentation of particles. From Moore and Reynolds, Jr 1997.

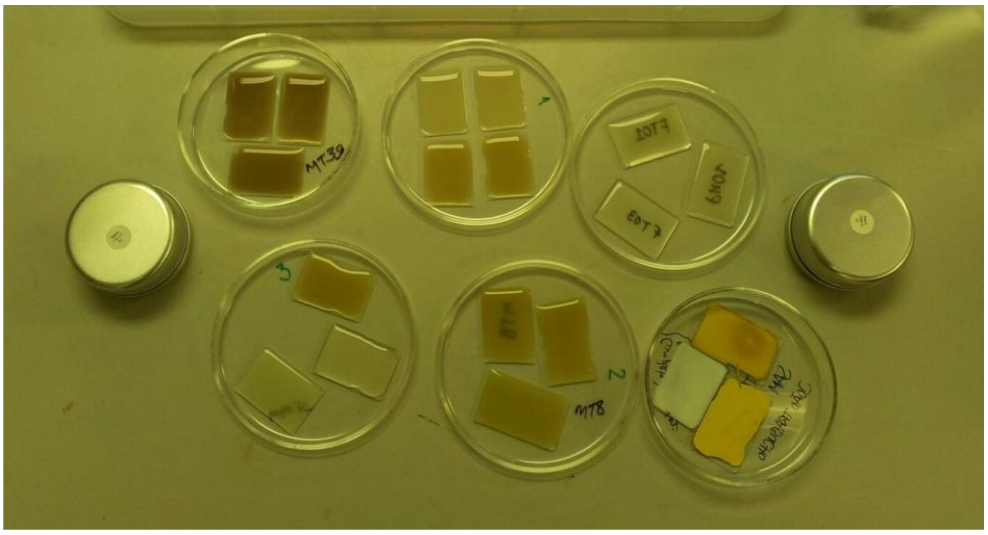

Figure 2.6: Clay fractions that have been pipetted onto glass slides. The three slides in the bottom right of the picture have air dried. Silver containers are 4.5cm in diameter.

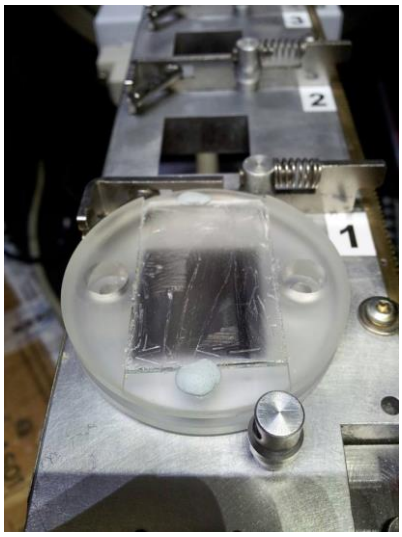

Figure 2.7: Custom made Perspex holder containing a glass slide. Note this slide is coated in a test solution not clays.

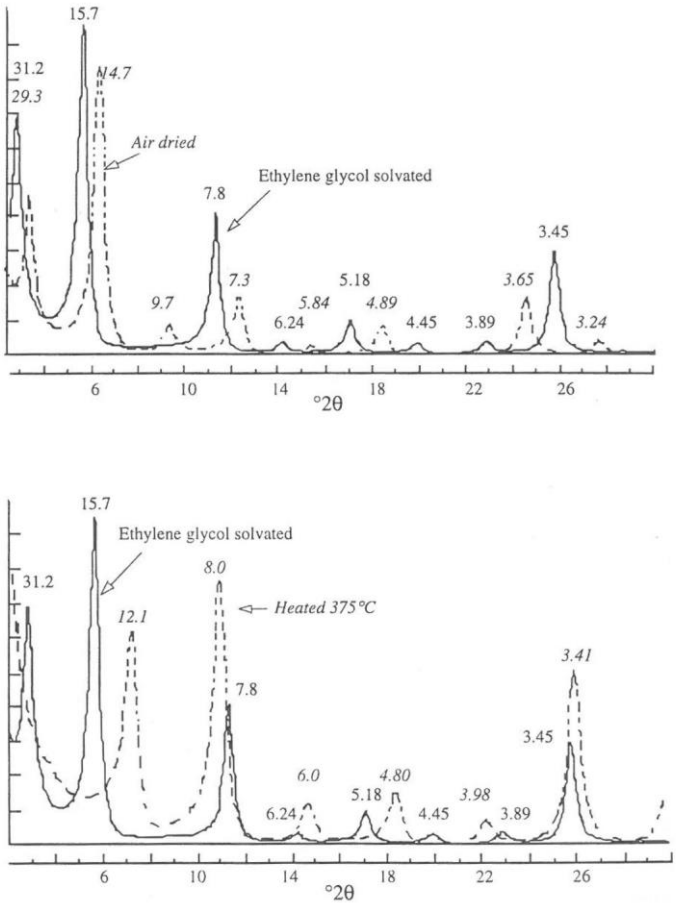

Figure 2.8: Example XRD trace showing the differences in air dried, glycolated and furnace in corrensite. Corrensite swells when gylcolated and therefore moves the peak at 14.7Å to 15.7Å. Heating the corrensite causes the interlayers to collapse moving the peak to 12.1Å. Therefore, how the peaks react to the different treatments can help identify which clay you have. Example scans from: Moore and Reynolds, Jr 1997.

2.6.2.2 Air dried technique

Samples were pipetted onto a glass slide as described above and covered to protect from dust and impurities, but to allow air circulation. Samples typically took 2 days to air dry. Some authors suggest heating the slide to 90°C before pipetting the solution on to the slide in order to compensate for particle-size segregation. This was tested in some sample repeats, but no resolvable difference in XRD results was noted.

2.6.2.3 Furnace dried technique

Samples were pipetted onto glass slides as described above and left to air dry before being heated in a furnace for 24 hours at 550°C. This drove off interlayer water within the clays, collapsed the D spacing and allowed for identification of certain clay types.

2.6.2.4 Glycol technique

Samples were pipetted onto glass slides and left to air dry as described above. Ethylene glycol was then added to the base of a porcelain dish. Sample slides were placed on a porcelain plate within the dish and the lid was added. Care was taken not to let the glycol touch the samples. Samples were then heated at 60°C for 12 hours in an oven. Most authors suggest a minimum of 3 hours, but Trabucho-Alexandre (2007) suggested a longer glycolation time. Once the glycolation was complete samples were analysed one at a time, because glycol can evaporate and its effects are negated.

2.6.2.5 XRD analysis

Samples were analysed in a Bruker D8 Advance Diffractometer. (CuKα radiation) counting from 2 to 60° 2θ with a 0.02° 2θ steps at 0.85 s per step. Lower angles were run than in bulk analysis in order to see low angle clay peaks. Results were then analysed as in section 2.6.1.3.

2.7 Quantitative X-Ray Diffraction (QXRD)

Quantitative XRD was undertaken at the Hutton Institute in Aberdeen under the supervision of Steve Hillier. Due to time constraints only 8 samples could be analysed. The samples were chosen to be representative of volcaniclastic and silicilastic rocks from Mull and Rosebank.

2.7.1 Rock Disaggregation

Samples were crushed by hand using a mortar and pestle. Approximately 3 grams of samples were placed in an agate mill. Ethonol was then added at a 1:6 or 1:8 ratio. The ratio of ethanol was calculated from Table 2.5 (Hillier, 2011) and is highly dependent on the nature of the sample. As the rock samples contain swelling smectite, ethanol was used instead of water. The mixture of sample and ethanol was then ground in a McCrone Mill for 12 minutes. The McCrone Mill shears samples and minimises damage to delicate clay structures.

Material	Liquid/solid ratio	Binder
Most non water-sensitive minerals	2:1 - 4:1	Normally required
Clay minerals, bulk un-fractionated samples	2:1 - 30:1	Not normally required
Bentonites	10:1 - 30:1	Not normally required
Smectite clay fractions <2µm	20:1 - 60:1	Not normally required
Shales	3:1 - 10:1	Not normally required
Sandstones	3:1 - 5:1	Depends on clay mineral content
Limestones	3:1 - 5:1	Normally required
Mineral soils	3:1- 7:1	Not normally required
Drilling muds/solids	3:1 - 20:1	PVA may interact with organic components
Peat	3:1 - 5:1	Normally required

Table 2.5: Guidelines on slurry compositions for spray drying (Hillier 2011).

2.7.2 Spray Drying

It is important during bulk powder XRD and QXRD methods to have random particle distribution. Crystals will only produce reflections in certain orientations and therefore platy minerals such as micas and clays may be over or under represented in a bulk sample (Figure 2.9). The size of the particles is also important. The smaller the size the more crystals there are (per unit volume) to produce reflections and hence the validity of the data will be improved. If all the crystals are roughly the same size powder-preferential packing of the sample will not occur, and the errors will be less. For the latter reason, the spray drying technique of Hillier (1999, 2002) was adopted. Once the sample and ethanol slurry had been ground down in the McCrone Mill it was placed in an air gun. This is the most critical part of the process. It is important at this stage to make sure that the consistency of the slurry is correct. If the slurry is too liquid then particles may evaporate or be forced upwards during the spraying process. Conversely, if the slurry is too thick the sample will simply drip through the air flow and the particles will not be randomly orientated. The sample is then sprayed through the air drying chamber, which contains a stream of air heated to 60°C. The slurry must be sprayed at the lowest possible pressures (typically 10–15 psi) because at high pressures, the slurry will be retained in suspension within the air flow and will be carried upwards

rather than reaching the base of the chamber. At very low pressures the sample will move through the air stream at a slower pace and will have more time to dry before reaching the base of the chamber. The air gun must be held vertically, in the centre of the chamber and there must be a continuous sample flux (Figure 2.10). Once the sample has been sprayed it can be collected from the base of the chamber.

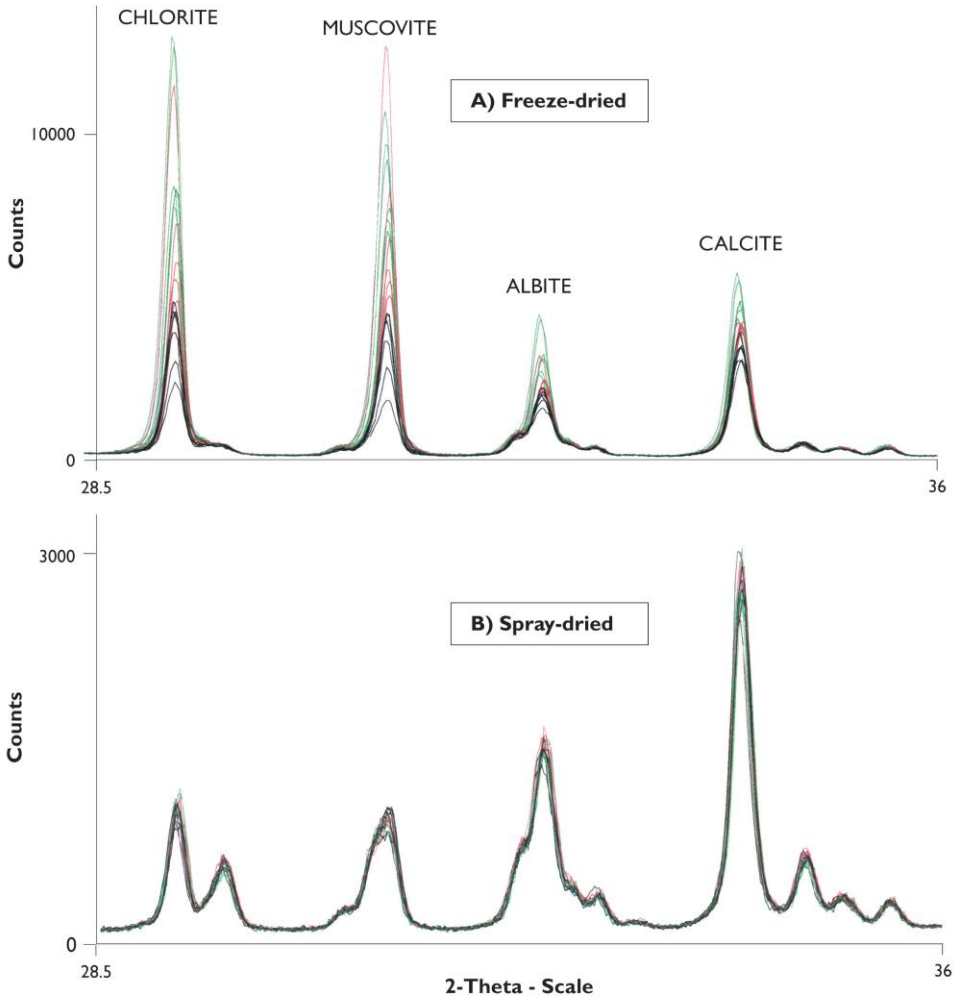

Figure 2.9: Difference between A) a freeze-dried bulk powder scan and B) Spray-dried bulk powder scan. The Spray-dried scans are much more reproducible in terms of relative insanity and therefore will significantly reduce the error in Quantification results. Hillier, 2011.

Figure 2.10: Spay gun held over the furnace vertically. Hillier, 2011.

2.7.3 Analysis

The QXRD analysis was undertaken by Steve Hillier using a Panalytical Expert Pro XRD. Full patterns were matched (as in section 2.6.1.3) to identify the main mineral phases. To quantify the mineral phases full patterns were matched to reference patterns. The reference patterns were created by spiking samples with 50 wt.% corundum so that relative peak intensity could be calculated. Hiller then used an EXCEL™ spreadsheet and the SOLVER™ add-in to calculate the difference between observed full patterns and a pattern that had been created from the sum of the standard reference patterns, as discussed in Omotoso et al., (2006).

2.8 Isotopic work

Stable isotope analysis can inform on the diagenetic history of the rocks. Meteoric waters are enriched in $\delta^{16}O$ relative to $\delta^{18}O$ and in ^{1}H relative to ^{2}D, whereas, igneous-derived and hydrothermal waters tend to be enriched in $\delta^{18}O$ relative to meteoric waters. Information about the pore water in the samples can be gained by analysing oxygen and deuterium ratios in clay minerals. The fractionation of O and H isotopes between a clay mineral and water is controlled primarily by temperature (Delgado and Reyes, 1996) and therefore, the temperature of clay formation can also be estimated.

The analyses were undertaken at the Scottish University Environment Research Centre, Stable Isotope Lab, under the supervision of Adrian Boyce.

2.8.1 Sample preparation

Samples were prepared following methods described in section 2.6.2.1. Approximately 10 mg of clay fraction was collected for oxygen isotope analysis and 50 mg for deuterium analysis.

A pure phase of clay is needed for isotopic work to be accurate and therefore, XRD analysis was undertaken on all clay separates to identify which mineral phases were present. The clay separates contained smectite, mixed layer corrensite and minor chlorite along with minor amounts of quartz. The amount of quartz was deemed to be nominal, however it will provide a further error that must be acknowledged. Gilg et al., (2004) have discussed ways in which clays such as smectite and chlorite can be separated. However, the effect of these separation techniques on the clays' isotopic signatures was poorly constrained and the techniques proved difficult and time consuming to achieve. It was therefore, decided to analyse the clay separates as a bulk separates and then analyse the results as end-member values.

2.8.2 Collecting the oxygen

Oxygen (in the form of CO_2) was collected using a glass oxygen fluorination line (Figure 2.11). Approximately 2 mg of sample powder was weighed and placed into a pre-baked sample block along with laboratory standards (Figure 2.12). The sample block was then placed into an oxygen line and evacuated before being reacted with Chlorine trifluoride ClF_3. On the first attempt samples were left to react with the reagent for approximately 2 hours to allow for moisture on the surface to react and for gases to be pumped away. However, the yields from this method were too low because the sample clays reacted very quickly with the reagent. It was therefore, decided not to pre-fluorinate. A larger shot of ClF_3 reagent was then released into the chamber and the sample was heated to > 1500 °C by a CO_2 laser (Sharp, 1990). The laser power was increased gradually. Combustion resulted in release of O_2 from the silica lattice. The gases from the fluorination process are passed through a slush trap (dry ice and acetone) and a further freeze trap (liquid nitrogen) to freeze impurities and left-over reagent,

which can be explosive on contact with air. All glass in the line is pre-heated and pumped prior to sending the sample through it in order to minimise sample contamination. The remaining O_2 was then then passed through a heated graphite rod that converted it to CO_2. This CO_2 gas yield was then measured before being collected in a mass spectrometer tube.

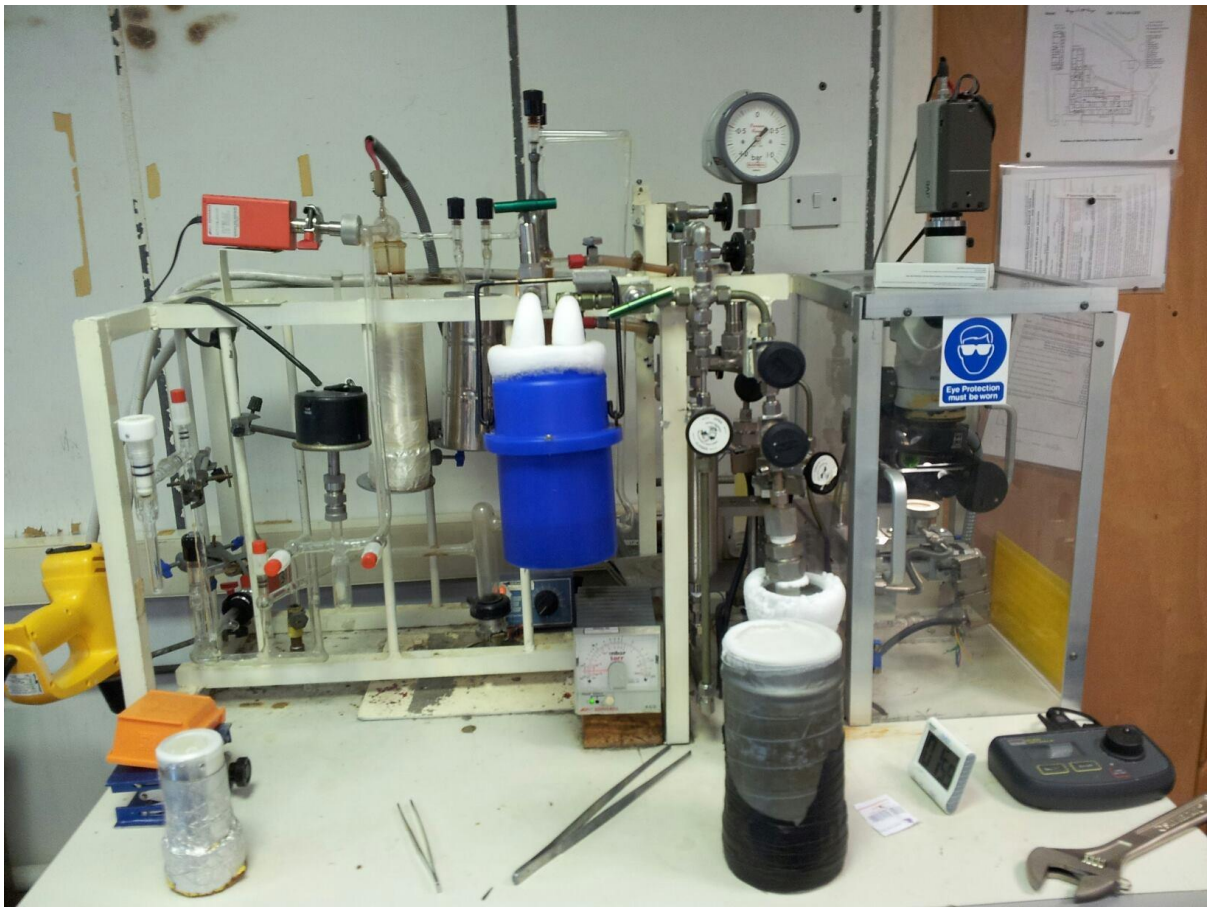

Figure 2.11: Oxygen fluorination line. SUERC.

Figure 2.12: Oxygen fluorination line sample holder containing approx. 2mg of clay sample (brown) and standards (white) in the wells. Sample block approx. 3cm in diameter.

2.8.3 Collecting the hydrogen

Hydrogen was collected using a glass hydrogen line (Figure 2.13). The sample Pt crucible was heated and left to outgas for 24 hours. Approximately 30 mg of sample was placed in the sample crucible and put under high vacuum, heated to 150 °C and left overnight to release labile volatiles. The samples were then placed in an evacuated quartz tube and heated to approximately 1200°C gradually by radiofrequency induction using a Cheltenham Induction Heater and coil for 30 minutes. The released gasses were then passed through a liquid nitrogen trap and frozen. The glass line is heated around the trap in order to collect any hydrogen that bonded to the glass. The liquid nitrogen trap is then removed and replaced with a slush trap. The slush trap is less cold and releases any CO_2 which can then be pumped away. The slush trap is removed and the remaining gas was passed through a chromium furnace at 800°C (Donnelly et al. 2001), which has the effect of reducing the water to H_2. The hydrogen is collected in a mercury monometer to measure the yield before it was collected in a mass spectrometer tube using a Toepler pump. Several international water standards; Greenland Ice sheet precipitate (GISP), Standard Mean Ocean Water (V-SMOW) and an internal lab specific standard (Lt Std) were run to calibrate the process. An international mineral standard NBS-30 (biotite) was also run.

Due to several problems with the hydrogen line only one sample was collected during two weeks. Tony Donnelly and Alison McDonald from SUERC performed the hydrogen collection at a later date.

Figure 2.13: Hydrogen Line. SUERC.

2.8.4 Analysis

The oxygen isotopes were analysed on-line by a VG SIRA 10 spectrometer by Alison McDonald. Reproducibility is better than ±0.3‰ (1σ). Results are reported in standard notation ($\delta^{18}O$) as per mil (‰) deviations from the Standard Mean Ocean Water (V-SMOW) standard.

Hydrogen isotopes were analysed by Tony Donnelly using a VG Optima mass spectrometer. Replicate analyses of water standards (mentioned above) gave a reproducibility of ±2‰. Replicate analyses of international mineral standard gave reproducibility around ±3‰.

2.9 Helium Porosity

Helium porosity was undertaken on a range of core and sidewall samples by Chevron. Helium gas at a known pressure was injected into the rock sample, the difference in pressure was then recorded and the porosity was calculated. Helium gas can penetrate

micro pores and so the helium porosity of a sample if often much higher than the visible porosity calculated from point counting. Chevron provided access to the helium porosity data set that was used within this thesis.

3 Geology of the Rosebank Field

This chapter aims to discuss the geology and hydrocarbon system within the Rosebank Field in the Faroe-Shetland Basin. Rock cores taken from the Rosebank wells are logged in detail providing context for the petrographic and diagenetic studies presented later in the thesis.

3.1 Introduction to the Faroe-Shetland Basin

The Faroe–Shetland Basin (FSB) is a series of northeast-southwest trending sub-rift basins that lie between Shetland and the Faroe Islands in the North Atlantic Margin, (Figure 3.1; Sørensen, 2003; Ritchie et al., 2011; Rateau et al., 2013). The evolution of these sub-basins was controlled by transfer zones during phases of rifting and compression that dictated sediment transportation and deposition in the depocentres (Figure 3.2; Dean et al., 1999; Jolley and Morton, 2007; Ellis et al., 2009; Moy and Imber, 2009; Fletcher et al., 2013; Wright, 2013).

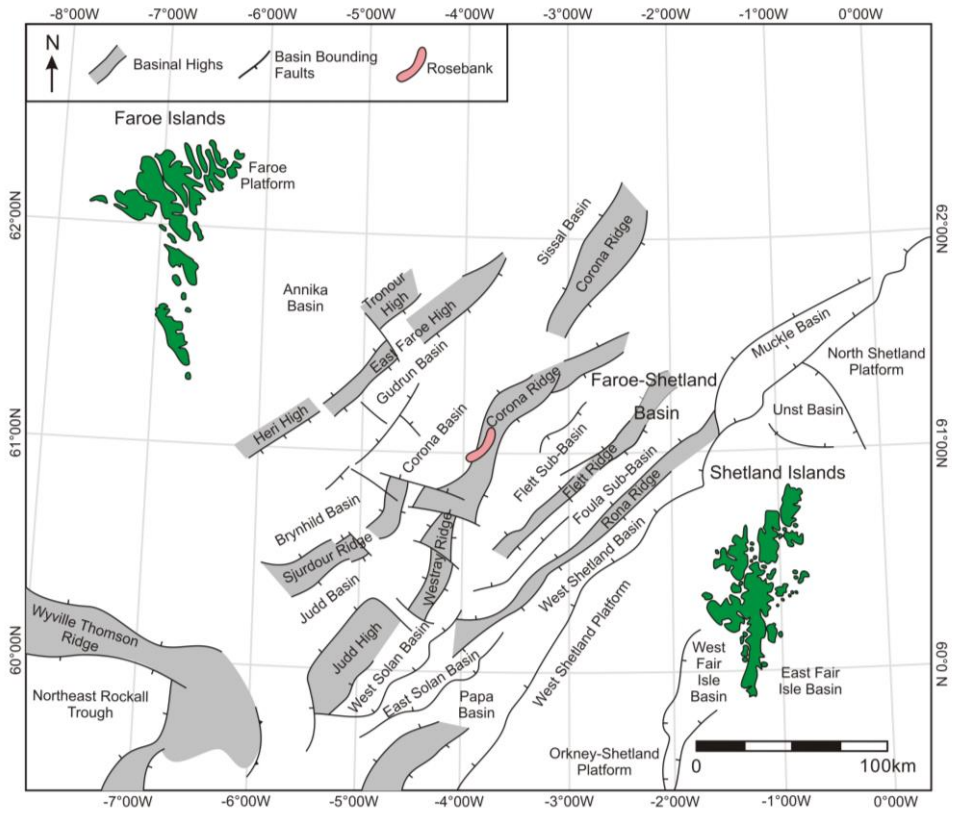

Figure 3.1: Location map of the Faroe-Shetland Basin and surrounding area, showing the highs and basins. Modified from Wright (2013) using from Stoker et al. (1993), Ritchie et al. (1996, 1999), Sørensen (2003), Ellis et al. (2009) and Moy & Imber (2009).

3.2 Geological history of the Faroe-Shetland Basin

The southern part of the FSB has had a complex geological history with a number of major tectonic events that influenced both sedimentation and the structural development of the basin (Figure 3.3 and 3.4; Dean et al., 1999).

The FSB is approximately 260 km wide by 460 km long and comprises a series of sub-basins divided by intra-basin highs (Ritchie et al., 2011). The basin floor is composed of late Archean to Paleo-proterozoic metamorphic crust from the Laurentian Terrane. During the early Palaeozoic the region was subjected to compression from northeast-trending Caledonian Orogenic thrust belts (McKerrow et al., 2000; Oliver, 2002; Strachan et al., 2002; Ritchie et al., 2011). Once the Caledonian Orogeny ended in the Late Devonian the compressional structural regime changed to an extensional inter-montane rift basin setting (Roberts et al., 1999; Soper and Woodcock, 2003; Ritchie et al., 2011).

The next major tectonic event to affect the FSB was the Variscan Orogeny caused by the closure of the Pangaean supercontinent in the Late Carboniferous to Permian, (Roberts et al., 1999; Glennie, 2002; Ritchie et al., 2011). This resulted in volcanism in the southeast of the FSB (Glennie, 2002; Ritchie et al., 2011). At the end of the Permian, the northeast trending Arctic Rift developed and was influenced by the inherited basement structures developed during the Caledonian Orgoeny (Roberts et al., 1999; Ritchie et al., 2011). This rift caused the development of peripheral sub-rift basins. Throughout the Jurassic, the Arctic Rift moved northwards (Roberts et al., 1999). During the late Jurassic rifting was responsible for a marine transgression (Dean et al., 1999).

The FSB was dominated by a northwest-southeast trending extensional regime, which coincided with the main phase of rifting in the Atlantic in the Early Cretaceous. This led to regional uplift of the margin and a fall in relative sea level (Naylor and Shannon, 2005; Mudge et al., 2009). This phase of rifting was the major control on the lateral distribution of sediments (Larsen et al., 2010): clastic material was shed into the FSB from the West of Shetland High and the emergent Crona, Judd, Westray, Rona and Flett highs (Figure 3.5) and deposition was dominated by mudstones and argillaceous limestones.

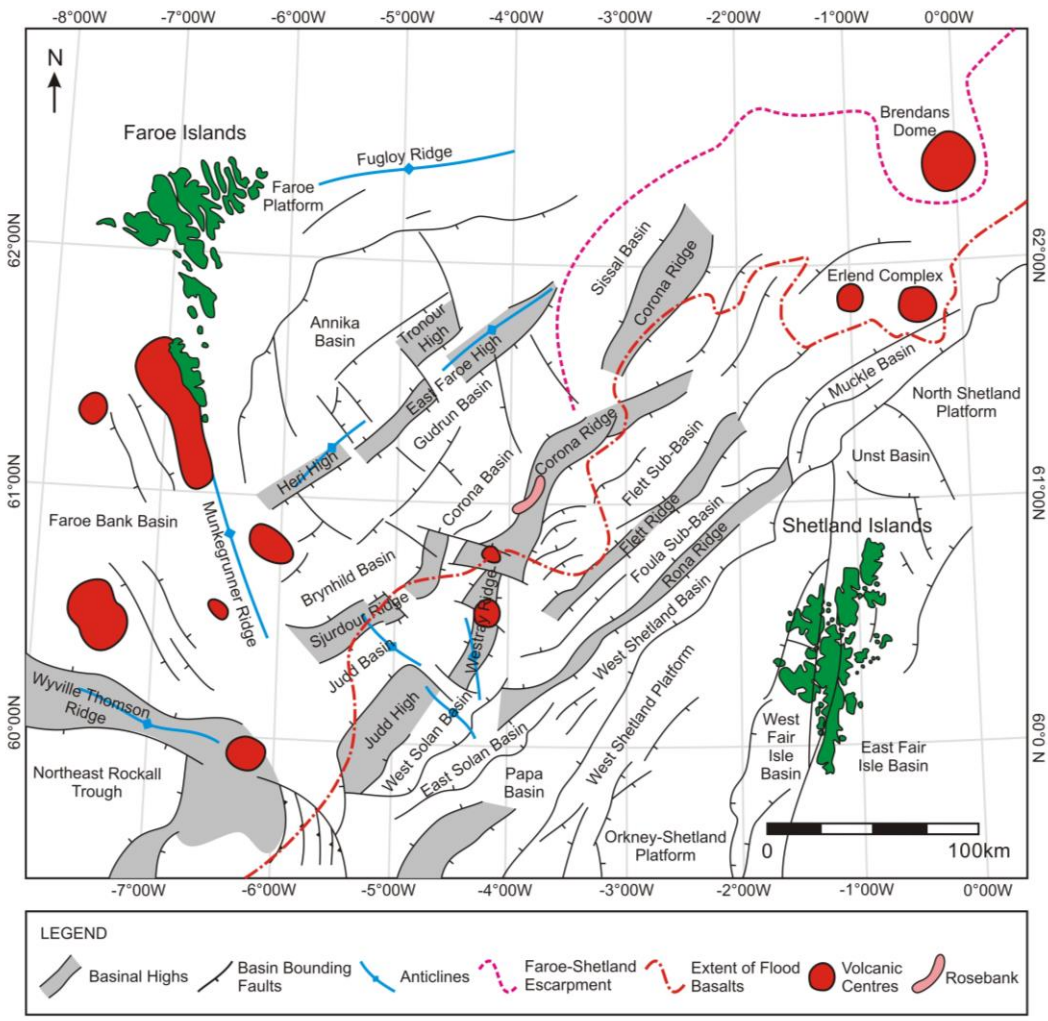

Figure 3.2: Map showing the basin structure within the Faroe-Shetland Basin. (Wright (2013) modified from Stoker et al. (1993), Ritchie et al. (1996, 1999), Sørensen (2003), Ellis et al. (2009) and Moy & Imber (2009)).

The Upper Cretaceous was marked by a period of tectonic quiescence accompanied by passive infill of early Cretaceous rift basins. A marine transgression submerged local highs, including the Corona Ridge (Figure 3.6) and a northward transition from carbonaceous siltstones and claystones to predominantly argillaceous limestone with rare carbonate shelf deposits, filled the Flett Sub-Basin (Mudge et al., 2009). The latter sequence is thicker in the northern part of the basin due to later inflation by igneous intrusions.

Localised rifting followed by regional uplift occurred in the Danian. Reactivation of Cretaceous faults led to a fault-driven topography, with a syn- to early post-rift phase leading to the creation of sub-basins (Mudge et al., 2009). In the Southern Flett Basin deep marine mudstones with mixed sandstone and mudstones marked the onset of deep water fan progradation into the FSB (Figure 3.7).

During the Upper Selandian, volcanic activity related to the rifting of the Atlantic began to the west of the FSB. Localised topography resulted in the development of submarine fans on the basin floor that extended to the Corona High to the west (Figure 3.8). A chaotic, submarine fan sequence with northwest-meandering channelised sands was deposited during this time (the Valia Formation). Later, the Lamba Formation, composed of progradational sands and mudstones, built out into the FSB from the SE (Mudge et al., 2009; Stoker and Varming, 2011).

The Icelandic plume is thought to have impacted 62 Ma ago and was responsible for the development of the North Atlantic Igneous Province (NAIP), which covers an area of 10^6 km^3 (White and McKenzie, 1989). Volcanism developed in areas of weakened crust along the rift margin, including East Greenland, the Faroe Islands, the west coast of Scotland, and eastern Ireland (Saunders et al., 1997).

During the Thanetian, basalt lavas erupted on the Faroe Islands and East Greenland and spread across ~12 0000 km^2 (Passey and Hitchen, 2011). The oldest Palaeocene volcanic unit (the Lopra Formation encountered in boreholes on the Faroe Islands) comprises a series of volcaniclastic rocks intruded by sills (Ellis et al., 2002; Passey and Jolley., 2009). The volcaniclastic rocks record the progradation of lava-fed, Gilbert-type hyaloclastite deltas into the FSB. These caused a rotational shift in the orientation of the shoreline (Kiørboe, 1999; Passey and Hitchen, 2011; Wright, 2013). The overlying Beinisvørð Formation is ~3.3 km thick, and 900 m of it are exposed on the Faroe Islands (Passey and Hitchen, 2011). It is composed of aphyric basalt lavas (Waagstein, 1988), fed from extensive fissure systems (Passey and Bell, 2007), that covered the western portion of the FSB covering local basin highs, including the Corona Ridge (Figure 3.9) (Boldreel and Andersen, 1994).

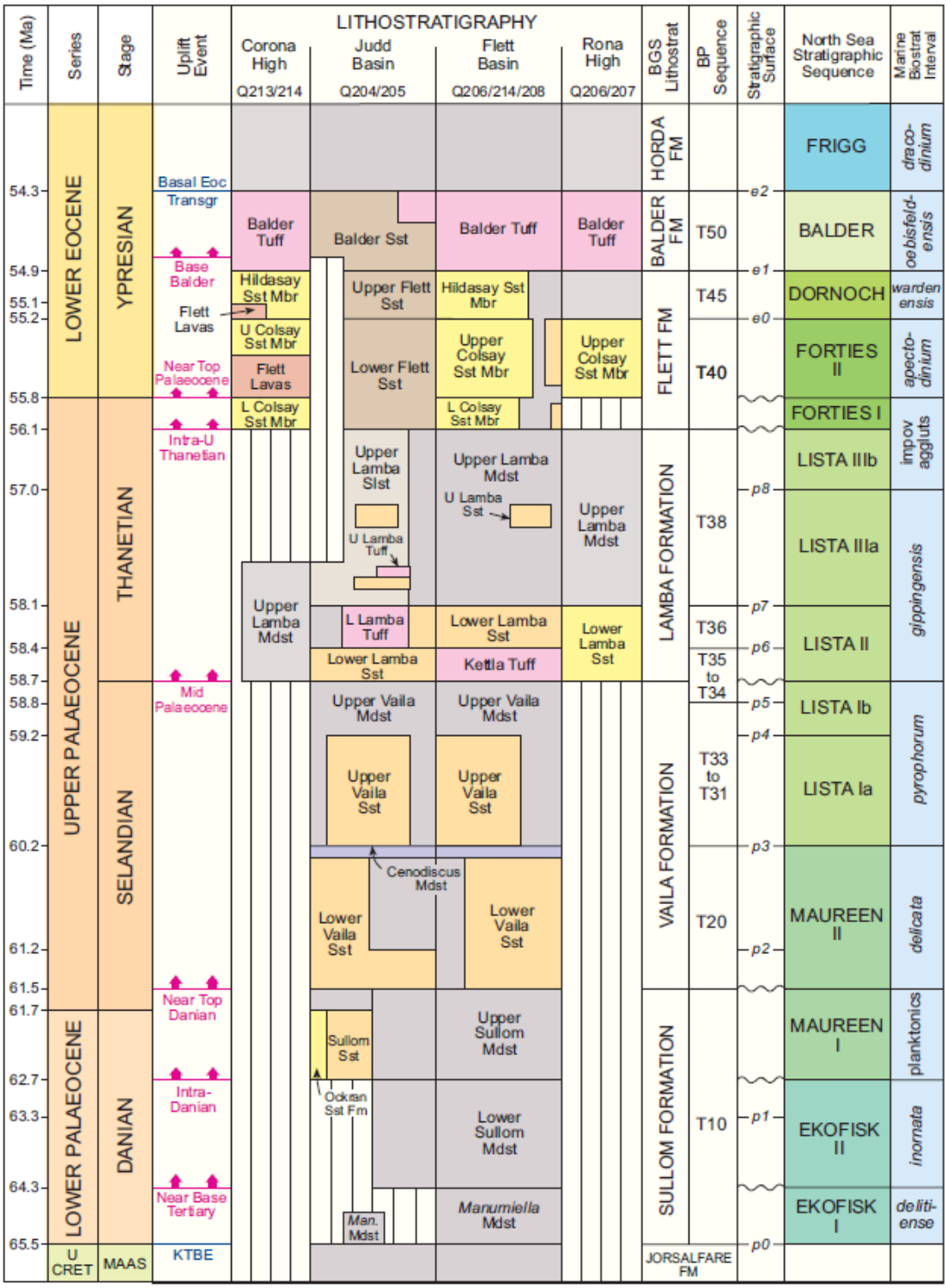

Figure 3.3: Stratigraphical column for the structural highs and basins within the Faroe-Shetland Basin. (Mudge et al., 2009).

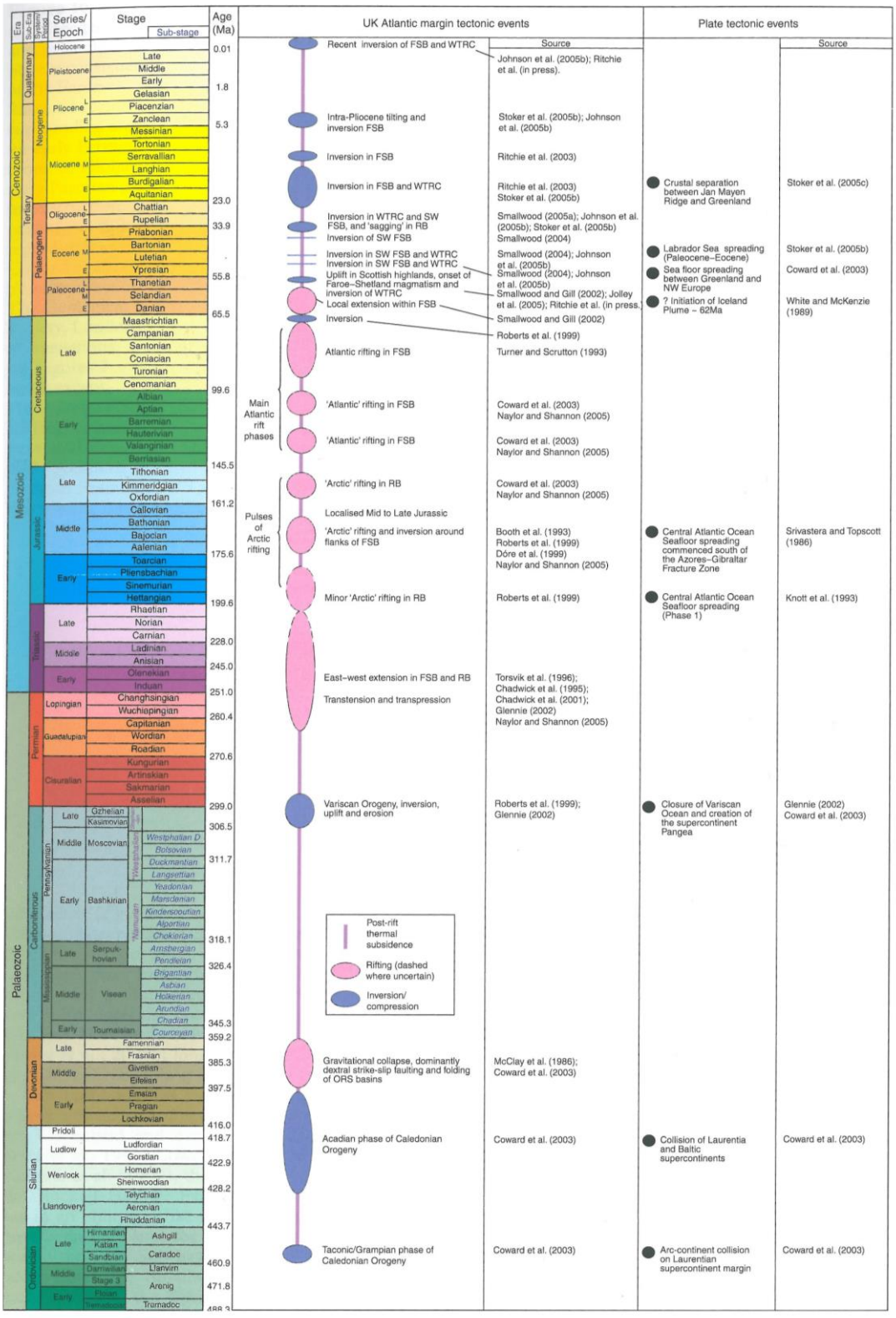

Figure 3.4: Generalised summary of the plate tectonic events within the Faroe-Shetland region. FSB- Faroe-Shetland Basin, RB- Rockall Basin and WTRC- Wyville Thomson Ridge. (From Ritchie and Ziska 2011).

The volcanic rocks are thought to have interacted with and deflected the existing siliciclastic input as the volcanic rocks progressed westwards (Mudge et al., 2009; Stoker and Varming, 2011). A hiatus in volcanism led to the back-stepping of lava flow fields and localised erosion. The Prestfjall Formation comprising of coals, claystone and volcaniclastic sandstones (Rasmussen and Noe-Nygaard, 1970; Passey and Jolley., 2009) were deposited onshore on the Faeroe Islands while its chronostratigraphical equivalent the Flett Delta (Flett Formation) was present in the FSB (Ellis et al., 2002; Jolley et al., 2002). The Hvannhagi Formation overlies the Prestfjall Formation on the Faeroe Islands (Passey and Jolley., 2009), comprises both pyroclastic and sedimentary rocks. These rocks are thought to be deposited in a terrestrial environment during quiescent inter-volcanic periods (Passey, 2004) and so correlate with the Colsay Formation found within Rosebank. The north westerly prograding sedimentary sequence initiated in the Selandian becomes a northerly prograding sequence that deposited the Colsay Sandstone Member: a predominantly terrestrial delta-top and fluvial sequence of rocks interbedded with lava flows (see Section 3.5 for more detail).

Volcanism recommenced on the Faroe Islands and is recorded by the Malinstindur Formation comprising thin anastomosing subaerial lava flows. However, this formation is not thought to have reached the FSB (Passey and Bell, 2007). The Enni Formation is the upper-most formation found on the Faroe Islands and is identified in the FSB. It is similar to the Beinisvørð Formation but comprises a mixture of compound and thin (<2.5 m) tabular flows suggesting it is sourced from point sources as well as fissures (Passey and Bell, 2007).

Volcanism began to wane in the Ypresian and lava flows retreated to the west (Figure 3.10) (Mudge et al., 2009). This allowed the fluvio-deltaic system seen during the Thanetian to once again dominate, and is recorded by the Hildasay Sandstone Member (Flett Formation); a predominantly terrestrial, delta-top and fluvial sequence of rocks (Mudge et al., 2009; Stoker and Varming, 2011). Transgression towards the end of the Ypresian resulted in the delta sediments backstepping into the basin.

Overlying the Flett Formation is the Balder Formation, which represents the final volcanism recorded within the basin. The formation is typically between 50–150 m thick (Passey and Hitchen, 2011), covers the FSB and marks a regional unconformity (Dean et al., 1999; Rateau et al., 2013). It is composed of silty, carbonaceous mudstone interbedded with reworked basaltic tuffs (Knox et al., 1988) sourced to the west of the FSB (Faroes and Greenland), with some volcanic input from the Scottish hinterland

(Morton and Knox, 1990). Volcanic glass within the tuffs has been extensively altered to palagonite and chlorite (Passey and Hitchen, 2011).

During the Late Eocene, volcanism ceased and the basin underwent a post-rift phase. Thermal subsidence led to thick (~550 m) accumulations of deep-water sediments (Brooks et al., 2001; Rateau et al., 2013). Sub-basinal highs became submerged leading to the formation of a large interconnected basin that forms the FSB seen today (Ritchie et al., 2011). The Eocene, Oligocene and Miocene were punctuated by basin-wide uplift that led to the formation of inversion structures (Smallwood and Kirk, 2005).

Volcanic activity in the FSB was also accompanied by the intrusion of large volumes of basaltic magma. The Faroe-Shetland Sill Complex (FSSC) is an extensive (~ 2.25×10^5 km^2) complex of sills and dykes that intrude the sedimentary rocks within the FSB (Hitchen and Ritchie., 1987). Most of the FSSC rocks intrude Upper Cretaceous strata, similar to the Palaeogene dyke swarm on Mull (Emeleus and Gyopari, 1992). There are also Thanetian aged sills intruded into Paleocene sedimentary rocks (Lamers and Carmichael, 1999). The majority of the intrusions occur towards the centre of the FSB, which has experienced the most crustal extension (Smallwood and Maresh, 2002).

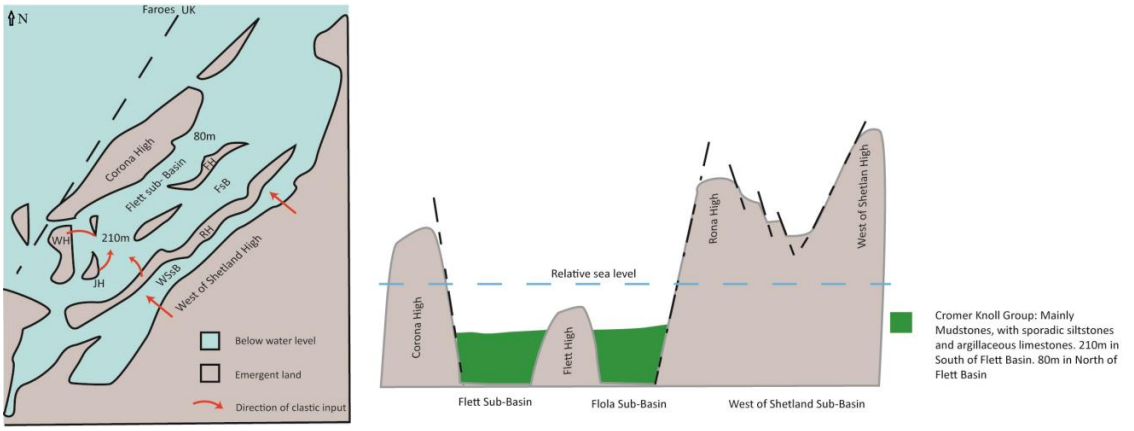

Figure 3.5: Schematic map and cross section of the Faroe-Shetland Basin, showing the relative sea level and sediment deposition during the Lower Cretaceous. Sketch map is orientated North. Line of section runs NW-SE. Scale of section ~80 km across. Modified from Mudge et al., (2009); Dean et al., (1999); Stoker and Ziska, (2011).

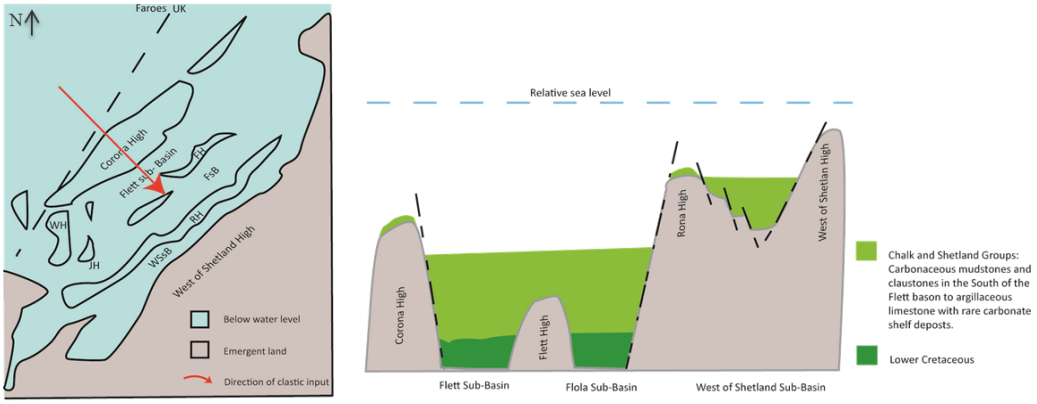

Figure 3.6: Schematic map and cross section of the Faroe-Shetland Basin, showing the relative sea level and sediment deposition during the Upper Cretaceous. Large red arrow indicates transgression. Sketch map is orientated North. Line of section runs NW-SE. Scale of section ~80 km across. Modified from Mudge et al., (2009); Dean et al., (1999); Stoker and Ziska, (2011).

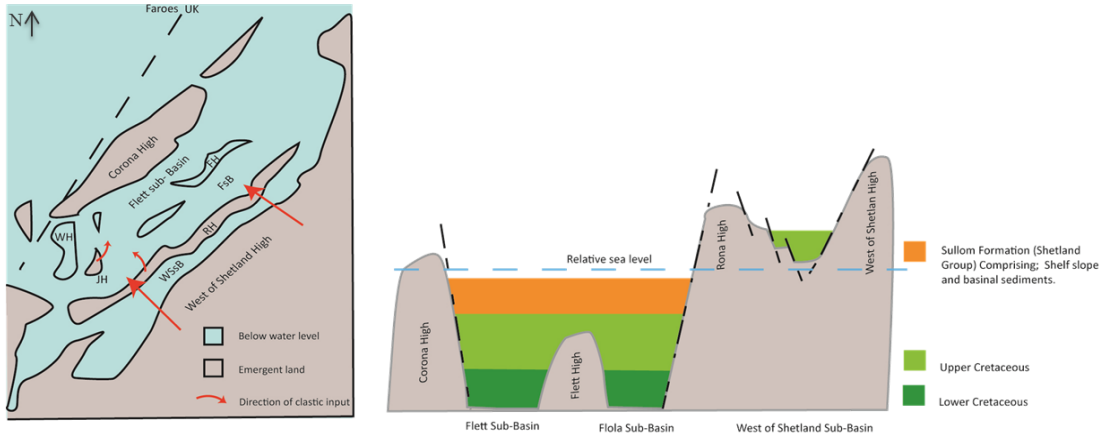

Figure 3.7: Schematic map and cross section of the Faroe-Shetland Basin, showing the relative sea level and sediment deposition during the Danian, Lower Palaeocene. Sketch map is orientated North. Line of section runs NW-SE. Scale of section ~80 km across. Drawn using information from Mudge et al., (2009); Dean et al., (1999); Stoker and Varming, (2011).

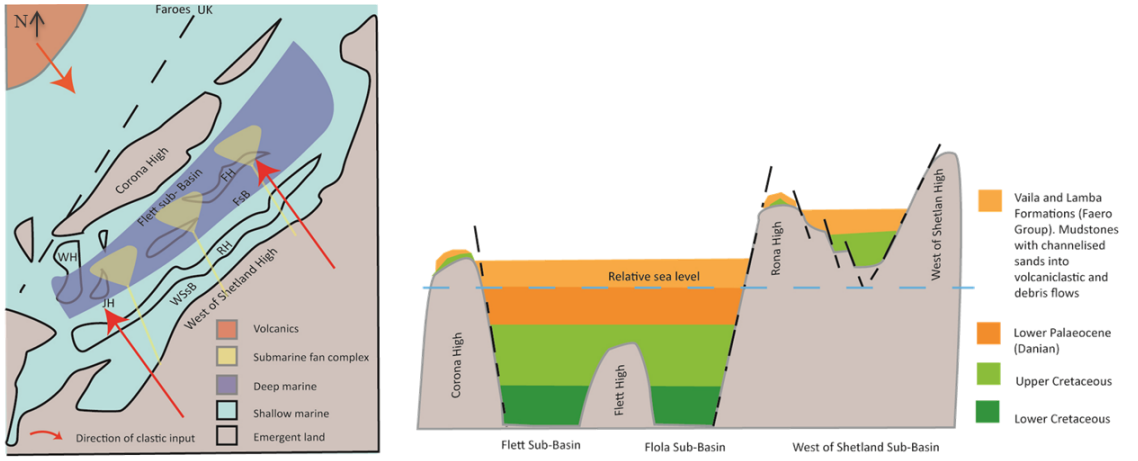

Figure 3.8 Schematic map and cross section of the Faroe-Shetland Basin, Upper Selandian, Palaeocene. Sketch map is orientated North. Line of section runs NW-SE. Scale of section ~80 km across. Modified from Mudge et al., 2009; Dean et al., 1999; Stoker and Varming, 2011.

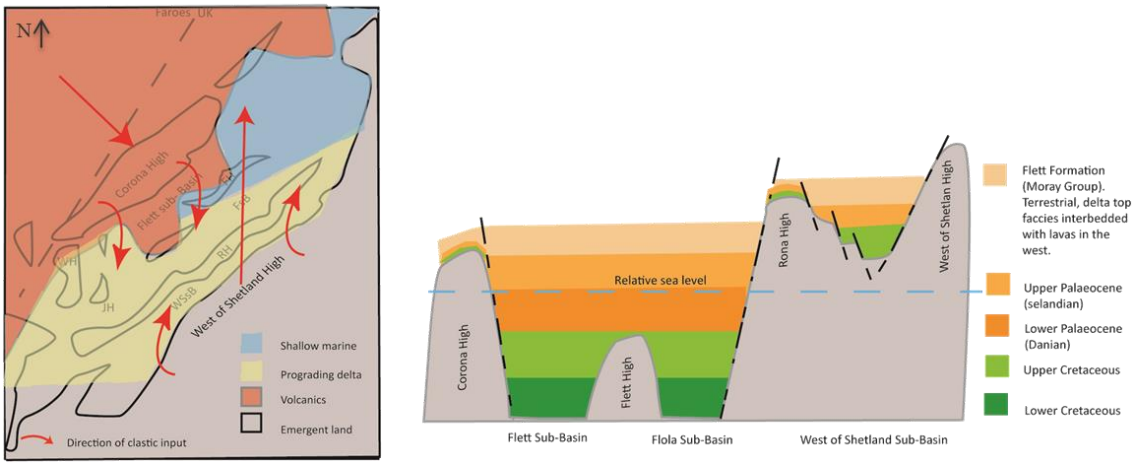

Figure 3.9 Schematic map and cross section of the Faroe-Shetland Basin, showing the relative sea level and sediment deposition during the Thanetian, Upper Paleocene. Sketch map is orientated North. Line of section runs NW-SE. Scale of section ~80 km across. Modified from Mudge et al., 2009; Dean et al, 1999; Stoker and Varming, 2011; Passey and Hitchen, 2011.

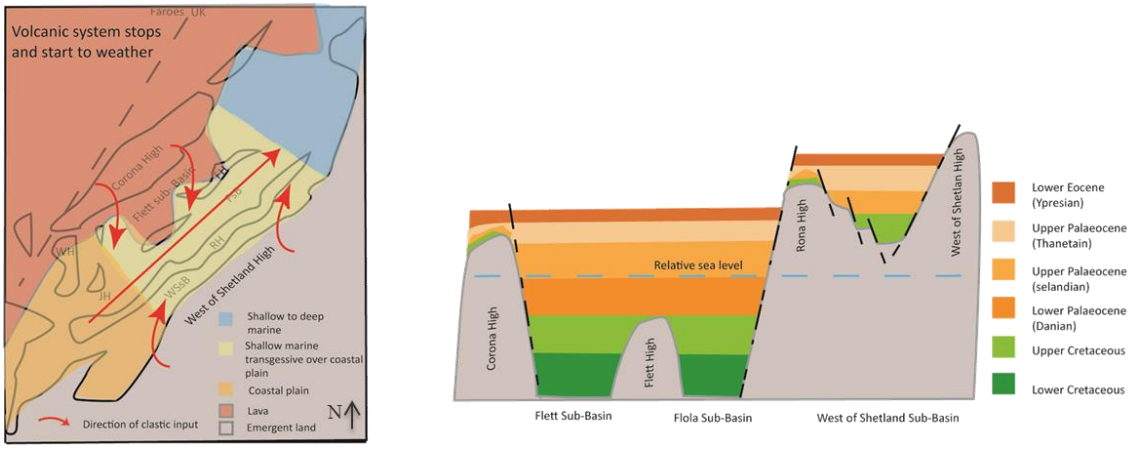

Figure 3.10 Schematic map and cross section of the Faroe-Shetland Basin, showing the relative sea level and sediment deposition during the Ypresian, Lower Eocene. Sketch map is orientated North. Line of section runs NW-SE. Scale of section ~80 km across. Modified from Mudge et al., 2009; Dean et al., 1999; Stoker and Varming, 2011; Passey and Hitchen , 2011.

3.3 Hydrocarbon system within the Faroe-Shetland Basin

The northeast-southwest trending depocentres within the sub-rift basins of the FSB contain commercially viable hydrocarbon reserves (Figure 3.11). All the elements of a typical hydrocarbon system can be found within the basin, however the large volume of volcanic and volcaniclastic rocks within the north west of the basin has limited oil exploration in the NW of the basin, to date.

3.3.1 Source rocks

Within the FSB nine potential source rocks have been identified, with four (Middle Devonian, Lower Jurassic, Middle Jurassic and Upper Jurassic) being linked to proven hydrocarbon resources (Peters et al., 1989; Bailey et al., 1990; Scotchman and Thomas, 1995; Bailey et al., 1987; Quinn et al., 2011). The organic-rich Kimmeridge Clay Formation (KCF) is the major source rock within both the FSB and the North Sea (Holmes et al., 1999). Local to the Rosebank area there are four distinct types of hydrocarbon fields (Gas, Gas and Concentrate, Oil and Oil and Gas), (Table 3.1). All the fields in the FSB have a Kimmeridge Jurassic Type II source rock.

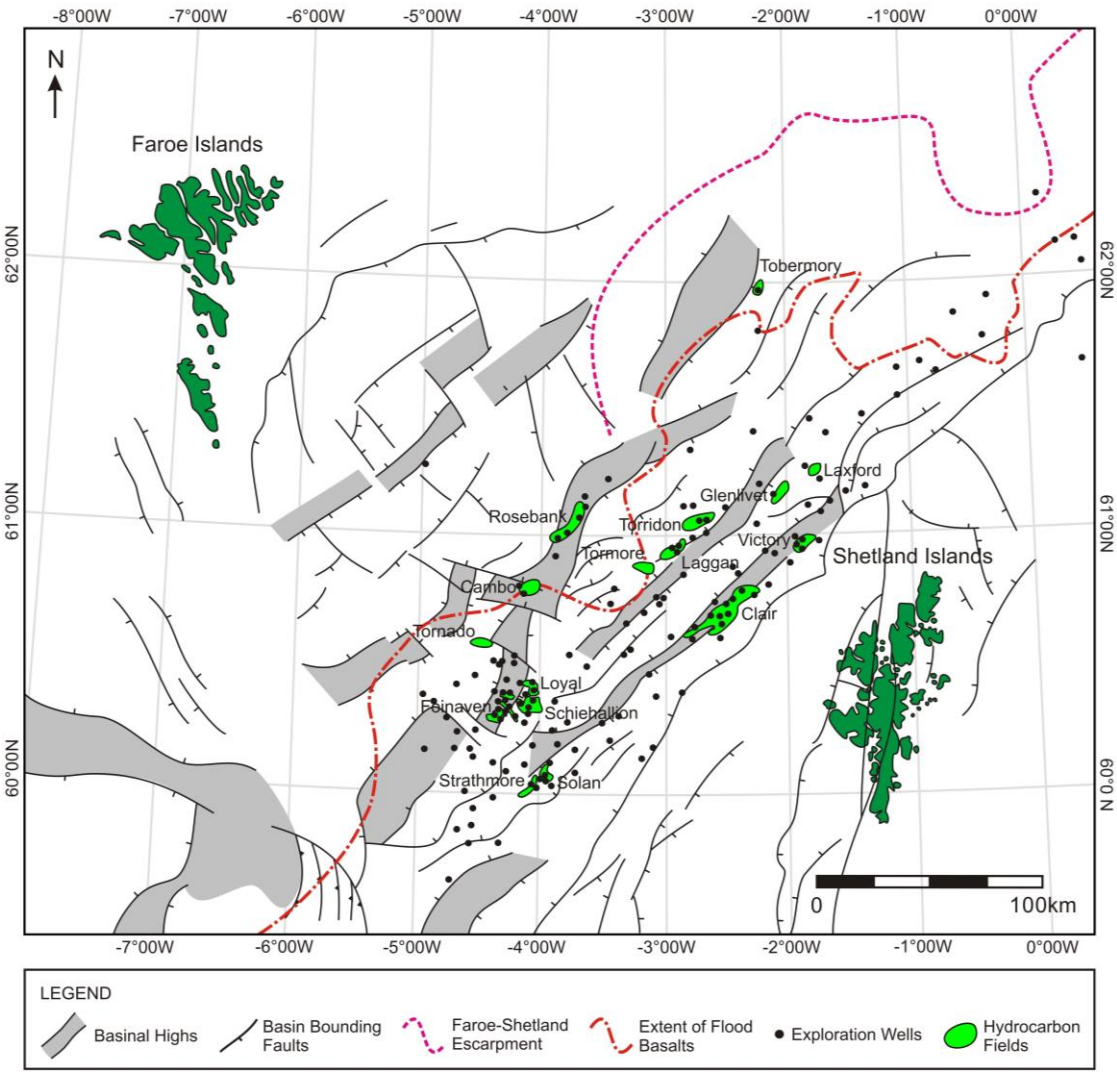

Figure 3.11 Map of hydrocarbon wells and fields within the Faroe-Shetland Basin, highlighting the economic potential of the area. Taken from Wright, 2013.

Name	Hydrocarbon type	Source
Victory	Gas	Multiple?
Laggan	Gas and condensate	Upper Jurassic type II source
Strathmore	Oil	Upper Jurassic type II source
Cambo	Oil	Upper Jurassic type II source (KCF)
Rosebank	Oil and gas	Upper Jurassic type II source (KCF)
Foinaven	Oil and gas	Middle Jurassic lacustrine source mixed with Upper Jurassic (KFC)
Clair	Oil and gas	Upper Jurassic type II source (KCF)

Table 3.1 Hydrocarbon fields within the Faroe-Shetland Basin (Clark and Campbell, 2011).

3.3.2 Reservoir rocks

There are a number of economically viable reservoir units of varying age and type found throughout the FSB (Table 3.2). The Upper Vaila Formation is the prime target in the majority of the fields. The Cambo field found along strike, has a similar aged discovery to the Rosebank field. High quality reservoir is found in the Cambo field with a permeability range of 100 mD to >1 Darcy (Fielding et al., 2014).

Field Name	Reservoir Unit	Age
Cambo	Hildasay/ Colsay Sandstone Mb	Ypresian
Rosebank	Colsay Sandstone Mb	Thanetian / Ypresian
Tornado	Lamba Fm	Thanetian
Tormore	Upper Vaila Fm	Selandian
Laggan	Upper Vaila Fm	Selandian
Glenlivet	Upper Vaila Fm	Selandian
Torridon	Upper Vaila Fm, Lower Vaila Fm	Selandian
Schiehallion	Upper Vaila Fm	Selandian
Suilven	Upper Vaila Fm	Selandian

Table 3.2: Reservoir units within the Faroe-Shetland Basin Data compiled by Rosebank Team, (2009).

3.3.3 Seal rocks

A number of rock units act as seals within the FSB basin. The majority of the basin is sealed by low porosity, low permeability shales; however Late Thanetian and Ypresian aged reservoir intervals (Colsay Sandstone Mb) are sealed by shale and silts deposited during and after the transgression and in the thermal subsidence phase of the basin. The Balder Formation is also a possible seal (Rosebank Team, 2009).

3.3.4 Expulsion, Migration and Charge

Expulsion of hydrocarbons began in the Early Cretaceous and continued until the early Eocene. Peak expulsion is estimated to have occurred in the Upper Cretaceous (Scotchman et al., 2006; pers comm. Value Creation Team, 2011). Hydrocarbon migration began shortly after expulsion started in the Early Cretaceous. A second period of migration started in the Late Cretaceous and continues to the present day. Three phases of charge have been identified within the basin, the first in the Early Cretaceous with the deeper reservoirs within fault blocks being charged and then two later phases within the Paleogene (Ritchie et al., 1999; Scotchman et al., 2006).

3.3.5 Traps

A number of different trap types occur within the FSB (Naylor et al., 1999), including inversion anticline structures (Doré et al., 1997), magmatic-driven uplift (Lamers & Carmichael, 1999), resulting in stratigraphic and fault bounded traps.

3.3.6 Timing

The timing of each element within the petroleum system in the FSB is shown in Figure 3.12. The basin has all the elements required with suitable timings from source formation in the Upper Jurassic up to trap formation during the Eocene, Oligocene and Neogene. The trap formation occurs well after peak expulsion and migration. A number of theories have been proposed to explain the discrepancy in timing. The first is that a large volume of hydrocarbons had already been lost from the system. The second is that the hydrocarbons had been temporarily stored in another deeper reservoir before re-migrating to their current position after trap formation. This model is named the Motel model (Lamers and Carmichael, 1999). The Whoopie Cushion model by Iliffe et al., (1999) suggests a similar system where hydrocarbons migrate laterally out of deep reservoirs. A build-up of pressure results in fracturing of the overlying seals and hydrocarbons can migrate through this fracture network into the present day reservoirs. Scotchman et al., (2006) however, highlight a number of problems with the above models stating that the models fail to consider the fluctuation in heat flow during rifting and therefore the influence of overpressure. As a result, they believe that the discrepancies in timing can be explained by delayed hydrocarbon generation due to overpressure.

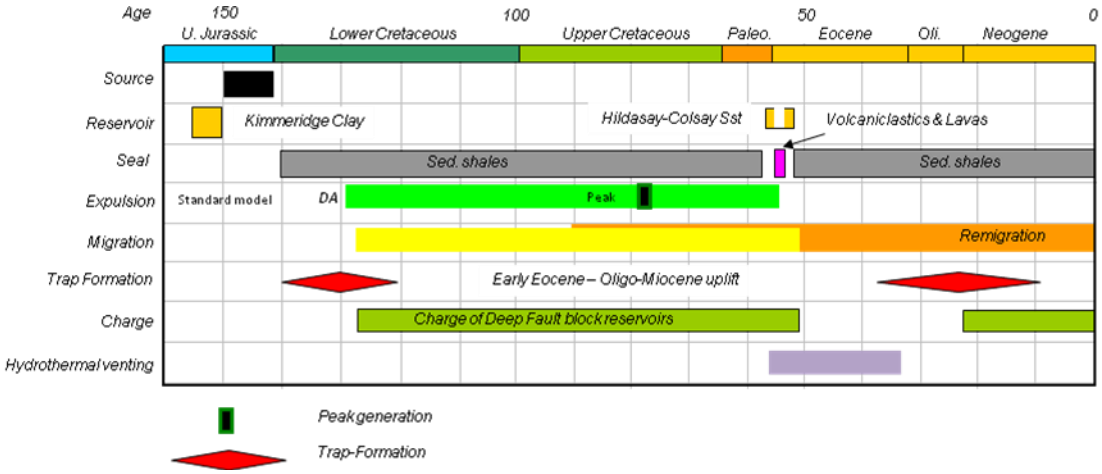

Figure 3.12 Timing of the different elements within the hydrocarbon system within the Faroe-Shetland Basin (Modified from Clark and Campbell, 2011).

3.4 The Rosebank Field

The Rosebank Field is approximately 20 km long by 5 km wide and sits on the Corona Ridge, ~125 km northwest of Shetland and close to the boundary between the UK and Faroese territorial waters (Figure 3.13). The field was discovered during the drilling of the 213/27-1z well by the Rosebank Partnership (Chevron 40% and operator, Statoil 30%, OMV 20% and DONG 10%) in 2004. The primary target was initially the Cretaceous sandstones below the basalt cover within a four way dip closure, however, oil shows were found within the overlaying Palaeocene rocks. From 2011 the Rosebank Partnership became OMV 50%, Chevron 40% and DONG 10%. The well encountered a series of petroleum bearing siliciclastic rocks with high porosity (up to 25 %) and permeability (~3.5 D). These reservoir intervals are interbedded with volcanic rocks. To date, six wells and two sidetracks have been drilled, orientated NE-SW along the crest of the Rosebank structure (Figure 3.14). All wells encountered oil shows at the Colsay Sandstone Member level (depth of ~2700 m), while only 213/27-3 in the north of the structure found a very thin interval of oil (approx. 6 m net pay) at the Hildasay Sandstone Member level (depth of ~ 2500 m).

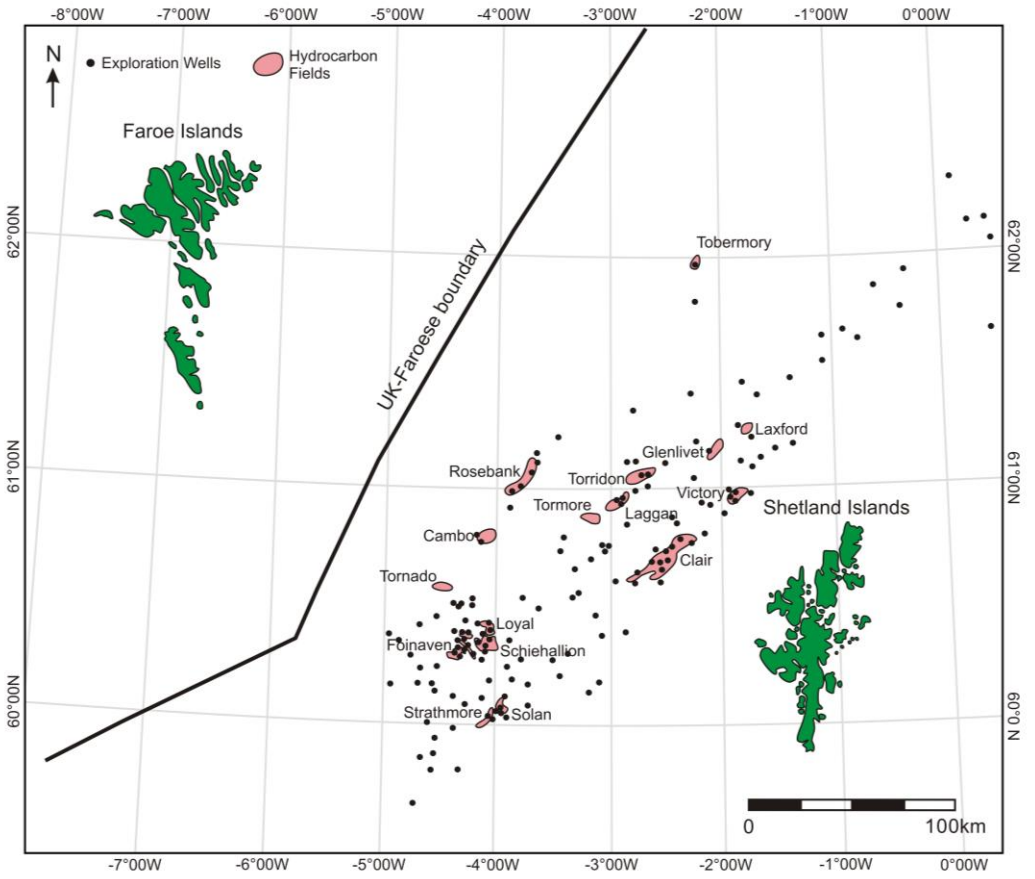

Figure 3.13: Location map Rosebank Field. Only UK wells plotted. Edited from Wright, 2013.

3.4.1 Rosebank petroleum system

The source rock in the Rosebank Field was proven in the 213/27-1z and 213/27-2 wells to be Upper Jurassic Kimmeridgian shale with an average Total Organic Content (TOC) of 5.8% and Type II kerogen (Rosebank Team, 2009). The average source rock thickness is 77 m, but it is thought to thicken off the Corona Ridge. A maximum thickness of 236.8 m occurs off the Westray High (Quinn et al., 2011).

Reservoir rocks occur in the Colsay Sandstone Member of the Flett Formation (Upper Thanetian and Lower Ypresian). These are typically fluvio-deltaic sands with high porosity (~20%) and permeability (up to 3.5 Darcies). The Hildasay Sandstone Member has similarly high reservoir qualities, however no oil and gas were found within this unit, other than a small 6 meter unit in the 213/27-3 well due to a possible breach in the seal (Rosebank Team, 2009).

The seal within the Rosebank Field differs slightly from surrounding plays such as Cambo, where the Hildasay Sandstone Member is thought to be sealed by silty

sediments seen within all the wells. However, no hydrocarbons occur within the Hildasay Formation indicating that the seal has been breached. A series of channels (the Breydon channels) cut into the overlying Balder Formation and this erosion, combined with faulting, is held responsible for the possible leak (Clark and Campbell, 2011). The Colsay Sandstone Member (which is the reservoir within Rosebank) is thought to be sealed by Late Thanetian T40-45 mudstones of the Flett Formation. However, the reservoir units were also periodically covered by basalt lava flows. The role of these volcanic rocks in sealing the system is still not fully understood.

3.4.2 Stratigraphy

Seismic data can be used to divide the field into four chronostratigraphic units, which equate to reservoir units (Colsay 1–4) interbedded with volcanic rocks. Figure 3.15 shows a chronostratigraphic correlation based on well log information. The Colsay units are named in reverse chronostratigraphical order: Colsay 4 is the oldest unit.

Colsay 4 is the oldest unit of the Colsay Sandstone Member. Its thickness is fairly constant across the reservoir ranging between ~30.5 – 46 m. Overlying this is a thick package of volcanic rocks named the Rosebank Lower Volcanic Unit, which at its thickest reaches ~91 m, comprising basaltic lavas and associated volcaniclastic rocks.

The Rosebank Lower Volcanic Unit is overlain by another thin layer of volcanic rocks, followed by the Colsay 3 reservoir unit. Colsay 3 varies considerably in thickness along the Rosebank structure. In the south it is approximately 5.5 m but thickens to 54 m in the north of the structure. It has volcanic facies (Net to Gross of 0%) in the south and siliciclastic sandstones with a (NTG) of 60% and porosities averaging 20% in the north. The Colsay 2 unit comprises volcanic rocks with rare, thin siliciclastic sands and silts found in the northern wells.

Overlying this another unit comprising basaltic lavas and above this is the Colsay 1 reservoir unit. Lithostratigraphically the unit varies along the crest of the structure from 48 m of silicilclastic sandstones in the south to 41 m of volcaniclastic rocks in the north (the exact opposite of Colsay 3). The porosity and NTG ratio of the unit also varies, ranging from 21% and 55% respectively, in the southernmost well (205/1-1) to 0% porosity and NTG in the northern wells. The uppermost unit in the Colsay Sandstone Member is the Upper Rosebank Volcanic Unit, which is composed of ~76 m of basalt lava flows and volcaniclastic rocks.

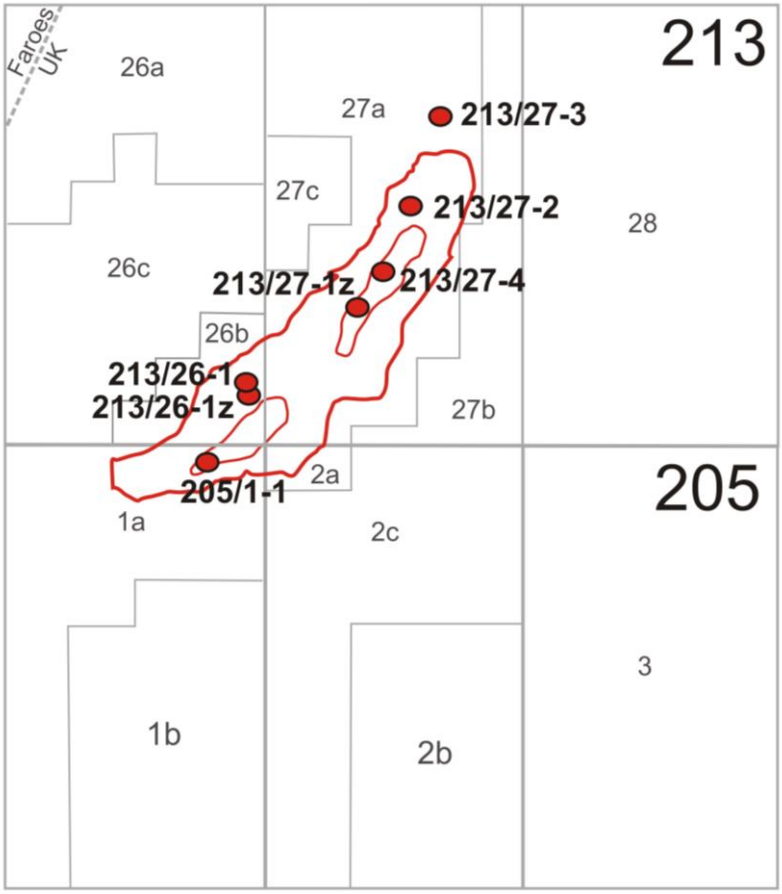

Figure 3.14: Map showing the relative locations of the Rosebank wells. Drawn using data from Duncan et al., (2009) and Fielding et al., (2014).

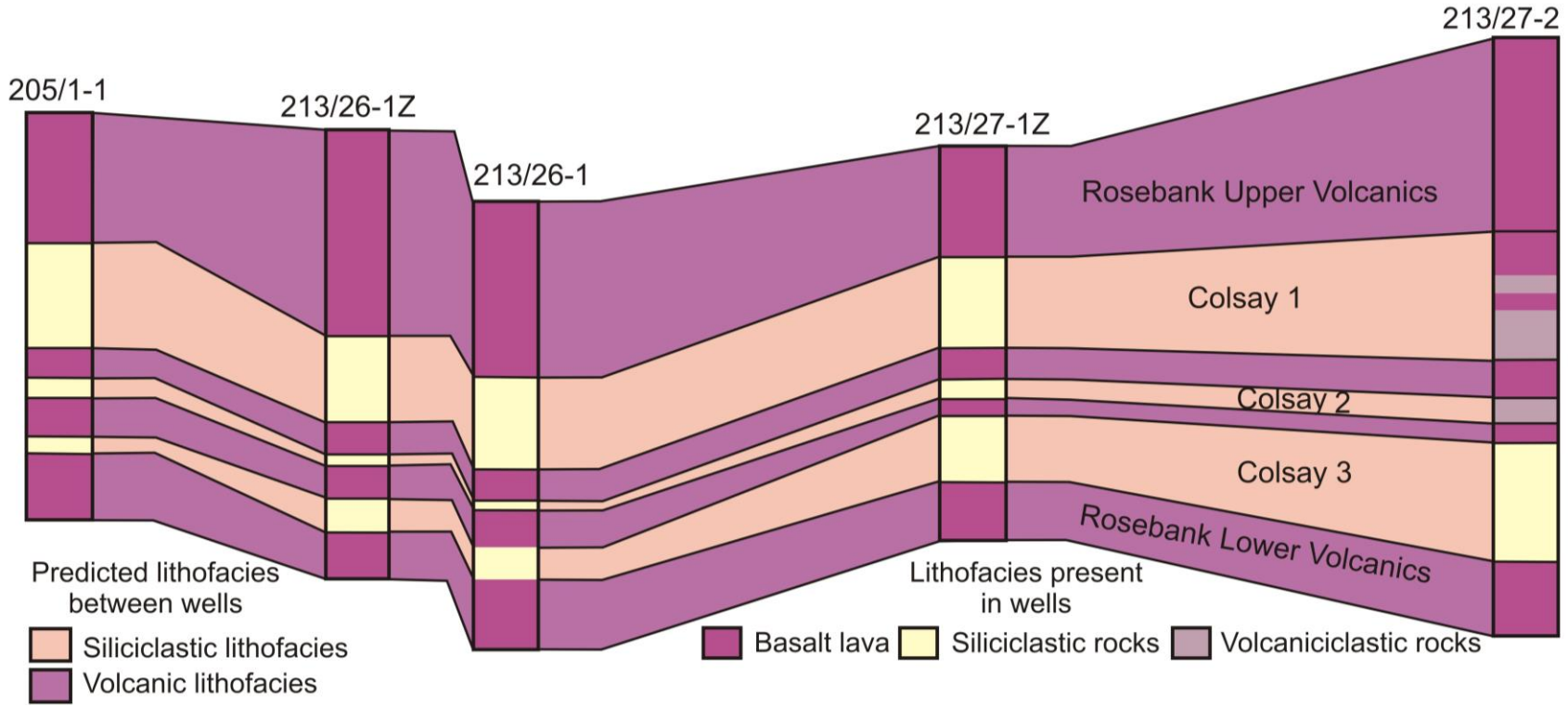

Figure 3.15: Schematic well correlation across the Rosebank Field. Purple colours represent volcanic lithofacies, sandy coloured units represent siliciclastic lithofacies. Units are correlated chronostratigraphically. The schematic highlights the alteration between volcanic and siliciclastic rocks vertically through the reservoir. Note variation also occurs along strike with volcanic rocks occurring in the 213/27-2 well in Colsay 1. Modified from Rosebank Team (2009).

3.4.3 Paleogeography

3.4.3.1 Upper Palaeocene – Colsay Sandstone Member

The Rosebank Field lies at the interface between two competing systems (Figure 3.16); the Greenland Platform to the northwest (which shed volcanic material into the basin) and the West Shetland Platform to the southeast (which shed siliciclastic material into the basin). Thermal uplift associated with North Atlantic rifting caused a relative lowering of sea level (Mudge et al., 2009).

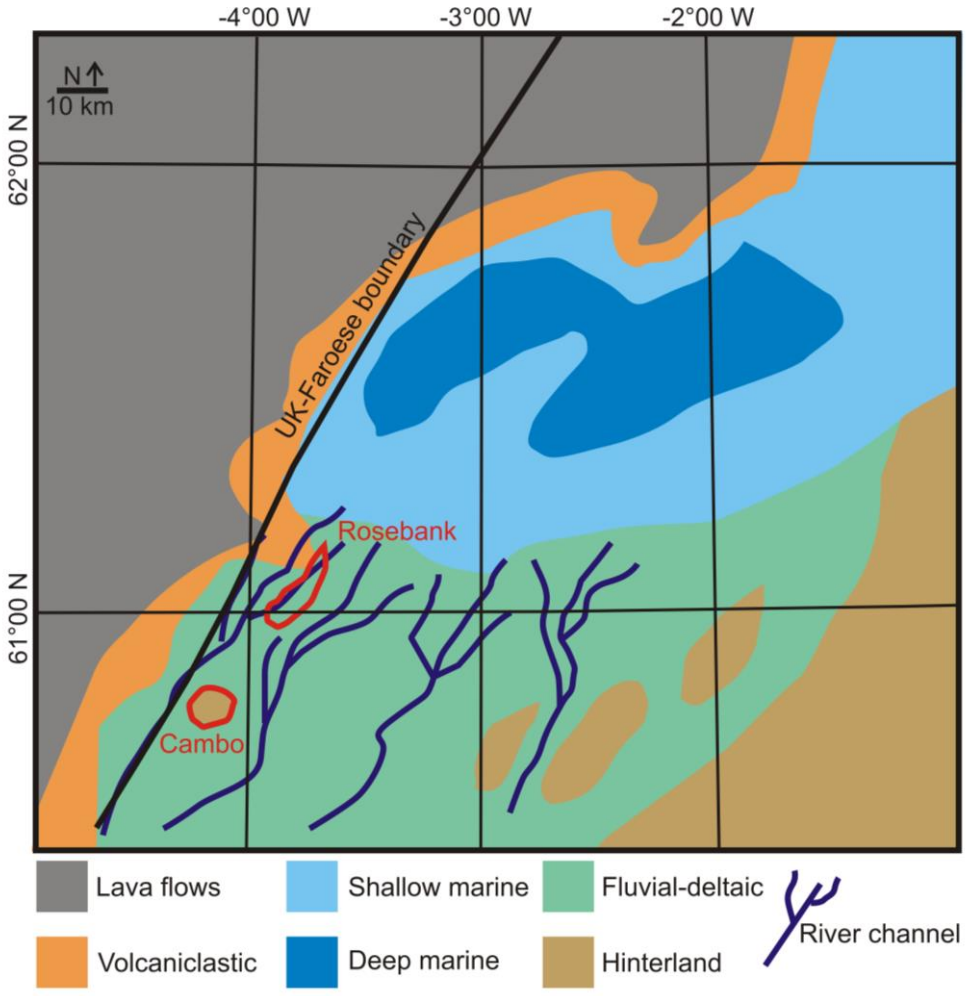

Figure 3.16**:** Paleogeography of the Rosebank Field during Colsay Sst Mb times. Elongate red field outline is Rosebank. Circular red outline to the south is Cambo. The depositional environment in Rosebank area changes from shallow water shoreface to lagoonal/estuarine to fluival-deltaic as the Flett Delta migrated north eastwards. Modified from Rosebank Team (2009) using information from gained from Mudge et al., (2009); Stoker and Varming (2011); Passey and Hitchen (2011).

The Rosebank Field lay at the axis of a fluvio-deltaic depositional system generated by the initiation of the north-eastwards progradation of the Flett Delta. Rivers were deflected around the Cambo High and entered the Rosebank area from the southwest (Schofield and Jolley, 2013; Wright, 2013). Throughout the deposition of the Colsay Sandstone Member the Flett Delta moved northeast. Evidence for this is found in rocks at the base of the most northern well, 213/27-1, which indicate that shallow marine sediments were deposited during Colsay 4 times. This sequence is then overlain by shoreface and deltaic sediments during Colsay 3 and 2. Colsay 1 contains mainly terrestrial sediments but some marine sediments are found in the North (pers. comm. Rosebank Team 2013). The palaeo-shoreline data runs NW-SE across the basin and can be seen in seismic surveys.

Basaltic lava flows erupted towards the Faroe Islands and flowed southeast towards the basin margin. Isolated volcanoes to the southeast of Rosebank also inputted volcanic material into the basin (Schofield and Jolley, 2013; Wright, 2013). The lavas reached their maximum extent ~20 km east of Rosebank: a thin 30 m lava flow reached the location of well 205/8-1 (Figure 3.17). After each phase of volcanism, the siliciclastic regime regained dominance. As a result the basin depocentre experienced cyclic switches in sediment provenance between siliciclastic and volcaniclastic material. For example, during the deposition of Colsay 3 sediments the southern part of the field was subject to the emplacement of volcanic rocks while in the north, siliciclastic sands were being deposited. This relationship was reversed during Colsay 1 times when volcanic rocks dominate wells in the north and siliciclastic rocks are confined to southern wells.

3.4.3.2 Lower Eocene – Hildasay Sandstone Member and Balder Formation

The long established drainage basin that deposited the Colsay Sandstone Member continued with the deposition of the Hildasay Sandstone Member (Mudge et al., 2009; Schofield and Jolley, 2013). Palynological data indicate that the fluvial system cut through mature swamp forests (Jolley, 2007). A transgression resulting from basin sag resulted in the deposition of shallow marine sediments across the Rosebank area (Figure 3.18). Volcanism in the basin came to an end, with tuffs in the Balder Formation deposited on regional highs. Both the marine sediments and the tuffs may act as seals in the Rosebank system (Figure 3.19).

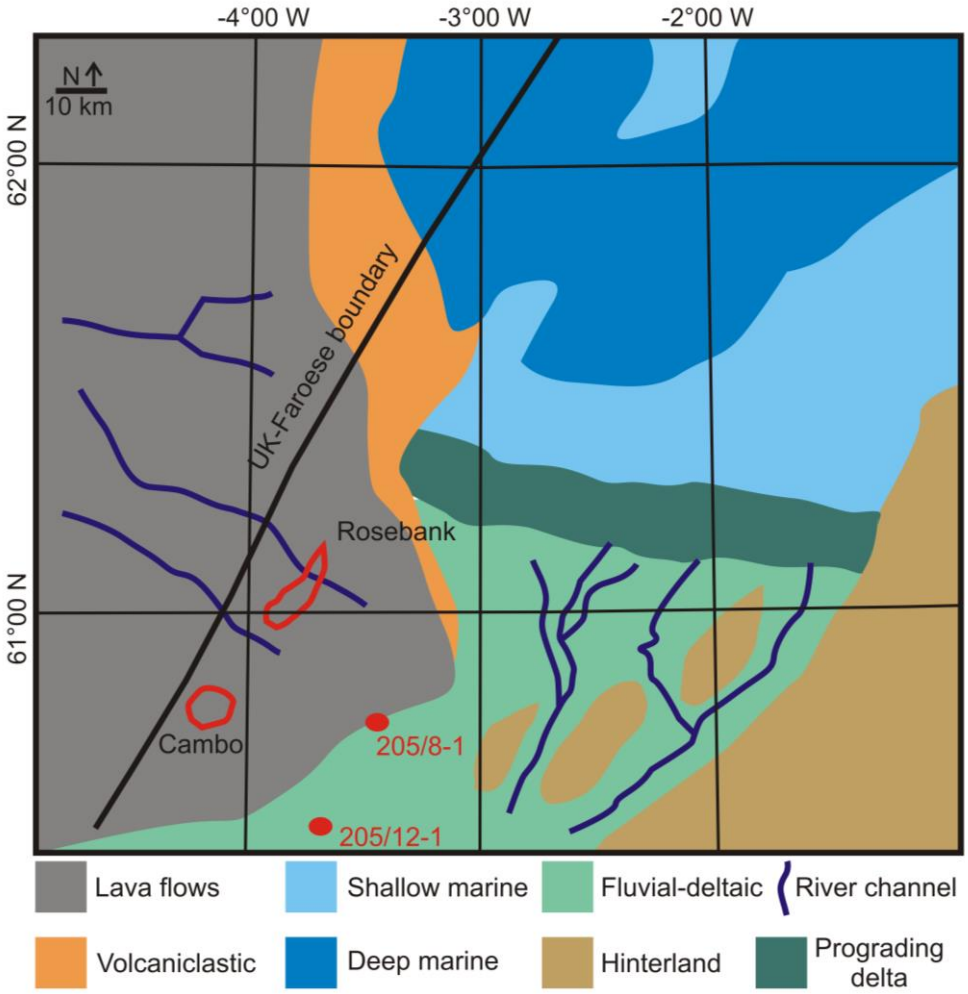

Figure 3.17: Paleogeography of the Rosebank Field during Colsay times. Elongate red field outline is Rosebank. Circular red outline to south is Cambo. As the delta progrades from SW- NE, pulses of volcanic material sourced from the northeast and potentially to south west migrate across the area. The maximum volcanic extent is shown as a thin lava unit is found in well 205/8-1 but no lava is found in 205/12-1. The lavas change the topography altering the drainage system. As the lavas retreat volcaniclastic material is shed into the basin (Modified from Rosebank Team, (2009) using information gained from Mudge et al., (2009); Stoker and Varming (2011); Passey and Hitchen (2011), Schofield and Jolley (2013)).

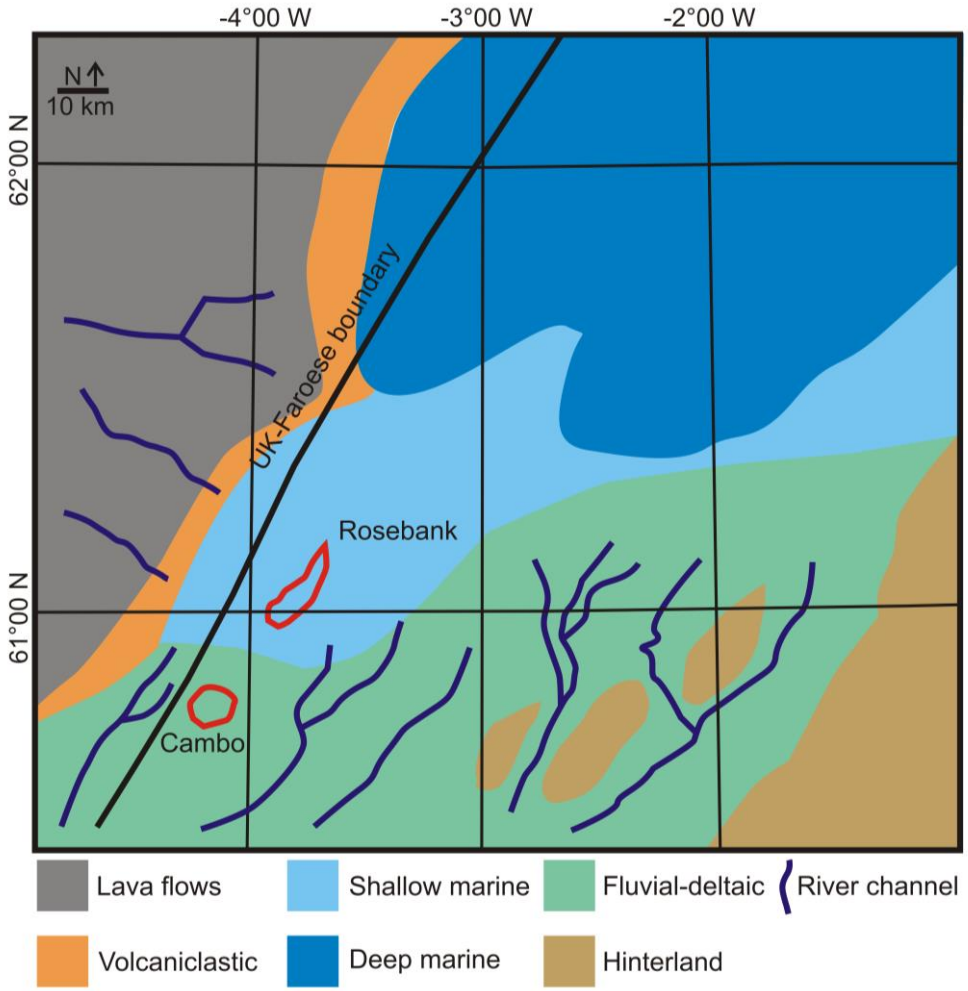

Figure 3.18: Paleogeography of the Rosebank Field during Hildasay times. Elongate red field outline is Rosebank. Circular red outline to south is Cambo. As the lavas retreat volcaniclastic material continues to be shed into the basin. A transgression causes shallow water rocks to be deposited during Hildasay times. Modified from Rosebank Team (2009) using information gained from Mudge et al., (2009); Stoker and Varming (2011); Passey and Hitchen (2011).

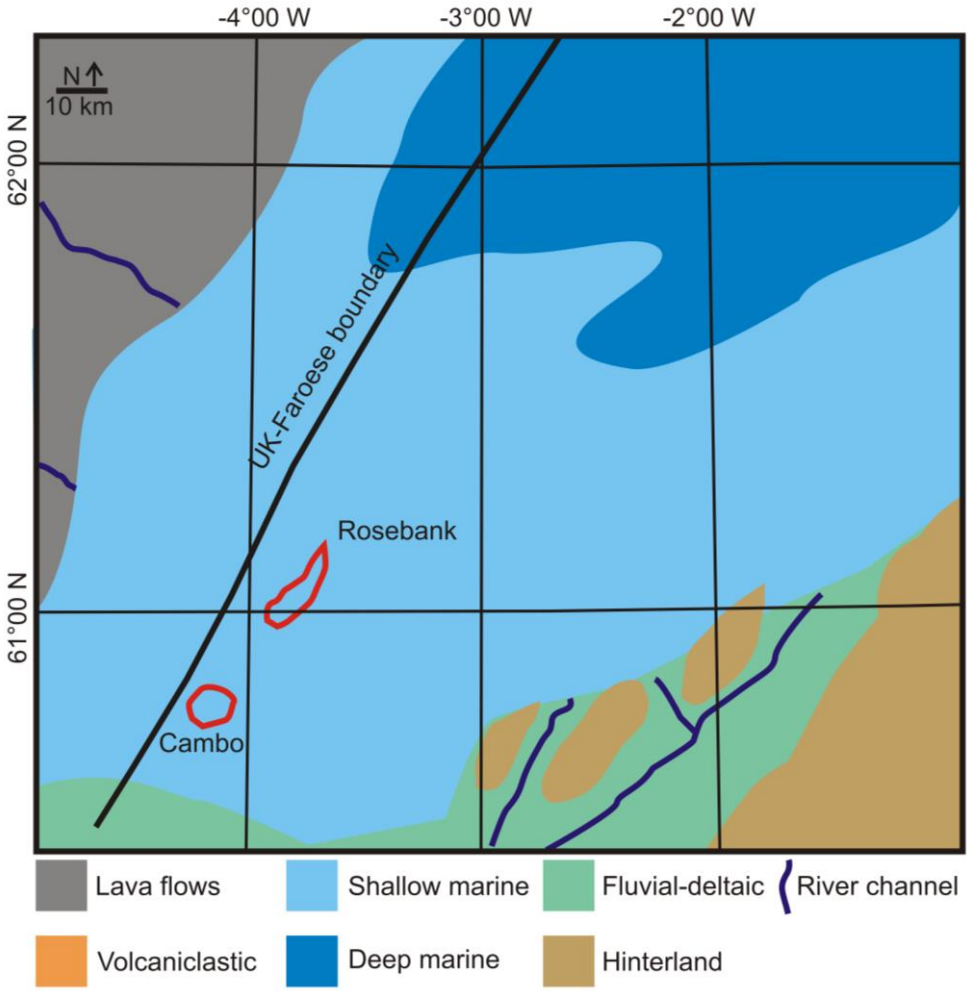

Figure 3.19 Paleogeography of the Rosebank Field during Hildasay times. Elongate red field outline is Rosebank. Circular red outline to south is Cambo. A transgression causes shallow water rocks to be deposited during Hildasay times. Modified from Rosebank Team (2009) using information gained from Mudge et al., (2009); Stoker and Varming (2011); Passey and Hitchen (2011).

3.5 Rosebank lithology

Lithological units within the Rosebank wells have been identified by combining wireline log data with observations from rock cores and sidewall cores. A number of cores, taken from the Rosebank wells, targeted reservoir units in Colsay 1 and 3 and some of the volcanic rocks (Table 3.3). Despite drawing on literature the following section is based on my own descriptions and interpretations.

3.5.1 Colsay 4

3.5.1.1 Lithofacies descriptions

The lithofacies present within Colsay 4 were determined using petrophysical data from wireline log and sidewall cores (Siggerud, 2008; Bell, 2008).

Colsay 4 is composed of well to poorly sorted, laminated sandstone and mudstone, which in places is bioturbated. The sandstones are fine- to medium-grained and show inverse grading. Also present are volcaniclastic claystone and fine-grained lithic arenite with abundant basalt lava fragments, feldspar, rarer quartz and lithic fragments.

Well Name	Chronostratigraphic unit	Core Number	Depth (m)	Lithology	No. Additional Sidewall cores
205/1-1	Colsay 2	1	2926.4 to 2938.3	Basalt lava flow	52
213/26-1	Colsay 1	1	2817.9 – 2819.7	Ripple laminated muddy sandstone	50
	Colsay 1	2	2820.3 – 2820.9	Ripple laminated mudstone	
	Colsay 3/2	3	2872.4 – 2888.9	Basalt lava flow overlying silty sediment	
213/26-1z	Colsay 1	1	2926.1 – 2927.0	Mudstone and siltstone	45
	Colsay 1	2	2942.5 – 2947.8	Mudstone and sandstone	
	Colsay 3	3	3005.3 – 3014.5	Mudstone and sandstone	
213/27-2	Colsay 1	1	2872.7 – 2878.2	Basalt lava flow with some silty sediment	n/a
	Colsay 3	2	2932.2 – 2959.4	Interbedded sandstones, mudstones and silts	

Table 3.3: Core and Sidewall Core information. Table compiled using well logs in conjunction with Siggerud (2008) and Bell (2008).

A thin sequence of volcanic rocks separates Colsay 4 from the overlying Colsay 3. The sequence is dominated by microcrystalline aphyric basalt lava flow and peperites. Lava flows contain euhedral plagioclase and pyroxene phenocrysts with minor amounts of altered olivine phenocrysts and abundant Fe-Ti oxides. Amygdales

are composed of clay minerals, calcite and zeolite. Peperite rocks comprise fluidal-shaped basaltic clasts in a fine-grained siltstone matrix.

3.5.1.2 Interpretation

Rocks in the Colsay 4 chronostratigraphical unit are interpreted to record a transition from shallow marine, bioturbated sediments up through shoreface to mouth bar and fluvial deltaic sediments as a result of the northward progradation of the Flett Delta into the basin. This interval was followed by the emplacement of subaerial basalt lava flows.

3.5.2 Colsay 3

3.5.2.1 Lithofacies description

The Colsay 3 chronostratigraphical unit was cored in well 213/26-1, 213/26-1z and 213/27-2. Within the 213/26-1 wells the unit is composed of both volcanic and siliciclastic rocks while in the 213/27-2 well to the north the unit is composed of siliciclastic rocks.

Well 213/27-2 core

Approximately 27 m of siliciclastic rocks were cored in the 213/27-2 well. The base of the cored section comprises well-sorted claystones, siltstones and sandstones. Heterolithic bedding is common in the fine-grained sub-arkose with the proportion of thin muddy laminations, alternating between flaser and lenticular. In places the beds are locally disturbed by bioturbation and syn-sedimentary faulting. These fine-grained rocks grade upwards into very coarse- to medium granule grained, poorly sorted sub-arkose composed of sub-rounded to sub-angular quartz, feldspar and lithic clasts. Coarse granule sized clasts (up 3 cm) are concentrated in normally graded bedsets that fine upwards to medium grained sand.

Well 213/26-1z core

Approximately nine metres of volcanic and siliciclastic rocks were cored in the 213/26-1z well (Figure 3.20). The base of the core is composed of dark siltstone

containing clasts of amygdaloidal basalt interpreted to be a basaltic breccia. Clasts are sub-rounded to sub-angular with sharp contacts but without glassy chilled margins. Amygdale composition and size changes from calcite macro-amygdales (up to 8 mm in diameter) in the interior, to clay-filled micro-amygdales (up to 2 mm in diameter) at the clast edges. Most have tear-drop shapes with thin tails that are aligned horizontally across the basalt clasts.

The basaltic breccia then grades into a dark grey, fissile mudstone with millimetre-scale flaser bedding. Anastomosing calcite veins are commonly displaced by small scale faults towards the base of the section.

Overlying the mudstone are pale grey sub-arkose, siltstone and claystone beds with abundant sedimentary structures including symmetrical ripples, cross-bedding (max. 5cm), and millimetre-scale, organic-rich, lenses. Bedding is heterolithic and switches from lenticular to flaser highlighting fluctuating energy in the system. Four distinct (max. 5 cm) bivalve horizons are present within the more mud-rich layers. Abundant *Apectodinium* specimens are also found (Jolley, 2007). Overlying this is approximately 0.3 m of massive mudstone.

The gravelly, very coarse sub-arkose comprises vein quartz (up to 1cm), feldspar, and lithic clasts. Grains are sub-angular to rounded with moderate sphericity. There is oil staining throughout the sequence.

Well 213/26-1 core

A log of the 213/26-1 core through Colsay 3 and into Colsay 2 is seen in Figure 3.21. At the base of the core there is fine grained pale yellow siltstone, with faint ripples, convoluted bedding and possible bioturbation. Some small discontinuous lenses of darker, more organic-rich material are also present. The rocks directly overlying this unit were not available for study. Above the removed section is a darker grey/brown fine grained siltstone, with some faint laminations and smaller flecks of darker, more organic-rich material. The siltstone also contains a large wood fragment.

The siltstone is overlain by 0.9 m of amygdaloidal basalt. The contact between the lava and sediment is sharp with no induration. Small veins of calcite (typically 5 mm wide and up to 4 cm long) bound the base of the lava and penetrate vertically into the sediment below. Directly at the contact, the basalt is discoloured with chilled margins and with abundant calcite and/or zeolite pipe vesicles (up to 2 cm long) and spherical dark, glass rimmed, mm scale clay-filled amygdales. Approximately 4 cm

away from the contact the basalt is finely crystalline with rare plagioclase phenocrysts up to 0.5 cm long. Amygdales range from ~1–4 cm in diameter and are dominated by calcite, zeolite and clay minerals. Irregular areas of fine to medium grained grey sandstone are mixed with basalt and in places fill the irregular surface of the lava completely surrounding the basalt clasts.

The amygdaloidal basalt grades into, approximately 4.6 m of greenish brown to grey massive basalt. The basalt has a glomeroporphyritic texture in places with randomly orientated clusters of euhedral plagioclase phenocrysts (up to 0.5 cm). Rare large (2 cm) aligned zeolite and smaller clay amygdales with glassy rims along with clay and calcite veins (max 5 mm wide but approx. 1 m long) are found at this depth.

The massive basalt grades into ~2.25 m of light grey amygdaloidal basalt that resembles the one described above (Figure 3.22). Overlying this basalt is a zone of fine to medium grained dark grey sandstone with faint parallel laminae. The contact is irregular and cross cuts the core at a high angle. A 2 – 5 mm darkened zone is seen within the basalt directly at the contact. As before, amygdales increase in size away from the contact. No thermal effects are seen in the sediment which fills fractures in the basalt. Small isolated blebs of basalt can also be found in the sediment.

Overlying this is a small isolated section of basalt dominated by zeolite amygdales, with clay-filled amygdales at contacts with the sediment. The basal lava contact resembles others described above, however the upper contact of the basalt is yellow and has flame like structures protruding into the overlying sediment, which is laminated.

Figure 3.23 shows the upper part of the core. Amygdaloidal basalt, with clay amygdales and large zeolite-filled regions, grades into grey non-amygdaloidal crystalline basalt with abundant plagioclase phenocrysts up to 1 cm long. Rare glomeroporphyritic texture with radial clusters of plagioclase phenocrysts is also present. This non-amygdaloidal basalt then grades into 1.5 m of light grey, amygdaloidal basalt with abundant (10%) plagioclase phenocrysts (up to 1.5 cm). Amygdales are teardrop shaped with tails and are aligned across the core along with small (up to 4 mm) lenses of glassy material and clay filled veins (max. 2 cm wide). A sediment fracture 10 cm long cuts into the basalt at the top of the core. The sediment is a fine to medium grained reddish brown sandstone.

3.5.2.2 Interpretation

The presence of fossils and palynoflora in the sedimentary sequence within the 213/26-1z core is indicative of a sub-tidal, estuarine environment seen in the Rosebank area at this time.

The alternation of amygdaloidal basalt with dense basalt seen throughout the cores represents alternations between pāhoehoe lava cores and crusts. As lava lobes inflate more vesiculated regions develop on the base and top of the flow (cf. Self et al., 1998; Passey and Bell 2007).

The nature of the sediment-lava interaction in the 213/26-1 and 213/26-1z cores is different. There are no thermal effects seen within the lava clasts in the 213/26-1z core which suggests that they were emplaced cold. This lava breccia could represent reworking of the cooled lava surface during a period of volcanic quiescence.

This contrasts with the contacts seen in the 213/26-1 core. At the base of the lava, minor chilled margins imply hot emplacement however no thermal effects are seen in the sediment. Pipe vesicles are seen at the base of the lava while veins cut down into the sediment; however, the lava does not disrupt sedimentary structures. Therefore, the lava was emplaced passively, infilling the topography of the underlying sediment. Amygdales nearer to the contact are filled by clays derived from the glassy chilled margin.

Interaction between the sediment and the top of the lava is peperitic. Fluidal basalt clast shapes with chilled margins locally disturb sedimentary structures, implying significant heat retention on deposition. Multiple faulting and vein forming events are evident, with relative displacement of veins.

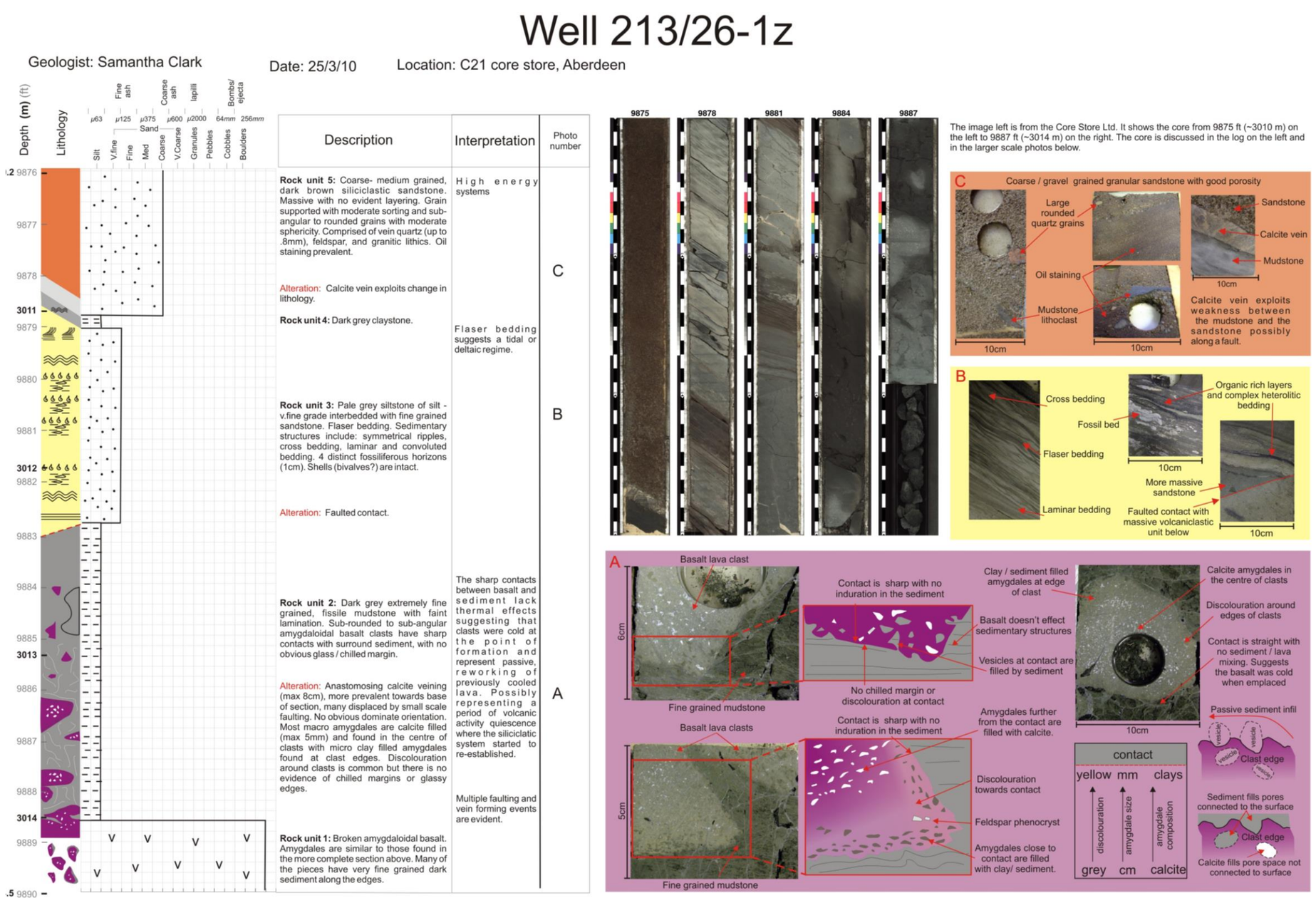

Figure 3.20 : Log of the 213/26-1z Colsay 3 core.

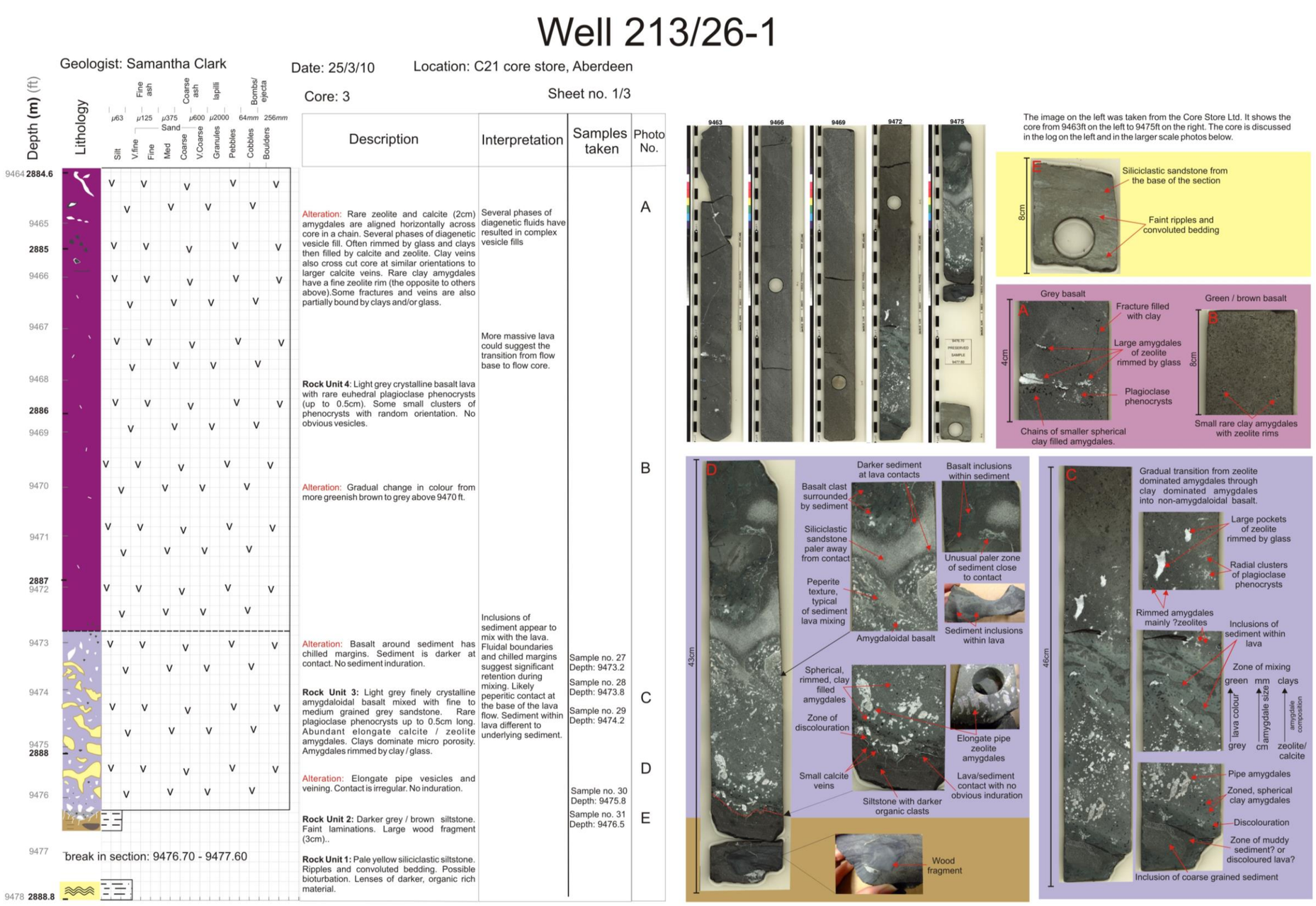

Figure 3.21: Base of Colsay 3 core log in well 213/26-1

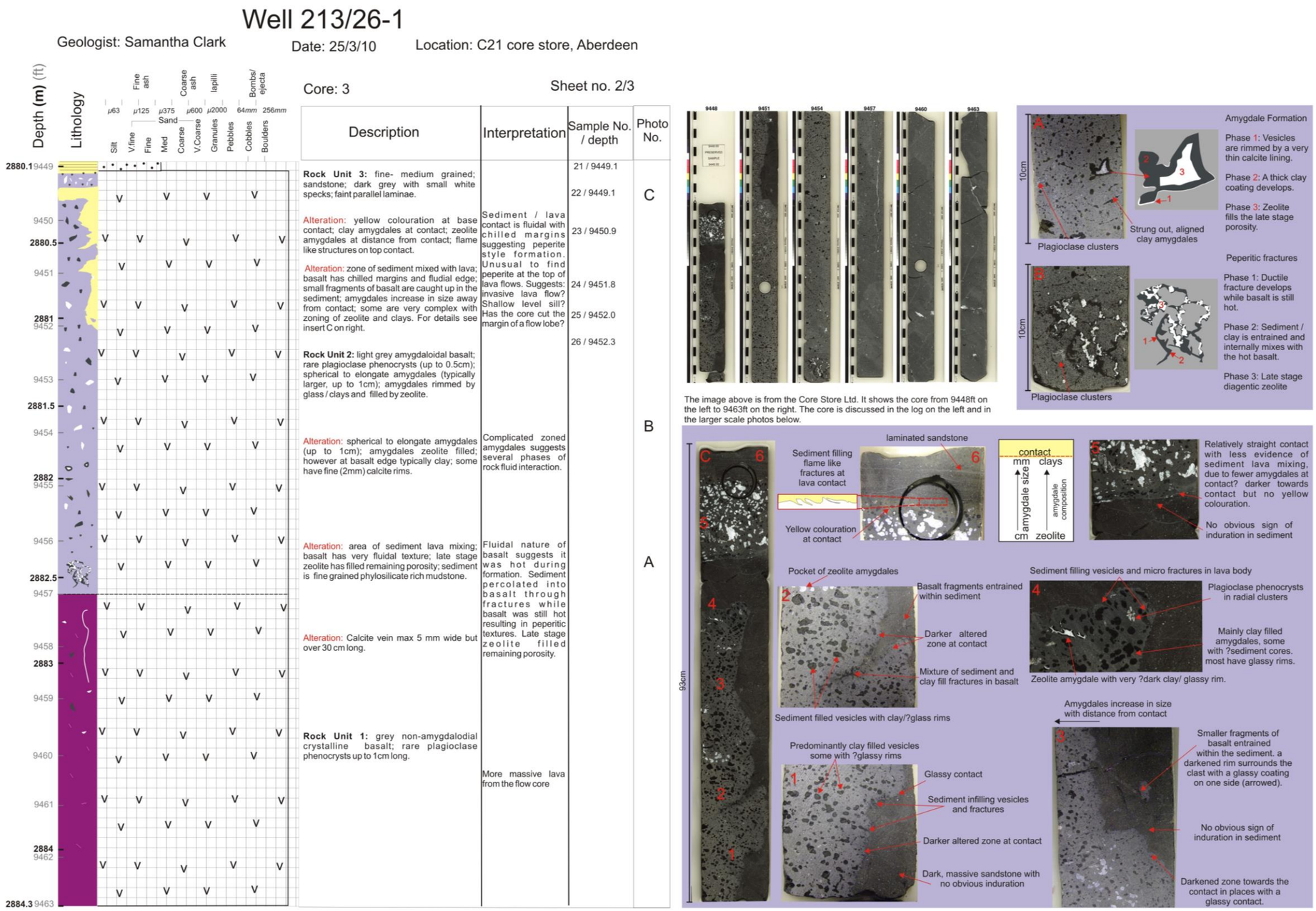

Figure 3.22: Colsay 3 core, well 213/26-1

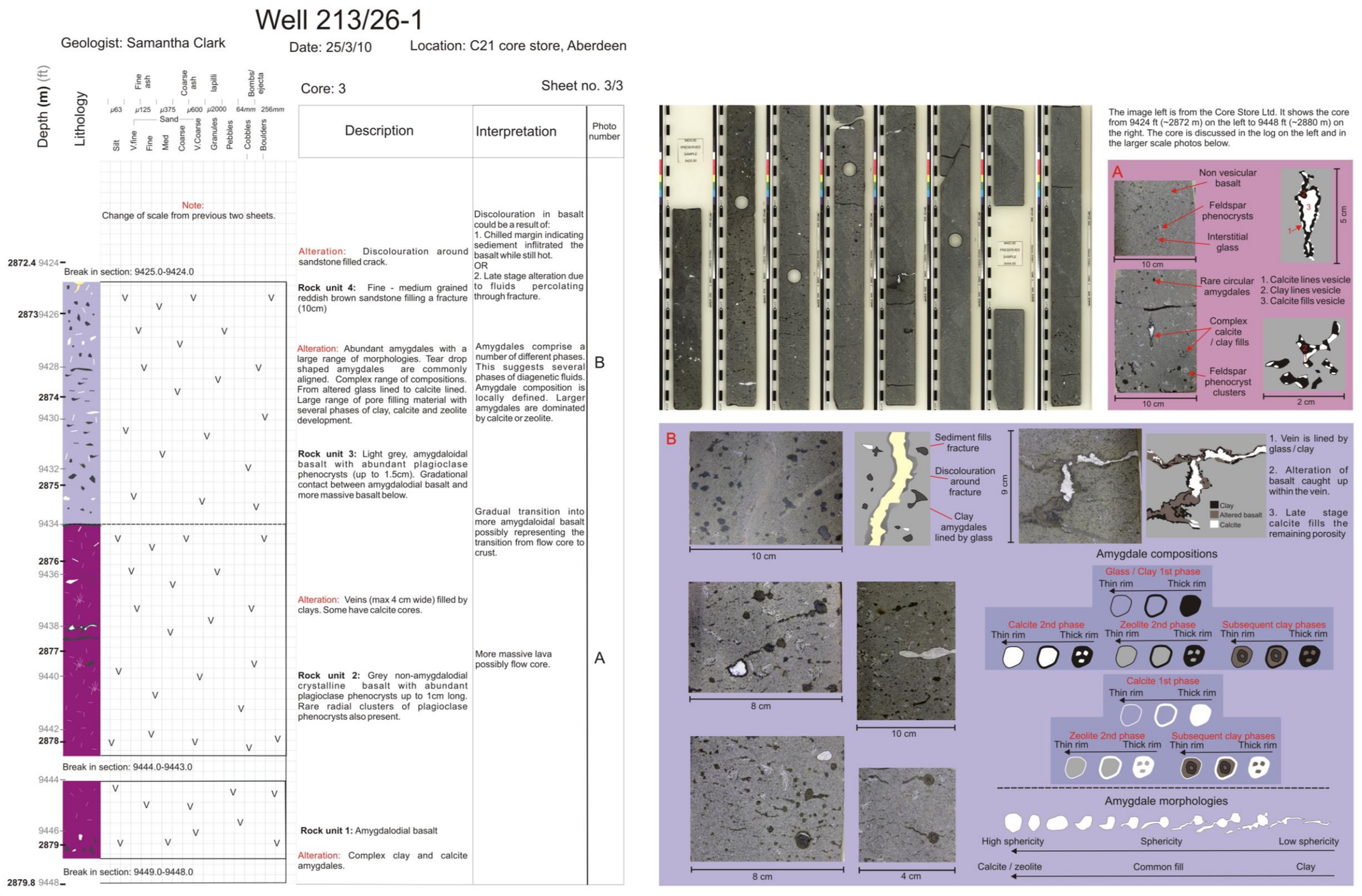

Figure 3.23: Top of Colsay 3 core, 213/26-1 well.

3.5.3 Colsay 2

3.5.3.1 Lithofacies description

The lithofacies present within Colsay 2 were determined using petrophysical data from wireline logs, sidewall cores (Siggerud, 2008 and Bell, 2008) and by examining core from Well 205/1-1.

The sedimentary rocks within the Colsay 2 unit are mainly moderately to poorly sorted, sub rounded to angular claystones and siltstones. A thin fine-grained, micaceous, bioturbated sublithic arenite occurs in well 213/27-1z. Volcanic lithofacies comprise basalt lava flows and volcaniclastic claystones and siltstones that resemble those described in Section 3.5.2.1.

The base of the 205/1-1 core comprises volcaniclastic claystone that has been heavily altered by calcite veins. Overlying this is a non-vesicular micro-crystalline basalt lava with rare (max. 5 cm) patches of coarser-crystalline basalt. Calcite veining is confined to the base of the lava. Overlying this is an amygdaloidal basalt similar to those described Section 3.5.2.1.

3.5.3.2 Interpretation

The absence of large sandstone units suggests that the emplacement of the lava flows diverted the fluvial channels seen in Colsay 3. Siltstone and claystone beds represent flood plain deposits. Volcaniclastic rocks may represent paleosols, while thin sandstones suggest that small rivers are present within the volcanic-dominated landscape.

3.5.4 Colsay 1

3.5.4.1 Lithofacies description

The Colsay 1 interval was cored in the 213/26-1, 213/26-1z and 213/27-2 wells. The 213/26-1 and 1z cores are described by Siggerud (2008) as being angular to well rounded fine sand to coarse granule grade sublithic arenites and conglomerates and fine grained laminated mudstones. Abundant sedimentary features such as ripple marks and

fining upwards sequences are also found. The core taken in well 213/27-2 is volcanic and is shown on Figure 3.24.

Well 213/27-2 Core

At the base of the core is dark grey, massive, non-vesicular aphyric basalt. Overlying this is an area of lava and sediment mixing. The sediment is a dark brown, immature, granular, volcaniclastic lithic wacke. It is typically fine - medium grained, moderately sorted, with sub-angular to rounded grains with moderate sphericity. In places it is matrix supported with a very fine grained muddy matrix. The interaction between the two rocks is complex with a variety of peperitic textures developed, including fluidal basalt clasts with chilled margins and blocky jigsaw fit clasts where chilled margins are not extensively developed. Both textures seem to coexist only centimetres apart.

Overlying the peperitic zone is grey fine grained amygdaloidal basalt. This basalt resembles that described above with a mixture of calcite- and clay-filled amygdales. Several small clay- and calcite-filled fractures at two orientations (vertically down and at 45°) cross cut the core.

The contact between this basalt and the overlaying dark grey/ brown, fine-medium grained, matrix supported volcaniclastic lithic wacke is similar to those described in the 213/26-1 Colsay 3 core. The grain size ranges from µ125- µ375 with occasional larger clasts up to 2 mm while the matrix is fine grained brown clay. Grains are poorly sorted, locally very heterogeneous and are angular to sub rounded with low sphericity. Lenses of darker finer grained muddy material up to 6 cm long and rare lenses of coarser grained material are intermingled with the wacke.

This unit grades into approximately 1.8 m of very fine grained grey, black lithic wacke and extremely altered basalt. The core here is very difficult to interpret. Areas of basalt are often only recognisable by areas of amygdales with clast boundaries being indistinguishable.

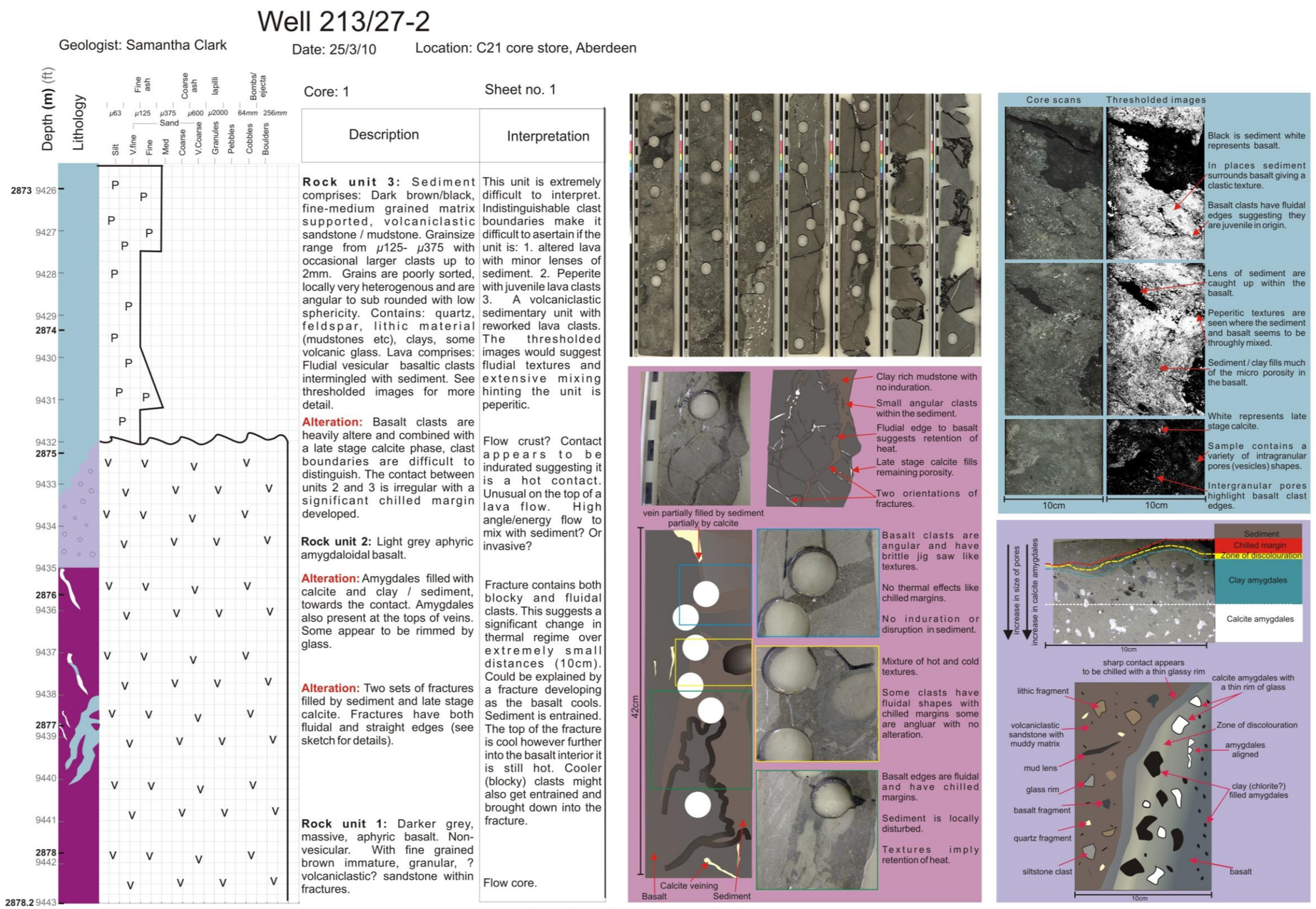

Figure 3.24: Colsay 1 core, 213/27-2 well.

3.5.4.2 Interpretation

Colsay 1 is interpreted as predominantly fluvial channel sandstones and overbank mudstones (Siggerud, 2008). The lack of shoreface and deltaic lithofacies indicates that the Flett Delta had migrated northwards.

Volcanic rocks in 213/27-2 can be interpreted in a similar way to those in 213/26-1 in Colsay 3. The aphyric lava represents the core while the amyalgdaloidal basalt represents the flow crust. Fractures filled with sediment cross cut the core leading to peperitic textures being developed.

The difficult to interpret volcanic – sedimentary unit at the top of the 213/27-2 core is interpreted to be a peperite comprising a mixture of basaltic material and very fine grained volcaniclastic mudstones. The small grain size however, and intense alteration makes interpretation at hand specimen level difficult. Peperites are not usually found at the top of lava flows as is discussed in Section 5.4.2.

3.6 Conclusions

The Rosebank Field lies at the orthogonal heart of two competing systems. Volcanic rocks in the form of basalt lava flows and volcaniclastic rocks dominantly enter the basin from the north-west, but also minor quantities may come from volcanic centres to the south east. These volcanic rocks directly compete with siliciclastic sediments sourced from a fluvial-deltaic system that progrades into the basin from the south-east. During periods of quiescence the volcanic activity wanes and the siliciclastic regime is re-established. The result is a complex stratigraphy that switches from volcanic to sedimentary and back again. As the lavas flow into the basin the evolving topography alters the drainage system, cutting off and diverting the siliciclastic system out of the area.

The reservoir quality of the rocks varies not only vertically through the stratigraphy, but also laterally across the field. High quality reservoir rocks with porosity on average of 20% can be found towards the north of the field during Colsay 3 times. However, by Colsay 1 times the system has reversed with the good quality reservoir rocks occurring in the southern part of the field.

3.7 Next steps

Thin section and sample plugs were taken from the core in order to characterise the petrography and analyse the paragenesis. Samples crossing contacts between the igneous and sedimentary rocks were also taken in order to better understand the interplay between the two competing systems. A field analogue has been used in order to better understand the facies architecture and field relationships that cannot be established when looking solely at the core.

3.8 Further work

Further work could be undertaken to correlate the lithofacies seen within these cores across the full Rosebank field area. A new ocean bottom seismic data (OBS) set have been acquired in the last year that will provide further precision in the mapping of lithofacies (e.g. identifying fluvial channel directions). Formation micro-imager (FMI) data could also be better linked to the wireline and core data, using the method outlined in Watton (2013) in order to better interpret the relationship between the volcanic and siliciclastic rocks.

4 Sedimentation of vent proximal pyroclastic and volcaniclastic deposits: Staffa Formation, Mull

The amount of rock samples from the Rosebank core is extremely limited leading to difficulties in understanding the lithofacies architecture especially when examining the igneous sedimentary contacts. An onshore analogue was chosen in order to try and understand the lithofacies relationships in a spatial context. The following chapter presents findings from fieldwork carried out on the Staffa Formation in the south-west of Mull.

4.1 Introduction to the BPIP

The British-Irish Palaeogene Igneous Province (BPIP) consists of a series of flood basalt provinces and associated rocks emplaced across northern Ireland and the west coast of Scotland (Figure 4.1). It is part of the North Atlantic Igneous Province (NAIP), which extends for a minimum of 1.3×10^6 km^2 (Eldholm and Grue, 1994) and includes the Rosebank Field. The igneous activity is associated with ocean-floor spreading in the north east Atlantic Ocean (Naylor et al., 1999), with the onset of volcanism at approximately 62 Ma (White and Lovell, 1997). The BPIP comprises three flood basalt lava fields in Scotland (the Skye, Eigg and Mull Lava fields; Figure 4.2), and the Antrim Lava Field in Northern Ireland, as well as a number of intrusive centres (Skye, Rum, Ardnamurchan, Mull and Arran) in Scotland (Figure 4.2), and (Carlingford, Mourne Mountains and Slieve Gullion) Ireland. Interbedded with the flood basalt lava fields are pyroclastic and sedimentary rocks that form the focus of this study.

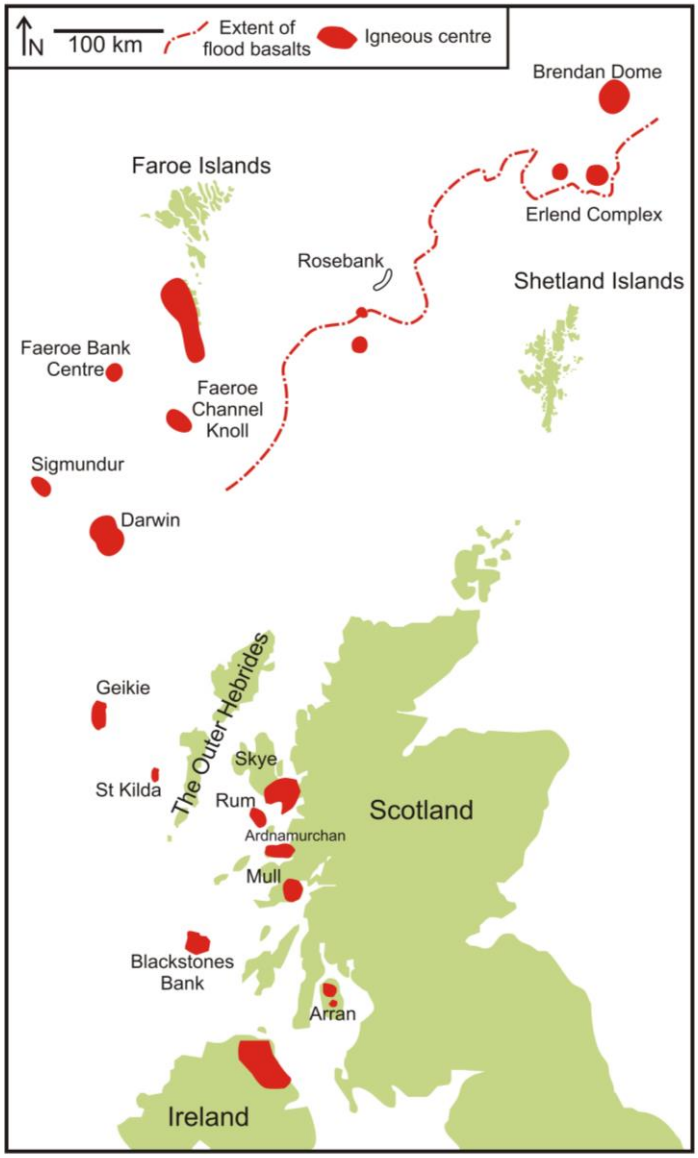

Figure 4.1: Map of the North Atlantic Igneous Provenance highlighting the igneous centres of British-Irish Palaeogene Igneous Province and the igneous centres in the Faroe-Shetland Basin. The extent of the flood basalts in the Faroe-Shetland Basin is also mapped. Map created using data from Bell and Williamson (2002), Ritchie and Hitchen (1996) and Wright (2013).

4.2 Introduction to the Isle of Mull

At approximately 940 km^2 the Isle of Mull's igneous centre (located off the west coast of Scotland) is one of the largest within the BPIP (Chambers and Pringle, 2001). The oldest rocks, the Neoproterozoic Moine basement, crop out on the Ross of Mull and comprise biotite schists and psammites that were metamorphosed during the Caledonian Orogeny. The basement rocks are intruded by Devonian granite (414 ± 3 Ma) surrounded by a well defined contact metamorphic aureole (Potts et al., 1995).

These rocks are confined to the south west of Mull and are separated from the rest of the island by the NW–SE trending Assapol Fault (Holdsworth et al., 1987). To the east of this fault lie Jurassic and Cretaceous sandstones and limestones. These are overlain by the Palaeogene volcanic rocks that crop out over most of the island. The

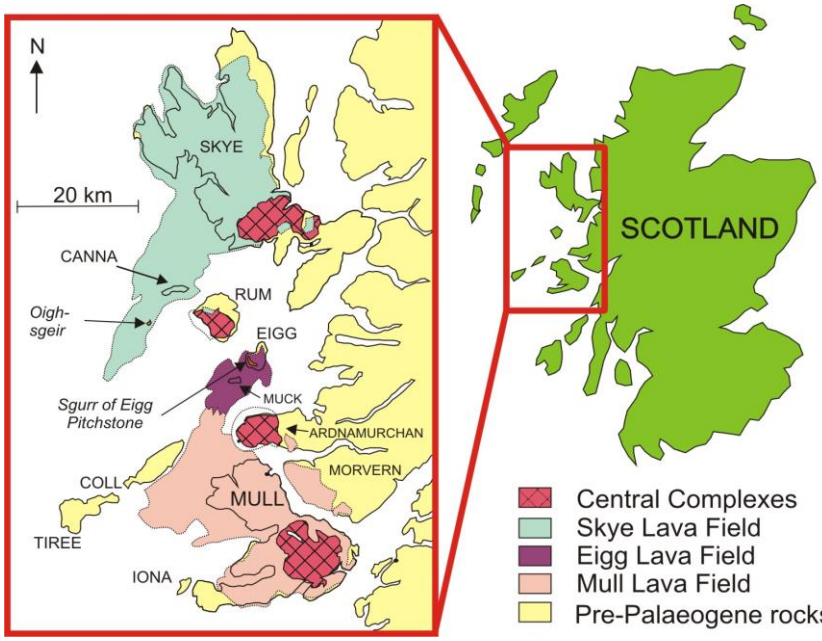

Figure 4.2: Map showing the Palaeogene central complexes and lava fields in NW Scotland. Redrawn from Brown et al., (2009).

volcanic rocks have been extensively studied (Bailey et al., 1924; Bailey and Anderson, 1925; Beckinsale et al., 1978; Morrison et al., 1980, 1985; Thompson et al., 1986; Kerr, 1995a, 1995b, 1997, 1998; Kerr et al., 1999 and Williamson and Bell, 2012). A ~2 km thick pile of fissure-fed lava flows (the Staffa and Plateau formations) were erupted 60.5 ± 0.5 Ma (Chambers and Pringle, 2001) before being intruded by three igneous centres. A geological map of the island can be seen in Figure 4.3.

4.3 The Staffa Lava Formation

The Staffa Formation crops out in the southwest of Mull (Figure 4.5). It comprises a ~275 m thick sequence of basalt lava flows interbedded with subordinate volcaniclastic and sedimentary rocks (Williamson and Bell., 2012). The formation is structurally bound to the west by the Assapol Fault, which separates it from the Moine basement rocks to the southwest. In the northeast it is bound by the Allt na Leacainn–Carraig Mhòr Fault. The formation unconformably overlies pre-Palaeogene Cretaceous and Jurassic rocks and is capped by the chemically and visually distinct lavas of the Mull Plateau Lava Formation. The Staffa Formation has been sub-divided into a genetic sequence of lavas and interbedded sedimentary rocks (Williamson and Bell, 2012). The sequences define extensive discontinuity surfaces rather than individual lithologies; packages of rocks of differing facies are grouped together. Each sequence contains a sedimentary unit overlain by volcanic strata. The sequence runs from GS-A1 to GS-A7, where A1 is the oldest package of rocks (Figure 4.4). The lavas and interbedded units have also been correlated across the island using palynological data (Jolley et al., 2009) and geochemistry (Kerr et al., 1999). Approximately 1.6km of basalt has been eroded off the top of the Mull Lava rocks (Holford et al, 2010) resulting in a minimum burial depth of ~2km.

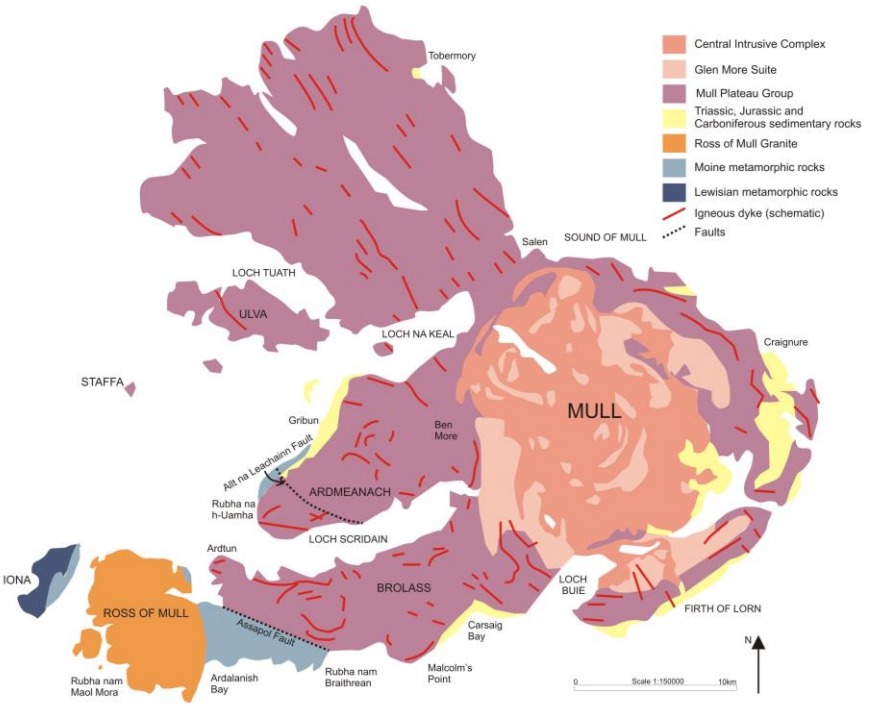

Figure 4.3. Geological map of Mull and surrounding islands. Edited from EDINA DigiMap with reference to Williamson and Bell (2012).

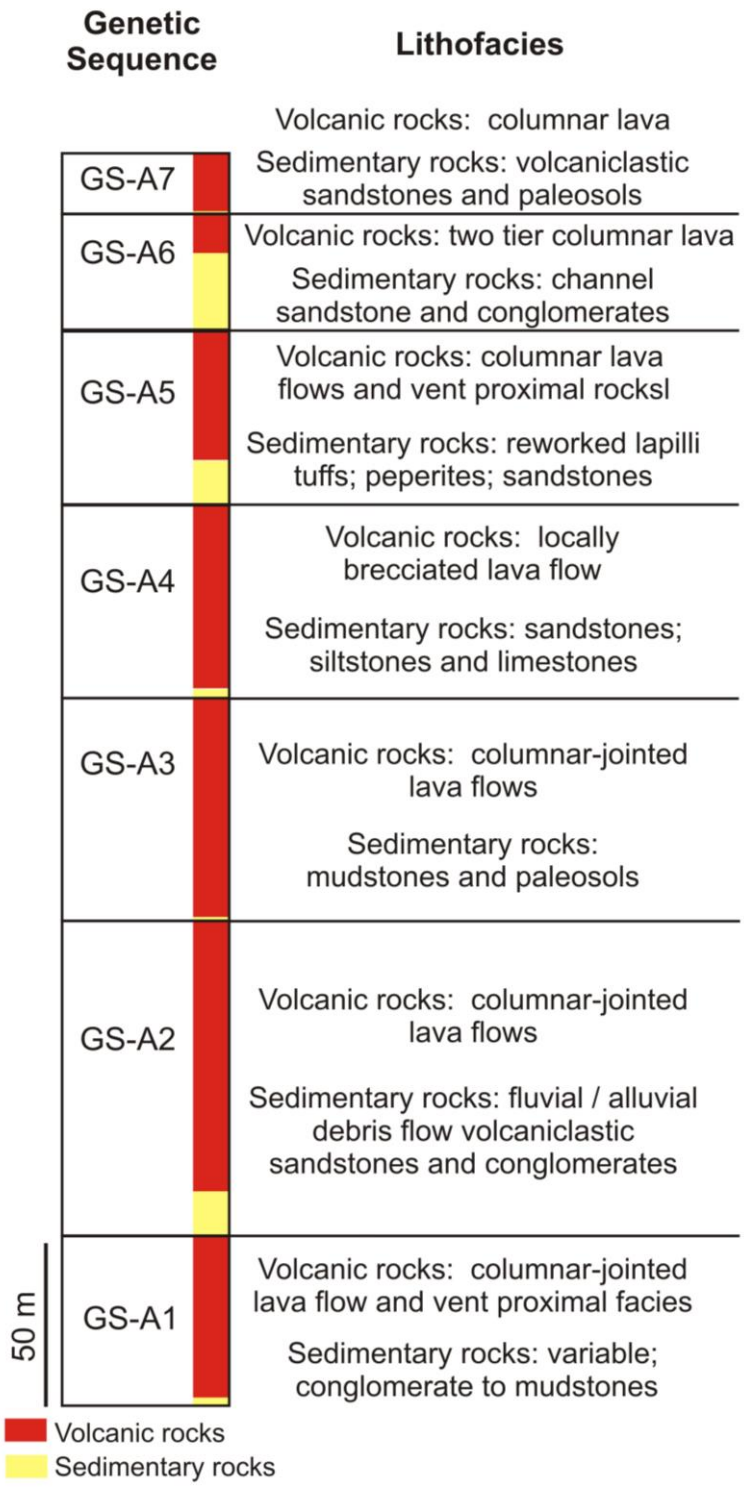

Figure 4.4. Genetic Sequences modified from Williamson and Bell (2012).

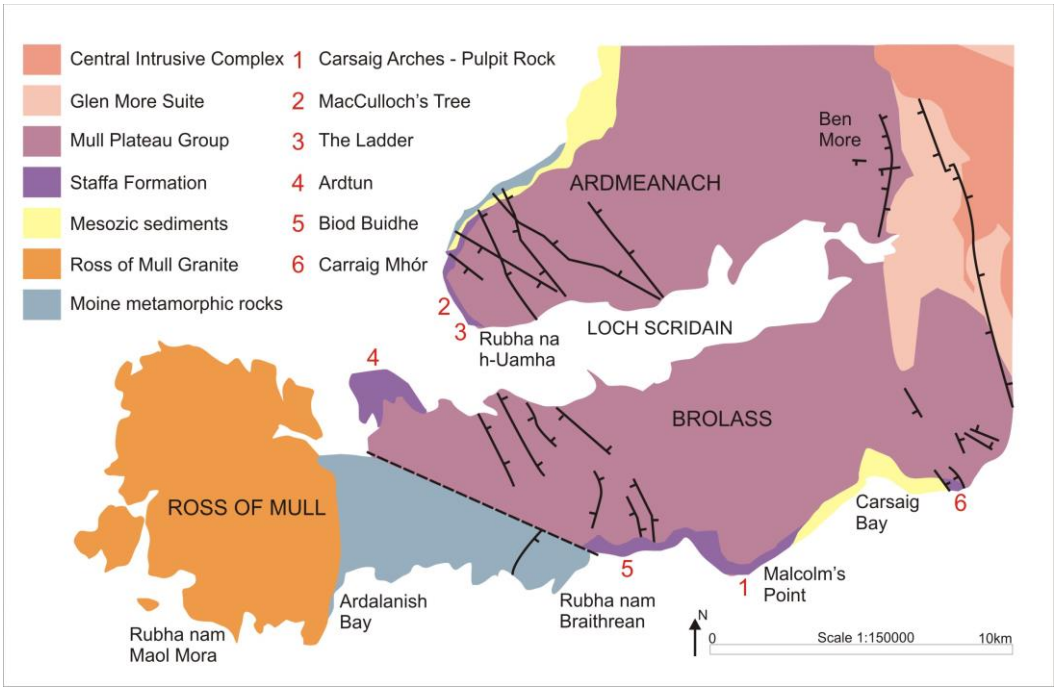

Figure 4.5. Map of the south-west of Mull. The Staffa Formation outcrops at the 6 locations named on the map. Edited from EDINA DigiMap with reference to Williamson and Bell (2012).

4.4 Lithofacies descriptions and interpretations

Nineteen lithofacies were identified from five locations within the Staffa Formation. These lithofacies are summarised in Table 4.1. The lithofacies descriptions are later combined with petrographical descriptions to quantitatively characterise the volcaniclastic rocks of the Staffa Formation. The following section builds on work by Williamson and Bell (2012). All lithofacies descriptions and interpretations have been directly made by the author with reference to the previous body of work, unless otherwise stated.

4.4.1 Basalt lava (L)

Several different basaltic lithofacies are observed on Mull but these have been grouped together for simplicity. Two phase (colonnade and entabular) basalt flows are most common (Plate 4.1.A) but pillows, hyaloclastite and more rubbly brecciated facies can also be found. Lavas are typically finely crystalline, with plagioclase and pyroxene. The predominantly tholeiitic basaltic lavas are classed as a geochemically defined group named the Staffa Magma sub-Type (SMsT) (Kerr, 1995; 1998). Towards the top of the

Staffa Formation the basaltic facies become more evolved. Basaltic hawaiite pāhoehoe lava flows are present at a number of locations (Beckinsale et al,. 1978).

The basaltic lava flows range in size from ~2 m to a ~80 m ponded flow at Carsaig (NM 493 186). The colonnade part at the base of the flow, is often obscured by the sea at sample locations. Regular spaced columns of varying sizes are often at sub-vertical angles. The upper entablature part of the flows are a chaotic mass of smaller-spaced columns; however, locally, these become more regular again in the upper colonnade.

Rubbly, chaotic basaltic lava (Plate 4.1.B), composed of weathered vesiculated lava clasts (up to 15 cm in diameter) is found in a number of locations. These rounded basalt clasts are highly altered and are set within a more coherent crystalline, lava matrix. Patches of clay are inferred to be completely altered lava clasts. More coherent lava blocks are punctuated with areas of isolated elongate and strung out vesicles that do not display a dominant orientation.

Lithofacies name	Facies code	Location of outcrop	Genetic sequence (Williamson and Bell, 2012)	Plate
Basalt lava	L	All locations	GS1-GS7	4.1
Peperite	P	Biod Buidhe, Carraig Mhòr	GS5	4.1
Clastogenic lava	cL	Carsaig Arches, Ladder	GS2, GS6	4.1
Basaltic tuff	T	Carsaig Arches	GS2	4.1
Massive scoria-rich breccia	mscBr	Carsaig Arches, MacCulloch's Tree	GS2, GS5	4.2
Massive scoria rich tuff	mscT	Carsaig Arches, MacCulloch's Tree, Ladder	GS2, GS5, GS6	4.2
Scoria rich volcaniclastic breccias	scvBr	MacCulloch's Tree, Ladder	GS5, GS6	4.3
Volcaniclastic siltstone	vS	MacCulloch's Tree	GS5	4.3
Massive clast-supported volcaniclastic breccias	mcvBr	Carsaig Arches	GS2	4.3
Massive matrix-supported volcaniclastic breccia	mmvBr	Carsaig Arches	GS2	4.3
Volcaniclastic lithic wacke	vlW	Carsaig Arches	GS2	4.3
Conglomerate	C	Ardtun	GS5	4.3
Volcaniclastic lithic arenite	vlA	Ardtun	GS5	4.4
Sublithic arenite	slA	Carsaig Arches	GS2	4.4
Flint dominated conglomerate	fC	Carsaig Arches	GS2	4.4
Organic rich Mudstone	M	All locations	GS1-GS7	4.4
Coal	Co	Carsaig Arches, MacCulloch's Tree, Ardtun	GS2,	4.4
Quartz arenite	Q	Carsaig Arches	GS2	4.4
Dolerite	D	All locations	GS1-GS7	4.1

Table 4.1: Table of Staffa Formation lithofacies, abbreviations and locations. Links to Williamson and Bell, 2012 GS scheme. Links to chapter figures.

Large 50 cm pillow lavas originally described by Geikie (1888), and chaotic, brecciated lithofacies also exist in several places, with internal chilled margins highlighting lava lobes or lava tubes (Williamson and Bell, 2012).

The multi-tiered lava flows found within the Staffa Formation are interpreted to be pāhoehoe lavas that have been ingressed by water. The presence of pillows in places also suggests that the lavas have been erupted into a terrain filled with localised bodies of water (Lyle, 2000; Williamson and Bell, 2012).

4.4.2 Peperite (P)

This lithofacies is composed of a mixture of dark grey, black fine grained siltstone and finely crystalline basalt lava fragments (Plate 4.1.C). The basalt clasts contain plagioclase phenocrysts (up to 5 mm in diameter) and are green due to clay alteration. Chilled margins and fluidal textures indicate the clasts are juvenile. The siltstone has faint laminations, which are locally disturbed by the basalt. Both blocky and fluidal peperite textures are present. These peperites are exclusively found at the bases of lava flows.

The presence of both fluidal and blocky peperite suggests complex intermixing between the lava and the underlying siltstone. The highly altered nature of the juvenile basalt clasts suggests alteration by fluids. The locally disturbed sediment also indicates a degree of fluidsation implying that the sediment was sufficiently wet when intruded (cf. Kokelaar, 1982).

4.4.3 Clastogenic lava (cL)

This facies comprises crystalline basalt lava with irregular zones of agglutinated vesicular spatter clasts. The dark grey, finely crystalline lava contains rare plagioclase phenocrysts (2 cm) and is devoid of structures or vesicles. Agglutinated zones reach 2 m in diameter and have irregular shapes. These zones are distributed throughout the facies but occur more commonly towards the top of the outcrops. Within these zones the outlines of spatter clasts are barely visible. Spatter clasts range in size, from 5 cm-30 cm long. The densely welded spatter shapes are irregular and are predominantly flattened horizontally throughout the zones. Vesicles are elongate and deformed, particularly at the edges of the agglutinated zones. In places the edges of the zones are irresolvable and appear to blend into the surrounding crystalline basalt lava (Plate 4.1.D). The clastogenic lavas are typically found in locations interpreted as vent proximal and reach a maximum thickness of around 5 m.

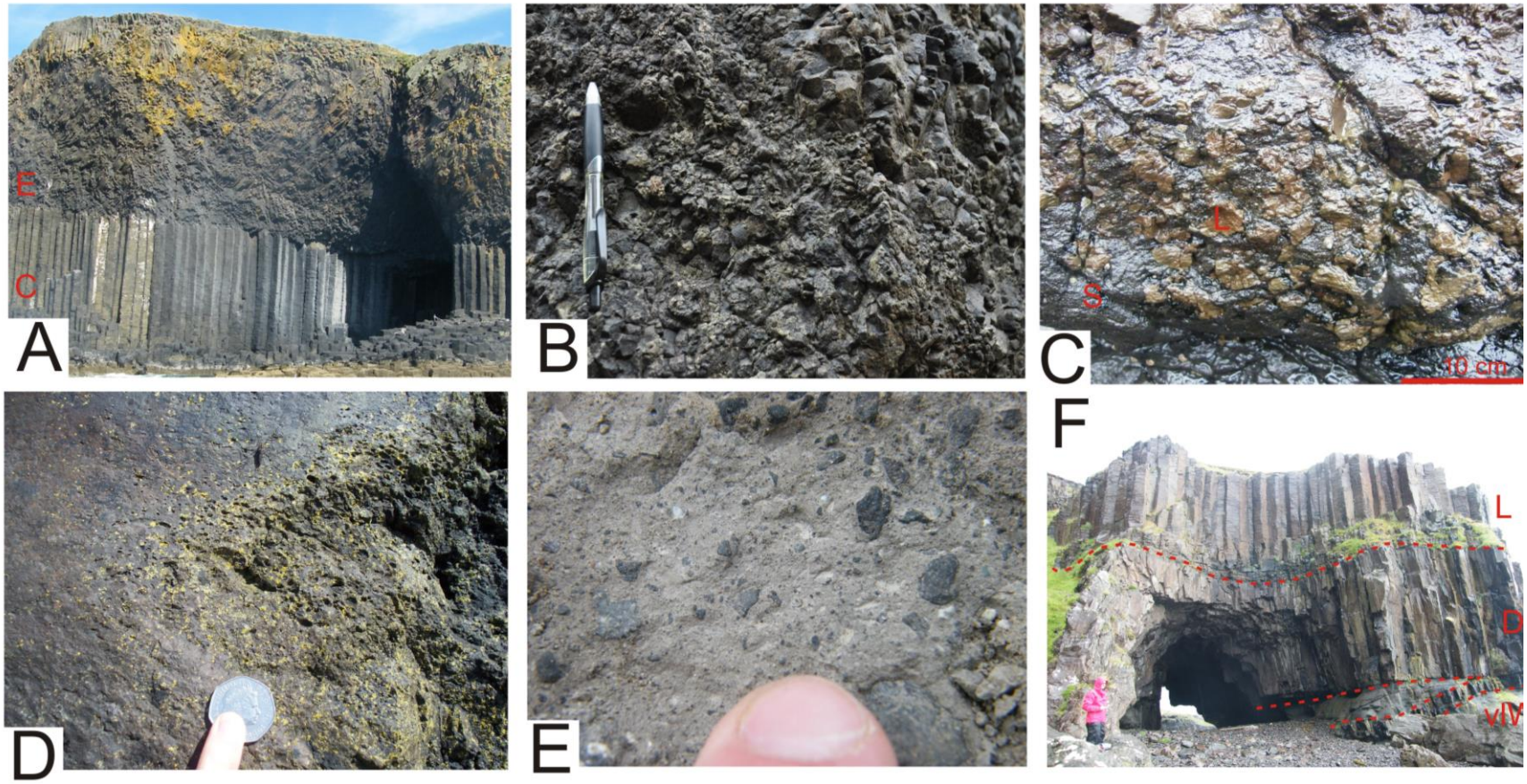

Plate 4.1 Volcanic lithofacies. A. Multi-tiered (colonnade (C) and entablature (E)) basalt lava flow, Isle of Staffa. Photo is 12 m across. B. Rubbly, chaotic basaltic lava, Ardtun, pen for scale. C. Blocky peperite, lava clasts (L) in a silt matrix (S), Biod Buidhe. D. Clastogenic lava (cL), The Ladder, 50p coin for scale. E. Basaltic tuff (T), Carsaig Arches, finger for scale. F. Dolerite sill (D) intruding between volcaniclastic lithic wacke (vlW) and basalt lava (L), Carsaig Arches, view to the east, person for scale.

This lithofacies is interpreted as the product of fountain-fed lava flows. High accumulation rates from lava fountains result in minimal radiative and convective cooling and can produce welded or agglutinated spatter deposits (cf. Walker, 1973). Accumulation rates of 20 cm/min can lead to densely welded spatter (Sparks and Wright, 1979; Sumner, 1998). Larger clasts cool at slower rates resulting in more welding and clastogenic textures (Thomas and Sparks, 1992). Two methods of clastogenic lava formation are envisioned by Sumner (1998). The first is simply an increase in accumulation rates under a lava fountain, and the second corresponds with the waning of the spatter column allowing spatter blocks to be carried or rafted upon an agglutinated layer below. Patches of more distinct spatter towards the top of the lava flow may represent rafted blocks; however, the Staffa Formation clastogenic lavas are not rubbly and there is little evidence for rotational slumping or failure as described by Sumner (1998).

4.4.4 Basaltic tuff (T)

This lithofacies comprises grey, poorly sorted, crystal-rich tuff (Plate 4.1.E) composed of fine-grained basaltic ash, minor quartz crystals (<5%), and fine (<5 mm in diameter.) basaltic scoria lapilli. The tuff displays faint milimetre scale laminations. This facies is only found in one location and forms a small 30 cm wide, laterally discontinuous unit.

The tuff is interpreted to be a fall deposit and is thought to represent a waning in the explosive activity.

4.4.5 Massive scoria-rich breccia (mscBr)

This lithofacies is composed of irregular rag-shaped basaltic spatter clasts that reach 30 cm in diameter, set in a matrix of palagonitised scoria clasts (1–2 cm diameter). Larger spatter clasts are mostly elongate and stand prominent from the exposure. They are highly vesicular with elongate, deformed vesicles and irregular fluidal edges (Plate 4.2.A). Alteration rims (possibly thin chilled margins) are present on some larger spatter clasts. Basaltic bombs up to 80 cm in diameter are found throughout the facies (Plate 4.2.B). These are commonly more spherical than the spatter clasts with more distinct, less fluidal edges. Typically, they have a finely crystalline groundmass and are less vesicular (Plate 4.2.C). Poorly-defined impact sags are present below some bombs.

There is no preferred orientation of the bombs but they typically occur in horizons with abundant large spatter clasts. The breccia is generally poorly sorted, clast-supported and massive, but locally exhibits diffuse bedding defined by layers of large spatter clasts and scattered bombs up to several metres thick, intercalated with layers of scoria lapilli. The larger spatter clasts exhibit a weak horizontal alignment of long axes within the finer scoriaceous matrix. Layering is sub-horizontal and mantles underlying topography. Lenses (up to 1 m long) of more rounded, scoria and rare quartz, are seen towards the top of the unit. This lithofacies is only found in vent proximal regions and is spatially associated with a number of other facies (mscT, scvBr and vS). The thickness of the lithofacies varies from the centimetre to decimetre scale.

The breccia is interpreted as vent proximal basaltic pyroclastic deposits that may have formed part of a scoria cone. The fluidal spatter rags and bombs indicate deposition in a Hawaiian style vent proximal eruption (Valentine and Gregg, 2008). The presence of fluidal spatter clasts (Plate 4.2.D,E) indicate a significant retention of heat when deposited and large ballistic clasts suggest deposition close to the vent (cf. Kuno et al., 1964; Cas and Wright, 1987). Impact sags indicate that the large clasts were emplaced on ballistic trajectories. The breccias are primary in origin with small lenses of localised reworking and syn-rift faults. Bedding within the spatter is thought to represent different pulses of volcanic activity from the vent (cf. Cas and Wright, 1987). Variations can be seen in welding vertically through the facies units indicating pulses in volcanism and welding intensity (cf. Valentine and Gregg, 2008).

4.4.6 Massive scoria-rich lapilli-tuff (mscT)

This lithofacies is composed of massive, well-sorted basaltic scoria lapilli and ash. Scoria clasts range in diameter from 0.1 to 7 cm, are vesicular, have irregular shapes and some display a degree of horizontal flattening (Plate 4.2.F). Diffuse bedding is defined by parallel layers of slightly coarser-grained scoria lapilli and blocks. Welding degrees vary but weakly welded deposits are most common, which tend to mantle the topography below. This lithofacies forms a laterally continuous unit associated with a number of other facies (mscBr, cL, scvBr and vS). Its thickness varies depending on location, but can reach 5 m.

This lithofacies is interpreted as vent proximal pyroclastic fall deposits. Accumulation rate and temperature of the eruption will define the type of scoria cones

produced (Head and Wilson, 1989). Fast accumulation rates with colder clasts will result in non-welded scoria. However, fast accumulation of warmer clasts leads to more welded scoria and spatter accumulations (Fisher and Schminke, 1984).

4.4.7 Scoria-rich volcaniclastic breccia (scvBr)

Small lenses of fine to medium grained sub-angular, yellowish quartz grains and lithic clast dominated sandstone can be found within finer-grained spatter-rich layers. Reworked scoria and spatter clasts (max. 6 cm) are mixed thoroughly with the quartz and lithic clasts (Plate 4.3.A). The lenses are typically no wider than 1 m x 1 m and pass gradationally into the adjacent mscT. Syn- and post-eruptive reworking and deformation of pyroclasts are locally preserved in the form of small scale sumps and loading.

Reworked spatter intervals indicate a break in volcanism, with angular, fractured quartz possibly sourced from the volcanic vent itself. As the explosive nature of the vent rips blocks of county rock free from the fissure walls it incorporates this into the eruption. However, it is unclear why this quartz would only be found in small lenses. During periods of relative quiescence, sedimentary derived quartz may have blown across the volcanic terrain and into cracks and depressions within the scoria. This may explain why lenses of more silicic material are found surrounded by a predominantly basaltic primary volcanic lithology.

4.4.8 Volcaniclastic siltstone (vS)

This facies is a dark grey silt layer, similar to the scvBr facies (Plate 4.3.B). It is much darker in colour with distinct layers of well sorted small (3 cm max.) spatter clasts and scoria, which appears more rounded and therefore reworked. Black organic fragments up to 5 cm long (likely to be wood-like plant material) make up around 10% of this facies. In places the facies is weakly laminated and fines upwards. This lithofacies is laterally continuous and often forms a 5-30 cm thick layer beneath lava flows.

The more continuous silty layers are often found towards the top of the scoria reworked horizons and sit below the basalt. These may also indicate a period of quiescence with fluvial/alluvial and lacustrine systems beginning to wane with the onset of the next phase of volcanism.

4.4.9 Massive clast-supported volcaniclastic breccia (mcvBr)

This facies comprises massive clast-supported, poorly sorted basaltic breccia containing angular to sub-rounded weathered basaltic blocks, <1 m in diameter, set in a dark black and red clay-rich matrix (Plate 4.3.C). Many of the blocks exhibit zeolite- and/or calcite-filled amygdales and have onion-skin style weathering. Unlike the mmvBr (section 4.4.10), the matrix is dominated by volcanic clasts and palagonitised and altered ash. This lithofacies is laterally discontinuous, with the maximum exposure being approximately 2 m wide by 3 m thick.

The mcvBr is interpreted as a debris flow due to the angular clasts within the deposit. The basaltic blocks are locally derived from the underlying and surrounding lava flows. The red nature of many clasts suggests a period of weathering. The lack of other clast types such as flint would suggest that the debris flow was a result of localised movement on a weathered basalt scarp and did not interact with the surrounding fluvial / alluvial system.

4.4.10 Massive matrix-supported volcaniclastic breccia (mmvBr)

This facies comprises poorly-sorted, matrix-supported, massive breccia with sub-rounded to angular blocks of basalt and flint as large as 1 m across (Plate 4.3.D). Two populations of basalt clasts are present: (1) highly vesicular basalt with calcite-filled amygdales; and (2) non-vesicular, dense lava that resembles corestones with exfoliation red-weathered surfaces. Two populations of flint clasts are also present: (1) a fossiliferous lithology; and (2) a non-fossiliferous altered lithology. The matrix ranges from fine to coarse grained quartz wacke. Most units fine upwards, although some outcrops do display localised reverse grading. This lithofacies varies in thickness but is typically 30 cm – 2 m thick.

The massive matrix-supported breccia is interpreted to be a debris flow. The large weathered basalt lava clasts are sourced from surrounding weathered lava flows. The laterally discontinuous nature of this lithofacies may result from a structural, fault bound localised control on deposition.

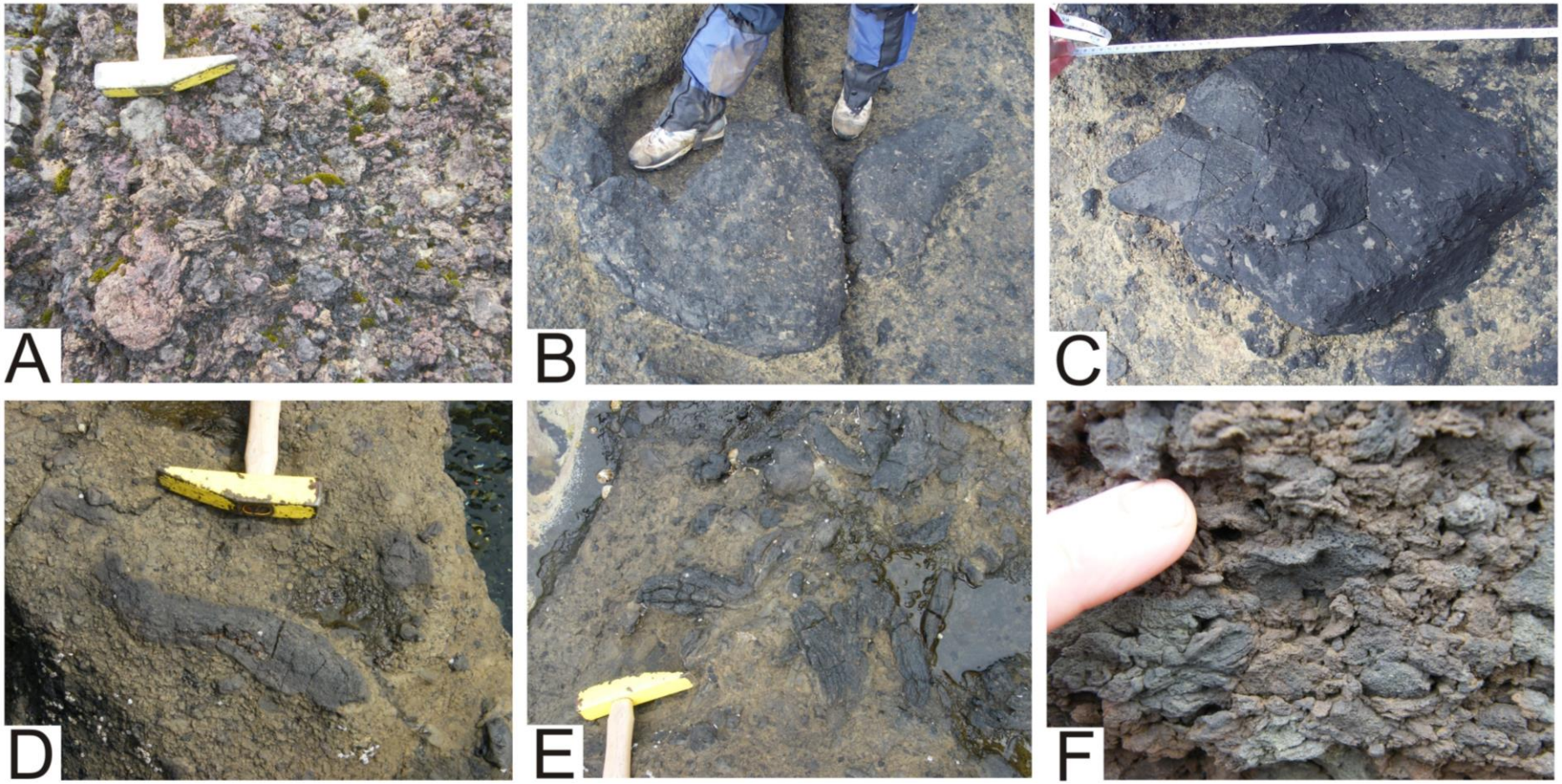

Plate 4.2. A. Massive scoria-rich breccia (mscBr). B. Fluidal basaltic bomb. C. Blocky basaltic bomb. D. Fluidal spatter clast within palagonitised scoria-rich matrix. E. Random orientation of fluidal shaped spatter clasts. F. Massive scoria rich tuff (mscT). All photographs from MacCulloch's Tree. Hammer head 12 cm long; tape 30cm long.

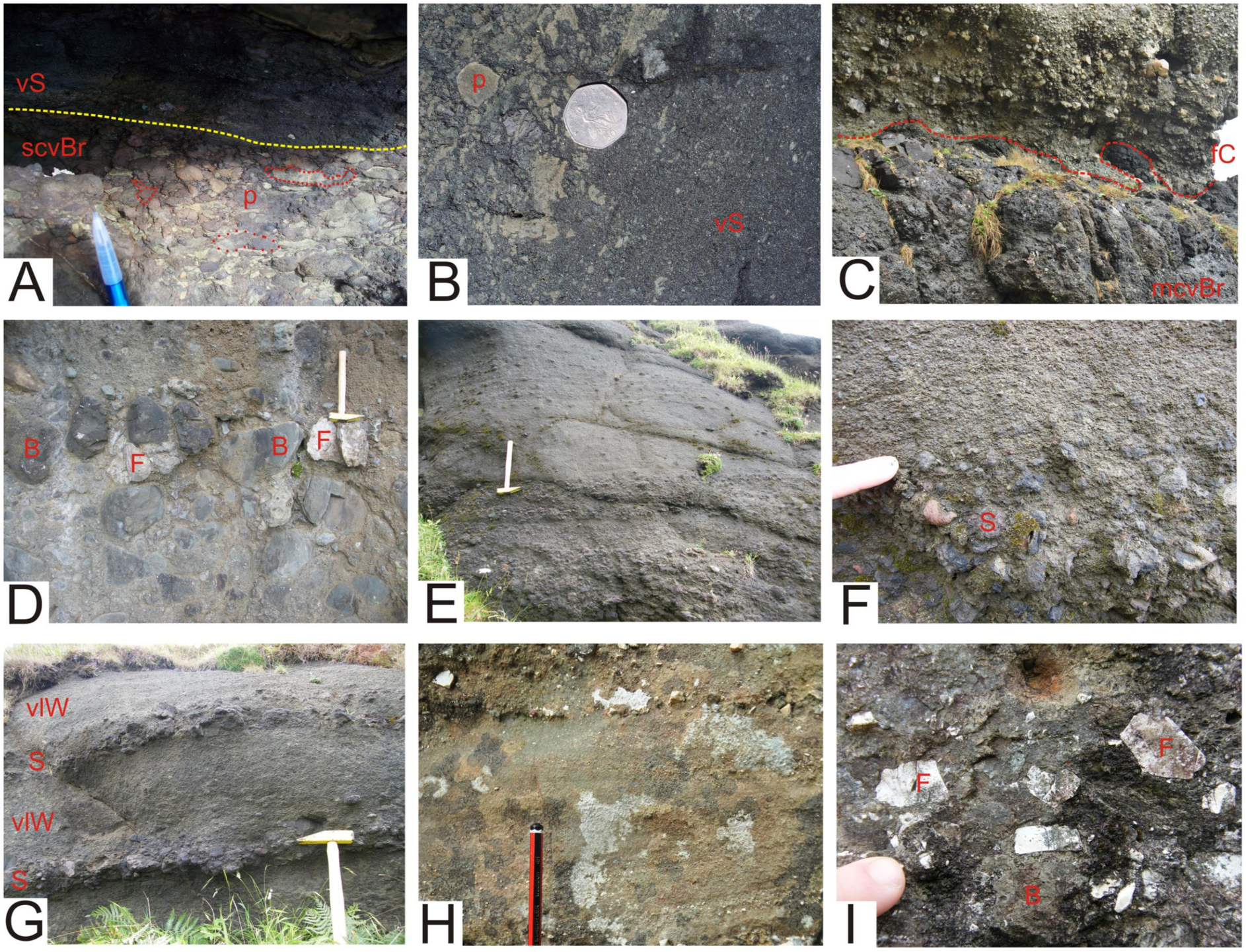

Plate 4.3. A. Scoria-rich volcaniclastic breccia (scvBr) with reworked rounded scoria pyroclasts (p and outlined), MacCulloch's Tree, pencil in view 3 cm. B. Volcaniclastic siltstone (vS) with some scoria clasts (p), MacCulloch's Tree. C. Massive clast-supported volcaniclastic breccia (mcvBr) underlying flint dominated conglomerate (fC), Pulpit Rock. D. Massive matrix-supported volcaniclastic breccia (mmvBr) with rounded basaltic clasts (B) and flint clasts (F). E. Massive volcaniclastic lithic wacke (vlW) fining upwards sequence from mmvBr at the base. F. Volcaniclastic lithic wacke (vlW) with rounded spatter and flint clasts. Fining upwards sequence. G. Volcaniclastic lithic wacke (vlW) with reworked spatter horizons (S). H. Volcaniclastic lithic arenite (vlA). I. Conglomerate dominated by flint clasts (F) and rare basalt (B), Ardtun. Images D-G taken east of Carsaig Arches. Hammer 30 cm shaft.

4.4.11 Volcaniclastic lithic wacke (vlW)

This lithofacies comprises massive grey and green, medium to coarse grained poorly sorted volcaniclastic lithic wacke composed of angular grains of quartz, feldspar, pyroxene, basaltic scoria, palagonitised ash, two types of flint (described in Section 4.4.10), calcareous sandstone / limestone and rare weathered basaltic lava, mica and glauconite. The clay-rich matrix gives the facies a distinctive green colour. Most units are normally graded and weakly laminated (Plate 4.3.E,F); however, rare coarsening upward sequences and sedimentary structures such as crossbedding and asymmetrical ripples are also present. Spatter and scoria rich beds up to 10 cm thick are interbedded with the vlW. The spatter in these beds shows a weak alignment along the long axis and in places is imbricated (Plate 4.3.G). This lithofacies is one of the most common found within the field area. It is laterally continuous and is often closely associated with mmvBr (Section 4.4.10). Beds vary in thickness from <10 cm to ~3 m.

These rocks are interpreted as alluvial fan deposits due to their poorly sorted and matrix supported nature (cf. Sohn et al., 1999). Scoria and spatter clasts have been locally reworked into horizons within these units.

4.4.12 Volcaniclastic lithic arenite (vlA)

These yellow-brown-grey lithic arenites are typically clast supported with rounded quartz and feldspar crystals, angular clasts of flint, scattered pebbles of heavily altered, red glassy vesicular basalt, and very rare schist clasts (Plate 4.3.H). Beds vary in competency due to the presence of a calcite cement and often form lenticular beds in surrounding conglomerates. Larger clasts are found towards the base of individual beds and truncate cross bedding in places. Fining upward sequences are prevalent. Most units contain cross bedding with Type 1 ripple drift cross laminations (cf. Walker, 1963), while other beds contain asymmetrical ripples associated with the cross bedding and rare coarsening upward sequences. This lithofacies is laterally continuous and can be traced for several metres along the foreshore. Beds range from 10 cm to ~2 m in thickness and are associated with the conglomerate (section 4.4.13) and mudstone (section 4.4.16) facies.

These rocks are interpreted as fluvial in origin due to the relatively mature nature of the sediment. The lenses represent channels, with normal and inverse grading

indicating waxing and waning of flow. Type 1 ripple drift cross lamination occurs when abandoned channels are filled, indicating an anastomosing braided stream system (cf. Walker, 1963). This interpretation is consistent with the presence of channels. Ripples can also be seen forming on the back of mid-channel dunes suggesting that the river system was relatively large and well established (cf. Frostick and Jones, 2002). The red colour and rounded nature of many of the basalt clasts suggests they were weathered from a lava flow before being incorporated within the sediment. More evolved lava clasts are also found and these are thought to be from Devonian lavas and not sourced from the underlying lithology (Bailey and Anderson, 1925; Williamson and Bell, 2012).

4.4.13 Conglomerate (C)

This lithofacies comprises clast supported conglomerate with sub-angular to rounded flint clasts (up to 10 cm in diameter), quartz and weathered basalt clasts set in a coarse-grained sublithic arenite matrix (Plate 4.3.I). At least two populations of flint are present as before. Cross bedding is prevalent, and elongate 1 m lenses of medium to coarse grained sublithic arenite with abundant organic fragments are also present. Cross bedded foresets form shallow angles of approximately 10° and are no greater than 30 cm in height. Larger conglomeratic layers scour into sandy units below and in places can be seen truncating cross bedding. Fining upwards sequences are prevalent. Clasts are predominantly randomly orientated (Plate 4.4.A); however, weak imbrication can be seen in places, tentatively indicating palaeo-flow direction to the south-east. Similar to the vlA (Section 4.4.12), this lithofacies is laterally continuous with a maximum bed thickness of 2 m.

The conglomerates are interpreted to be fluvial channel deposits. The rounded nature of the clasts suggest it is a mature deposit, while the low angle cross bedding foresets indicates that the conglomerate was deposited in a lower river regime (cf. Frostick and Jones, 2002). The 30 cm maximum height of the foresets suggests a maximum water depth of ~75 cm (cf. van de Neut and Eriksson, 2009), while the presence of possible obstacle clasts suggests a perennial river system (Stuart Jones, pers. comm). Waxing and waning energy as the braided river channel system moves would lead to the normal and reverse grading, and erosional surfaces.

4.4.14 Sublithic arenite (slA)

This lithofacies comprises sublithic arenite composed of pale yellow to grey, coarse to medium grained, well-sorted, sub-rounded quartz with angular flint clasts and minor quantities (<5%) of feldspar grains (Plate 4.4.B). Fining upward sequences are common with fine (mm scale) asymmetric ripples. In places, the unit has faint bedding, and is often interbedded with finer organic-rich silty or muddy layers with occasional flaser bedding. Many of these layers are disturbed by dewatering textures. This lithofacies is localised and cannot be traced for more than a few metres, with a maximum thickness of ~30 cm.

The sublithic arenites are interpreted to be fluvio-deltaic deposits. The deposits are relatively mature, demonstrated by the lack of abundant feldspars, and are most likely derived from a source area lacking volcanic rocks. Flaser bedding can be found in fluvial settings often on point bars within the lower part of the rivers course (cf. Davis, 1983; Bhattacharya, 1997; Martin, 2000). Dewatering structures may be due to liquefaction but are most likely to be due to the loading of the lava flows above.

4.4.15 Flint-dominated conglomerate (fC)

This lithofacies comprises well sorted, massive, clast-supported cross-bedded conglomerate composed almost exclusively of flint clasts up to 40 cm in diameter (Plate 4.4.C). The matrix comprises coarse sand to pebble grade flakes of flint, minor amounts of quartz and rare feldspar crystals. Flint clasts are sub rounded to sub angular and of high to medium sphericity. No imbrication is present although a weak alignment of more elongate clasts can be seen in some beds. Clasts are weathered, many are fractured at grain contacts, and some are cross-cut by calcite veins that do not extend into the surrounding sediment. Cross bed foresets reach over 1 m in height and indicate transport to the southeast. Fining upward sequences are prevalent with coarser conglomeratic layers often pinching out against medium to coarse-grained flint dominated arenite layers. This lithofacies is only found at one location within the field area, with a maximum thickness of 4 m.

Two populations of flint are present within the monolithic congolmerates indicating that initial reworking occurred before being deposited. Although well sorted,

clasts are angular and so transportation distances are thought to be low. The large cross-bedding foresets indicate a maximum water depth of around 2.5 m. The deposit may be a large fluvial channel; however, no evidence such as obstacle clasts, could be found indicating a perennial river system and is therefore thought to be deposited by a hyperconcentrated flow regime. This is in agreement with Williamson and Bell's (2012) interpretation that the conglomerate is a proximal fan deposit.

4.4.16 Organic-rich mudstone (M)

This lithofacies comprises grey to very dark grey/black, fine grained, fissile mudstone (Plate 4.4.D) with fine parallel laminations and abundant organic matter. A wide range of fossil plants and pollen are found within the mudstones (Boulter and Kvacek, 1989; Cleal et al, 2001; Jolley et al., 2009). This lithofacies is common throughout the field area; however it is limited to thin layers (typically less than 30 cm thick) and often occurs underneath lava flows.

The mudstones are thought to be low energy, terrestrial, floodplain overbank deposits, which is consistent with the latest interpretation in Williamson and Bell (2012). The abundant fossils found within these deposits indicate a swampy or lacustrine environment, with a mature forest located nearby (Jolley et al., 2009).

4.4.17 Coal (Co)

This lithofacies comprises thin beds (max. 10 cm thick) of very dark grey/black coal (Plate 4.4.E). Units are weakly bedded, occasionally fissile and are often located beneath lava flows. These coals may have been further matured due to heat of the above lava. This lithofacies is commonly seen at the interface between lava flows and underlying sedimentary or pyroclastic sequences. It is typically a laterally continuous unit, with lenses ~ 20 m across.

4.4.18 Quartz arenite (Q)

This lithofacies comprises pale yellow, fine to medium grained siliciclastic sandstone composed almost entirely of quartz with very rare feldspar and flint clasts, and devoid of volcanic lithoclasts (Plate 4.4.F). Quartz grains are sub-rounded to rounded and well

sorted. The facies is poorly lithified, with no obvious sedimentary structures; however, in places there is a quartz cement giving an almost nodular appearance to the sandstone. This lithofacies is only exposed at one locality on the Carsaig foreshore. It sits towards the top of a sedimentary package and reaches a maximum of 30 cm in thickness.

The mature nature of the quartz arenite suggests deposition in a well established fluvial regime, with the lack of feldspar and clast roundness suggesting large transport distances relative to the more immature volcaniclastic sandstones.

4.4.19 Dolerite (D)

Shallow, finely crystalline dolerite intrusions are present within the Staffa Formation (Plate 4.1.F) (Bailey et al., 1924; Preston et al., 1998). They vary in thickness from a few cm to several metres, with plagioclase phenocrysts up to 2 cm long. They exhibit chilled margins and some have disturbed the adjacent sedimentary structures. Straight, undulating, fluidal and peperitic texture contacts are found.

The intrusions often exploit the lava / sediment interface. For example, at the Carsaig Arches (NM49798 18549) a sill intrudes between the top of the volcaniclastic sediment and the base of the lava above. However, this is not always the case; at Ardtun (NM 3773 2479) the sill initially intrudes into the sedimentary sequence, but then ramps upwards into the overlying lava, presumably following an original line of weakness such as a fault.

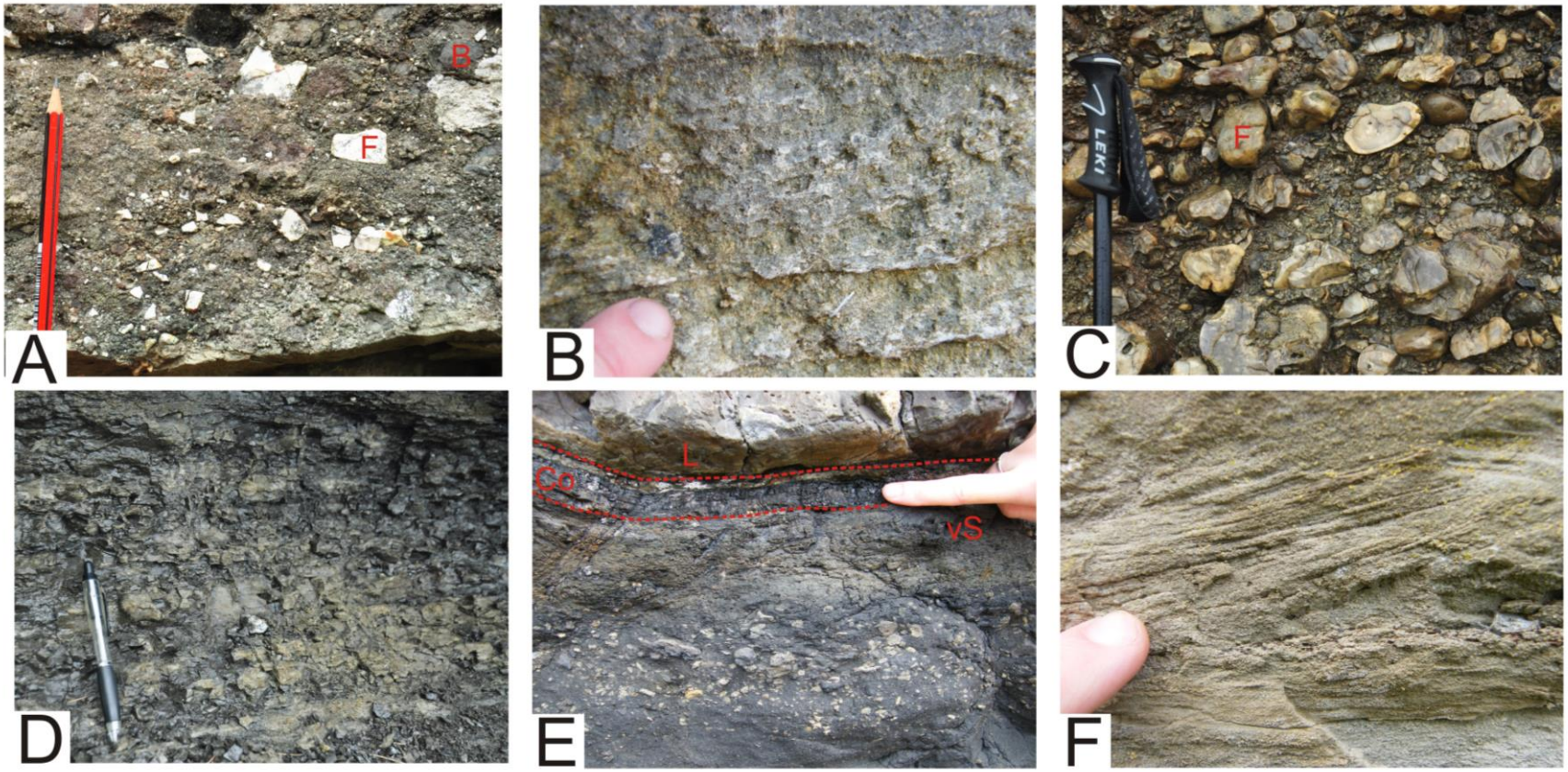

Plate 4.4. A. Conglomerate with randomly orientated clasts of flint (F) and basalt (B), Ardtun. B. Sublithicarenite (slA). C. Flint (F) dominated conglomerate (fC), Pulpit Rock, Walking stick in view 20cm. D. Organic rich Mudstone (M). E. Coal (Co) overlaying volcaniclastic siltstone (vS) at the base of a lava flow (L), MacCulloch's Tree. F. Cross bedding in quartz arenite, Carsaig Arches. Photographs A,B, D and E, taken at Ardtun.

4.5 Field Locations

Five field locations were chosen to examine the Staffa Formation in detail. Locations were chosen due to their accessibility and to allow the study of how the lithofacies interact laterally and vertically along the sediment interbeds to be undertaken.

4.5.1 Carsaig Arches – Pulpit Rock

The Carsaig Arches to Pulpit Rock (NM 49209 18557 – NM 50192 18816) sedimentary and pyroclastic sequence crops out on the south-west coast of Mull, to the west of Carsaig Bay (Figure 4.6). This complex sequence of sedimentary and pyroclastic rocks can be traced for one kilometre along the coast allowing vent proximal to vent distal rocks to be studied as summarised in logs 1-12 (Figures 4.6; 4.7). The sequence is assigned to the GS-A2 sedimentary unit in Williamson and Bell (2012).

At the Carsaig Arches (NM 49209 18557) the lowermost unit within the clastic sequence is a massive scoria-rich breccia (mscBr). In places this is overlain by an almost 4 m thick section of densely welded spatter and clastogenic lava (cL). The spatter units grade both vertically and horizontally into a massive volcaniclastic lithic wacke (vlW). Spatter- and scoria-rich beds up to 10 cm thick are interbedded with the wackes. Locally overlying this unit is a ~2 m thick matrix-supported volcaniclastic breccia (mmvBr). The breccia unit grades up into a series of vlW beds which vary in thickness along the sedimentary sequence. A small, max 10 cm, tuffacous unit (T) can be found at Carsaig Arches.

Towards the eastern end of the outcrop the vlW beds pass upwards into a fine grained mudstone (M) which in turn is overlain by a thin, coal (Co). Above this unit is a pale yellow quartz arenite (Q), which stands out from the volcanic dominated succession below. Overlying this unit is another bed of dark, fissile mudstone (M).

Further, east at Pulpit Rock the clastic succession comprises a basal massive clast-supported volcaniclastic breccia (mcvBr), which overlies the weathered rubbly flow top of a pahoehoe lava, distinguished by a reddened weathering surface. Overlying the breccia is a clast-supported cross-bedded flint conglomerate (fC) that fines upwards into a poorly consolidated sublithic arenite (slA). The whole sedimentary sequence is cut by a number of dolerite (D) sills and dykes. The best example of this is at Carsaig Arches itself (NM49796 18549).

The sedimentary and pyroclastic rocks found at Carsaig are interpreted as a vent proximal to vent distal sequence (Figure 4.6 log 5 to12). Although no vents are preserved on Mull the primary deposits such as the massive scoria-rich breccias indicate a close proximity to a fissure. Syn- and post-eruptive reworking of these deposits indicate breaks in volcanism.

The fining upwards sequence from the mmvBr to the vlW could represent switches between debris and hyperconcentrated flow deposits (cf. Lirer et al., 2001) common in alluvial fan settings (cf. Sohn et al., 1999) but may also be a result of localised flooding events (Williamson and Bell, 2012). Layers of spatter included in the volcaniclastic lithic wacke may represent periodic increases in explosive activity at the fissure, reflecting a switch of source area from volcanic spatter-rich to poor or may simply reflect an increase in channel energy. Cross-bedding within the volcaniclastic sandstones yield palaeoflow directions towards the south east (Williamson and Bell, 2012). The yellow quartz arenite is devoid of volcanic material despite sitting at the top of a volcaniclastic rock package. This indicates that the fluvial system had re-established itself over the volcanic terrain and the provenance has switched to a more distal location. The mudstone beds may represent overbank deposits and highlight the switch from a volcanic-dominated provenance to a more siliciclastic one. The massive matrix-supported breccias seen at the Pulpit Rock are interpreted as a debris flow deposit, linked to localised tectonic activity. The flint conglomerate that overlies this breccia is completely devoid of volcanic material. The switch from one regime to the next is sharp indicating a sudden and total change in provenance The historically tectonic nature of the graben could potentially have exposed chalk and flint escarpments that would provide sudden influxes of siliciclastic material into the system, allowing for the switching of source regions (Williamson and Bell, 2012).

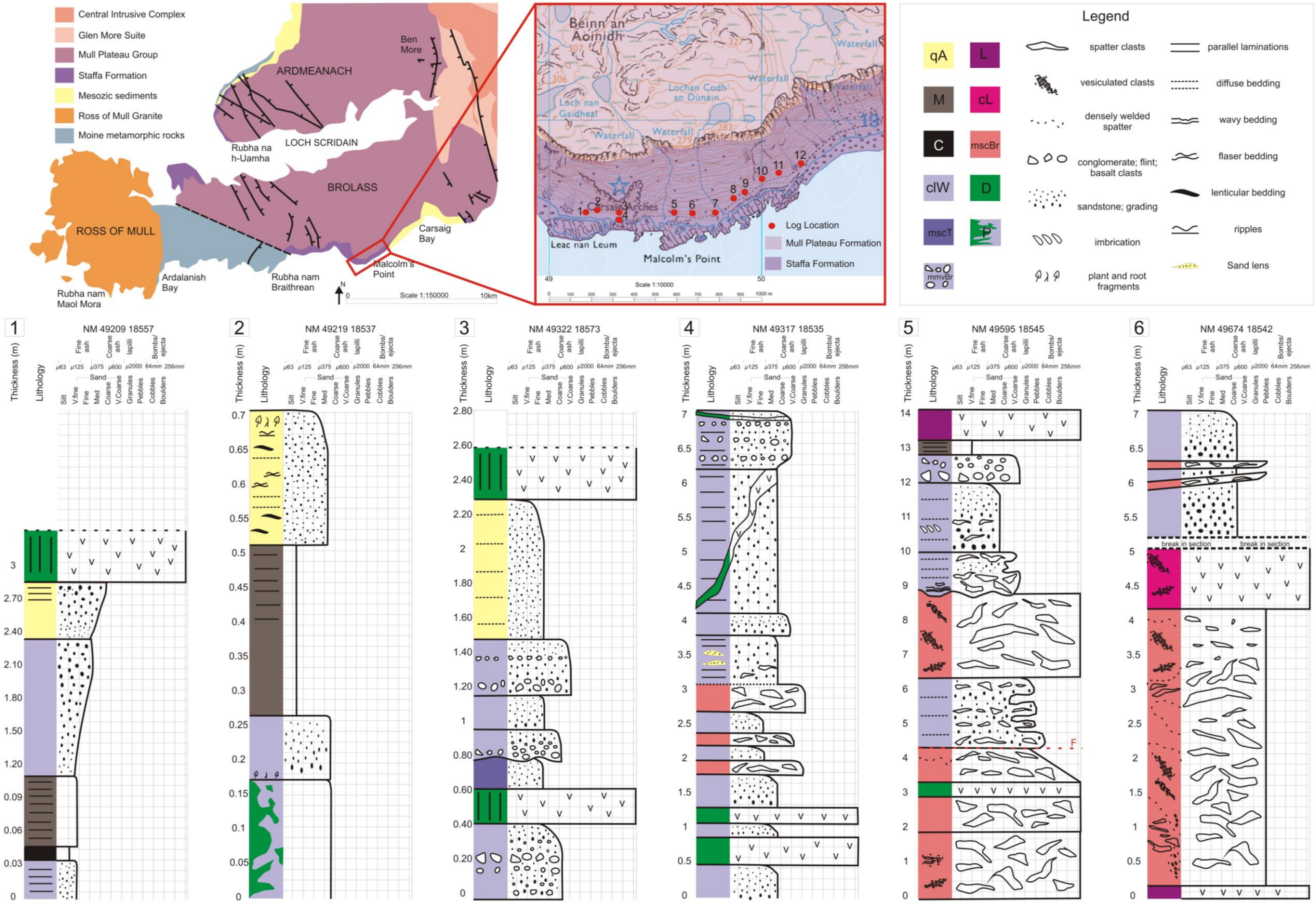

Figure 4.6. Schematic logs taken at the Carsaig Arches to Pulpit rock section. Logs 1 to 6 are shown with their locations on the map. Note the scale differs on each log. More vent proximal volcaniclastic rocks such as spatter rich rocks and clastogenic lavas are found towards the Carsaig Arches. Lithofacies codes match those in Table 4.1.

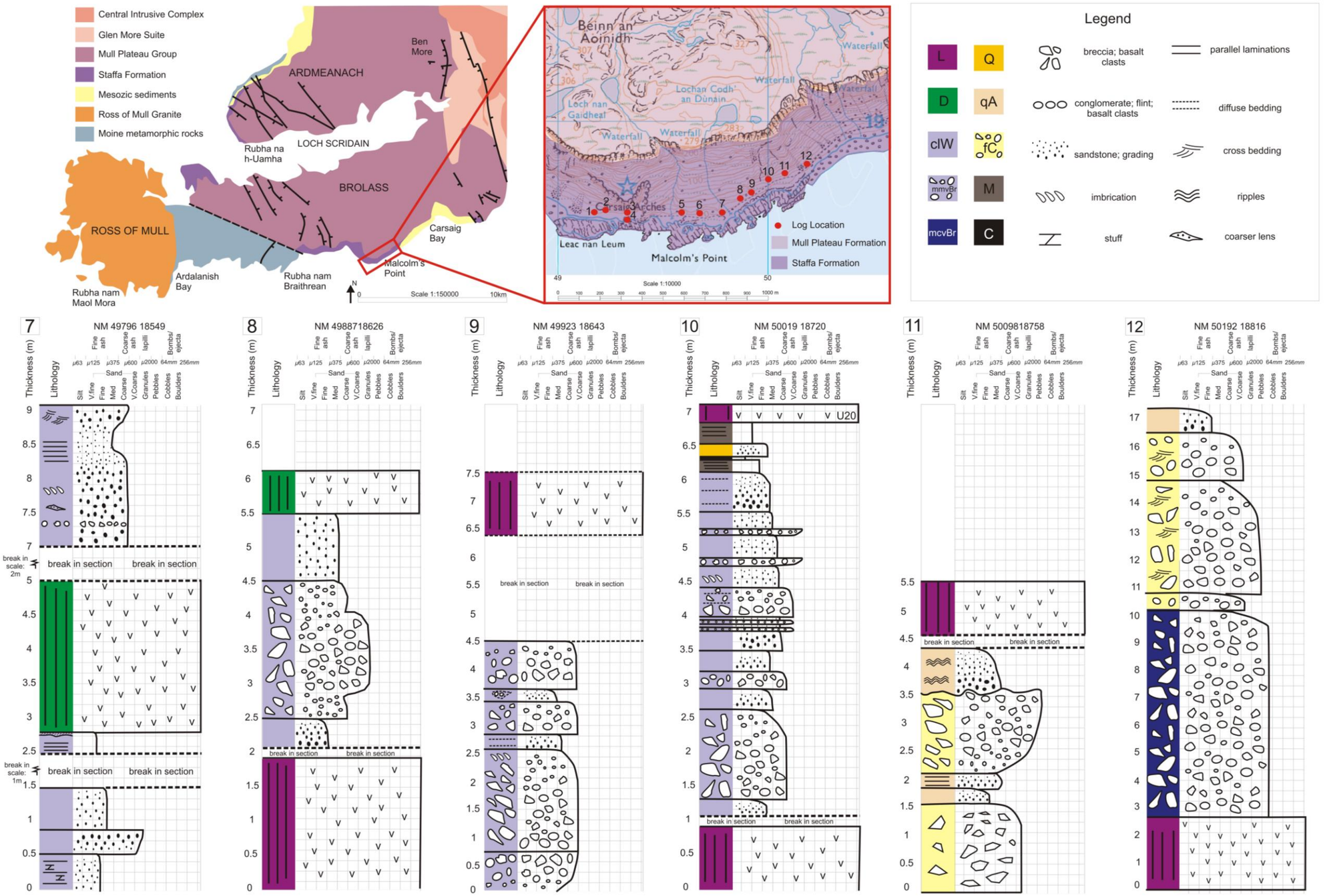

Figure 4.7. Continuation of Figure 4.6. chematic logs taken at the Carsaig Arches to Pulpit rock section. Logs 7 to 12 are shown with their locations on the map. Note the scale differs on each log. There are no primary pyroclastic rocks within this section. Spatter and scoria are reworked and mixed with sillicilastic components such as quartz and flint. Towards the Pulpit rock the volcaniciclastic rocks pinch out and sillicilastic rocks begin to dominate.

4.5.2 MacCulloch's Tree

The MacCulloch's Tree outcrop is found at the south-west end of the area called the Wilderness on Mull (NM 4025 2785) (Figures 4,3; 4.8). The outcrop consists of a large wave cut platform, which can only be seen in full at very low tides and the associated cliff section. The outcrop is named after a large tree mould in a lava flow at the base of the cliff. The sequence is part of the GS-A5 sedimentary and GS-V5 volcanic units (Williamson and Bell, 2012).

The basal unit comprises a thick succession of basaltic spatter and scoria-rich pyroclastic breccias (mscBr). Thin lenses of scoria-rich volcaniclastic breccia (scvBr) can be found towards the top of the spatter unit within finer-grained spatter-rich layers. These lenses are up to 1 m wide and 30 cm thick and pass gradationally into the adjacent mscBr facies. Locally, towards the top of the spatter unit a 1 m by 40 cm lens of reworked vS can be found although this was only apparent during one field session as it is often masked by the boulder field. The mscBr fines upwards and passes into a distinct more continuous layer (max. 30 cm thick) of scvBr. Williamson and Bell (2012), noted the presence of cross bedding and other sedimentary structures, which they cited as evidence of reworking; however, these features were not observed in the present study. The mscBr in turn grades into a thin (5 cm thick max.) highly organic rich coal layer (Co), which is, in turn, overlain by the lava flow (L) which contains the famous MacCulloch's Tree. The contact between the Co and the overlying lava flow is sharp with no evidence of peperitic textures; in places however, the lava does load the sediment with small scale (5 cm) dish-and-pillar structures. The nature of the lava flow is complex and changes considerably over a few metres. In places the lava flow directly above the organic layer is columnar-jointed while further to the east it forms pillows. The nature of the sediment-lava contact will be discussed in the contact section (Section 4.8).

In one location, to the west of the MacCulloch's Tree the Co unit is missing and instead the unit is capped by a 2 m thick steeply-dipping spatter dome. The relatively fresh unaltered nature of this spatter contrasts with the surrounding deposits. Above the high tide mark it has been spared erosion from wave action; however, the high porosity preserved differs from similar deposits elsewhere on Mull. Similar textures are evident in the much younger deposits of the Columbia River (pers. comm. Richard Brown). The overlying lava flow appears to chill against the dome as it mantles the topography. The

lava at this location is chaotic and brecciated with several internal chilled margins highlighting lava lobes or lava tubes (Williamson and Bell, 2012).

The basaltic spatter and scoria-rich pyroclastic breccias (mscBr) found at MacCulloch's Tree are similar to those seen at Carsaig Arches and are also interpreted as proximal pyroclastic fall deposits associated with a scoria cone, but with less reworking. No evidence for extensive hyaloclastite and channelised volcanic breccias as described in Williamson and Bell (2012) were noted, but these rocks may have been obscured by unusually high storm surge tides during fieldwork. Spatter is vesiculated and lacks quenched fragmentation textures common in hyaloclastite depoists. However, localised fall deposits into standing bodies of water are present. Freshwater algae microfossils and woody macrofossils in the mudstone layers indicate that the area was dominated by well-established upland coniferous swamps (Jolley et al., 2009). The presence of a large mature tree within the flow indicates a significant time gap between at pulse of volcanism in order for mature vegetation to colonise the substrate. The presence of pillow lava again suggests large areas of standing water.

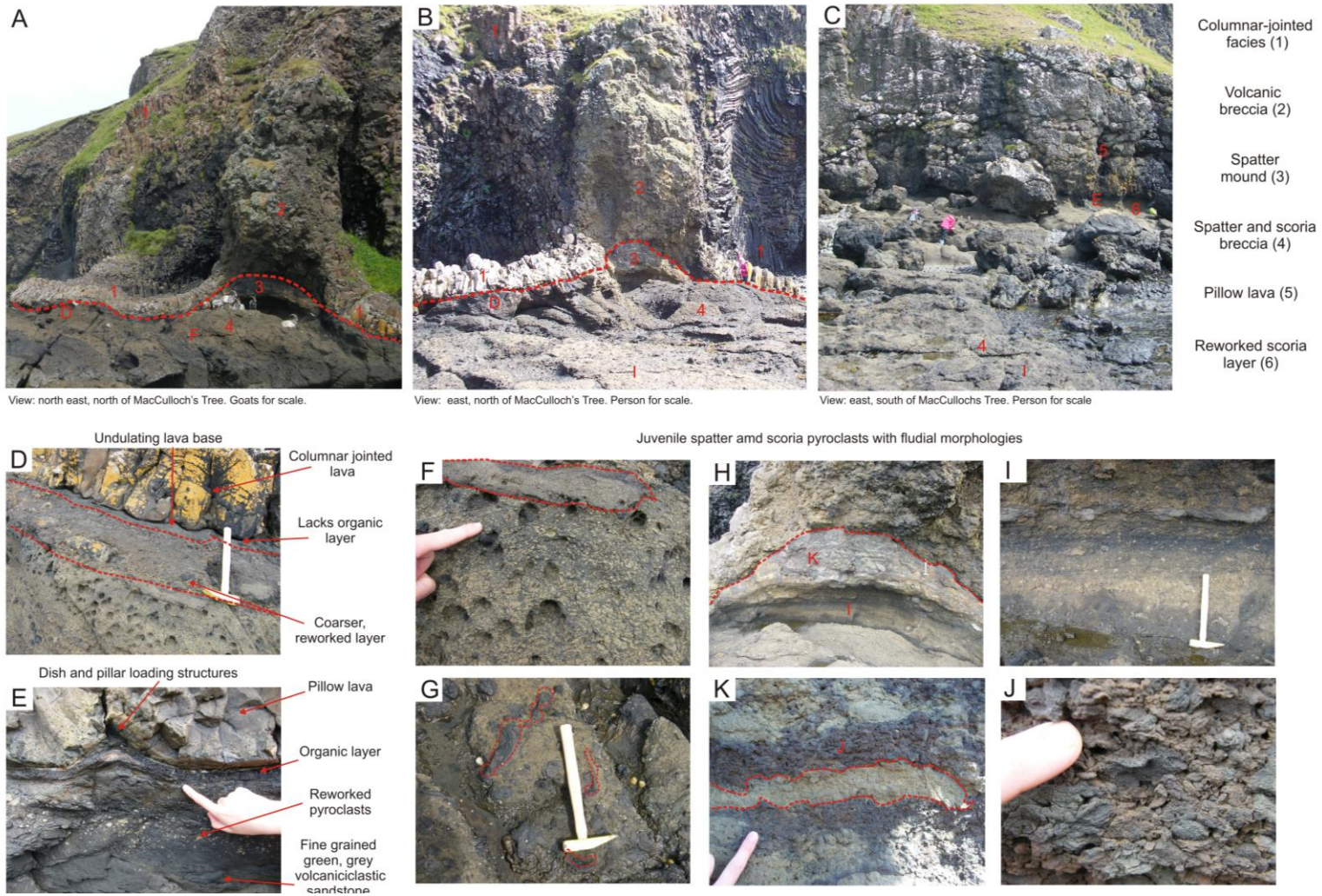

Figure 4.8. Field photographs from MacCulloch's Tree. A: Undulating contact (dashed red line) between the columnar jointed lava and the underlying spatter and scoria breccia. B: The irregular columnar joints are perpendicular to the lava breccia. C: The Spatter and scoria breccia grades up into a layer of reworked scoria. Overlaying this is a pillow lava facies. D: Loaded lava contact. E: Loaded contact overlaying organic layer. F: Scoria rich breccia with large spatter rag. G: Fluidal spatter rag morphologies. H: Spatter mound. I: Bedded spatter in spatter mound. K: Large altered spatter rag. J: Fluidal, vesiculated scoria.

4.5.3 The Ladder

The Ladder sequence is situated 700 m south east of MacCulloch's Tree (NM 40506 27309) (Figure 4.9). It comprises a 26 m high exposure composed of sedimentary and pyroclastic rocks sandwiched between basalt lava flows. It is part of the GS-A6 unit (Williamson and Bell, 2012). Although the sequence cannot be traced laterally along strike it gives an insight into the interplay between sedimentary, pyroclastic and volcanic systems vertically through time.

At the base of the sequence is a columnar-jointed pahoehoe lava flow (L) with a vesiculated upper crust. This is overlain by a 1.5 m thick series of sublithic arenites (slA) interbedded with organic-rich mudstone (M); however, the contact is not exposed. In general, the sedimentary unit is clast supported; however, a 10–40 cm lens of quartz cemented arenite is seen within the upper units. The slA are overlain by a massive, well-sorted massive scoria-rich tuff (mscT) but the contact is not seen. The contact between this scoria and the overlying clastogenic lava (cL) unit is complex. In places the contact is fairly well defined and straight. The overlying unit comprises a more coherent lava with very few vesicles and the boundary between this and the brecciated facies below is sharp. In places however, this boundary is much more irregular and the more vesiculated brecciated lava appears to grade into the coherent unit above. Overlying this clastogenic lava there is a sharp transition into a 10 m thick well-jointed, basalt lava flow with a prominent colonnade (L). Columns at the base of the flow are tight, separated by 10–15 cm compared to the more regular spacing towards the centre of the flow. The cliff section is completed by a 3 m thick rubbly, brecciated vesicular basaltic lava with zeolite filled amygdales.

The Ladder allows a unique opportunity to study an almost complete vertical cross section through a sedimentary sequence from the bounding lava at the base, to the one at the top. The sublithicarenites and mudstones at the base of the section are interpreted to be of fluvial origin (Williamson and Bell, 2012). The palynoflora found within the mudstone units suggest deposition in a fluvial marginal mire setting (Jolley et al., 2009). These rocks lack a significant volcanic component with only minor (<5%) altered glass shards present. The glass shards retain their vesicle wall structure and some retain fluidal shapes indicating minimal transportation distances. This rock therefore represents the transition from dominantly silicilastic rocks to rocks that are dominated by volcanic clasts.

The overlying massive scoria-rich tuff (mscT) indicates that there was direct volcanic input into the system. As the volume of spatter ejected from the vent increases spatter on the ground begins to coalesce and flow as lava (Valentine and Gregg, 2008). This explains the complex transition from the basal brecciated unit into the more coherent clastogeneic lava unit punctuated by vesiculated areas. The closely spaced glassy nature to the base and top lava flow suggests it cooled quickly (cf. Grossenbacher and McDuffie, 1995).

Location: The Ladder. NM 40506 27309

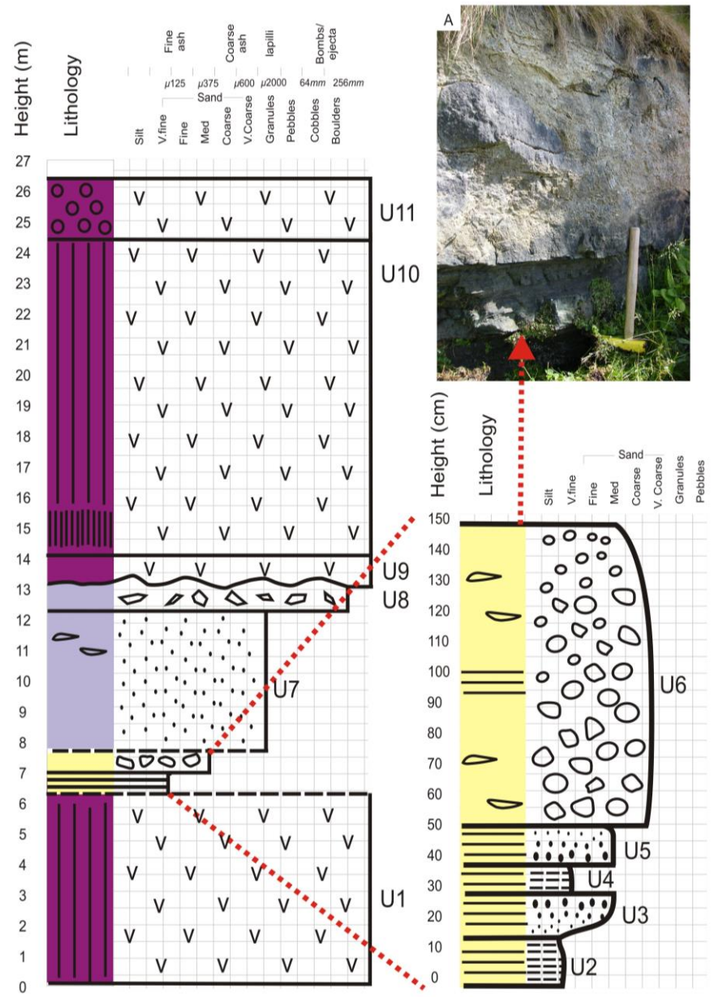

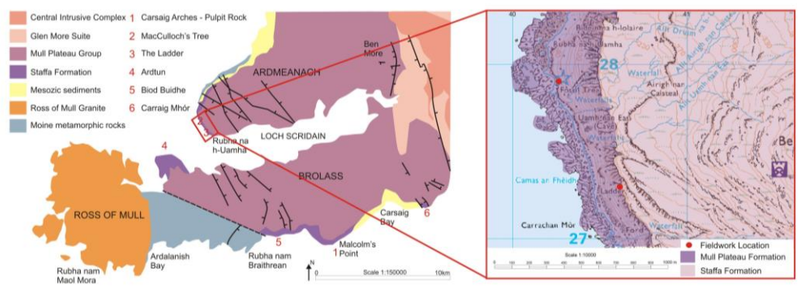

Description	Interpretation
U11: Crystalline basalt lava. Brecciated and vesicular.	U11 interpreted to be crustal region of U10.
U10: Crystalline basalt lava. Columnar jointing tighter and more irregular at base.	
U9: Contact between U8 and U9 irregular; In places straight / defined but in others undulating and graded. Clastogenic lava.	
U8: Dark grey; black volcanic breccia; rubbley texture; vessiculated clasts of basaltic lava (<15 cm); elongate randomly orentated vesicles; red staining around basalt edges; clast supported but with some areas of red/brown clay matrix.	As the proporiton of scoria and spatter increases a clastogenic lava forms
U7: Contact between U6 and U7 not exposed. Dark grey; purple; massive scoria-rich tuff; containing: basaltic socria (mm to 7 cm);weathered/altered highly porophyritic basaltic clasts; scoria preserves primary textures: welding and is flattened; very altered; minor ?clay matrix?; original clast supported porosity is retained; coarser layers present; lens of paler grey; fine grained; granular sediment.	Volcanic regime begins to dominate with primary pyroclastic rocks
U6: Medium- coarse grained; sandy matrix; supported conglomerate; matrix consists of: predominately quartz; flint; rarer feldspar; clasts of flint up to 6cm; rarer clasts of basalt up to 30cm.	Direct volcanic input as sandstones have a volcanic material within them.
U5. Medium - coarse grained; pale yellow; green; sandstone; interbedded with silty layers; Resembles U3 but has normal grading.	
U4: Sharp possibly erosional contact between U3 and U4. Dark purple/grey siltstone; parallel laminations; organic rich layers; coal like; interbedded with silty material; unit thins laterally.	Fluvial sandstones with overbank mudstone deposits.
U3: Medium to coarse grained; pale yellow; grey; sandstone. occasional finer grained; silty; parallel laminations. Clast supported; coarsening upwards; contains flint; quartz; rare feldspar; organic fragments; red ?weathered basalt; fairly well sorted; sub-rounded to sub-angular grains; no sedimentary structures or imbrication.	
U2: Very dark brown/ black mudstone; high organic content; parallel laminations; extremely fissile.	
U1: Columnar-jointed pahoehoe lava flow; vesiculated upper crust; Contact between U1 and U2 is not exposed.	

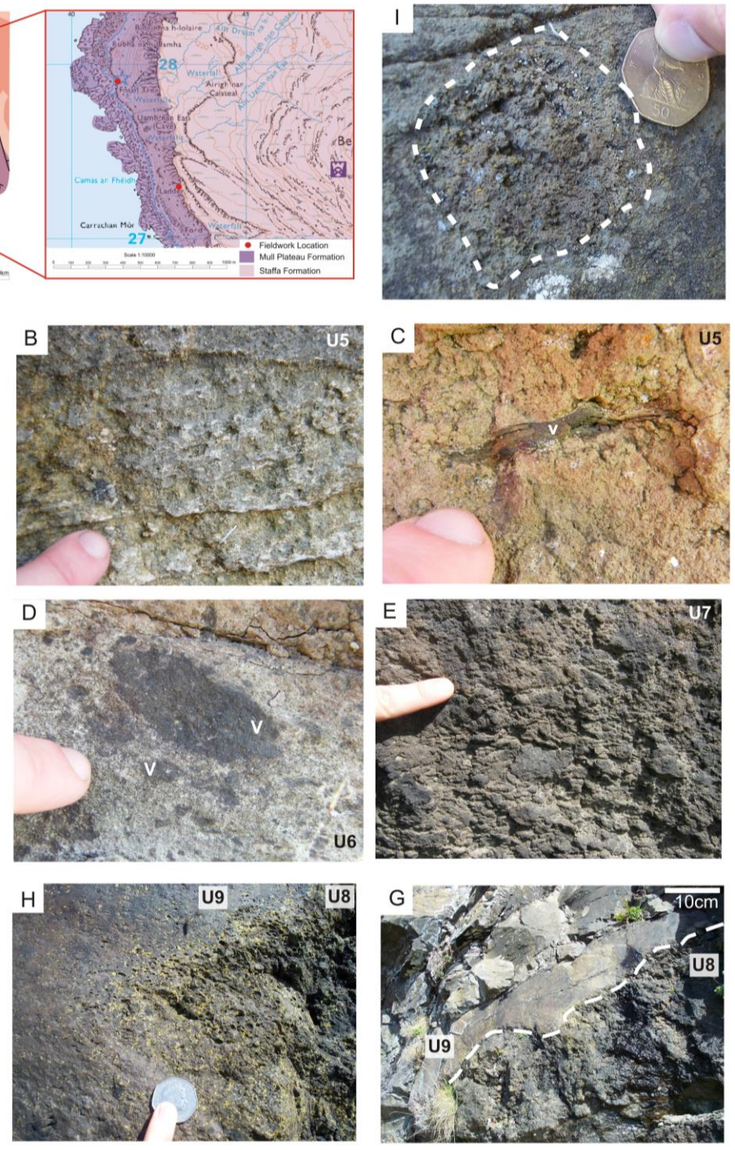

Figure 4.9. Map showing the location of the Ladder section in relation to the MacCulloch's Tree locality and schematic log. A: Photograph of U2–U6 (hammer shaft 30 cm). B: Laminated sublithicarenite (U5). C: Volcanic glass shard within a sublithicarenite. D: Altered, rounded scoria clasts reworked in asublithiarenite. E: Massive scoria rich lapilli tuff. H: Graded contact between U8 and U9. G: Sharp contact between U8 and U9. I: vessiculated clast within U9 clastogenic lava unit. Photographs: B, C, D and E have a finger for scale. Photographs: H and I have a 50 pence coin for scale.

4.5.4 Ardtun

The Ardtun sequence is situated in the south west of Mull and is the location of the famous Ardtun Leaf Beds (Duke of Argyll, 1851; Bailey et al., 1924). It comprises ~ 15 m thick sedimentary unit interbedded between two lava flows. The exposure can be traced along the coast for several metres; however, access is limited to a steep gully which was artificially enhanced by the Duke of Argyll in the 1850s. A series of logs were taken through the Ardtun sequence providing a composite log for the section (Figure 4.10).

At the base of the sequence is a basaltic hawaiite multi-tiered pāhoehoe lava flow (Beckinsale et al., 1978). The colonnade part of the flow is mainly under sea level although in places large mounds of regular spaced columns sweep out of the water. The upper entablature part of the flow is a chaotic mass of smaller-spaced columns; however, locally, these become more regular towards the very top of the flow. Overlying the entablature is a dark black, massive basaltic breccia flow top, with no obvious jointing. Large, 50 cm broken pillow lavas are also present within this unit (Geikie, 1888). The contact between the rLBr and the underlying lava unit is irregular and steep in places.

The rubbly flow top is overlain by a thin (max. 30 cm thick) organic-rich mudstone (M), which is the first of the famous Ardtun Leaf Beds. In places the basal leaf bed is a thin coal horizon (Bailey et al., 1924). The contact between the two units is passive with the mudstone simply mantling the rubbly lava topography with no obvious erosional surfaces. There is no evidence of a bole or soil horizon above the lava. Directly overlying the first leaf bed is a massive volcaniclastic lithic arenite (vlA) (~ 1 m thick). The contact between the mudstone and arenite is sharp. The arenite then fines upwards into another ~10 cm thick mudstone (Leaf Bed 2). Between the second and third mudstones (Leaf Bed 3) there is another package of vlA, this time interbedded with conglomerates (C). This package is thickest (~3 m) towards the centre of the gully and thins on either side (Bailey and Anderson, 1925). The conglomerates form channel shape deposits within the vlA units. The sedimentary sequence grades up into a third mudstone, approximately 20 cm thick, towards the top of the gully. The sedimentary sequence is capped by a regular-spaced columnar jointed lava flow (L) (Beckinsale et al., 1978; Thompson et al,. 1986). The contact again appears to be passive with no evidence of the lava interacting with the mudstone below. A dolerite (D) sill initially

intrudes at the junction between the upper mudstone and the lava flow; however, this sharply ramps up to intrude directly into the flow.

The chaotic brecciated lava flow at the base of the Ardtun outcrop resembles a slump or debris flow type deposit. The large angular blocks and steep undulating, contact with the lava flow below may be erosional and would fit with this interpretation. The fragmented pillow lavas indicate the presence of water and suggest that pillows may have been caught up within the slump deposit. However, Williamson and Bell (2012) however, note the presence of pahoehoe tube-like structures and state that the inclined contact between the brecciated unit and the underlying flow suggests an intrusive-invasive relationship. The pahoehoe tube-like structures may simply be inflated pahoehoe lobes and therefore an invasive relationship may not be required.

The overlying sedimentary sequence is interpreted as a fluvial/lacustrine/ riparian sequence (Gardner, 1887; Bailey et al., 1924; Bailey and Anderson, 1925; Boulter and Kvacek, 1989; Cleal et al., 2001; Jolley et al., 2009) based on palynological data from the fossiliferous mudstone beds. The sequence of channelized conglomerates and arenites are interpreted to be a series of large well established anastomosing braided stream deposits with the fine grained leaf beds representing low energy, terrestrial, flood plain over bank deposits (Williamson and Bell, 2012). The cross-bedding shows a palaeo flow direction to the east / north east with the sedimentary source to the south west. The Assapol Fault was likely to have influenced sediment deposition at Ardtun due to its proximity. A lack of granite–schist–gneiss basement clasts within the Ardtun sequence, however, suggests the fluival system did not traverse the fault (Williamson and Bell, 2012).

Ardtun sediments lack significant volcanic detritus (<10%). Weathered volcanic clasts that are present may be Silurian–Devonian in age and derived from south east Mull and the Scottish Mainland rather than from the underlying Staffa Formation flow(s) (Bailey and Anderson, 1925). Therefore, the river system has passively filled the topography of the hardened lava flow surface. The channelised nature of the sedimentary rocks indicate the river was in its lower course and was therefore, less likely to actively erode down into the lava flow below. Despite being deposited during a thermal maximum when erosion rates were expected to be high (Jolley at al., 1999 estimates the full Ardtun sedimentary sequence may have been deposited within 10 thousand years) no volcanic boles are developed above the Ardtun lavas despite being

evident at other locations. This may be explained by prolonged and focused river currents effectively stopping weathering of the underlying lava flow.

4.5.5 Biod Buidhe

A thin (max. 1.5 m thick) sedimentary sequence can be found at Biod Buidhe (Figure 4.11). At the base of the sequence is a thin (10 cm thick) mudstone (M), which passes vertically upwards into 1 m of medium- to coarse-grained dark grey volcaniclastic lithic arenite (vlA). Overlying this is a basalt lava flow with a blocky peperitic (P) contact.

4.5.6 Carraig Mhór

At Carraig Mhór there is a 250 m wide wave cut platform of mudstones, sandstones and ignimbrite. These are intruded by a dolerite sill which has peperitic margins (Figure 4.12). Overlying the peperitic unit there is a sedimentary sequence (~1 m thick). The sequence consists of a series of sub lithicarenites (slA) and mudstones (M) overlain by a thick volcanic package (Brown and Bell, 2007). The contact between the mudstone and the overlying lava flow is undulating. Overlying this is an extensive peperitic sequence, which is graded with both blocky and fluidal textures (Brown and Bell, 2007).

Location: Ardtun, South Mull. NM 37733 24799

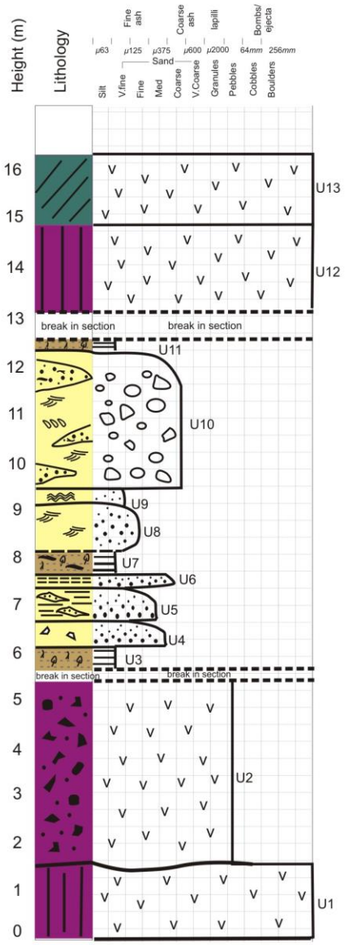

Description	Interpretation
Rock unit 13: Sill intruded into basalt at a slight angle; columnar jointing evident.	
Rock unit 12: Columnar jointed basalt; regular columns.	
Rock unit 11: Thin; fissile mudstone (M); dark grey/black; rich in organic content.	Individual channels with relatively high energy possibly a braided stream? Unusual lack of volcanic detritus. Source not contaminated by basalt.
Rock unit 10: Conglomerate (C) with coarse sandy matrix; clasts of angular to rounded flint (up to 10 cm); rare basaltic well rounded clast (up to 5 cm); clast imbrication; elongate lens typical 1 m long of med- coarse- sandstone; some organic fragments; Figure C,G,H.	
Rock unit 9: Dark brown/green; fine grained volcaniclastic lithic arenite (vlA); clast supported; rounded quartz grains; asymmetrical ripples; Figure E.	Flow direction towards East/North East
Rock unit 8: Brown/green volcaniclastic lithic arenite (vlA); clast supported; rounded quartz grains; relatively mature; rare coarsening upwards; occasional larger clasts present at base; cross bedding; Figure F.	
Rock unit 7: Dark grey/black, fissile mudstone (M) with organic rich layers and abundant woody fragments	Normal grading would indicate pulses of higher energy with periodical waning. Inverse grading indicating a pulse in energy.
Rock unit 6: Dark grey/green; coarse- grained; volcaniclastic lithic arenite (vlA); faint laminations.	
Rock unit 5: Dark grey/green; med- coarse- grained; volcaniclastic lithic arenite (vlA); faint laminations; sporadic angular flint clasts; lens of more resistant (cemented?) sandstone.	
Rock unit 4: Dark grey/green; med- coarse- grained; volcaniclastic lithic arenite (vlA); sporadic angular flint clasts: Figure D.	U3/7/11:Low energy, terrestrial possible flood plain over bank deposit?
Rock unit 3: Dark grey/black; fissile; extremely fine- grained mudstone (M); parallel laminations; woody fragments; Figure D.	
Rock unit 2: chaotic; massive; dark black/grey basaltic breccia flow top (rLBr); rubbly texture; no obvious jointing; clast supported, angular, large clasts ~1 m; pillow lavas.	Pillows indicating presence of water.
Rock unit 1: grey non-amygdalodial crystalline columnar jointed basalt lava flow (L); jointing chaotic at the base of the flow; regular towards the top.	

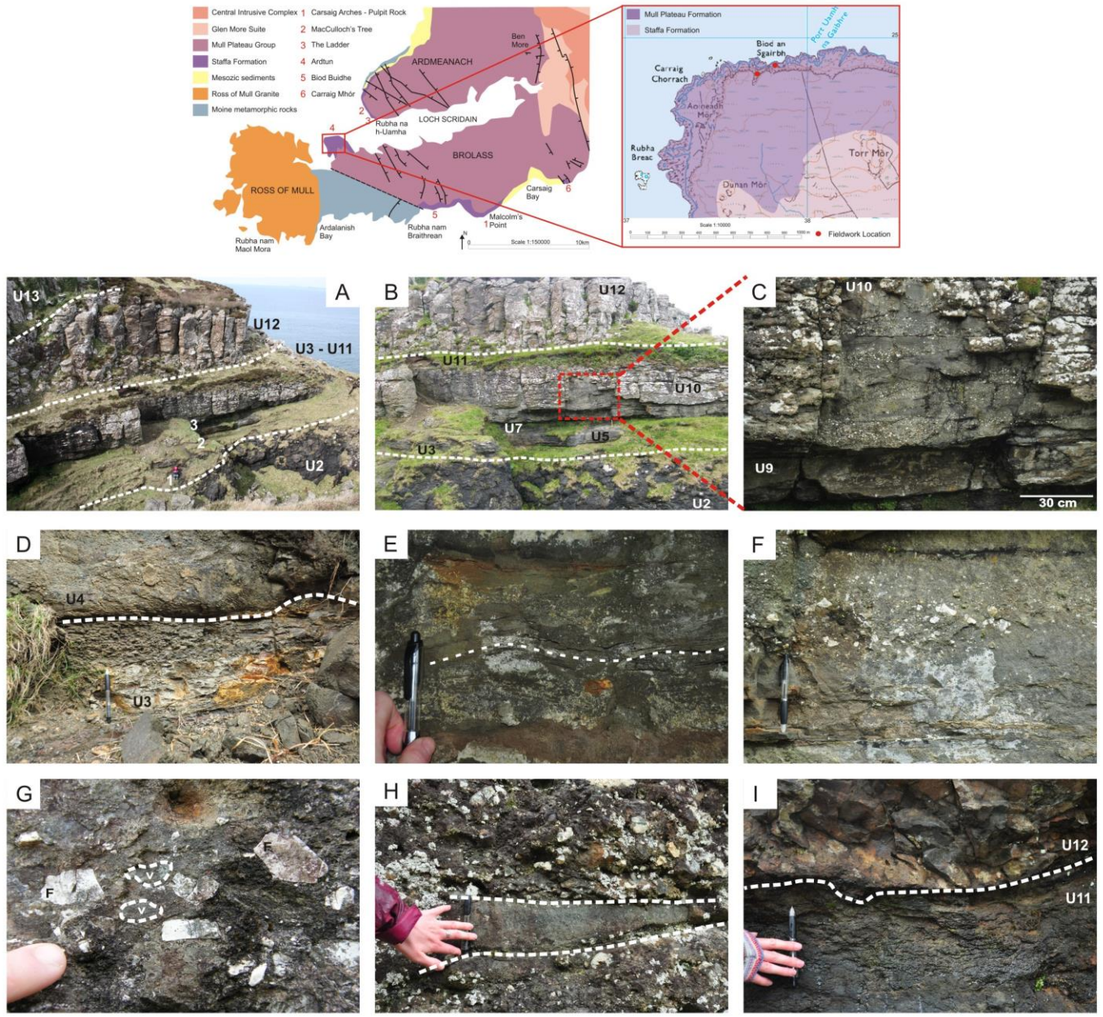

Figure 4.10. Location map and schematic log from the Ardtun locality. A: Ardtun gully, looking east showing the interbedded sediments between the lava units. B: Close up showing the relationship between the sediments and the volcanic lavas. C: Close up of U10 showing crossbedding. D: Contact between the fissile fine grained U3 and the more massive coarser U4. E: Ripples within the U9 sandstone. F: Coarser grained flint scours into the finer grained unit below. G: Angular flint and rounded volcanic clasts. H: Sandstone lens within the coarses conglomerate layers within U10. I: Relatively passive contact between the fine grained (U11) mudstone and the overlying basaltic lava (U12).

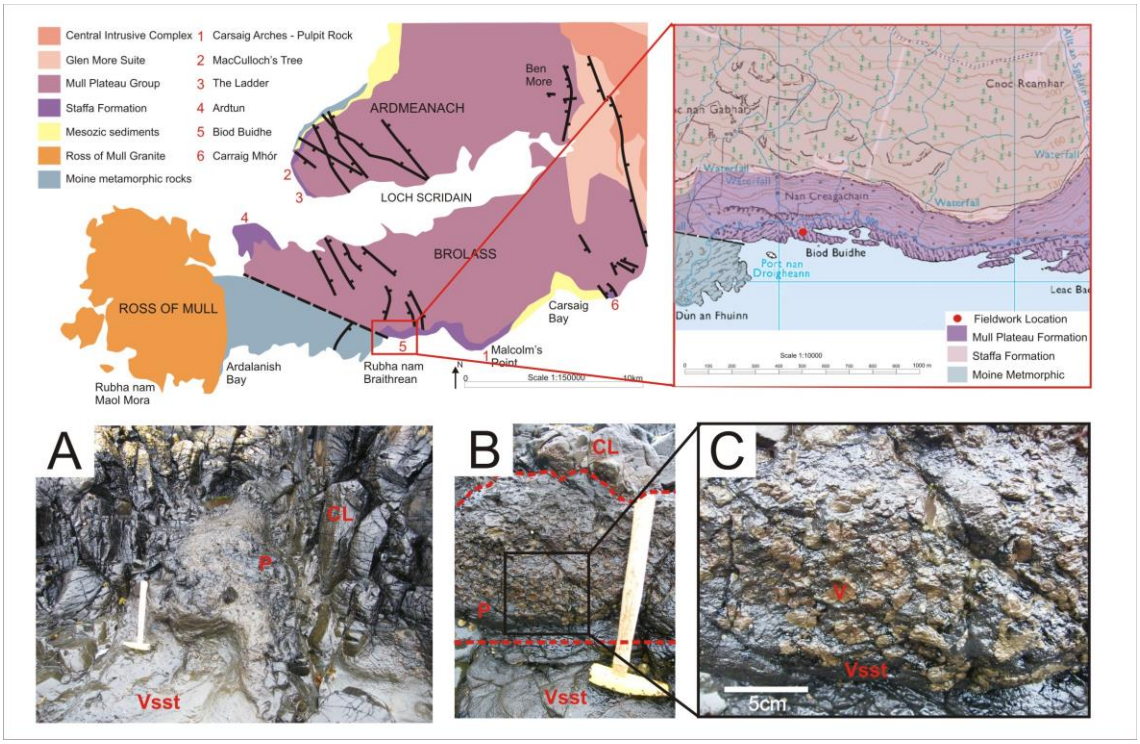

Figure 4.11. Location map showing the Biod Buidhe locality. A: Photograph showing the contacts between the volcaniclastic sediment (vsst) and the overlying lava (CL). At the contact is a peperitic zone (P). Hammer shaft is 30 cm. B: Close up showing the straight nature of the contact between the peperite zone and the underlaying sediment. While a more irregular contact exists between the lava and the peperite. C: Close up of the peperite unit showing the amoeboid morphology of the juvenile lava clasts.

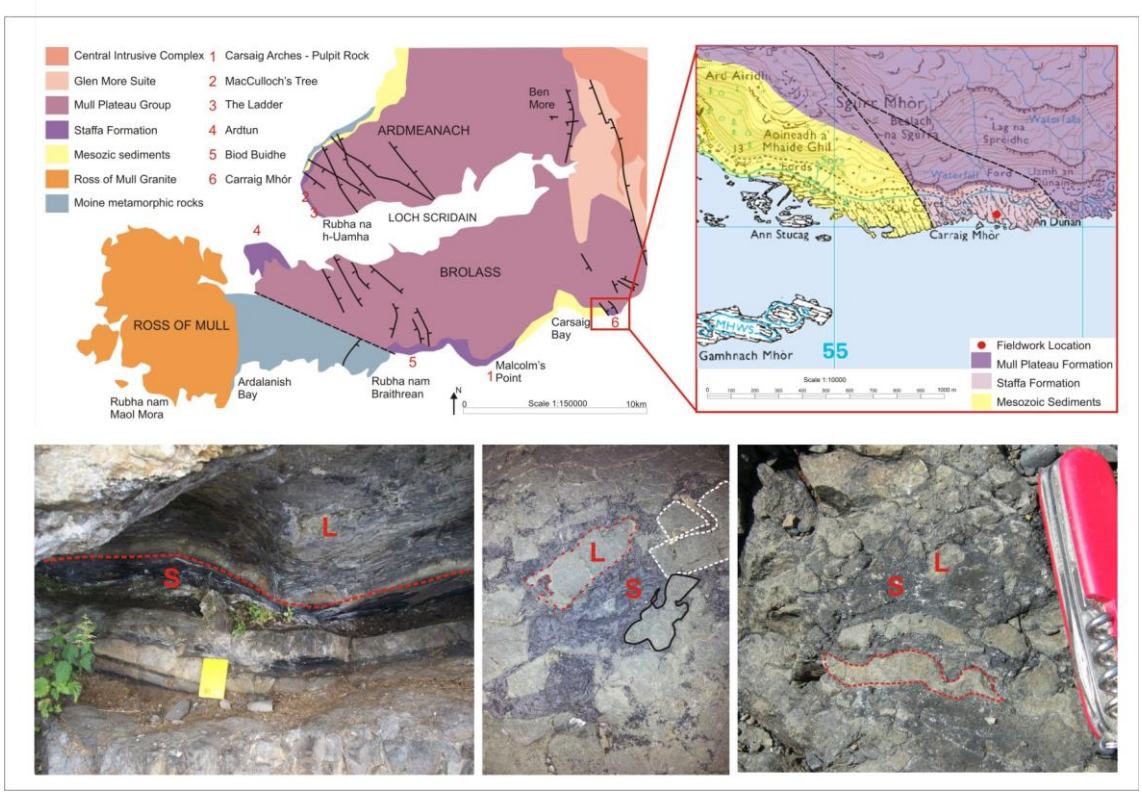

Figure 4.12. Map showing the location of the Carraig Mhór locality. Photograph (left) shows the undulating, loaded contact between the underlaying sediment and the lava flow (note book is 15 cm). Photograph (middle) shows the range in peperite morphologies. L = lava; S= sediment; dashed red = fluival clast with a sub planner margin; dashed white = blocky jig saw fit; black = fluidal-amoeboid. Photograph 20 cm wide. Photograph (right) shows an elongate fluidal juvenile peperitic clast. Pen knife = 10 cm long.

4.6 Model of formation

4.6.1 Carsaig Arches to Pulpit Rock mode of formation

The Carsaig Arches to Pulpit rock exposure allows a transect along strike through a sedimentary and pyroclastic sequence to be recorded. The model shows a vent proximal to vent distal transition. Figure 4.13 shows a model of emplacement for the sedimentary interbeds at the Malcolm's Point to Puplit Rock sequence. The model is split into four distinct zones that are characterised below:

Zone 1

Basalt lava flows were erupted from fissures in an actively subsiding graben and interacted with wet substrates and localised bodies of standing water. Volcanism was predominantly effusive and periodically explosive. Although volcanoes and their vents are not preserved, proximal deposits (<100s m from source) crop out at Malcolm's Point. This zone is characterised by primary pyroclastic rocks, such as thick accumulations of non-welded and welded spatter and scoria and rare clastogenic lavas. The presence of volcanic bombs and spatter rags up to 40 cm in size suggest a proximity of no more than 200 meters from the vent (Richard Brown pers. comm.). Rocks found within this zone are dominated by volcanic detritus and have little to no siliciclastic input.

Zone 2

During periods of volcanic quiescence some of the primary material was locally reworked by the re-establishing fluvial/alluvial system into spatter- and scoria-rich horizons resulting in rocks that although still dominated by volcanic detritus, contain minor siliciclastic grains such as quartz and low abundances of flint.

Zone 3

Within this zone the volcanic and siliciclastic regimes are competing. Reworked primary pyroclasts are mixed with weathered basalt blocks and quartz, feldspar and flint from the newly established fluival/alluvial systems. Tectonic activity and vent wall collapse released large blocks into the system and cause localised debris flow deposits.

Zone 4

At distal locations (~1 km) the siliciclastic regime begins to dominate as the fluvial system re-establishes over the volcanic terrain. Fluvial channel deposits dominated by quartz and flint with little to no volcanic component indicate a switch in provenance. The volcanic clasts are locally altered to clay, but are relatively fresh compared to the proximal equivalent, and overall poroperm is retained. The proportion of scoria begins to decrease and is replaced by clasts of aphyric and amygdaloidal basalt (< 1 m in diameter) from weathered lava flows.

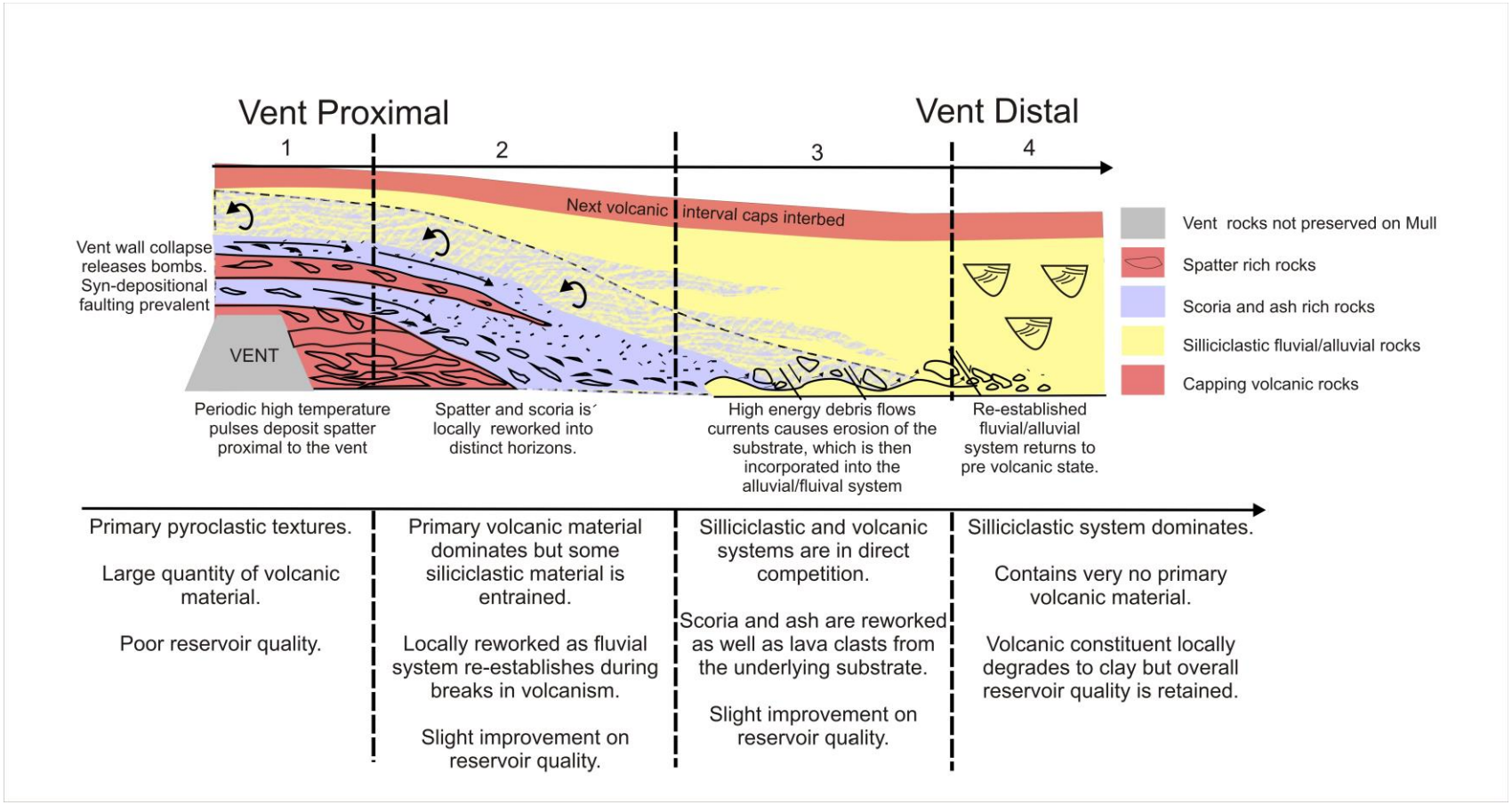

Figure 4.13. Model of deposition for the Carsaig Arches to Pulpit Rock section. Zone 1 (Carsaig Arches) is characterised by vent proximal deposits with primary pyroclastic textures. In zone 2 the proximal deposits are reworked. Volcanic rocks still dominate. Zone 3 represents competing systems between the reworked volcanic rocks and the re-establishing siliciclastic system. Zone 4 (Pulpit Rock) marks the transition to a system dominated by silicilastics and background pre volcanic processes. Distance between zone 1 and zone 4 is ~1 km.

4.6.2 MacCulloch's Tree model of formation

Model – Vent Proximal

The exposures at MacCulloch's Tree preserve a sedimentary and pyroclastic sequence typically comprised of vent proximal rocks, similar to that of the Zone 1 deposits found at Carsaig Arches. The spatter lithofacies found at the MacCulloch's Tree deposit is synonymous with the Fingal's Cave Flow on Staffa (Williamson and Bell, 2012). Figure 4.15 shows all three locations lie along a NW-SE trend, similar to the regional Paleogene dyke swarm trends (Emeleus and Gyopari, 1992). The rocks are produced by periodic pulses of explosive Hawaiian style volcanic activity along a fissure-fed system with localised vents and is concurrent with the Williamson and Bell (2012) interpretation that the lavas are dyke-fed. However, according to the genetic sequences outlined in Williamson and Bell, 2012, the Malcolm's Point rocks are defined as GS2 while the MacCulloch's Tree and Staffa rocks are GS5. If this correlation is correct, these rocks are not temporally related.

Periods of quiescence in the volcanic activity allowed for localised reworking and for lenses of more siliciclastic material to be included. Organic rich mudstones are commonly found directly underlying lavas throughout the Staffa Formation. These represent the last remnants of a siliciclastic sedimentary system before the volcanic rocks again begin to dominate. The low energy deposits indicate a waning of the siliciclastic system as it is diverted by the emerging volcanic topography. The MacCulloch's Tree Flow and the underlying organic-rich layer contains well established palynoflora indicating vegetation had time to establish after the initial volcanic activity. Large lake-like bodies of water, were created in part due to damning of the existing fluvial system by the evolving volcanic topography.

4.6.3 The Ladder model of formation

Model – Vertical transect through a sedimentary and pyroclastic sequence between lavas.

The transition from basalt lava flow into relatively basalt-poor sediment indicates that a fluvial system developed across the surface of the lava flow during a period of volcanic

quiescence, and that the river was transporting and depositing sediment from a non-volcanic source. The inclusion of reworked scoria in the upper beds within the fluvial unit suggests the partial re-establishment of the volcanic source or onset of another phase of volcanism. As the volcanic activity increased it began to overhaul and dominate the fluvial system. Lava dams may have blocked rivers further up stream or the evolving new volcanic topography caused the fluvial system to divert, as described in the Faeroe-Shetland Basin (Schofield and Jolley 2013) at St. Cyrus, North East Scotland (Hole et al., 2013) and Owyhee River, Oregon (Ely et al., 2012).

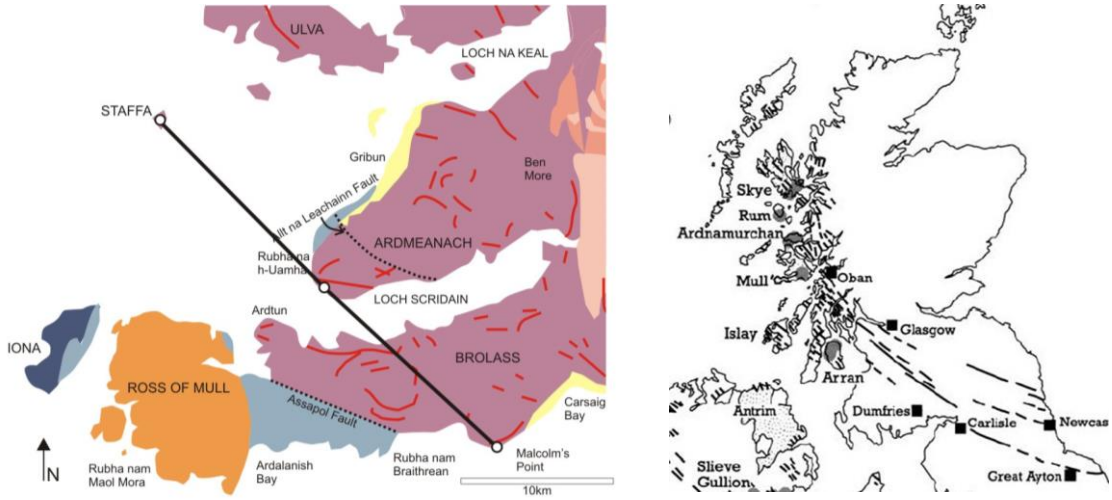

Figure 4.14. Vent proximal deposits are found at three locations; Staffa, MacCulloch's Tree and Carsaig Arches. All of these locations line up indicating that they may have been periodically erupted from a fissure system. The north west – south east direction of the potential fissure lines up with regional Paleogene dyke swarm as seen in the map on the right (Emeleus and Gyopari, 1992). Note locations are limited by exposure.

4.6.4 Ardtun model of formation

Model – Sedimentary interbed at distance from volcanic source.

The Ardtun sedimentary sequence was deposited during a thermal maximum (Jolley et al., 2009) when weathering rates were thought to be high, and the full Ardtun sequence could have been deposited within a few thousand years (Bell, pers comm.). It is envisioned that during a period of quiescence in volcanic activity the sedimentary system re-established over the volcanic terrain. Palynoflora indicate the presence of early stage colonizing vegetation, rather than the mature forests as seen at MacCulloch's

Tree (Jolley et al., 2009). Hence the sedimentary system was still in early stages of development when the next pulse of volcanic activity flowed over the area, supporting the potentially geologically rapid deposition of the sedimentary rocks.

The Ardtun outcrop therefore, allows sampling of sedimentary interbed rocks at a distance from volcanic source. For the purpose of this thesis they are defined as being sedimentary rocks deposited within a volcanic terrain but not near the volcanic source and therefore have been brought in from outside the volcanic catchment area. They by definition contain little to no volcanic component derived from the surrounding volcanic rocks.

4.6.5 Flint Provenance

The origin of the flint within the Staffa Formation remains open to debate. There are currently no exposures of flint on Mull. As described earlier, two populations of flint are present (see Section 4.4.15). Larger flint clasts are fractured, with two sets of fractures evident. The first set is randomly orientated across clasts and are often filled by calcite, which does not extend into the matrix of the rock. Therefore, this set of fractures is thought to pre-date deposition in the Staffa Formation. Moldic porosity from the dissolution of fossil remains within the clasts has also partly been filled by calcite. The second set of fractures are found at grain edges, indicating the rocks have experienced some compaction. The flint-dominated conglomerate at Pulpit Rock best illustrates the flint enigma. The conglomerate was deposited within a volcanic terrain, directly overlying a volcanic derived breccia but lacks *any* inclusion of volcanic material. The monolithic nature of the conglomerate implies that it is derived from a source area solely of flint. Bell and Williamson (2012) suggest that the flint is derived from Cretaceous strata that have been locally uplifted in a fault scrap and then eroded. However, the sheer volume of flint included in the conglomerate and in other Staffa Formation exposures suggest that the source area must have been relatively extensive. Martin Lee, (per comm.) suggested that there may be two populations of flint within the samples. Lee suggested that the non-fossiliferous variety may be Jurassic in origin due to the lack of significant fossils within it. This would suggest several cycles of flint may have been incorporated into the deposit.

4.7 Comparison of Rosebank and Staffa lithofacies

The Staffa Formation acts as a comparable analogue to the Rosebank Field (see Section 2.1). Although differences with basin architecture exist, both localities consist of interbedded sedimentary and volcanic rocks.

4.7.1 Volcanic lithofacies

Both the Rosebank and Staffa Formation flows. have vesiculated crusts and more crystalline cores. Limitations of the Rosebank core mean it is difficult to ascertain if Rosebank lava flows have the characteristic colonnade and entablature displayed in the Staffa Formation lava flows. Amygdales in both localities are very similar with a wide range of complex fills, including calcite and clays. Peperitic lithofacies are found in both localities with similar fluidal and blocky textures. In both cases the peperite mixes with fine grained mudstone and locally sedimentary structures are disturbed.

The most obvious difference is the lack of primary pyroclasts within the Rosebank sequence. No evidence for primary spatter or scoria clasts are found in the Rosebank core leading to the conclusion that the wells are not located within 200 m of a vent. However, the chance of reworked scoria and ash being within some of the non-cored volcaniclastic units within Rosebank cannot be eliminated.

4.7.2 Sedimentary lithofacies

The rocks at Ardtun provide the best analogue within the Staffa Formation for the Rosebank siliciclastic lithofacies. Differences in the mineralogy and cementation of the lithofaces are noted. The most obvious of these being the lack of flint and calcite cements within the Rosebank lithologies.

The depositional setting of the rocks is similar however. In both cases the rocks are devoid of a significant volcanic component despite being within a volcanic terrain. The fluvial and deltaic systems have passively established on top of lava flows without eroding and entraining material from the underlying lava and sediments are sourced from outside the volcanic catchment area. This process is not limited to the BPIP. Sediment devoid of volcanic material is found within the Columbia River Basalt Provenance in Washington State, USA (Brown, 2012). This river system traversed

hundreds of kilometres into the volcanic terrain without the inclusion of volcanic material. The drainage network includes both localised wasting of volcanic rocks and clean siliciclastic sediment brought into the volcanic terrain.

Very fine grained organic rich mudstones are found in both the Rosebank and Staffa Formation rocks at the base of lava flows. Volcanic activity has the potential to alter significantly the drainage basin (Hole et al., 2013). At a critical point the volcanism in the basin will overpower the pre-existing fluvial system. Unlike siliciclastic systems, lavas have the potential to form positive topography (Passey and Varming, 2010) and therefore could cause a deflection or damming of the river course leading to a sudden cessation in silicilastic input (Stollhofen and Stanistreet, 1994; Ely et al., 2012). This would explain the fining upwards sequences and change from the fluvial and alluvial lithofacies to lower energy lacustrine deposits in both on and offshore settings.

4.8 Igneous – sedimentary contacts

Another important aspect of this research is the influence of the igneous material on the sediment directly at the contact. A number of igneous / sediment contact relationships can be seen within the Staffa Formation. These contacts have been categorised into seven styles as seen in Figure 4.14. These are then linked to the contact relationships seen in the Rosebank cores.

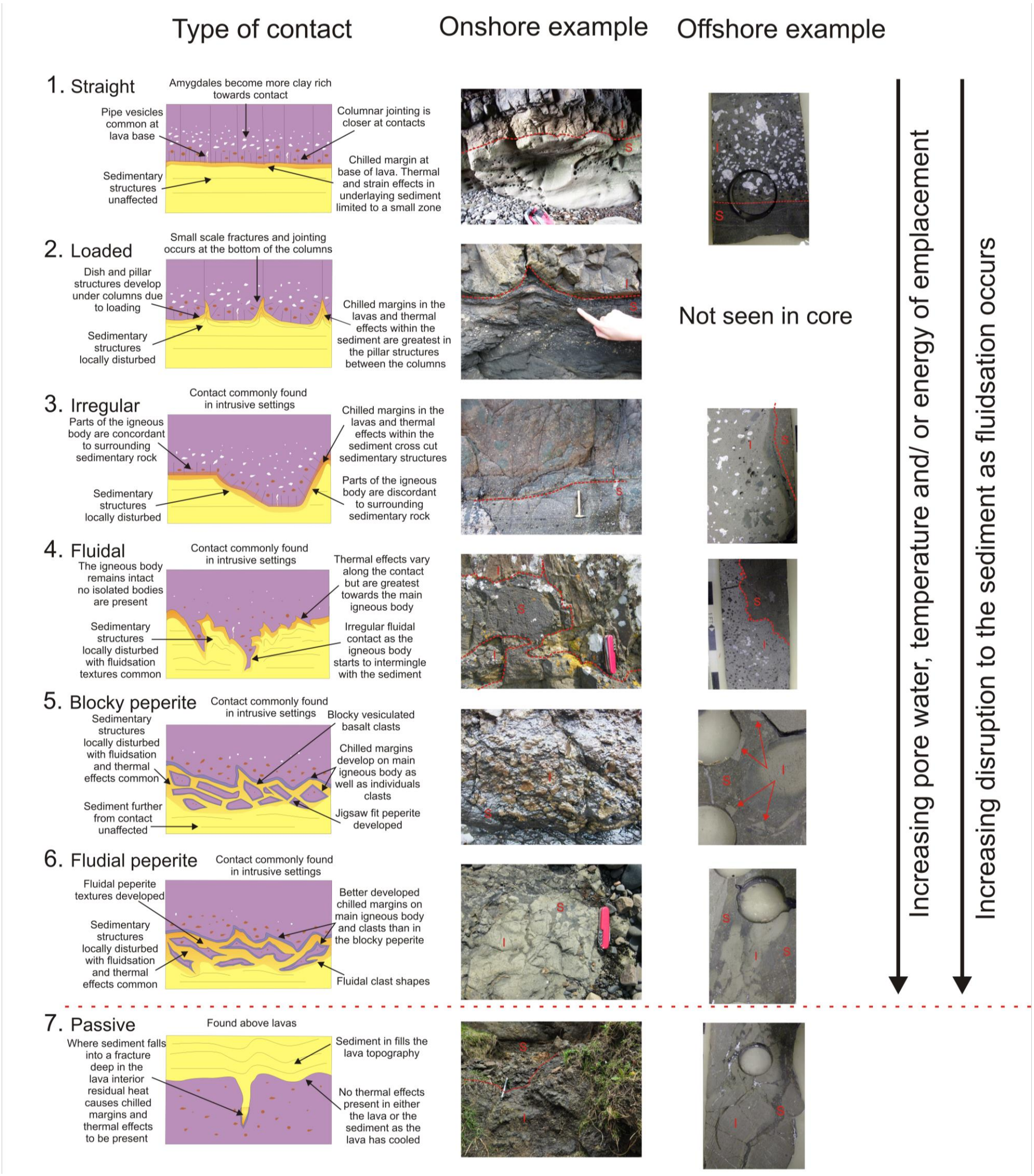

Figure 4.15. Igneous- sediment contacts. Type 1: Straight contacts. Mull – Carsaig Arches, (Rucksack 50 cm). Rosebank- 213/26-1, 2880.2 m. Type 2: Loaded contacts. Mull – MacCulloch's Tree. Type 3: Irregular contact. Mull – Malcolm's Point (hammer shaft 30 cm). Rosebank- 213/27-2, 2875 m. Type 4: Fluidal contact. Mull- Carsaig Arches (pen knife 15 cm). Rosebank- 213/26-1 2881 m. Type 5: Blocky peperitic contact. Mull- Biod Buidhe (photo width 1 m). Rosebank (blocky clasts are arrowed) 213/27-2, 2877 m. Type 6: Fluidal peperitc contact. Mull – Carraig Mhór. Rosebank- 213/27-2, 2877.2 m. Type 7: Passive contact. Mull- Ardtun (pen for scale). Rosebank- 213/27-2 2877.3 m. In all photographs I- igneous, S- sediment. Rosebank core photographs 1,3,4 and 7 are 30 cm wide. Rosebank photographs 5 and 6 are 20 cm across.

4.8.1 Straight contacts

The contact is defined as being a sharp transition from igneous body to sediment with no mingling textures developed. Contacts are generally concordant to bedding, but can occasionally have interconnecting lobes or fingers, which display an irregular contact relationship with the surrounding sediment (see below). Chilled margins are prevalent on both intrusive and extrusive examples. The maximum chilled margin found within this study was at the Carsaig Arches. Here the chilled margin was ~6 cm thick, associated with a 3 m thick intrusion. The size of the chilled margin depends on the thermal history of the magma (Huppert and Sparks, 1989). Indurated margins have been found surrounding intrusive rocks and at the base of lava flows in a number of other localities including Namibia (Jerram and Stollhofen, 2002; Grove, 2014,) and on the Faroe Islands (Simon Passey, pers. comm.). No evidence of significant indurated zones were found within the Staffa Formation rocks. This will be discussed more in following chapters.

Mainly found in intrusive settings on Mull but also at the base of pāhoehoe lava flows in the Rosebank core. Columnar jointing is often developed with closer spaced joints towards the contacts. Vesicles are common within the extrusive examples, with pipe vesicles and veins acting as later stage fluid pathways between the lava and the underlying sediment. In places, mm scale fractures are present perpendicular to the contact. Within the Staffa Formation the majority of these fractures and columnar joints remain open. Minor clay, calcite and zeolite fill some fractures but possible fluid pathways remain. However, fractures at depth may behave differently to outcrops examples (Walker et al., 2012). All fractures found within the Rosebank core are filled, however a full Formation Micro-Imager Log (FMI) investigation in the future may aid understanding by allowing fractures to be mapped.

A range of sedimentary rocks are found beneath straight igneous-sedimentary contacts within the Staffa Formation. There appears to be no correlation between sediment type and the straight contacts developed. In extrusive settings the base of the lava is broadly concordant with sedimentary beds beneath. The underlying sedimentary beds have actively controlled the geometry of the lava base, while sedimentary structures remain unaffected. The lack of mingling textures implies that the sediment was fully to partially consolidated before lava ingress.

4.8.2 Loaded contacts

Loaded contacts form dish and pillar structures as the weight of the lava flows over the partially consolidated sediment. This type of contact is found at a range of scales from 2 – 5 cm thick at MacCulloch's Tree to ~30 cm at Carraig Mhór. The transition from the sediment to the igneous body is sharp and well defined with no mingling. Chilled margins are common within the lava and are best developed adjacent to the pillar structures. Here the sediment shows signs of discoloration, perhaps providing evidence of minor thermal alteration. No induration or thermal effects are seen below the thin coal and organic-rich mudstone layers. No loaded contacts are seen within the Rosebank core.

Loaded contacts are commonly found at the base of columnar jointed lava flows but also occur under pillow facies within the Staffa Formation. The columnar jointing is well developed; however, unlike in straight contact examples there is no change in scale of the joints at the contact. Small internal jointing and fractures occur within each of the columns. Pipe vesicles are common at contacts similar to those seen in straight contact types.

Loading contacts are commonly associated with very fine- to fine- grained mudstones and coal horizons. Sedimentary structures are locally disturbed around the edges of the basalt columns however no fluidisation or mingling occurs. It is likely that the sediment was partially consolidated in order to accommodate the loading.

4.8.3 Irregular contacts

Irregular contacts have complex geometries. They can be concordant but also cross cut bedding at sharp sub-vertical angles. An example of this is seen at the Carsaig Arches where a dolerite sill runs concordantly to bedding in the underlying volcaniclastic sediment before cross cutting bedding at a sharp angle of approximately 35°. The transition from the sediment to the igneous body is sharp and well defined with no mingling. However, margins are irregular, sub-planar and curvilinear. Chilled margins similar to those seen in straight contacts are prevalent. Near the contact vesicles and fractures are often filled by a mixture of sediment and igneous micro-clasts, due to mechanical stress induced auto-brecciation (c.f. Skilling et al., 2002) as the igneous

body is emplaced. Similar textures are present within the Rosebank cores alluding to the presence of shallowly invasive flows or magma lobes at the base or edge of the main flow body.

Irregular contacts within the Staffa Formation most commonly form within intrusive settings; however, they can occur as invasive fingers or lobes of lava at the base or edge of a lava flow. Columnar jointing is much less well developed or absent; however, vesicles are common. Fracturing is present but is not confined to being perpendicular to the contact.

As with straight contact settings irregular contacts develop with a wide range of sedimentary units. There does not appear to be any correlation between sediment type or grain size and this contact type. Where the igneous body is concordant sedimentary structures are unaffected. Where the irregular contacts cross cut bedding sedimentary structures are locally truncated or disturbed. No evidence of fluidisation, induration or sediment mingling is seen within the sediment. It is likely that the sediment is fully to partially consolidated.

4.8.4 Fluidal contacts

Fluidal contact types have highly irregular geometries. Lobes of interconnected magma can isolate and trap large bodies of sediment. Rafts of sediment and broken bridges are present where sediment has been caught up between igneous flow lobes as they coalesce. The irregular nature of the contact may be a small-scale version of the magma finger propagation method (Schofield et al., 2010). Chilled margins on these lobes are prevalent. Sediment must be partially unconsolidated as fluidisation occurs (Kokelaar, 1982). Fine-grained fragments of igneous material within the sediment may be explained by pore-water steam explosions and localised magma-sediment density contrasts (c.f. Skilling et al., 2002). Both processes combined with the fluidal morphology of the contact would suggest the emplacement deformed the contact in a ductile fashion. Fluidal contacts often grade into peperite style contacts.

Fluidal contacts only occur within intrusive settings in the Staffa Formation; however, Skilling et al. (2002) and Hole et al. (2013) suggest similar textures can develop on invasive lava flows. In the Staffa Formation, igneous bodies with fluidal contacts normally lack columnar jointing and fractures associated with the contact zone. All fluidal contacts within the Rosebank core are vesiculated as are the majority of

Staffa Formation examples; however, rare non-vesiculated areas are also found. Vesicles towards the contact are commonly filled by sediment and in places by small fragments of igneous material.

Fluidal contacts are most commonly associated with fine grained sediment but can also occur with the volcaniclastic sandstones in the Staffa Formation. Sedimentary structures are locally disturbed with evidence of sediment fluidisation; however, no sediment mingling occurs.

4.8.5 Peperitic contacts

Peperites are well documented in the literature and occur in a variety of sediment-igneous interfaces. They are classed as hot contacts and result in mixing of juvenile lava clasts and surrounding sediment. They typically develop in wet sediment; however, a number of authors report the presence of peperite in dry aeolian settings (Jerram and Stollhofen, 2002; Petry et al., 2007; Waichel et al., 2008). Therefore, peperite is used as a general term to mean any sediment-igneous body interaction in which mingling occurs (White et al., 2000). An extensive review in which peperites were subdivided into a number of distinct groups, was undertaken by Skilling et al. (2002). Four styles of peperite are identified within this study: 1) blocky; 2) irregular angular; 3) amoeboid; and 4) fluidal elongate (c.f. Busby-Spera and White, 1987; Skilling et al., 2002).

Peperite is found surrounding both intrusions and invasive lava flows in the Staffa Formation and the Rosebank core. The majority of the peperite within the Staffa Formation is non-vesiculated; however, vesiculated basaltic clasts are present within the peperitic facies in the 213/27-2 Rosebank well. Peperitic texture may be partly dependant on the volatile content of the parent magma (Skilling et al., 2002) with several authors reporting the presence of highly vesiculated juvenile clasts (Rawlings, 1993; Doyle 2000). Peperitic textures can also develop at the base of fractures within a lava flow crust.

The peperite lithofacies found within the Staffa Formation and the Rosebank core occur exclusively in fine-grained mudstones. Sedimentary structures are disrupted, with extensive fluidisation suggesting the sediment was unconsolidated and wet at the time of mixing.

Four types of sediment-lava mingling occur within this study:

Type 1: Juvenile clasts have a blocky, jig-saw fit morphology. Clasts are angular and irregular with sharp and well defined edges. Clasts within type 1 peperite, found at Carraig Mhor, have well developed chilled margins. Heavily altered clasts have a distinct yellow green discolouration due to alteration.

Type 2: Juvenile clasts are irregular and angular but lack jig-saw fit morphology and lack extensively developed chilled margins. This type of peperite is found within the 213/27-2 well in Rosebank as well as at Boid Budhe on Mull.

Type 3: Juvenile clasts have an amoeboid morphology and lack extensively developed chilled margins. Juvenile clasts range from 2–8 cm across. On Mull, this peperite type is best developed at Biod Buidhe.

Type 4: Juvenile clasts have an elongate fluidal morphology. Clasts have complex edges with evidence of fluid-fluid shearing. They are often elongate and are connected by small thin necks. They are also often deformed around ridge framework grains within the sediment (Skilling et al., 2002). Fluidal clasts are found in both Rosebank cores and in the Staffa Formation.

The type of peperite developed depends on a number of factors including magma temperature, flow rate, sediment grain size and fluid composition. Busby-Spera and White (1987) and Skilling et al. (2002) state that fluidal peperite types exist when magma is intruded into fine grained wet sediment where full mixing can occur. It is common in a basaltic regime for stable vapour films to surround clasts and act as a barrier to pore fluid allowing complex mixing to occur (Skilling et al., 2002). Magma-sediment density contrasts can also lead to mixing (Donaire et al., 2002).

Blocky, jigsaw fit style peperite occurs at lower temperatures where the magma behaves in a less ductile fashion but can also result from a higher sediment water content, where phreatomagmatic reactions can occur producing sharp angular clasts (Skilling et al., 2002).

At Carraig Mohr, blocky, amoeboid and elongate fluidal peperite types occur in close proximity (within 1 m), despite no obvious change in sediment or magma type.

The change in peperite type is thought to relate to the water content of the sediment. The underlying sediment can also affect the type of peperite produced. Surface depressions that collect more water resulted in thicker peperites with a higher degree of mingling (c.f. Waichel et al., 2007).

4.8.6 Passive cold contacts

Passive contacts are defined as cold contacts found at the top of a lava flow. Once the lava flow has cooled the sedimentary system can re-establish over the lava surface. This can be after a period of time in which the top surface of the lava is weathered and eroded, or can be relatively quickly where the sediment mantles the top surface of the lava flow. In both cases the sediment passively fills depressions in the surface of the underlying flow. This can be seen at Ardtun where the sediment is seen to mantle the underlying flow. Sediment filled fractures are also observed in the Rosebank core. As the pahoehoe lava develops sediment could be incorporated into the crust, filling fractures and vesicles. If the sediment entered the fracture shortly after the lava was emplaced then the centre of the flow may retain heat. Therefore, thermal effects such as chilled margins and fluidal peperite textures could develop at the base of the fracture (Figure 4.15). As the flow progresses autobrecciation could cause already cooled, angular clasts of lava to be incorporated into the fracture.

Sediment can also be incorporated into the base of the flow as it moves over the substrate, leading to isolated bodies of sediment, which have undergone brittle deformation, caught up within the flow crust (Figure 4.16). Other examples of sediment filling fractures within lava can be seen in Brazil (Waichel et al., 2007; Holz et al., 2008), in St Cyrus, Scotland (Hole et al., 2013) in the Faroes (pers comm. Simon Passy) and inflation clefts as described by Walker (1991) and Self et al., (1998).

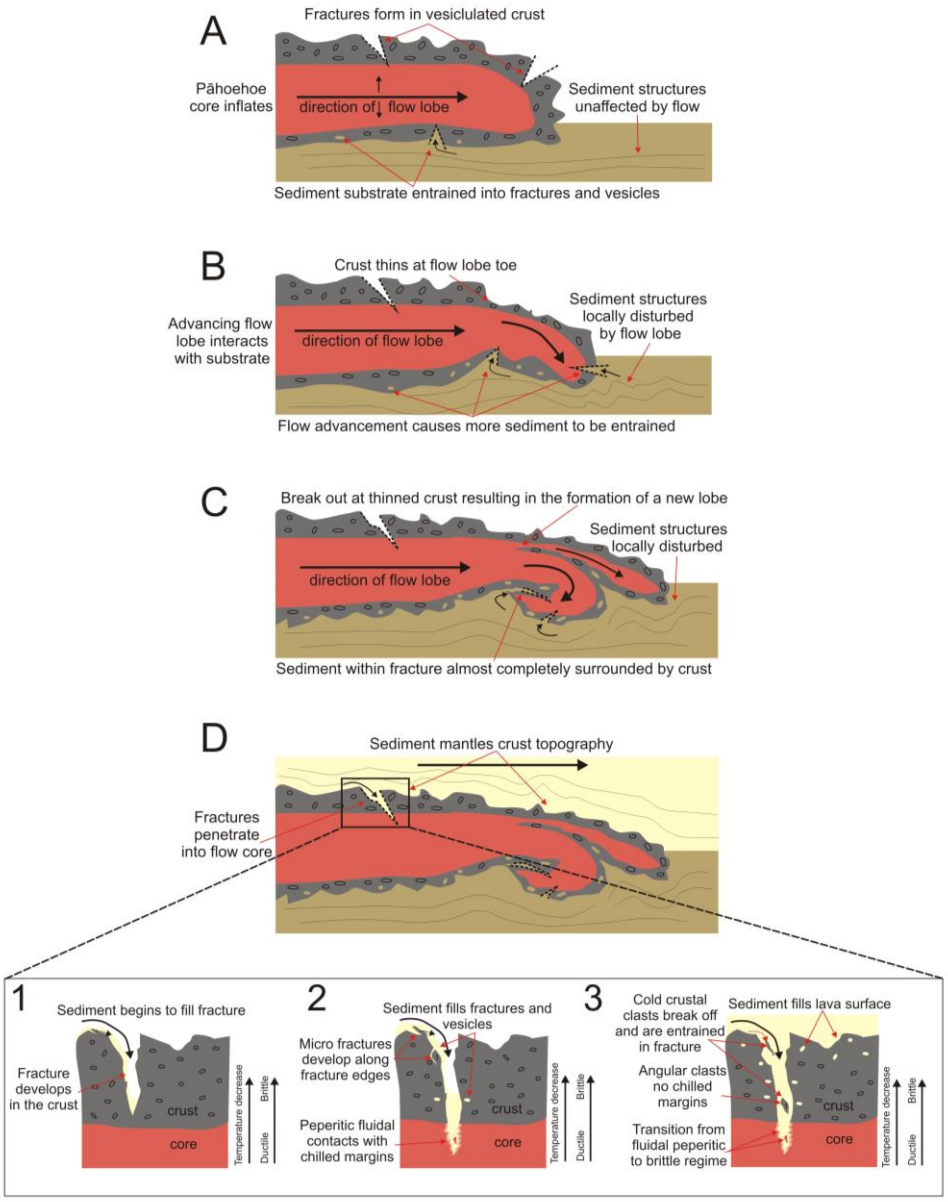

Figure 4.16. Lava-sediment contacts. A: As the lava advances over the substrate fractures form in the lava crust. B: The toe of the lava lobe starts to advance. This causes a thinning of the lava core and causes fractures in the crust to be extenuated. Sediment becomes entrained within the vesicles and fractures at the contact. C: Another lava lobe breaks out where the previous crust had being thinned. This process causes more sediment to be entrained and completely surrounded by lava. D: Sediment passively infills the surface of the cooled lava flow. Sediment falls down inflation clefs (Self et al., 1998) in the lava crust. The core however may retain heat for longer, causing a fluidal peperitic effect at the base of the fracture. Previously cooled crust can also be eroded and entrained into the fracture resulting in a mixture of both fluidal and blocky clasts.

4.8.7 Factors controlling the type of contact produced

The type of sediment-lava contact produced depends on a number of factors.

The nature of the igneous body

Intrusive bodies and invasive lava flows will differ from subaerial lava flows. The nature of the contact is highly dependent on how the igneous body interacts with the surface. In this study intrusive and invasive contacts (such as the fluidal contacts at the Carsaig Arches, see Section 4.8.4) were more disruptive to surrounding sediment than lava flows which flowed passively over the substrate.

The type of lava

This will have an effect on the nature of the contact. The surface of a ropey pāhoehoe lava is very different from that of an aa flow and so will interact with the sediment differently. Brecciated lava flow bases typically form more irregular contacts than that of a columnar jointed flow. The physical form the lava flow takes is often highly associated with the environment which it is traversing, and this will also affect the nature of the contact produced. For example, pillow lavas form in water and are rounded, tending to spall off into soft water laden sediment (Yamagishi, 1985) and so will form a completely different contact type to that of a thick pāhoehoe inflated flow that has traversed dry desert sands.

The angle of the contact

Lava flows can form peperite textures in dry environments highlighting that the energy and angle of intrusion are equally important in contact formation as the water content of the sediment (Jerram and Stollhofen, 2002). If a lava flows down a steep sided dune surface or fault scarp it will gain energy allowing it to effectively plough into surrounding sediment (Petry et al., 2007). Sediment deformation and peperitic contacts are therefore, more likely to develop in a setting with large slope angles than if the lava were to creep passively along a relatively flat river bed.

The temperature of the igneous body

Localised melting of surrounding sedimentary rocks and the development of a limited metamorphic aureole are seen at intrusion edges. Their formation depends on a number of inherent factors, including the temperature and duration of the igneous body (Mckinley et al., 2001). The temperature of the igneous body can also influence whether the contact is likely to behave in a ductile or brittle fashion (Skilling et al., 2002). At Carraig Mhór and in the 213/27-2 Rosebank core, the nature of the igneous contact changes significantly from brittle to ductile style morphologies within a few centimetres.

The location of the contact relative to the igneous body

Different effects are seen at the top and basal contacts of a lava flow. This is also applicable in intrusive bodies. For example, heat and fluids associated with saucer shaped sills will focus on sill tips as the body propagates (Schofield et al., 2010). Therefore, fluidisation of sediment is more likely to occur towards the leading edges of sills than directly above or below. Hydrothermal systems are also more likely to develop at sill tips (Schofield et al., 2010). Evidence for this is seen in seismic sections where areas of seismic disturbance can often be correlated around the edges of sill.

Sediment consolidation

Different effects are seen depending on whether the igneous body interacts with soft unconsolidated sediment or is intruded into hard sedimentary rock. If the sediment is unconsolidated peperitic textures are more likely to develop (Skilling et al., 2002). Where sediment is partially consolidated loading can occur. This is seen onshore at MacCulloch's Tree where the contact changes from a straight contact to a loaded contact within 5 meters.

Sediment regime

The type of sedimentary regime that develops over a volcanic terrain will influence the type of contact produced. Large energy, upper flow, fluidal systems would be more likely to be erosive and entrain underlying volcanic material than a meandering or braided, lower flow system that may passively fill underlying topography.

Water content of the sediment

A number of authors have linked sediment-water content to the type of igneous contact produced (Skilling et al., 2002; Wacichel et al., 2007; Hole at al., 2013). Higher sediment water contents are linked to more intense mingling due to the formation of vapour films around igneous clasts (Skilling et al., 2002; Waichel et al., 2007).

Original sediment type

Within this study all of the contacts involving sediment mingling occurred in fine grained relatively well sorted sediment. Fluidisation occurs when fluid can move freely through the sediment without being trapped or hindered by grains or being focused into elutriation pipes (Skilling et al., 2002). Therefore, sediment with good initial porosity, permeability and sorting should promote the development of fluidisation textures.

4.9 Conclusions

The Staffa Formation of the Palaeogene Mull Lava Field, NW Scotland, comprises a ~275 m thick sequence of basaltic lavas interbedded with a variety of subordinate volcaniclastic and sedimentary units. The complex inter-relationship between these rocks provides an excellent analogue for similar hydrocarbon producing offshore sequences (e.g. Rosebank, Faroe-Shetland Basin).

Lavas were erupted in an actively subsiding graben and interacted with wet substrates and localised bodies of standing water. Volcanism was predominantly fissure fed and periodically explosive. Although vents are not preserved, proximal deposits are found at Carsaig Arches, MacCulloch's Tree and on the Isle of Staffa (NW of Mull). Here massive scoria-rich breccias display characteristics of primary volcanic origin,

with large spatter rags up to 60 cm long and well developed eutaxitic textures within scoria-rich horizons. These horizons are dominated by highly vesicular, fluidal-shaped, glassy scoria indicating the primary nature of the deposit.

During periods of quiescence some of the primary material was locally reworked into spatter- and scoria-rich horizons and contains quartz grains and low abundances of flint clasts. At more distal locations (1 km) the proportion of quartz and flint increases as a siliciclastic regime re-establishes over the volcanic terrain. The proportion of scoria begins to decrease and is replaced by clasts of aphyric and amygdaloidal basalt (< 1 m in diameter) from weathered lava flows. These are interpreted as debris flow deposits within a tectonically active basin. At very distal locations (~3 km) the siliciclastic regime begins to dominate. Fluvial channel deposits dominated by quartz and flint with little to no volcanic component indicate a switch in provenance. The volcanic clasts are locally altered to clay, but are relatively fresh compared to the proximal equivalent, and overall poroperm is retained.

A wide range of igneous- sediment contact types are found both onshore within the Staffa Formation but also offshore in the Rosebank cores. The type of contact produced is dependent on a number of factors including; nature of the igneous body, the rate and angle in which it intrudes, the composition, porosity, perambility and ridgity of the sediment, temperature and water content. Contact types can change over centimeter distances if one of the above factors changes. On Mull the most common lava-sediment contact is lava overlaying fine grained mudstone or coal. This may be because the siliclclastic sedimentary system has been damned or diverted by the impending volcanic lavas, resulting in swampy overbank type deposits with low energy to be deposited. These coal or fine grained units effectively protect the sediment below from the thermal effects of the overlaying sediment. No obvious induration or thermal effects are seen within the sediment in this study.

4.10 Next steps

Samples were taken from all of the localities in order to characterise the petrography and analyse the paragenesis. Samples crossing contacts between the igneous and sedimentary rocks were also taken in order to better understand the interplay between the two competing systems.

5 Petrographic and SEM characterisation of volcaniclastic rocks

5.1 Introduction

The previous two chapters discussed the large range of lithofacies found in the Rosebank cores and in the Staffa Formation. These chapters highlighted the field and core relationships between the different lithofacies and linked these to modes of formation and to depositional setting. To further understand these rock types petrographical analysis was undertaken using the methods described in Chapter 2.

5.2 Petrography

A total of 50 thin sections were made from samples collected from the Staffa Formation and 40 from the Rosebank core (see sample list in appendix). Each sample was extensively studied under a petrographic microscope as described in Section 2.3.4. Point counting results for each lithofacies can be found in be found in the appendix.

5.2.1 Rosebank

Point counting results for each Rosebank Formation lithofacies can be found in Figure 5.1 and tabulated results can be found in the appendix.

5.2.1.1 Rosebank basalt lava

There are subtle differences in the lava petrography across the Rosebank cores. The basalt lava from well 205/1-1 core contains predominantly euhedral plagioclase feldspar (~0.5 mm), altered interstitial glass and rare pyroxene (Figure 5.2.A). The basalt is relatively fresh with only minor alteration to the plagioclase crystals. None of the interstitial glass remains isotropic and instead displays brown to yellow interference colours. The glass has altered to gel palagonite around crystal surfaces and fibrous palagonite fills any visible intragranular porosity left from the alteration of the glass. Amygdales are also typically rimmed by gel palagonite and filled by lighter fibrous palagonite (Figure 5.2. Type 1).

Basalt in the 213/26-1 well has a much lighter appearance, with a greater amount of pyroxene and with large feldspar phenocrysts that often occur in glomeroporphyritic textures. Phenocrysts have embayed grain boundaries with a pitted sieve texture (Figure 5.2.B). Abundant iron and titanium oxides are also found. As in the 205/1-1 core all interstitial glass is similarly altered to orange-brown fibrous palagonite. Porosity created from the alteration of plagioclase phenocrysts is also filled by palagonite. Within the 213/26-1 well there a number of different amygdale fills. Type 1 (Figure 5.2.1) are lined by gel palagonite and filled by fibrous palagonite. Type 2 (Figure 5.2.2) is very similar to Type 1 with the only difference being small colourless spherical features that develop towards the edge of the vesicle. These spherical features resemble spherulitic textures formed by the devitrification of rhyolitic glass. However, rather than being composed of quartz and k feldspar as is common in rhyolitic varieties these spherical features are thought to be composed of calcite rich zeolites. Type 3 (Figure 5.2.3) have zeolite coating occurs completely around the outer amygdale edge (Figure 5.2.C).

The fourth type (Figure 5.2.4) of amygdale present within the 213/26-1 basalts is very similar to Type 1 amygdales but fibrous palagonite forms a regular coating with coarse crystalline calcite filling the interior of the amygdale (Figure 5.2.D). Amygdale types 5 (Figure 5.2.5) and 6 (Figure 5.2.6) are also filled by calcite. Type 5 has similar spherical structures developed around the edge of the vesicle but in this case the spherical structures are composed of fibrous palagonite instead of zeolite (Figure 5.2.E).

In most cases the palagonite has started to alter to clays, such as pore filling smectite and chlorite. This is most common in the 213/26-1 core, especially close to areas of sediment. The basalt is a more distinctive green colour due to the phyllosilicate clay presence. Amygdales are typically more complex with several different phases of fill, alternating between altered palagonite, clays, zeolite and calcite, Type 7 (Figure 5.2.7) and Type 8 (Figure 5.2.8). Figure 5.3.A.B, shows an example of a complex amygdale fill. The vesicle is rimmed by a thin white layer in ppl that displays undulating low order interference colours in xpl (Figure 5.3.C,D,G,H). This is then lined by a thin layer of light brown amorphous material that displays very dark colours under xpl. There is then a thicker fibrous layer that has bright colours under xpl. These layers resemble similar textures seen in core of volcaniclastic rocks taken during the Ocean Drilling Program (Calanchi et al., 1994) and therefore, are identified as zeolite, altered gel palagonite and altered fibrous palagonite, respectively. The palagonite is now altered to clays. The centre of the vesicle is filled with spherulitic style clays with

high interference colours (Figure 5.3.E,F). This marks a distinctive switch from wall nucleation to point source nucleation. It is unknown why such a switch would occur. If conditions within the pore filling fluid suddenly favoured clay growth, wall based nucleation might be expected to accelerate causing the fibres to grow and meet in the middle of the vesicle, resulting in an axiolitic style texture. However, this has not happened and instead a switch to point source nucleation has occurred.

Figure 5.4.A,B, shows another example of a common amygdale type. Here, layers of gel and fibrous palagonite are present, but this vesicle lacks the outer zeolite rim. The colour of the palagonite is much more orange perhaps reflecting its less altered state. The centre of the amygdale is filled by an amorphous brown material that appears to have zones (Figure 5.4.C). Under xpl the amygdale appears to be sector zoned and has a fibrous appearance (Figure 5.4.D).

Most of the amygdales within the basalt lava flows are completely filled. However, occasionally partially filled amygdales that retain some porosity can be found (Figure 5.4.D1,D2). Where the clay spherulites are closely packed porosity is lost; however, where the spherulitic clays are less tightly packed interstitial porosity remains. Therefore, with the same apparent clay material two different structures are present. If the vesicle had been completely filled by the wall nucleation type all porosity would have been destroyed; however, the point source nucleation has resulted in some minor porosity remaining. Axiolitic texture is common within the amygdale clay fills (Figure 5.4.E1,E2).

Porosity in all of the offshore basalt lava flow thin sections is less than 10% and most have no porosity at all. All fractures and vesicles are partially filled with clays resembling those found within the Staffa Formation samples and while interstitial glassy material is less altered, porosity is still severely reduced.

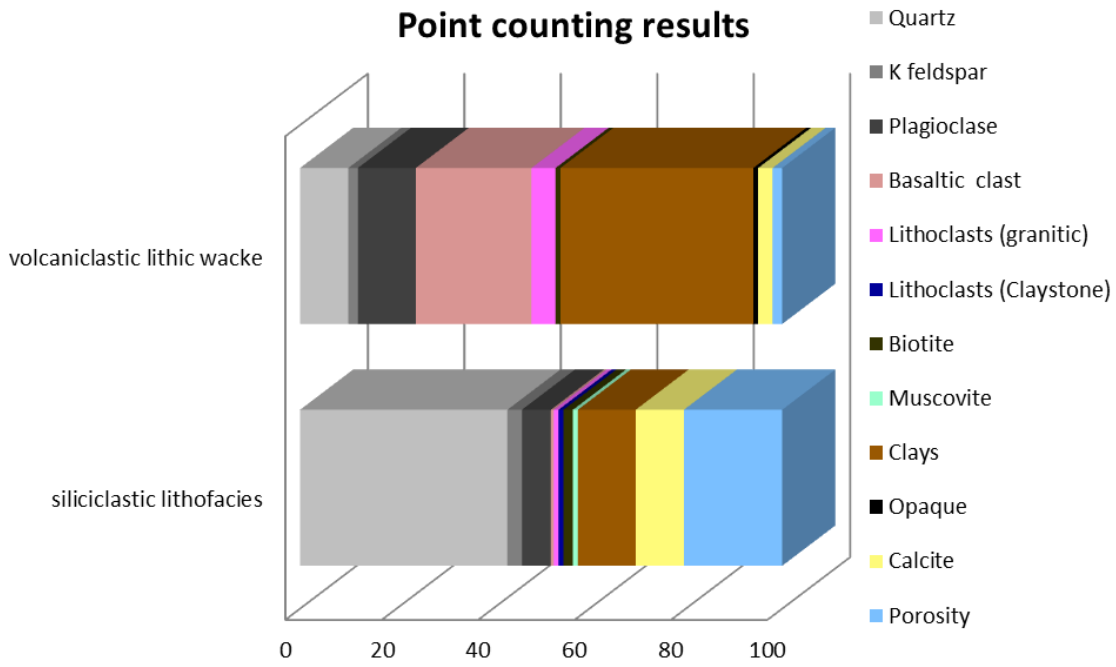

Figure 5.1: Average point counting results for each offshore lithofacies, based on 500 points. For full results see the "Point counting" file in the appendix.

5.2.1.2 Rosebank volcaniclastic lithic wacke

The volcaniclastic lithologies within the Rosebank core are similar to the volcaniclastic lithic wackes found within the Staffa Formation. Two dominant rock types are found within the core; a siliciclastic poor rock type that is dominated by volcanic clasts and a second type where the proportions of siliciclastic clasts and volcanic clasts are almost equal. The sediment in both cases is a dark brown colour resulting from thorough alteration of the volcanic components (Figure 5.5.A1,2).

The volcanic rich wacke is dominated by angular volcanic clasts. As in the onshore equivalents, a range of alteration is present within the volcanic clasts. The glassy groundmass of clasts is often altered to fibrous and gel palagonite, while quartz and feldspar are rounded with some dissolution of grain boundaries (Figure 5.5.B1), However, relatively fresh basaltic fragments are also present where the glass remains isotropic (Figure 5.5.C1). Almost all of the porosity is filled by altered palagonite and clays. Fibrous palagonite forms grain coats that are easily seen under cross polarised light (Figure 5.5.C2). Dissolution of framework grains is more prevalent than in onshore equivalents with all interstitial porosity and vesicles commonly filled by palagonite and/or clays. Layering can be seen within some pore fills (Figure 5.5.D1,2). As in

onshore examples, some volcanic clasts appear to have more altered cores than grain boundaries (Figure 5.5.E1,2). It is unclear why the centre of the grain would alter more that the outside. It is thought that aggressive dissolution of the glass could cause moldic porosity, which could later be filled by remobilised palagonite and clays. Another possibility is that material could be precipitated on the outside of clasts, which may be more resistance to alteration.

The more siliciclastic clast dominated wackes have a more heterogeneous petrography. They have almost equal parts quartz, feldspar and volcanic clasts, as well as biotite, sandstone and mudstone lithoclasts, and pollen and plant fragments (Figure 5.6.A,B). As in the more volcanic rich sediments, they comprise a range of volcanic clasts with similar alteration textures to those already described (Figure 5.6.C). Despite the siliciclastic grains having more of an influence in the sediment, than in the volcanic-rich rocks, the porosity is very low. All inter- and intra-granular porosity is filled by palagonite and clays (Figure 5.6.D). Compaction of the sediments is similar to onshore equivalents; however, more crystalline clasts tend to retain their original structure better than the glassy clasts found in the Staffa rocks (Figure 5.6.E1,2). Spherulitic and axiolitic clay textures are also commonly found in the Rosebank vlW rocks; however, no pyroclastic textures were found indicating that the volcanic clasts are not of a pyroclastic origin. Zeolites are found as a pore lining in some samples (Figure 5.6.F1,2).

5.2.1.3 Rosebank siliciclastic lithofacies

As in the onshore equivalents these facies are dominated by quartz grains ranging from 25– 51%. The quartz ranges in length from 0.1 mm in the more silty facies to 2 cm in the conglomeratic units. The quartz is mono crystalline and ranges from very angular to sub-rounded with minor dissolution boundaries. Plagioclase and microcline feldspar are abundant but is highly dissolved with minor sericitic alteration. Subordinate biotite and muscovite mica and granitic and muddy and granitic lithoclasts are also found.

Visible porosity in these facies ranges from 2% in the silty facies up to 26% in the well-sorted sandstones. (Figure 5.7.A1,2,3,4). Pores are well connected and are often oversized with floating grains. Moldic porosity is also present where feldspars have dissolved. Dark green clay is a minor phase coating some quartz grains. It is often associated with areas of more muddy lithoclasts. Patchy calcite cement is present in

some of the samples (Figure 5.7.A5). The irregular morphology of the calcite cement regions closely resembles the quartz cemented region within the quartz arenite samples, onshore (Figure 5.7.A6). The edges of these calcite cement areas, while irregular do not show significant dissolution (Figure 5.7.A7, A8). Calcite completely fills the pore space in these areas, which contrasts with the oversized pores found throughout the rest of the sample (Figure 5.7.A9).

There are at least two possibilities as to why the pores may be oversized. Firstly, the calcite may have originally completely cemented the rock protecting it from compaction. At a later stage, this calcite was then dissolved out leaving only isolated small patches behind. However, as previously discussed the remaining calcite does not show any evidence of dissolution. To remove large quantities of calcite from the rock would also require prolonged interaction with diagenetic fluids (Blatt, 1979) and for the diagenetic system to be open. Removal of this quantity of calcite appears unlikely. The second explanation is that the sediment never experienced widespread calcite precipitation and that pores were held open due to over pressure. This scenario seems more likely as protection from compaction could be provided by the volcanic lavas above and below each of the sandstone layers. However, evidence of compaction is noted in some samples, with mica and organic fragments being deformed around framework grains (Figure 5.8). Where calcite has filled intra granular porosity grains have not compacted, indicating the importance of an early calcite cement.

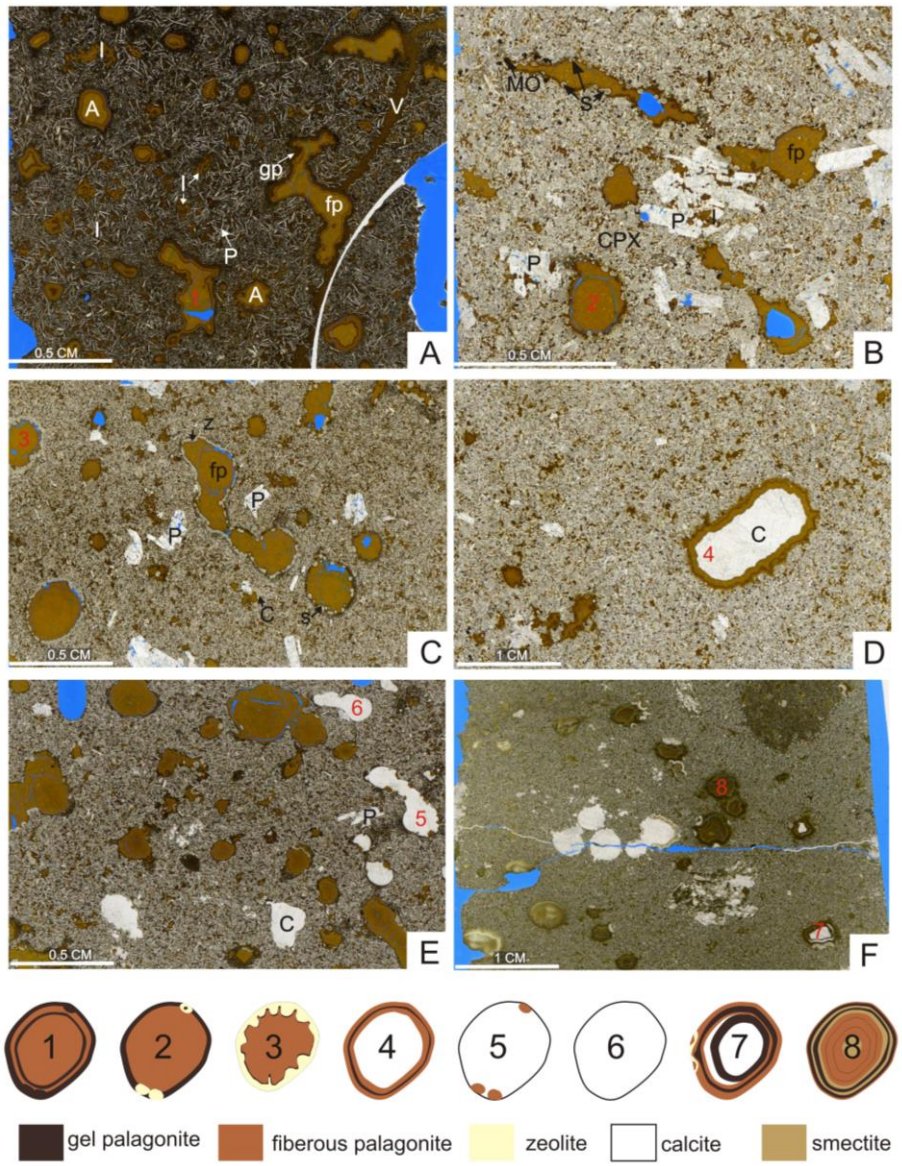

Figure 5.2: Basalt lava flows with a range of amygdale fills. Annotations- A = Amygdale; P = Plagioclase; CPX = clinopyroxene; I = altered interstitial glass; MO = metal oxides (Fe, Ti); gp = glass palagonite; fp = fibrous palagonite; v = vein; s = spherical structures; numbers correlate to amygdale fill types. **5.1.A:** well 205/1-1 depth of 2931.2 m. All other images are from the 213/26-1 well with depths of 2874.4 m; 2879.5 m; 2879.4 m; 2881.1 m and 2887.6 m respectively.

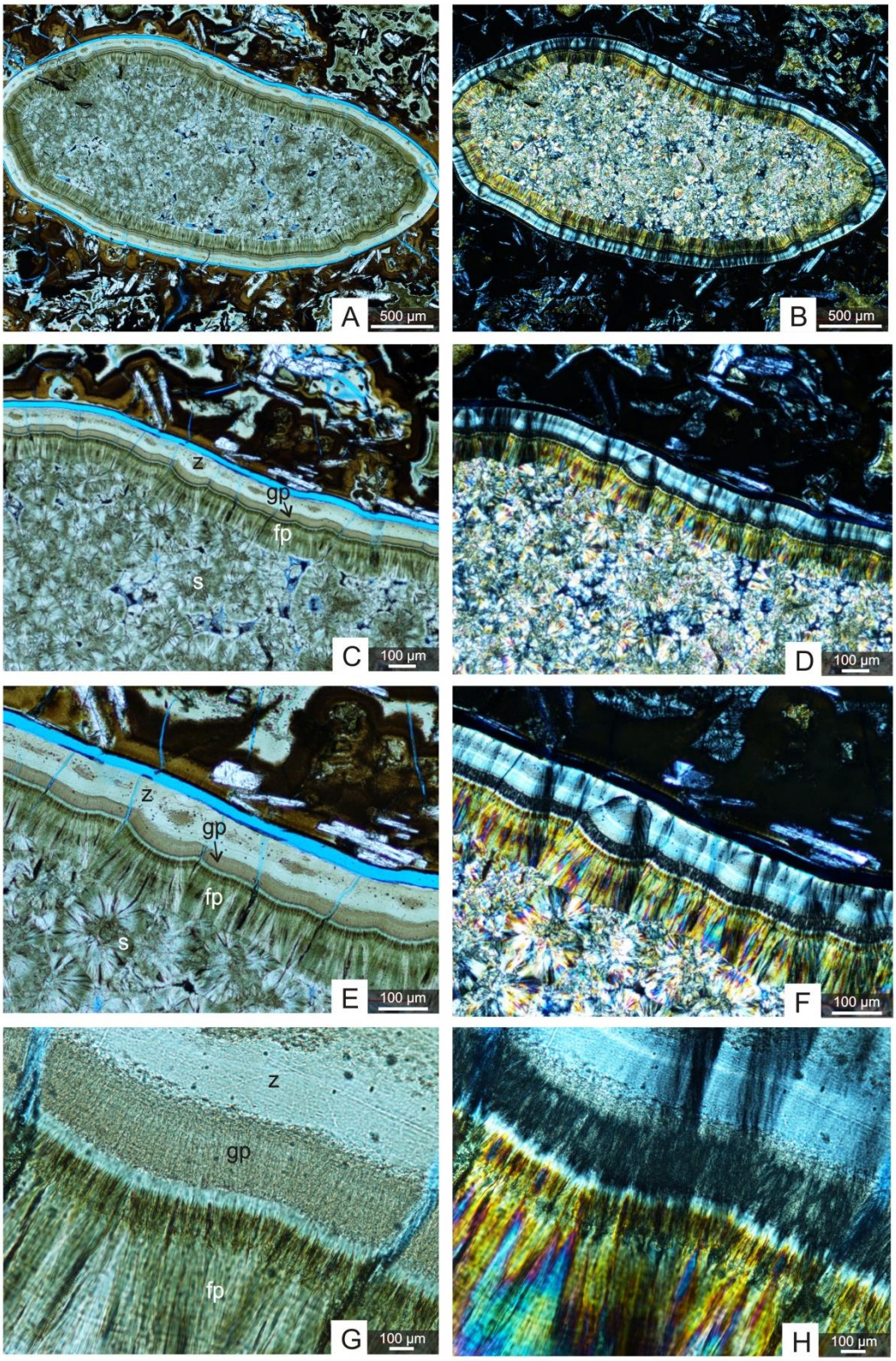

Figure 5.3**:** Complex amygdale fill. Sample Chev 8. **A** (ppl); **B** (xpl): Amygdale within altered basalt. **C** (ppl); **D** (xpl): Some interstitial porosity remains between the spherulitic clays. The basalt has also altered. **E** (ppl); **F** (xpl): Amygdale is rimmed by a thin white layer, possibly zeolite (z). A thin layer of altered gel palagonite (gp) from the alteration of the volcanic glass and coasts the zeolite layer. A thicker layer of fibrous palagonite (fp) grows outwards into the centre of the vesicle. Spherulitic clays grow in the centre of the amygdale (s). **G** (ppl); **H** (xpl): Close up of the transition from zeolite to amorphous gel and then fibrous palagonite.

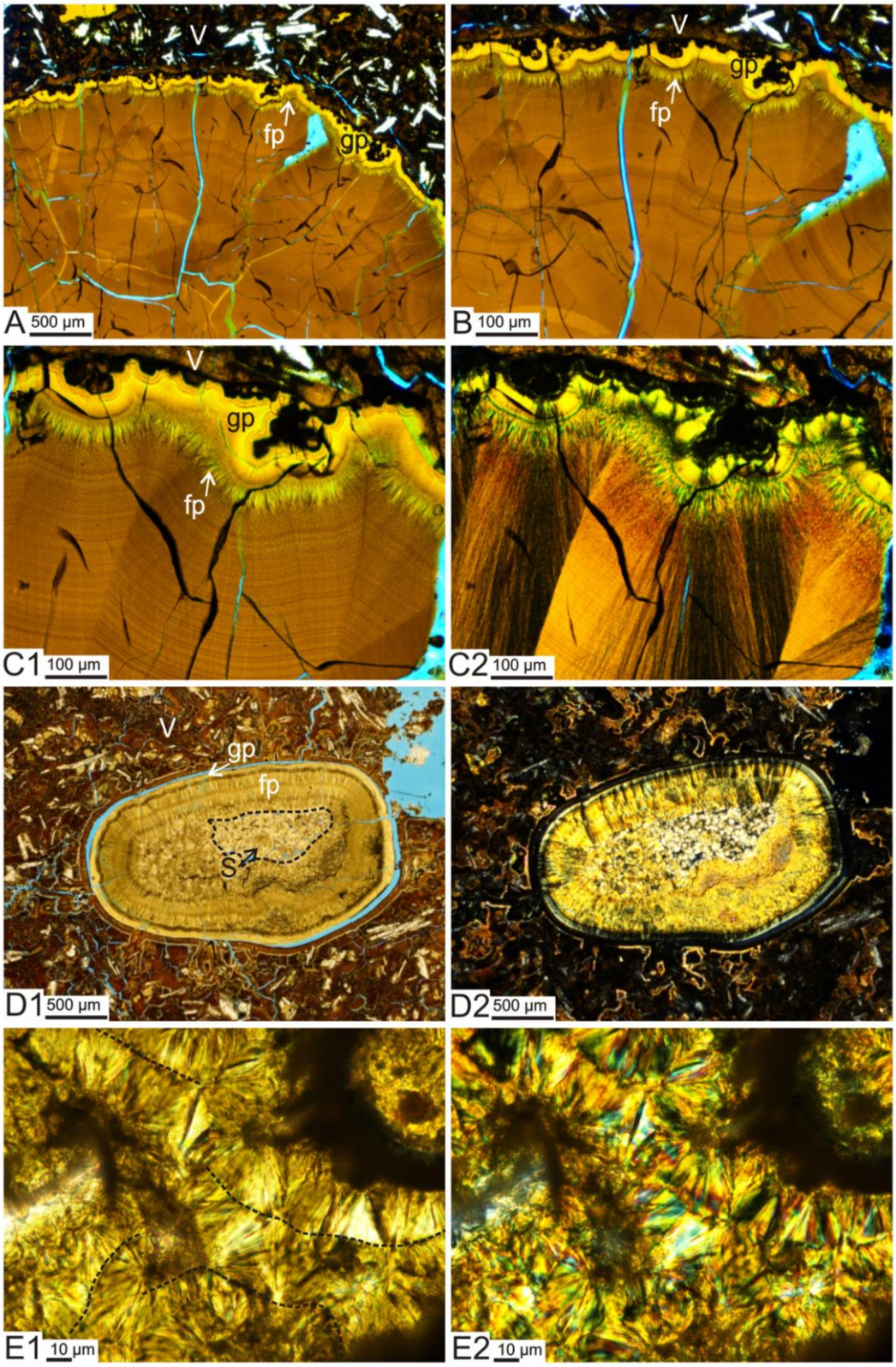

Figure 5.4: **S**pherulitic clay amygdale fills. Sample: Chev 9. **A:** Amygdale within a basalt. **B**: More magnified view, showing the basalt groundmass is altered to a similar material as the amygdale fill. **C1**: Amygdale is rimmed by gel palagonite (gp) and then fibrous palaognite (fp). **C2**: Core of the amygdale (xpl) is filled by fibrous, sector zoned orange clay minerals. **D1** Amygdale in altered volcanic glass (v) with spherulites (S) (ppl); **D2** (xpl): Amygdale centre is filled with tightly packed spherulitic clays. Where the spherulites are loosely packed (outlined with dashed line) interstitial porosity is retained. **E1** (ppl); **E2** (xpl): Axiolitic texture (dashed lines) developed within the clay fill.

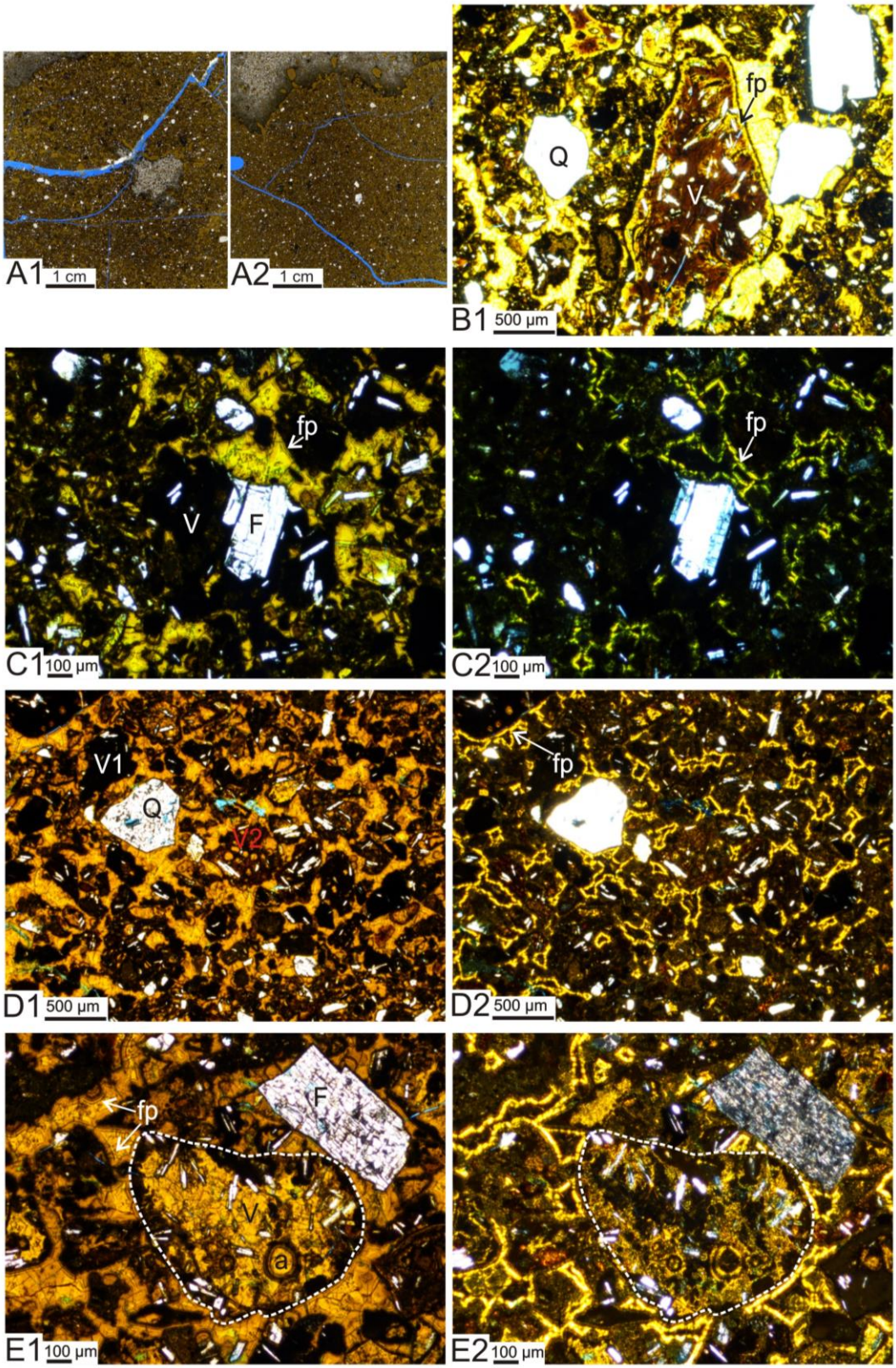

Figure 5.5**:** Rosebank volcanic rich vlW. **A1,2:** Thin section scans of example vlW. **B1**: Angular volcanic clast (V) with altered fibrous palagonite (fp) coating and quartz (Q) in a clay rich matrix. **C1** (ppl): Relatively fresh basaltic clast with plagioclase phenocryst (F). **C2** (xpl): Fibrous palagonite grain coats. **D1** (ppl), **D2** (xpl: Fresh glassy volcanic clast (V1) and altered vesicular volcanic clast (V2). **E1** (ppl); **E2**(xpl): Volcanic clast with altered core (outlined by dashed white line). Note: fibrous palagonite (fp) layering in pore filling material (arrowed).

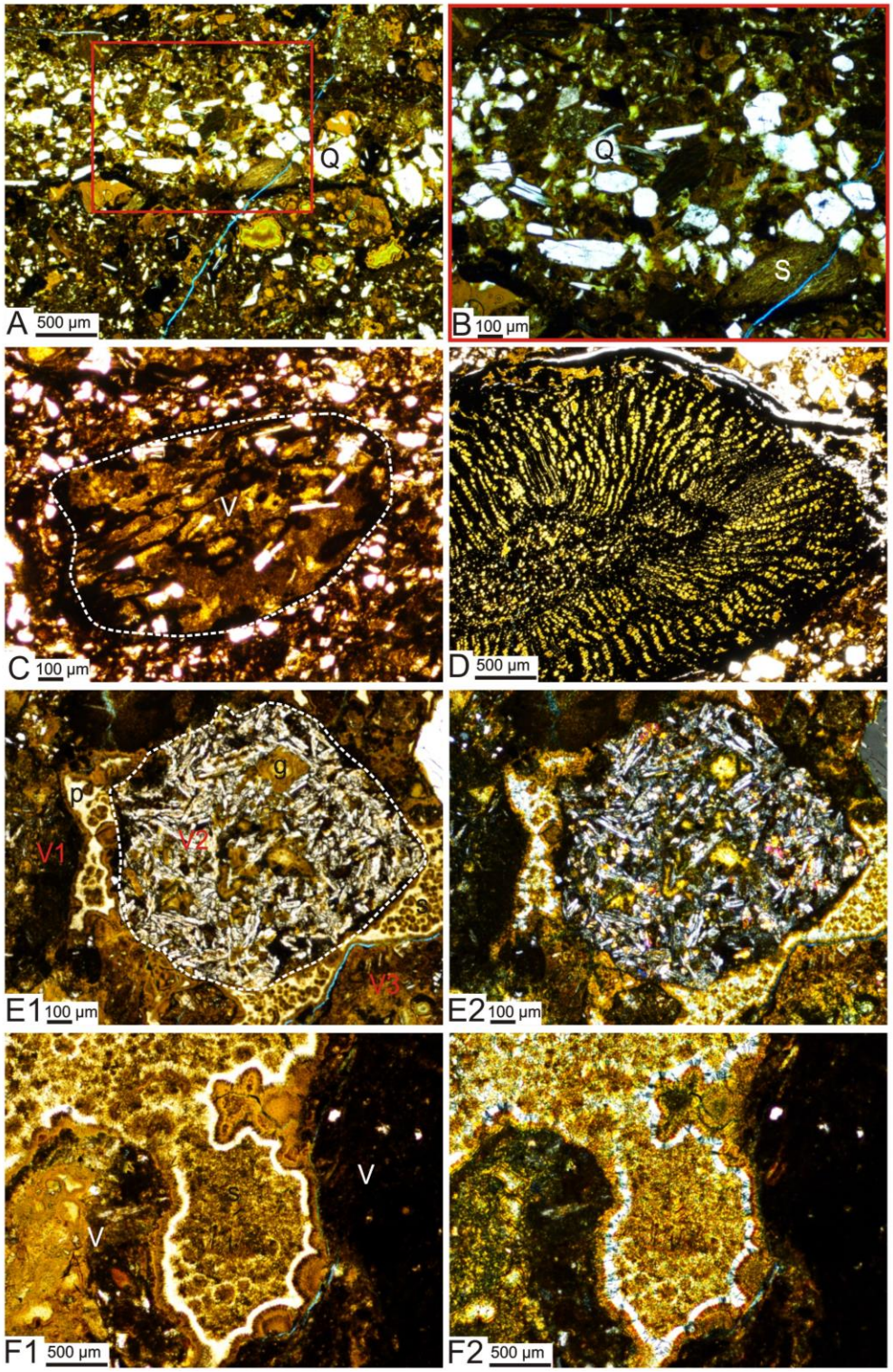

Figure 5.6: Rosebank vlW. **A**: Layer of siliciclastic grains; quartz (Q), feldspar, mica, mudstone and sandstone lithoclasts (S) in between more volcanic rich layers. Box is location of B. **B:** Magnified image of the siliciclastic rich layer. **C:** Rounded altered volcanic clast showing similar texture to onshore examples. **D:** Pollen fragment where intragranular porosity has been filled by clays. **E1** (ppl), **E2** (xpl): Three types of volcanic clast (V1-3). V2 is a lava clast that is altering but retains overall shape and structure. **F1** (ppl), **F2** (xpl): spherulitic clay texture between lava clasts. Possible zeolite (white) pore rim.

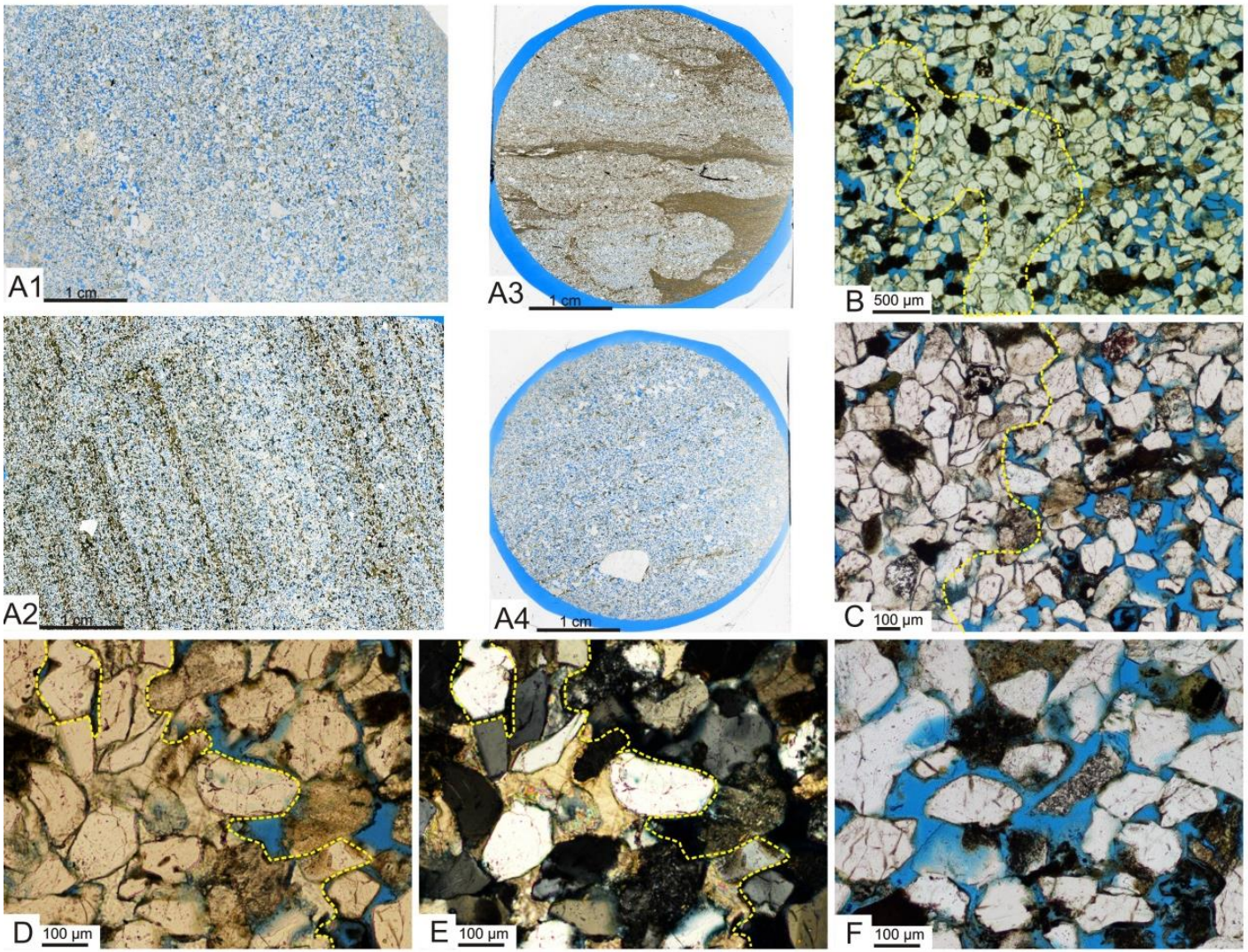

Figure 5.7: Rosebank sublithic and quartz arenites. **A1-A4**: Blue stained thin sections showing the range in visible porosity within the Rosebank sublithic arenite samples. **B:** Irregular patchy calcite cement (dashed yellow line). **C:** Difference in calcite filled pores (left of yellow line) and oversized uncemented pores. **D**(ppl); **E**(xpl): Irregular calcite edge but with no obvious dissolution textures. **F:** Further from calcite-cemented areas sandstone has well developed, oversized pore network.

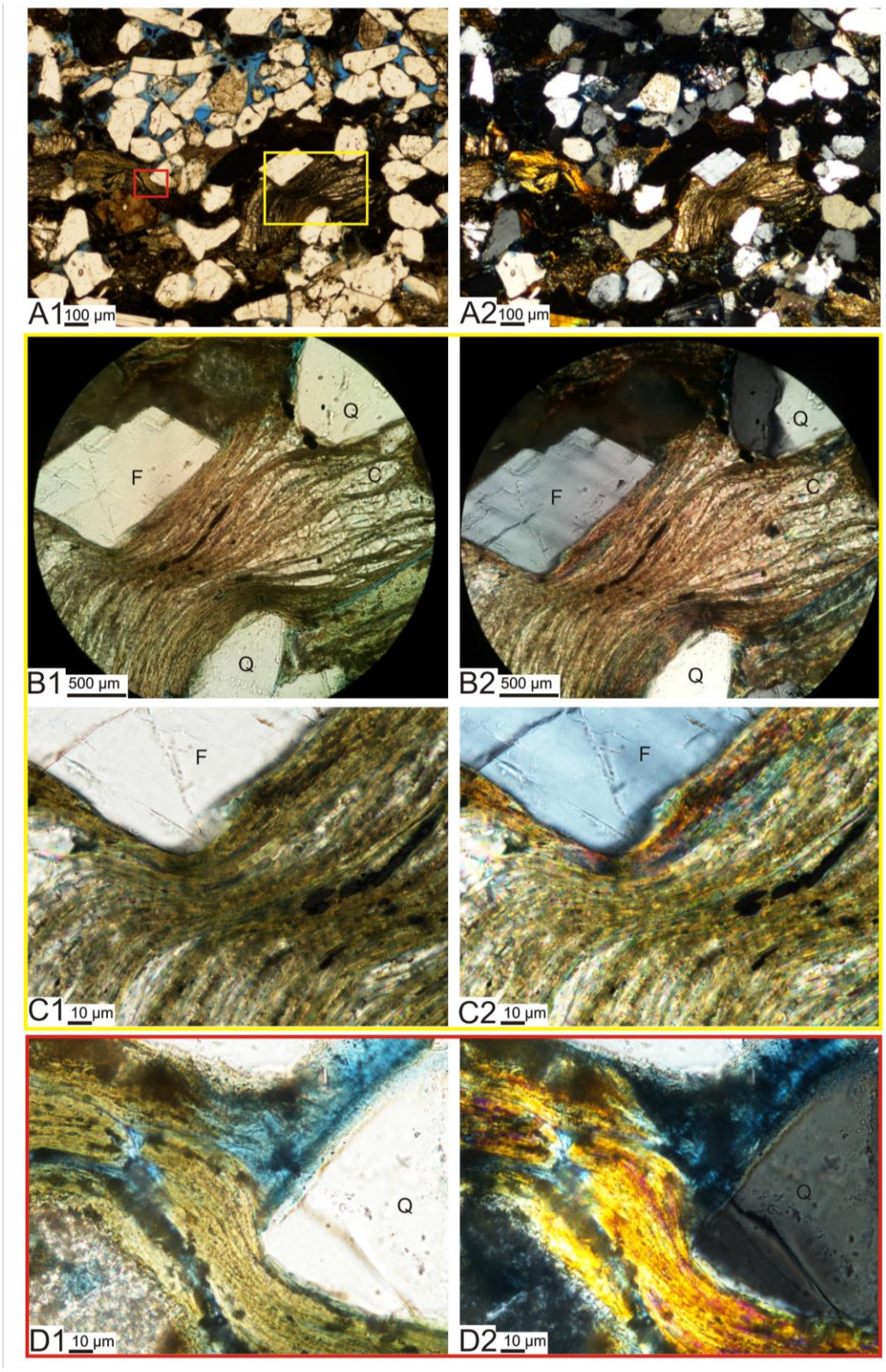

Figure 5.8: Evidence of compaction in the Rosebank siliciclastic samples. **A1**: Photomicrograph showing the location of other photomicrographs in yellow and red boxes. **A2**: Mica deformed around framework grains. **B1** (ppl); **B2** (xpl): Mica deformed between framework grains; quartz (Q) and feldspar (F). Where calcite cements intragranular porosity the grain is not compacted to the same degree. **C1** (ppl); **C2** (xpl): Magnified image showing mica compacted around the quartz grain. **D1** (ppl); **D2** (xpl): Altered biotite grain compacted around quartz grain; however, some porosity remains.

5.2.2 The Staffa Formation

Point counting results for each Staffa Formation lithofacies can be found in Figure 5.9 and tabulated results can be found in the appendix. Volcanic clast type abundance is seen in Figure 5.10

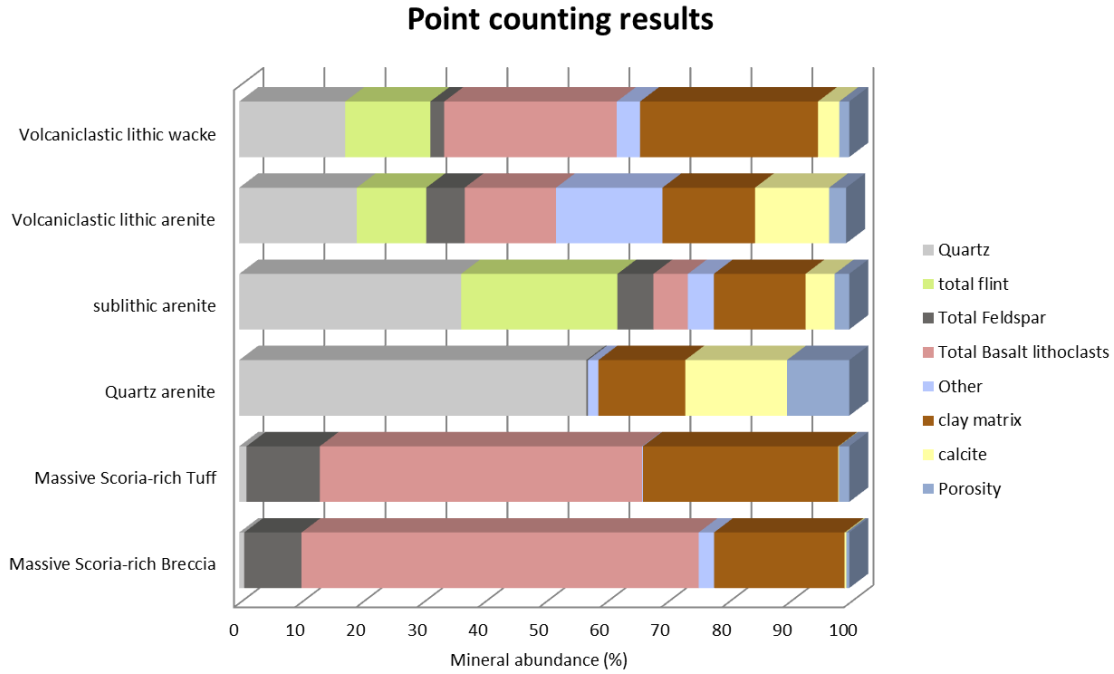

Figure 5.9: Average point counting results for each onshore lithofacies, based on 500 points. Other includes organic material, mica, pyroxene, lithoclasts, glaucophane, zeolite and opaque's. For full results see the "Point counting" file in the appendix.

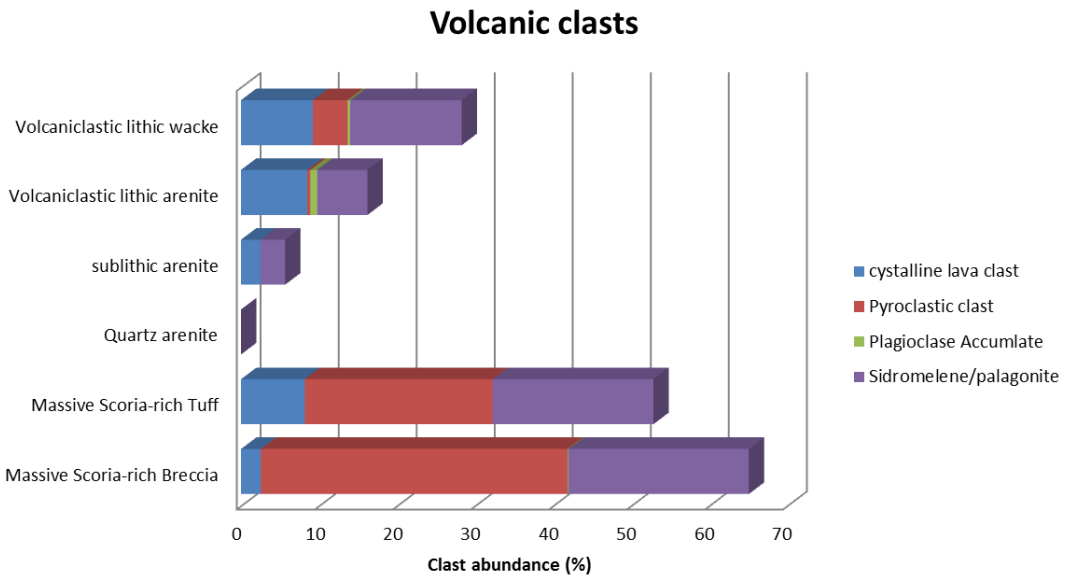

Figure 5.10: Average volcanic clast types within each lithofacies based on 500 points. For full results see the "Point Counting" file in the appendix.

5.2.2.1 Basalt lava (L)

The Staffa Formation basalt flows are aphyric and comprises plagioclase and pyroxene set in a glassy groundmass. Plagioclase phenocrysts (1 mm – 2 cm) is sub-euhedral to euhedral with minor resorption textures. Pyroxene (0.2 mm – 2mm) is commonly zoned and extremely altered. Most samples are amygdaloidal with abundant circular, teardrop and pipe shaped, calcite- and clay-filled amygdales (0.1 mm – 5mm). Amygdales are more prevalent in crustal regions (~20%) than in the cores (~5%).

5.2.2.2 Massive scoria-rich breccia (mscBr)

Several samples from the massive scoria- rich breccias were taken from the proximal deposits at the Carsaig Arches and MacCulloch's Tree localities. The samples comprise irregular rag-shaped basaltic spatter clasts up to 15 cm in diameter, set in a matrix of palagonitised scoria lapilli (1–2 cm diameter).

A wide variety of textures are evident from aphyric glass-rich scoria through to scoria clasts abundant in microcrystalline plagioclase laths to others with well-developed plagioclase phenocrysts up to 2 cm in length. The scoria pyroclasts are dominantly yellow to brown in plane polarised light. Under cross polarised light the scoria is rarely isotropic and birefringence colours range from dark browns and yellows to reds with undulating extinction patterns. Spatter pyroclasts have rag shaped morphologies with glassy chilled margins and are often aligned within the samples. The spatter pyroclasts range from yellow and brown through to black in plane polarised light. Localised autobrecciation of less vesiculated spatter clasts occurs within some of the samples.

Most pyroclasts have circular to flattened amygdales filled by a complex alternating sequence of clay minerals, calcite and rarely zeolites. A thin layer of fibrous clays that have high order interference colours commonly rims the outer edge of each amygdale. Blocky calcite or clays with large radial interference colours fill amygdale interiors.

Rare quartz crystals (<2%) are also scattered throughout the samples. They are often fractured and have a strained, undulose extinction; however, they lack evidence of significant dissolution or overgrowth textures. Pyrite is found as an accessory mineral in some samples.

Alteration is prevalent throughout the samples. All volcanic clasts are highly altered to yellow brown clay like material. In places, this alteration is so prevalent that original primary textures are overprinted and clast boundaries are difficult to distinguish. Vesicles are filled by a number of different minerals indicating several diagenetic phases. This paragenesis is difficult to unravel optically as many of the alteration phases are a similar dark brown.

The ~visible porosity of the samples is less than 2%. Much of the original pore space is filled by clays with minor calcite and zeolite. The initial porosity within the pyroclastic facies varied dependant on grain welding.

5.2.2.3 Massive scoria-rich tuff (mscT)

Petrographically the mscT samples are a fine-grained equivalent of the mscBr samples (Figure 5.11). They are composed of basaltic scoria lapilli (0.1 to 6.4 cm) and ash with rare basaltic lava bombs. Scoria clasts have fluidal morphologies and are often very vesicular (Figure 5.12.A1,2; Figure 5.13.A). Amygdales within the clasts are predominately spherical, but some show evidence of flattening (Figure 5.12.B1,2). The amygdales are typically lined with bands of yellow brown material that under plane polarised light (ppl) appears to have no structure (Figure 5.12.C1). However, under cross polarised light (xpl) these bands have brighter yellow – brown interference colours with distinctive fan-like structures and undulating, wave-like extinction when the stage is rotated (Figure 5.12.C2). These minerals are tentatively identified as altered gel and fibrous palagonite and zeolite. The vesicles are commonly filled by a darker brown to green clay mineral that fans out into the centre. Plagioclase feldspars within the more crystalline pyroclasts display a wide variation in alteration textures. Some appear fresh with euhedral crystal shapes, well developed cleavage and twinning while other feldspars have heavily dissolved sutured grain boundaries. Rare quartz and flint grains are also found within some of the samples (Figure 5.12.F.1,2). This resembles the quartz in the mscBr.

Basaltic glass that makes up the matrix is highly altered and no longer isotropic (Figure 5.2.D.1,2). Instead, it has yellow to brown low order birefringence with concentric rings. Glass surfaces are pitted with abundant inclusions and twinning is undulose. Axiolitic textures are prevalent throughout, and are often associated with spherulitic like textures at grain contacts. Faint perlitic fractures can also be seen within

the altered glass shards. Fractures are filled with brown to yellow palagonite similar to the matrix material (Figure 5.12.E).

As in the mscBr, samples were difficult to analyse due to their dark appearance under the petrographic microscope. Therefore, a variety of image analysis techniques were adopted to interpret the samples (Figure 5.13.A). The matrix and amygdales can be highlighted allowing the fluidal-shaped basalt clasts to be better identified. In some samples the location of the quartz and feldspar could be used as a proxy for the location of scoria clasts (Figure 5.13.B). The scoria and ash is often flattened resulting in the occlusion of surrounding pore spaces. The porosity of these samples is very low with only minor intragranular porosity present within some of the larger scoria pyroclasts.

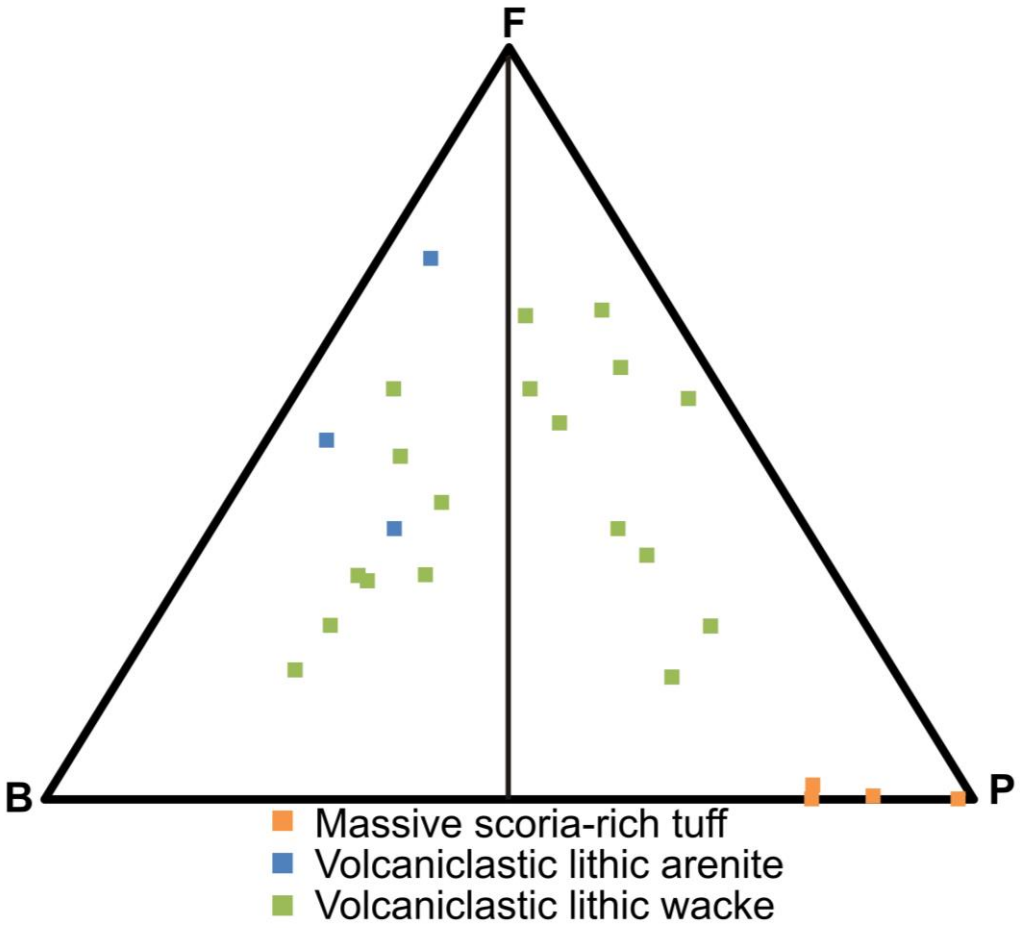

Figure 5.11: Plot of proportion of lithoclast type. End member types: flint (F); basalt lava clast (B); pyroclasts (P). Samples plotted all contain more than 10% total lithoclasts. Data points are based on point counting.

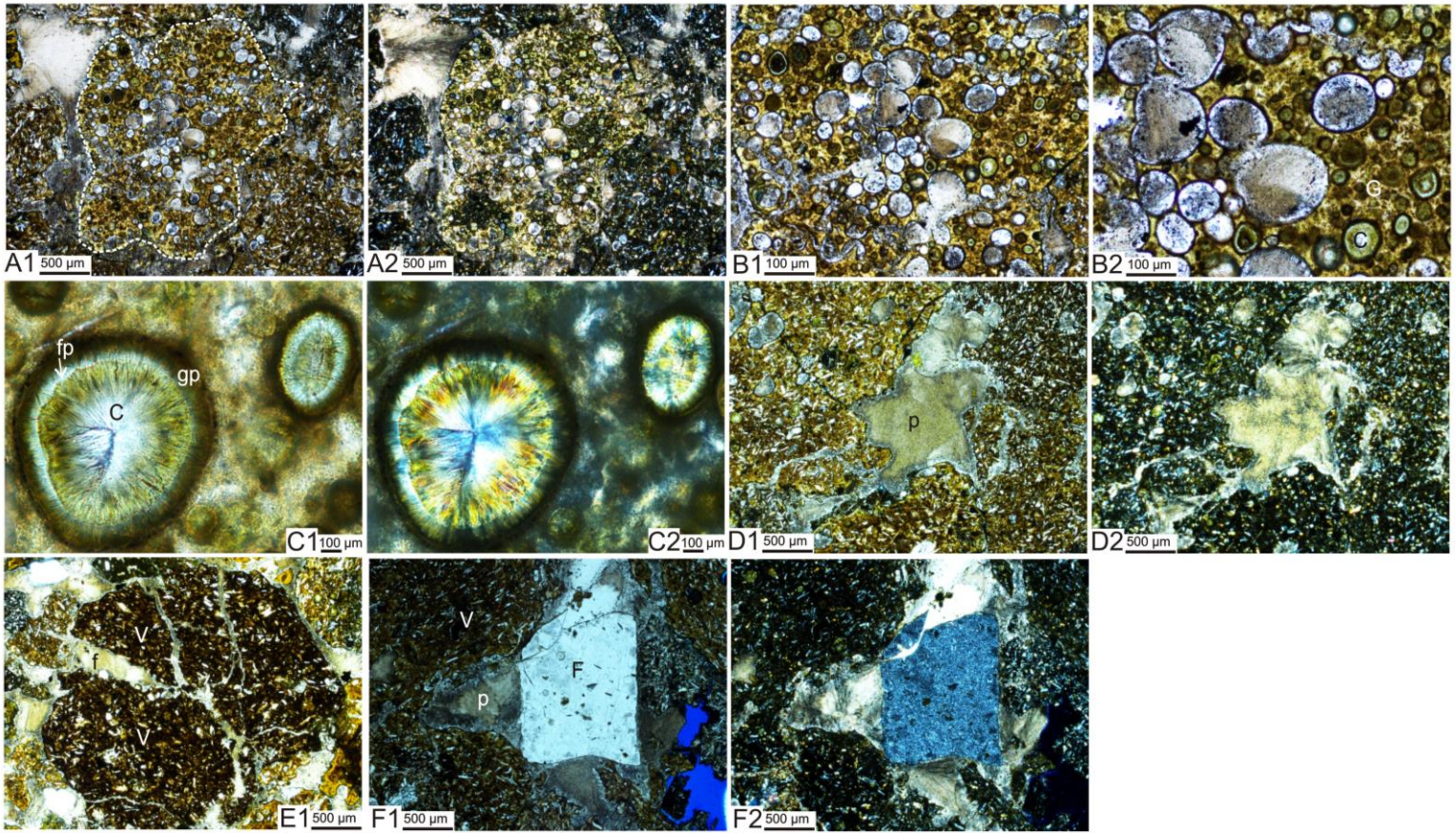

Figure 5.12: mscT photomicrographs. **A1:** Vesiculated basalt clast (ppl). Note the zeolite pore filling material surrounding the clast. **A2:** Glassy groundmass (xpl) has altered and is no longer isotropic. Note fibrous nature of pore filling material. **B1:** Amygdale morphologies (ppl). **B2:** Range of amygdale fills (ppl). **C1**: Amygdale (ppl) comprising; a gel palagonite (gp) rim, a fibeous palagonite coating (fp) and a clay pore fill (C). **C2:** Interstitial glass outside the vesicle has also altered (xpl). **D1** (ppl); **D2** (xpl): Pore space (p) filled by fibrous clays. **E1**: Filled fractures (f) within a scoria clast (V). **F1** (xpl); **F2** (ppl): Flint clast within the mscT sample.

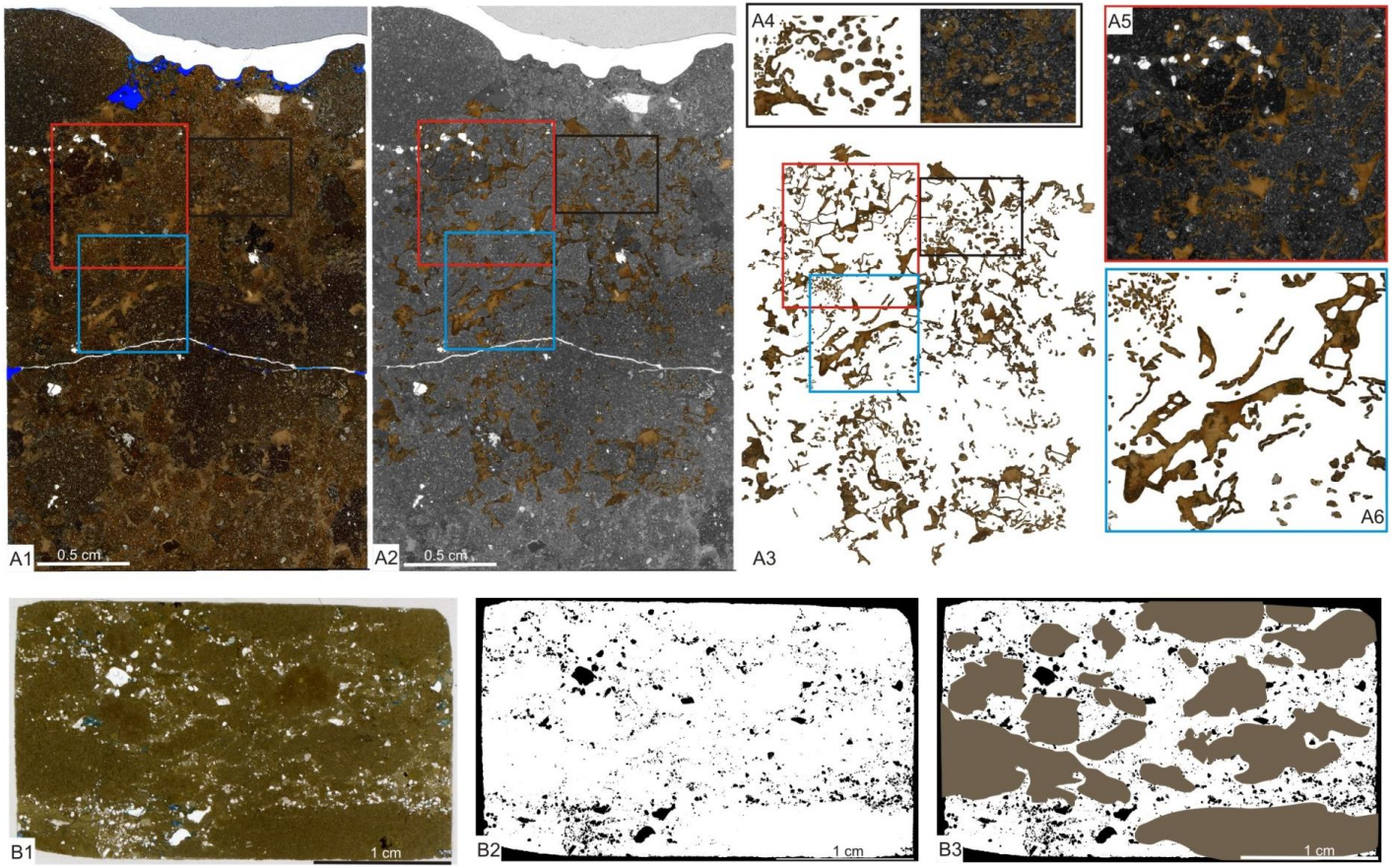

Figure 5.13: Image analysis of proximal mscT. **A1**: Thin section scan from MacCulloch's Tree. **A2**: Desaturated image with clay matrix highlighted. **A3:** Matrix highlighted showing locations for close up figures in red, blue and black. **A4**: Amygdales within a juvenile lava clast are filled by clays. **A5**: Intergranular pore space filled by clays. Note fluidal nature of basaltic clasts. **A6**: Clay filled amygdales (top left) and intergranular pore space. Internal structure of pore fill can be seen. **B1:** Thin section scan from Carsaig Arches of locally reworked mscT. **B2:** Quartz and feldspar (black) highlight edges of spatter clasts. **B3:** Juvenile, fluidal shaped spatter clasts are highlighted.

5.2.2.4 Massive volcaniclastic lithic wacke (vlW)

Massive volcaniclastic lithic wacke was sampled from the Carsaig – Pulpit Rock sequence and also from The Ladder. These samples are heterogeneous and contain a complex mineralogy (Figure 5.14).

Quartz is abundant in all these samples and ranges from sub angular to rounded, is monocrystalline and shows minor dissolution with convex-concave boundaries. It is a relatively fresh phase devoid of extensive alteration or inclusions; however, undulose extinction is common, indicating the quartz has been stressed.

Fossiliferous and non-fossiliferous populations of flint are present within this lithofacies, (Figure 5.15). Type 1 is a fossil-rich variety that is extensively altered with highly dissolved grain boundaries. Alteration is focused on fossils resulting in moldic porosity where fossil material has dissolved and in many cases the pores are filled by brown clay material resembling that found in the matrix. Type 2 is a non-fossiliferous variety that appears fresher with grain interiors remaining intact and dissolution around grain boundaries less severe. Fractures within both flint types have been annealed by calcite and minor quantities of calcite can be found in places around grain edges. A second set of clay-filled fractures are focused at grain boundaries emanating out from flint-flint or flint-quartz point contacts.

Both biotite and rarer muscovite mica can be found within these samples. In both cases the mica appears relatively fresh with little alteration other than radiation spots within the biotite. The mica is often bent around other more ridged framework grains. Rare organic fragments such as pollen and silicified wood occur throughout the samples.

A wide variety of volcanic clasts are found with most samples containing 10–50 % volcanic clasts. The clasts range from reworked pyroclasts to basalt lava clasts (Figure 5.11; Figure 5.16). The lava clasts range from aphyric to hyalopilitic to ophitic in texture. Alteration varies from relatively unaltered clasts to clasts that have been completely replaced by clays. Some clasts no longer have isotropic groundmass as the glass has altered to brown clays with low order yellow to brown interference colours. Some clasts have been extensively weathered and have Fe rich rims. Rarely clasts show chilled margins. The more crystalline clasts are usually the least altered although exceptions do occur.

In the more volcanic-rich parts of the samples the matrix has been compacted (Figure 5.17.A, B). Here, glassy/tuffaceous grains are typically deformed around more ridged framework grains (Figure 5.17.C). Pseudo-pyroclastic textures can also be found such as perlitic fractures within clasts (Figure 5.17.D). In most cases however, the alteration is so prevalent that primary pyroclastic textures within clasts/grains and pseudo-pyroclastic textures in the matrix are destroyed. It might be expected that alteration would be more prevalent at clast edges especially on any clast with a chilled margin. This is because the amorphous glass will preferentially alter over the more crystalline interior. However, several clasts were found throughout the vlW sample range that had the opposite texture, with the clast cores altering more than the edges (Figure 5.17.E). Where alteration is extreme, volcanic clasts can only be identified from the plagioclase pseudomorphs (Figure 5.17.F).

Field and petrographic observations indicate that the vlW represent the complex interplay between competing volcanic and sedimentary systems. The siliciclastic input includes clasts that have been through several cycles of weathering and transportation and so come with inherited diagenetic phases, which complicates the history of the vlW. The petrography of the samples is highly variable and while the main constituent minerals discussed above can all be found, their individual quantities can vary significantly through individual samples as well as between samples. The heterogeneity of the system adds to the complexity to the diagenetic regime the samples undergo.

The visible porosity of the vlW samples ranges from zero to ~5%. The porosity reduction can mostly be attributed to the presence of clays and less crucially calcite. The abundance of pore filling clays appears to be directly correlated with the amount of volcanic clasts within the facies (discussed in Section 6.5.4.5). Figure 5.18 shows a selection of thin sections taken from the vlW samples. Vent proximal samples (Zone 2-3, see the Carsaig model of formation, Section 4.6.1) have a greater proportion of volcanic clasts and associated pore filling clays, and therefore, are low porosity. Samples at more distal locations, where the siliciclastic regime has begun to dominate (e.g. Zone 3 rocks) have a much lower proportion of volcanic clasts and therefore, have greater porosities. At very distal locations, small quantities of ash and scoria can alter to clays; however, this appears to fill only localised pores (Figure 5.19). Zone 4 rocks have very little (<10%) volcanic material and so the porosity remains unaffected.

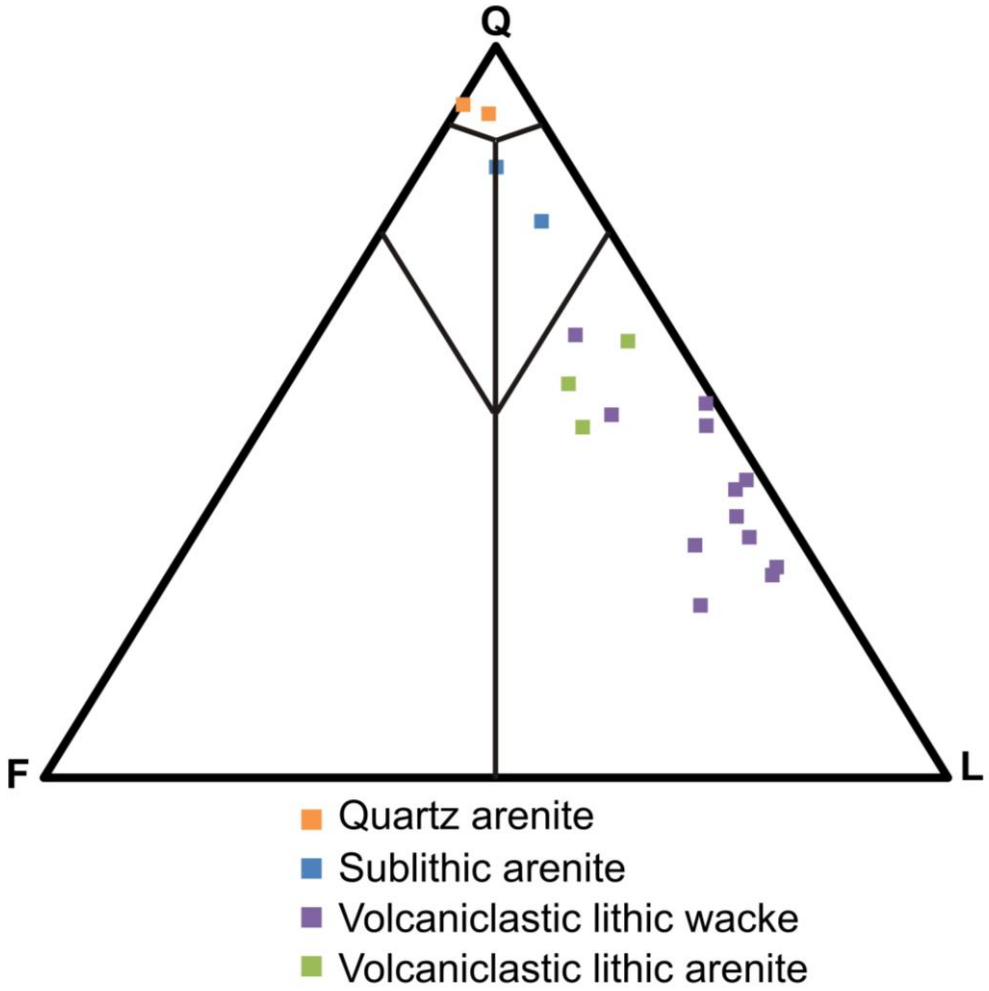

Figure 5.14: Quartz, feldspar and lithic plot for sedimentary lithofacies. Data based on point counting data using the Q,F,L regions defined in Pettijohn et al., 1987.

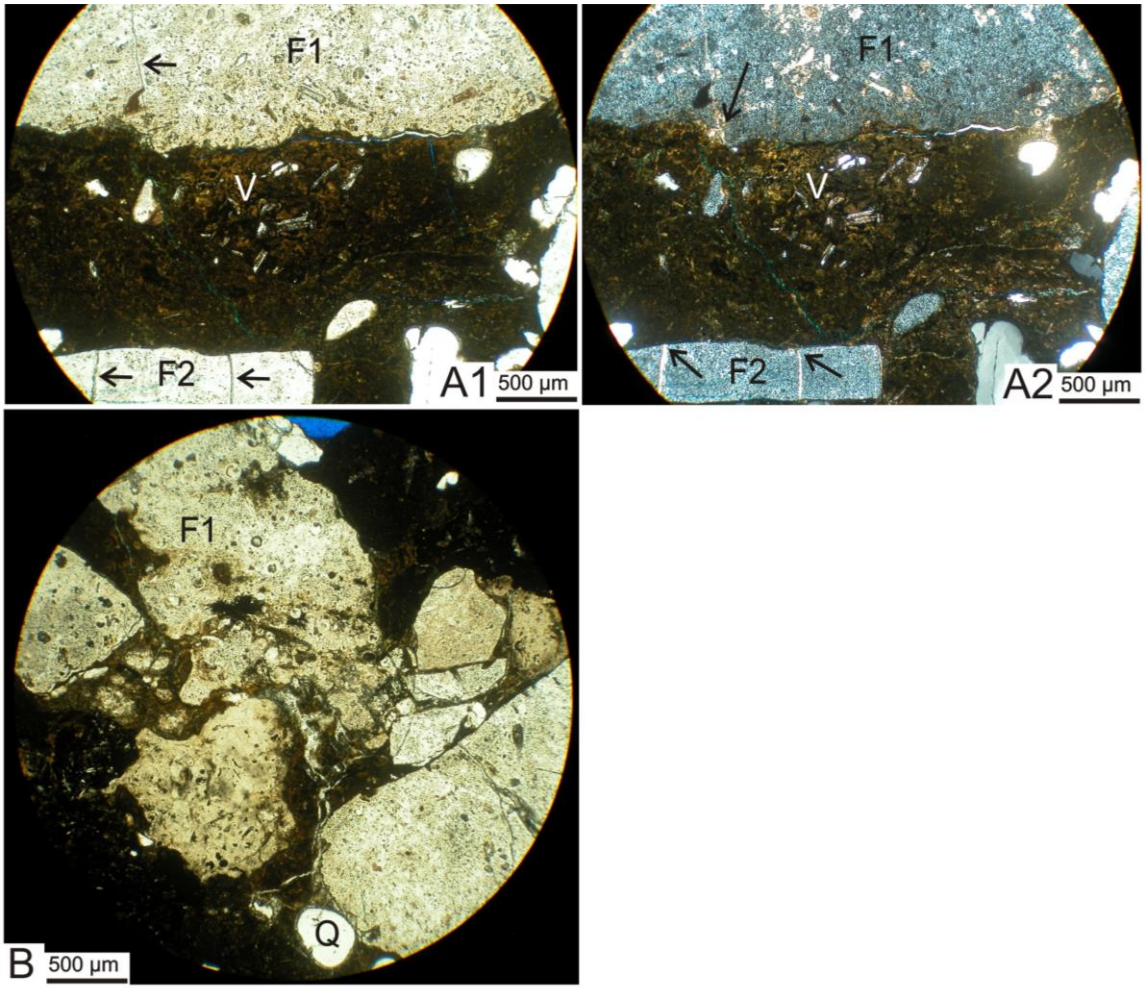

Figure 5.15. Flint clasts within the vlW. **A1** (ppl); **A2** (xpl): Type 1 fossiliferous flint (F1), Type 2 (F2) non fossiliferous flint and an altered volcanic clast (V) set within a clay matrix. Calcite fractures (arrowed) occur in the flint but do not continue into the matrix. Therefore, the filled fractures predate the rock formation. B: Type 1 flint (F1) has highly irregular dissolved grain boundaries in comparison to the rounded quartz grain (Q).

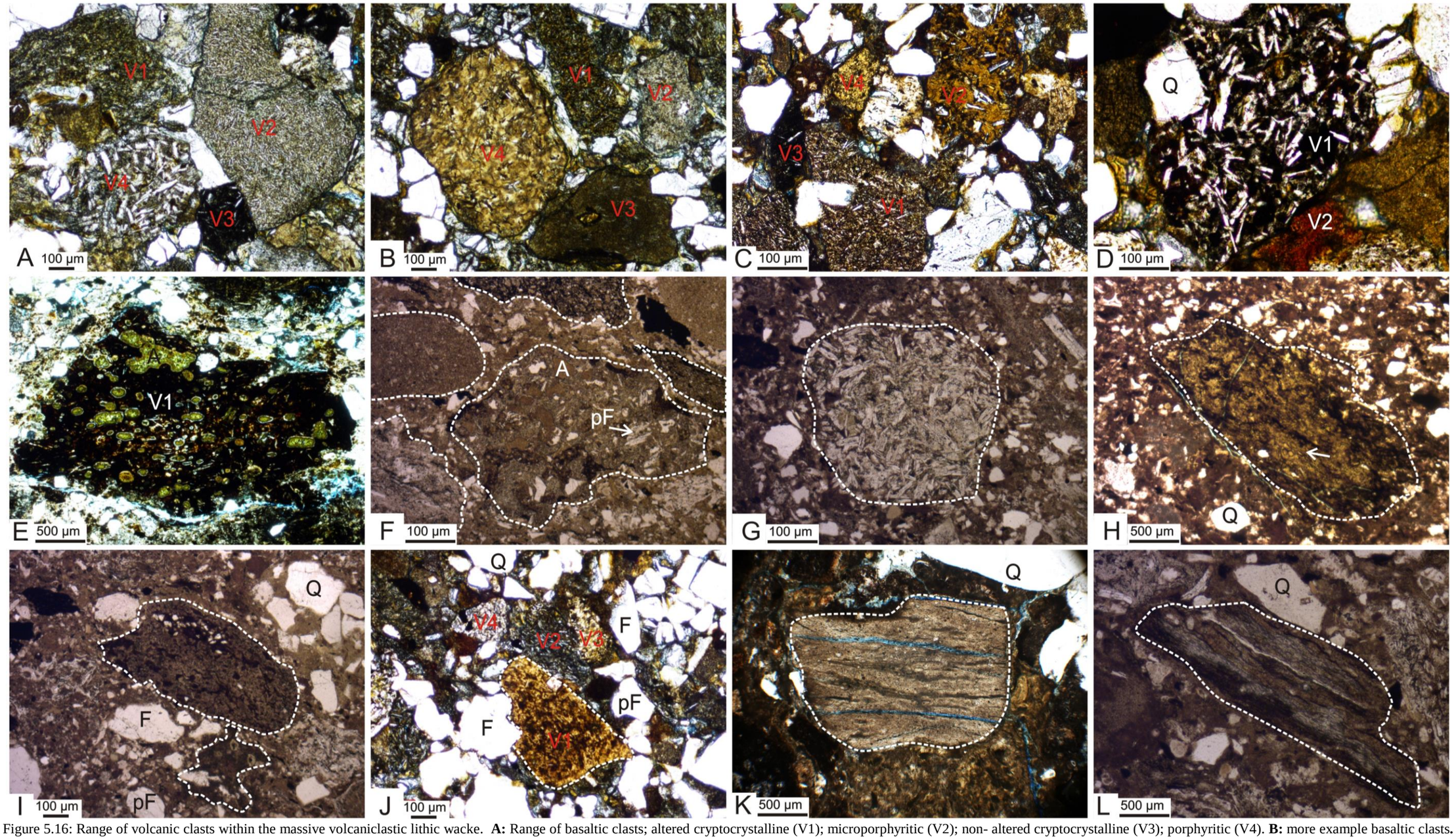

Figure 5.16: Range of volcanic clasts within the massive volcaniclastic lithic wacke. **A:** Range of basaltic clasts; altered cryptocrystalline (V1); microporphyritic (V2); non- altered cryptocrystalline (V3); porphyritic (V4). **B:** more example basaltic clasts**. C:** Range in alteration stages; semi altered (V1); interstitial glass completely altered but phenocrysts preserved (vs); non altered (V3); alteration reached completion (V4). **D:** Variation in weathering; non- weathered basalt clast (V1); weathered basaltic clast with Fe rich staining (V2). **E:** Porphyritic fluidal shaped reworked scoria clast with clay filled Amygdales (A). The groundmass is only partially altered. **F:** Porphyritic fluidal shaped reworked scoria clast (outline in white) with clay filled amygdales (A). The groundmass has completely altered to clays; however, plagioclase feldspar phenocrysts (pF) show only minor resorption. **G:** Crystalline dolerite clast. (outlined in white). Plagioclase crystals remain relatively fresh. **H:** Altered glassy scoria clast (outline in white) with eutaxitic texture and altered amygdales (arrowed). **I:** Altered scoria clast (outlined in white). The more crystalline core of the clast is less altered. **J:** More siliciclastic rich sediment that comprises quartz (Q); flint (F) and plagioclase feldspar (pF) as well as a range of volcanic clasts with varying stages of alteration (V1-4). **K:** Altered tuffaceous clast with relict eutaxitic texture. **L:** Rounded reworked scoria clast (outlined in white) with eutaxitic texture.

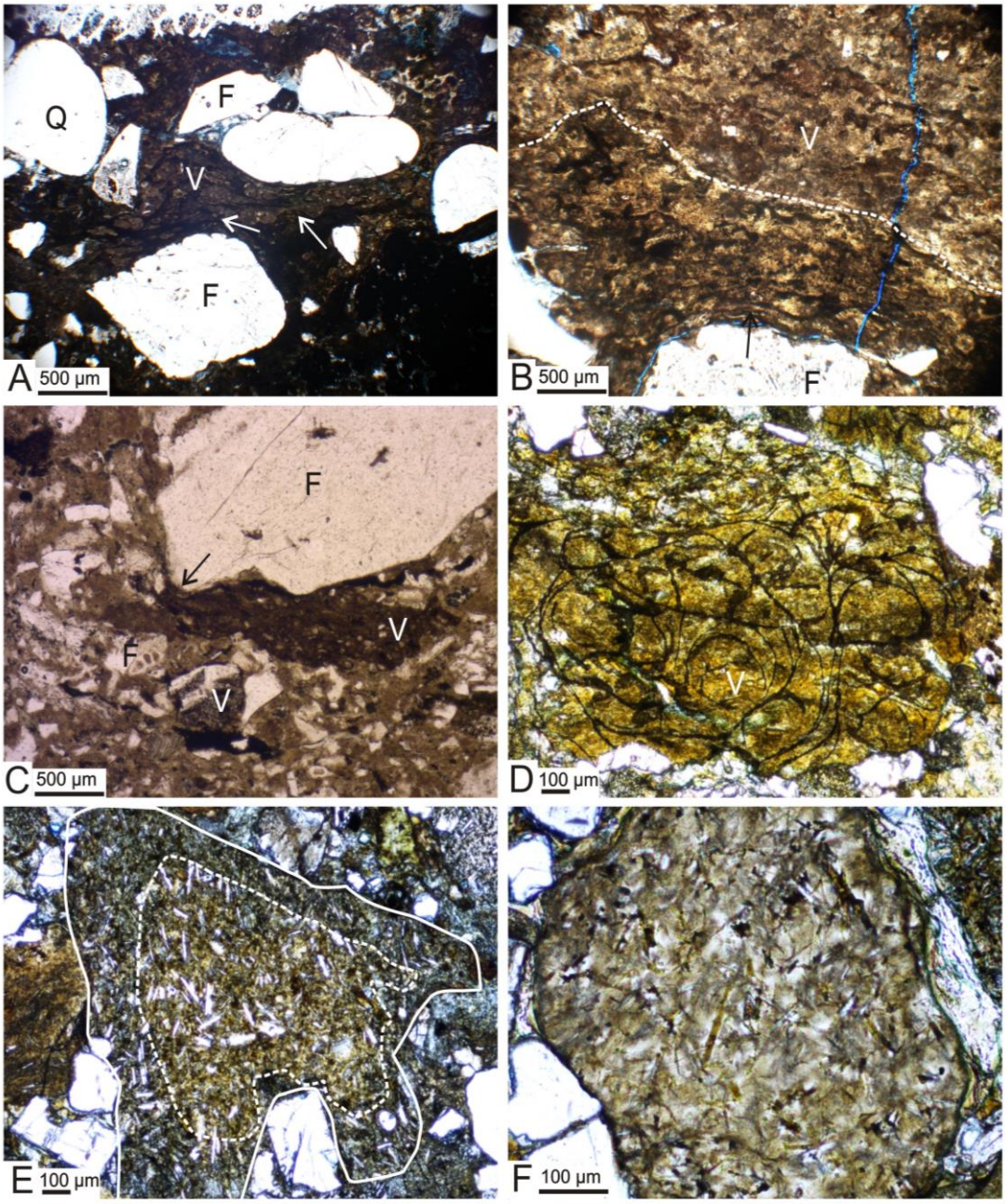

Figure 5.17: Volcanic textures within the vlW samples. **A:** Compaction textures (arrowed). Volcanic clast (V) is bent around framework grains, quartz (Q) and flint (F). **B:** Pseudo-eutaxitic texture in clast (arrowed) between a flint grain (F) and an altered volcanic clast (V). **C:** Volcanic glass shard (V) compacted around flint grain (F). **D:** Relict perlitic fractures in altered glass shard. **E:** Volcanic clast (outlined in solid white) with more altered core (outlined in dashed white). **F:** Extensive alteration resulting in clay pseudomorphs of plagioclase feldspar phenyocryts.

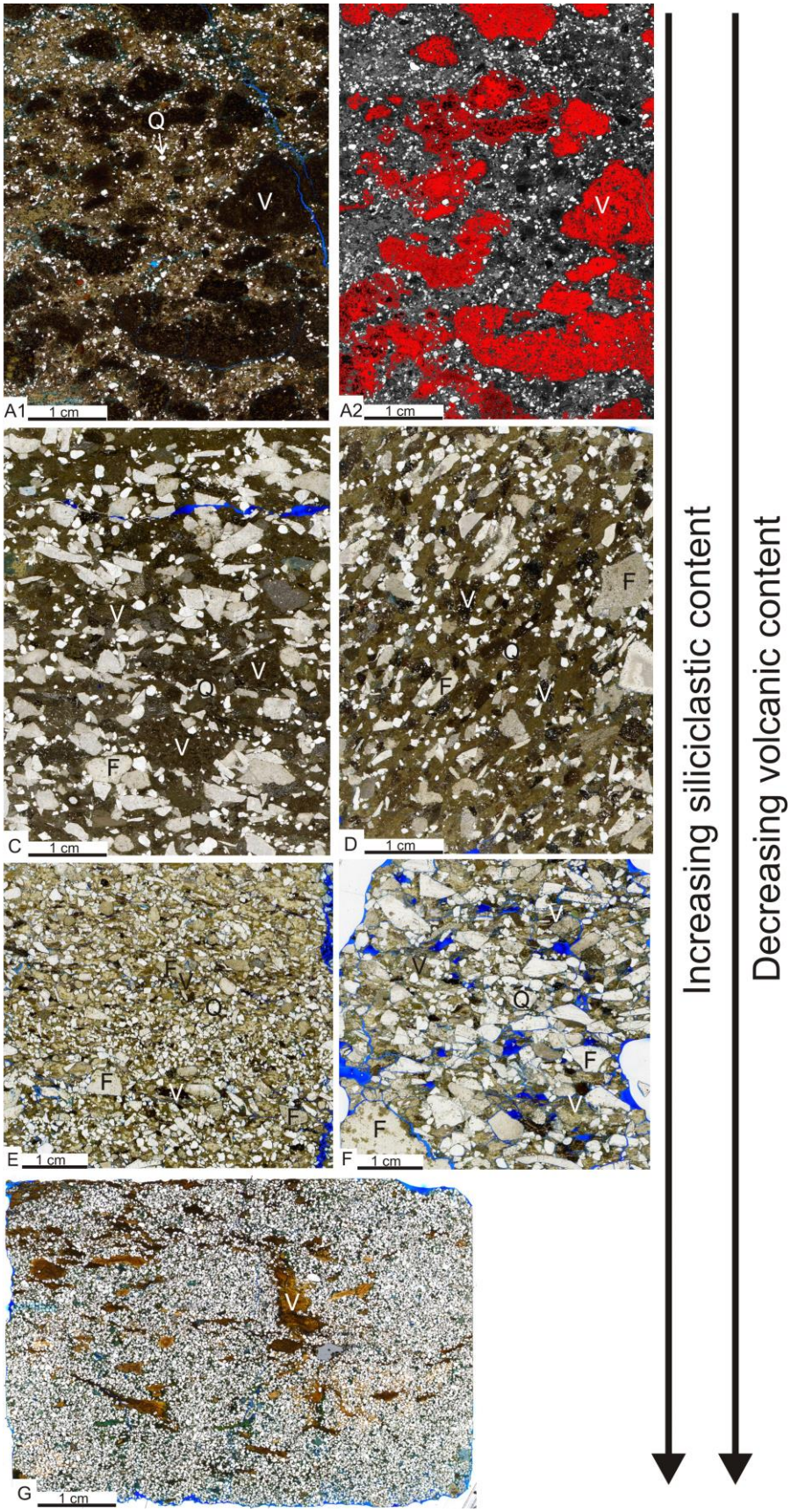

Figure 5.18**:** Heterogeneity in porosity of vlW samples. Thin section scans from most proximal (**A**) to most distal (**F**). Proportion of volcanic clasts decreases with distance from the vent. Proportion of quartz (Q) and flint (F) increase with distance from vent. **A2**: Image processed to distinguish volcanic clasts (red) from clay matrix.

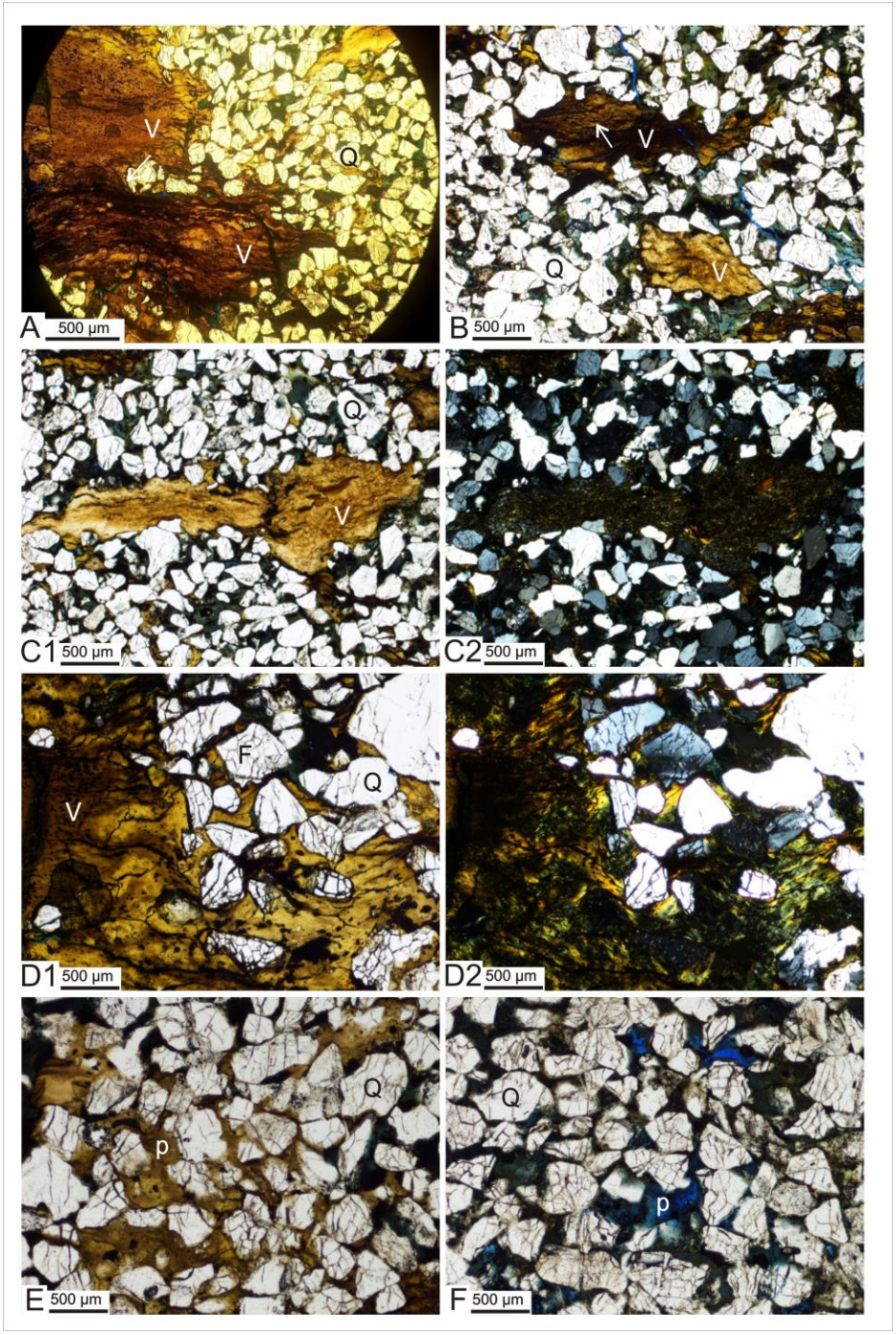

Figure 5.19: Vent distal vlW. **A:** Altered volcanic scoria (V) within a quartz (Q) rich vlW. **B:** Volcanic clasts retain relict eutaxitic texture (arrowed). **C1** (ppl); **C2** (xpl): Volcanic clast surrounded by localised pore filling clays. **D1** Flint (F) and quartz surrounded by volcanic matrix (V) (ppl); **D2** (xpl): Quartz grains are caught up within the edge of the altered scoriaceous fragments. **E:** Within the sample, porosity (p) near volcanic clasts, is locally filled by pore filling clays. **F:** Further from the volcanic clasts porosity (p) is retained with only minor clay fill.

5.2.2.5 Volcaniclastic lithic arenite (vlA)

Volcaniclastic lithic arenites were sampled at Ardtun. The clast-supported samples comprise quartz, feldspar and flint (Figure 5.11; Figure 5.20) that have similar

compositions and textures to those described in Section 5.2.2.4. Small fragments of zoned clinopyroxene are present, as are very rare schist clasts; however, the variety of volcanic clasts found is much less. Reworked pyroclasts are rare and instead samples contain scattered pebbles of glassy fine-grained and heavily altered red coloured vesicular basalt lavas (0.5 – 2cm) and rarer more evolved clasts (Figure 5.11). The volcanic clasts are sub-rounded to well-rounded. As in the vlw samples there is a range of alteration present within the basalt clasts but most seem fresher than their vlW equivalents. The glass in most clasts has altered; however, plagioclase phenocrysts have only minor dissolution textures. The lava clasts often have iron stained edges and lack chilled margins.

The matrix within these samples is mainly a mixture of clays and calcite. The clays are predominantly green in ppl and are only brown when situated near to a volcanic clast. Calcite is a much more abundant pore fill than in the vlW samples.

Initial porosity in these samples is generally higher than those of the more volcanic rich rocks due to less heterogeneity and better sorting. Compaction is evident by convex-concave boundaries and undulose extinction in quartz grains. Porosity reduction as before is mainly due to clays and calcite. In areas of the thin sections where there were abundant volcanic grains, clay inhibits visible porosity, while in the more siliciclastic regions the porosity is reduced by calcite.

These samples tend to only include one or two volcanic clasts types resulting in a simpler diagenetic history.

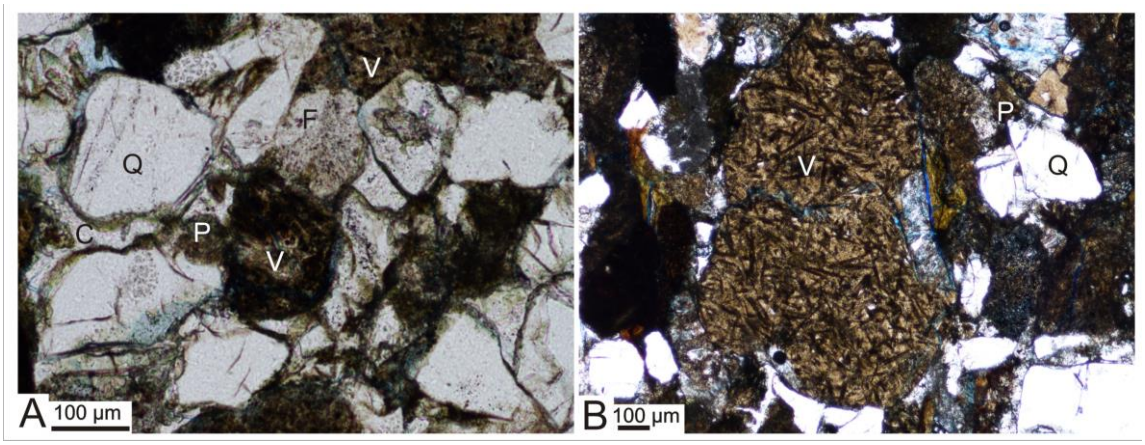

Figure 5.20: Photomicrographs from vlA samples. **A:** Quartz (Q); flint (F); volcanic clasts (V) are cemented by calcite (C) and minor pre filling clays (p). **B:** Weathered basalt lava clast (V).

5.2.2.6 Sub-lithic arenite (slA)

Sub-lithic arenites were sampled at Pulpit Rock. The samples resemble the volcaniclastic arenites with the only real difference being the lack of volcanic clasts (Figure 5.14; Figure 5.21).

The main mineral phase is quartz, which has both poly- and mono-crystalline varieties. Minor dissolution occurs in some of the grains with convex-concave boundaries. Overgrowths of an unknown accreted material can be found around some grains, which is out of optical continuity. The quartz however, typically appears relatively fresh compared with the surrounding rock with only rare fractures, inclusions and undulose extinction. The second most predominate phase is flint as described above. Other phases include: plagioclase and microcline feldspars, which are in many places extensively altered; rare mica; organic material such as woody fragments and pollen; sandstone and mudstone lithoclasts; and in some samples rounded fragments of glauconite. Crucially these samples contain virtually no volcanic material of any description.

Visible porosity in the samples ranges from 1–10%. Pores are, in most cases, filled by clays and blocky calcite. The clays are a deep green to brown colour with high order interference colours. They coat quartz and flint grains and block pore throats. Thin rims of calcite can also be seen coating some grains and filling fractures in flint clasts. This calcite appears more altered with heavily dissolved grain boundaries and a pitted texture.

Compaction is seen within these samples reducing initial porosity. The strained undulose extinction and convex-concave boundaries seen within the quartz imply that the sediment had been compacted as the lava pile grew above. Mica and elongate woody fragments are folded around quartz and flint grains again implying the sediment has been compacted. The presence of glauconite would suggest a marine environment and may support the suggestion that the sea may periodically have entered the basin (Williamson and Bell, 2011). However, the fragmental and well-rounded nature of the glauconite suggests that it is more likely to have been recycled into the sediment from another source. Much of the porosity is reduced by late stage calcite cement discussed in more detail in Section 6.5.4.3.

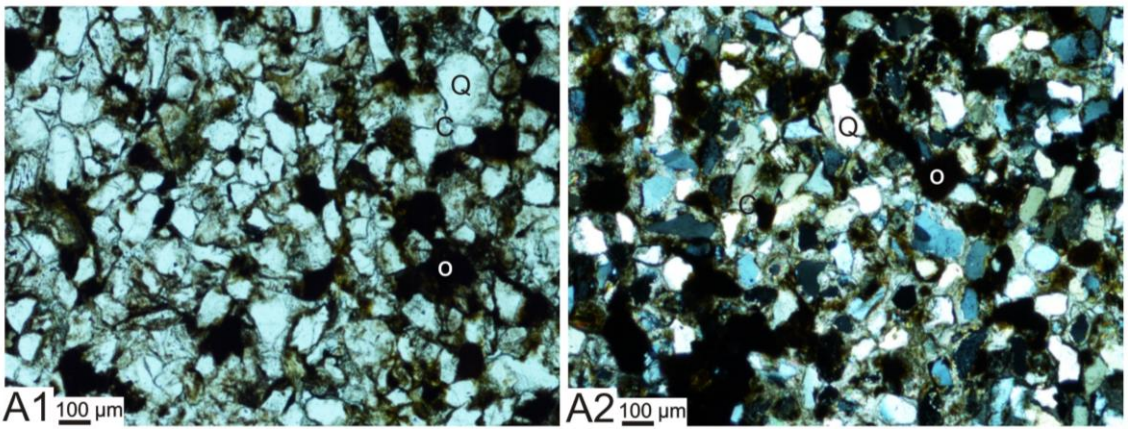

Figure 5.21: Photomicrographs of slA samples. **A1** (ppl); **A2** (xpl): Quartz (Q), flint, feldspar and fine grained organic material (O) is cemented by calcite (C).

5.2.2.7 Quartz arenite (Q)

One sample of quartz arenite was sampled at Carsaig. The rock is poorly lithified and so made sampling difficult. Mineralogically, the sample is much simpler than the other rocks and is dominated by mono-crystalline, angular to sub-rounded, well sorted quartz grains (Figure 5.14; Figure 5.22.A). Many of the quartz grains were artificially fractured during thin section manufacture due to the friable nature of the rock. The key difference between this rock type and the sublithic arenite is the lack of flint, feldspar and lithoclasts as well as the lack of matrix material. The quartz arenite sample has a high visible porosity (40%) and has no pore filling clays. Pores in places are oversized (Figure 5.22.A2) hinting the rock was once over pressured with only limited compaction. In places however, sutured grain contacts are noted (Figure 5.22.B1,2) suggesting minor compaction did occur. Two small areas of the sample are quartz cemented (Figure 5.22.C1,2). The quartz cement may have initially been prevalent throughout the sample protecting framework grains and pore space from significant amounts of compaction. If parts of this cement were then dissolved this could lead to the over-sized secondary porosity. The rock is devoid of volcanic clasts and is also devoid of pore fillings clays.

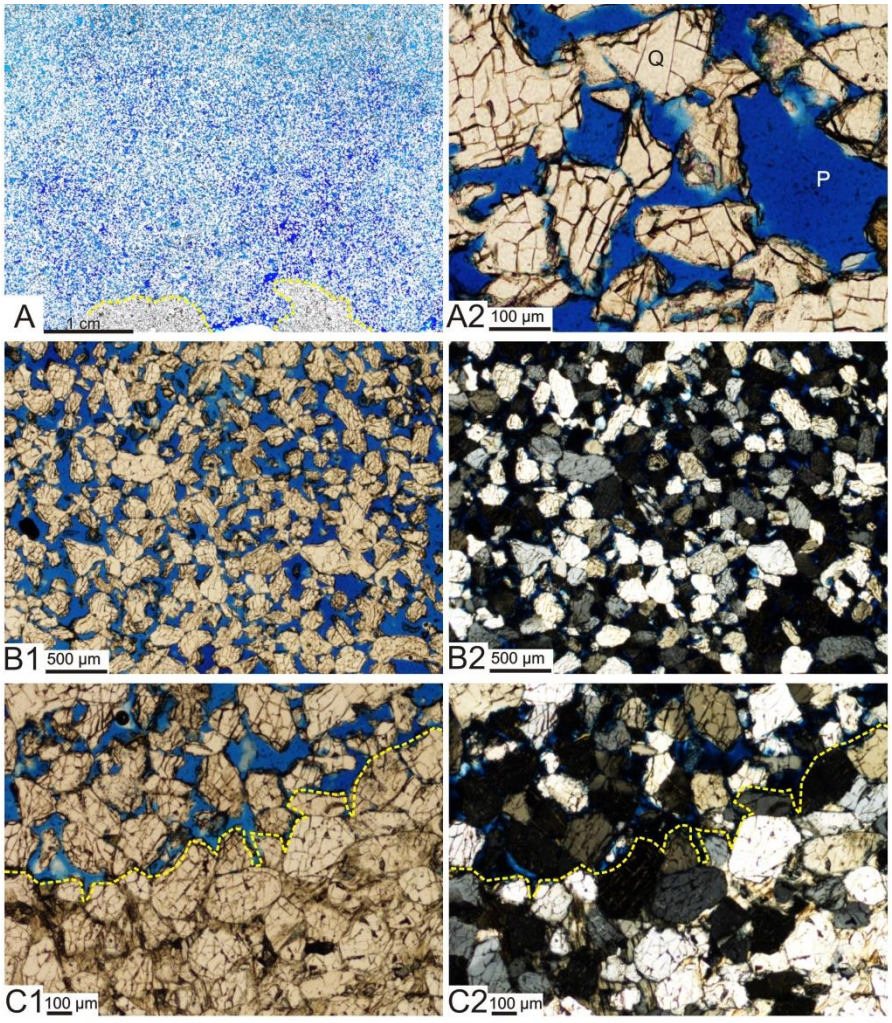

Figure 5.22: Photomicrographs of quartz arenite. **A:** Thin section scan showing the two quartz cemented areas (outlined in dashed yellow). **A2:** Oversized pore (P) surrounded by quartz. **B1** (ppl); **B2** (xpl): Quartz rich sediment with large well developed pore network. Some quartz grains have sutured grain contacts. **C1** (ppl); **C2** (xpl): Contrast in porosity between the quartz cemented region (below yellow dashed line) and the excellent reservoir quality region above. Note: grain fractures are man-made during thin section manufacture.

5.3 Igneous-sedimentary contacts

One of the key aims of the thesis was to establish the direct and indirect diagenetic effects at igneous-sedimentary contacts. A number of samples were, therefore taken across a variety of igneous-sedimentary contacts both from the Rosebank core and the Staffa Formation.

5.3.1 Peperite (P)

Rosebank

Thin sections of the igneous-sedimentary contacts within the Rosebank cores were examined in order to better characterise the contact types.

The top lava contact on the 213/26-1 core was shown to be a fluidal contact with small isolated juvenile clasts of lava within the sediment. These small clasts show highly fluidal, elongated and stretched morphologies (Figure 5.23.A) and range in size up to ~ 15 mm long. They are composed of finely crystalline basalt with plagioclase microcrysts. Well developed chilled margins are seen on both the main lava unit as well as the clasts. The surrounding sediment is very fine grained volcaniclastic lithic wacke comprising sub-rounded to sub-angular quartz (up to 2 mm across), feldspar crystals (up to 1 mm across) and dark black to brown basalt clasts set in a palagonitised glass and clay-rich matrix. There is no change in the mineralogy of the sediment closer to the igneous contact. Vesiculated regions (up to 2 mm across) are present within the matrix of the sediment. These regions contain several circular amygdales linned by palagonite and filled by clays.

Samples at the top of the 213/26-1 core were initially interpreted as a fluidal contact; however, on closer inspection, several small clasts of basalt observed within the sediment indicating the more peperitic nature of the contact. The fluidal shapes to the clasts along with the well developed chilled margins suggest hot emplacement. The clasts are well dispersed throughout the host sediment indicating intimate mixing between the volcaniclastic sediment and the igneous component.

The vesiculated regions within the sediment could be explained in a number of ways. Firstly, they may represent altered vesiculated scoria that has been incorporated

into the sediment. This scoria has then altered to palagonite and then to clay minerals. Alteration has reached completion so that only the fluidal shape and vesiculated texture remain and the clast is largely indistinguishable from the matrix of the sediment. These scoria fragments may be associated with the basalt lava; however, much of this lava appears fresher with alteration having not reached completion. It is possible that small fragments entrained within the sediment could experience greater alteration due to the greater surface area and therefore, a greater rock to fluid ratio. However, there are basalt clasts caught up within the sediment that are smaller than the vesiculated regions but have not been completely altered. A second possibility is that the vesiculated ash may be unrelated to the basalt contact and could simply have been reworked into the sediment, and therefore explaining the range in alteration levels. However, the regions have fluid morphologies with little evidence of erosion or transportation. The final possibility is that vesiculated areas could represent sediment vesiculation (c.f. Skilling et al., 2002; Hole et al., 2013). This would indicate that the sediment had been fully fluidised and would agree with the dispersed nature of the juvenile basalt clasts. However, it is unclear why vesiculation would be limited to small well-defined regions within the sediment.

The peperite at the base of the 213/26-1 core (Figure 5.23.B) is slightly different to the peperite observed at the top of the lava flow. Small isolated regions of sediment are entrained into the base of the lava. The lava itself has a greater degree of alteration and has a green/brown colour as a result of clay alteration. Amygdales are either filled by calcite, complex layers of clays, a mixture of both or in places, sediment. The sediment comprises predominantly rounded to sub-angular grains of quartz and feldspar, with rare siltstone lithoclasts in calcite cement. The sediment is mixed with finer grained sediment that has a clay rich matrix. There are no induration effects (discussed in Chapter 4) at the contact.

The multiple amygdale fills suggest that there have been several phases of pore-filling fluids. Amygdales closer to the contact tend to be filled with either sediment or clays, whereas amygdales further from the contact tend to be filled with calcite. The amygdales that are a mixture of both phases tend to have linings of clay and are filled by calcite implying that the calcite was a late stage diagenetic phase.

Staffa Formation

These peperite textures are also found onshore within the Staffa Formation. Both fluidal and blocky lithofacies are present. The peperite from the Carraig Mhor locality resembles that of the 213/26-1 well peperite. The lava is similarly altered to clay minerals and has a greenish appearance. Lava clast shapes are fluidal (Type 4) with inclusions of sediment caught up within the lava (Figure 5.23.C). Where the peperite facies is more blocky (Type 2) the sediment appears to be more coherent with rafted blocks being caught up within the lava. Many of the blocks retain sedimentary structures such as bedding or laminations. The lava itself is much less altered and often lacks significant chilled margins (Figure 5.23.D).

At Carraig Mhor, the peperite changes from a fluidal type to blocky types over cm scales. As discussed in Section 4.8.7, this change in texture may be due to a number of factors. For the Carriag Mhor peperite, sediment competency and water content have the largest influence on the type of peperite produced. Where sediment is more coherent, fluidisation cannot occur and insulating vapour films do not protect lava clasts resulting in brittle fragmentation (Skilling et al., 2002.)

5.3.2 Straight contacts

Straight contacts are seen in several places throughout the Rosebank core and within the Staffa Formation. At a mineralogical scale the contact is defined as being a straight sharp transition from the igneous rock into the sedimentary rock. The igneous rock often has a glassy chilled margin at the contact. This glass in most cases has extensively altered to palagonite and then to pore filling clays. The number of amygdales also increases towards the contact, with their morphology becoming smaller and more elongate. Amygdale fill consistently switches from calcite to clay and or sediment filled towards the contact (Figure 5.24.A1).

The sediments underlying straight contacts in this study ranged from very fine grained mudstone and coals, which were common onshore, to volcaniclastic lithic wackes more commonly found offshore. All of the sediment rock types were sampled and examined petrographically, to determine the effects of the igneous body. None of the sediment rock, regardless of composition, showed any significant thermal effects

across the contact. No evidence of melting or calcite cementing that has previously been found in other studies (Grove et al., 2014). Increased compaction was noted due to the weight of the overlying igneous body. Quartz and feldspar grains often showed signs of strain and grain boundaries showed evidence of dissolution with suture contacts. However, the amount of dissolution to the framework grains does not appear to significantly decrease with distance from the contact. In more porous lithologies there was a slight increase in the amount of clay matrix towards the contact. However, this may be a result of later stage dissolution and remobilisation of the glassy chilled margin within the igneous body rather than a direct effect from the contact. Diagenetic fluids may also be focused along contacts heightening dissolution and clay precipitation

The contact between the lava crust and the overlying volcaniclastic / peperitic unit in the 213/27-2 well was examined in more detail. The contact was interpreted as a straight contact due to its straight nature and well developed chilled / altered margin (Figure 5.24.A2), however this interpretation is limited by the width of the core. This contact is unusual in that the peperitic unit "overlies" the lava. The nature of the contact implies that the lava intruded the overlying volcaniclastic sediment and chilled against it. Therefore, the juvenile basalt clasts within the peperite may be related to the main body below.

5.3.3 Irregular and fluidal contacts

In Section 4.8.3, irregular contacts were defined as resembling straight contacts that were locally discordant to bedding, whereas fluidal contacts are characterised by their fluidal morphology. Petrographically, irregular contacts are difficult to identify if no sedimentary structures can be accurately determined. The top of the 213/26-1 core was identified in hand specimen as being an irregular contact as it appears relatively straight but cross cuts the sediment at an oblique angle even when well deviations are taken into account. However, at a microscopic scale the contact was revealed to be more fluidal in nature (Figure 5.24.B1) with minor peperitic textures developed.

Fluidal contacts are characterised by irregular edges of the igneous body which display well-developed chilled margins (Figure 5.24.B2). As observed at straight contacts amygdales become smaller towards the contact and are often filled by sediment or pore filling clays. Fluidal contacts occur most commonly in association with fine

grained sediment that shows very little evidence of thermal effects. Similar to straight contacts, no melting of framework grains, such as feldspars, occurs. However, alteration within these sediments is prevalent, especially in the offshore examples (213/26-1 well). Therefore, any direct thermal effects may have been overprinted by later diagenetic fluids.

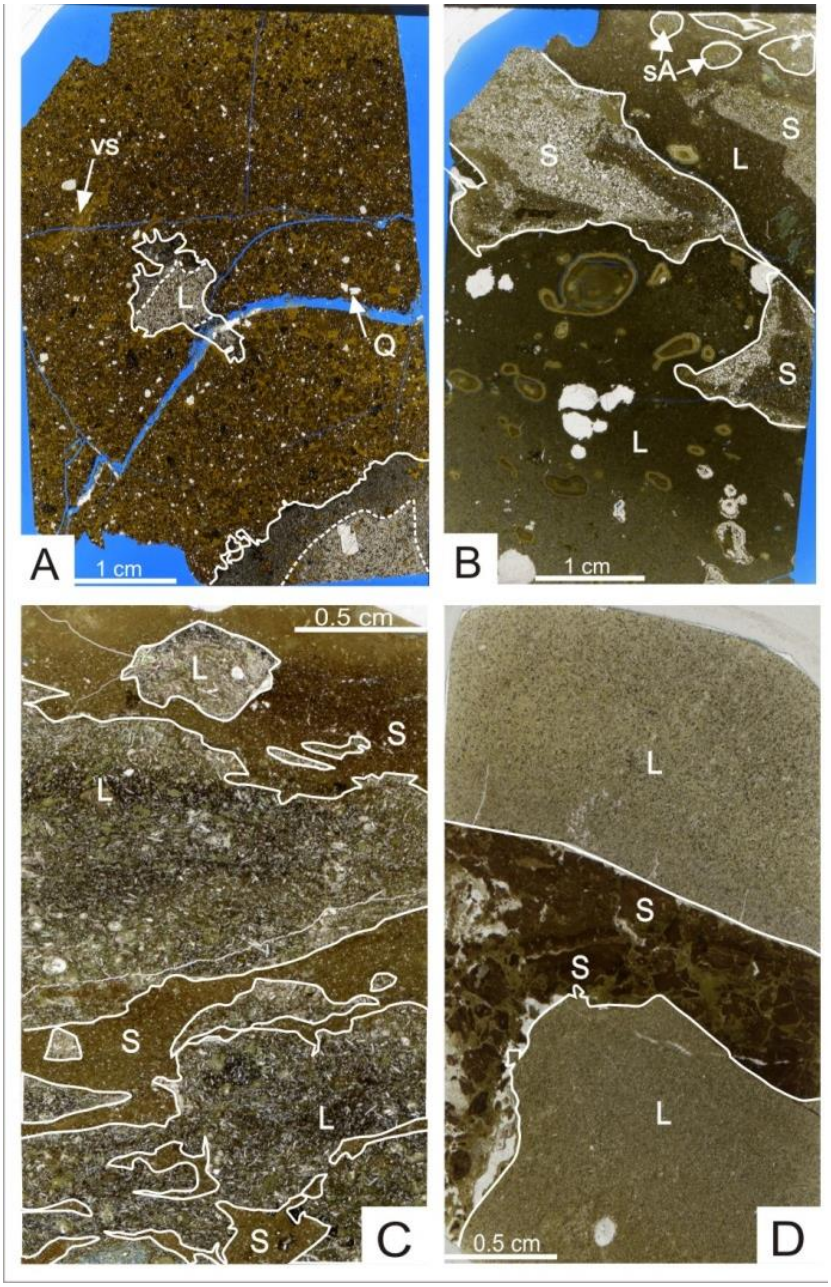

Figure 5.23: Peperitic contacts**. A:** Peperite from the 213/26-1 well, depth of 2881 m. Fluidal basalt clast completely surrounded by volcaniclastic sediment. Note the chilled margin on the basalt (L) denoted as a dashed line. Quartz (Q); possible sediment (VS). **B:** Peperite from the 213/26-1 well, depth 2887.7 m. Altered basalt lava (L) with complex clay and calcite filled amygdales; sediment filled amygdales (sA); fluidal shaped inclusions of sediment (S). Sediment matrix is mixture of clay (brown) and calcite (white). **C:** Fluidal peperite from the Carraig Mhor section. Fluidal, shape, altered basalt lava (L – outlined in white) surrounded by fine grained volcaniclastic sediment (S). **D:** Blocky peperite from the Carraig Mhor section. Bedding can be seen in some of the sediment "clasts". All thin sections have been stained blue for porosity.

5.3.4 Passive contacts

Passive contacts were identified in a number of locations both on and offshore. They are characterised as being sharp, sometimes erosional contacts and differ to straight contacts because they form when the igneous body is cold. Sediment in fills the lava topography but no direct mixing between the lithologies occurs. Both the lava and the sediment show no thermal effects such as chilled margins or baking.

The igneous-sediment contacts at the base of the 213/26-1z core comprise clasts of lava within a siltstone matrix (Figure 5.24.C). Some lava clasts have an alteration halo around the edge of the clast; however, there is no evidence to state that this is a chilled contact.

Two passive igneous-sediment contacts occur at the base of the 213/27-2 core. The base of the lava passively fills depressions in the underlying sediment without disturbing sedimentary structures such as bedding (Figure 5.24.D1), similar to the passive contacts seen on Mull. A small darkened layer is seen at the base of the lava, which was originally interpreted to be a chilled margin at its base of the lava; however, closer inspection of the thin section reveals small fragments of rounded quartz and therefore the blackened horizon is now interpreted as sediment. Calcite veins cut down through the base of the basalt. In the basalt, these take the path of least resistance noticeably along vesicle walls. The veins then cut down into the sediment at a uniform angle suggesting they developed under tensile shear stress (pers. comm. Eddie Dempsey). The veins are consistent through the darkened sediment but fan out within the underlying sediment. Here quartz grains are totally surrounded by the calcite. This suggests that the sediment was not fully lithified with the calcite vein was injected. However, through the darkened sediment the vein is confined suggesting that the dark sediment has a higher rigidity than the underlying sediment. This could be evidence for minor sediment baking below the lava, similar to that found in Namibia and the Faroes as discussed in Section 4.8.5. However, as the sediment is so fine grained it is difficult to tell if there are any thermal effects on the sediment, or what is causing the extra rigidity.

Amygdales at the contact are partially filled by sediment (Figure 5.25). As the lava moved over the substrate sediment was entrained within the vesicles. Pore filling clays then filled the remaining pore space within the vesicle.

The second passive contact seen within the 213/27-2 core is shown in Figure 5.24.D2. It is unusual as the contact is between siliciclastic sediment with no volcanic detritus. A darkened halo can be seen within the sediment, which was initially thought to be due to pore filling clays; however, this was not the case. Instead, the sediment is completely cemented by calcite (Figure 5.26) and the darkened zone simply represents a slightly smaller grain size.

5.4 Identifying the Rosebank contact types

A number of contacts within the Rosebank core proved difficult to identify at hand specimen scale. Each of these contacts were sampled, to better characterise the contact type.

5.4.1 213/27-2 peperite identification

While the peperite in the 213/26-1 well and onshore was easy to identify some other rocks proved more challenging. The rocks above the basalt lava flow in the 213/27-2 core were tentatively identified as peperite during core viewing. Thin section scans where subjected to image analysis techniques which can strip out alteration and allow the original primary mineralogy to be examined (Figure 5.27).

Basalt lava clasts have extremely fluidal shapes and were thoroughly mixed with the altered clay rich sediment (Figure 5.27.A2). In places alteration appears to be focused along the edge of the juvenile basalt clasts (Figure 5.27.B2). The basalt lava is extremely altered with much of the interstitial glass having completely altered to pore filling clays. The sediment is extremely fine-grained claystone that contains darker more, organic-rich regions. Calcite alteration is prevalent throughout the samples. In places, the calcite fills vesicles within the basalt clasts (Figure 5.27.A3) but can also be found filling porosity within more organic rich layers in the sediment.

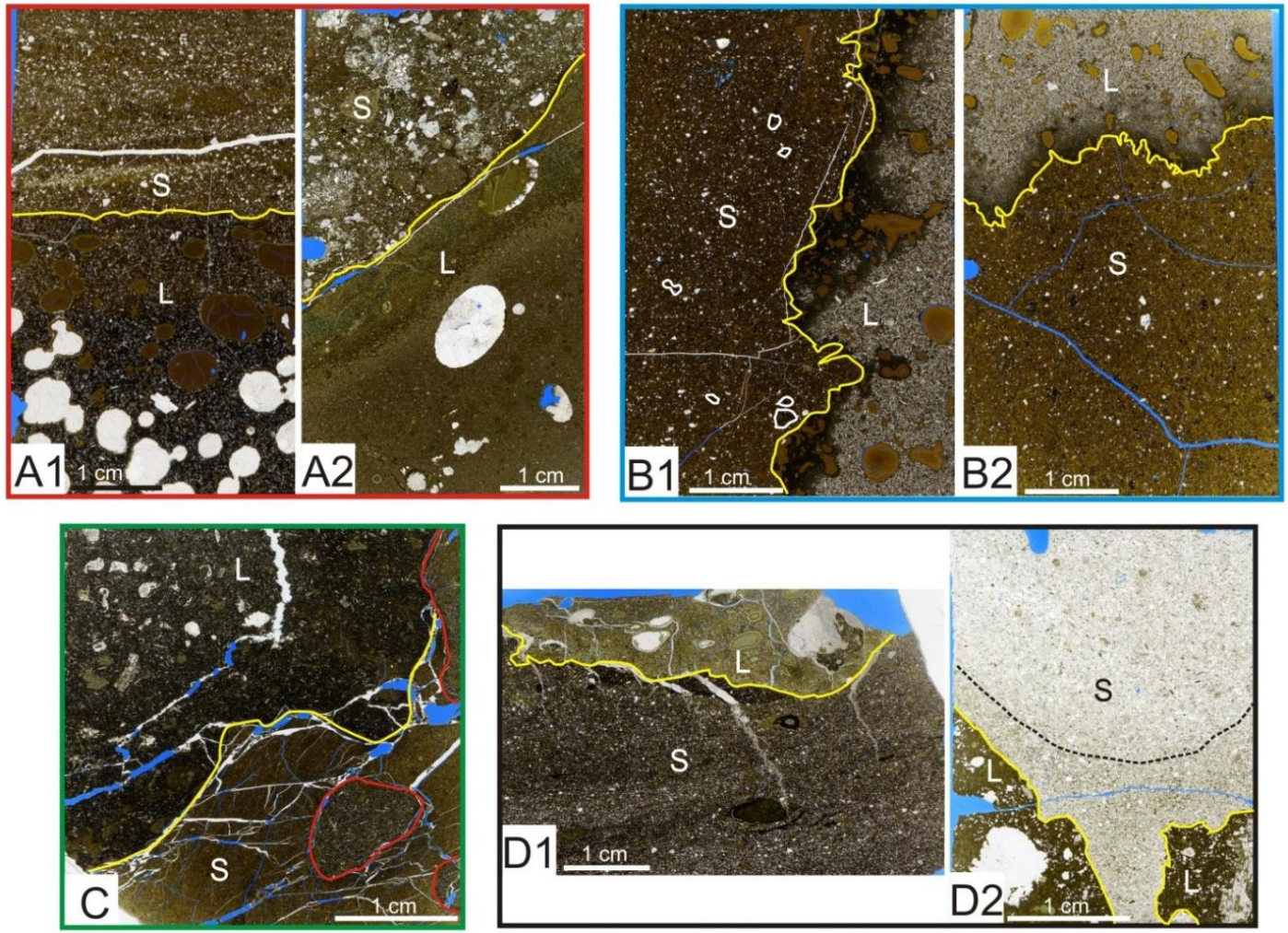

Figure 5.24. Basalt- sediment contacts are shown in yellow. **A1:** Straight contact where sediment passively in fills lava surface. Transition from calcite to clay amygdales approaching contact. Well 213/26-1, 2880.2 m. **A2:** Straight contact between sediment and lava. Well 213/27-2, 2875.1 m, deviation ~ 25°. **B1**: Irregular – fluidal contact with well-developed chilled margin. Dispersed peperite as juvenile lava clasts in sediment (outlined in white). Well 213/26-1, 2880.6 m. **B2:** Fluidal – irregular contact with chilled margin. Well 213/26-1, 2880.9 m. **C:** Irregular contact. No evidence of thermal effects. Lava clasts are outlined in red. Well 213/26-1z, 3014 m, ~ 34.5° deviation. **D1:** Passive lava-sediment contact. Glassy chilled margin has completely altered to clays. Sediment comprises quartz, feldspar, organic and woody fragments and shows no thermal effects, with bedding undisturbed. Note unusual calcite veining. Well 213/26-1, 2888.4 m. **D2:** Passive cold contact. Quartz and feldspar rich sediment has filled fracture within the basalt. Lava is altered to clays. Sediment matrix changes from calcite to clay at contact (dashed line). Well 213/26-1, 2888.2 m.

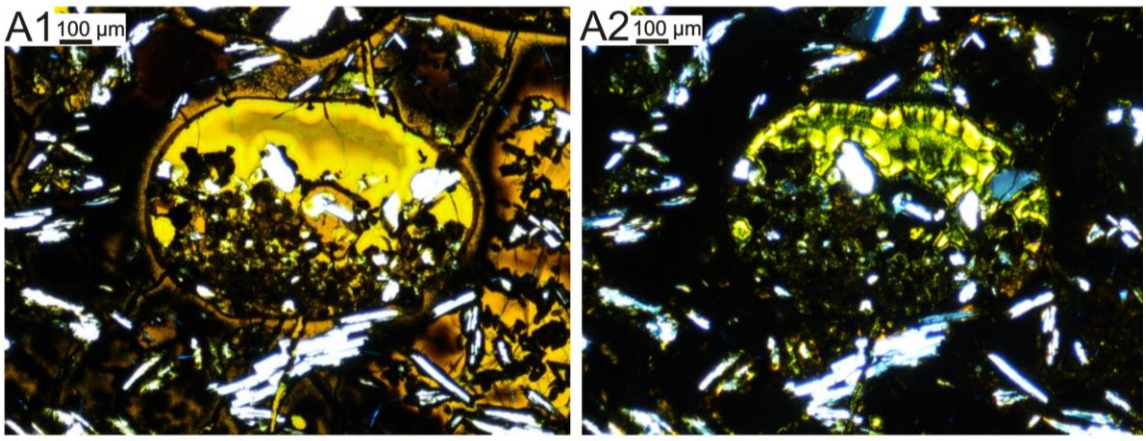

Figure 5.25**:** Amygdales partially filled by sediment in 213/27-2 core**. A1** (ppl): Quartz and feldspar (white grains within amygdale) collect in the base of the vesicle. **A2** (xpl): Altered palagonite and clays (bright yellows) fill the remaining porosity around the sediment grains.

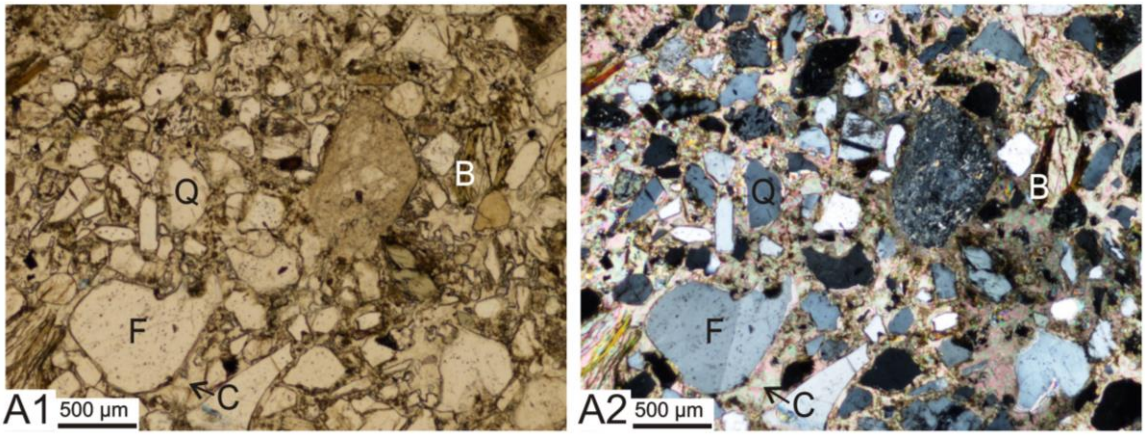

Figure 5.26: Photomicrograph of sediment 1 cm above a passive contact within the 213/27-2 core. **A1** (ppl): Quartz (Q), feldspar (F), biotite (B) and lithoclasts with a calcite cement (C), ppl. **A2**: Calcite cement fills all porosity, xpl.

The fluidal nature of the basalt clasts would suggest their juvenile origin and suggests the rock is a peperite rather than a volcaniclastic epiclastic sediment or altered lava flow top. The alteration is much greater than in the other peperite facies found within the Rosebank cores as well as onshore peperite. Much of the basalt clasts have started to alter with often only the cores of the clasts having not reached completion (Figure 5.28.A1,2). Vesicles have been lined by palagonite and filled by clays. Porosity created by dissolution of the basaltic glass, towards the edges of clasts, has been filled by clays. Pore space in the host sediment, has also been filled by clays. Any remaining interstitial porosity within the basaltic clasts has been filled by late stage calcite. In places zeolites fill moldic porosity (Figure 5.28.B1,2).

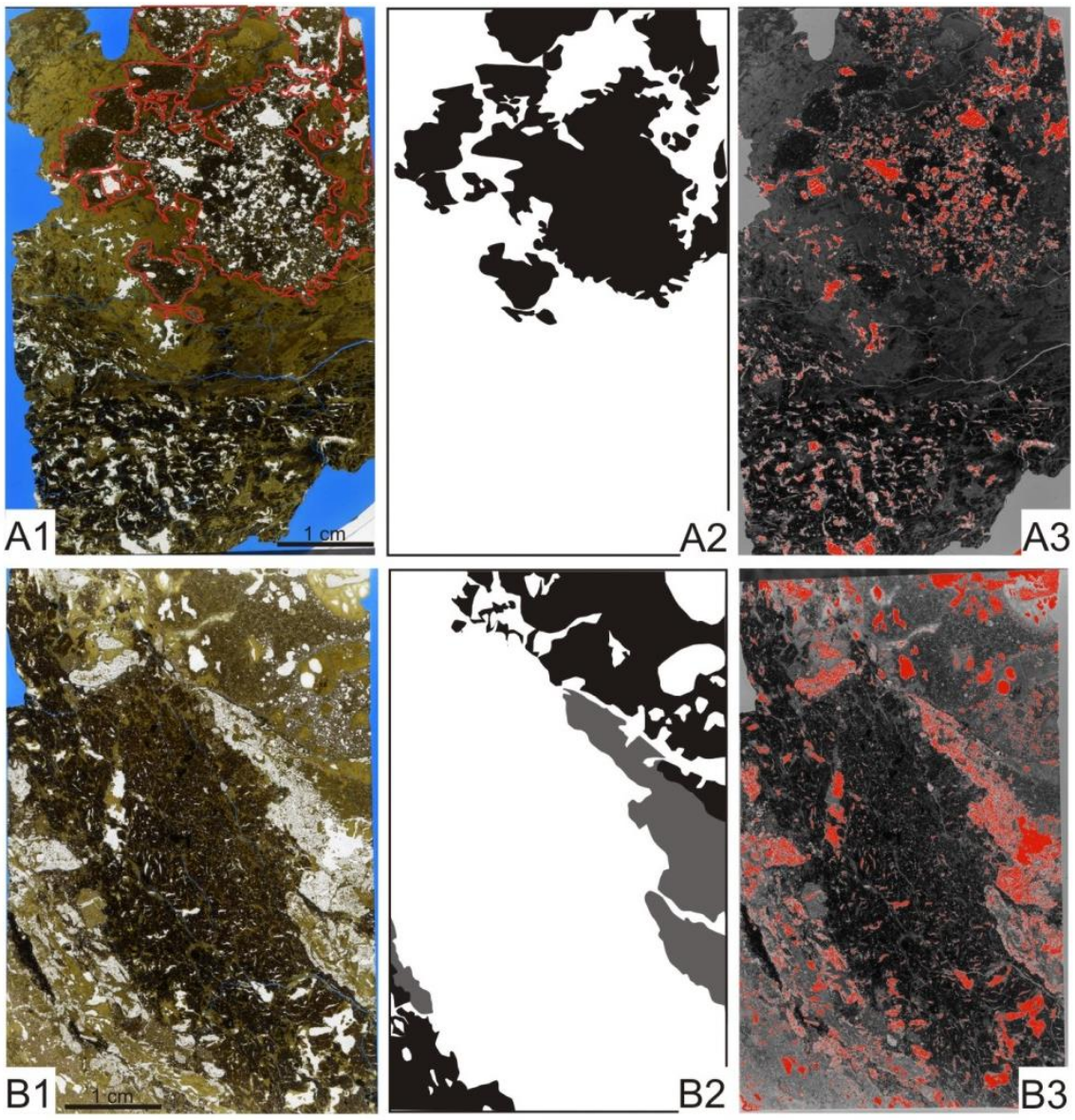

Figure 5.27: Peperite from the 213/27-2 well. **A1:** Scan of thin section from a depth of 2874.1 m. Juvenile basalt clast outlined in red. **A2:** Black area highlights the fluidal texture of the juvenile basalt clast. White areas are sediment. Grey areas are so altered that they cannot be properly identified. **A3:** Red highlights calcite alteration over print. Circular amygdales are noted as well as clays minerals replacing areas of altered matrix. **B1:** Scan of thin section from 2874.5 m. Juvenile texture is difficult to identify due to alteration. **B2:** Black highlights juvenile basalt clast. Grey areas are possible basalt but alteration overprint makes identification difficult. **B3:** Red highlights the prevalent calcite alteration.

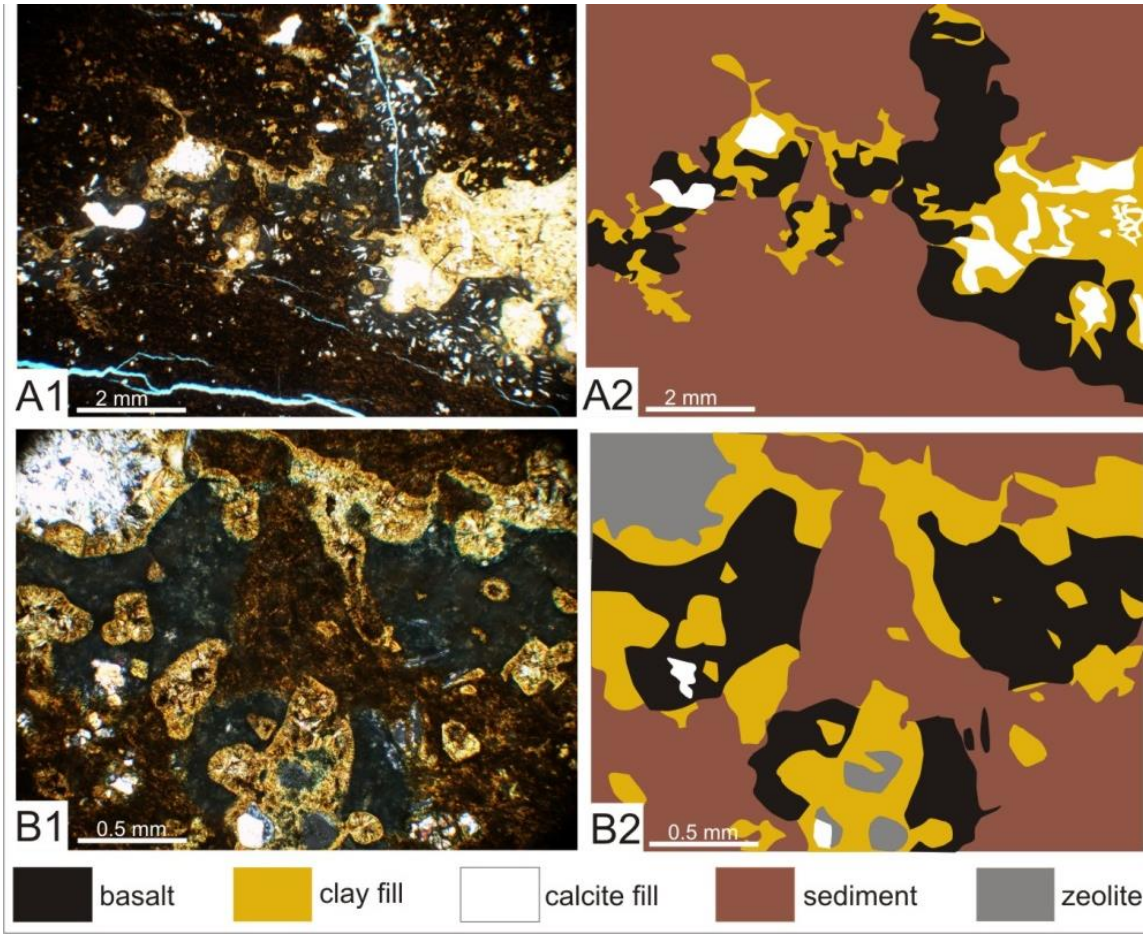

Figure 5.28: Photomicrographs of peperite (**A1**(ppl) **B1**(xpl)) and sketch maps of phases (A2, B2). from the 213/27-2 well at a depth of 2872.9 m. In both images the fluidal shape of the basalt is seen. Clay, calcite and zeolite alteration is focused towards the edges of clasts. Spherical clay alteration is seen in B1.

5.4.2 The top contact peperite problem

Peperite with a chilled lava flow contact, was identified at the top of lavas in the 213/26-1 and 213/27-2 cores. This is unusual as in order for peperite to form here the lava must intrude into the sediment. The 213/26-1 well has a deviation of ~ 0.93 – 1.59° at the depth of the peperite while the 213/27-2 well has a larger deviation of around 25.57° (pers. comm. Rosebank Team 2013). Despite the larger angle of deviation in the 213/27-2 well the peperite unit will still sit above the underlying lava. Therefore, the lavas must be invasive or alternatively, represent a shallow sill. The lavas are not interpreted to be an apophysis of an overlying flow (c.f. Vosgerau et al. 2010) as in both cases the overlaying crystalline lava is more than ~10 m above.

5.4.3 213/27-2 fracture contact

The igneous-sediment contact at depth of 2877 m in the 213/27-2 core was interpreted to be sediment entrained within a basalt fracture. Parts of the fracture appear to have formed in a cold, brittle regime with sharp, angular edges to the basalt lava clast (Figure 5.29.A1,2). There is no evidence of chilled margins or thermal alteration of either the basalt or the sediment. Small angular fragments of basalt can also be found entrained within the sediment infill. Further into the fracture both brittle clasts and fluidal shaped clasts are present (Figure 5.29.B1,2). The more rounded clasts have a distinctive altered margin, while more angular clasts show no obvious alteration. At the base of the fracture the lava behaves in a more ductile fashion and displays a fluidal morphology, indicating it was still hot during emplacement (Figure 5.29.C1,2).

In the centre of the fracture both fluidal and brittle clasts exist side by side. Therefore, these contacts were sampled to better understand them (Figure 5.30.A). The chilled margin at the edge of the fluidal clasts comprises more interstitial glass than the crystalline clast core. This glass appears to have altered more than the clast interior (Figure 5.30.B). The fresher lava clasts have irregular contacts that passively interact with the surrounding substrate. The cold crystalline clasts display much less alteration than the fluidal shaped clasts (Figure 5.30.C1,2). The fluidal contacts appear to have no influence on surrounding sediment, with no evidence of thermal effects (Figure 5.30.D1,2). However, the supposedly cold angular crystalline clast has a small layer of fine grained darkened sediment underlying it (Figure 5.30.E1,2). This sediment resembles that found under the lava at the base of the 213/26-1 core as described earlier. As this sediment differs from the underlying sediment it is suggested that it was transported attached to the basalt clast. If this sediment does represent a small, indurated layer beneath the volcanic clast this would imply the clast was hot. However, no thermal effects such as chilled margins or alteration zones are seen surrounding the basalt clast itself making a thermal influence unlikely.

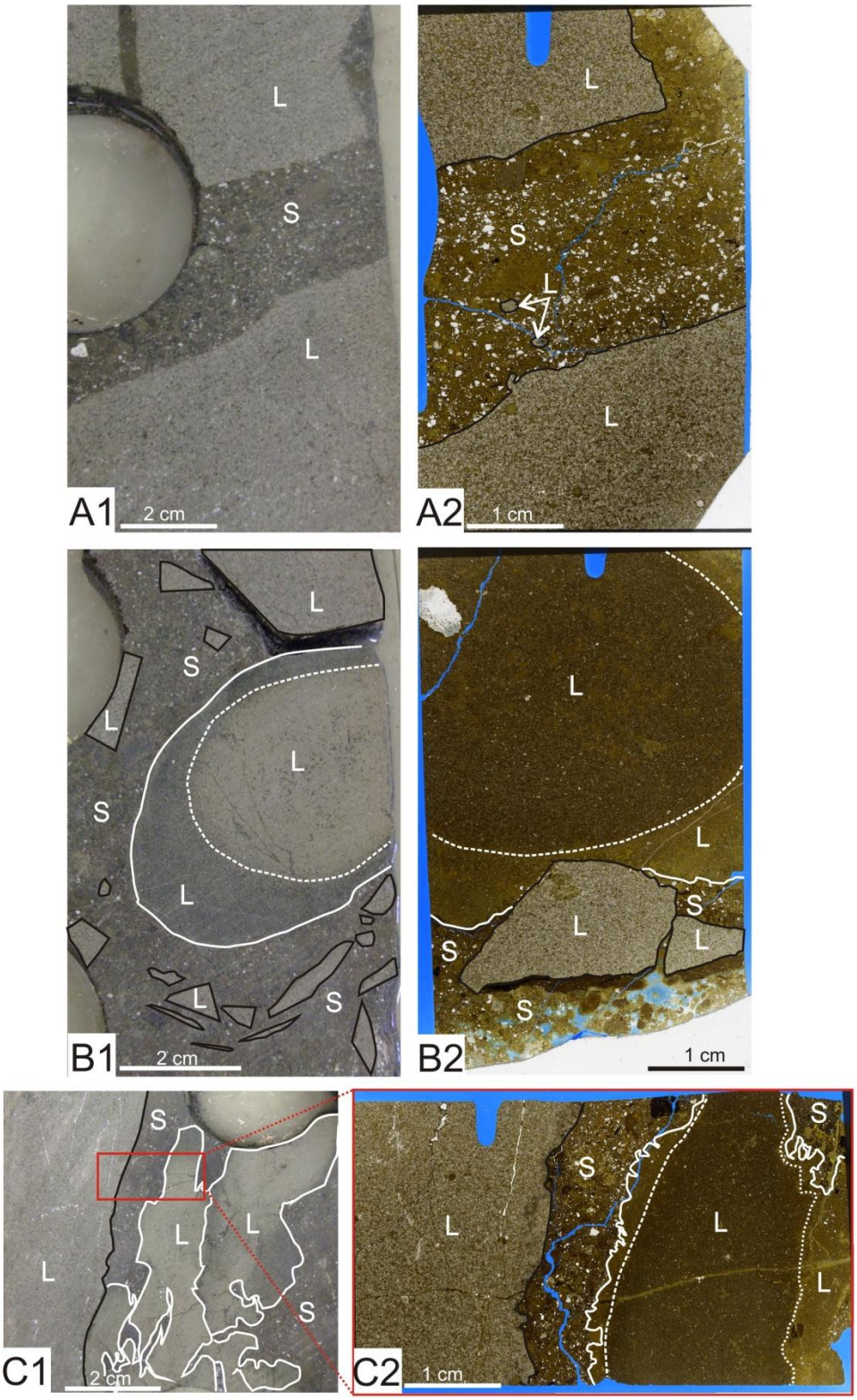

Figure 5.29: Lava (L) sediment (S) contacts in well 213/27-2 between depths of 2876.7 m – 2877 m. Cold contact (brittle) shown in black. Hot contacts (ductile) shown in white. Chilled margin defined by dashed line. **A1:** Core photo of brittle fracture (2876.7 m). **A2:** No chilled margin on lava implying cold contact. Angular clasts of lava entrained in sediment. **B1:** Core photo showing the close proximity of cold and hot lava clasts (2876.9 m). **B2**: Cold lava clasts appear fresher than altered hot clasts. Chilled margin has altered to clays. Thin section taken from half cut so does not precisely match the core photo. **C1**: Core photo of relationship between fluidal hot and brittle cold contacts (2876.7m). **C2**: Thin section scan of area within red box. Fluidal lava is much more altered than brittle cold lava.

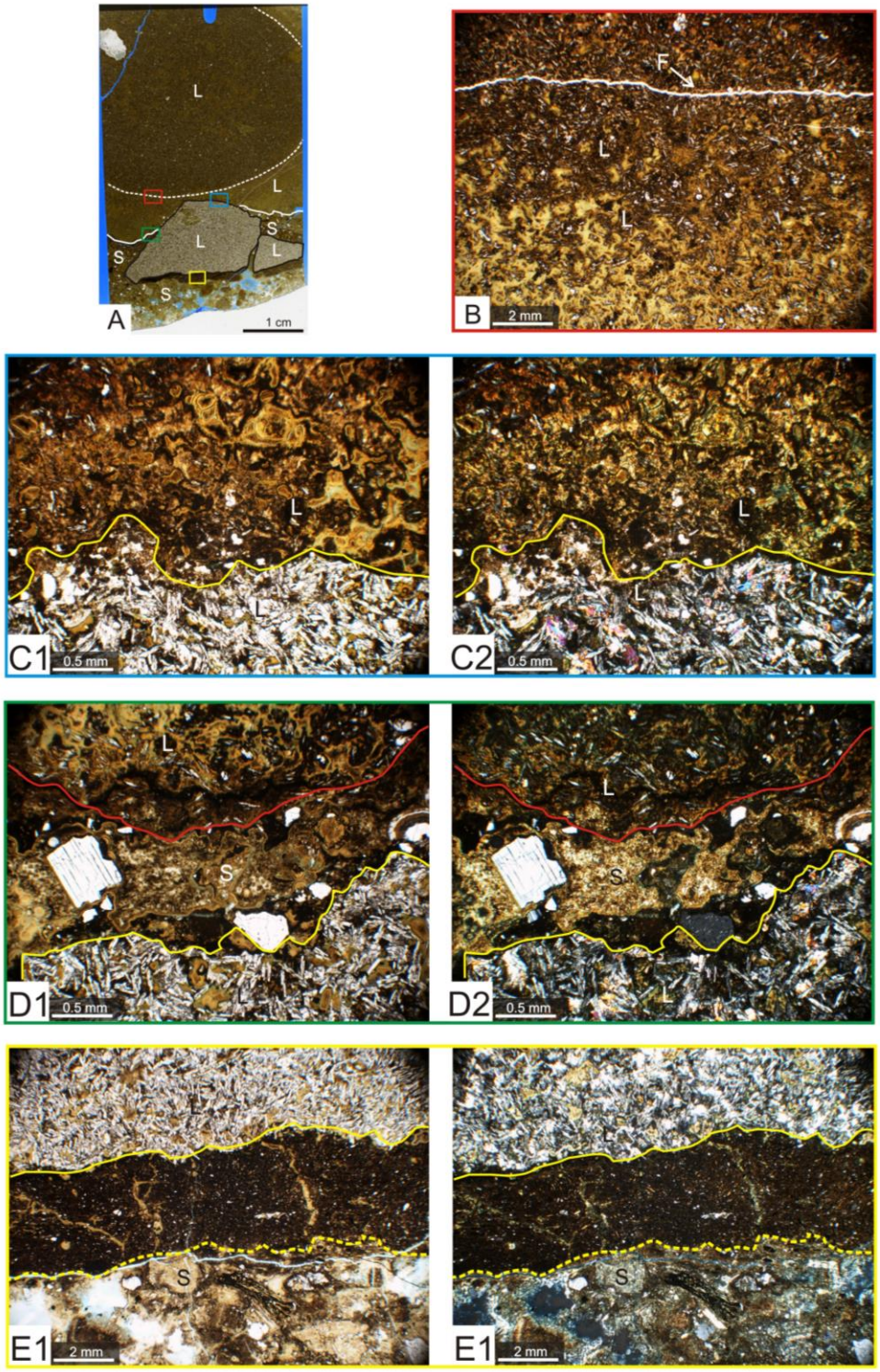

Figure 5.30**:** Photomicrographs highlighting the contrast between the hot and cold contacts within the 213/27-2 well. Red line defines the edge of the altered hot clast, while yellow defines the edge of the more crystalline clast. Darkened, fine grained sediment is outlined in dashed yellow. **A:** Thin section scan with coloured boxes highlighting the locations of the photomicrographs (F- a fracture in the slide). **B:** Altered margin on a hot contact. The upper portion of the image is more crystalline and alteration of interstitial glass is less prevalent. At the clast margin all of the glass has been altered to palagonite (ppl image). **C1** (ppl); **C2** (xpl): Highlights the contrast in alteration between more crystalline lava clast and the very altered glassy lava clast above. **D1**: Relationship of both clast boundaries with the surrounding sediment. Sediment matrix comprises clays similar to those forming from the interstitial glass in the upper volcanic clast. **E1** (ppl); **E2** (xpl): Darkened sediment layer underlying the crystalline clast.

5.5 SEM characterisation of mineral phases and textures

Considerable alteration of the rocks leads to difficulties in identifying grain boundaries, original pore space and clay mineral phases. The Scanning Electron Microscope (SEM), using the method outlined in Section 2.5.1, allowed these issues to be better resolved and the main diagenetic phases to be identified. Each mineral phase will be described and interpreted in detail and the diagenetic sequence determined. Rosebank core samples experienced significant charging (Section 2.5.1) and therefore backscatter and EDAX analysis were limited within these samples.

5.5.1 Quartz

Mull

Quartz grains in all samples exhibited minor dissolution at grain boundaries, but suture contacts are common. Quartz overgrowths and cements are not generally present, with the exception of a patchy quartz cement in the siliciclastic quartz arenite found at the Carsaig Arches (Section 4.5.1).

Rosebank

All quartz grains in the samples exhibit minor dissolution similar to that seen onshore. Suture contacts are common between quartz grains. Embayed contacts are also more common in the siliciclastic lithofacies in Rosebank than onshore.

5.5.2 Quartz interpretation

The quartz dissolution and minor suture contacts imply that the sample has undergone some compaction. Quartz overgrowths are a common diagenetic phase in sandstones and are often responsible for a reduction in porosity (Pittman 1972, Worden and Morad 2000, Zhou and Friis 2013). Quartz overgrowths form from pore waters saturated in silica (Leder and Park, 1986). Bloch et al., (2002) suggest that development of early clay rims will impede overgrowths as they eliminate nucleation sites for the silica. Therefore, the lack of quartz overgrowths within the samples could be due to the early stage development of clays.

5.5.3 Flint

Mull

Two types of flint clasts occur in the Mull samples (Figure 5.31.A) as described above. Type 1 flint exhibits extensive dissolution along grain boundaries but only limited alteration within the interior which results in a pitted texture. Type 2 flint has similar dissolution along grain boundaries but the grain interiors are more altered. Calcite and phosphorous-rich minerals (e.g. fluorapatite) replace clasts margins Figure 5.31.B,C) while alteration in the interior is focused on fossils. Moldic porosity is commonly filled by clay minerals and calcite (Figure 5.31.D,E). Delicate lace-like structures within the flint are commonly preserved (Figure 5.31.F).

Rosebank

No flint is found within the Rosebank samples.

5.5.4 Flint interpretation

The greater degree of alteration in Type 2 flint may be a result of the moldic porosity providing better pathways for diagenetic fluids to infiltrate the clast. The flint is Cretaceous in age (Williamson and Bell, 2012) and has been previously buried, uplifted and eroded, and therefore, has been exposed to earlier diagenetic fluids prior to being included within the Staffa Formation rocks. Evidence for this is further discussed within Section 5.5.12. It is unlikely that even with minimal transport, delicate lace-like structures such as the one seen in Figure 5.31.F would survive erosion and consequently silica dissolution may have occurred. Dissolution may have exploited the flint, and in particular the pre-altered fossiliferous variety, over that of the quartz, due to its microcrystalline structure (Siever 1962).

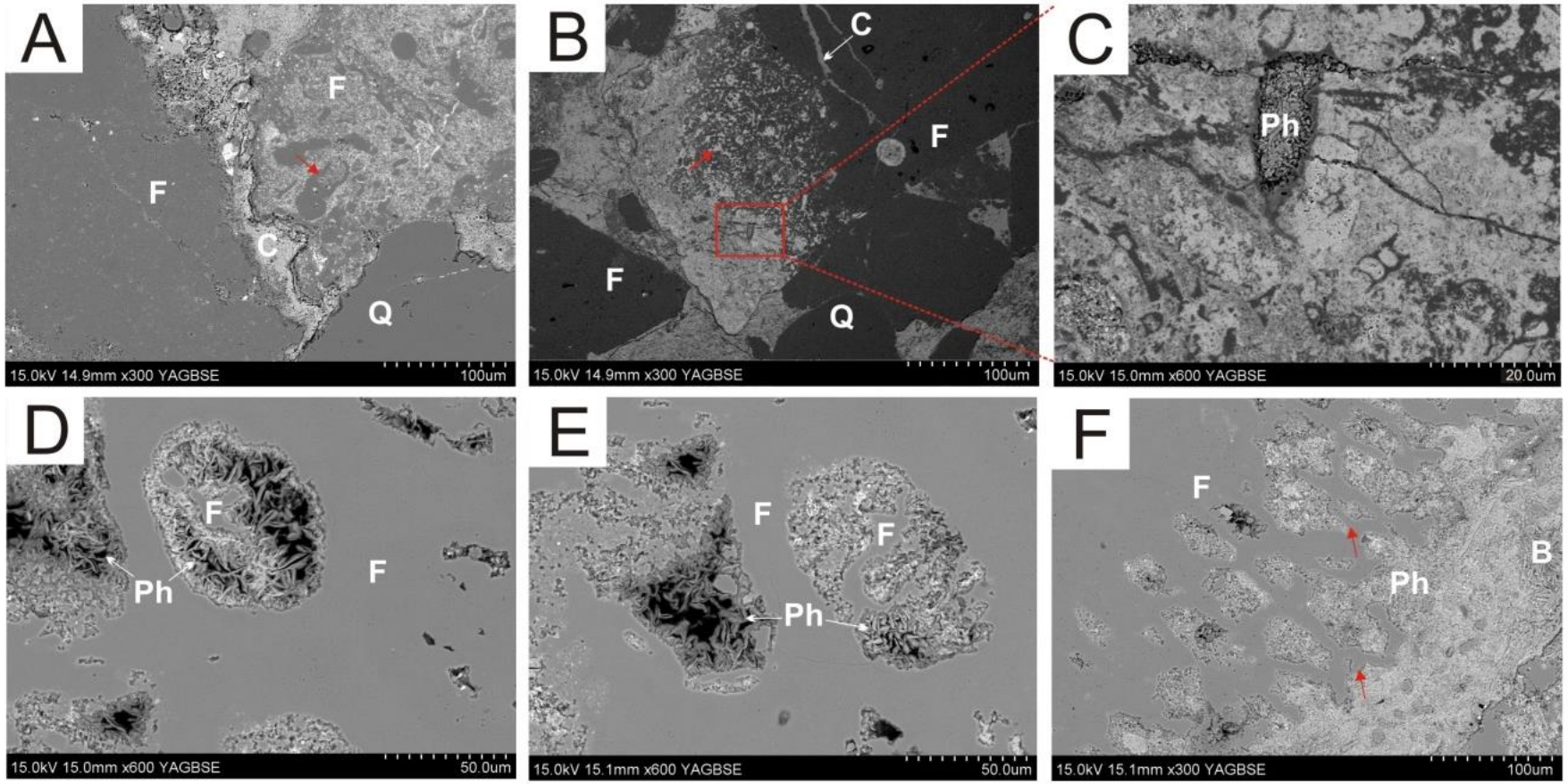

Figure 5.31: Backscatter images of flint. **A.** Flint (F); type 1 on left; type 2 on right; fossil arrowed; quartz (Q); calcite (C). Note type 2 flint is much more altered**. B**. Fluorapatite replaces flint clast. Fractures are filled by calcite (white arrow). Moldic porosity filled by calcite (red arrow). **C**. Close up of flint clast with considerable alteration. Moldic porosity filled by phyllosilicates (Ph). **D.** Moldic porosity filled by phyllosilicates. **E**. Intra granular flint dissolution. **F**. Delicate lace-like structures at the edge of the flint clast.

5.5.5 Volcanic Clasts

A variety of predominantly basaltic volcanic rock clasts are present within the samples. These are divided into three main types: crystalline lava clasts, crystalline pyroclasts, and ash. All three clast types are found in the Mull rocks, whereas only lava clasts and ash are found within the Rosebank rocks. There are no obvious differences in alteration between Staffa and Rosebank, and, therefore both rock will be examined together.

5.5.5.1 Crystalline basaltic lava clasts

The crystalline lava clasts are generally the least altered of all the basaltic clast types, but they still show a variety of alteration textures. The groundmass in the more-altered clasts has completely altered to clay minerals. In some cases, clasts can only be identified by clay pseudomorphs and by remnants of plagioclase phenocrysts. A common alteration texture identified in Section 5.4.3 was where clasts cores altered more than at the grain boundaries. Under the SEM this texture was often used to distinguish relict basaltic lava clasts from the altered rock matrix. While clast margins do show some concave-convex dissolution textures they remain crystalline and are composed of a sodium-rich silicate such as albite. In places this material appears to have been precipitated on the outside of the basalt clast or could form from leaching of mobile trace elements towards the edges of the clast (Figure 5.32.A). Despite the high levels of alteration, clasts typically retain their strength and do not easily compact around framework grains. In the less altered basaltic clasts the interstitial glass has partially altered; however, the feldspars crystals are unaltered and only exhibit minor dissolution at grain boundaries (Figure 5.32.B).

5.5.5.2 Scoria lapilli pyroclasts

This clast type is only found in Staffa Formation samples. They are generally more altered than the crystalline lava clasts, and there is less variation in alteration textures. Extensive dissolution and replacement has resulted in complex diagenetic textures that overprint much of the original igneous textures. Clast boundaries even at the micron scale are difficult to resolve (Figure 5.32.C). As in the crystalline lava clasts, the glassy groundmass has been replaced by large, randomly orientated, clays that fill relict pore space. Clay plates nucleated on plagioclase feldspar microcryst surfaces and have grown into pores.

Intra-granular porosity has developed between clay fibres towards the centre of the pores. Figure 5.32.D). Axiolitic textures developed as clay nucleation fronts met; thus creating an interconnected network of clay minerals that have effectively destroyed localised porosity as the clays swelled (Figure 5.32.E). Plagioclase feldspar microcrysts within the pyroclasts are generally much more altered than those in the lava clasts, and have highly dissolved crystal boundaries. Diagenetic fluids exploited the dissolved regions of the feldspar crystals which has produced clay fibres that appear to have grown from inside the feldspar clast. Typically, only small remnants of feldspars remain (Figure 5.32.F). Titanium-rich minerals are dispersed throughout the groundmass. Commonly, the amygdaloidal clasts are the most altered as alteration is focused at vesicle walls.

5.5.5.3 Basaltic ash

A large amount of basaltic ash particles occur within the more vent-proximal primary pyroclastic rocks of Mull. Rare glass shards are found within the Rosebank volcaniclastic samples. Very little fresh volcanic glass was seen within the samples; with most completely altered to fibrous clays with radial titanium-rich bands (Figure 5.33.A). Tightly packed clay minerals coat the ash particles, presumably replacing gel palagonite, whereas more fibrous clays replace the fibrous palagonite and grow into pore space from the glass shard walls (Figure 5.33.B). Titanium oxides are concentrated into "strings" along glass shard edges as they cannot be incorporated into the clay minerals as they grow. This extenuates any relict dissolution textures present within the samples (Figure 5.33.C). Shard-like axiolitic textures are found highlighting a change from Fe to Mg rich clay minerals (Figure 5.33.D). This most likely represents alteration/ devitrification of the glass shards. The structures do not resemble those formed from microbial action (c.f. Cockell 2009) or root structures found in paleosoils.

5.5.6 Volcanic clast interpretation

Basaltic ash clasts are the most susceptible to alteration due to their glass texture and high surface area. Mafic glasses are more reactive than their silicic counterparts (de Gennaro et al. 2000).The chemical composition of the glass controls the authigenic facies produced and affects the kinetics of the alteration process (Khalaf, 2013). Vesicular pyroclasts are

more susceptible to alteration than less vesicular varieties. If vesicles are interconnected more diagenetic fluids can percolate through the clast, aiding alteration from the interior, out to the margins of the clast. Vesicle walls are also likely to be weaker and less crystalline, thus promoting vein development, as fluids follow the path of least resistance. The larger surface area of the vesiculated clasts results in greater rock to water ratios. Particles composed of volcanic glass are also more susceptible to compaction during diagenesis than crystalline lava clasts.

After burial basaltic volcanic glass first alters to gel palagonite, which lines pores. Fibrous palagonite then nucleates on this and grows outwards into the pore space. With increasing depth and temperatures (~80°C) palagonite is transformed into clay minerals such as smectite (Gifkins et al., 2005).

In vent proximal regions rocks are dominated by pyroclasts that were produced within a short time period and should have relatively uniform alteration. In medial and distal locations the range of alteration textures of volcanic clasts in the volcaniclastic lithic wackes is much higher, due to the greater range in clast compositions, morphologies and ages. Therefore, the clasts are all at different alteration states. Due to severe alteration it is typically impossible to separate out weathering alteration that may form at the surface, from the diagenetic alteration the clast experiences at depth.

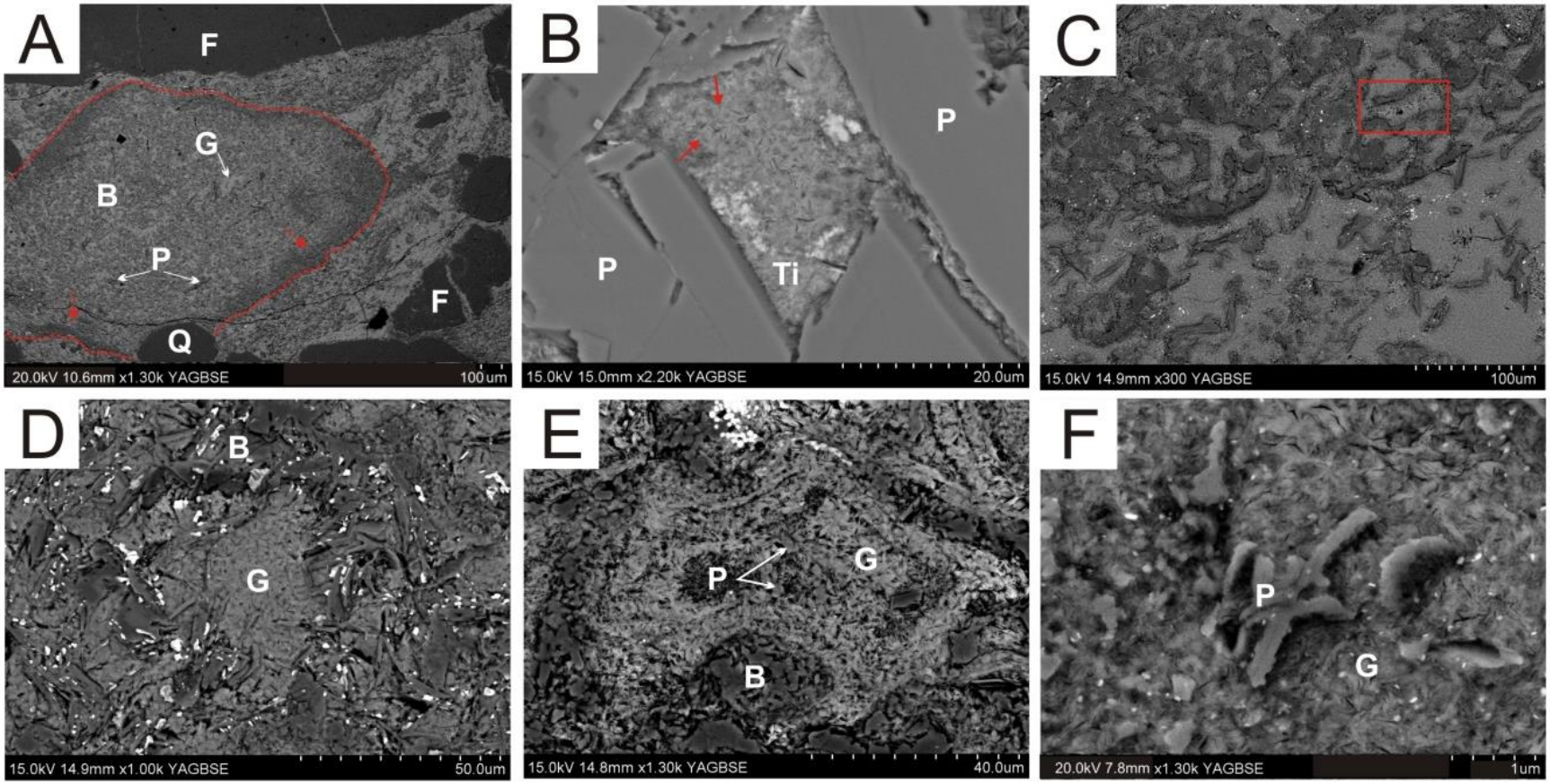

Figure **5.32**: Crystalline basaltic clasts and basaltic pyroclasts. **A:** vlW sample comprising: flint (F) and quartz (Q) and basaltic lava clast (B) with altered groundmass (G) and relict plagioclase pseudomorphs (P). The clast appears fresher towards the boundaries with K-rich material possibly accreted around the edge of the clast (red line and arrowed). **B**: Altered interstitial glass between plagioclase crystals (P). Clay grows from crystal walls into pore (arrowed). Titanium (Ti) from the glass is concentrated in titanium oxides. **C**: Extremely altered pyroclasts with relict feldspar. Clays replace the groundmass and grow into pores (red box). **D**: Interstitial glass (G) within a basalt crystalline pyroclasts (B). **E:** Small fragments of plagioclase form isolated islands within the fibrous network of clays (G). **F**: Small altered plagioclase microcrysts (P).

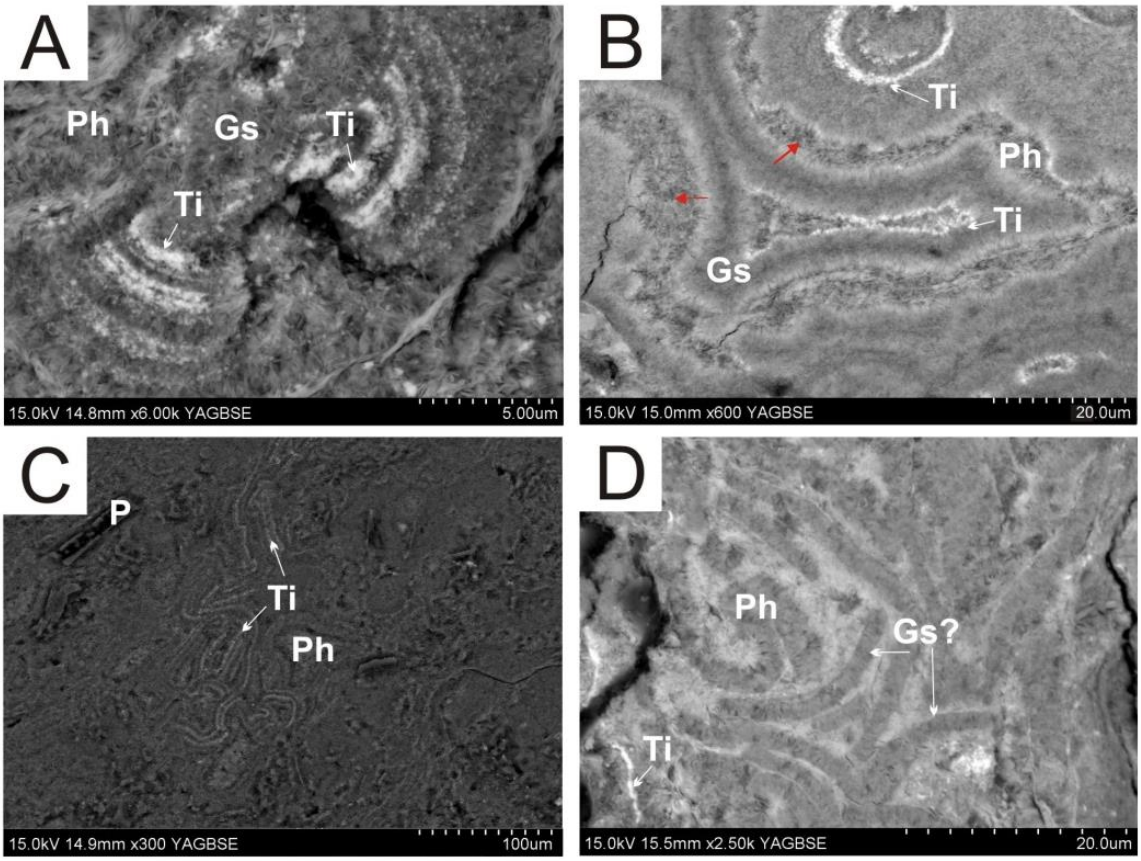

Figure 5.33: Backscattered SEM image of altered volcanic glass textures. A: Glass shard (Gs) that has altered to clays (ph) with titanium banding (Ti). **B:** Altered glass shard (Gs). Titanium (Ti) coats vesicle and shard edges. Dark Mg-rich tightly packed clay coats the shard, possibly replacing gel palagonite. More fibrous clays (Ph) grow from the vesicle walls into dissolved pore space (red arrows). **C:** Titanium (Ti) highlights relict dissolution texture. Pseudomorphs of plagioclase phenocrysts (P) are replaced by clays (Ph). **D:** Axiolitic texture developed in altered glass shards (Gs). Mg rich clays (dark), Fe rich clays (light).

5.5.7 Feldspars

Plagioclase and alkali feldspar crystals occur in most rocks types within the Staffa Formation and Rosebank samples. In common with the volcanic clasts, there are no notable differences in feldspar alteration between on and offshore samples.

Siliciclastic samples

Within siliciclastic samples plagioclase feldspar is the dominant feldspar, with only minor quantities of alkali feldspar. Alteration is less advanced than for the volcanic clasts, with only minor dissolution to crystal boundaries. Alkali feldspars are typically more strongly altered.

Volcaniclastic samples

Plagioclase feldspar crystals are the dominant feldspars found in the volcaniclastic rocks. EDAX results indicate that Na-rich feldspar is most common and there are only minor quantities of Ca-rich feldspar. The extent of alteration of plagioclase feldspar crystals varies from relatively fresh with only minor dissolution along cleavage planes to extreme alteration resulting from intense dissolution (Figure 5.34.A). In most cases, plagioclase crystals are very altered with only isolated fragments remaining in a "matrix" of phyllosilicate minerals. Figure 5.34.B shows one such isolated fragment surrounded by smectitic clay fibres, which bridge outward into the pore space from the crystal edges.

Commonly, the Ca- and Na-rich plagioclases are replaced by patches of K-rich material. Figure 5.34.C, shows a Na-rich albite feldspar with K-rich zones, which appear to form along the cleavage (Figure 5.35). However, the K-rich zones are more commonly found in randomly distributed patches (Figure 5.36). Dissolution on this crystal is extensive and it has pitting on the surface. Dissolution is focused within the K-rich areas leaving isolated Na-rich feldspar fragments (Figure 5.34.D).

Smectitic clay fibres fill inter and intra granular pore space, growing from Na-rich plagioclase grain boundaries, while fragments of K-rich feldspar are dispersed between the smectitic clays (Figure 5.34.E). In some samples, the smectite appears to directly interact with the highly irregular dissolution boundaries of the feldspar crystal (Figure 5.34.F). More rarely plagioclase feldspars crystals are replaced by calcite (Figure 5.34.G).

5.5.8 Feldspar crystal interpretation

The majority of the feldspar crystals have been extensively dissolved, which would have created an initial secondary porosity (e.g. Schmidt and McDonald 1979), that was then filled by smectitic clays, or more rarely, calcite. Differing feldspar alteration states can be explained in a similar way to the volcanic clasts; feldspar crystals are derived from a range of sources and have therefore experienced variable amounts of alteration. Albitisation is prevalent throughout the samples. K-rich zones could be attributed to exsolution and solid-state solution of the feldspars. However, such alteration tends to be focused along cleavage lines in well-ordered zones, but in many samples, the K-rich zones are scattered randomly

throughout the crystals. Potassium is a relatively mobile element and hence it is suggested that the K-rich fluids could have been focused in the areas of maximum alteration rather than being a by-product of the feldspar alteration itself. Alternatively, the most highly altered areas of feldspar could be attributed to secondary diagenetic feldspar produced as a result of analcime alteration (c.f. Surdam, 1977).

Volcanic grains are often rimmed by alkali feldspar. It is unlikely that grains are altering from the inside out, as much of the alteration will be focused on grain boundaries that are in contact with pore fluids. These original grain boundaries could act as a focus for diagenetic fluids. The feldspar may be diagenetic in origin and have been precipitated around the edge of the grains, which are then later extensively dissolved. The result is that the clast is more structurally rigid than volcanic ash and suffers less under compaction. The alteration appears to be contained within the clast and so pore spaces surrounding the basaltic clasts remain unaffected.

5.5.9 Amygdales

Amygdales within basaltic clasts are present within the samples from both on and offshore, and these are described earlier (Section 5.2.2.1). There appears to be no correlation between amygdale fill and sample location, with amygdales in both on and offshore setting being similar. Clast type can also not be correlated with amygdale fill composition with similar amygdales being found in all three basaltic clast types as defined above. However, the groundmass surrounding the amygdales tends to be more altered in glassy clasts than in crystalline clasts (Figure 5.37.A,B).

Amygdales are partially to totally filled by a complex mineral assemblage of clay, calcite and zeolites. Commonly, the sequence of pore filling material changes considerably from amygdale to amygdale within the same basaltic clast (Figure 5.37.C). Regardless of the fill composition, most amygdales have a thin lining of tightly packed fibres, identified as smectite using EDAX. This lining follows the vesicle wall, replacing the surrounding glass groundmass rather than growing into the vesicle centre. The clay coating has also nucleated around small feldspar fragments resulting in spherulitic masses of clay at vesicle edges (Figure 5.37.D). These clay phases are often followed by larger fibres of corrensite to chloritic composition clay that nucleates on the vesicle lining and grow into the vesicle centre in a randomly orientated, sinuous fashion. Visible porosity in the vesicle is severely

reduced, but not completely occluded (Figure 5.37.E). In some vesicles the pore coating clay precipitation is prolonged, resulting in thick fan-like structures rather than the randomly orientated sinuous fibres (Figure 5.37.F). Some amygdales have several layers of clay lining before the later-stage fibrous fill (Figure 5.37.G).

Titanium-rich minerals are commonly concentrated around the edges of vesicles (Figure 5.37.H,I,J), as the glass alters to palagonite and then later smectitic clays. Titanium rims were much more common in vesicles within glass shards rather than in crystalline lava clasts. Zeolite minerals were only found in a small number of vesicles and always occurred as a late stage fill. Tightly packed Fe-rich smectitic clay commonly formed a pore coat in the vast majority of samples. In samples where the lining was restricted to a few microns, larger pore filling clay of a more chloritic and corrensite composition commonly filled the vesicle, with minor amounts of intra-fibre porosity retained in the vesicle centre.

Zeolite occurs more commonly as a late stage vesicle fill in the offshore volcanic rich samples (Figure 5.37.K).

5.5.10 Amygdale interpretation

The range of pore filling material is complex and can vary within millimetres in the same sample, with neighbouring amygdales having different mineral assemblages highlighting the complex interplay of pore waters and surrounding mineralogy. The examples presented are the most common in both on and offshore samples with the exception of calcite-filled vesicles, which were encountered during SEM, but due to charging issues with the sample an image of significant quality was unable to be taken. Titanium found within the glass is considered to be immobile (Brimhall and Dietrich, 1987) and therefore is not taken into the clay and instead is concentrated at vesicle walls.

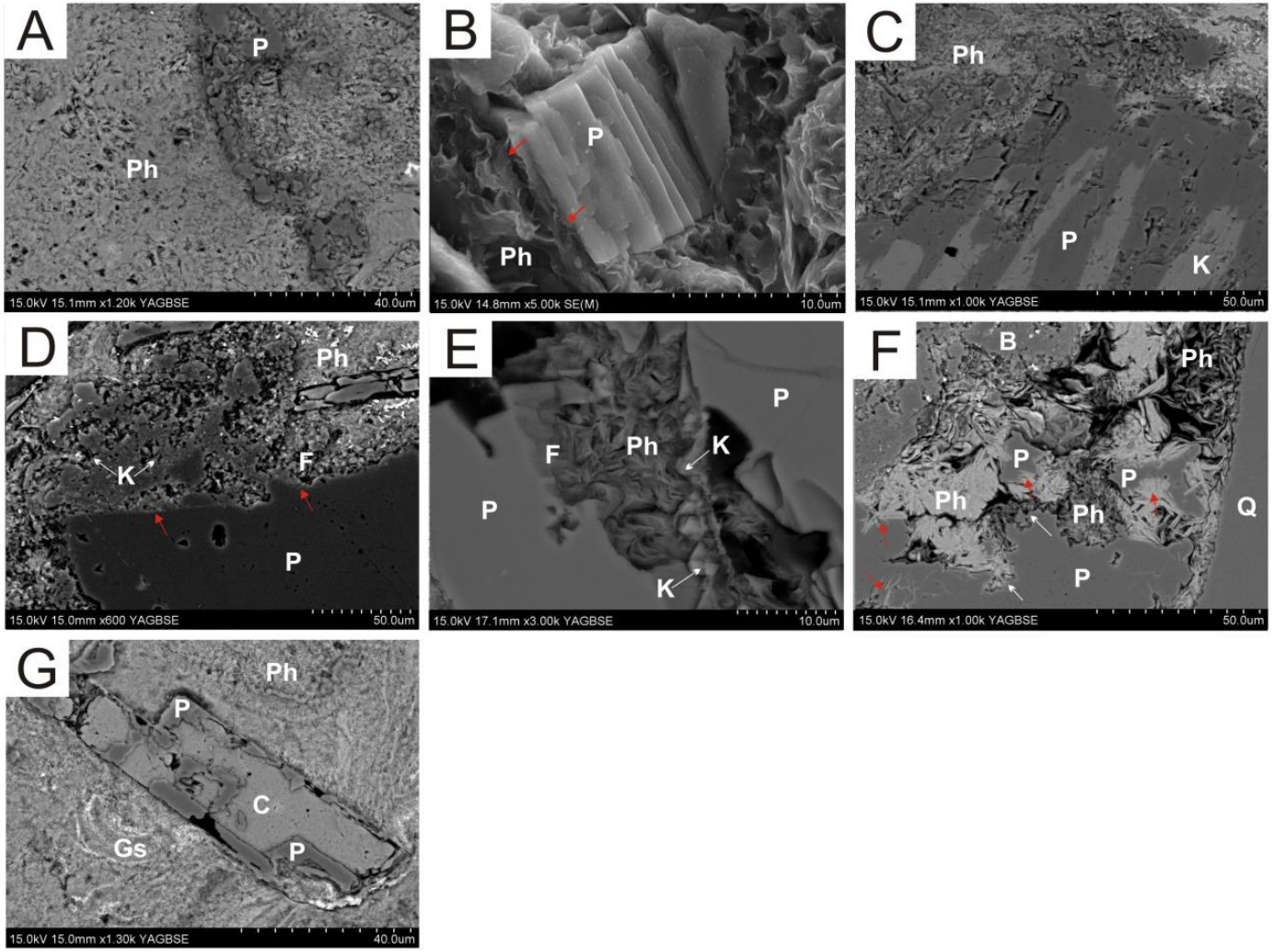

Figure 5.34: SEM feldspar images. All backscatter apart from B which is secondary electron. Abbreviations: plagioclase (P); clays (Ph); K-rich feldspar (K); feldspar dissolution (F); basalt clast (B); quartz (Q); calcite (C); Gs (altered glass shard). **A:** Extremely altered plagioclase crystal surrounded by clays**. B:** Smectitic coating growing from the plagioclase surface (arrowed). **C**: K-feldspar alteration along cleavage plane within a plagioclase crystal. **D:** K-rich feldspar areas are more altered than Na-rich plagioclase areas. **E:** Small isolated K-feldspar fragments within clay fibres. **F**: Clays appear to exploit weaknesses within the feldspar crystal structure (arrowed). **G**: Calcite replaces plagioclase feldspar.

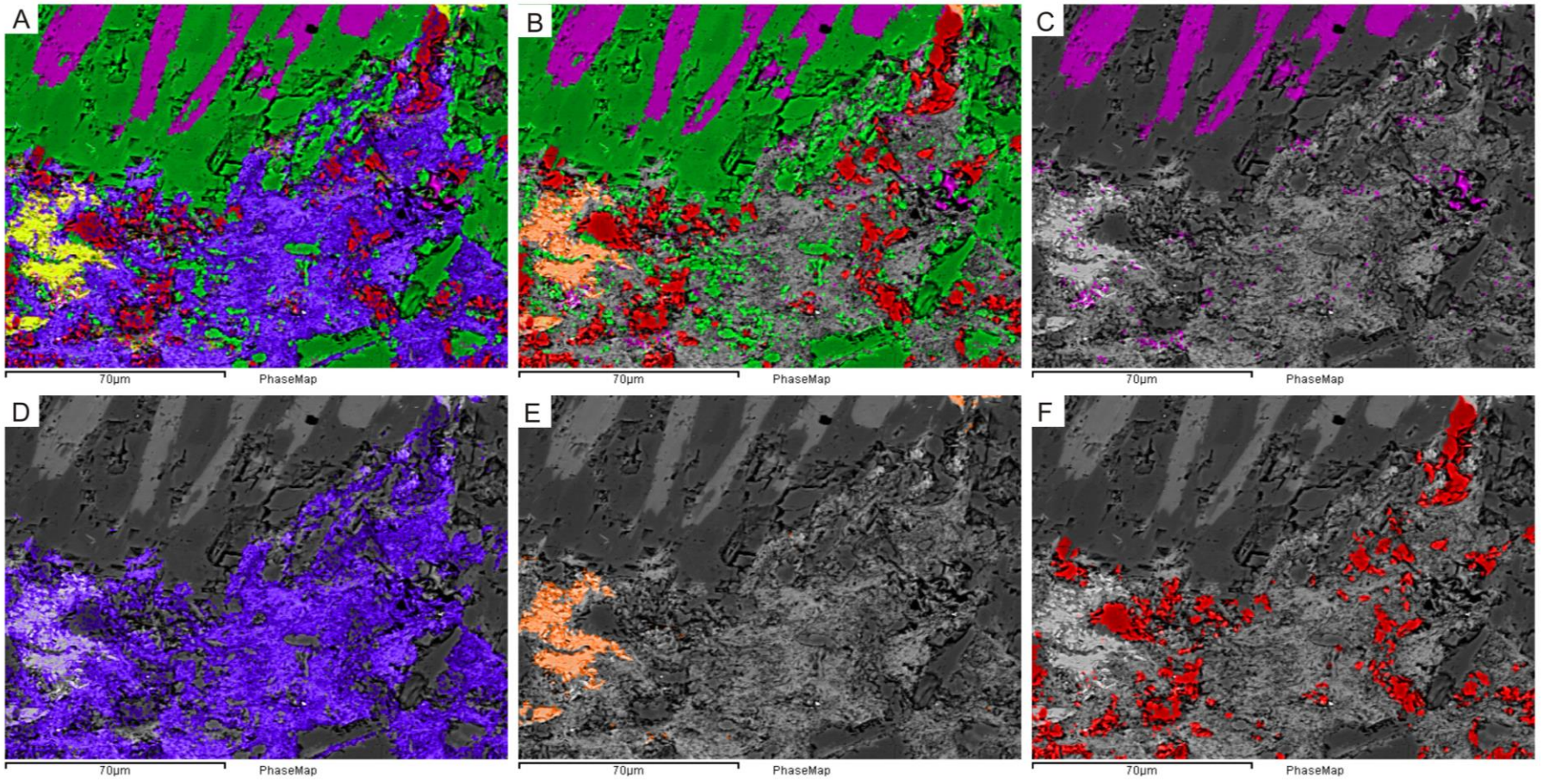

Figure 5.35: SEM phase map of a vlw sample. **A:** Composite image made from all phases. **B:** Na-rich feldspar is highlighted in green. **C:** K-feldspar is highlighted in pink. Note the K-feldspar is focused on the cleavage of the Na-rich feldspar. **D**: Mg- and Fe-rich clay minerals. **E**: Ca- and Ti-rich minerals. **F:** Quartz.

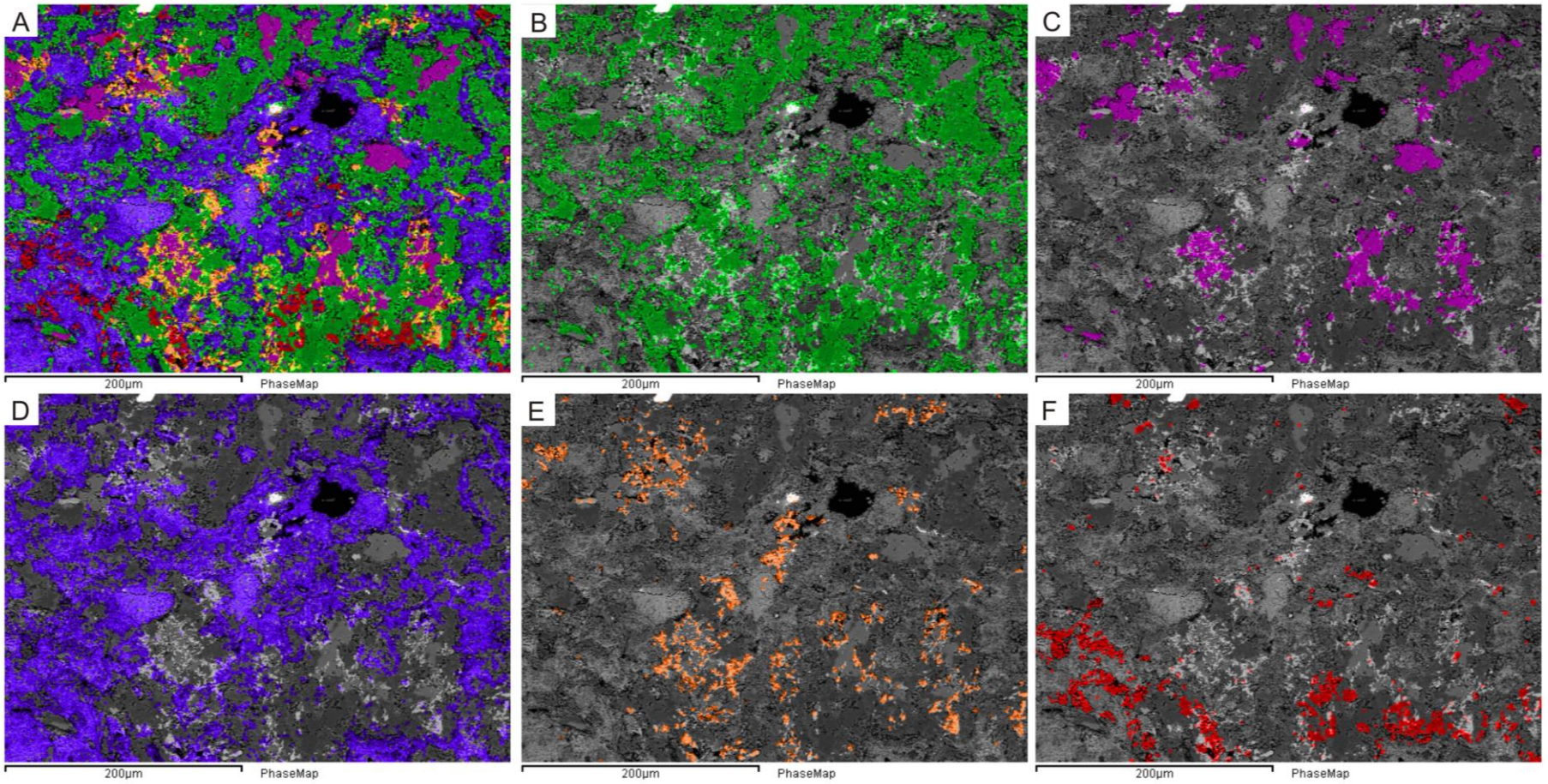

Figure 5.36: SEM phase map of a vlw sample. **A:** Composite image made from all phases. **B:** Na-rich feldspar is highlighted in green. **C:** K-feldspar is highlighted in pink. Note the K-feldspar appears as patches within the Na-rich feldspar.. **D**: Mg- and Fe-rich clay minerals. **E**: Ca- and Ti-rich mineral. **F:** Quartz.

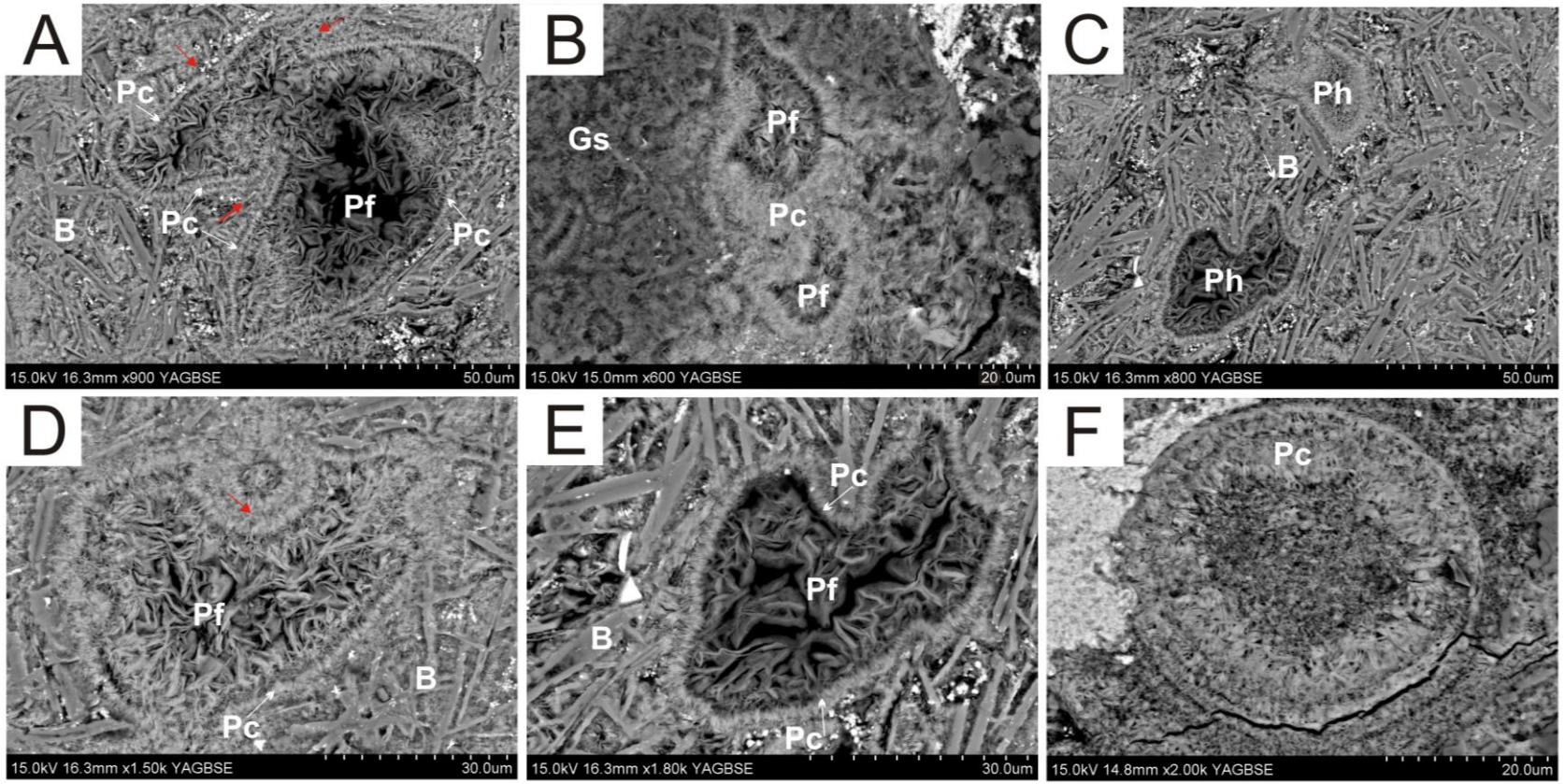

Figure 5.37: SEM backscatter images of amygdales in a range of basalt clasts. Annotations: basalt (B); altered glass shard (Gs); Titanium oxides (Ti); zeolite (Z); phyllosilicate minerals (Ph); pore coating smectite clay (Pc); Pore filling clay (Pf) typically corrensite or chloritic in composition. **A**: Flattened amygdale within a crystalline basalt clast. Clast shows only minor alteration. Note: amygdale shows evidence of flattening highlighted by Pc clay (red arrows). **B:** Amygdale within an altered glass shard. Clays replace clast groundmass. **C:** Top amygdale has a thick clay coating with little remaining porosity, bottom vesicle has thin coating and more porosity preserved. **D:** Pc point nucleates creating a spherulitic texture at the amygdale edge. **E:** Thin, tightly packed Pc layer. Randomly orientated Pf then grows into vesicle space. **F**: Thick Pc layer grows into the amygdale. Figure continued on next page.

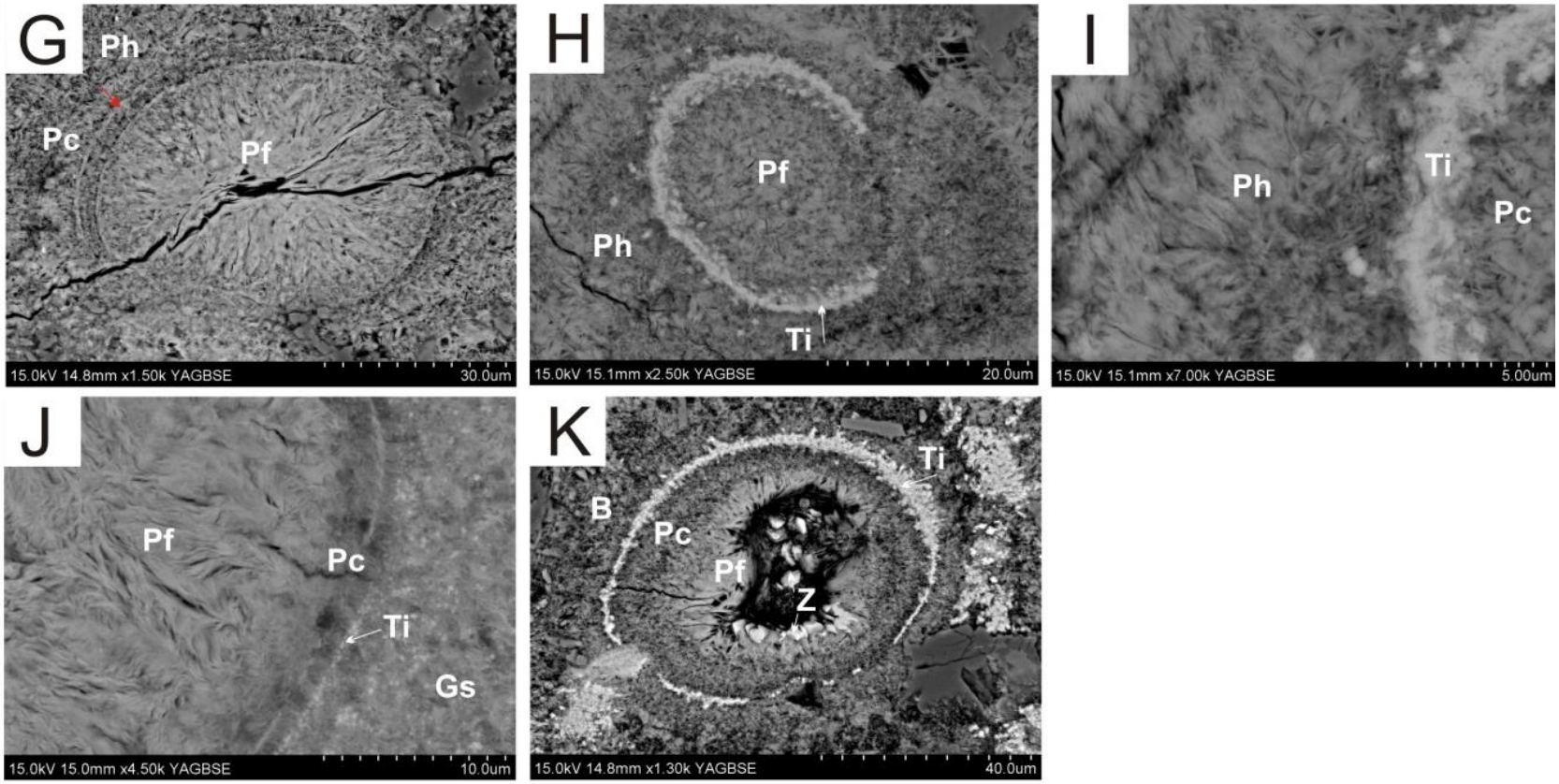

Figure 5.37 cont. **G**: Pf reaches completion filling the amygdale with only minor inter-fibre porosity. **H:** Titanium oxides concentrated at amygdale edge. I: Magnified view of H. Amygdale centre to right of image**. J:** Titanium concentration within the altered glass increases towards the amygdale edge. Note the large size of chlorite clays (Pf) filling amygdale. **K:** Late stage zeolite fills the pore.

5.5.11 Zeolite minerals

Zeolite minerals were identified optically in a number of volcaniclastic samples in both the Staffa Formation and Rosebank samples. They occurred as late-stage pore and vesicle fills in some vent proximal pyroclastic samples (e.g., MacCulloch's Tree and the Carsaig Arches). However, very little zeolite was identified in the volcaniclastic lithic wackes. In the offshore samples zeolite occurred only as a rare vesicle fill, most commonly in the lava flows.

However, evidence for extensive zeolite minerals were not found within the SEM analysis. Severe charging effects occurred in the majority of the volcanic Rosebank samples (see Section 2.5.1 for discussion). Therefore, the SEM accelerating voltage had to be lowered and this resulted in no adequate secondary electron images of zeolite minerals. At low voltages the electron signal was also too low for the backscatter detector to function efficiently and accurate identification of the zeolite under the SEM proved difficult.

5.5.12 Calcite

Several phases of calcite occur within the samples. Each phase enters the rock at a different stage within the diagenetic sequence and therefore, affects the porosity in a slightly different way. Calcite textures between on and offshore samples are similar; however, differences do exist between siliciclastic and volcaniclastic samples.

Siliciclastic samples

Onshore samples from the volcaniclastic lithic arenites and the sublithic arenites both have extensive calcite cements. Offshore, a patchy calcite cement was found within some of the reservoir rocks. This cement may have contributed to the protection of framework grains from compaction and that subsequent dissolution of this calcite phase led to a well-developed oversized pore network. Within the calcite patches porosity is completely eliminated and in places the calcite fills aggressively dissolved framework grains (Figure 5.38.A). Outside these cemented areas, framework grain boundaries are better preserved with sharp contacts and euhedral shapes (Figure 5.38.B). Pores are oversized and well

connected. Some point grain contacts show minor dissolution with suture contacts; however, this texture is not extensive. Minor clay coats occur on framework grains within the high porosity zones (Figure 5.38.C), and are typically illite and more rarely kaolinite. The clay mineral coats nucleate on grain boundaries and grow out into the pore but stop growing well before porosity is eliminated (unlike the amygdale examples). Areas of sample where clays and calcite co-exist were identified. Unfortunately, no obvious cross cutting relationships could be established between the two (Figure 5.38.D).

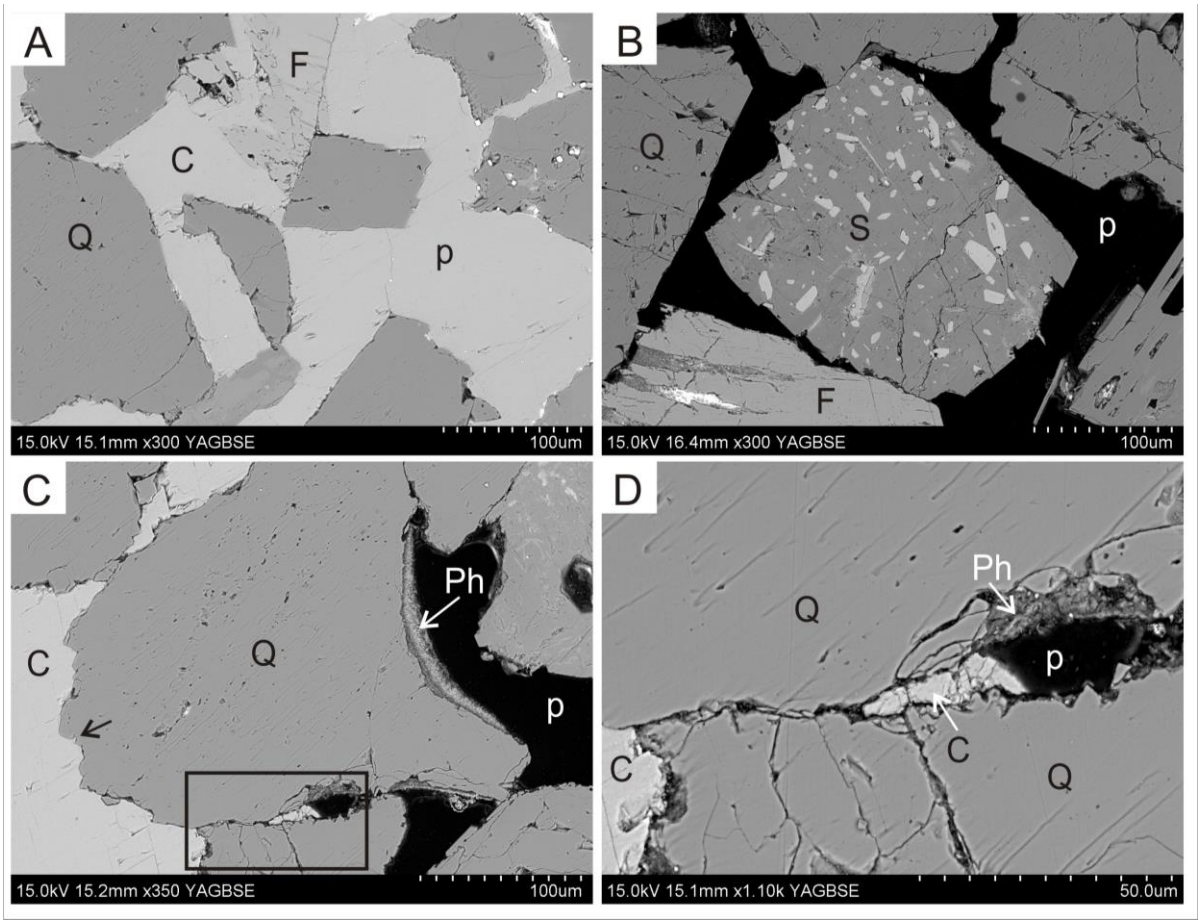

Figure 5.38: Backscatter images of calcite in Rosebank siliciclastic samples. Annotations: quartz (Q); feldspar (F); siltstone lithoclast (S); phyllosilicate minerals (Ph); calcite (C); pore space (p). **A**: Calcite cement fills all porosity. **B**: Oversized and well-connected pore network exists away from calcite areas. Grain boundary dissolution is less than in calcite cemented regions. **C**: Calcite aggressively dissolves framework grains (arrowed) while phyllosilicate minerals line grains in uncemented areas. Box shows location of D. **D**: Calcite and clays within the same pore. No cross cutting relationships are evident.

Volcaniclastic samples

Calcite is much more common in the onshore sample suite. There are six different phases of calcite, which result in complex relationships between calcite and surrounding minerals.

Type 1 calcite is exclusively associated with the flint clasts (only found within onshore samples). This calcite fills fractures and vugs within the flint grains but is not seen surrounding the grain or in the adjacent matrix. Figure 5.39.A,B shows examples of fractures through flint clasts that have been annealed by calcite. The calcite in both examples does not continue into the surrounding matrix.

Type 2 calcite predominantly fills pores, fractures and in some cases acts as a grain coat. Aggressive dissolution has modified grain boundaries and leaves the calcite with a pitted rough appearance (Figure 5.39.C). The calcite does not appear to have interacted with surrounding mineralogy as clays can be seen growing outwards from its irregular surface.

Type 3 calcite is very similar to Type 2 in that it is also highly corroded with dissolution pits. There is also little interaction between clay fibres and the edge of the calcite. However, unlike Type 2, Type 3 calcite appears to fill porosity created by the extremely altered volcanic mineralogy (Figure 5.39.D).

Type 4 calcite shows highly altered grain boundaries and a pitted texture. Here surrounding clays grow up into the calcite edge and fibres grow directly into it (Figure 5.39.E).

Type 5 calcite similarly interacts more with the surrounding mineralogy. Figure 5.36.F shows how the calcite and fibrous clay display a complex interwoven texture, with clay fibres appearing to compartmentalise the calcite. A more magnified image of this relationship (Figure 5.39.G) shows clay fibres cross-cutting the calcite. Small pore spaces do still exist along the edge of some of the calcite fibres.

Finally, Type 6 calcite replaces plagioclase feldspar phenocrysts in some samples (Figure 5.39.H).

5.5.13 Calcite interpretation

Calcite found within the offshore siliciclastic samples is interpreted as an early diagenetic phase, which may have helped to lessen the effects of compaction. Calcite is susceptible to dissolution in acidic fluids (Ehrenberg, 1990). Therefore, the calcite may have been aggressively dissolved in the non-cemented areas. However, the presence of clay coats may further dispute this theory. If the calcite cement was dissolved leaving only small patches behind before the onset of the clay formation, clays might be expected to coat calcite grains at the edges of the cemented areas. Therefore, this suggests that the clay grain coats may have formed first, inhibiting wide spread calcite precipitation and resulting in a patchy calcite cement. At a later stage this already patchy calcite cement may have been dissolved leaving only minor amounts remaining within the sample. Therefore a combination of early clay and later patchy calcite cement and later dissolution, could explain why the siliciclastic offshore samples are less compacted than would be expected.

The calcite found within the onshore samples is much more complex. Type 1 calcite is only associated with flint clasts with no evidence of it affecting surrounding grains. It is highly unlikely that fluid pathways were restricted to the flint grains only and therefore, that the calcite may originate from a first cycle diagenetic fluid (pre-Paleogene). The flint had previously been buried and silicified. During burial fractures within the flint clasts may have been annealed by a late-stage calcite cement. Following this, localised tectonism of the basin led to the flint being uplifted and eroded. These clasts were incorporated into the Staffa Formation rocks and were then buried for a second time. The calcite cemented fractures survived the process whereas pore filling material was lost with erosion.

The order of the other calcite phases is difficult to determine. Type 2 calcite appears to pre-date the onset of the clays and is an early stage diagenetic phase. The calcite was aggressively dissolved before later stage clay fibres grew outwards from the surface filling pore spaces. Type 3 calcite is very similar in texture, but appears to fill the pore space around altered volcanic clasts and therefore postdates the clay alteration.

Type 4 and Type 5 calcite timings are difficult to determine, for example the altered volcanic grain in the upper part of Figure 5.39.H, has clay that fans outwards from this grain towards the calcite surface. This clay could be interpreted as growing out into an open pore space because clay fibres increase in size towards the centre of the space. Late-

stage pore fluids could then precipitate the calcite around the delicate clay fibres, leading to the complex intergrowth. There is no evidence of clay growing from the calcite surface as seen in the Type 2 example, indicating that the calcite may post date the clay. However, the small circle in the bottom left of the image appears to show clay fibres growing from the calcite to fill the hole. This would imply that the calcite was already in place before the clays grew and the fibrous intergrowths were simply exploiting fractures and weaknesses in the calcite crystal structure. The magnified image (Figure 5.39.F) could be interpreted in either way. If the calcite was a late stage fluid filling the space between the clay fibres it might be expected to completely fill the pore. However, the clay structures would undoubtedly restrict pore throats leading to pore scale compartmentalisation and partial calcite precipitation. Conversely, if the calcite pre dates the clay fibres, it might be expected that the fibres would be orientated parallel to the cleavage and fracture regime in the calcite crystals, or that the edges of calcite crystals would show dissolution or alteration along their boundaries. Neither scenario is observed as fibres are randomly distributed and calcite crystal edges are straight and run parallel to clay fibres. An alternative theory is that the calcite may have precipitated simultaneously. The 3D shape of the pore must also be considered. If the pore was relatively shallow then the SEM thin section could show fibrous clay from below growing upwards, resulting in the illusion that the calcite and clays were intermixed. However, as this feature is fairly common and occurs in several different samples it is thought that the relationship is not just an optical anomaly.

Finally, Type 6 calcite is thought to represent a late stage replacement of feldspar phenocrysts.

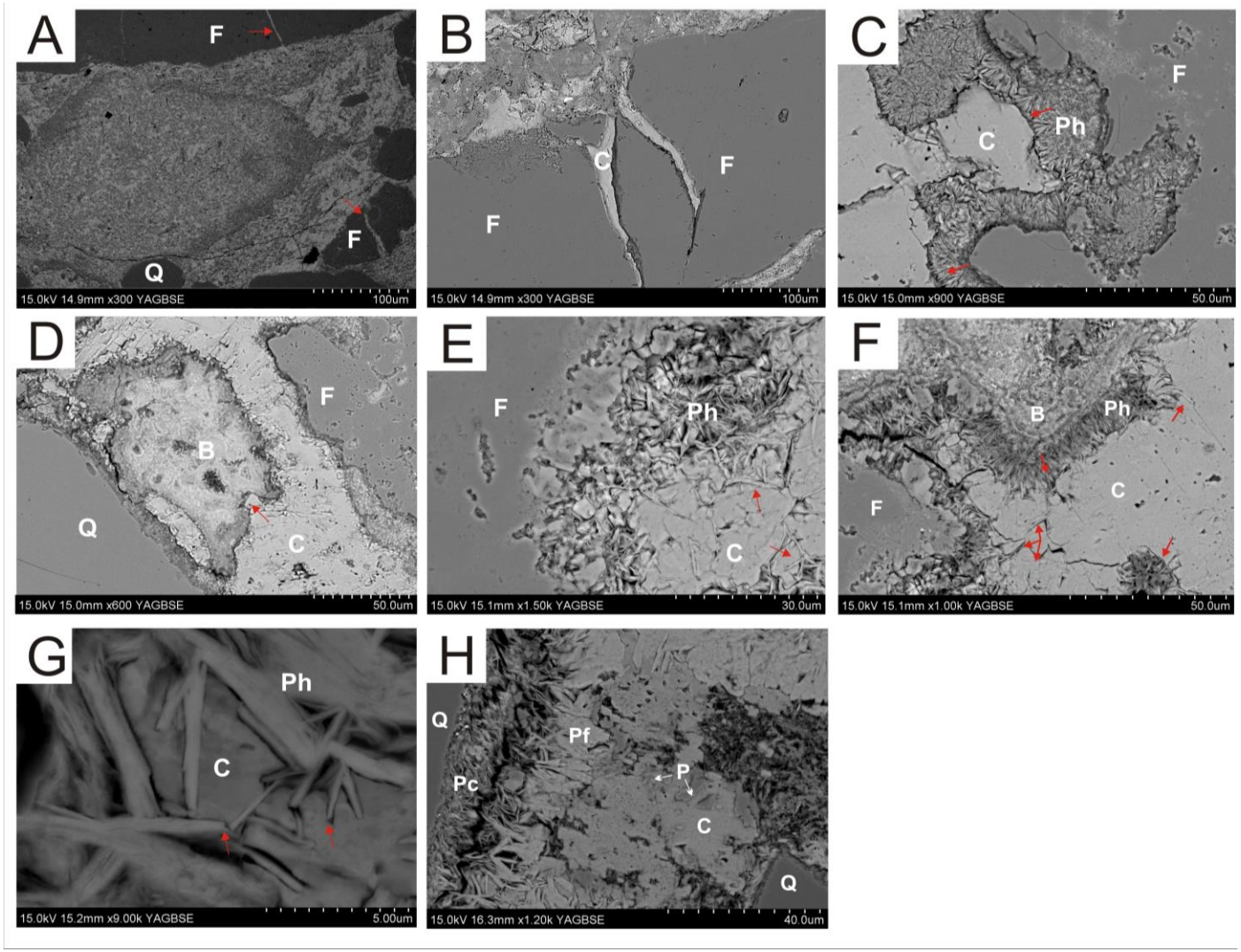

Figure 5.39: Backscattered images of calcite in volcaniclastic samples. Annotations: flint (F); quartz (Q); calcite (C); basalt (B); plagioclase feldspar (P); clay (Ph); pore coating clays (Pc); pore filling clays (Pf). **A:** Calcite filled fractures terminate at flint grain boundaries (arrowed). **B:** Calcite fills fractures in flint. **C:** Clays grow out from dissolved flint grain boundaries to meet dissolved calcite (arrowed). **D:** Calcite aggressively attacks altered basaltic clast (arrowed). **E:** Clay fibres mixed within calcite pore fill (arrowed). **F:**. Clays grown from altered basaltic clast to calcite (top of image). Clays grow into calcite (top right and bottom centre). Clays grow from calcite into pore (bottom right). **G:** Magnified image showing calcite compartmentalised by clay fibres. **H:**). Pore coating clays line framework grains. Pore filling grains grown into interstitial pore space. Highly dissolved feldspar grains replaced by calcite

5.5.14 Clay minerals

A range of different clay mineral compositions and morphologies were found in all samples. There were no obvious differences between clay minerals found in offshore samples versus those found onshore.

Siliciclastic samples

Siliciclastic samples (sublithic arenites and quartz arenites) have only minor amounts of clay. Detrital clay minerals that were found within these samples typically formed grain coats on framework grains (see Section 5.5.14.2, Figure 5.38.C). While these clay minerals do limit permeability by clogging pore throats, overall visible porosity is retained.

Volcaniclastic samples

Clay minerals are more abundant in the volcaniclastic samples, both on and offshore. A wide range of compositions, morphologies and textures are present and these are discussed below.

5.5.14.1 Identification

Clay minerals are the dominant pore space and amygdale fill within all of the volcaniclastic samples, regardless of lithofacies type. They are most abundant in vent proximal rocks that contain high proportions of basaltic pyroclasts. The proportion of clay minerals reduces with distance from the volcanic source and can be correlated to a reduction in the abundance of glass-rich volcanic clasts in the samples.

Optically these clays appear as a brown-green masses leading to difficulties in identification. However, four different clay structures were identified using the SEM.

Type 1 clays comprise tightly packed randomly orientated fibres and are abundant in almost all of the volcanic rich-samples. The clay is Fe-rich and often forms fan structures, and platelets are typically less than 5 μm long (Figure 5.40A). It is predominantly associated with the altered groundmass of basaltic clasts and ash, and forms pore linings on vesicles.

Type 2 clay appears to transition between more fibrous material and more blocky platelets (Figure 5.40.B). This clay generally has less Ca and Na than the previous type.

Type 3 clay is present within samples as long elongate fibres that, locally, form radial fans (Figure 5.40.C). These plates are much larger (5–10 μm) and reach (20 or 30 μm) in length (Figure 5.40.D) where they appear less blocky and slightly more elongate. This clay type lacks Na and Ca.

Type 4 clay is more Fe-rich than the others. This clay has long elongate aligned plates, which are commonly orientated in large fan structures. The plates are typically over 50 μm (Figure 5.40.E).

The different clay structures were tentatively identified using EDAX spectra in combination with examples in literature, (Welton, 1984). Type 1 clays are rich in Si and Al, Na and Ca, as well as minor amounts of Fe and Mg, and have been identified as smectitic clay. Type 2 clay minerals represent a transitional clay from smectitic to chloritic composition, possibly corrensite, due to the mixture of both platy and fibrous structures. Chemically, they are similar to Type 2 clay but contain less Na and Ca and more Fe and Mg. Type 3 clays contain Si, Al, Fe and Mg, but lack Na and Ca, and represent chloritic material. Type 4 clays are of very similar in composition to Type 3, but are relatively enriched in Fe.

The identification of clay minerals proved difficult as limitations on the EDAX beam spot size (1 μm) and accelerating voltage resulted in a significant error within results. The complex heterogeneity in the samples may lead to surrounding mineralogy being included within the EDAX results. Therefore, XRD and QXRD analysis was undertaken in order to better identify the clay phases.

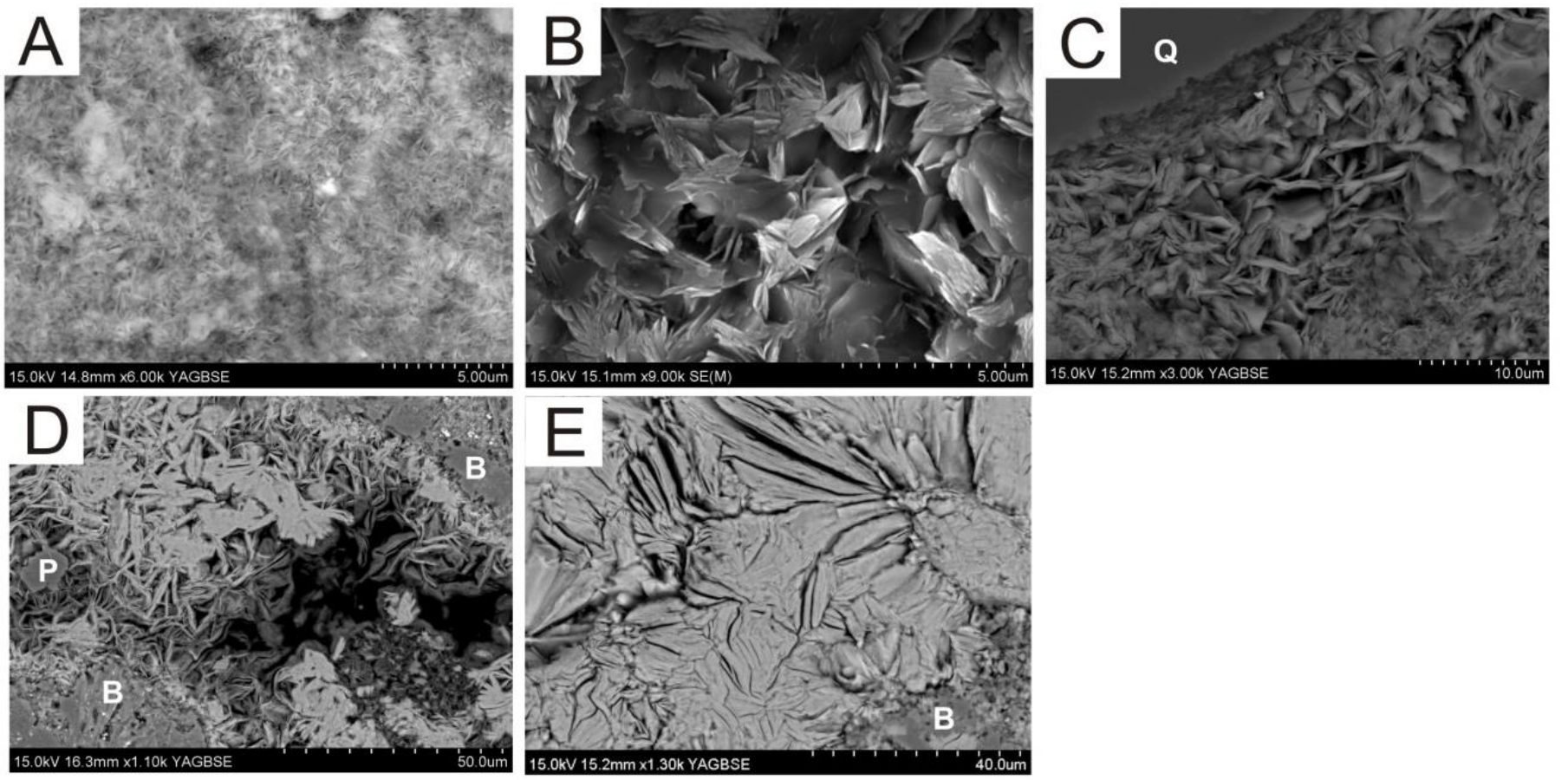

Figure 5.40: SEM images of clay types found within volcaniclastic samples. Annotations: quartz (Q); basalt clast (B); plagioclase feldspar (P). All images are backscatter except B which is secondary electron. **A:** Type 1, smectite. **B:** Type 2, possibly corrensite. **C**: Type 3, chlorite. **D**: Type 3, chlorite. Note larger size up to 30µm. **E**: Type 4, chlorite with platelets exceeding 50µm.

5.5.14.2 Grain coats

The clay phases are partly responsible for the decrease in visible porosity in the samples. Therefore, the nature of how the clays interact with the surrounding mineralogy was examined.

Clay grain coats in the volcaniclastic rich samples (volcaniclastic lithic wacke), were all identified as Type 1 smectite clays. A number of previous studies have linked the presence of volcanic glass with the formation of similar smectitic grain coats (Davies and Ethridge, 1975; Khalaf, 2013). A sample of volcaniciclastic lithic wacke from the Staffa Formation was taken in order to assess the relationship between the smectite grain coats and the volcanic ash. The sample (mt3d) from a vent medial location contains ~15% reworked basaltic pyroclasts but is mostly composed of quartz and flint grains. Visible porosity within the sample is estimated to be ~15%. Localised areas of pore lining and filling clay are randomly distributed throughout the sample.

In areas rich in volcanic clasts (Figure 5.41.A), the grains are coated in tightly packed smectite coating that severely reduces porosity and permeability of surrounding pores and reduces the visible porosity within the thin sections to 0%. Secondly, an area towards the edge of a volcanic clast rich zone was examined (Figure 5.41.B). Here, smectite coats the volcanic clasts as before; however, some quartz and feldspar grains have incomplete grain coats. Therefore, the smectite grain coats seem to be associated with the volcanic grains and hence only locally reduce the visible porosity and permeability of the pore network. Visible porosity in the thin section here is ~ 3%. Finally, an area of sample mt3g devoid in volcanic clasts was examined (Figure 5.41.C). Here, framework grains completely lack the smectite grain coats and the pore network remains unaffected, with viable porosity of ~ 15%.

As the basaltic clasts and ash start to alter to smectite, grain coats can form. In samples that contain abundant glass the smectite appears to coat the vast majority of grains. In samples such as the one described above only grains directly in contact and proximal to volcanic grains are likely to be affected by the smectite grain coats. In most cases the grain coats acted as the precursor to later stage pore filling clays. Therefore, pores surrounding grains that have a substantial grain coats, are likely to be filled.

Several authors (Imam, 1986; McBride, 1989; Worden and Morad, 2003) suggest that early chlorite formation can lead to the preservation of porosity during burial. They suggest that early pore coating chlorite inhibits the formation of quartz overgrowths by

limiting the nucleation sites in which the silica can form, thus protecting the pore network. Figure 5.42 (Bloch et al., 2002) shows a breach in a similar type of clay rim leading to the nucleation of an overgrowth and a reduction in porosity. Early grain coats may also inhibit nucleation of other early cements such as calcite.

Why therefore, in previous studies has clay formation stopped resulting in porosity preservation, but continued in the rocks in this study, until the visible porosity has been eliminated? Firstly, pore rims imaged within this study are significantly thicker than those seen in previous studies, indicating that grains were exposed to clay favourable diagenetic fluids for relatively long time scales. Secondly, large amounts of altered volcanic glass within the samples may have resulted in pore waters enriched in Fe and Mg and this may have promoted the formation of phyllosilicate minerals. The chloritic clays may also develop from a smectitic precursor (e.g. García-Romer et al., 2005). However, previous studies (Zou et al., 2008, 2012) also suggest volcanic clasts as the origin of their clay coats. If the samples in these studies contain only lava clasts with little amounts of ash or pyroclasts, then clay development may be localised and therefore lead to incomplete pore fill. Hydrothermal circulation affecting the rocks in this study may also promote clay growth and lead to more reservoir damaging clay growth.

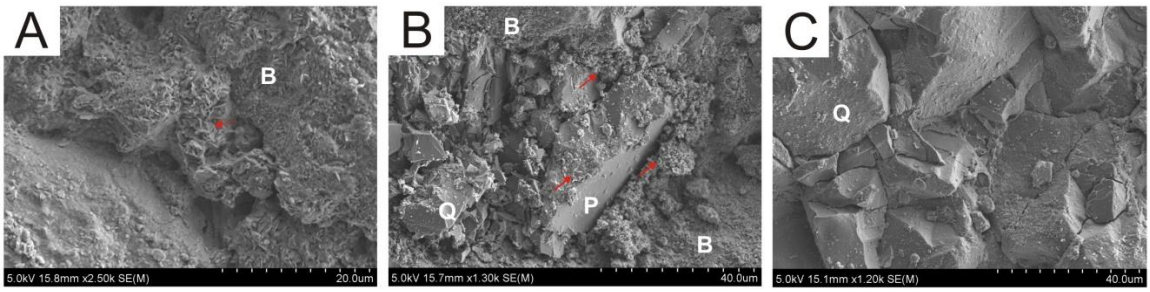

Figure 5.41: Secondary electron images of smectite grain coats within sample mt3g. **A:** Volcanic clast (B) is coated with smectite, which clogs localised pore space (arrowed). **B:** Volcanic clasts have smectite grain coating but quartz (Q) and plagioclase feldspar (P) only have incomplete grain coats (arrowed). **C:** Quartz rich area of the sample devoid of volcanic grains. No extensive smectite grain coats are present.

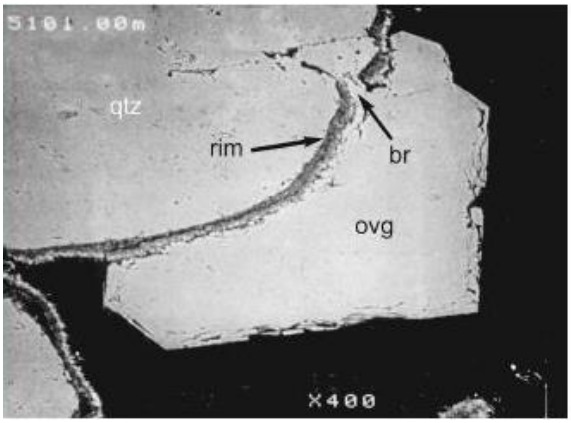

Figure 5.42: Breach in clay coats leading to quartz overgrowth development. Abbreviations: Quartz (qtz); Clay coat (rim); breach in clay coat (br); quartz overgrowth (ovg). From Bloch et al. (2002).

5.5.14.3 Pore throats

Pore throats are the most important part of the pore network because they control permeability (Doyen, 1998; Bryant, and Blunt, 1992). The reservoir quality of a rock can be reduced by only limited amounts of clay in pore throats. All volcaniclastic samples exhibited reduced permeability due to clogged pore throats. Figure 5.43.A shows an example of how smectite grain coats grow outwards into the centre of the pore to occlude the porosity and reduce permeability.

5.5.14.4 Pore-filling clay

The majority of pores within the volcaniclastic samples are filled by pore-filling clays. The pore-filling clay comprises corrensite or chlorite fibres, which have nucleated on the grain coats and grew into the centre of the pore. In most volcanic clast rich samples the pore filling clay has completely filled the surrounding pore space (Figure 5.43.B). Where the pore-filling clay has not reached completion intergranular porosity between the fibres is present (Figure 5.43.C). While limited porosity is retained, these fibres can significantly reduce permeability.

While there does not seem to be significant differences in pore-filling clay textures between on and offshore samples, some differences are seen between rock types. Samples with abundant scoria and ash clasts, such as the massive scoria rich lapilli tuff, typically have much greater amounts of pore-filling clay than samples that contain lava clasts. Figure 5.43.D shows a typical pore-filling texture in the scoria-rich samples. Glass has altered to smectite and are also often coated by smectite, which appears to have been remobilised and lines the pores parallel to the edges of the glass. Pore-filling corrensite has

then grown with a blocky fan like structure, and filled the pore. The blocks are randomly orientated and often appear to radiate from a point source or to form an axiolitic texture. In samples dominated by altered lava clasts, pores are typically filled by more fibrous clay that grows perpendicular to the framework grains and into the pore in a more regular and ordered fashion (Figure 5.43.D). The visible porosity is therefore, reduced with time until clay fibres meet in the centre of the pore (Figure 5.43.E).

The extent of the pore-filling clay minerals appears to correlate with the amount of volcanic material (in particular volcanic glass) in the sample. The pore filling clay is tentatively identified as chlorite and corrensite. Therefore, the transition from pore-coating to pore-filling marks a textural change from tightly packed to wider spaced fibres, but also reflects a compositional change from Ca- and Na- rich smectite to Fe- and Mg- rich chlorite. This transition is discussed in Section .

The difference in clay textures in samples containing abundant pyroclasts versus samples that contain lava clasts might be explained by pore architecture. Firstly, lava clasts are generally more resistant to compaction and so retain their shape. As a result the surrounding pores are held open for longer during compaction. These pores are often larger and therefore will take longer time scales to fill, resulting in incomplete pore fills. Glassy pyroclasts are structurally less rigid than lava clasts and so will compact more easily leading to an early reduction in porosity. As a result pores are smaller and therefore will fill faster. Secondly, glass rich pyroclasts alter more than lava clasts resulting in more material being available within the diagenetic fluids to be taken into the clays.

5.5.14.5 Unusual clay textures

Clay patches

Type 4 clay is almost exclusively found as patches within volcanic rich samples. This clay is Fe rich, very large (in the order of 50 μm) and commonly forms a distinctive texture. Fibres grow outwards from sinuous line point sources that curve through the patch forming a complex replacement / pore filling texture. The edges of the patches are very sharp and there is no evidence of pore coating material (Figure 5.44.A). All clay patches have an almost euhedral shape (Figure 5.44.B).

Initially these clay patches were thought to be amygdales within basalt clasts. However, the nature of the clay is different from other vesicles. No pore-rimming clays

could be found and clays growing into the centre of the vesicle were absent. The patches were then thought to be altered glass clasts with clay minerals growing off relict perlitic fractures that developed when the glass started to alter. However, the overall euhedral shapes of the patches make them unlikely to be glass. The patches also seem to withstand compaction unlike the majority of the observed glass shards. It is therefore thought that Type 4 clay is more likely to be replacing a mineral phase, because the majority of the patches occur within basaltic clasts these may have originally been pyroxene phenocyrsts. It is not clear why the clay has grown in this orientation; however, it is assumed that this is an artefact of the pyroxene alteration. The axiolitic texture of the clay may be artificially accentuated. As the clays grow and meet, the remaining pore fluid will be enriched in elements not taken into the clay structure such as Ti or excess Fe. These elements could then precipitate out in the remaining pore space, resulting in long thin strands that join clay fibres on either side. Both Ti and Fe are bright under the SEM these strands would stand out against the surrounding clays resulting in the unusual wavy axiolitic texture developed.

Large clay areas

Large areas of clay are more commonly found within the Rosebank volcaniciclasic samples. Unlike the more commonly tightly packed smectite clay matrix that has formed from altered glass, these areas have extremely large clay minerals that appear to be growing into open pore space. The fibres are Mg and Fe rich and have been interpreted as chlorite. The fibres have grown in fan-like shapes and appear to radiate out from single point nuclei (Figure 5.45.A1). They are extremely large, and often exceed 50 μm, which is unusual in itself as the clay fraction of a rock is, by definition, <2 μm. Some pore space is retained between fibres; however, overall permeability is reduced. Veins of tightly packed clays are often found cross-cutting the clay areas. Original framework grains have been extensively dissolved with only minor fragments of feldspar remaining (Figure 5.45.A2). This feldspar often has patchy K alteration zones as described in Section 5.5.7. Extensive dissolution of framework grains has taken place in the large clay areas, with very little of the original rock structure remaining. The chlorite has then grown into the large open voids nucleating on the remaining fragments of framework grains.

The large >50 μm platelets may have most likely grown from a sustained high temperature fluid (cf. Hillier, 1994). As there is no apparent correlation between these clay areas and hot igneous – sediment contacts samples it is though they are not a direct result

of contact effects. Therefore, it is more likely that the clay areas are a result of circulating hydrothermal fluids that resulted in extensive dissolution of framework grains and then rapid chlorite growth at elevated temperatures.

Spherulitic clay alteration

Spherulitic clay textures were noted in vesicles in several samples. However, in places spherulitic clay structures also appear to aggressively attack surrounding feldspar framework grains (Figure 5.45.B1) leaving isolated fragments of feldspar with irregular margins. The formation of these textures is not yet understood.

5.5.14.6 Clay evolution

Several clay phases are present throughout the samples. Often one phase appears to have grown into another (e.g. smectite grain coats transform into larger clay fibres of chloritic composition that fill the pore, Figure 5.46). This relationship is common in many of the volcanic rich samples, both on and offshore. Chang et al., (1986) explain that most basaltic volcaniclastics alter to trioctahedral smectites. Gifkins et al., (2005) have reported a transition from smectite to chlorite with increasing depths and temperatures. The evolution of the clay phases is discussed further in Chapter 7.

5.5.15 Compaction

Evidence of compaction can be found within all the samples, but is most common in the volcanic clast rich, onshore samples (minimum burial depth of ~ 2km).

Siliciclastic samples

The sublithic and quartz arenites found onshore show signs of compaction, mainly within the flint grains. Sutured contacts are common and altered flint clasts are often deformed around stronger quartz grains (Figure 5.47.A). Fractures are also common within the flint clasts and they radiate out from point grain contacts (Figure 5.47.B).

Volcaniclastic samples

Compaction is greatest in samples containing significant amounts of volcanic glass and pyroclasts, such as the massive scoria lapilli tuffs. Compaction can be seen in the volcaniclastic lithic wackes, as ash clasts are flattened and deformed around framework grains (Figure 5.47.C,D,E). Lava clasts are more resistant to compaction and retain their structure better, preserving surrounding porosity. In examples where the clasts have been completely replaced, but have an unaltered coating or rim, this rim seems to protect the clast from further compaction (Figure 5.47.F).

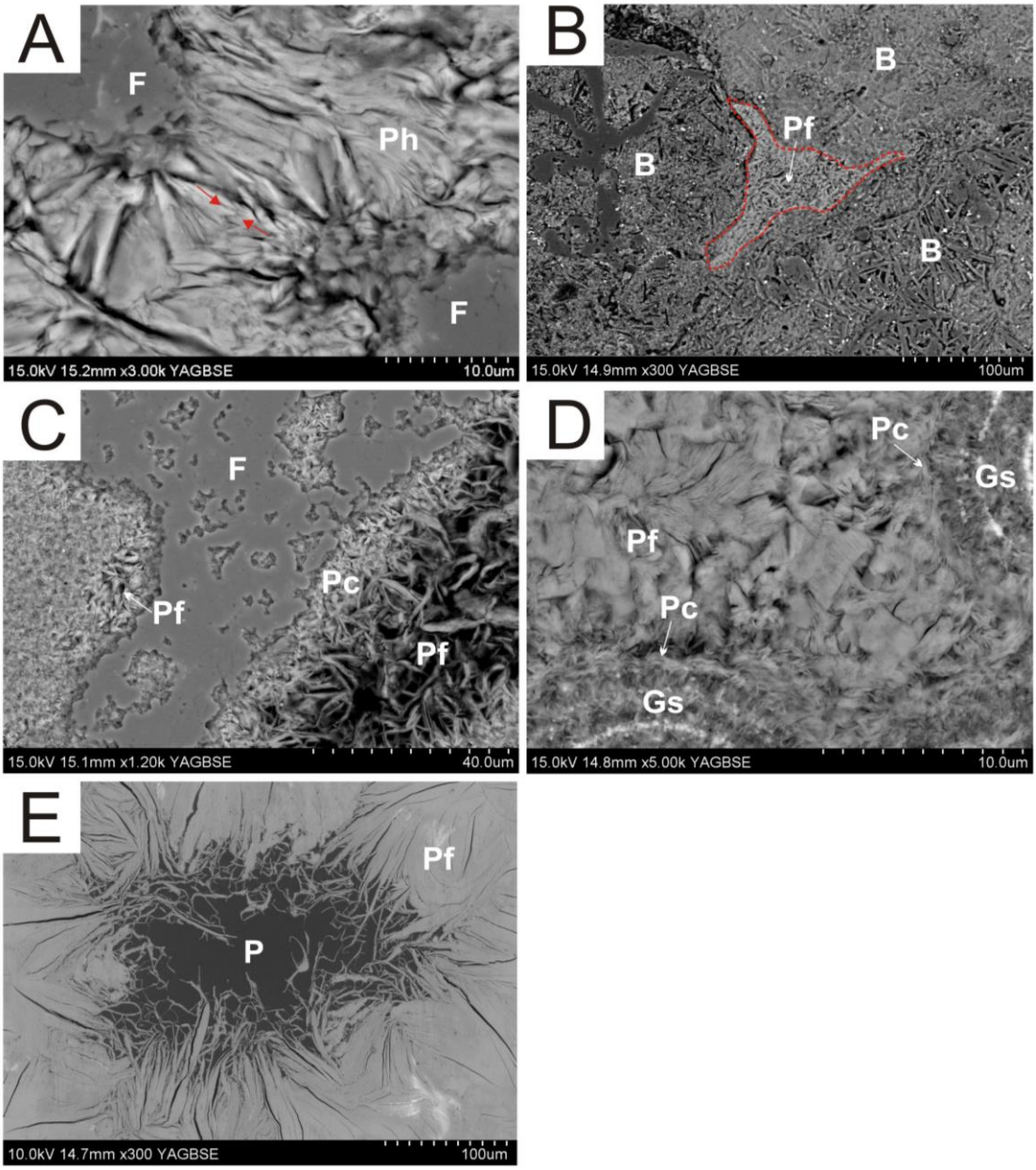

Figure 5.43: Backscatter SEM images of pore filling clays. **A:** Clays (Ph) coat flint gains (F). Clays meet in the centre of the pore throat reducing the permeability of the sample. **B:** Pore (outlined in red) in between three basaltic clasts (B) that is filed by pore filling clays (Pf). **C:** Highly dissolved flint grain (F) that is coated by pore coating clays (Pc) before larger and more fibrous pore filling clays (Pf) grow into remaining porosity. **D:** Pore space between two altered glass shards (Gs) has been filled firstly by remobilised smectite pore coats (Pc) and then by more blocky corrensite (Pf). Note titanium banding in glass shard. **E**: Larger scale pore space (P) being filed by fibrous pore filling chlorite (Pf).

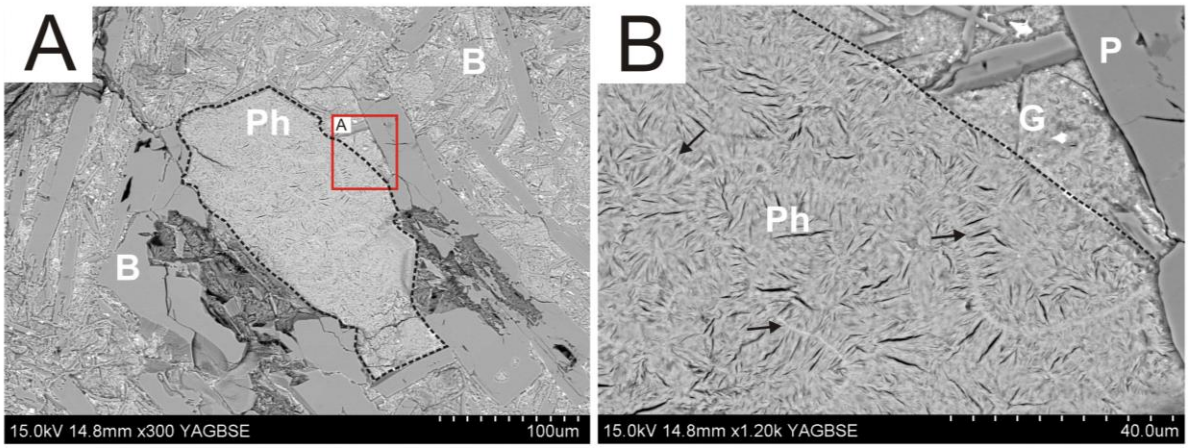

Figure 5.44: Backscattered SEM images of the clay patches. **A:** Clay patch (Ph- black dashed outline) with euhedral shape within a basalt clast (B). Red box shows location of magnified imaged B. **B:** Dashed line shows sharp transition from the basalt clast into the clay patch. Plagioclase (P) within the basalt clast is relatively fresh, while the groundmass (G) is altered to smectite. Note the axiolitic texture within the clay (Ph) patch (arrowed).

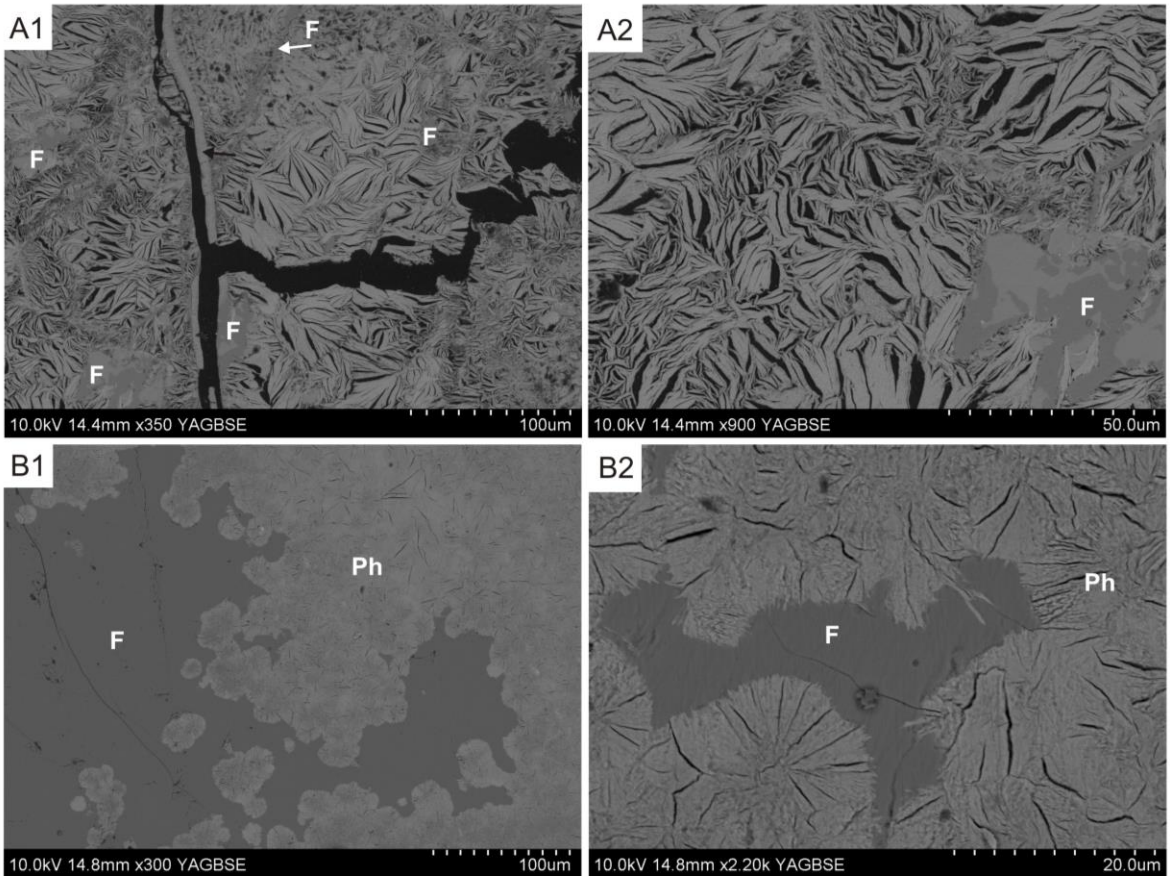

Figure 5.45: Backscatter SEM images of unusual clay textures. **A1**: Clay with large fibrous platelets. Fragments of feldspar (F) are interdispersed throughout clays. Tightly packed vein (black arrow). Artificial fracture (black resin) produced during thin section manufacture. **A2**: Magnified image showing clay texture. Note light areas on feldspar (F) are K rich, whereas dark areas are Na rich. **B1**: Feldspar (F) being aggressively attacked by spherulitic clays (P). **B2**: Remaining fragments of feldspar have irregular boundaries.

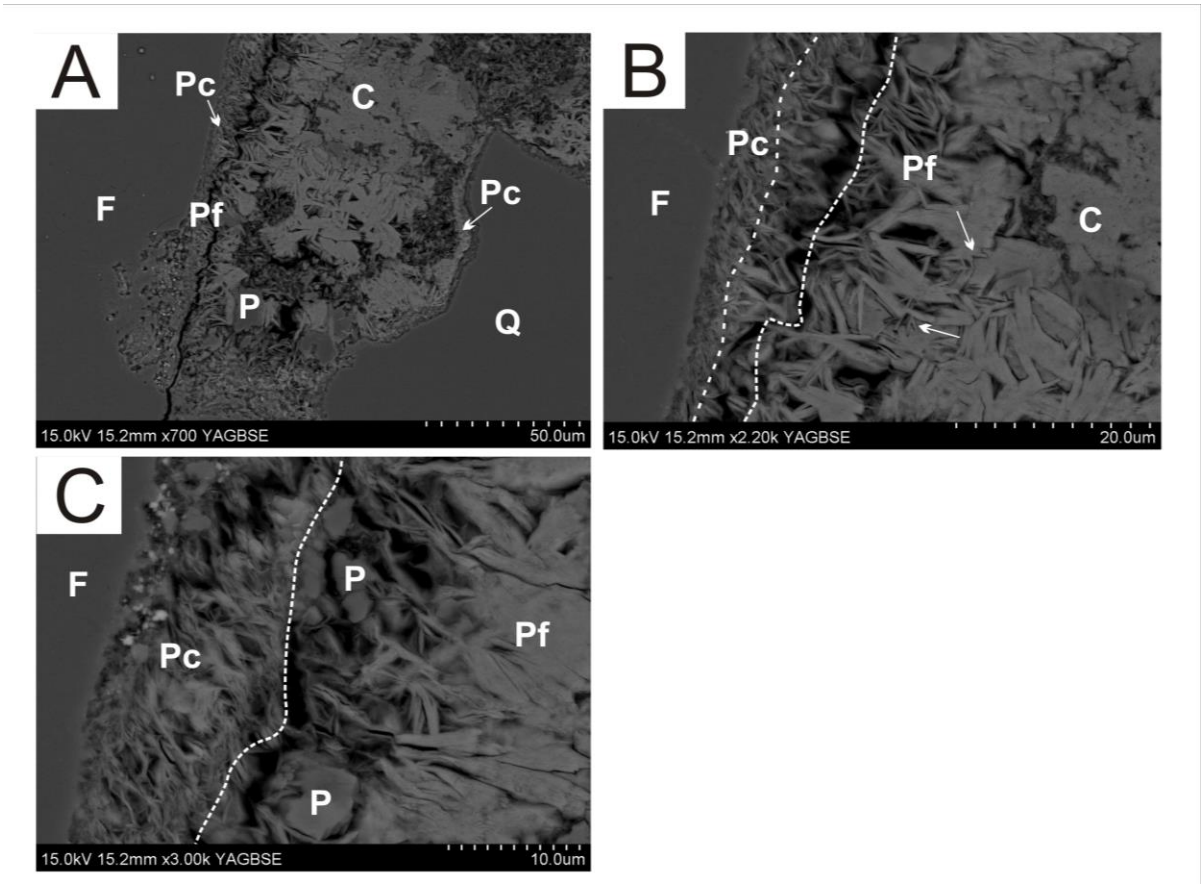

Figure 5.46: Backscattered SEM images of clay evolution. Annotations: flint (F); plagioclase feldspar (P); quartz (Q); calcite (C); smectite clay coat (Pc); corrensite pore fill (Pf). **A:** Framework grains are firstly coated by smectite. Chlorite then fills old pores. Calcite fills the remaining porosity. **B:** Magnified image showing the pore coating layer on flint grain, then a transition layer (between dashed lines), before chlorite fills the pore. Note the relationship between the Pf clay and the calcite (arrowed). **C:** Magnified image showing the tight structure of the Pc clay, contrasting with the larger well formed fan structures in the Pf clay. Relict feldspar exists between the layers.

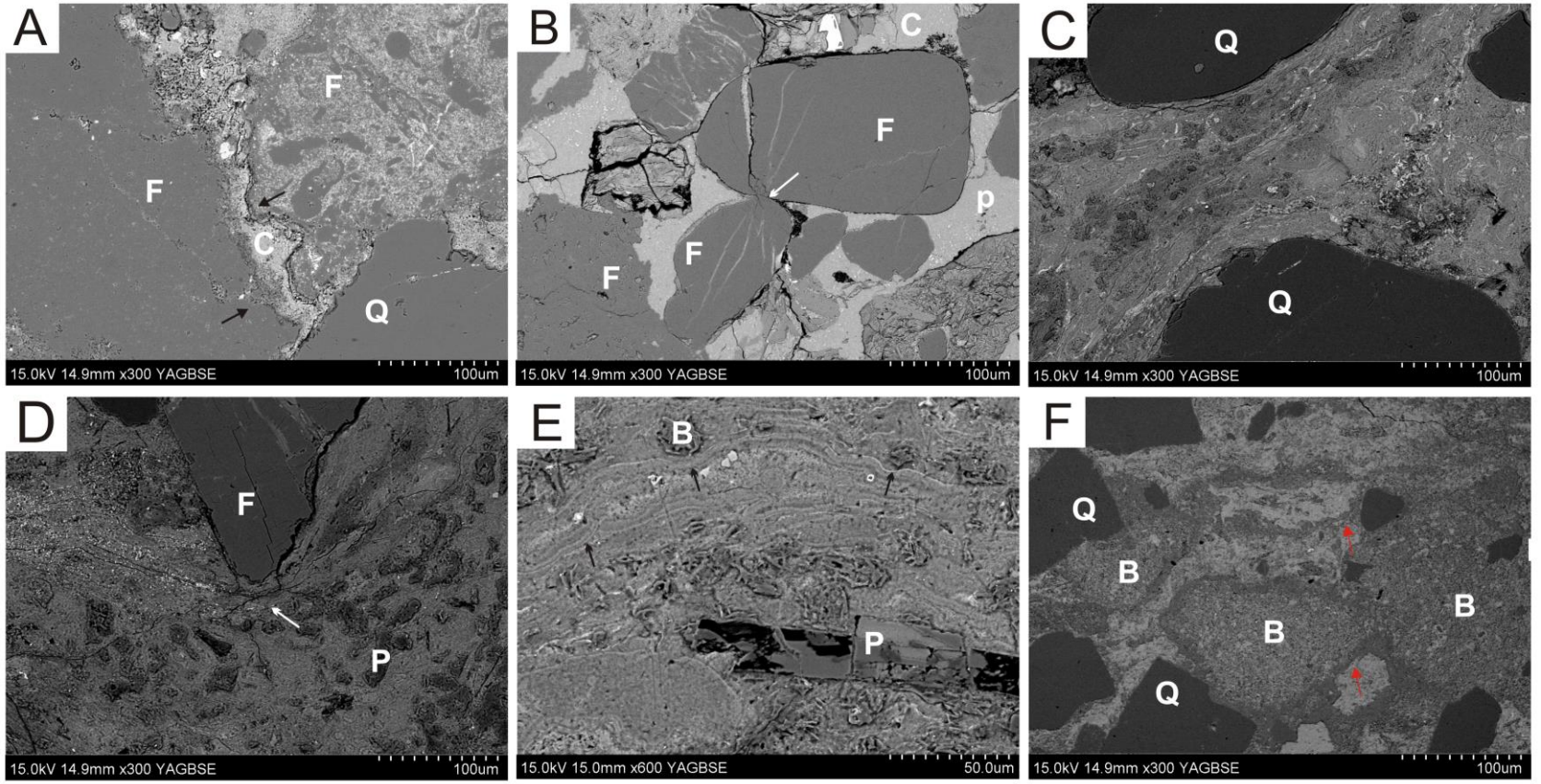

Figure 5.47: Backscattered SEM images of compaction. **A:** Sutured contact (arrowed) between two flint clasts (F). The more altered type 1 flint is deformed around the more resistant quartz grain (Q). **B:** Fractures within flint clasts (F) emanating from point contacts (arrowed). Large pores (P) are typically retained, but in this case have been filled by calcite (C). **C**: Altered ash clasts are bent around quartz grains (Q). **D**: Altered volcanic clast is deformed around a flint clast (F). Altered plagioclase feldspar (P) remnants remain. **E**: Compaction texture, scoria fragments are deformed round remaining plagioclase fragments. (B). Note plagioclase (P) has been replaced by calcite. **F:** Basaltic lava clasts (B) have completely altered, but retain their shape due to the feldspar coating or rims (arrowed). Matrix comprising altered ash deformed around the basalt lava clast and quartz (Q) framework grains.

5.6 Conclusions

Petrographical and SEM analysis has revealed a large number of diagenetic phases within the samples. The offshore samples from Rosebank were very similar to the samples found onshore from the Staffa Formation.

Staffa Formation siliciclastic samples

All of the non-volcanic samples from the Staffa Formation (e.g. sublithic and quartz arenites) have much simpler mineralogy than the volcanic-rich samples. Framework grains are preserved, showing only slight dissolution at grain contacts, with the exception of Type 1 flint that is often much more altered. Evidence for significant compaction is seen throughout with more malleable grains such as micas being deformed around framework grains. Very little authigenic clay can be found within the samples; most forms thin grain coats and is locally confined to areas containing mud lithoclasts or organic material. A wide range of porosity exists within the samples. The quartz arenites have the highest porosities (discussed in the next chapter) with good quality oversized pore networks. The sublithic arenites however, have limited porosity due to a pervasive calcite cement.

Rosebank siliciclastic samples

The Rosebank siliciclastic samples have the most simple petrography of all the samples, being dominated by quartz with rarer feldspar and micas. Evidence of compaction can be found in places, with micas being deformed around framework grains, similar to that seen in the Staffa Formation samples. Some minor dissolution of quartz grains is seen and rare suture contacts also show the sample has experienced some compaction. However, the porosity of these samples is very good with well developed pore networks often with oversized pores. Clays are rarely found coating framework grains and may help protect pores from later stage diagenetic fluids by providing a barrier to nucleation. A patchy calcite cement is found through the samples that locally reduces porosity. This calcite cement may have also influenced the pore network. The timing of this cement could then prove crucial. If early, the cement could protect pores from compaction, with later dissolution of this calcite resulting in pores being preserved. However, significant amounts of diagenetic fluids would be required to dissolve and transport the calcite out of the

reservoir making this sole explanation unlikely. Conversely, a simpler explanation would be that the cement has only ever been patchy with very limited amounts of dissolution.

Staffa Formation volcaniclastic samples

The volcanic-rich samples have a much more heterogeneous mineralogy than the siliciclastic samples due to variable input from volcanic and fluvial/alluvial sources. Vent proximal samples are dominated by pyroclasts that were produced instantaneously, resulting, therefore in more uniform alteration states across the sample. In the reworked samples such as the volcaniclastic lithic wacke, a greater range of volcanic clasts are present and therefore, the range of alteration textures produced is more complex. Grain dissolution is prevalent and in some cases so severe that original rock textures have been completely obliterated. Feldspar alteration is unusual with evidence of K metasomatism.

Clays are abundant in all samples, and the proportion of clay increases with the abundance of volcanic clasts (see Figure 6.33). The basaltic glass firstly alters to gel and fibrous palagonite, which in time is replaced by smectite. Titanium is concentrated into layers as it is not taken into the smectite. More blocky clays tentatively identified as corrensite then grow from the smectite grain coat precursor into the pores. In most cases, pores are completely filled; however, in places extremely large chlorite clays represent a late stage clay fill. Several phases of calcite also exist within the samples with different timings. Late stage calcite fills the last remaining porosity within the samples. A minor phase of zeolite was also found within the samples. The diagenetic paragenesis is difficult to unravel due to the large amounts of phases, complex timing and amount of alteration. Diagenetic phases are locally defined and highly dependent on surrounding mineralogy.

Rosebank volcaniclastic samples

The Rosebank samples have very similar textures to those found onshore. Their petrography is slightly different in that they do not contain flint or primary pyroclasts; however, they do show similar alteration textures, such as axiolitic and spherulitic clay textures and rare perlitic fractures within altered glass samples. Visible porosity is also similarly reduced with clay grain coats and pore fills resulting in rocks with poor reservoir quality. However, the low porosities of these rocks may make them good seals.

5.7 Next steps

Some correlations have been made between volcanic clast abundance and visible porosity and these relationships are explored and quantified in the next chapter. Clays were also only tentatively identified using SEM images and EDAX. QXRD was therefore undertaken to better identify and quantify the diagenetic phases and is discussed in Chapter 6.

6 Quantification of diagenetic phases in volcaniclastic and siliciclastic rocks and their role in hydrocarbon reservoir quality

6.1 Introduction

In the previous chapter a number of diagenetic phases were tentatively identified using the SEM and EDAX. However, clay minerals proved particularly difficult to identify and so X-ray Diffraction (XRD) was undertaken, using the methods described in Section 2.6. As discussed below the XRD results posed a number of further questions and due to limitations with the techniques, Quantitative X-ray Diffraction (QXRD) was undertaken. QXRD allowed the quantification of mineral phases and aided the identification of the authigenic clays, which resulted in a better understanding of the paragenesis of the samples.

The second part of the chapter uses point counting data to discuss the relationship between porosity and permeability with each of the main diagenetic phases (e.g. pore filling clay minerals and calcite cements). The final part of the chapter presents isotopic data that better constrain temperatures and the chemistry of the water in which the pore filling clays grew.

6.2 X-ray Diffraction

For the purpose of this study, all of the samples were separated into six categories depending on volcanic clast content and lithofacies (Table 6.1): Group 1 - vent proximal, comprises vent proximal rocks that are dominated by primary pyroclasts; Group 2 – volcanic-rich epiclastic, comprises rocks that have <20% volcanic clasts, which have clearly been reworked; Group 3 – volcanic-poor epiclastic lithofacies, comprises rocks that have between 10%-20% volcanic clasts; Group 4 - siliciclastic lithofacies, comprises rocks that contain <10% volcanic clasts; Group 5 - Rosebank volcaniclastic rocks, comprises all of the volcaniclastic facies encountered within the Rosebank cores; Group 6 - Rosebank siliciclastic, comprises all of the siliciclastic facies sampled from the Rosebank cores.

Note that flint is not easily resolvable by XRD, as it is composed of recrystallized silica and therefore crystalline varieties appear as quartz in XRD traces.

More amorphous silica varieties will result in a vitreous halation at angles between 20° and 30° (Verstraete et al., 2004). In many cases this will be undetectable in samples that have larger background intensities due to volcanic glass and / or accidental interference from the Perspex sample holders. Therefore, within this chapter the term "quartz" is used to include all crystalline silica, including flint.

Group name	**Lithofacies**	**Samples**	**Dominant characteristic**
Group 1: Vent proximal	Massive scoria-rich breccias (mscBr)	MT2, MT8, MT9,	Primary pyroclasts: vesicular scoria lapili and ash
	Massive scoria rich tuff (mscT)	MT4, MT5,	
	Scoria rich volcaniclastic breccias (scvBr)	MT1, MT3e, MT3f	
Group 2: Volcanic rich epiclastic	Volcaniclastic lithic wacke (VLw) (volcanic clast rich samples)	CA1a, CA1b, Ca1c, Ca1d, Ca2, Ca3, Ca5a, Ca5b, MP03d, MP03e	Mix of reworked pyroclasts, lava clasts, quartz, flint. More than 20% volcanic clasts.
Group 3: Volcanic poor epiclastic	Volcaniclastic lithic wacke (vlW) (volcanic clast poor samples)	MT3g, MT3d, BB1, BB2, BB3	Dominated by quartz, flint with rare mica and lithoclasts. Volcanic clasts are mainly lava clasts but rare ash pyroclasts. Volcanic clasts 10-20%
	Volcaniclastic lithic arenite (vlA)	AT1, AT2, AT3, AT4	
Group 4: Siliciclastic rocks	Sublithic arenite (slA)	MT3a, MT3b, MT3c	Dominated by quartz, flint and feldspar with rare mica and organic material. Volcanic clasts <10%
	Quartz arenites (Q)	MP04	
Group 5: Rosebank volcaniclastic	Volcaniclastic lithic wackes	CHEV 1, CHEV 6, CHEV 8, CHEV 13	Dominated by lava clasts with some ash, quartz, feldspar
Group 6: Rosebank siliciclastic	Sublithic arenites	CHEV 16, CHEV 17, CHEV 25	Dominated by quartz and feldspar with rare mica and mudstone lithoclasts. No volcanic clasts.
	Quartz arenites	CHEV 19	

Table 6.1: Summary of groupings used within this chapter

6.2.1 Bulk XRD

Bulk XRD analysis was undertaken on the majority of the samples. Initially, the smear method was used, but due to poor results and a high background signal, the packing method was then utilised (both methods are described in Section 2.6.1). It was hoped that bulk analysis could be used to quantitatively predict the minerals within each sample. Peak positions correlated well with literature, allowing the main mineral phases within each sample to be identified. While absolute peak intensities are arbitrary, relative peak intensities can be used to quantify the amounts of mineral phases. However, due to poor instrumentation set up and preferential alignment of minerals in the samples during sample preparation, reproducibility of the relative peak sizes was poor. This lowered the confidence of the data and as a result accurate quantification was not attempted with this data set. The results from bulk analysis are described below using the groupings as described in Table 6.1.

Group 1 – Vent proximal samples results

Seven samples from the vent proximal grouping were analysed by bulk XRD (Figure 6.1). Generally, there is a good correlation between the scans for each sample, although minor differences do occur. All samples comprise rock-forming minerals such as feldspar (albite and anorthite) and minor quantities of quartz, while diagenetic phases include calcite and clays. The peak labelled K was initially identified as kaolinite; however, this peak may represent chlorite or a mixture of both minerals (discussed in Section 6.2.2). Samples MT1, MT5 and MT8 and MT9 all contain the zeolite, analcime. A high background intensity is seen in all of the group 1 samples, making identification of minerals difficult.

Group 1- Vent proximal samples interpretation

The bulk XRD results correlate well with the mineralogy seen in the previous chapter. The high background intensity within the scans implies the presence of an amorphous material. This could be explained by the large quantities of altered volcanic glass within the proximal samples. The large, broad peak at low angles indicates an abundance of several phases of clay minerals

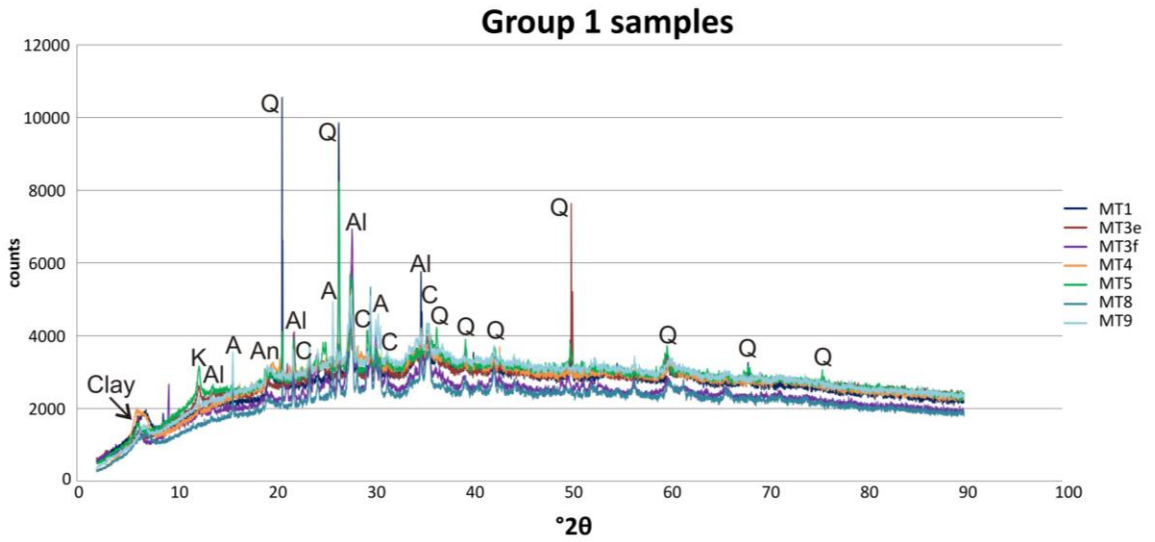

Figure 6.1: Bulk XRD traces for representative Group 1 samples. Annotations: quartz (Q); anorthite (An); albite (Al); calcite (C); analcime (A); kaolinite / chlorite (K).

Group 2 - Volcanic rich epiclastic

Six samples from the volcanic rich epiclastic grouping were analysed by bulk XRD (Figure 6.2). Correlation between these scans was better than that of Group 1 samples, with most samples containing the sample mineral phases. Group 2 traces have less noise than the Group 1 scans allowing for easier identification of mineral phases. The samples comprise quartz and anorthite (albite was not found). Diagenetic minerals are similar to Group 1, with clay minerals found in all samples.

Group 2 - Volcanic rich epiclastic interpretation

The large well defined quartz peak in the Group 2 results indicates a greater proportion of quartz than in the Group 1 samples, which correlates well with the petrography data (Section 5.2.2.4). The broad peak at low angles again indicates the presence of a large amount of clay minerals. The large background within the scans suggests the presence of large amounts of volcanic glass. Notable differences between these results and the Group 1 samples are the lack of calcite and albite. If clay pore fill has been extensive this could explain the lack of calcite within samples. The lack of albite however, is harder to explain as Na-rich feldspars were found in the SEM data.

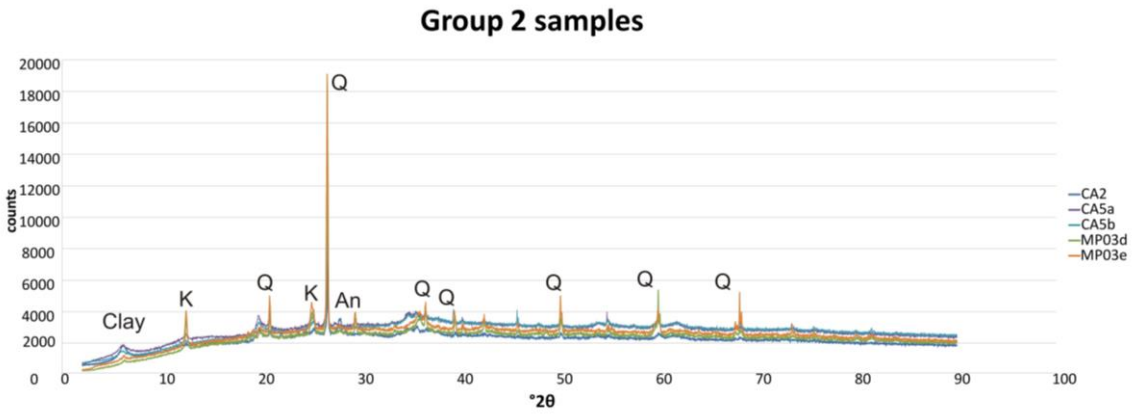

Figure 6.2: Bulk XRD traces for representative Group 2 samples. Annotations: quartz (Q); anorthite (An); calcite (C); kaolinite / chlorite (K).

Group 3 - Volcanic poor epiclastic

Five samples from the volcanic poor epiclastic grouping were analysed by bulk XRD (Figure 6.3). The background in all samples is much lower than the previous two groups. Correlation between all the Ardtun (AT) samples is very good. Quartz and albite are the main rock forming minerals found within the samples, and calcite is the dominate pore filling phase in the Ardtun samples. No calcite is found within sample MT3d.

The presence of a small broad low angle peak indicates that minor amounts of clay minerals can be found within the samples. There is no distinctive kaolinite/ chlorite peak at 12.5°, as found in the previous two groups; however, a minor peak may just rise above the background. Analcime was only present within sample MT3g.

Group 3 - Volcanic poor epiclastic interpretation

The lower background levels indicate less amorphous material within the samples and therefore less volcanic glass than in the previous groupings. The smaller, broad clay peak and minor peak at 12.5° indicate that the proportion of clay within the sample is much less than in previous groupings. This correlates well with the SEM data, which identified calcite as the main pore-filling phase within the volcaniclastic lithic arenites.

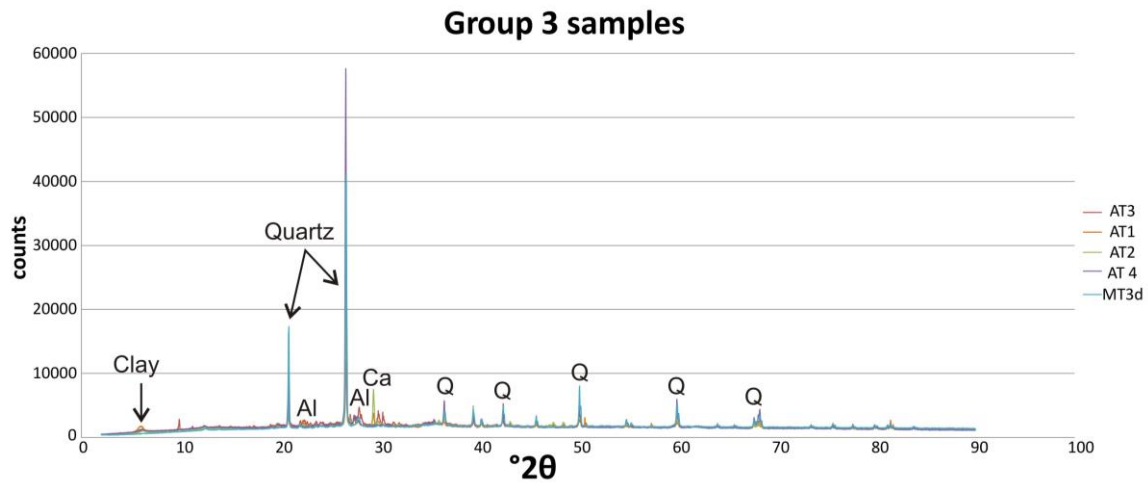

Figure 6.3: Bulk XRD trace for typical Group 3 samples. There is good correlation between all of the traces. Annotations: quartz (Q); calcite (Ca); albite (Al).

Group 4: Siliciclastic rocks

Four samples from the siliciclastic rock grouping were analysed by bulk XRD (Figure 6.4) and correlation between the samples is very good. The background within the samples is relatively low, especially within the MT samples (The Ladder locality). These samples are dominated by quartz. The MT samples have very little clay with no obvious low angle peaks. MP04 (Malcolm's Point locality) has a visible clay peak but also has calcite.

Group 4: Siliciclastic rocks interpretation

The low background counts indicate low amounts of amorphous volcanic glass within the sample. The MT samples have very little clay or calcite, which correlates well with the petrographic and SEM data for quartz arenites in the previous chapter. MP04 has a small amount of calcite, which also correlates to the patchy calcite cement found within the sublithic arenites.

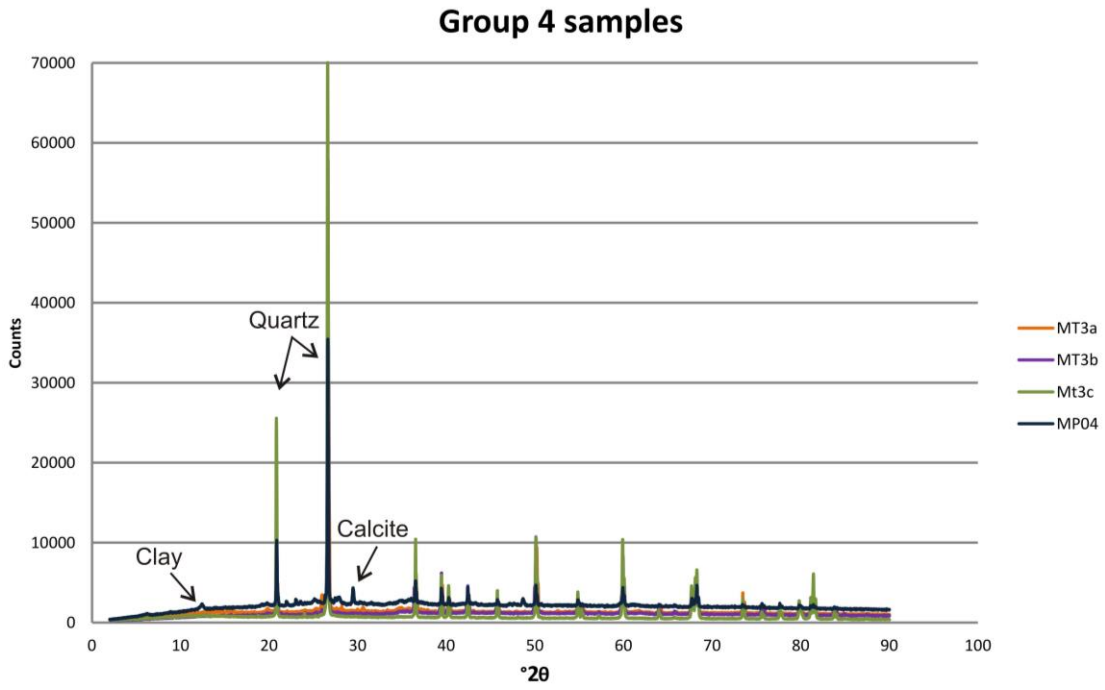

Figure 6.4: Bulk XRD trace for typical Group 4 samples. Large unlabelled peaks are secondary quartz and calcite.

Group 5: Rosebank volcaniclastic samples

Two representative samples from the Rosebank volcaniclastic rock group display significant differences in their traces and represent end member samples (Figure 6.5). CHEV 1 represents a quartz-rich volcaniclastic wacke. The sample comprises quartz, Ca- and Na-rich feldspar (anorthite and albite) and calcite. CHEV 13 represents a volcanic clast-rich sample comprising albite and calcite but lacking quartz and anorthite. It also contains significant quantities of analcime. A sharp peak at 6° in both samples, is identified as smectite. The background in all samples is high and resembles that seen in the volcanic-rich onshore rocks.

Group 5: Rosebank volcaniclastic sample interpretation

The background is higher in CHEV 13 indicating the presence of more volcanic glass than in CHEV 1. The more volcanic-rich sample is also the zeolite-rich sample, that has very little quartz. The very high quantities of clay (in this case smectite) are similar to the onshore volcanic clast-rich rocks (groups 1 and 2).

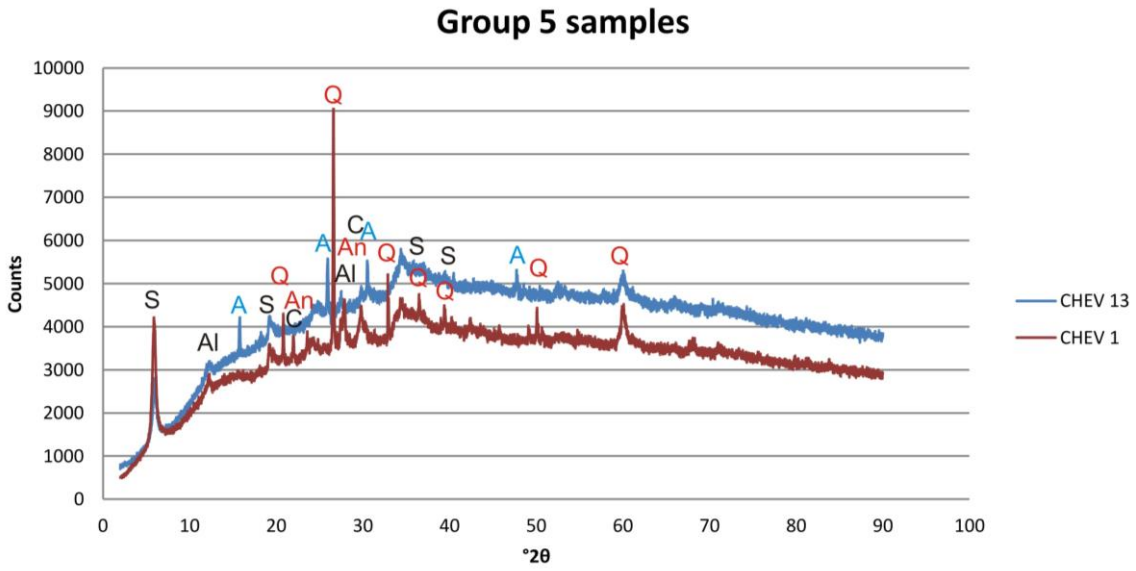

Figure 6.5: Bulk XRD traces for representative Group 5 samples. Annotations: quartz (Q); anorthite (An); albite (Al); calcite (C); analcime (A); smectite (S). Red annotations = minerals only found in CHEV1, blue are only found in CHEV 13, black are found in both.

Group 6: Rosebank siliciclastic

Four samples from the Rosebank silicilastic rock grouping are shown in Figure 6.6. These samples correlate well with most minerals being identified in each trace, and have very low background readings, similar to group 4 samples. They comprise quartz and feldspar (anorthite and albite) but lack calcite, which was found in onshore equivalents. A very small peak is noted at 12.5° indicating the presence of minor amounts of clay.

Group 6: Rosebank siliciclastic interpretation

The low background counts indicate the samples lack volcanic glass. The small clay peak indicates very minimal amounts of clay minerals similar to the onshore equivalents (Group 4). Calcite was found within these samples in Section 5.2.1.3; however, no calcite appears within the group 6 bulk XRD traces, which may be explained by the patchy nature of this cement.

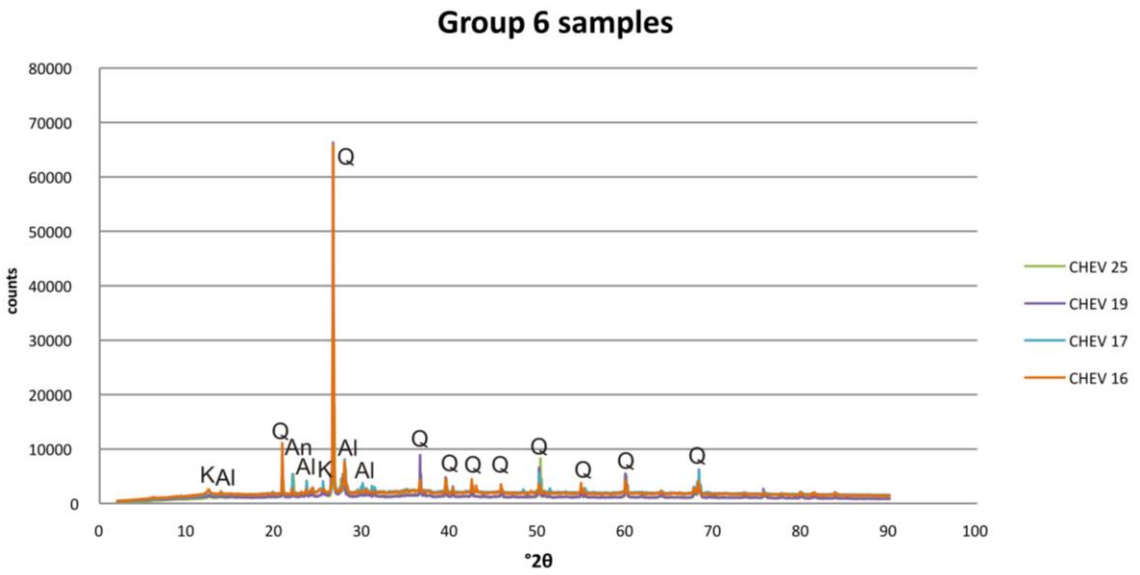

Figure 6.6: Bulk XRD traces for representative Group 6 samples. Annotations: quartz (Q); anorthite (An); albite (Al); kaolinite / chlorite (K).

Bulk XRD discussion

Most of the major phases were identified and confirmed by using the bulk XRD method. Siliciclastic samples (groups 4 and 6) contained few phases and had a lower background, leading to more accurate and easier identification. However, volcanic-rich samples (group 1, 2 and 5) all have large backgrounds with multiple peaks, resulting in a difficult identification process.

Some minerals (e.g. pyroxene, alkali feldspar, mica) identified in the previous chapter (Section 5.2.2.5) were not identified in any of the XRD traces. There may be several reasons for this. Firstly, the missing minerals are all fairly minor components of the rocks and therefore may have been lost in the sampling process. Secondly, poor instrumental set up may result in larger backgrounds which could obscure smaller peaks. As already stated samples containing large amounts of amorphous glass will cause an increase in the background and may also contribute to smaller peaks being obscured. Finally, sample orientation may lead to some phases being overestimated while others may be reduced. Bulk XRD samples were prepared using firstly the smear method and then a packing method (as described in Section 2.6.1.2). Roughening of the sample surface within the packing method aims to reduce preferential orientation and keep the power randomly orientated. However, the technique is limited and some preferential alignment may occur. It is likely that missing minerals are due to a

combination of all three of these factors. In the future I would recommend that bulk samples be prepared by using the spray drying method discussed in Section 2.7.2.

6.2.2 Clay separate XRD

A broad peak at low angles was found in the majority of the bulk XRD traces. This peak was identified as clay minerals but could not be further subdivided. Similarly a sharp peak at 12.5° was found in several traces. However, the resolution of the bulk scans was such that differentiation between kaolinite and chlorite could not be achieved. For these reasons clay orientated XRD was undertaken.

The clay fraction (<2μm) was separated out using the method described in Section 2.6.2.1. The samples were examined under the SEM to ensure clay platelets were adequately orientated. These samples were then analysed in three ways; air dried, etholene glycollated, and furnace to 550°C. Clay types will react differently to the treatments and therefore identification can be made (Carroll, 1970; Thorez, 1976; Moore and Reynolds, 1997). Using the groupings defined above, the typical clay separate scans are displayed below.

Group 1 – Vent proximal

An example of a Group 1 sample, MT5, is seen in Figure 6.7. The small sharp peaks at 26.65° and 20.85° seen in all three scans are identified as quartz. The peaks at 12.5° and 25° could either be chlorite or kaolinite or a mixture of both mineral types. The sample was heated to 550°C in order to differentiate between the two minerals. Kaolinite becomes amorphous to X-rays at this temperature and therefore the diffraction pattern will disappear (Moore and Reynolds, 1997). The peak in MT5 is reduced but still visible indicating that it is more likely to be chlorite than kaolinite. The broad peak around 6° swells to ~ 5.2° under glycollation and collapses to ~8.4° after heating. This would indicate that the peak is smectite.

Group 2 - Volcanic rich epiclastic

An example of a Group 2 sample, CA1d, is seen in Figure 6.8. Quartz peaks are identified at 26.65° and 20.85°. The peaks at 12.5° and 25° can be identified within the

furnace trace indicating the presence of chlorite rather than kaolinite. Smectite is also identified within the Group 2 samples. The chlorite peak is relatively much larger than the smectite peak, indicating a greater proportion of chlorite within the sample.

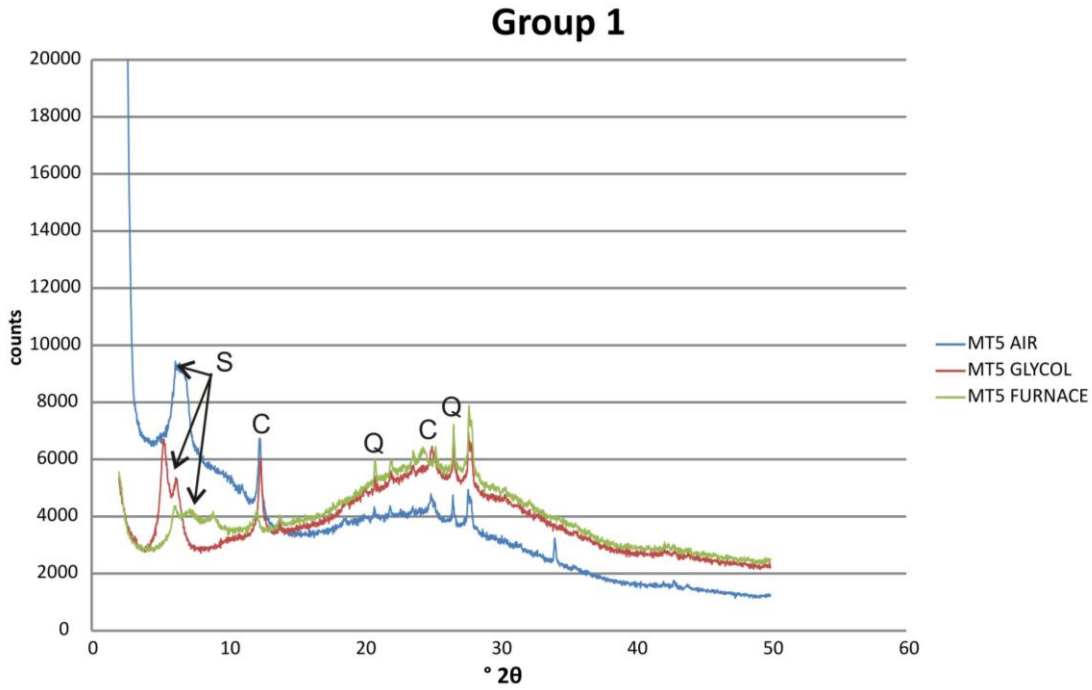

Figure 6.7: Clay separate XRD traces for Group 1 sample, MT5. Air (blue),glycollated for 18 hours (red), furnace at 550°C for 24 hours (green). Annotations: quartz (Q); chlorite (C); smectite (S).

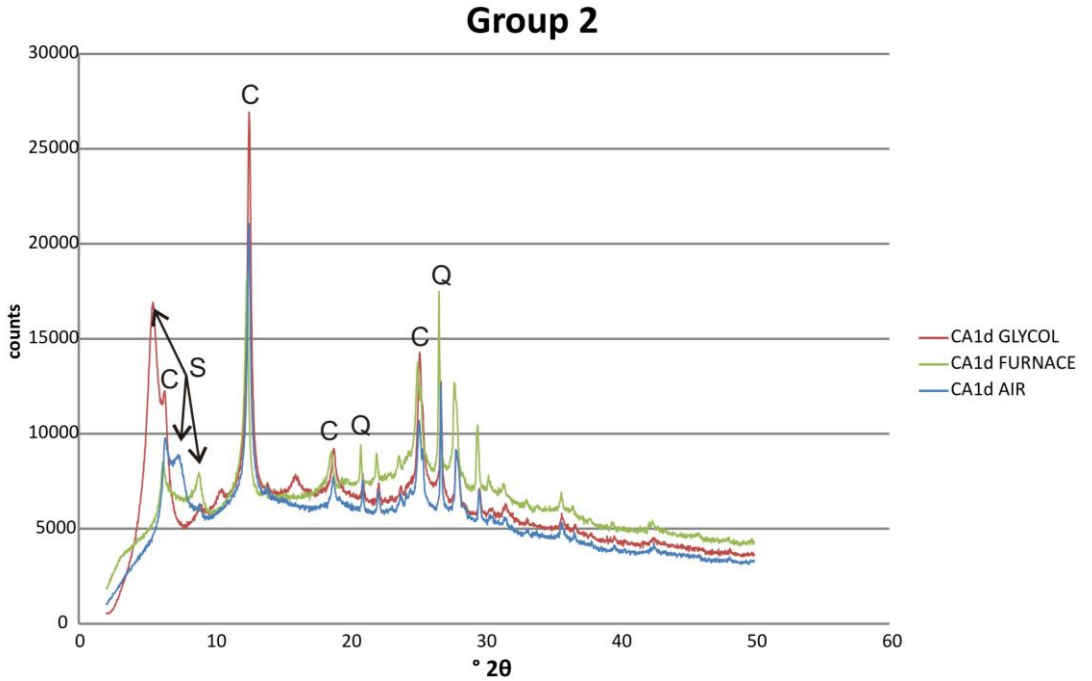

Figure 6.8: Clay separate XRD traces for Group 2 sample, CA1d. Air (blue), glycollated for 18 hours (red), furnace at 550°C for 24 hours (green). Annotations: quartz (Q); chlorite (C); smectite (S).

Group 3 – Volcanic-poor epiclastic

An example of a Group 3 sample, Ca5b, is seen in Figure 6.9. A very small amount of quartz is identified within this sample. The dominant clay phase is smectite; however, the collapse of the 12.5° and 25° peaks in the furnace trace indicates the presence of kaolinite instead of chlorite.

Group 4: Siliciclastic rocks

An example of a Group 4 sample, CA4, is seen in Figure 6.10. As in the Group 3 example the 12.5° and 25° peaks collapsed in the furnace trace indicating the presence of kaolinite, which is the most dominant clay type. Smaller peaks of smectite are also identified.

Group 5: Rosebank volcaniclastic

Despite the slight differences in the mineralogy of the Group 5 bulk traces, clay peak positions were constant throughout the sample set. Analysis of all the Group 5 samples showed very similar clay separate results. An example of a Group 5 sample, Chev 1, is seen in Figure 6.11. Quartz peaks are again identified, as is chlorite and smectite. The sharp peaks at 8.8° and 17.73° that are unaffected by glycollation or heating indicate the presence of illite.

Group 6: Rosebank siliciclastic

An example of a Group 6 sample, CHEV 16, is seen in Figure 6.12. Quartz peaks are identified as is chlorite, which is the dominant clay type. Illite is also identified; however, smectite peaks are absent.

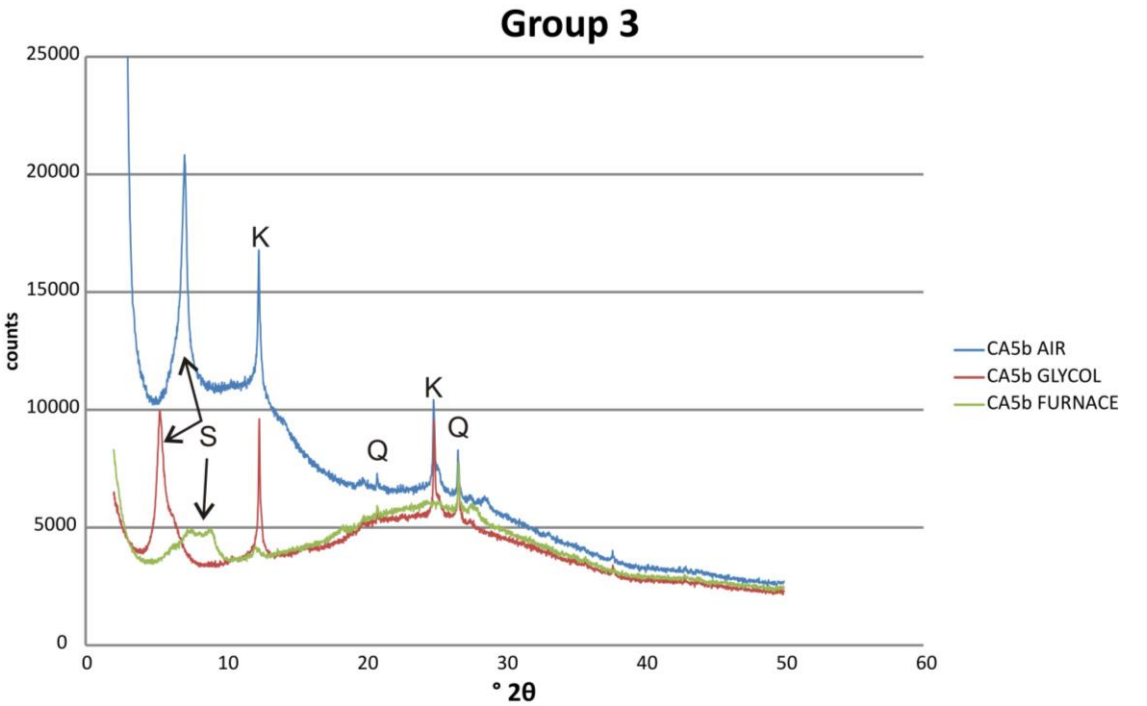

Figure 6.9: Clay separate XRD traces for Group 3 sample, CA5b. Air (blue), glycollated for 18 hours (red), furnace at 550°C for 24 hours (green). Annotations: quartz (Q); kaolinite (K); smectite (S).

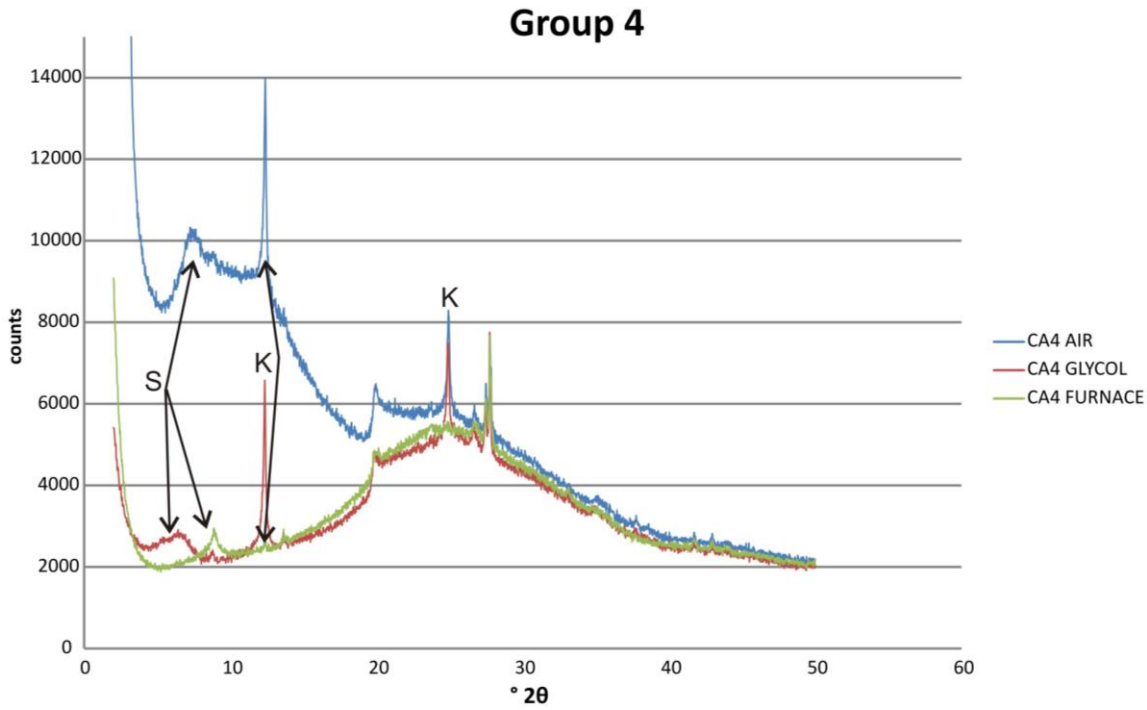

Figure 6.10: Clay separate XRD traces for Group 4 sample, CA4. Air (blue), glycollated for 18 hours (red), furnace at 550°C for 24 hours (green). Annotations: kaolinite (K); smectite (S).

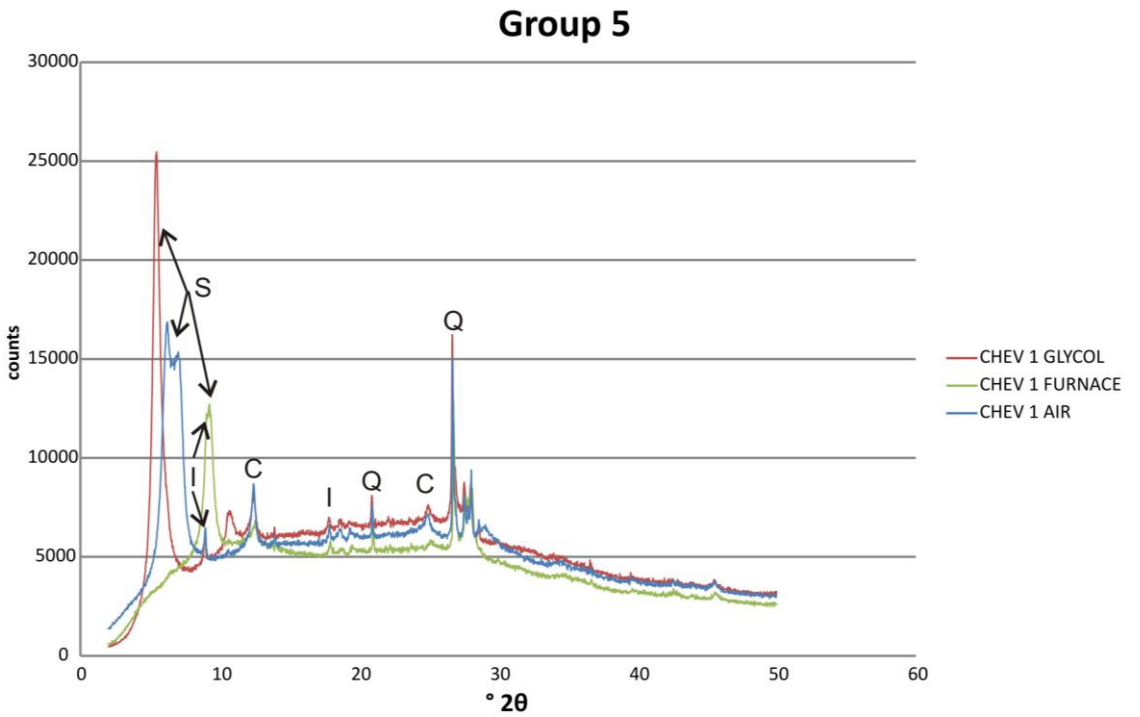

Figure 6.11: Clay separate XRD traces for Group 5 sample, CHEV 1. Air (blue), glycollated for 18 hours (red), furnace at 550°C for 24 hours (green). Annotations: quartz (Q); chlorite (C); smectite (S); illite (I).

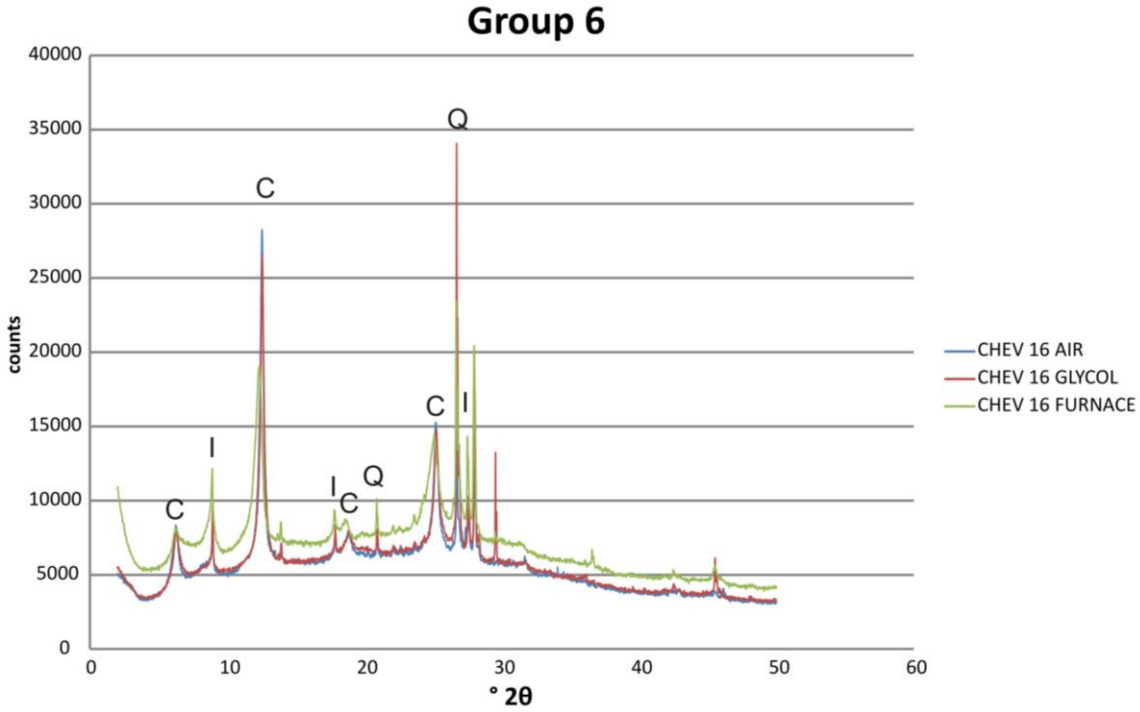

Figure 6.12: Clay separate XRD traces for Group 6 sample, CHEV 16. Air (blue), glycollated for 18 hours (red), furnace at 550°C for 24 hours (green). Annotations: quartz (Q); chlorite (C); illite (I).

Clay orientated XRD discussion

All of the samples comprising volcanic clasts contain smectite. Volcanic clast-rich samples (groups 1, 2 and 5) were dominated by smectite and chlorite. Group 3 samples still contain a significant smectite component; however, instead of chlorite, they contain kaolinite. Despite the lack of volcanic clasts within Group 4 samples, they still contain minor amounts of smectite; however the dominant clay is kaolinite. Offshore group 6 samples are devoid of smectite and instead comprise chlorite. Illite is found as a minor phase in both offshore sample sets, but is not found within the onshore samples.

The clay separate analysis followed standard protocol found within the literature. By definition the clay fraction of the rock is material under 2 μm in size (Moore and Reynolds, 1997). Samples were separated into size fractions by centrifugation, using times calculated according to Stokes' Law (Jackson and Barak, 2005). Stokes' Law describes the relationship between the gravitational force acting on a spherical particle as it falls against the resistive forces of the fluid it is falling through. This relationship is only relevant for spherical particles under 20 μm (Moore and Reynolds, 1997). The samples in this study are unusual in that clay fibres as large as 50 μm long were observed using the SEM. Clay particles are also not spherical in shape meaning that they will take longer to settle in a resistive fluid and will stay in suspension longer. As a result, clay particles larger than 2 μm will be included within the analysis. However, the 50 μm chlorite platelets may still be too large to be included within the separate.

Four samples were re-analysed but this time the < 5 μm size fraction was analysed. This size fraction should include more of the larger clay platelets. The results from the re-analysis of a Group 2 sample (Ca1d) is shown in Figure 6.13, and shows a relative increase in the chlorite and quartz peaks compared to Figure 6.8. This indicates more chlorite was present within the sample suggesting that some of the large 50 μm platelets have been lost from the original analysis. However, the increase in quartz indicates that small quantities of crystalline minerals were included in the size fraction. The well-formed crystalline nature of these minerals produces relatively large peaks which obscured smaller clay peaks and made identification of the mineral phases harder.

The "lost" chlorite is not thought to significantly change the overall conclusion of this study; however, the presence or absence of very large metosamatic or hydrothermal clays is an important consideration during clay separate analysis.

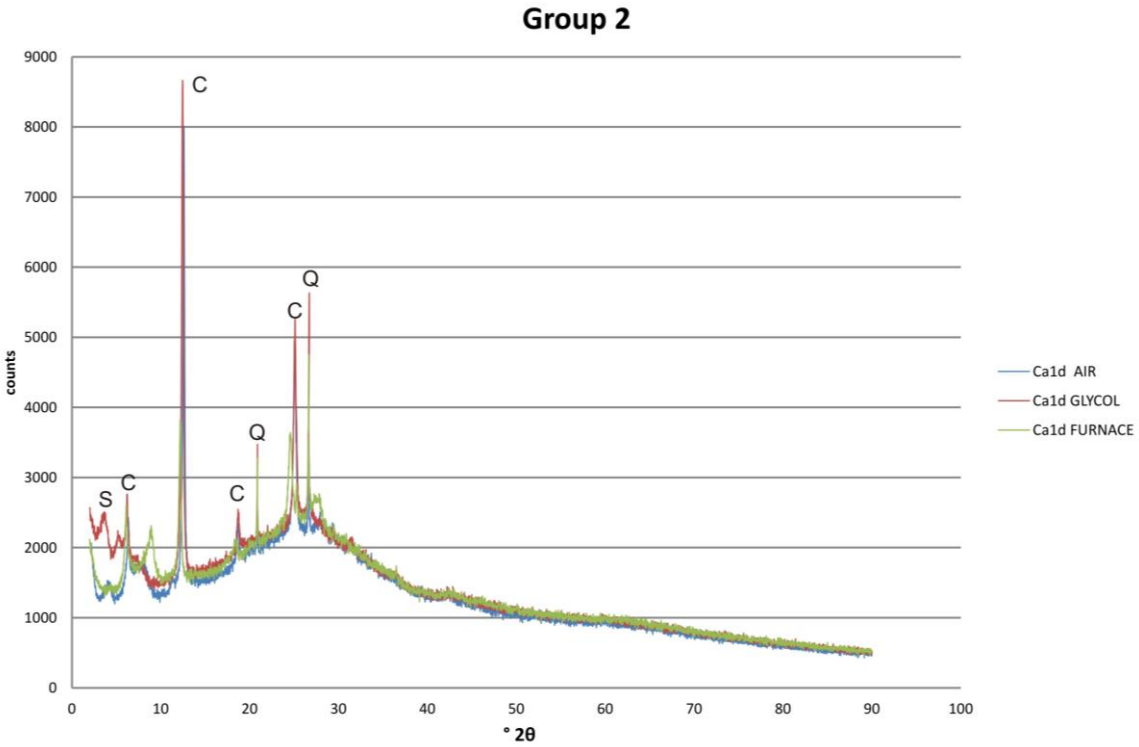

Figure 6.13: XRD trace for the < 5 µm fraction. Note the more prominent chlorite and quartz peaks compared to Figure 6.8.

6.3 Quantitative X-ray Diffraction (QXRD)

Bulk and clay separate analysis allowed the main mineral phases to be identified within each sample grouping; however, only tenuous semi-quantification could be attempted based on relative peak heights. In order to better quantify mineral amounts, QXRD was attempted on 8 samples (Table 6.2), which were chosen to represent the spectrum of lithofacies seen both on Mull and Rosebank. The correlation between offshore and onshore mineralogy is very good. The samples can be classified into the facies groupings discussed in Table 6.1.

SAMPLE ID	LOCATION	FACIES TYPE	LITHOFACIES GROUPING
MT8	Onshore: MacCulloch's Tree, Mull	Massive scoria-rich breccia	Group 1: Vent Proximal
MT5	Onshore: MacCulloch's Tree, Mull	Massive scoria rich tuff	
Ca1d	Onshore: Carsaig Arches, Mull	Volcaniclastic lithic wacke (volcanic rich)	Group 2: Volcanic-rich epiclastic
MT3g	Onshore: The Ladder, Mull	Volcaniclastic lithic wacke (volcanic poor)	Group 3: Volcanic-poor epiclastic
MT3a	Onshore: Ardtun, Mull	Sublithic arenite	Group 4: Sililciclastic rocks
CHEV 6	Offshore: Well 213/27-2	Volcaniclastic lithic wacke	Group 5: Rosebank volcaniclastic
CHEV 13	Offshore: Well 213/27-2	Volcaniclastic lithic wacke	
CHEV 16	Offshore: Well 213/27-2	Sublithic arenite	Group 6: Rosebank siliciclastic

Table 6.2: 8 samples analysed by QXRD.

6.3.1 Results from this study

Table 6.3 shows the simplified QXRD results where all compositions of minerals have been grouped together under one heading (e.g. compositions from albite to anorthite are all included under plagioclase).

Sample name	% Quartz	% Plagioclase	% K-feldspar	% Pyroxene	% Glass	% Other
MT8	3.9	33.1	4.7	10.6	18.1	1.5
MT5	3.0	12.7	3.4	10.9	15.2	2.3
MT3g	31.5	14.4	1.3	1.4	11.0	1.4
CHEV 6	0.6	2.1	3.1	5.5	25.1	1.9
Ca1d	11.2	7.0	3.0	2.8	11.3	1.9
CHEV13	0.7	0.7	2.6	4.0	20.9	2.5
MT3a	38.8	10.5	8.2	10.0	8.2	0.6
CHEV16	57.8	20.1	7.1	0.8	2.3	0.6

Sample name	% Calcite	% Analcime	% Corrensite	% Saponite	% Nontronite	% Di-smectite	% Illite/smectite	% Kaolinite	Sum
MT8	0.0	1.2	16.0	10.9	0.0	0.0	0.0	0.0	100
MT5	1.1	1.4	6.4	24.8	9.0	4.0	5.8	0.0	100
MT3g	2.1	0.8	26.9	2.3	4.8	0.0	0.0	2.1	100
CHEV 6	0.2	13.2	32.6	15.7	0.0	0.0	0.0	0.0	100
Ca1d	0.0	9.8	24.5	3.5	8.8	0.0	13.8	2.4	100
CHEV13	0.2	8.0	42.2	13.3	4.9	0.0	0.0	0.0	100
MT3a	0.0	0.5	7.0	4.7	0.0	4.8	6.7	0.0	100
CHEV16	0.0	0.4	9.5	0.0	0.0	1.1	0.3	0.0	100

Table 6.3: QXRD summary results. % Other includes; amphibole and pyrite.

Group 1

MT8 and MT5 are both proximal vent facies and so contain abundant primary pyroclastic lithoclasts. The QXRD data suggests they contain high proportions of plagioclase (33.1% and 12.7%), pyroxene (10.6% and 10.9%) and glass (18.1% and 15.2%). Minor amounts of quartz (<4 %) and zeolite are present. MT5 also contains minor amounts of calcite (1.1%) as well as traces of amphibole and pyrite. The proportion of total clay is much higher than in siliciclastic equivalents. MT5 has 50% total clay whereas MT8 has 26.9%. The clay phases reported differ in the samples. MT8 is dominated by corrensite (16%) but also contains saponite (10.9%), whereas MT5 is dominated by saponite (24.8%) with only 6.4% of corrensite. MT5 also contains several other types of clay such as nontronite (9%), illite/smectite mixed layer clay (5.8%) and dioctrohedral smectite (4%).

The QXRD data set broadly correlates with the point counting results for Group 1 samples (see the "Point counting" file in the appendix). Portions of clay and glass were higher in point counting results while plagioclase and zeolite were found in higher proportions within the QXRD data set. The QXRD data set cannot distinguish between plagioclase clasts and plagioclase phenocrysts within basalt clasts therefore QXRD data sets will have higher plagioclase feldspar proportions relative to point counting data. One key difference is the proportion of pyroxene. Less than 1% pyroxene was identified during point counting however ~10% was found in the QXRD analysis. This may be explained by the degree of alteration. If the pyroxene was highly altered then in may be difficult to identify optically and could have been classed as clay.

Group 2

Onshore sample Ca1d, represents a much more transitional volcaniclastic facies as it contains a significant siliciclastic component as well as a volcanic component. Ca1d, based on QXRD, comprises 11.2% quartz and 10% feldspar, both significantly greater than the offshore examples; however, the zeolite and total clay components are similar, with 9.8% and 5.3% respectively. Corrensite is the dominant clay phase (24.5%), with illite/smectite mixed layer (13.9%), nontronite (8.8%) and minor, kaolinite and saponite present.

Group 2 samples also loosely correlate to point counting values (see the "Point counting" file in the appendix). Here the main difference was the proportion of clay, which was underestimated in the point counting data set with respect to the QXRD data set. The volcanic clasts however were over estimated. This again highlights the difficulties associated with classifying minerals during point counting. Where a relect basalt clast edge was present the clast was counted as basalt however, the clast may have been partially replaced by clays resulting in the QXRD data having a higher clay content.

Group 3

Sample MT3g is transitional between volcanic-rich and volcanic-poor (31.5% quartz, 15.7% feldspar, 11% glass and a minor calcite phase of 2.1%). Less volcanic rich facies have a lower percentage of total clay than the more volcanic rich facies at 36.1%. Corrensite is the dominant clay phase (26.9%), with minor quantities of nontronite (4.8%), saponite (2.3%) and kaolinite (2.1%) also present.

Group 3 QXRD results correlate well with point counting data. The only slight difference is the proportion of clay which was slightly underestimated in the point counting (25%) compared to the QXRD results (36.1%).

Group 4

Quartz is found in all samples and in this case can be used as a good inverse proxy to volcanic content. MT3a, based on QXRD, has a high proportion of quartz (38.8%) and although is classified as siliciclastic, it does contain rare (<2%) of weathered basalt clasts. This results in a more complex mineralogy than that of samples devoid of volcanic material (e.g. CHEV 16). MT3a contains low proportions of feldspar (11% plagioclase and 8% k-feldspar) but also contains pyroxene (10%). The clay mineralogy of MT3A is complex with a total clay content of 23%. This is made up of corrensite (7%), saponite (4.7%), illite/smectite (6.7%) and nontronite (4.8%).

Group 4 rocks correlate well with point counting data. Again the proportions of feldspar and pyroxene have been underestimated however the proportion of quartz and total clay is within 5% in both data sets.

Group 5

Offshore samples CHEV 13 and CHEV 6 are volcanic-rich samples. These rocks, based on QXRD, have very little quartz (<1%), feldspar (<5.2%) and pyroxene (<6%), but much higher proportions of volcanic glass (21–25%). Both rocks also have a significant zeolite component with CHEV 6 containing 13.2% analcime and CHEV 13 containing 8%. CHV6 has a total clay mineral content of 48.3% while CHEV13 is as high as 60.4%. The clays in these rocks are very similar with corrensite being the dominate phase in both (32.6% – 42.2%) followed by saponite (15.7% – 13.3%). Sample CHEV13 also contains 4.9% of nontronite.

The proportion of zeolite and clay minerals is much higher in QXRD results than in the point counting data. Some zeolite may have been misidentified during point counting as calcite. Difficulties again arise in distinguishing between and characterising altered volcanic clasts under optical conditions.

Group 6

CHEV 16 has based on QXRD data, high proportions of quartz (58%), together with high proportions of both plagioclase (20%) and k-feldspar (7%). The only clay phase present is corrensite (10%). Group 6 QXRD results correlate well with the point counting data set.

6.4 QXRD discussion

The QXRD results generally correlate well with the bulk XRD results. Some discrepancies such as the lack of pyroxene and K-feldspar in the bulk XRD results can be explained by the more accurate sample preparation techniques and machine set up in the QXRD method, resulting in better resolution of peaks and therefore more detailed and accurate identification. The higher precision method and extensive custom made clay trace database and expertise at the Hutton Institute, allowed smectite phases to be separated.

However, one significant difference between the XRD undertaken at Durham and that undertaken at the Hutton Institute remains unexplained. Clay separate XRD

and SEM analysis both indicated the presence of well-formed chlorite. Small quantities of chlorite were lost in the clay separate sample preparation. However, no chlorite was identified in the QXRD samples. These samples were not prepared by separation techniques and so should still contain all of the chlorite. Mixed layer chlorite-smectite are often difficult to resolve due to peak interference (Moore and Reynolds, 1997); however, very sharp chlorite peaks were observed in the clay separate results indicating that chlorite close to pure phase was present. This anomaly remains unexplained.

6.4.1 Volcanic glass

The relationship between quartz and volcanic glass is linear, although the sample small sample set must be considered (Figure 6.14). The relationship between the proportion of volcanic glass and the total amount of clay is shown in Figure 6.15. This highlights that having large quantities of volcanic glass within a sample will result in high proportions of clays. There is a threshold relationship with all samples over 10% glass having significant proportions (> 26%) of clay minerals.

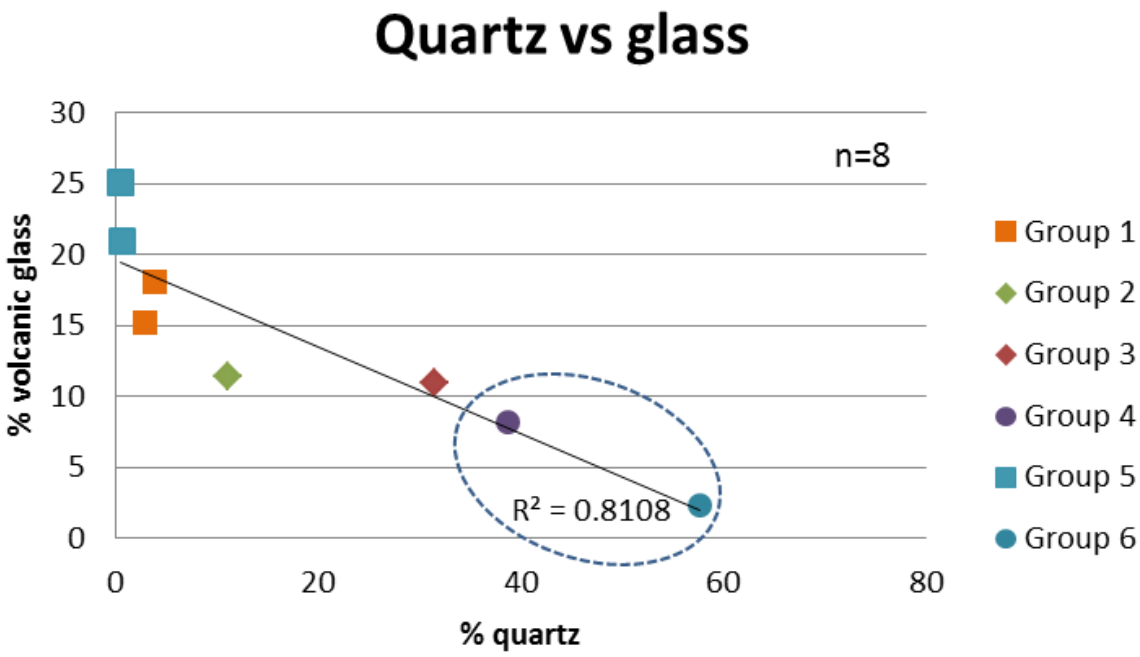

Figure 6.14: Relationship between % of quartz and % of volcanic glass using QXRD data. Square points are volcanic rich samples, diamonds are intermediate samples and circles are volcanic poor samples. Dashed line defines siliciclastic samples.

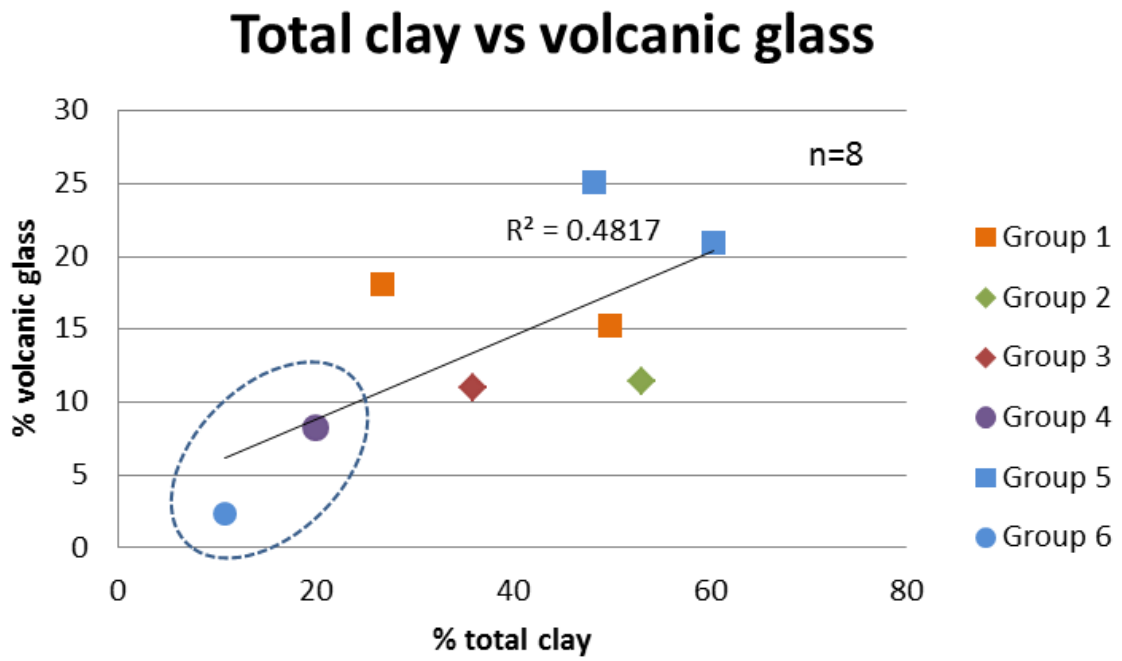

Figure 6.15: Relationship between % of total clay minerals and % of volcanic glass using QXRD data. Square points are volcanic rich samples, diamonds are intermediate samples and circles are volcanic poor samples. Dashed line defines siliciclastic samples.

6.4.2 Phyllosilicates

Understanding the composition of clay within a reservoir is important in the hydrocarbon industry (Eslinger and Pevear, 1988). Different clay minerals have different structures and therefore, affect the porosity and permeability of the sample differently (Moore and Reynolds, 1997). Smectite can swell in the presence of water, and fill surrounding pore spaces, while chlorite can be dissolved in acid resulting in precipitation of iron hydroxide and amorphous silica – aluminous gel that can reduce permeability (Moore and Reynolds, 1997). Therefore, an understanding of the type of clay is crucial during hydrocarbon extraction.

The QXRD results allowed the difference in the smectite clays to be resolved and quantified. Therefore, the relationship between clay minerals and other mineral phases could be explored.

Corrensite

Large quantities of corrensite (a mix layer smectite-chlorite clay) were identified in the QXRD results, but not in the clay separate XRD. Corrensite is difficult to identify using XRD (Reynolds, 1988). It forms peaks at very low angles (~3°), which would be obscured by the high background within the clay separate samples. Other corrensite peaks overlap with the smectite peaks and so could contribute to the width of these peaks within the clay separate results. The effect of glycollation on corrensite peaks is hard to identify due to peak interference with smectite. Corrensite also hydrates very quickly (within minutes) meaning that the effects of heating are often lost before analysis is complete (Moore and Reynolds, 1997). A combination of all these factors has most likely resulted in corrensite peaks being unresolvable in the clay separate traces.

Corrensite has been found in volcanic rocks in a number of studies (e.g. Schulte, 1963 and Whitney and Northrop, 1986) with several linking the presence of corrensite to the weathering and alteration of basaltic rocks (Smith, 1960 and Shau et al., 1990). Figure 6.16 shows the relationship between corrensite and volcanic glass within the QXRD results. With the exception of one Group 1 sample all samples containing volcanic glass contained large quantities (>15%) of corrensite.

There are currently two differing opinions on corrensite. Some authors consider corrensite to be a mix layer phyllosilicate on the saponite to chlorite continuous (Chang et al, 1986, Reynolds, 1980; Robinson and Bevins 1994) or discontinuous (Inoue et al. 1988; Inoue and Utada, 1991) conversion series, bridging the large compositional difference between saponite and chlorite. Brigatti and Poppi, (1984) hypothesize that the continuous chemical variation of corrensite between chlorite and smectite is due to Mg and Fe mobilization by hydrothermal fluids. Other workers consider corrensite to be a single phase and itself, an end member (Reynolds, 1988; Roberson, 1988; Beaufort et al., 1997). These authors found the composition of corrensite was constant throughout their sample sets and was only very rarely found with saponite. Figure 6.17, shows the relationship between saponite and corrensite found within this study. Both phases were found in all of the samples apart from the Group 6 offshore silicilclastic sample. Samples that contain higher percentages of corrensite also contain high proportions of saponite. Apart from in Group 1 rocks that have low levels of corrensite.

Several authors have reported that different compositions of smectite / chlorite mix layer clays are found in vesicle lining versus amygdale fills. Typically mix layer smectite chlorite / expandable clay is found as a vesicle lining, whereas a phase approaching the chlorite end member fills the amygdale centre (Boles and Coombs, 1977; Viereck et al, 1982; Shau et al., 1990). This is consistent with the SEM results and explains the presence of both clay phases within the QXRD results. If the origin of the chlorite identified in the clay separate does result from a smectite or corrensite precursor then this could in part explain why this material was identified as corrensite during QXRD analysis.

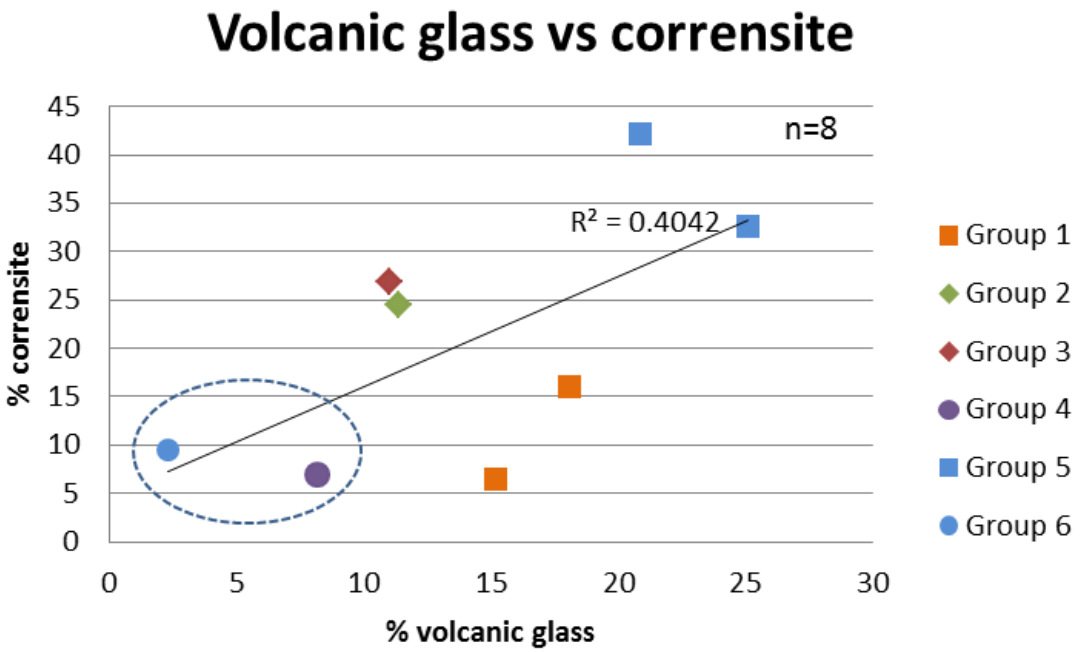

Figure 6.16: Plot of % volcanic glass against % corrensite using QXRD data. Dashed line defines siliciclastic samples.

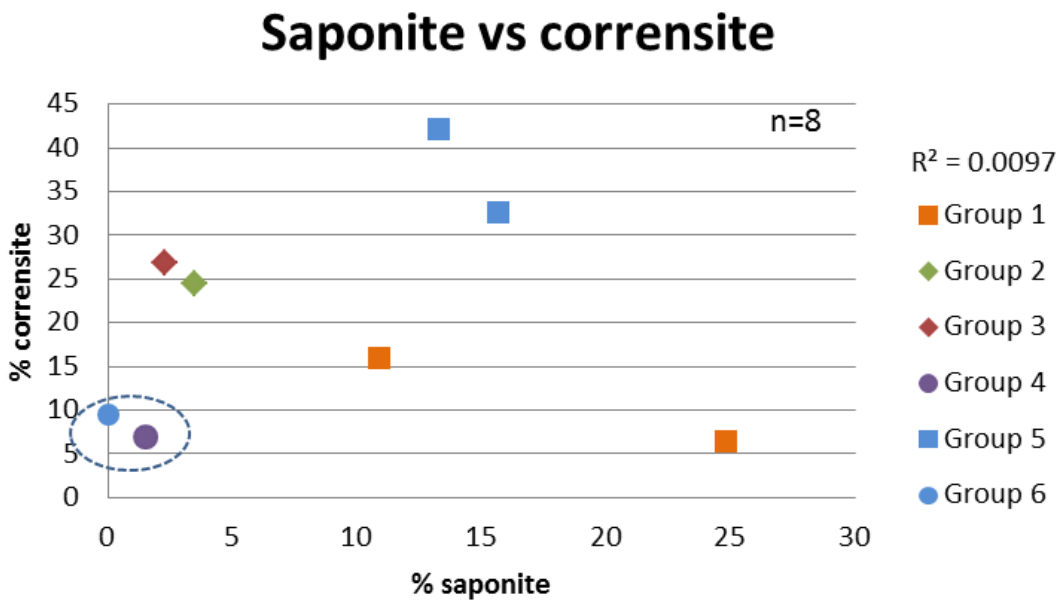

Figure 6.17: Plot of % corrensite against saponite using QXRD data. Dashed line defines siliciclastic samples.

Smectite

Several authors have reported volcanic glass as a precursor to smectite formation (Nadeau and Reynolds, 1981; Bohor and Triplehorn, 1993; Moore and Reynolds, 1997; Stroncik and Schmincke 2002; Gifkin et al., 2005 and references therein). Excluding one sample, a strong relationship exists between volcanic glass and total smectite composition in this study (Figure 6.18).

The type of smectite produced is dependent on the precursor material (Moore and Reynolds, 1997). Banfield et al., 1991 suggests that smectites that form from pyroxene and basaltic glass are likely to contain high amounts of Fe and Mg, but low amounts of Al, whereas smectites that are produced from the weathering or alteration of plagioclase are more likely to result in di-smectites that have higher Al contents. Smectites containing the highest amounts of Al are likely to have been produced from the alteration of other minerals such as kaolinite (Moore and Reynolds, 1997).

Three types of smectite were found within this study: 1) saponite, an Mg-rich tri smectite; 2) nontorinite, a relatively poor Al di-smectite; and 3) other undifferentiated di-smectites such as montmorillonite, an Al-rich smectite (Smykatz-Kloss, 1974). Therefore, all three of the smectite types discussed in Banfield et al. (1991) are present, which can be linked to the precursor material. Firstly, the relationship between saponite and the di-smectites is examined (Figure 6.19). Volcanic clast-rich samples (e.g. Group

1 onshore and Group 5 offshore) all have greater amounts of saponite than di-smectites. The inverse is true for siliciclastic, volcanic poor samples (groups 4 and 6) and for intermediate samples (groups 2 and 3).

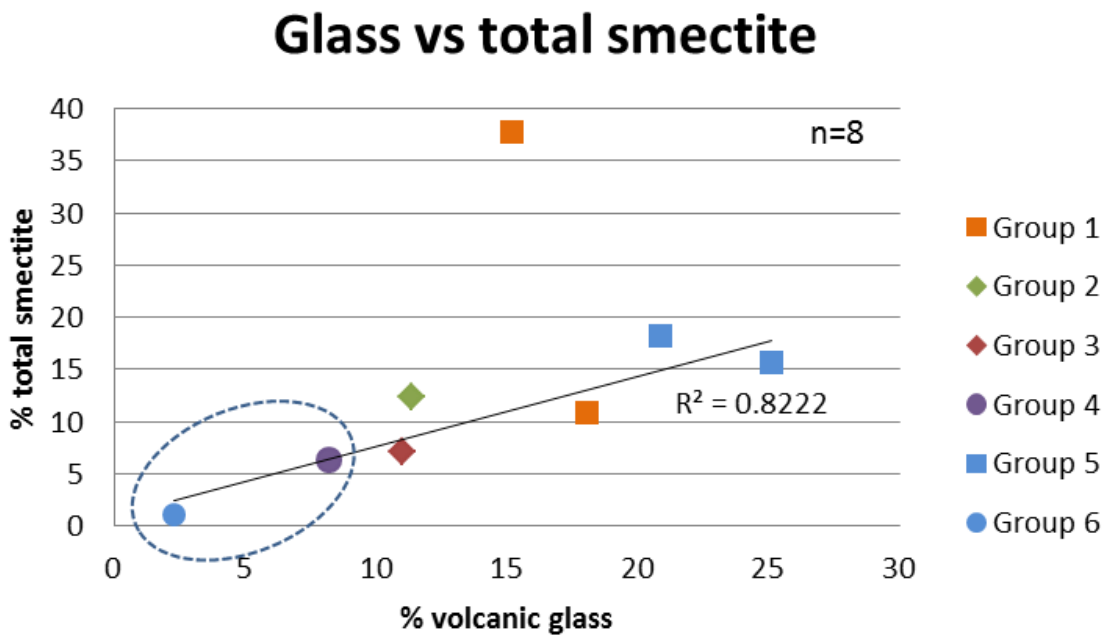

Figure 6.18: Plot of % volcanic glass against % total smectite using QXRD data. Dashed line defines siliciclastic samples. Liner Trend line and R^2 value calculated excluding the Group 1 proximal point from analysis.

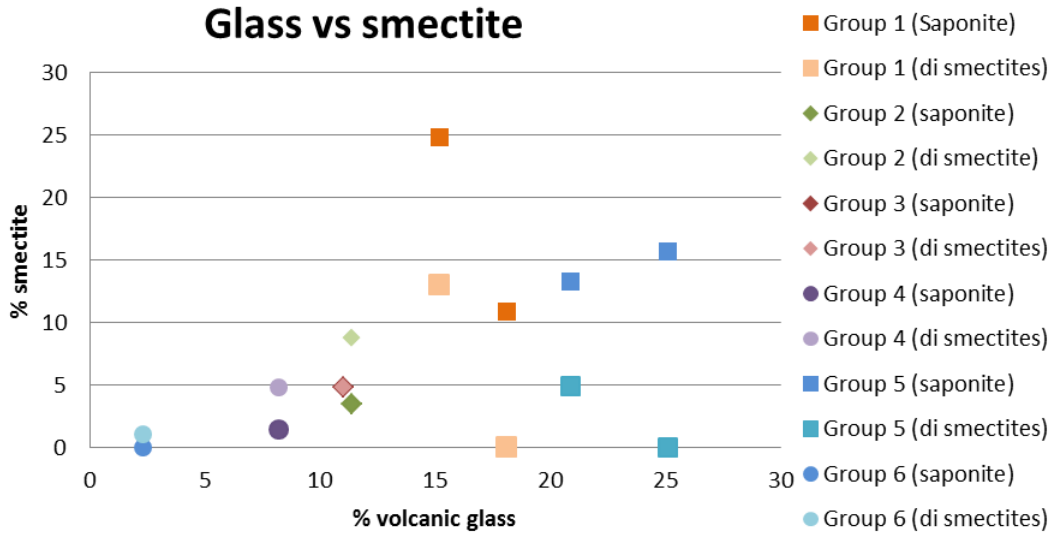

Figure 6.19: Plot of % volcanic glass against smectite. Bold colours represent saponite % whereas light colours represent the di smectite percentage. Note: volcanic glass rich samples are dominated by saponite, whereas other samples are dominated by di smectites.

The relationship between saponite and volcanic glass is strong, with the samples containing greater than 15% volcanic glass having more than 10% saponite (Figure 6.20). This suggests that the saponite within the samples grew from the alteration of volcanic glass. No clear relationship is seen between volcanic glass and nontronite (Figure 6.21). Four samples do contain nontronite including the two intermediate samples (group 2 and 3). These samples are the most likely to contain a mixture of both volcanic glass, plagioclase and kaolinite.

An inverse relationship between di-smectites and volcanic glass was found within this study (Figure 6.22). One exception is sample MT5 (Group 1), which contains a larger percentage of all the smectite clays. According to Moore and Reynolds (1997) Al-rich di-smectites are associated with alteration of kaolinite and plagioclase. Kaolinite was only identified in the intermediate group 2 and 3 rocks within these samples. However, kaolinite was identified in other Group 4 samples in the clay separate analysis. Large quantities of plagioclase were found within the siliciclastic phases (groups 4 and 6); however, these feldspars were fresher than those found within the volcanic samples. Therefore, alteration to smectite may be occurring but is not as extensive as within volcanic rich samples.

Other clay phases

Mix layer illite-smectite and kaolinite were dominantly found in the non-volcanic clast rich samples. The smaller amounts of clay found in the Group 6 offshore samples explains why their porosity is higher than onshore (Group 4) equivalents. These clay phases are likely to be detrital rather than authigenic.

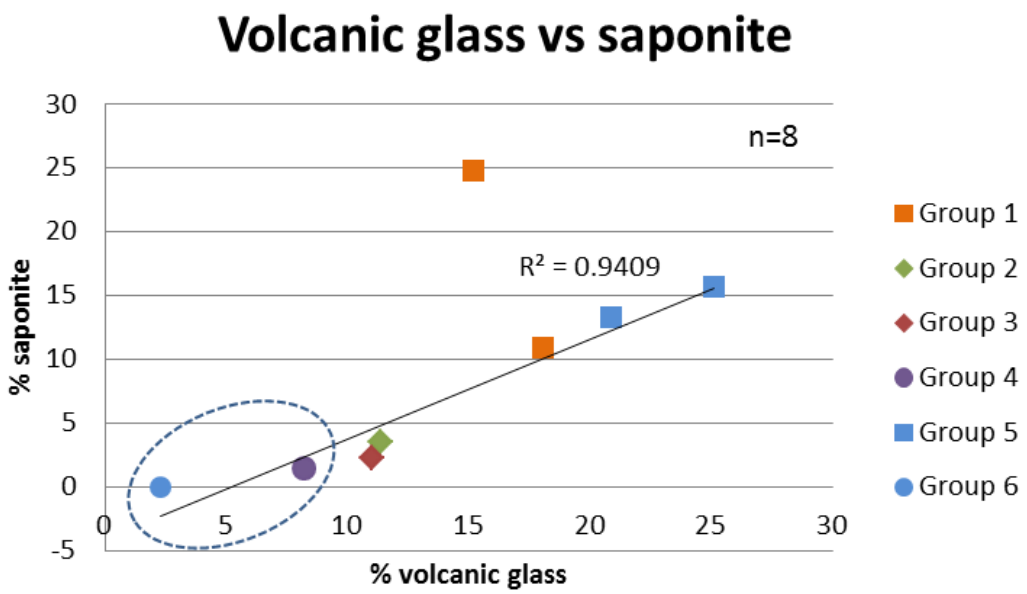

Figure 6.20: Plot between % volcanic glass and % saponite using QXRD results. Dashed line defines siliciclastic samples.

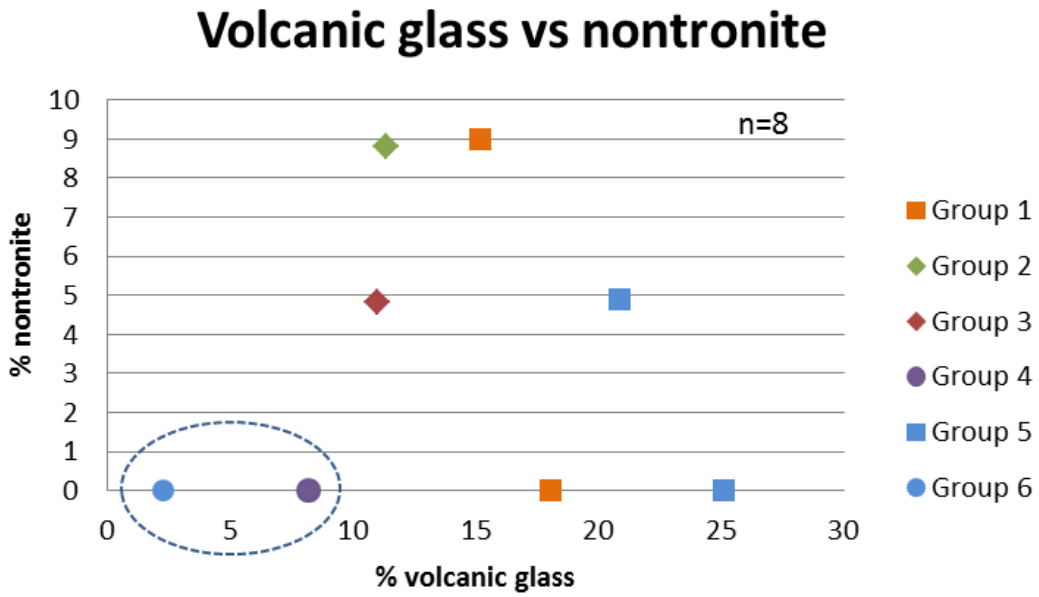

Figure 6.21: Plot between % volcanic glass and nontronite using QXRD results. Dashed line defines siliciclastic samples.

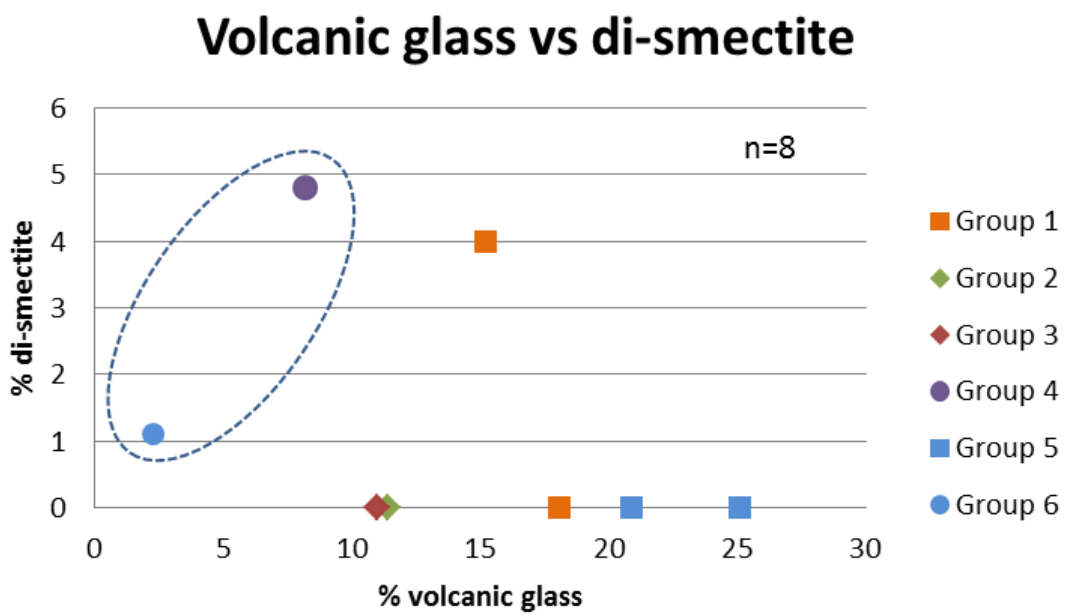

Figure 6.22: Plot between % volcanic glass and di-smectite using QXRD results. Dashed line defines siliciclastic samples.

6.5 Porosity

6.5.1 Previous work

A considerable body of work has been undertaken on the porosity of siliciclastic sandstones; however, very little work has been undertaken on volcaniclastic rocks. Some authors have indicated that it is possible to have a volcaniclastic reservoir, as some porosity and permeability is retained within volcaniclastic rocks during diagenesis (Seeman and Scherer, 1984 and Vernik, 1990). More recently work has focused on the diagenetic paragenesis (Mathisen and McPerson, 1991) and geophysical responses (Revil et al., 2002). The association with volcanic rocks and pore filling zeolites is also outlined in Iijima (2001). A number of factors affect the porosity of a sample as outlined below. The visible porosity for each lithofacies was estimated during point counting, see Figure 5.9 and the "Point Counting" file in the appendix.

Compaction

Typical compaction curves for a normally pressured, lightly to un-cemented sandstone are seen in Figure 6.23. The curves show the typical porosity reduction due to compaction for different percentages of rigid grains. The reduction in porosity is greater for samples with high proportions of plastic grains, such as mica or volcanic glass.

Therefore, samples rich in volcanic glass shards should experience greater compaction than quartz rich lithologies.

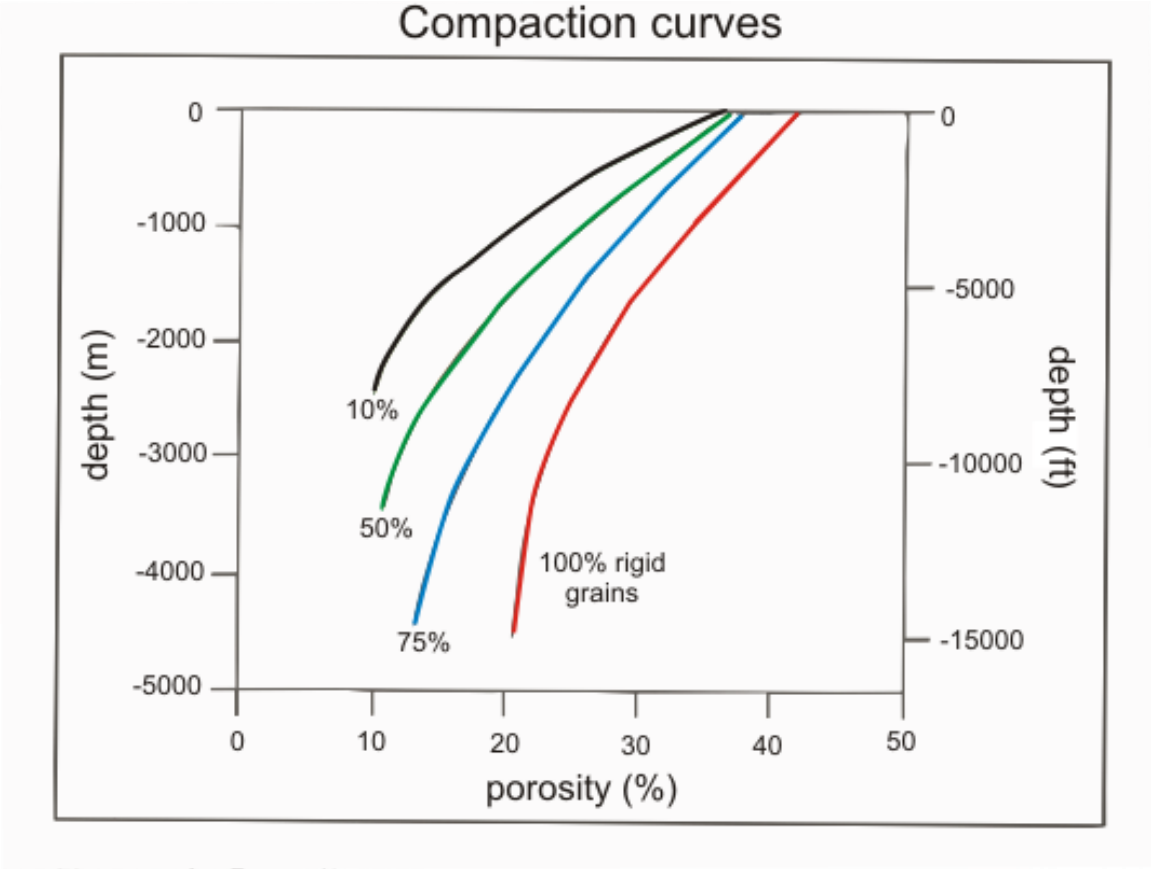

Figure 6.23 Compaction curves for a non-cemented sandstone. Porosity in a sandstone with only 10% rigid grains will be reduced at shallower depths (modified from Oxtoby and Grant, 1992)

Grain size and sorting

The relationship between grain size, sorting and porosity is complex. While fine-grained sediments typically have lower visible (but higher micro) porosity, this is dependent on other factors such as cementation and grain packing. Poorly sorted rocks will have lower initial porosities than well-sorted rocks (Brayshaw and Hogg, 1992). Volcaniclastic samples are often more heterogeneous and have poorer sorting than siliciclastic equivalents and so have lower initial porosity (Selley, 1978). This however, is completely lithology dependant, as a strongly welded pyroclastic rock will have a much lower initial porosity than a non-welded rock. Houseknecht and Hathon (1987), suggested that at depth, porosity reduction was less in poorly sorted rocks than well

sorted examples as the stresses of compaction are more equally spread across a large number of grain contacts.

Porosity in volcaniclastic rocks

Porosity can also be altered at depth due to a number of diagenetic phases such as quartz and/or calcite cementation, clay and zeolite growth, and dissolution. Figure 6.24 shows a number of diagenetic phases associated with volcaniclastic sediments, which will potentially alter the overall porosity compaction curves (Figure 6.25). Cements will greatly reduce the porosity, whereas dissolution will create secondary porosity in the form of moldic or intra-granular pores.

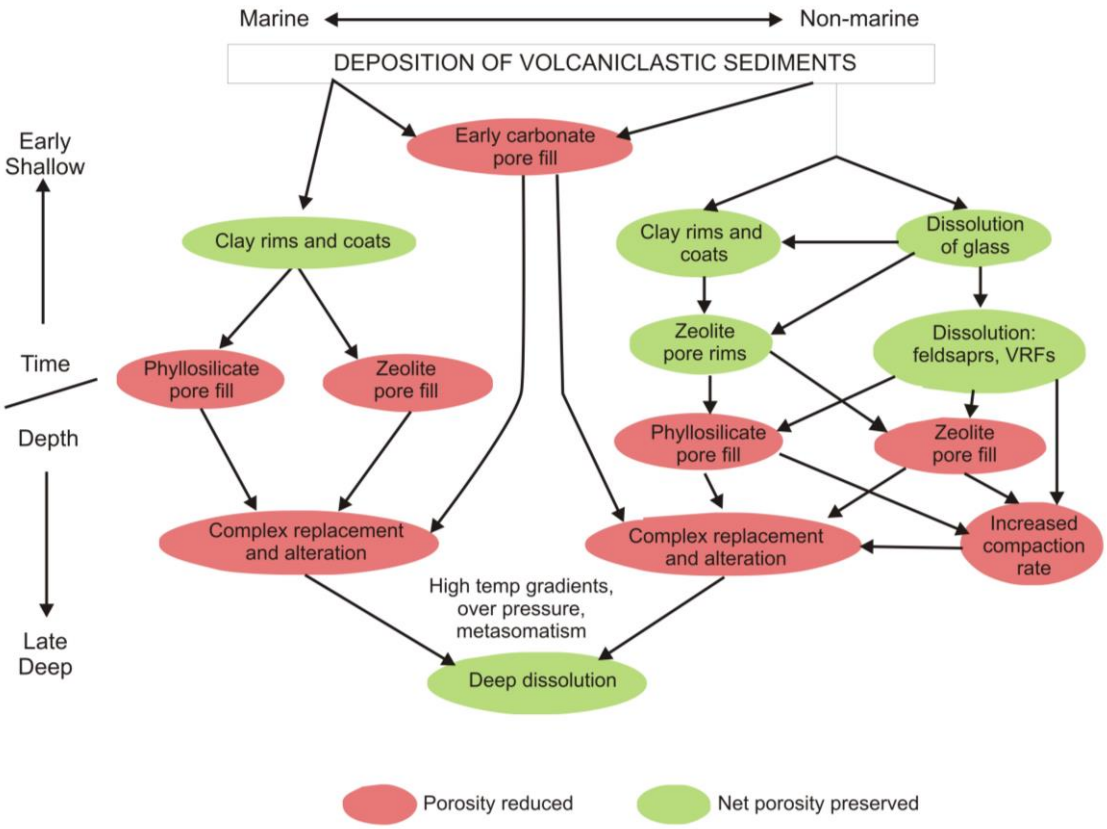

Figure 6.24: Flow chart showing the complex paragenesis that leads to the destruction and creation of porosity within volcaniclastic rocks (modified from Mathiesen and McPherson, 1991).

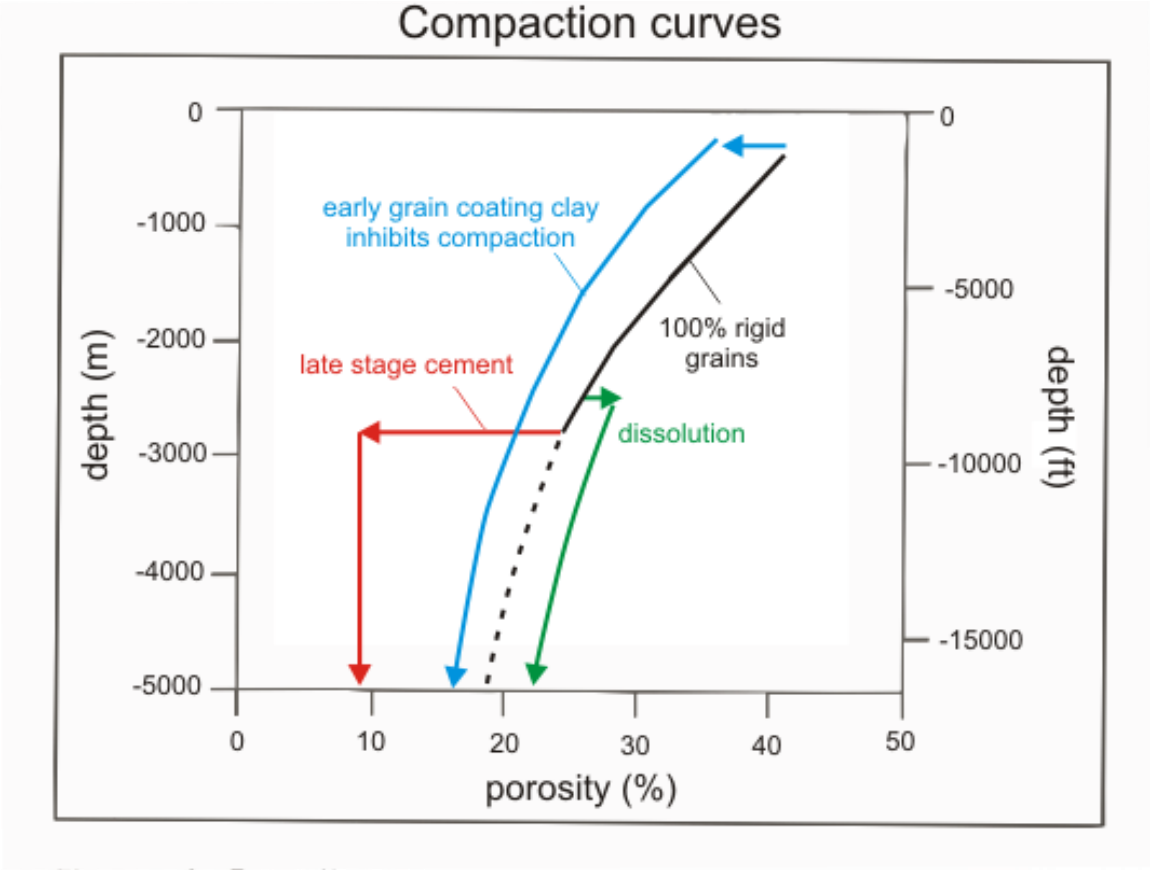

Figure 6.25: Alteration of simple compaction curves by diagenetic effects such as late stage cements or early grain coats. Curves are based on 100% ridged grains with normal reservoir pressure (modified from Oxtoby and Grant, 1992).

6.5.2 Relationship between porosity and depth

As the Staffa Formation samples now crop out at the surface their relationship to depth cannot be properly analysed. No correlation was found between depth and porosity from the offshore Rosebank samples however, as the samples have been taken from cores and so the depth range is relatively small. To better understand the true relationship between the samples and depth, sidewall core data covering the full length of the wells (provided by Chevron) was plotted (Figure 6.26). On a whole these data show no obvious relationship between porosity and depth, and that porosities vary considerably throughout the chronostratigraphical units. Colsay 4 samples do show some correlation is, where porosity drops from 24.3% at 3131 m to 11.3% at 3199 m. There is a week increase in helium porosity with depth if only the volcanic samples are considered. This can be explained by the breakdown of volcanic glass into clays. The clays restrict pore throats but often do not completely occlude pores with micro-porosity between clay structures being created.

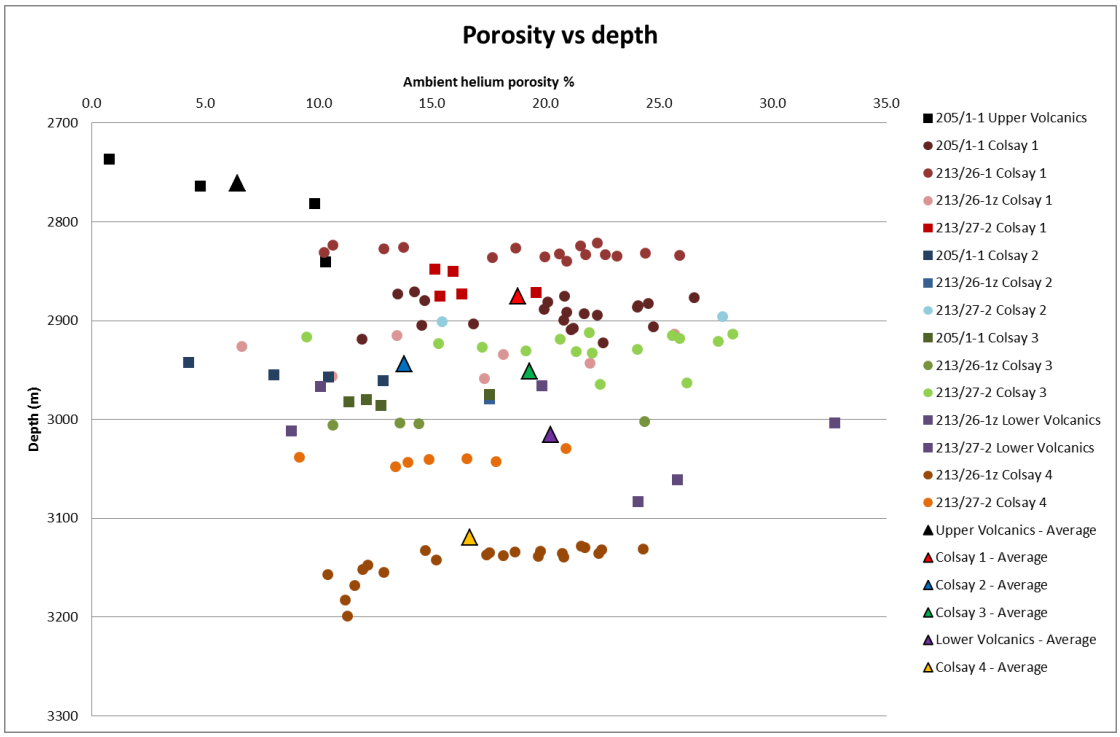

Figure 6.26: Plot of porosity against depth for the Rosebank wells (data plotted is sidewall core data provided by Chevron). Circles are siliciclastic samples, squares are volcaniclastic samples.

6.5.3 Relationship between total volcanic clasts and porosity

Offshore

Figure 6.27 shows the percentage of total volcanic clasts versus visible porosity calculated from point counting data for the offshore samples. The Rosebank samples are split into chronostratigraphical groups, as described in Chapter 2. Square points represent volcanic rich (Group 5) samples, whereas circles represent the siliciclastic (Group 6) samples.

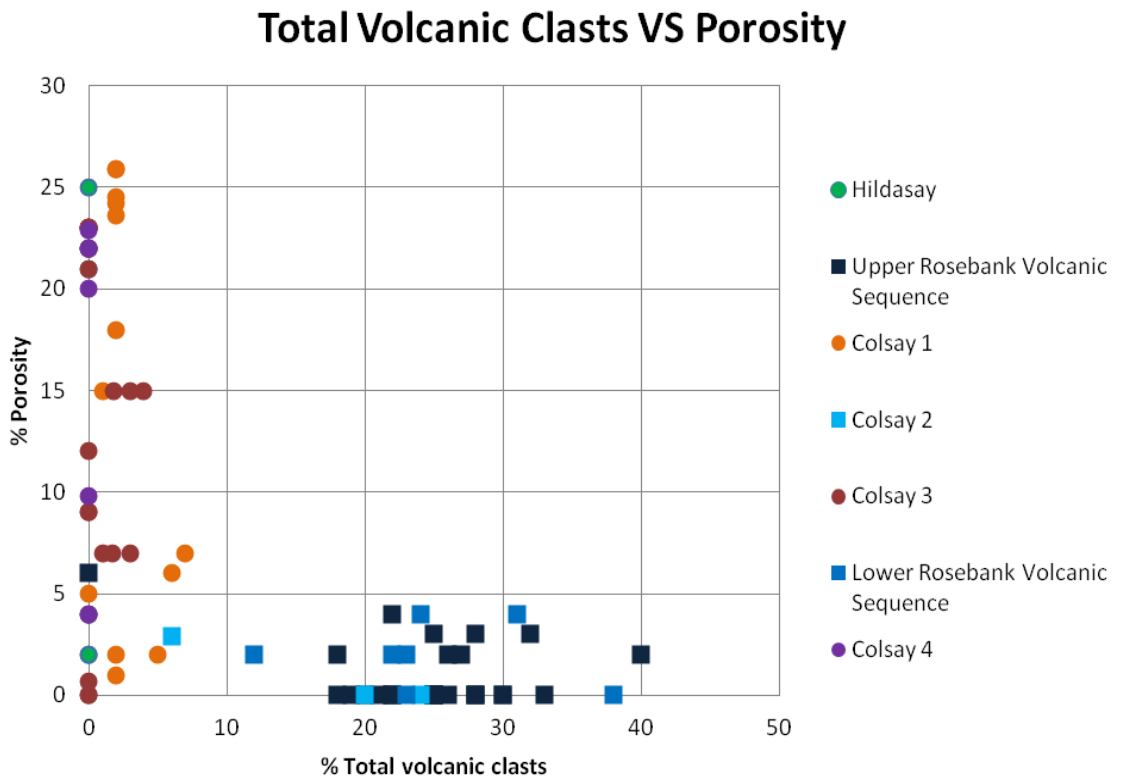

Figure 6.27: Plot of total volcanic clasts against visible porosity for the Rosebank rocks. Squares represent Group 5 volcanic rocks, whereas circles represent Group 6 rocks. Note all samples comprising more than 10% volcanic clasts have less than 4% porosity.

A large range of porosities are present within the samples. Group 6 siliciclastic samples (Colsay 4 and Hildasay) contain less than 1% volcanic clasts and have very similar porosity distributions, ranging from 1–25%. Lower porosities represent finer grained units that often have interbedded clay and silt facies. Colsay 1 and 3 samples contain a higher percentage of volcanic clasts (up to 8%) but have a similar range in porosity (2-25%).

The more volcanic-rich samples from Group 5 show a strong relationship between the proportion of volcanic clasts in each sample and porosity. The rocks within the Upper and Lower Rosebank Volcanic Sequence and Colsay 2 groups all have a high proportion of volcanic clasts ranging from 6 – 40% with the exception of one rock found within the Upper Rosebank Volcanic sequence, which was found to be a small quartz rich siltstone that contained no volcanic clasts. Excluding that sample from the analysis, all volcanic rich samples have porosities < 4%. There does not appear to be a direct correlation between the percentage of volcanic clasts in the rock and porosity. There is however, a threshold limit: all rocks containing more than 10% volcanic clasts

have less than 5% porosity, whereas rocks that contain less than 10% volcanic clasts have variable visible porosities of up to 26%.

Onshore

These findings are compared to the results from the onshore Staffa Formation samples, (Figure 6.28). The onshore samples generally plot on the same trend as the offshore data. The majority of rocks with abundant volcanic clasts (above 10%) fit the 5% threshold porosity with the exception of three samples that plot between 6 – 10% porosity. Rock samples with less than 10% volcanic clasts have lower porosities than their offshore equivalents. This is explained below, when the nature of the pore-filling material is examined.

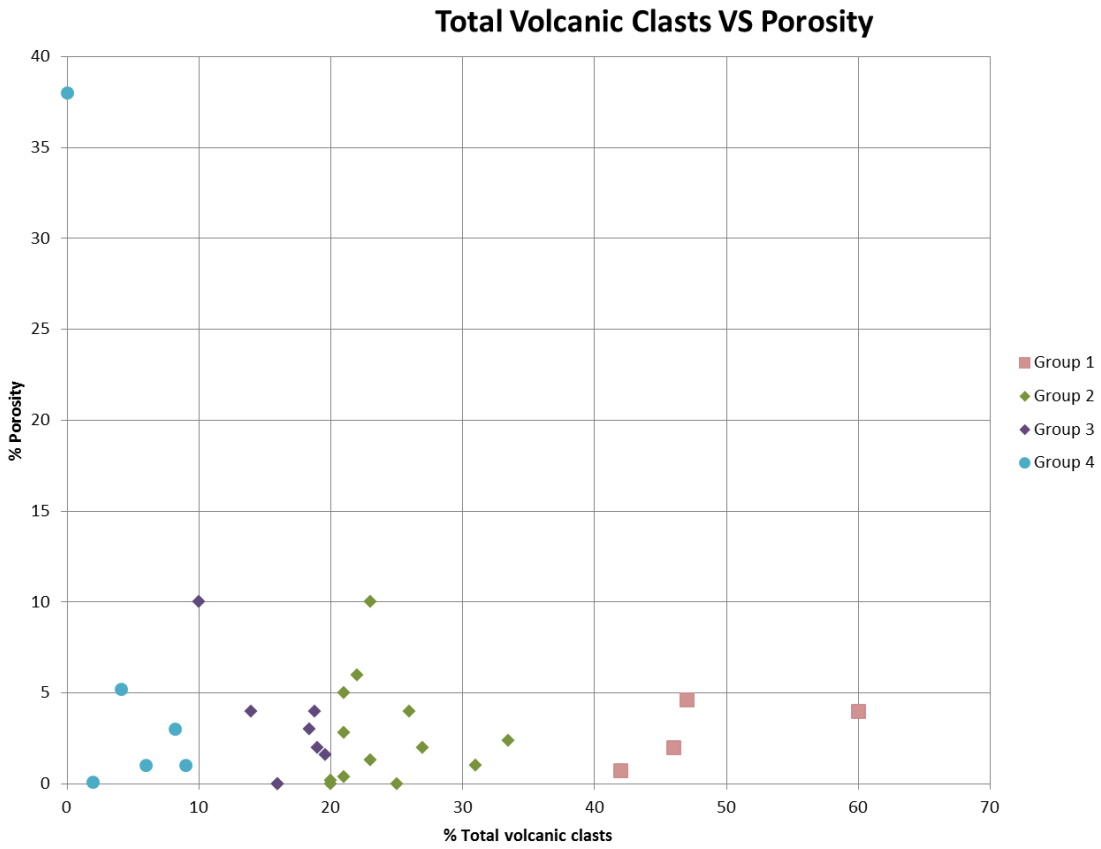

Figure 6.28: Plot of total volcanic clasts against visible porosity for all samples. Onshore samples are generally similar to offshore samples; however, onshore samples all have much lower porosities.

6.5.4 Porosity reduction within the samples

Both onshore and offshore samples were analysed optically in order to assess the nature of the pore filling materials and the relationship between phases and visible porosity.

6.5.4.1 Quartz

In both the Staffa Formation and Rosebank rocks quartz cements are a relatively minor phase. Only one sample within the Staffa sample suite exhibits evidence of a quartz cement that has been aggressively dissolved at a later stage. This represents a relatively minor phase and contributes to less than 1% of the overall visible porosity reduction.

6.5.4.2 Zeolite

Zeolites commonly fill vesicles and fractures in volcanic rocks (Hay, 1978; Fisher and Schmincke, 1984) and were therefore expected to contribute to significant porosity reduction in the study samples. Zeolites zones surrounding the Mull Central Complex have previously been mapped out by Walker (1971) and suggest that mesolite and laumonite should be present within the Mull samples (see Section 7.5, Figure 7.9). Similarly, Jørgensen (2006) indicates the presence of a wide range of zeolites on the Faero Islands and uses these to predict geothermal gradients across the Faero-Shetland Basin. Therefore, it was expected that Rosebank samples would contain similar zeolite minerals. However, the only zeolite found was analcime, which was slightly more abundant in the Rosebank volcanic-rich samples, and typically filled intragranular porosity in basalt clasts. In one proximal pyroclastic Staffa Formation sample analcime was the dominant pore filling material. However, this sample is anomalous as in all other Staffa Formation samples, regardless of rock type, zeolites contribute less than 2% of total visible porosity reduction. The discrepancy between the zeolite found in this study and those in the literature is further discussed in Section 7.5.

6.5.4.3 Calcite

Minor calcite cements are present in many of the samples and were discussed in Section 5.5.12.

Offshore

Figure 6.29 shows the proportion of calcite in the Rosebank samples versus visible porosity. Three samples (two points overlay each other at 15% calcite) comprise 15–20% calcite cement, which is the main porosity reducing factor. Excluding these samples the majority of rocks have less than 5% calcite cement, and so these cements play only a minor role in porosity reduction (or secondary porosity was created by dissolution of these cements).

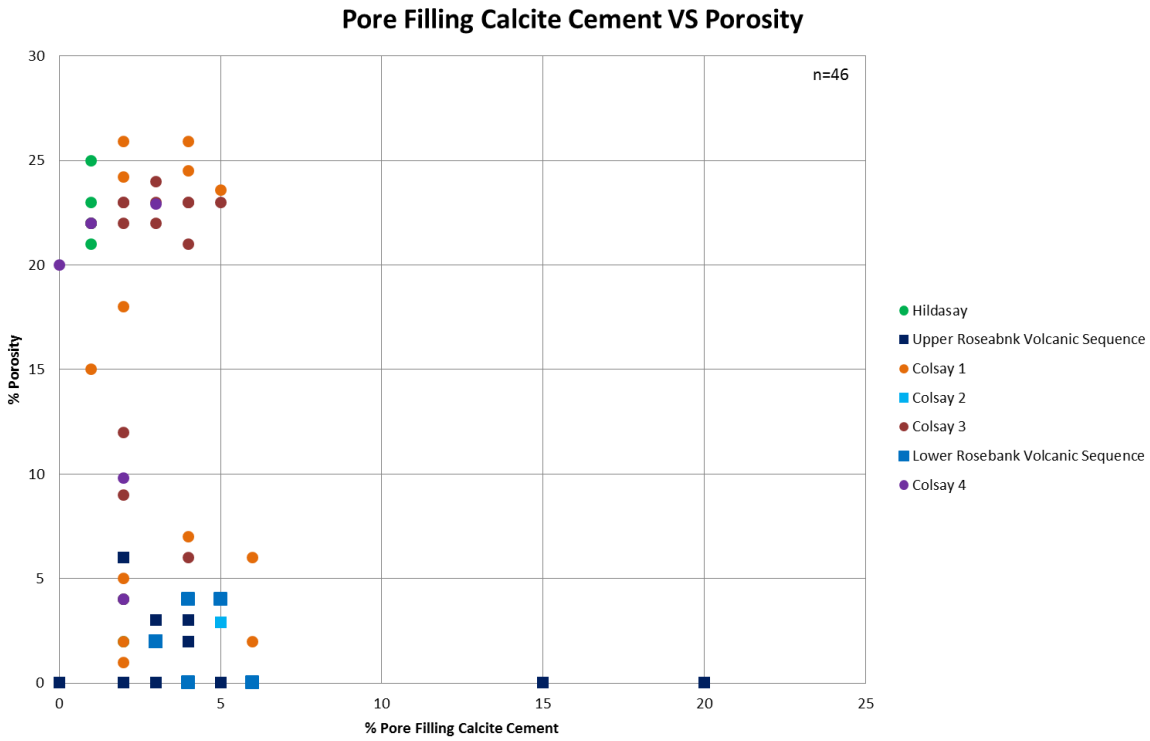

Figure 6.29: Plot of pore filling calcite (%) against visible porosity for the Rosebank samples. Group 5 samples (squares) and Group 6 samples (circles) show a wide range of porosities. Calcite is the main pore filling phase in 3 samples (2 overlie at 15% calcite).

Onshore

The Staffa Formation rocks with lower proportions of volcanic clasts have higher proportions of calcite cements. This, in part, explains why some of the onshore rocks, the Ardtun samples in particular, do not fit the volcanic porosity trend (Figure 6.28). The rocks at Ardtun have lower than expected visible porosity due to precipitation of a late stage calcite cement. Similar lithologies at other locations on Mull, such as the rocks at Malcom's Point have much lower percentages of calcite cement. Here, larger quantities of volcanic ash have resulted in higher percentages of authigenic clays, which reduce visible porosity and limit pathways for later fluids. As a result, these rocks have only minor quantities of calcite. If this late stage calcite cementation had not occurred the siliciclastic Staffa samples their visible porosities would be in line with their offshore equivalents (Figure 6.30).

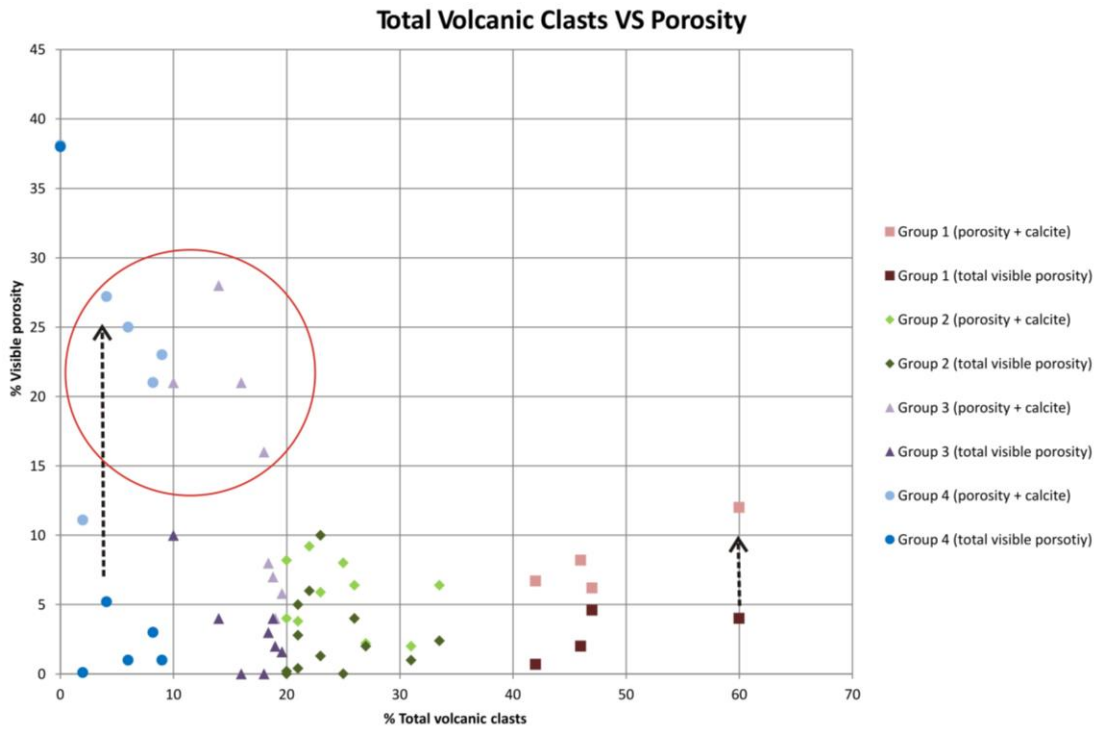

Figure 6.30: Plot of total volcanic clasts (%) against visible porosity (+ calcite) for the Staffa Formation samples. Bold colours represent actual visible porosity values. Light colours represent the equivalent samples where the effect of late stage calcite cementation on porosity has been removed. This is achieved by adding the total calcite pore fill to porosity. Dashed arrows indicate large differences in porosity when calcite is removed. Red circle highlights Ardtun samples.

6.5.4.4 Phyllosilicates

Offshore

Figure 6.31 shows the percentage of pore filling clay minerals versus visible porosity in each of the rock samples. The siliciclastic Group 6 samples, Hildasay and Colsay 1, 3 and 4, all show a strong inverse trend between clay pore fill and visible porosity, with the most porous rocks containing the least amount of pore-filling clay minerals. The majority of the samples have less than 40% pore-filling clay, with the exception of two Colsay 3 samples that have high proportions of pore-filling clay (up to 60%). Rocks that contain less than 10% pore filling clays have a wide range of porosities, from 4 – 26%, the same relationship as is seen with volcanic clasts. Group 5 samples with more than 10% pore filling clays typically have less than 10% porosity, with the exception of two samples. The volcanic-rich rocks have high proportions of pore-filling clays, ranging from 20–48%, and low porosities, below 6%.

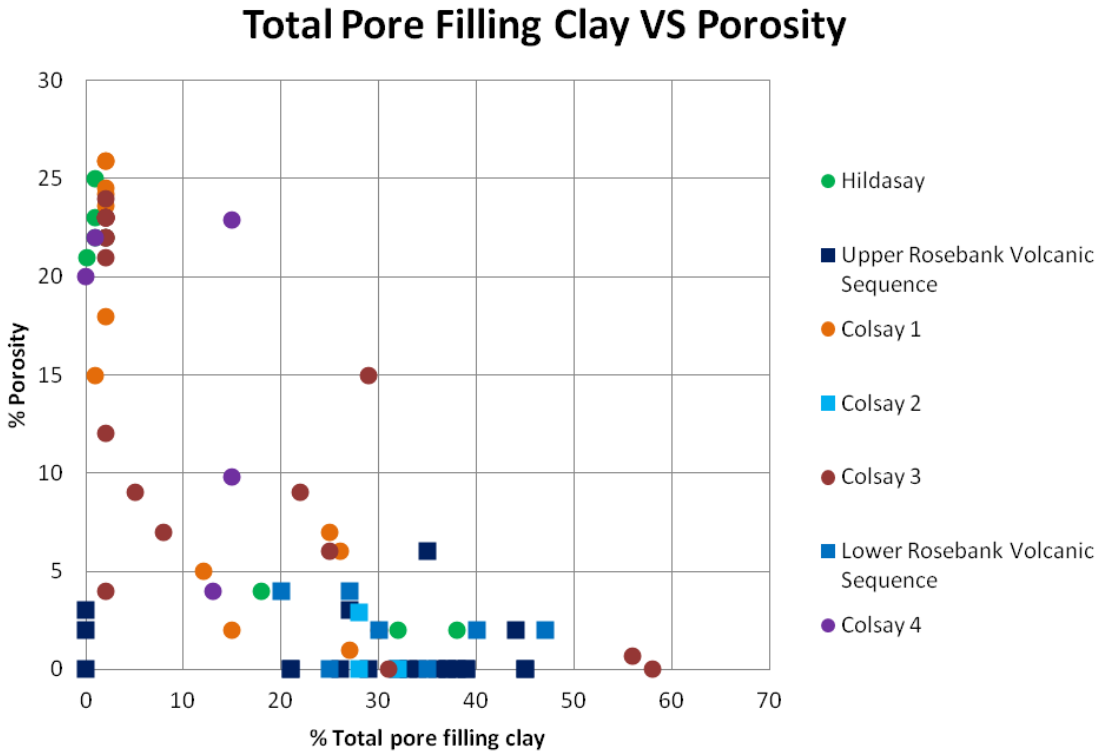

Figure 6.31: Plot of total pore filling clay against visible porosity for the Rosebank rocks. Samples that contain a lot of pore filling clay have lower porosity. N=46

Onshore

No direct link between pore filling clay and visible porosity could be made in the Staffa samples. However, a patchy calcite cement in some samples resulted in lower porosity. When the effects of this late-stage calcite are removed the relationship between porosity and clay pore fill closely resembles that of the offshore samples, with samples containing less than 20% pore filling clay retaining porosity of over 15% (See section 6.5.4.3 and Figure 6.30).

6.5.4.5 Relationship between volcanic clasts and pore filling clay.

Offshore

Figure 6.32 shows the proportion of volcanic clasts plotted against pore filling clays. The majority of the siliciclastic Group 6 units with less than 10% volcanic clasts have variable proportions of pore filling clay, ranging from 0 – 39%; however, two Colsay 3 samples have higher proportions of clay, up to 58%. The more volcanic rich Group 5 samples have pore filling clay proportions up to 48%, but critically, all volcanic rich samples have more than 12% pore filling clays. This implies that a rock with more than 10% volcanic clasts will have a significant amount of porosity reduced by clays. The relationship between volcanic clast type and pore filling clay will be dealt with in Section 6.5.4.7.

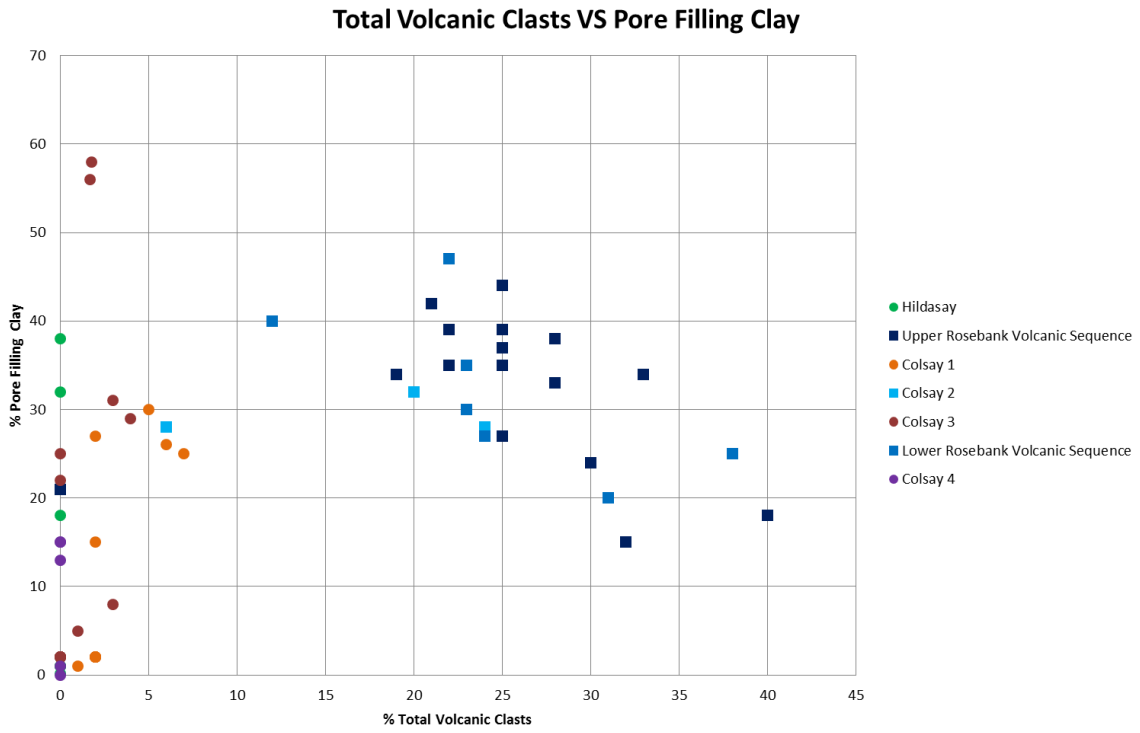

Figure 6.32: Plot of total volcanic clasts against % pore filling clay. All samples that contain more than 10% volcanic clasts contain more than 12% pore filling clay.

Onshore

The onshore samples show a positive linear relationship (r^2=0.58) between the proportion of pore filling clays and volcanic clasts. Group 1 and 2 samples comprise the greatest amounts of volcanic clasts and also the largest proportions of pore filling clays (Figure 6.33). This is different from offshore volcanic samples that had a weak negative relationship. This difference can be explained if the total amount of volcanic clasts and rate of alteration is considered. If a rock has a large proportion (>60%) of volcanic clasts then the amount of clay produced will also be high leading to a positive relationship. In a closed system such as the offshore samples most of the volcanic fragments have altered resulting in rocks that only have a few volcanic clasts remaining but high proportions of clay.

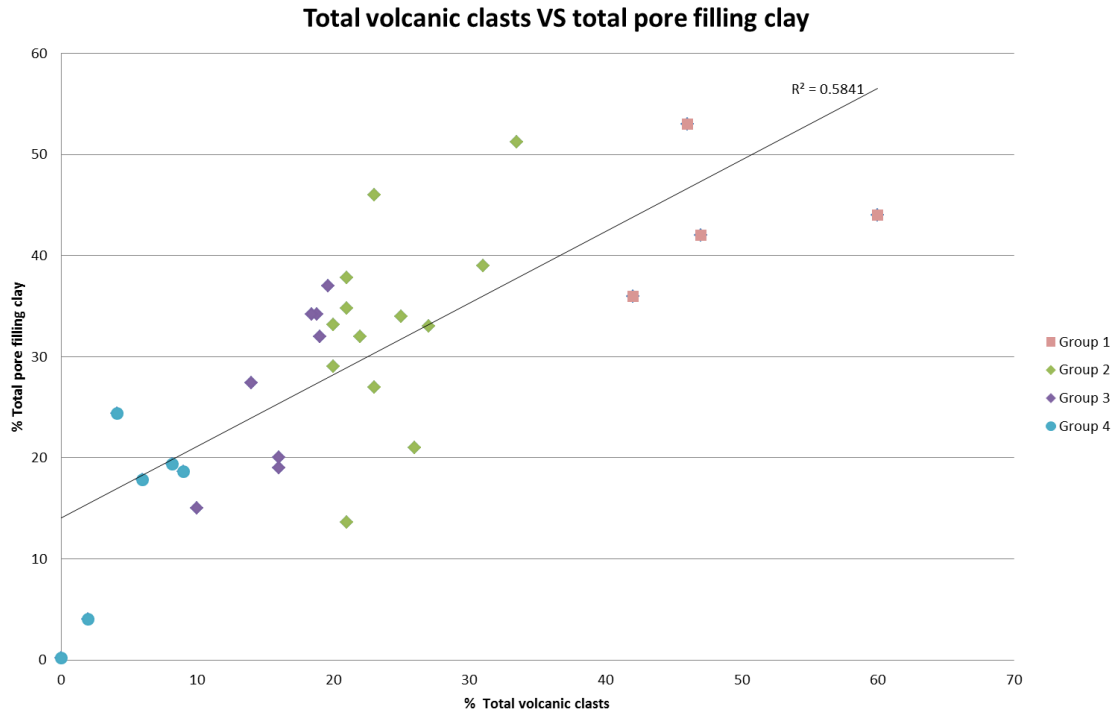

Figure 6.33: Plot of total volcanic clasts against % pore filling clay for the Staffa samples. There is a linear relationship between total volcanic clasts and total % of pore filling clay.

6.5.4.6 Relationship between volcanic clasts and pore filling clay type

Offshore

Within the Rosebank samples, two groups of clay could be identified optically; a dark brown green clay (Type 1) and a lighter brown yellow clay (Type 2). Using XRD and SEM techniques, Type 1 clays were identified as smectitic and chloritic clays as well as mix layer varieties such as corrensite, whereas Type 2 clays were identified to be illite-smectite mix layer clays with minor kaolinite.

Figure 6.34 shows the proportion of volcanic clasts against Type 1 clays. The siliciclastic Group 6 samples (Hildasay and Colsay 4) have less than 15% of Type 1 clays. The majority of Colsay 3 samples also have less than 15% Type 1 clay with only one rock sample having a value of 23%. Colsay 1 samples are slightly more variable with three samples containing more than 25% Type 1 clays. For the Group 5 volcanic rich samples, Type 1 clay content varies from 9% to as much as 47%.

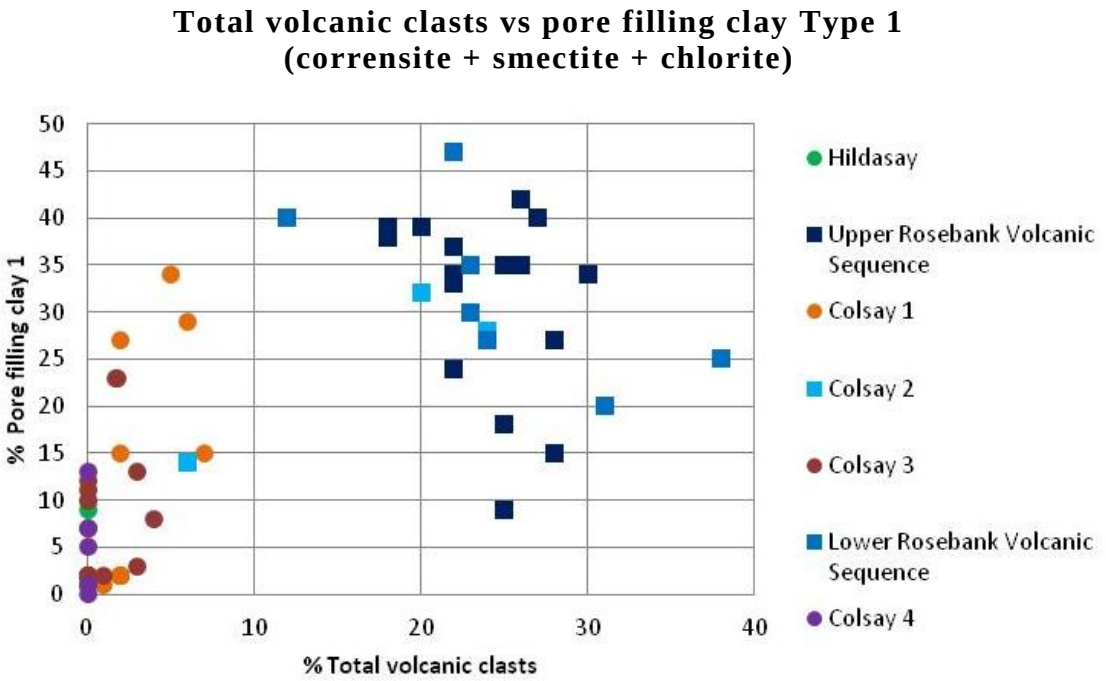

Figure 6.34: Plot of % total volcanic clasts against % Type 1 pore filling clay. n=46.

Figure 6.35 plots the proportion of volcanic clasts against Type 2 pore filling clays. Group 6 samples again display a wide range in clay amounts from 0 – 50%; however, the volcanic rich Group 5 samples have less than 5% of Type 2 clays with the vast majority of samples containing less than 1%.

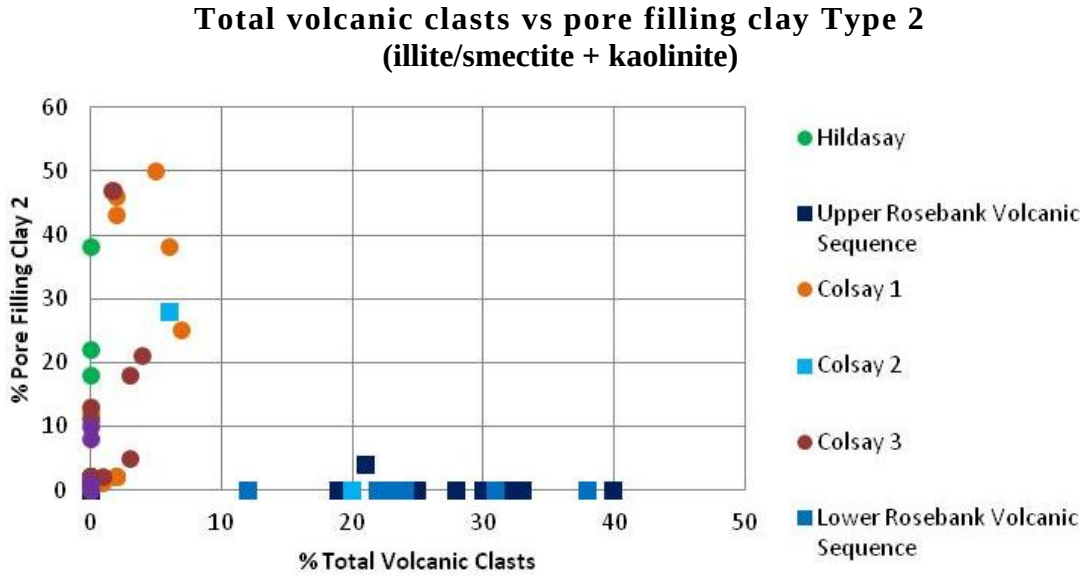

Figure 6.35: Plot of % total volcanic clasts against % Type 2 pore filling clay. n=46.

The average proportion of Type 1 clays in the Group 6 samples is 7%, whereas the average proportion of Type 2 clays is 11%. This shows that both clay types can be found in low proportions in siliciclastic rocks, but Type 2 clay is more commonly associated with rock samples that have low proportions of volcanic clasts. The average proportion of Type 2 clays in group 5 samples is 28% while the average proportion of Type 2 clays is 1.5%. Hence rocks rich in volcanic clasts are much more likely to be dominated by Type 1 (smectite + corrensite + chlorite) clays than by Type 2 (illite/smectite + kaolinite).

Onshore

The relationship between Type 1 clay minerals and total volcanic clasts is shown in Figure 6.36. Group 1 rocks are the most volcanic rich but also contain the highest proportions of Type 1 clay minerals (>30%). The inverse is true of Group 4 rocks, which have less than 10% volcanic clasts but also have less than 4% Type 1 clay minerals and are abundant in Type 2 clay minerals (Figure 6.37). Group 2 and 3 rocks typically have a combination of both clay types.

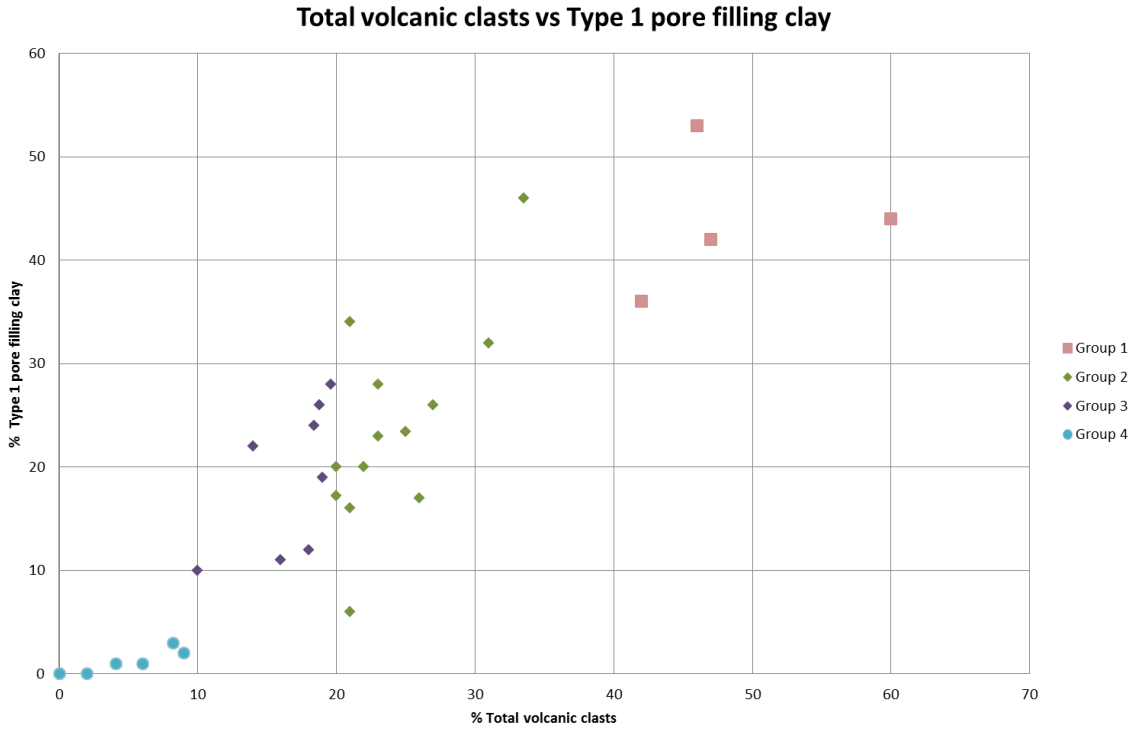

Figure 6.36: Plot of total volcanic clasts against % of Type 1 pore filling clay. n=32.

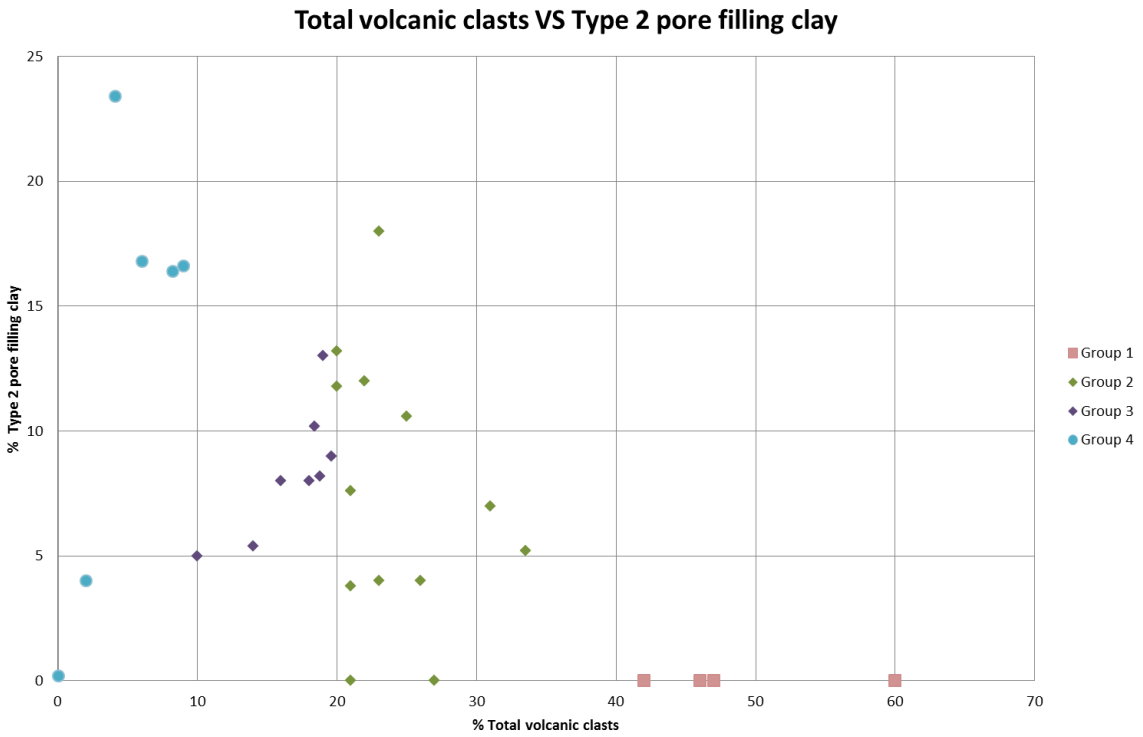

Figure 6.37: Plot of total volcanic clasts against % of Type 2 pore filling clay.

6.5.4.7 Relationship between volcanic clast type and pore filling clays

Figure 6.38 plots volcanic clasts against percentage of pore filling clays for the onshore Staffa Formation samples and shows a positive relationship. However, the type of volcanic clast influences this relationship. Several different volcanic clast types were identified in Chapter 5. To simplify the analysis these clasts have been sub-divided into two groups. Group 1 is 'Basaltic Clasts' and contains all dominantly crystalline basaltic lithoclasts regardless of their alteration / weathering state. Group 2 is named 'Basaltic Glass' and contains all basaltic ash fragments and glassy pyroclasts that lack abundant micro crystalline material. This group contains both vesicular and non-vesicular glass shards regardless of alteration states. The different clasts types were also plotted against different clay types however there was no correlation.

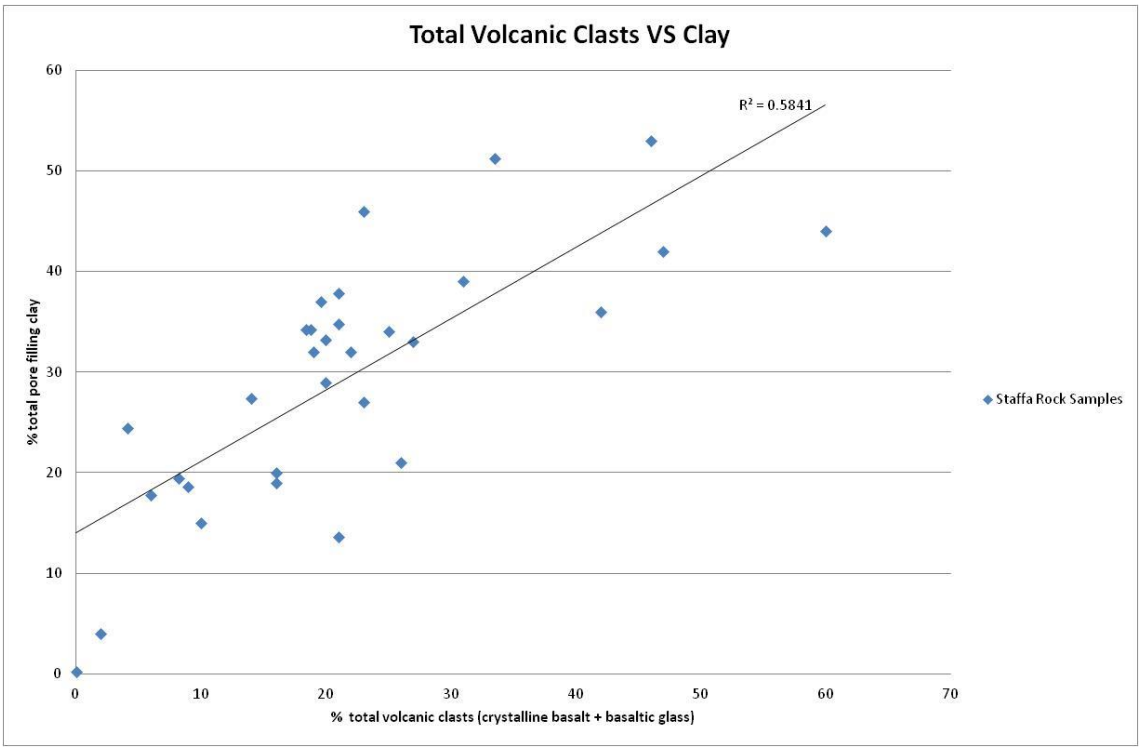

Figure 6.38: Plot of % total volcanic clasts against % pore filling clay for the Staffa samples. There is a linear relationship between total volcanic clasts and pore filling clay.

Figure 6.39 plots the proportion of 'Basaltic Clasts' against pore filling clay, and a weak positive relationship is observed. Samples containing higher proportions of basaltic lava clasts typically have higher proportions of pore filling clay; however, some scatter does occur.

Figure 6.40 plots 'Basaltic Glass' against pore filling clay, and a strong positive linear relationship is observed. Therefore, the proportion of volcanic ash and pyroclasts in the rock has a much larger influence on porosity reduction than the proportion of basalt clasts

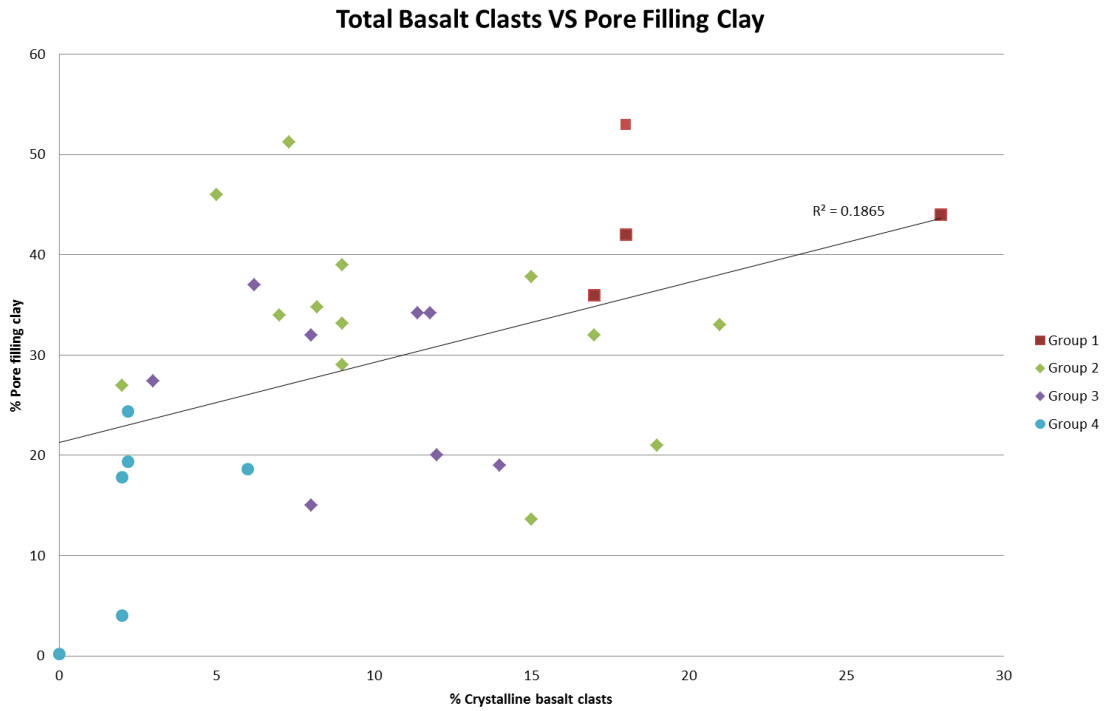

Figure 6.39: Plot of % basalt clasts against % pore filling clay. There is a weak linear relationship between basalt clasts and pore filling clay. n=31.

.

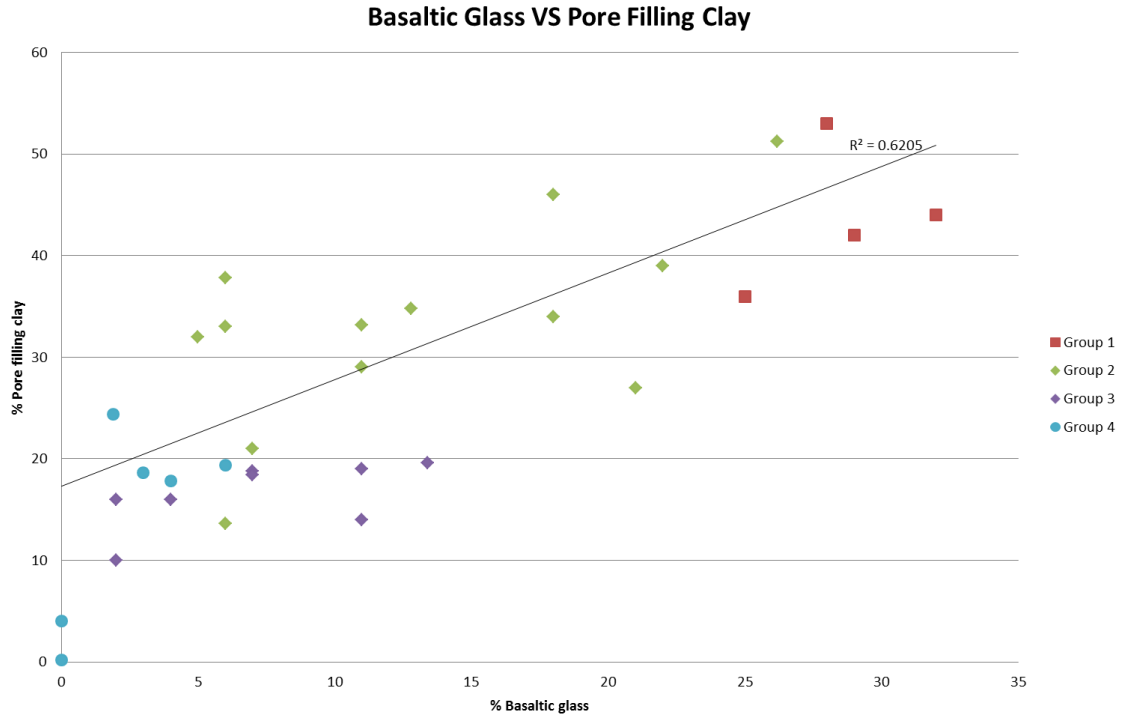

Figure 6.40: Plot of % basaltic pyroclasts and ash against % pore filling clay. There is a strong liner relationship between basaltic glass and pore filling clay. n=31.

There are a number of reasons for this relationship (Figure 6.41). Crystalline basalt clasts retain their structure under compaction better than glass-rich pyroclasts and ash, preserving surrounding pore space. The glassy groundmass of the lava clasts is protected by the crystalline component and therefore, alteration is contained within the general structure of the basaltic clasts resulting in only limited, localised porosity fill.

In sediment containing basaltic ash and glassy pyroclasts, the basaltic glass shards are more reactive than the crystalline basalt. Therefore, glass shards are more likely to start altering to clays and blocking pore throats, more rapidly after burial than crystalline clasts. The crystalline lava clasts may take longer to alter, resulting in pore throats being left open and being exposed to diagenetic fluids for longer. Basaltic glass shards have lower compressive strength and may behave in a more plastic way when subjected to compaction. As the rock is buried, ash and glass rich scoria fragments can become flattened and strung out along their axis (Branney and Sparks, 1990.) As a result the clast can deform around surrounding grains obstructing pore throats and filling surrounding pores. The effects of the alteration are therefore, far wider reaching than those seen with basaltic lava clasts. Together, this means that a volcanic rich sediment composed of crystalline basaltic clasts will retain initial porosity under compaction better than a sediment composed of basaltic pyroclasts.

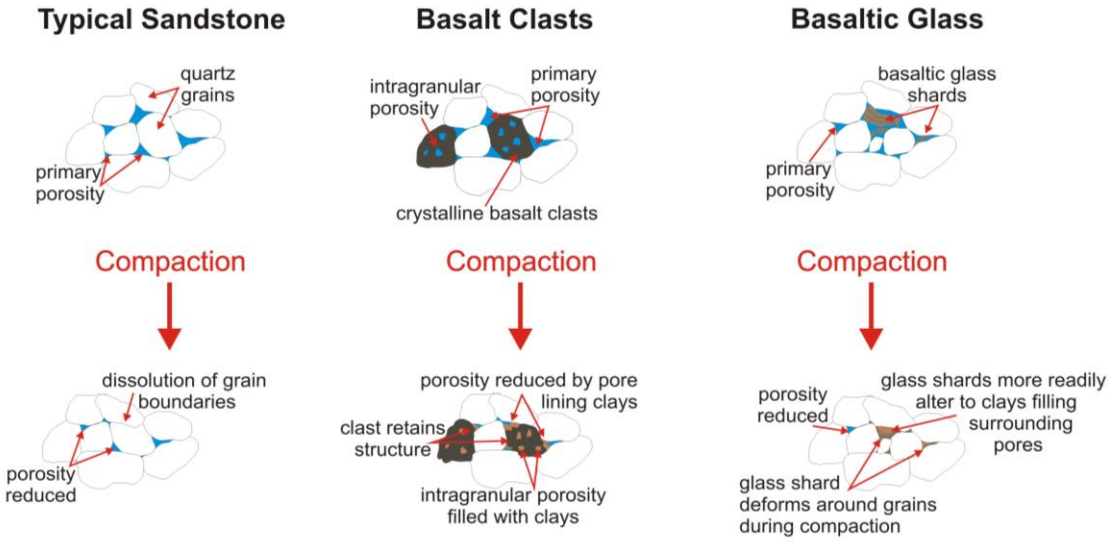

Figure 6.41: Schematic interpretation of the behaviour of basaltic lava clasts and glassy pyroclasts under compaction.

6.5.4.8 Relationship between depositional environment and porosity reduction

It has already been shown that factors such as sorting, maturity and grain size effect porosity and so depositional environment can influence the rocks behaviour during diagenesis. As a general correlation between volcanic clast type and porosity can be distinguished and links can also be made to depositional setting. On Mull, the highest proportions of volcanic glass and therefore lowest porosities occur in rocks that are proximal to a vent. Samples taken close to a volcanic vent are likely to contain higher abundances of volcanic clasts in particular volcanic glass rich pyroclasts and ash and therefore, it will have lower porosity after initial burial than rocks at more distal locations. The rocks at Ardtun contain a low percentage of basaltic lava clasts and therefore porosity reduction is localised and not the deterministic factor of final porosity values.

6.5.4.9 Relationship between igneous-sediment contacts and porosity

Previous studies have linked destruction of porosity to direct induration effects found at igneous-sediment contacts (Girard et al., 1989; Merino et al., 1997; Doyle, 2001; McKinley et al., 2001; Lima and De Ros, 2002; Bernet and Gaupp, 2005). Figure 6.42 shows a series of thin sections taken at varying distances from the base of a lava contact with sandstone, Namibia (Dougal Jerram, unpublished). The photomicrographs show an aggressive calcite cement filling porosity at the lava contact; however, at a distance of 4 m there is no calcite cement and the porosity of the sediment matches background levels. (Grove and Jerram, 2011), also found similar porosity reduction due to calcite cements and contact metamorphic effects surrounding intrusions in Namibia.

In both of the previous studies the effects of the contacts appear to be reduced to nominal at a distance of 4 m from the contact. In offshore samples, limitations such as contact angle and core size, meant sampling of rock 4 m from the contact could not be achieved. Therefore, background porosity levels could not be defined and pore filling phases could not be directly linked to contact effects. No notable differences in porosity or mineralogy occurred over the small centimetre scale distances from contacts that could be measured in the Rosebank cores.

Systematic sampling of units at igneous-sediment contacts was possible for the Staffa Formation. Figure 6.43 shows a series of thin sections taken at progressive

distances from the base of the 3 m thick sill at the Carsaig Arches (Section 4.4.1). No changes in mineralogy are seen within the 4 samples, and porosity is predominantly filled by pore filling clays with only very minor amounts of calcite. Throughout the Staffa samples no significant porosity reduction or induration was seen at any of the contact types.

There are a number of key differences between the sediment in this study and that of the previous studies. Firstly the Namibian examples are within aeolian rocks with high initial porosity (~30%), whereas in this study the rocks have much more variable initial porosity (generally < 10%). Where the underlying sediment has poor porosity this may act as a barrier to any fluids associated with the igneous body, and force them to percolate up through fractures within the body or along the contact towards the margins of the body rather than down into the sediment below (Schofield et al., 2010). Many of the Staffa contact examples have thin layers of organic rich sediment, coal or low permeability volcaniclastic sandstone layers underlying the lavas, and these units may act as an insulating layer protecting the sediment below.

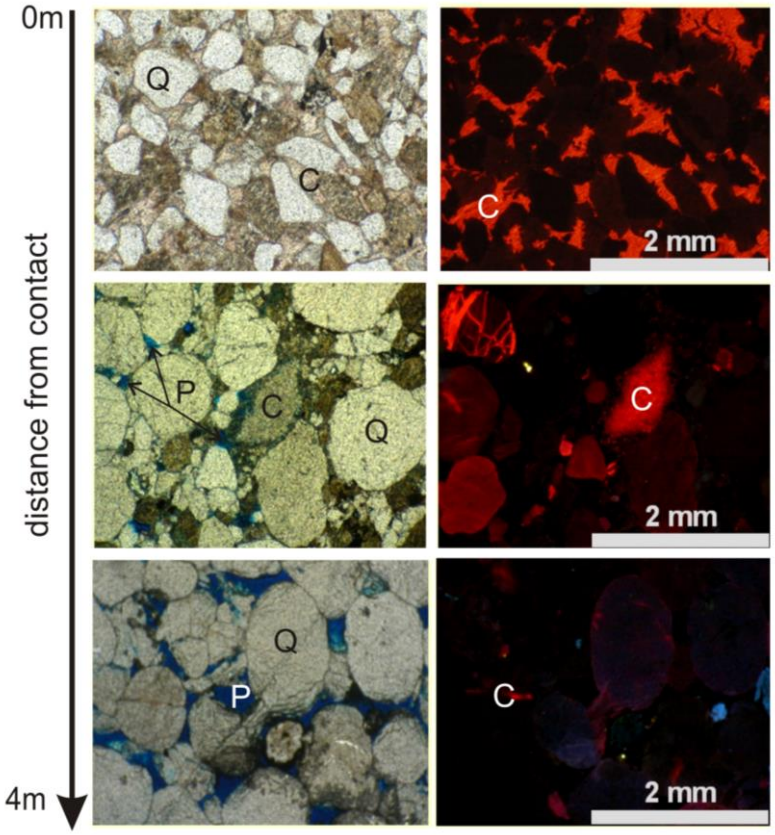

Figure 6.42: Photomicrographs (left) and cathodoluminescence images (right) taken at increasing distances from the base of a lava contact. A calcite cement fills porosity at the contact, but at 4 m calcite cement is minimal and porosity is unaffected. Annotations: quartz (Q); pore space (P), calcite (C). Modified from Grove (2014).

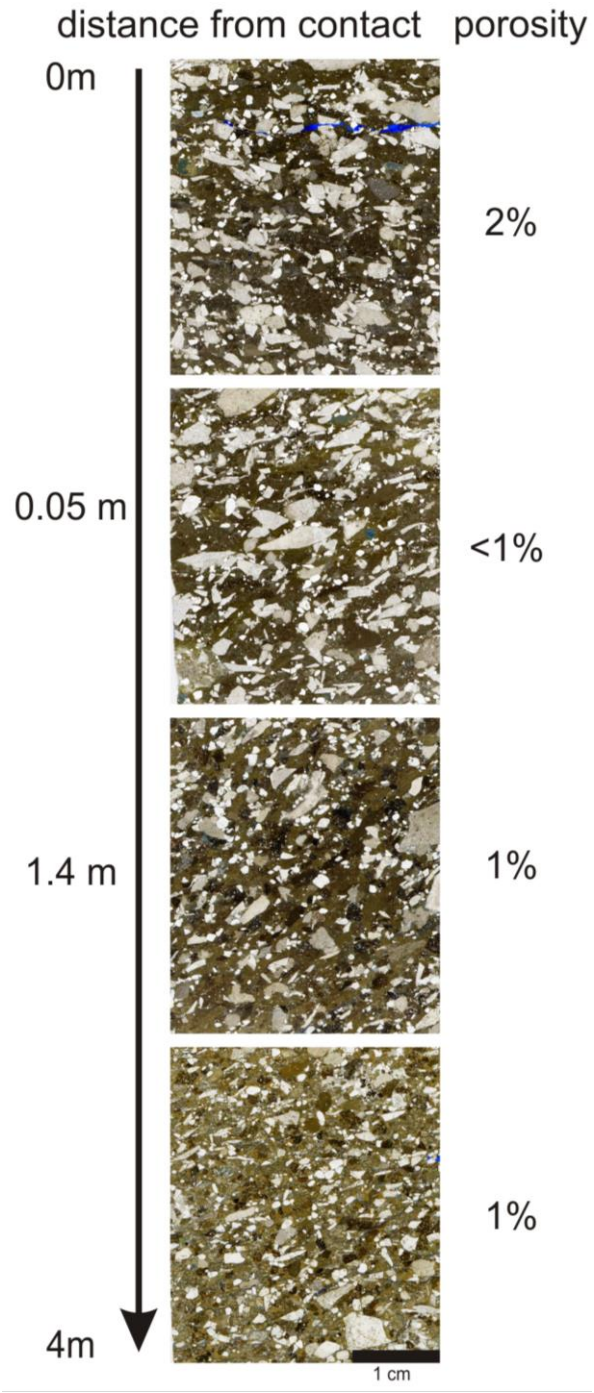

Figure 6.43: Scans of thin sections taken at distances from the base of an intrusive contact (Carsaig Arches, Staffa Formation). Samples are taken at 5 mm, 5cm, 1.4 m and 3.9 m beneath contact. No notable differences in mineralogy or porosity are seen throughout the samples, although the proportions of clay, calcite, flint and quartz does alter slightly.

6.6 Permeability

6.6.1 Previous work

The permeability of a rock is equally as important in a hydrocarbon reservoir as porosity. Very fine-grained rocks tend to have lower permeabilities, whereas very coarse grained rocks have much higher permeabilities (Hogg et al., 1996; Evans et al,

1997). Clay growth generally has a detrimental effect on reservoirs with as little as 1% needed before pore throats are clogged and permeability is reduced (Moore and Reynolds, 1997).

6.6.2 Onshore samples

Analysis of several samples from the Staffa Formation using a permeameter from the University of Aberdeen proved unsuccessful, due to difficulties in creating a seal with polished blocks. On samples that an adequate vacuum could be reached, permeability was very low, in the order of 0–2 mD. Permeability in all samples has been significantly reduced by clay coatings or, in the case of the onshore siliciclastic units, calcite. Further information on the permeability of these samples could have been acquired using mercury injection techniques or examining the pore network under the FIB-TEM; however, it was decided that such low permeability would not be of commercial significance with regards to reservoir quality. Such permeability may have a significant effect on long term seal integrity; however, this was deemed to be beyond the scope of the project.

6.6.3 Offshore samples

Permeability data were obtained by Chevron for a number of wells, typically from sidewall cores and plugs. Figure 6.44 plots the permeability of sidewall samples versus depth. The permeability of the samples varies considerably, independent of depth, and highlights the importance of facies type on permeability.

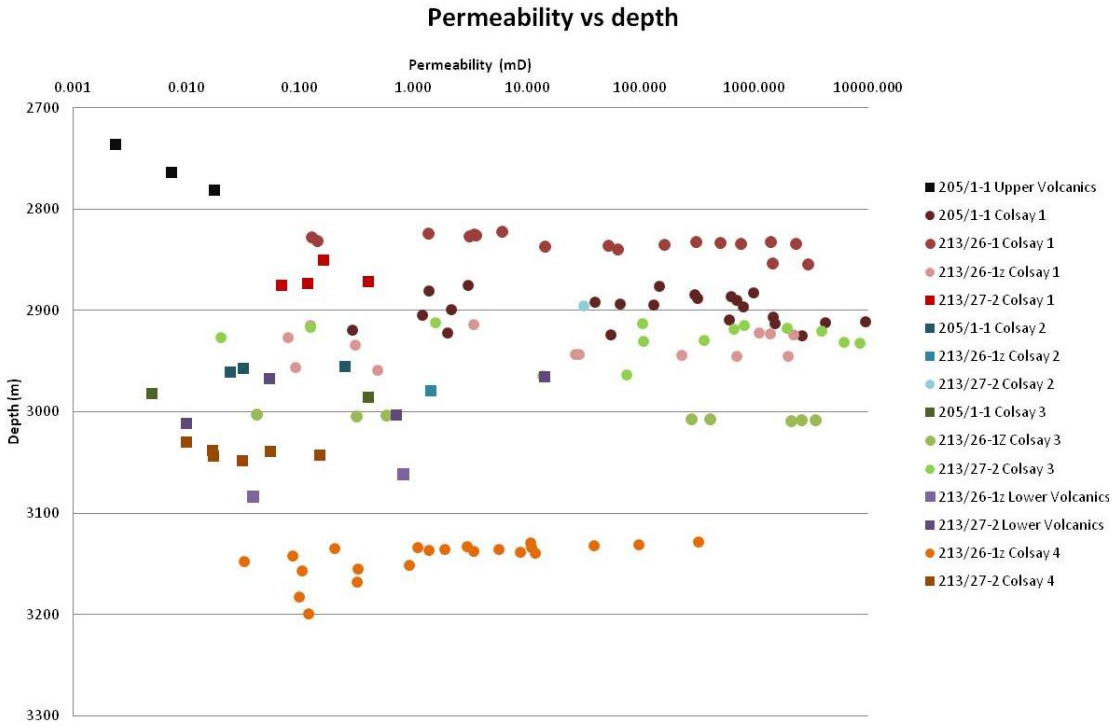

Figure 6.44: Permeability against depth. Squares are volcanic rich samples, whereas circles are siliciclastic samples. Colours represent stratigraphical units: Upper Volcanics (black); Colsay 1 (reds); Colsay 2 (blues); Colsay 3 (greens); Lower Volcanics (purples); Colsay 4 (oranges). Plot shows no correlation between depth and permeability. n=126.

Figure 6.45 shows helium porosity and permeability values for sidewall cores taken in four wells. There is a large range in permeability throughout the samples from 0.002 mD to as high as 8.6 D, and the data show a strong exponential relationship between porosity and permeability.

Figure 6.46 shows the ambient horizontal air permeability plotted against ambient helium porosity in core plug samples. Here the importance of lithofacies type on poro-perm relationships is clear. Core 3 from the 213/26-1 well and the 205/1-1 are both taken in volcanic intervals: helium porosity is low with the majority of samples plotting below 15%, as is the permeability, with most samples in the range of 0.01–1 mD and all lying below 10 mD. In the siliciclastic lithofacies the samples have 12-30% helium porosity and permeability typically greater than 10 mD and up to as high as 24.5 D.

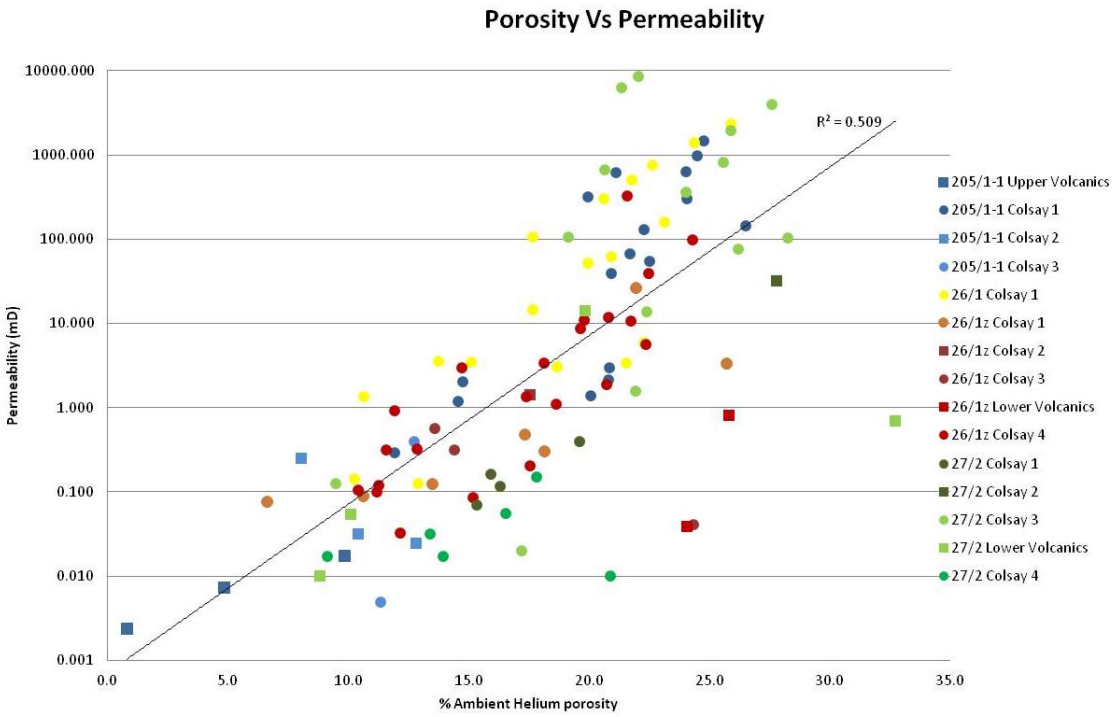

Figure 6.45: Plot of ambient helium porosity against permeability for core plug samples. Squares represent volcanic rich Group 5 samples. Circles represent the siliciclastic Group 6 samples. n= 106.

Basalt lava flows inherently have a lower porosity due to their crystalline nature, whereas volcaniciclastic rocks have higher percentages of pore filling clays, and therefore lower permeability, making them undesirable reservoirs. The siliciclastic units within the Rosebank core do however, have desirable porosity and permeability values. The pore network in these rocks has remained open. The lower permabilites of the 26/1 well core 1 samples can be explained by the percentage of interbeded silty material seen within this core. This again highlights that facies mineralogy exerts a strong control on the resultant poro-perm relationships.

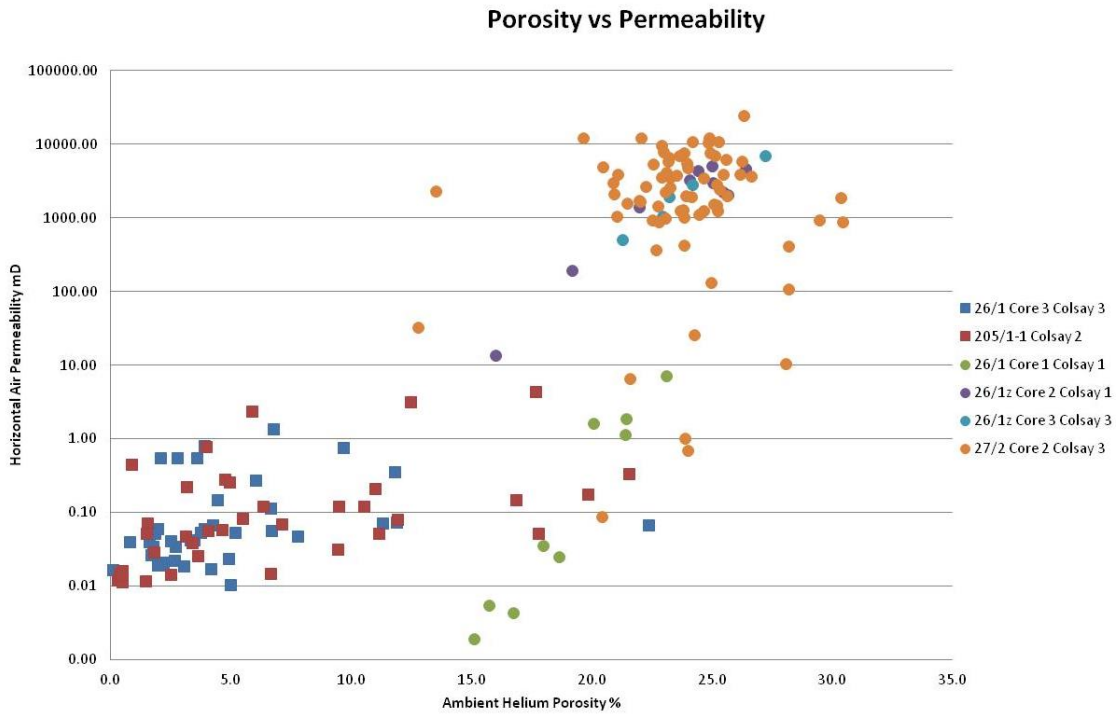

Figure 6.46: Plot of ambient helium porosity against horizontal air permeability in the Rosebank cores. Squares represent volcanic samples, whereas circles represent siliciclastic samples. Two distinct groups can be identified. The volcanic clast rich samples have low porosity and permeability, whereas the volcanic poor reservoir rocks have porosity and permeability values an order of magnitude higher. n=165

6.6.4 Permeability of basalt lava flows

The permeability measurements taken in the volcanic facies were collected on small plugs and sidewall cores and therefore, do not accurately measure potential permeability within fractures or jointing over the entirety of a basalt lava flow. As noted in Chapters 3 and 4 the basalt lava flows often have significant columnar jointing. On Mull the vast majority of the jointing was partially sealed by clays and in places zeolite and calcite; however, it is unclear how joints and fractures will behave at depth. At greater depths, joints and fractures may be annealed leading to poor conductivity between pore waters below and above a lava flow. However, fluid pathways could develop through open joints and fractures, and therefore, lava flows cannot automatically be assumed to act as a seal.

6.7 Isotopic work

The clay fraction of a number of samples was analysed for stable isotopes in order to understand the pore water chemistry and temperatures in which the clay minerals formed. Nineteen samples were analysed for oxygen and hydrogen, using the method described in Chapter 2, for a representative range of rock types (Table 6.4).

6.7.1 Creating a pure phase clay

Obtaining a pure phase of clay to analyse is an important factor when undertaking isotopic work (Morad et al., 2003). All minerals have different fractionation factors and will exchange isotopes with pore fluids at different rates. It is therefore important, to have only one phase of material present in the analysis. The sub 2 μm phase was separated out from the sample and analysed by clay separate XRD as discussed in Section 2.8.1. Care was taken to avoid samples thought to contain large abundances of detrital clays as only authigenic clays will provide information on diagenetic conditions. However, as already discussed in Section 6.4.2 all clay separates contained a complex range of clay minerals, some of which are thought to be mix layer. SEM analysis showed that the clays phases are often complex intergrown phases, for example the transition from grain coating clays to pore filling clays. Separation of such clay phases is an extremely difficult and time consuming process with large errors and uncertainties in results, and therefore, all of the clay within each separate was analysed. This however, also introduces errors into the data as several clay phases could be present within each sample, including minor quantities of detrital clays.

A small quantity of quartz was also present within some clay separates. The crystalline nature of quartz means it will produce large XRD peaks even when miniscule amounts are present. Therefore, samples with small quartz peaks relative to the clay peaks are likely to contain negligible amounts of quartz. Care was taken to only select samples with very low amounts of quartz. However, the presence of small quantities of quartz within a sample will contribute to the overall error within the isotopic data and must be considered when interpreting results.

Sample Name	Lithofacies Group	Sample Location	Sample Preparation	Analysis Undertaken
MT8	1	MacCulloch's Tree	Air	Hydrogen/ Oxygen
MT8f	1	MacCulloch's Tree	Furnace	Hydrogen / Oxygen
MT5	1	MacCulloch's Tree	Furnace	Hydrogen / Oxygen
MP03d	2	Malcolm's Point	Furnace	Hydrogen / Oxygen
MP03d (R)	2	Malcolm's Point	Furnace	Hydrogen / Oxygen
MP03e	2	Malcolm's Point	Furnace	Oxygen only
Ca1d	2	Carsaig Arches	Furnace	Hydrogen / Oxygen
Ca1d (R)	2	Carsaig Arches	Furnace	Hydrogen / Oxygen
Ca1d	2	Carsaig Arches	Air	Hydrogen / Oxygen
Ca5b	2	Carsaig Arches	Furnace	Hydrogen / Oxygen
MT3d	2	The Ladder	Furnace	Hydrogen / Oxygen
MP02	3	Malcolm's Point	Furnace	Hydrogen / Oxygen
MP02 (R)	3	Malcolm's Point	Furnace	Hydrogen / Oxygen
MT3g	3	The Ladder	Air	Hydrogen / Oxygen
AT1	3	Ardtun	Furnace	Hydrogen / Oxygen
AT4	3	Ardtun	Furnace	Hydrogen / Oxygen
MT3b	4	The Ladder	Air	Hydrogen / Oxygen
Ca4	4	Carsaig Arches	Furnace	Hydrogen / Oxygen
CHEV 1	5	213/27-2	Furnace	Hydrogen / Oxygen
CHEV 1(R)	5	213/27-2	Furnace	Oxygen Only
CHEV 13	5	213/27-2	Furnace	Hydrogen / Oxygen
CHEV9	5	213/26-1	Furnace	Oxygen only
CHEV8	6	205/1-1	Furnace	Hydrogen / Oxygen
CHEV 25	6	213/27-2	Furnace	Hydrogen / Oxygen
CHEV 19	6	213/27-2	Furnace	Hydrogen / Oxygen

Table 6.4: Table showing all samples and repeats (R) and the type of isotopic analysis.

6.7.2 Choosing a fractionation factor

As all of the samples had a mix of clay minerals the fractionation factors for the end member clays were calculated and plotted. Both XRD and QXRD results were used to determine relative abundances in each sample. The main clay phases were smectite, corrensite and chlorite; however, corrensite is a mix layer smectite-chlorite mineral and therefore, does not have its own fractionation factor. Fractionation will occur at different rates across the different smectite and chlorite layers within the corrensite

structure. If the proportion of smectite to corrensite layers in the corrensite and the exact chemical composition of these layers is known then a new oxygen fractionation factor could be calculated using the methods described in Zheng (1993a, 1993b). However, accurate information on the structure and composition of the corrensite and mix layer chlorite smectite minerals were not available in this study. For this reason, only the smectite and chlorite end-member fractionation factors were used, which adds significant error into the data.

Hydrogen fractionation is poorly defined for smectite and chlorite clay minerals (Morad et al, 2003). Fractionation is highly dependent on clay composition (Graham et al., 1987; Sheppard and Gilg, 1996) and therefore, a large error in hydrogen isotope values must be taken into account within this study as clay compositions are unknown.

6.7.3 Error

Low standard errors (maximum ± 0.3‰) and good reproducibility of data indicate high precision in the results of this study. However, as discussed above there are a number of factors that affect the accuracy of the results, as the following assumptions have to be made:

- Each of the samples contain only one clay mineral type or a mixture of several end member clay minerals that formed at the same time from the same conditions.
- Each sample contains only authigenic clay minerals.
- All inter layer water within the clay mineral structure has been removed.
- Clay minerals are similar compositions to the end member phases quoted in the literature.
- Fractionation coefficients quoted in the literature are applicable to these samples.

None of the above assumptions can be guaranteed within this study and therefore, all results must be treated with caution and only considered a best estimate of formation water conditions.

6.7.4 Smectite

Oxygen

Water-smectite and saponite oxygen fractionation coefficients are plotted in Figure 6.47. Saponite follows the same general trend as smectite but is shifted due to higher fractionation differences at low temperatures.

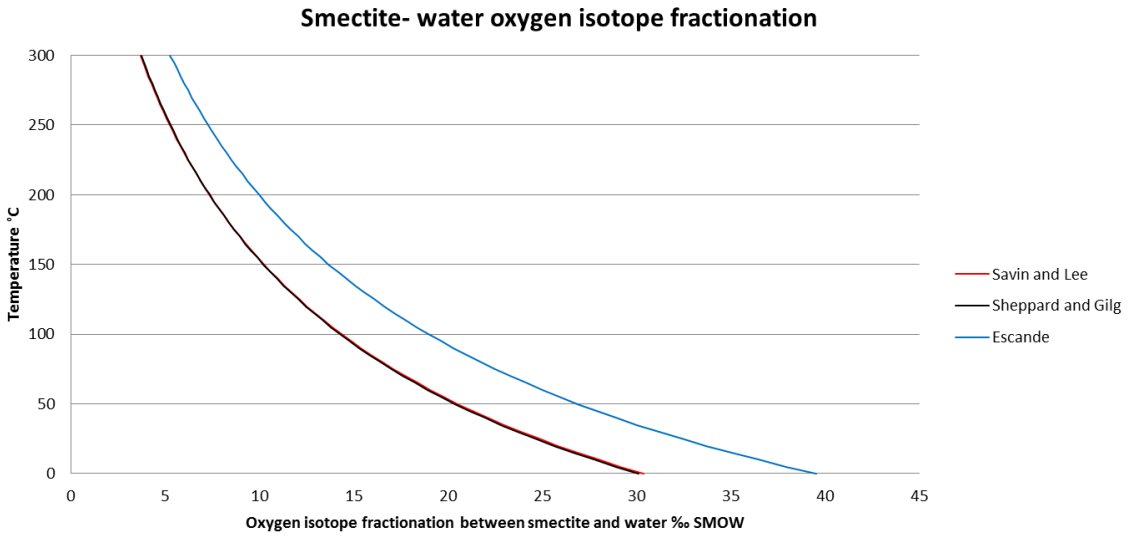

Figure 6.47: Experimentally derived smectite clay-mineral – water oxygen isotope fractionation factors (adapted from Morad et al.,2003). Data for smectites: Savin and Lee (1980), Sheppard and Gilg (1986). Data for saponite: Escanda (1983).

The fractionation factor was plotted against temperature for different isotopic values of smectite found within this study, using the Sheppard and Glig (1986) fractionation factor (Figure 6.48). If the samples formed from meteoric water (~6 –8‰ SMOW) this would indicate formation temperatures ranging between ~70°C and 300°C. The fractionation factor was plotted against temperature for different values of saponite found within this study (Escanda, 1983), (Figure 6.49). Assuming the saponite formed from meteoric waters the temperature range is higher than that of smectite, with samples forming at temperatures above ~140 °C.

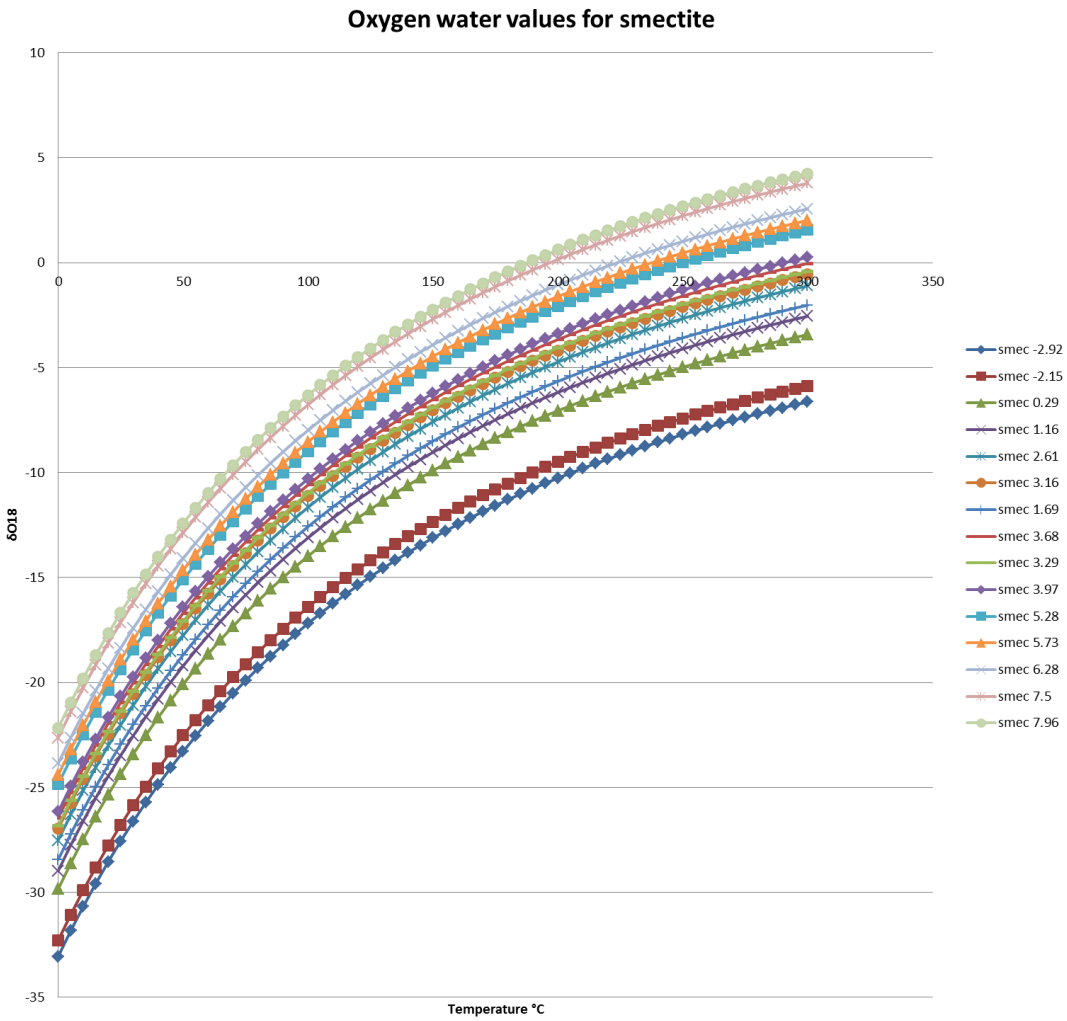

Figure 6.48: Plot of smectite – water fractionation for each sample using the Sheppard and Glig (1986) fractionation factors.

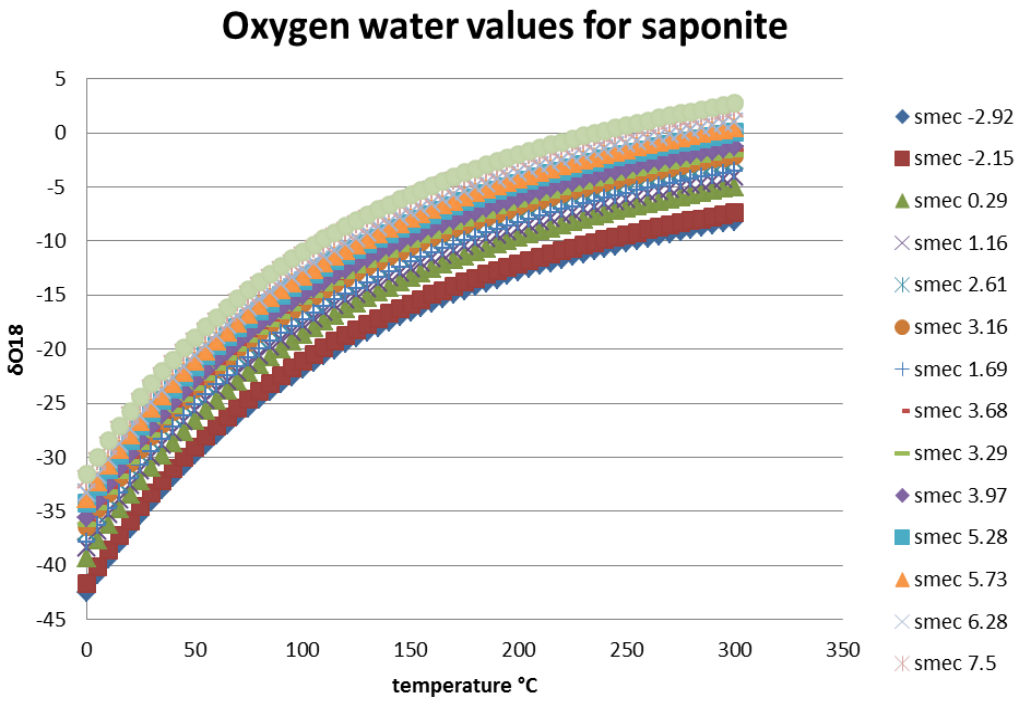

Figure 6.49: Plot of saponite – water fractionation for each sample using the Escanda (1983) fractionation factors.

Hydrogen

The only available hydrogen smectite fractionation factor was for temperatures between 25- 120°C (Yeh, 1980). This temperature range is likely to be too low for this study and therefore, hydrogen results must be viewed with caution.

6.7.5 Chlorite

Oxygen

Water-chlorite oxygen fractionation coefficients are plotted in Figure 6.50. Despite differing Mg and Fe contents the majority of the sources have similar results, with the exception of Cole and Ripley (1999) who have much heavier oxygen isotope ratios at lower temperatures; however, their equation is only suitable for temperatures between 170-350°C. The Fe content of the clays within the study samples is not known although they are expected to be Fe rich. A conservative mid-range Fe equation was selected from Savin and Lee (1988).

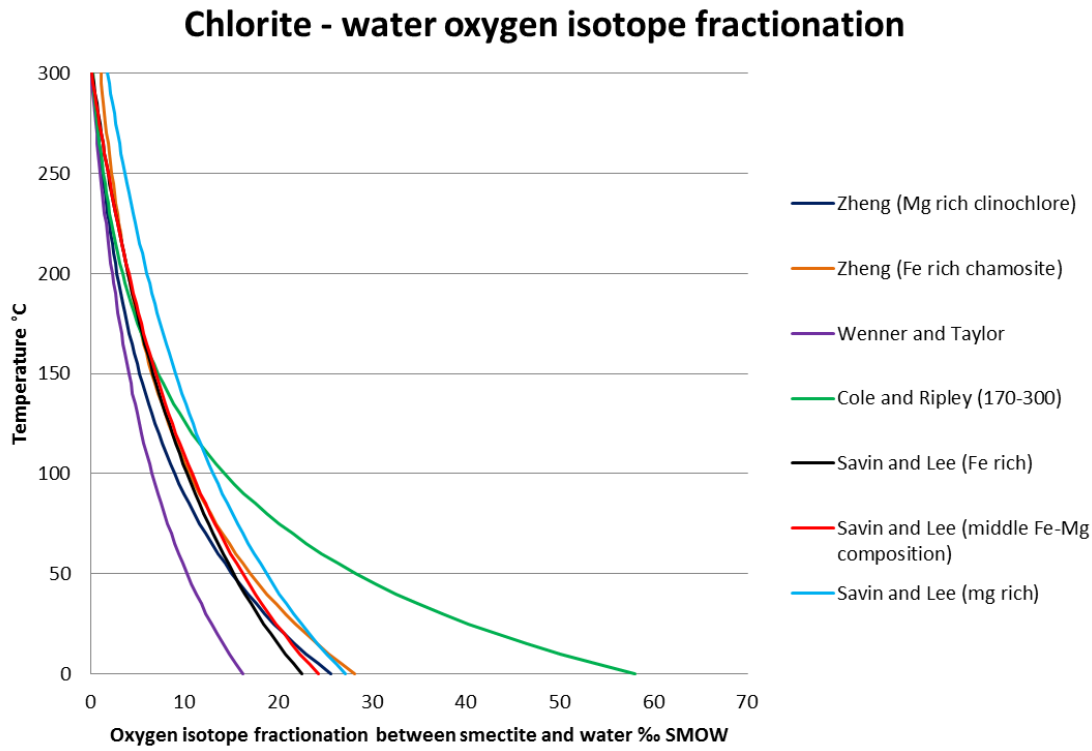

Figure 6.50: Experimentally derived chlorite clay-mineral – water oxygen isotope fractionation factors (Zheng, 1993b; Savin and Lee, 1988; Wenner and Taylor, 1971; Cole and Ripley, 1998).

The Savin and Lee (1988), fractionation factor for each of the samples is plotted in Figure 6.51. Assuming the chlorite formed from meteoric water (~6– 8‰ SMOW) the temperature range of formation would be between ~50– 200°C.

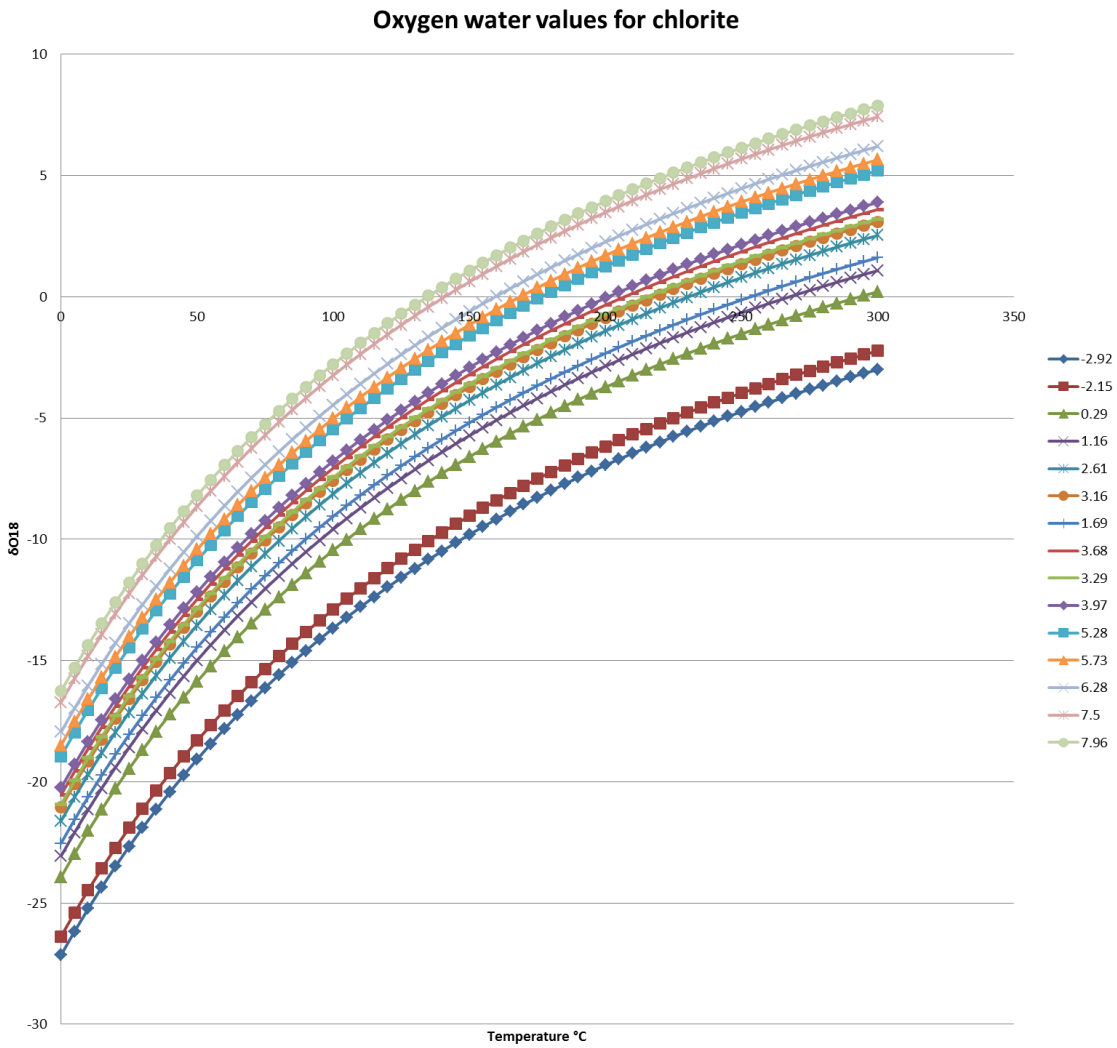

Figure 6.51: Plot of chlorite – water fractionation for each sample using the Savin and Lee (1988) fractionation factors.

Hydrogen

The fractionation factor for chlorite was taken from Graham et al. (1984b); however, Graham et al. (1987) state that hydrogen fractionation for chlorite is highly dependent on mineral chemistry.

6.7.6 Temperature range

The wide temperature ranges calculated from the fraction factors have shown the difficulty in contrasting temperature of formation within the samples. The fractionation factors estimate that the formation of smectite and saponite could occur at higher temperatures than chlorite. However, this directly conflicts spatial relationships observed in the SEM analysis, which indicated that the smectite and saponite formed first as grain coats, before the late stage chlorite pore fill. The maximum temperatures of smectite formation within the literature is ~ 100 °C (see Section 7. 4, Figure 7.8). Within this study much of the smectite has altered into corrensite or chlorite and therefore, may have lost its original isotopic composition during the chloritisation process (Morad et al., 2003).

6.7.7 Results

The isotopic data for each of the three main end member clay minerals were plotted for a formation temperature of 200 °C (Figure 6.52). The data plots in a roughly delta shape primarily, in the meteoric to hydrothermal water fields (as defined by Sheppard, 1986). As samples are bulk compositions they will lie somewhere within this end member field. Therefore, it is likely that samples formed from a mixture of meteoric and magmatic waters. The difference between clay end members results in a spread of ~16 ‰ $\delta^{18}O$ and ~95 ‰ δD from 100 % smectite to 100 % chlorite.

Figure 6.53 shows the smectite end member plotted at a range of temperatures. The spread in the oxygen data is greater at 20 ‰ $\delta^{18}O$, however the spread in hydrogen values remains similar to the clay end members value at 95 ‰ δD. Therefore, temperature exerts a greater effect on oxygen isotopic ratios than clay composition.

Figure 6.54 shows the samples labelled in their respective lithofacies groups, and indicates no correlation between lithofacies type (and therefore clay type) with the isotopic result. No correlation between the isotopic ratio of the clay minerals and their position relative to lava / sediment contacts was found. Therefore, within this study, lava-contacts have not significantly changed pore waters in terms of temperature or chemistry. It is likely that the hydrothermal waters are a result of intrusions (more information in Section 7.5). Figure 6.55 plots sample locations for 100% chlorite compositions. Three offshore samples have much higher deuterium values. The Group 6

sample was found to contain very low levels of chlorite. Therefore, in reality this point will plot at lower values, closer to the meteroirc – hydrothermal water field. However, both Group 5 samples do contain significant amounts of chlorite indicating these samples were influenced by metamorphic and/or seawater. Sample CHEV13, is Colsay 1 in age and comes from the 213/27-2 well. CHEV 8 is Colsay 2 in age and comes from the 205/1-1 well. There is a marine influence in the northern Colsay 1 samples (Rosebank Team, 2013), which may be responsible for the elevated deuterium values. However, the high Colsay 2 point currently remains unexplained.

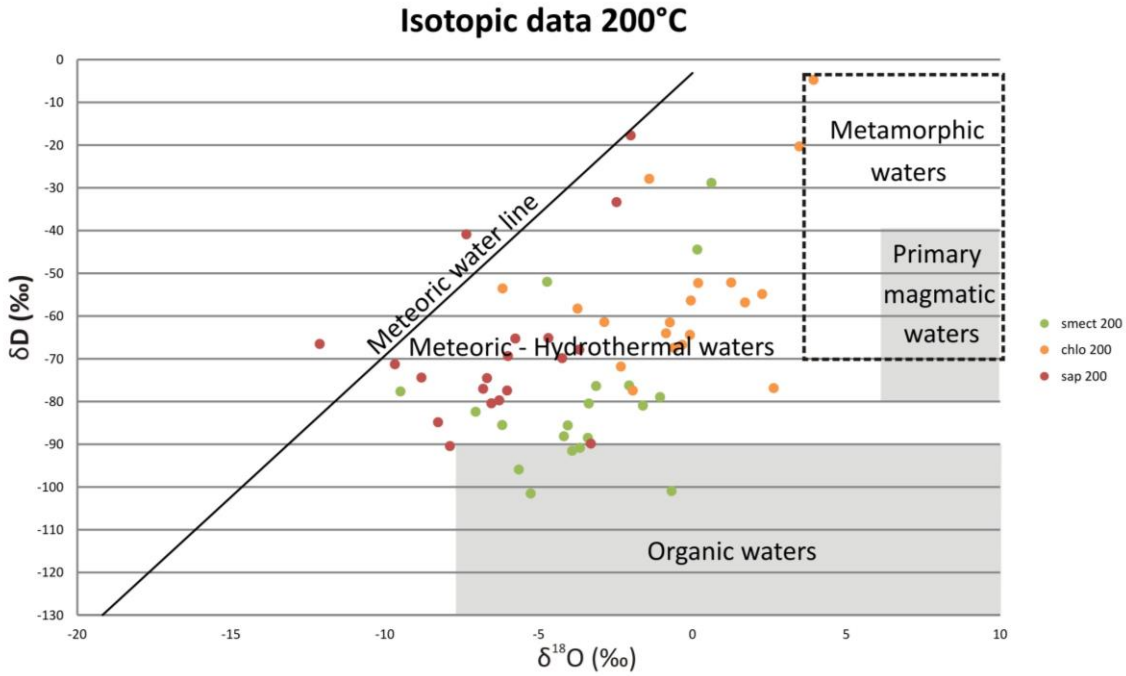

Figure 6.52: Plot of isotopic results for three end member clay types; 100% smectite, 100% saponite 100% and chlorite all at 200 °C. The data plots within the meteroric hydrothermal waters field and implies that meteoric water has mixed with magmatic water. Water fields reproduced from Sheppard et al. (1986). n=15.

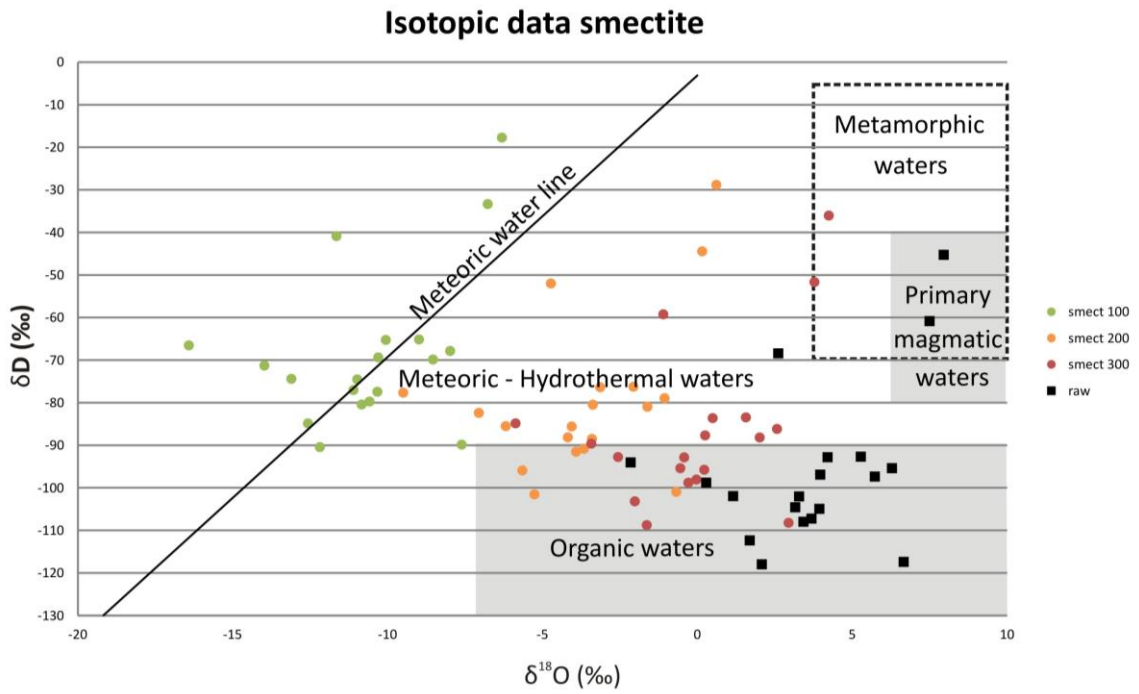

Figure 6.53: Plot of isotopic results assuming samples are 100% smectite for different temperatures; 100, 200 and 300°C. The raw uncorrected data are also plotted in black. Water fields reproduced from Sheppard et al. (1986). n=19

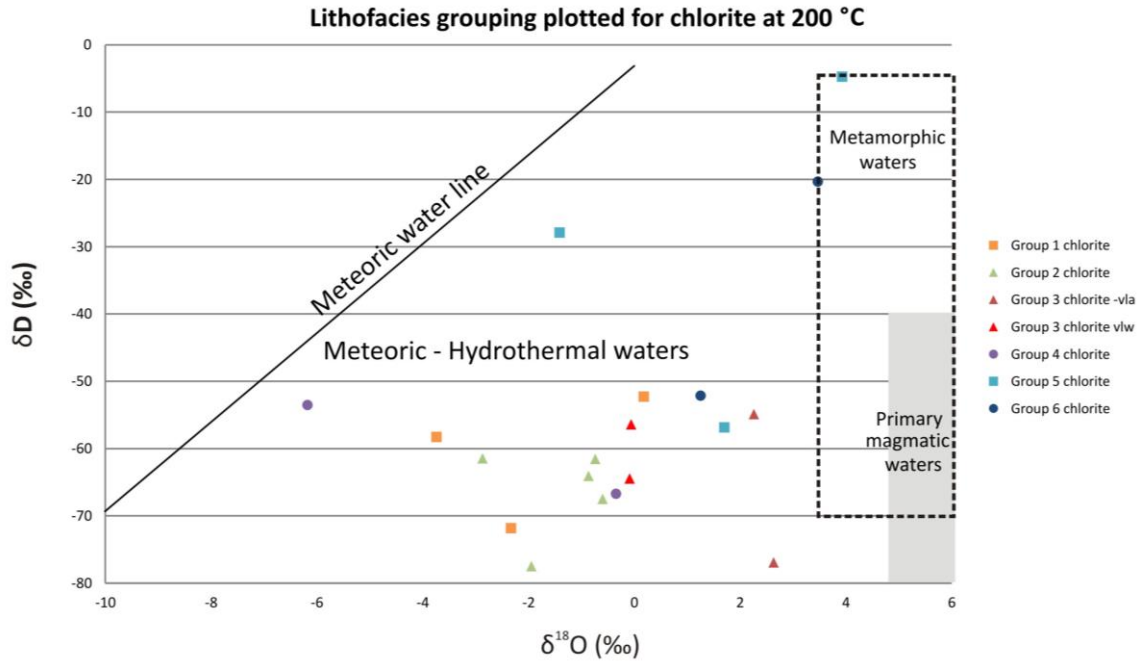

Figure 6.54: Plot of isotopic results for different lithofacies groups. All values are plotted at 200 °C. Water fields reproduced from Sheppard et al. (1986).

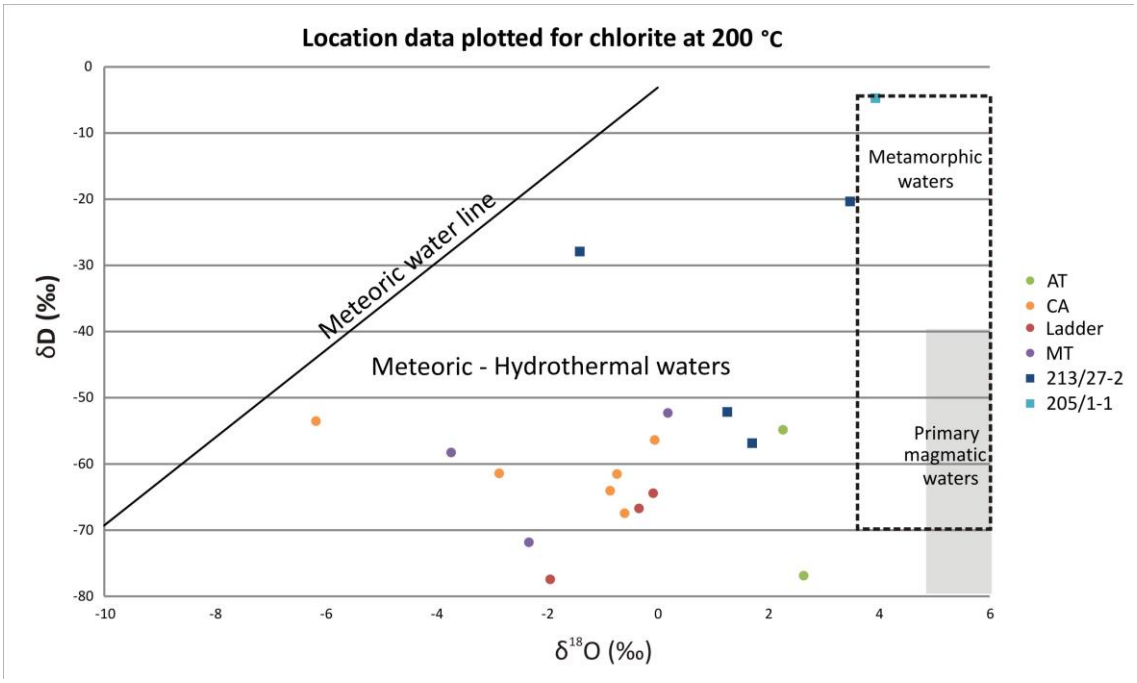

Figure 6.55: Plot of isotopic results for different localities. All values are plotted at 200 °C. Water fields reproduced from Sheppard et al. (1986).

6.8 Conclusions

Bulk XRD allowed the main minerals to be identified in each of the main lithofacies groupings, while clay separate XRD allowed the main clay minerals to be identified. The traditional method of clay separate XRD using the clay size fraction of the sample resulted in larger clay minerals being lost from the analysis. The mineralogy is summarised in Table 6.5 below.

Group name	Point counting data	Bulk XRD	Clay separate XRD
Group 1: Vent proximal	Volcanic glass, crystalline lava clasts, clay minerals, zeolite, opaques, calcite and quartz	Volcanic glass, chlorite, abundant clay minerals, albite, anorthite, calcite and quartz	Smectite and chlorite (potentially mix layer smecite / chlorite)
Group 2: Volcanic rich epiclastic	Volcanic glass, crystalline lava clasts, clay minerals, quartz, flint, calcite, feldspar, organic material, mica, pyroxene, lithoclasts, zeolite, opaques and glauconite	Volcanic glass, chlorite, abundant clay minerals, quartz, anorthite and analcime	Smectite and chlorite (potentially mix layer smecite / chlorite)
Group 3: Volcanic poor epiclastic	Quartz, flint, volcanic glass or crystalline lava clasts, feldspar, organic material, mica, pyroxene, lithoclasts, zeolite, opaques and glauconite	Quartz, albite, calcite, minor clay	Smectite and kaolinite
Group 4: Siliciclastic rocks	Quartz, flint, calcite, minor clay, minor volcanic lithoclasts, minor feldspar	Quartz, calcite, minor clay	Kaolinite and minor smectite
Group 5: Rosebank volcaniciclastic	Volcanic glass, crystalline lava clasts, clay minerals, zeolite, opaques, calcite and quartz	Volcanic glass, abundant clay minerals (including smectite), albite, anorthite, calcite, analcime, and quartz,	Smectite, chlorite (potentially mix layer smecite / chlorite) and illite
Group 6: Rosebank siliciclastic	Quartz, calcite, feldspar and minor clay	Quartz, albite, anorthite, chlorite	Chlorite (potentially mix layer smecite / chlorite) and illite

Table 6.5 Summary of point counting, bulk XRD and clay separate XRD results. Minerals are ordered in relative abundance.

QXRD allowed the quantification of mineral phases in each grouping. The following relationships were established:

- There is a strong correlation between on and offshore samples.
- There is a direct relationship between the amount of volcanic glass within a sample and the proportion of clay.
- Samples containing high amounts of volcanic glass (>15%) had the highest proportions of saponite (>10%). Intermediate samples had the highest proportions of nontronite and samples containing very few (<10% volcanic glass) contained di-smectites.
- Large pore filling chlorite was not seen in QXRD results but corrensite (mix layer chlorite / smectite) was observed.

Point counting data allowed the relationship between minerals and visible porosity to be established. The following conclusions were made:

- In Rosebank sample lithology has more of an effect on porosity than burial depth.
- Samples containing more than 10% volcanic clasts have less than 5% visible porosity.
- Clay is the primary pore-filling material.
- Onshore samples that lack abundant volcanic clasts have had their porosity reduced by a late-stage calcite cement.
- Samples containing high proportions of volcanic clasts (>20%) also contain abundant pore-filling clays (>20%).
- Rocks containing abundant volcanic clasts (>10%) tend to have corrensite, smectite and chlorite clay minerals.
- Rocks with <10% volcanic clasts have higher proportions of mix layered illite-smecite and kaolinite.
- Distance from source affects the porosity of the sample. Rocks closer to volcanic sources tend to contain more volcanic glass and therefore, more pore filling clay.
- Basaltic glass and pyroclasts have a much higher influence in surrounding porosity than crystalline lava clasts due to their reactive nature and plasticity.

- No direct contact diagenetic effects could be ascertained on the samples surrounding intrusions or beneath lava flows.

Permeability data for the offshore samples provide the following conclusions:

- In the Rosebank samples lithology exerts a greater control on permeability than depth, but the small depth range in which the samples have been taken must be taken into account.
- Volcaniclastic rocks have lower permeabilities (<10 mD) than the siliciclastic rocks (up to 10000 mD).

Isotopic data provide the following conclusions:

- Although the precision of the isotopic data are good (max. error 0.3‰), the accuracy of the data has a very large error with many assumptions and therefore, the data can only be used as an estimate.
- Offshore and onshore samples have experienced similar diagenetic histories.
- The samples formed at relatively high temperatures from a mixture of meteoric and hydrothermal waters.
- Lithofacies cannot be correlated to the isotopic results.
- Sample location does have an effect on the isotopic results, with some offshore samples having elevated δD values, potentially due to an influx of sea water.

6.9 Further work

Further work is required to accurately assess the permeability of the onshore samples. Mercury injection methods, (for example, Pittman, 1992; Tang et al., 2008) may provide more accurate data; however, it is anticipated that all volcaniclastic and pyroclastic samples would have similarly poor permeability to their offshore equivalents of under ~ 5 millidarcies.

7 The diagenetic evolution of onshore Staffa Formation rocks and offshore Rosebank rocks

7.1 Introduction

A simplified paragenetic sequence has been determined for the various diagenetic phases identified in each of the lithofacies groups described in previous chapters. Links to regional heat flow and burial are then identified. A simplified model of volcaniclastic basaltic rock diagenesis is provided and a risk chart introduced, which applies the findings from this study to further exploration in flood basalt provinces.

7.2 Diagenetic paragenesis of the Staffa Formation rocks

7.2.1 Group 1 – Vent Proximal

Stage 1

Alteration is abundant within the Group 1 – vent proximal pyroclastic lithofacies. This is due to the abundance of reactive volcanic glass and its thermodynamic instability, and the lack of more chemically inert forming minerals such as quartz (Figure 7.1, Stage 1).

Stage 2

Basaltic glass in the samples starts to alter soon after deposition (Figure 7.1, Stage 2) (e.g. Stronick and Schmincke, 2002; Gifkins, et al., 2005). Element mobility during alteration leads to changes in the water-rock chemistry, which dominates diagenetic paragenesis thereafter. As water interacts with the glass, micro dissolution and precipitation cause the development of amorphous gel palagonite as seen in Figure 5.3 (c.f. Peacock 1962; Hay and Iijima 1968; Staudigel and Hart 1983; Furnes 1984; Thorseth et al., 1991; Stroncik and Schmincke 2001). The composition of the palagonite is highly dependent on the initial glass and water composition (Stroncik and Schmincke 2002). During gel palagonite formation, there is a relative reduction in the volume of the glass as SiO_2, Al_2O_3, MgO, CaO and Na_2O are lost to pore waters

(Stronick and Schmincke, 2002; Gifkins, et al., 2005). Within this study, alteration is more common in the glass-rich pyroclasts than in crystalline bombs and lava clasts. Feldspar alteration also starts to occur.

Stage 3

As the sediment is buried diagenetic compaction of basaltic scoria and ash occurs (e.g. Branney and Sparks, 1990). This compaction is responsible for a large reduction in visible porosity as the scoria and ash are strung out and deformed around more rigid grains (Figure 5.8; Figure 7.1, Stage 3). More crystalline clasts retain their structure, resulting in surrounding porosity being preserved (see Figure 6.41).

As the rocks were buried and experienced higher temperatures, the amorphous palagonite altered to more structured and crystalline fibro-palagonite. This process is volume constant and results in CaO and Na_2O being lost into the pore water. However, SiO_2, Al_2O_3, MgO and K_2O are all gained from the pore water. Some authors suggest that K-rich palagonite could result from interaction with seawater (Staudigel and Hart, 1983; Fisher and Schmincke, 1984; Zhou and Fyfe, 1989; Jercinovic et al., 1990; Thorseth et al., 1991). However, Stroncik and Schmincke (2001) have demonstrated that no relationship between K concentration and water type exists in the early phases of alteration. The Ti banding found during SEM analysis is a result of low water/rock ratio, which concentrates immobile Ti and Fe^{3+} into concentric bands (Crovisier et al., 1992; Stroncik and Schmincke 2002).

The Na released during palagonitisation causes the pore waters to become increasingly alkali, which in turn accelerates the dissolution of volcanic glass (Stroncik and Schmincke 2002). Therefore, the process of palagonitisation results in a complex feedback loop (Gieskes and Lawrence, 1981; Gislason and Eugster 1987; Gislason and Arnórsson, 1993; Steefel and Lasaga, 1994; Stroncik and Schmincke 2002). The Na released during the palagonitisation process may also have aided the albitisation of feldspars, for example seen in Figures 5.32 and 5.33.

Stage 4

Increasing depth and elevated temperatures and pressures in the samples resulted in the alteration of palagonite to Fe-rich smectites (cf. Zhou and Fyfe 1989) (Figure 7.1, Stage

4). Small spherical features within the fibro-palagonite (see Figure 5.28 for reference) are identified as "stevensitic smectite", which is interpreted as an unstable Mg-rich smectite-like material that acts as a precursor material to smectite (Eggleton and Keller, 1982; Zhou and Fyfe, 1989; Stroncik and Schmincke 2002). Stevensitic smectite has been previously identified on Mull (Davison, 1989)

Smectite forms from volcanic glass under alkaline conditions provided there is a sufficient source of Ca, Mg and Na ions (Deer et al., 1966). Therefore, the Ca and Na realised during the palagonitisation process is incorporated into the smectite structure (Zhou and Fyfe 1989). The abundance of Fe in the scoria and ash fragments within this study results in formation of Fe-rich end member smectites. Palagonite may be replaced by K-rich smectite initially (Honnorez, 1978). Zhou and Fyfe (1989) identified an increase in K from glass to the palagonite; however, no K-rich smectite is recognised within the Group 1 samples.

Similar Fe-rich smectites have been reported in basaltic sequences in the Faero Islands (Sabine, 1971). The formation of these clays has been attributed to hydrothermal fluids causing argillisation of volcanic tuffs and from meteoric alteration of basalts (Parra et al., 1986).

The link between saponite and volcanic glass was shown in Figure 6.20, and Stroncik and Schmincke (2001) note that saponite and nontronite form from a palagonite precursor. Smectite is by definition a swelling clay (Moore and Reynolds, 1997; Worden and Morad 2003) and therefore, the process of palagonite to smectite formation is not isovolumetric, resulting in surrounding pore space being impeded by smectite. The smectite forms tightly packed grain coats (e.g. Figure 5.37) that mimic the earlier palagonite structure.

Zeolites are the second most common mineral formed from the alteration of volcanic rocks after smectite (Fisher and Schmincke, 1984). The zeolite, analcime, is reported in some Group 1 samples. Analcime ($16NaAlSi_2O_6$-H_2O, Si/Al ratios vary) is one of the most common zeolites and can form in a wide range of geological environments over a large range of temperatures (Gaines et al., 1997), but is typically formed from the alteration of volcanic glass (Hay, 1966). Analcime can form from a range of silica glass compositions, but typically forms from Na^+ rich basaltic glass or in rocks that experienced hydrothermal waters that were high in Na^+ (Höller and Wirsching, 1978). Therefore, Na released in the palagonitisation process may be incorporated into the analcime. Zeolite does not replace the glass directly but will

crystallise around the vitroclasts (Hay, 1966). Some authors (Surdam, 1977; Gifkins, et al., 2005) suggest that analcime can only be formed from the alteration of precursor zeolites such as clinoptilolite, phillipsite and erionite and cannot form directly from the volcanic glass. This would imply that a precursor zeolite forms during Stage 4 and is altered later (Stage 5) to analcime. Palagonitisation and the albitisation of feldspars (see Figure 5.35 for reference) leads to fluctuations of Ca and Na ions in the pore waters that can promote the formation of these precursor, calcic zeolites (Utada, 1991).

Stage 5

At further increased depths and temperatures, there is a switch from smectite to corrensite or mix layer smectite chlorite formation (Figure 7.1, Stage 5). The corrensite nucleates on the smectite grain coats and grows perpendicular from the grain surface, further reducing pore space (see Figure 5.46). High Fe and Mg varieties indicate they formed from hydrothermal waters (Höller and Wirsching, 1978).

During SEM analysis anomalous patches of K-rich material of unknown origin were found in albitised feldspars and surrounding some clasts (Figure 5.32A). Munhaetal (1980) suggests that interaction of volcanic glass with Na-rich sea water could exchange K and result in the formation of alkali feldspar. Several authors also report a transition from zeolites such as analcime to diagenetic alkali feldspar (Surdam, 1977; Hay, 1978), however, this normally results in crystalline overgrowths around plagioclase feldspars, which is not observed in this study. K liberated in the formation of zeolites and in the transition from earlier formed zeolites into analcime, may release K into the pore waters (Surdam, 1977) resulting in alkali feldspar formation (cf. Gifkins et al., 2005) or K-metasomatism. Noh and Boles (1989) note the formation of a K-rich gel like glass as a transitional mineral during the transformation from silicic glass to crystalline K-feldspar. Such material is identified in this study (e.g. Figure 5.32.A); however, Group 1 samples contain basaltic glass, which is unlikely to contain large quantities of K and therefore, another mechanism of releasing K into pore waters may be required. Mica, K-feldspar and organic material can all release K during burial (Berner and Berner, 2012) leading to K-metasomatism; however, none of these minerals were found within the Group 1 lithofacies. Therefore, the K may have been brought into the rocks from hydrothermal waters (e.g. Chapin and Lindley, 1985). At this stage, the porosity and permeability of the rock was severely reduced, limiting potential fluid

pathways, which contradicts the suggestion of large amounts of pore water accessing the rock.

Stage 6

Several authors report chloritisation of smectite (and corrensite) during burial diagenesis (Hillier, 1994; Worden and Morad, 2003; Gifkins et al., 2005). Mg, Fe and Al are increasingly concentrated into pore waters as the volcanic glass alters, during smectite and zeolite formation, and from the dissolution of pyroxene in more crystalline clasts (Worden and Morad, 2003). Mg is fixed in corrensite resulting in pore waters that are enriched in Al and Fe (Biron et al., 1999), explaining the pore filling Fe-rich chlorites in the Group 1 samples (Figure 7.1, Stage 6). The clay patches (Chapter 5, section 5.5.14.5, Figure 5.3.1.B) may grow into pore space formed by late stage albite and pyroxene dissolution. The porosity of these samples is reduced to less than 5%.

The chloritisation process results in the production of quartz (Worden and Morad, 2003); however, no diagenetic silica is found within the samples. Giles et al. (1992) and Bjørlykke et al. (1994) suggest burial depths of >2 km are required before a significant quartz cement is developed and therefore, the Staffa Formation samples may have been too shallow for this to occur. Alternatively, the extensive clay development earlier in the paragenetic sequence limited the availability of silica nucleation sites. McKinley et al. (2003) suggest that Ca can be released during chloritisation resulting in the formation of carbonate, and some Group 1 samples do display minor late stage calcite cements.

Ti is not incorporated into the chlorite structure and is concentrated within pore waters. Therefore, Ti oxides such as rutile and its alteration product, leucoxene, are the last minerals to form within the pores. The Ti oxides fill spaces around the chlorite platelets as they meet, resulting in the anastomosing textures seen in many pores and vesicles within Group 1 rocks.

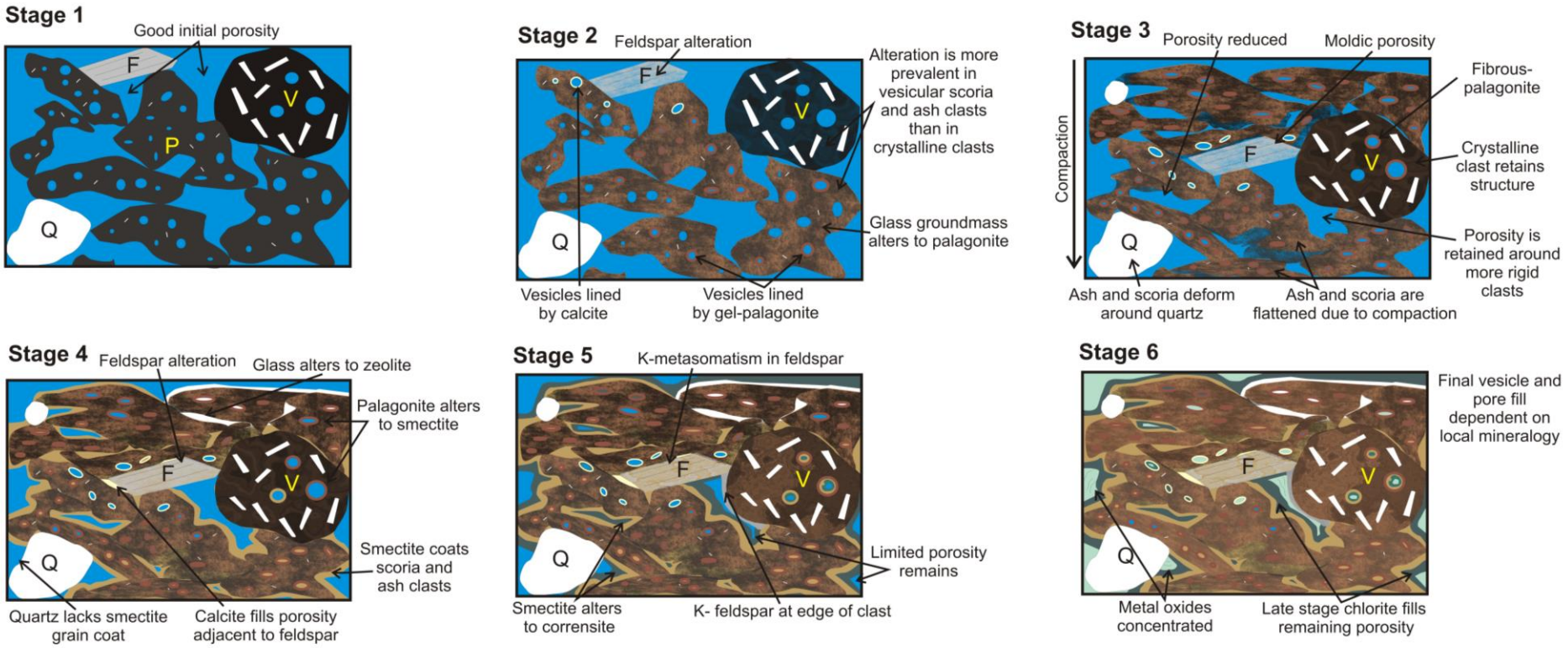

Figure 7.1: Simplified paragenetic sequence for Group 1 rocks.

7.2.2 Group 2 – Volcanic rich epiclastic rocks

Stage 1

The diagenetic paragenesis of Group 2 volcanic rich epiclastic samples is the most complex of all the rocks in this study, due to their heterogeneous nature. More variations in parent material will result in a wider range of phyllosilicate compositions (Khalaf, 2013). Volcanic clasts of several different compositions, textures and ages are found, together with feldspar, quartz, flint, mica and organic material (Figure 7.2, Stage 1).

Stage 2

Initially, paragenesis is similar to the Group 1 rocks, as the glass-rich reworked pyroclasts alter to palagonite and feldspars are altered (Figure 7.2, Stage 2). However, the range of alteration in volcanic clasts is much greater in Group 2 samples due to the heterogeneity of clast compositions.

Some flint clasts already have inherent diagenetic phases, such as calcite filled fractures (see Figure 5.39B). Alteration is more pronounced in fossiliferous Type 1 flint (see Section 5.5.3). Amorphous silica within the flint is partially dissolved creating intragranular, moldic porosity.

Stage 3

During compaction, the reworked pyroclasts, mica and organic fragments are deformed around framework grains such as quartz, resulting in the localised reduction of visible porosity (Figure 7.2, Stage 3). Crystalline basalt lava clasts retain their structure better and so adjacent pores remain open (see Figure 6.41). Sutured grain boundaries are common as compaction causes limited dissolution at grain boundaries.

Stage 4

Smectite coats scoria clasts and partially fills vesicles within less altered lava clasts (Figure 7.2, Stage 4), where the glassy groundmass starts to alter to palagonite. Flint alteration and the albitisation of feldspars continue to create moldic porosity and a patchy calcite cement replaces the palagonite in places (e.g. Dimroth and Lichtblau, 1979). This calcite may form from Ca released during feldspar alteration and from the remobilisation of calcite in fractures within flint clasts.

Stage 5

An influx of localised acidic pore waters caused partial dissolution of the calcite cement (e.g. Bjørlykke 1984; Mathisen 1984), resulting in the creation of secondary porosity (Figure 7.2, Stage 5). The groundmass and grain coats of the more crystalline lava clasts alter to smectite. As in Group 1 rocks this smectite then alters to corrensite, which fills the surrounding porosity. Some samples also contain limited amounts of analcime, formed by the alteration of volcanic glass, similar to that formed in Group 1 samples.

Stage 6

Similar to the Group 1 samples, K-metasomatism results in patchy K-feldspar like material, which is then preferentially altered (Figure 7.2, Stage 6). Alteration in all clasts is now so extreme that identifying initial clast boundaries can prove challenging. Another phase of calcite precipitation, potentially linked to the release of Ca during the palagonitisation of the remaining crystalline clasts and/or the albitisation of feldspars, re-cements localised porosity.

Stage 7

A further phase of calcite dissolution creates secondary porosity (Figure 7.2, Stage 7). Some authors (e.g. Siebert et al. 1984; Surdam et al. 1984) suggest late stage calcite dissolution may result from fluids associated with clay minerals. Similar to the Group 1 rocks, the chloritisation of corrensite and smectite leads to much of the remaining porosity being filled by chlorite.

Stage 8

Similar to the Group 1 rocks, much of the remaining porosity is filled by a calcite cement thought to be a result of the release of Ca during chloritisation of corrensite. As a result samples have less than 10% porosity (Figure 6.28).

Several phases of precipitation and dissolution of calcite are present but these are not evenly spread throughout all the samples, or even within one sample. Diagenetic paragenesis is therefore, strongly dependent on the localised, surrounding mineralogy which can variably considerably throughout individual samples.

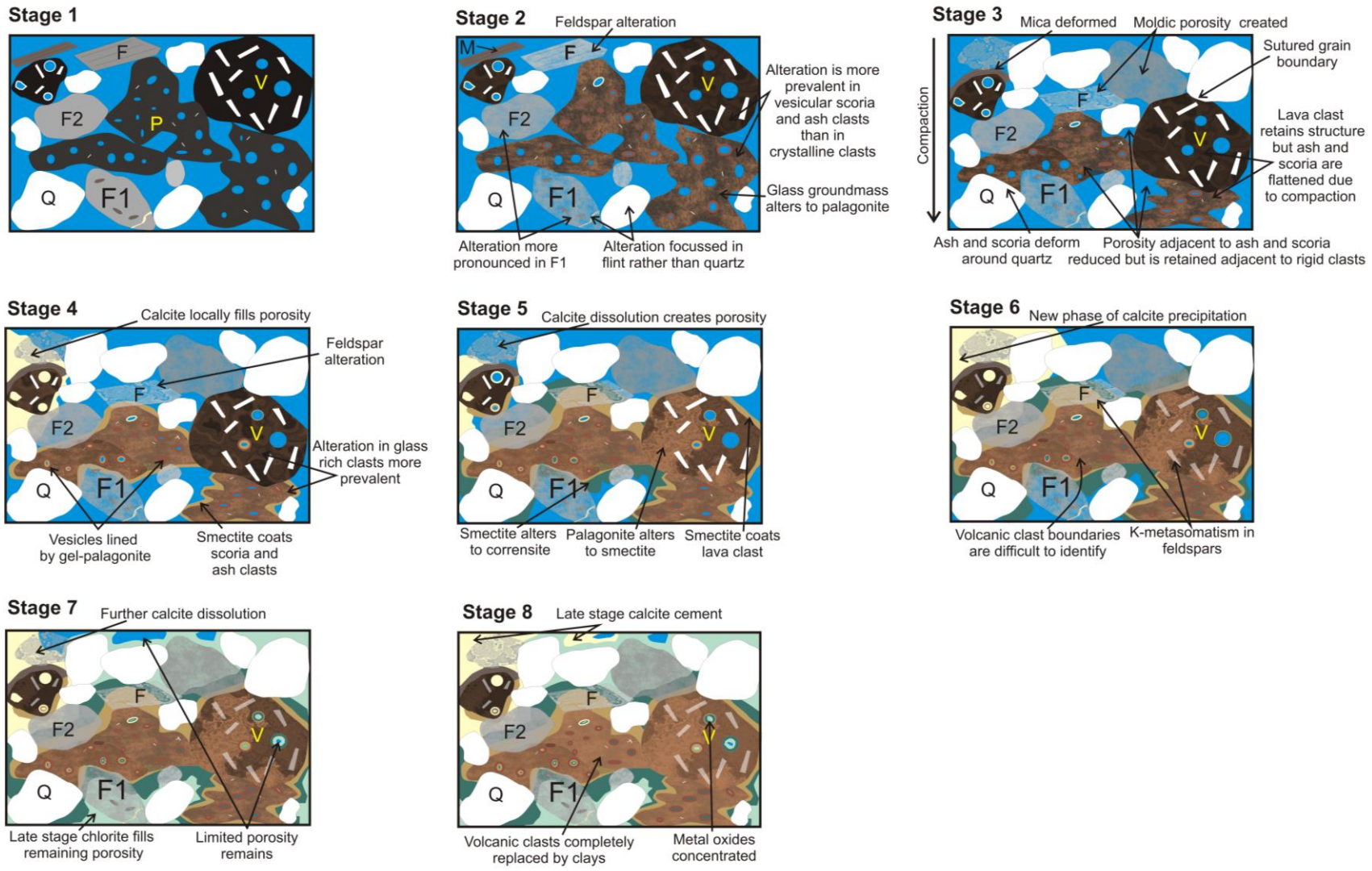

Figure 7.2 Simplified paragenetic sequence for Group 2 rocks.

7.2.3 Group 3 – Volcanic poor epiclastic rocks

The Group 3 volcanic poor epiclastic samples from Ardtun have a different diagenetic paragenesis than those sampled at other Staffa Formation locations and therefore, the volcaniclastic lithic arenites will be discussed separately from the volcaniclastic lithic wackes.

7.2.3.1 Volcaniclastic lithic arenites (vlA)

Stage 1

The vlA samples are characterised by basalt lava flow clasts, quartz, flint, mica and organic material and contain no pyroclasts (Figure 7.3, Stage 1). Porosity within these samples is initially good with the rocks being less heterogeneous than Group 2 rocks.

Stage 2

Under compaction feldspar and flint are altered, resulting in the formation of moldic porosity (Figure 7.3, Stage 2). Mica is deformed and sutured boundaries are common. Some of the lava clasts have inherited diagenetic phases such as calcite vesicles, or Fe stained rims due to weathering.

Stage 3

Lava clasts altered to palagonite and smectite formed grain coats (Figure 7.3, Stage 3). If formed early during compaction the smectite may help to protect porosity from compaction. Alteration of feldspars and flint resulted in moldic porosity.

Stage 4

Alteration of the basalt lava clasts continued with smectite altering to corrensite, and chlorite. However, only the porosity immediately surrounding the volcanic clasts is

affected (Figure 7.3, Stage 4). Visible porosity at this stage are estimated to up to 25% (Section 6.5)

Stage 5

The Ardtun samples have lower than expected visible porosity (<10% see Figure 6.30). This is due to an aggressive late stage calcite cement that almost completed filled porosity (Figure 7.3, Stage 5). The source of this calcite remains unexplained, however Ca was added to pore waters during feldspar dissolution. The amount of volcanic clasts is limited, resulting in fewer clay grain coats. Fluid pathways remain open therefore, resulting in the circulation of late stage pore fluids that could lead to calcite precipitation. Williamson and Bell (2011) suggest that the Ardtun calcite may be hydrothermal in origin.

7.2.3.2 Volcaniclastic lithic wackes (vlW)

Stage 1

Initially the vlW resemble the vlA samples, with the main difference being the presence of reworked scoria and ash pyroclasts (Figure 7.4, Stage 1). They contain more quartz and flint than Group 2 samples.

Stage 2

During initial compaction the vlW display a mixture of compaction textures seen in the Group 2 and vlA samples (Figure 7.4, Stage 2). The scoria, ash, mica and organic fragments deformed more than the crystalline clasts causing a localised reduction in porosity, whereas the lava clasts retained their structure and preserving surrounding porosity.

Stage 3

Similar to the vlA samples, feldspar and flint dissolution occurred (Figure 7.4 Stage 3). Volcanic clasts also altered to palagonite, with reworked pyroclasts showing the most alteration.

Stage 4

Porosity is reduced by the formation of smectite and corrensite locally around volcanic clasts (Figure 7.4, Stage 4). The reduction is most extreme surrounding the pyroclasts with pore throats being occluded. Overall porosity is higher than in the Group 2 rocks. Zeolite was also rarely found within the samples, and is thought to form in the same way as described in the Group 1 rocks.

Stage 5

Late stage calcite has not affected these samples, unlike the vlA (Figure 7.4, Stage 5). Late stage chlorite and kaolinite formed minor grain coats and filled porosity surrounding volcanic grains. Further from the volcanic clasts porosity was retained, perhaps due to minor clay coats blocking potential silica nucleation sites and halting late stage quartz cements.

7.2.4 Group 4 – Siliciclastic rocks

Stage 1

Siliciclastic sandstone diagenesis history is typically much simpler to understand due to less authigenic phases forming and less heterogeneity within the system. Unlike the volcanic rich samples, the Group 4 samples are composed predominantly of stable minerals such as quartz (Figure 7.5, Stage 1) so they are less likely to alter.

Stage 2

While volcanic minerals can add a wide range of ions into the system, alteration of quartz and flint can only provide silica. Ca could be provided by the dissolution of feldspars and from the remobilisation of calcite from fractures within the flint. Sutured boundaries are common indicating some compaction, and visible porosity, although reduced, is preserved (Figure 7.5, Stage 2). A patchy quartz cement resulting from the mobilisation of silica from suture grain contacts and the dissolution of flint, helped to protect some grains from further compaction. Feldspar was also dissolved leading to the formation of moldic porosity.

Stage 3

Minor kaolinite and illite authigenic clay grain coats developed due to the alteration of feldspars and mica (Figure 7.5, Stage 3). These grain coats may have helped to preserve porosity during further compaction.

Stage 4

A late stage patchy calcite cement filled pores; however, it did not significantly alter the overall porosity of the rock with visible porosity up to 38% being retained (Figure 7.5, Stage 4).

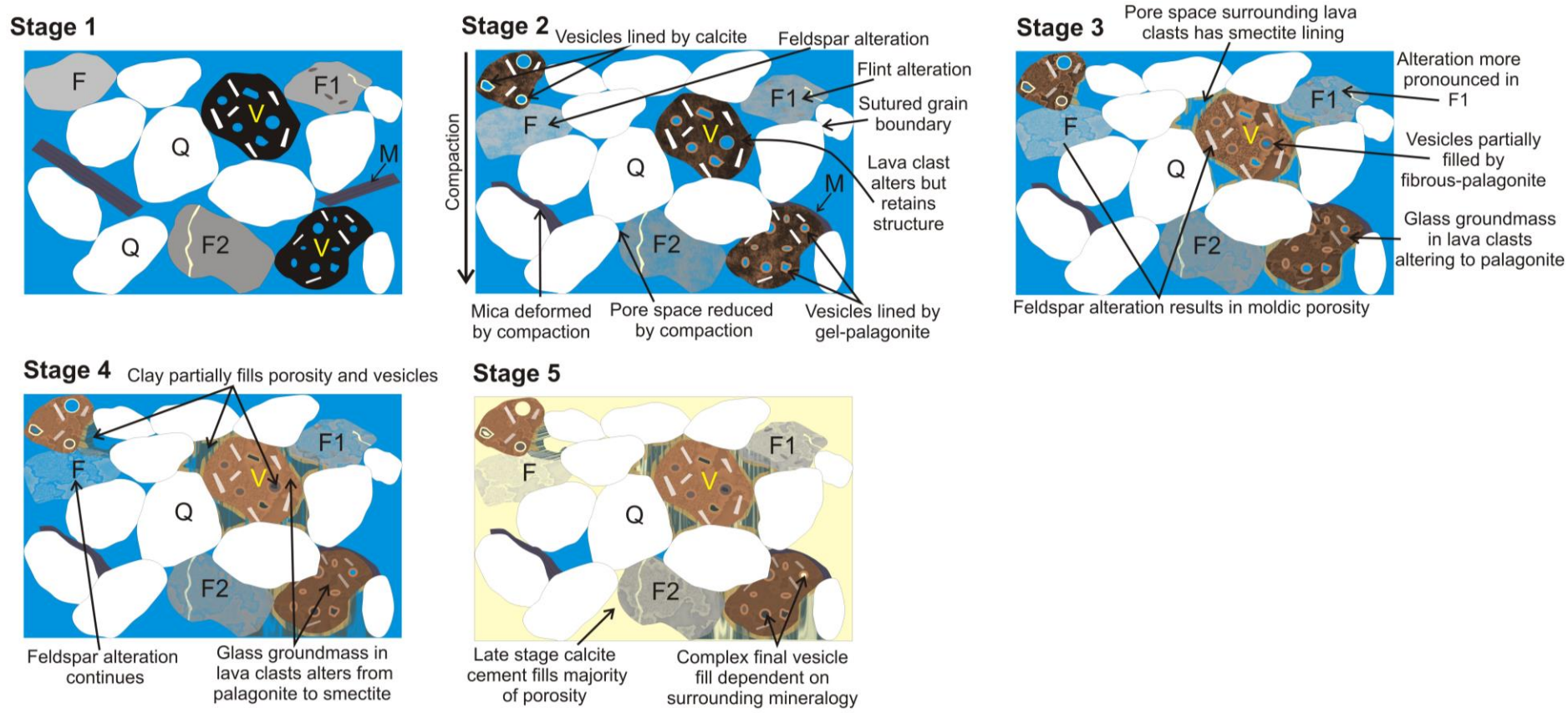

Figure 7.3: Simplified paragenetic sequence for Group 3 vlA rocks.

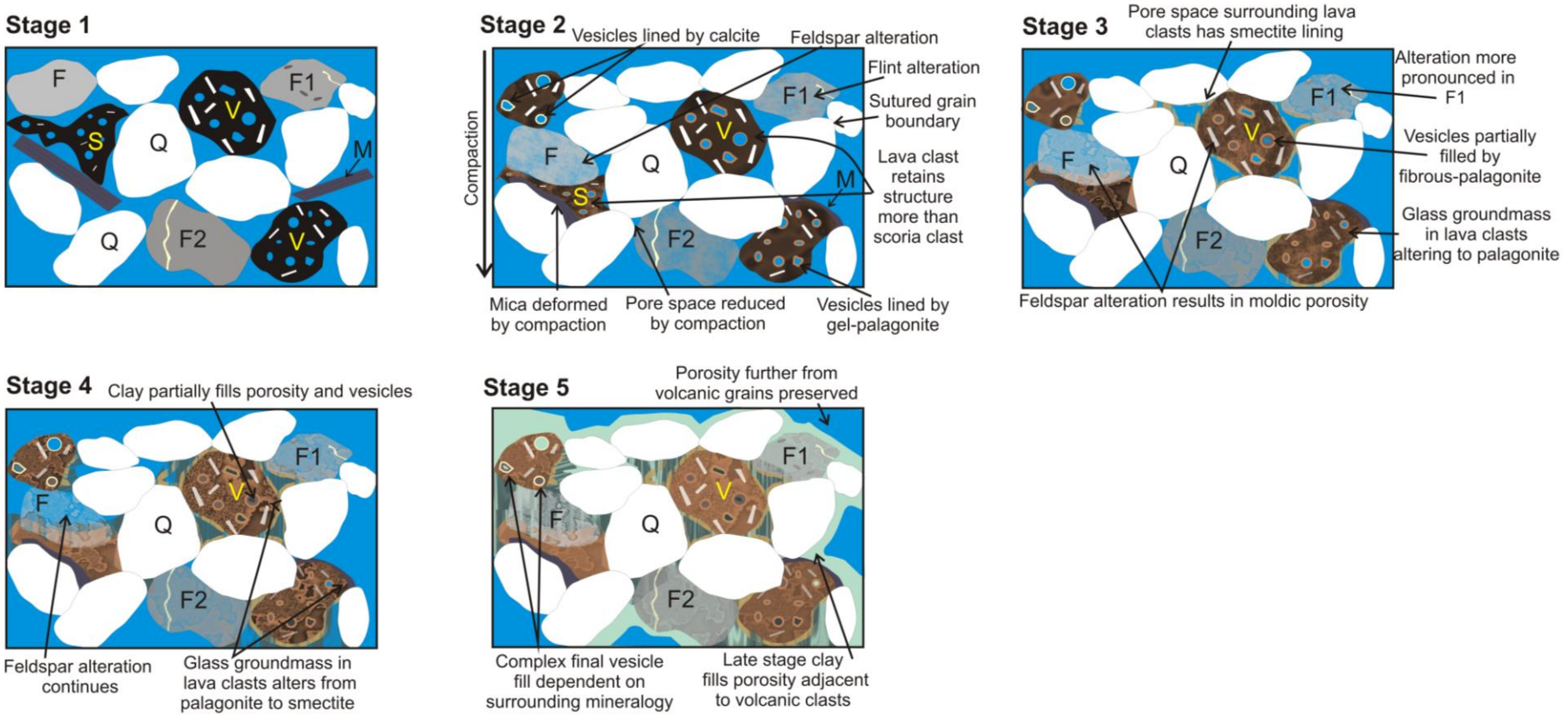

Figure 7.4: Simplified paragenetic sequence for Group 3 vlW rocks.

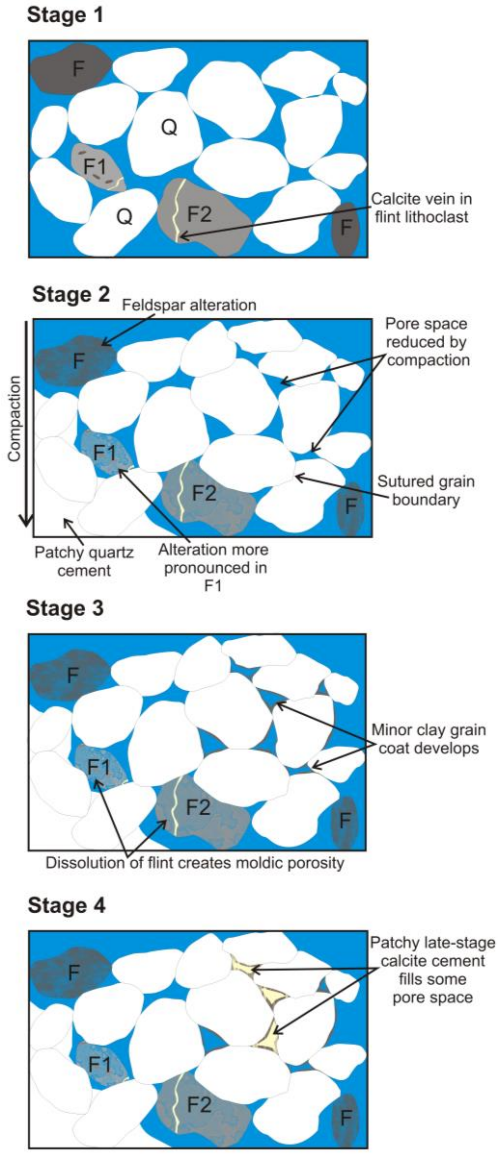

Figure 7.5: Simplified paragenetic sequence for Group 4 rocks.

7.3 Diagenetic paragenesis of the Rosebank rocks

7.3.1 Group 5 – Volcaniclastic rocks

Stage 1

The volcanic facies within the Rosebank field exhibit many similarities to those seen in onshore equivalents. This indicates that within this study, that the diagenetic paragenesis of the volcaniclastic facies was dependant more on localised mineralogy than by basin wide fluctuations in pore water chemistry (Figure 7.6, Stage 1).

Stage 2

The Group 5 samples resemble the Group 3 vlA samples, but with much greater quantities of basalt lava clasts and no flint. Alteration of the volcanic clasts varies considerably across the samples due to variations in clast composition, size and age (Figure 7.6, Stage 2).

Stage 3

Group 5 rocks behaved similarly under compaction to the onshore equivalents. The amount of compaction experienced was greater than in the Staffa examples, due to greater burial depths (Figure 7.6, Stage 3). Sutured contacts are common between grains and mica was deformed around framework grains. Albitisation and feldspar dissolution resulted in significant secondary porosity. Volcanic clasts altered to palagonite, locally reducing visible porosity and permeability by clogging pore throats.

Stage 4

Similar to the onshore equivalents extensive smectite grain coats formed from the alteration of palagonite (Figure 7.6, Stage 4). The K-metasomatism found in onshore rocks is also present within the Rosebank samples. This would indicate that metasomatism was related to the alteration of volcanic clasts rather than an external source of K being brought into the rock. Microcline crystals were rarely found within the samples; however, any early alteration of this feldspar would result in K being included in the pore waters and could explain the K-metasomatism. Similar textures are seen in Group 1 samples where alkali feldspar was not present and therefore, the exact nature of the K-metasomatism is not fully understood.

Zeolite is much more common in the Group 5 samples than in onshore equivalents. The Rosebank rocks are currently at depth of over 2000 m, which is deeper than the estimated maximum burial depth of the Staffa Formation (Williamson and Bell, 2012). If the Rosebank rocks were buried to greater depths than the Staffa rocks earlier in their paragenesis, then greater quantities of analcime could form before the onset of clay formation.

Stage 5

At greater depths, the smectite altered to corrensite (as explained in the Group 1 section above) resulting in only limited porosity remaining (Figure 7.6, Stage 5).

Stage 6

Late stage chlorite formed from the chloritisation of smectite and corrensite, and filled remaining visible porosity (Figure 7.6, Stage 6). Ca produced from the chloritisation of smectite resulted in the development of a patchy late stage calcite cement. Visible porosity is reduced to < 6%.

A key similarity between Group 5 rocks and their Staffa equivalents is the variability of the diagenetic assemblage produced. Although the processes that affect each group are similar, these models have been simplified and large variations exist in the diagenetic mineral assemblage within each sample, on a millimetre scale. Vesicles and pore spaces near to glassy groundmass are dominated by smectitic clay minerals, whereas vesicles located closer to feldspar rich areas are more likely to be filled by zeolite or calcite. Complex fluid pathways were established throughout the volcanic rich Group 5 samples as vesicles towards the centre of basalt clasts were filled with calcite, whereas ones on the periphery were clay filled. The outer edge of the clasts are likely to alter earlier in the paragenetic sequence. This leads to the production of clays filling vesicles towards the edge of clasts. Vesicles within the centre of the clasts are likely to retain their porosity for longer and therefore remain open as fluid pathways. Late stage calcite then fills vesicles in the centre of the clasts.

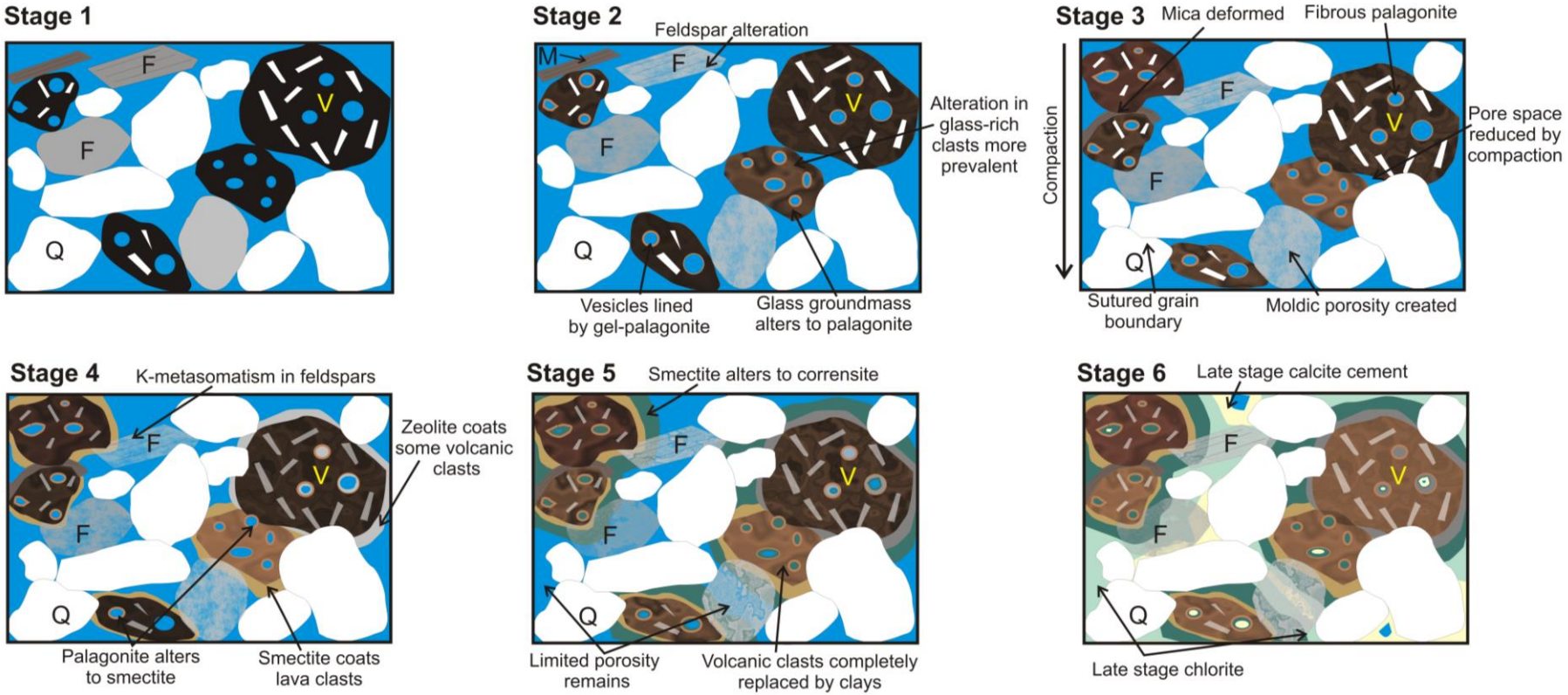

Figure 7.6: Simplified paragenetic sequence for Group 5 rocks.

7.3.2 Group 6 – Siliciclastic rocks

Stage 1

Group 6 samples are generally homogenous with a relatively simple mineralogy and therefore, have the simplest paragenesis. The samples have good visible porosity (up to 25%) with large oversized pores and floating grains (Figure 7.7, Stage 1).

Stage 2

An early calcite cement partially filled pores prior to significant compaction. Alteration and dissolution of feldspar grains resulted in limited moldic porosity being created (Figure 7.7, Stage 2).

Stage 3

At greater burial depths the calcite cement protected grains from compaction (Figure 7.7 Stage 3). Where the calcite was not present compaction resulted in sutured contacts at grain point contacts. Porosity was also reduced as mica and organic material were deformed around framework grains. The formation of minor smectite and illite grain coats in non-cemented areas locally reduced porosity however, the grain coats later helped to preserve porosity. Feldspars within cemented areas were less altered as the calcite provided protection from pore fluids.

Stage 4

At a later stage, changes in pore water chemistry resulted in the dissolution of this calcite, which allowed significant secondary porosity to develop (Figure 7.7, Stage 4) and therefore visible porosities as high as 36% are retained (Section 6.5). This alone however, cannot explain the apparent floating grains. It is postulated therefore, that the large package of lava flows above the sandstones protected the underlying reservoir from compaction, creating overpressure in the sandstone units. Overpressure has been recorded in other places within the Faeroe-Shetland Basin Alternatively, the timing of hydrocarbon entry into the system may have affected any clay coats that developed, as

hydrocarbons entering sandstone units can significantly reduce production of authigenic clays, and therefore protect porosity. Several of the sandstones within the Rosebank core are stained with oil although the exact timing of hydrocarbon entry, compared to mineral paragenesis is unknown.

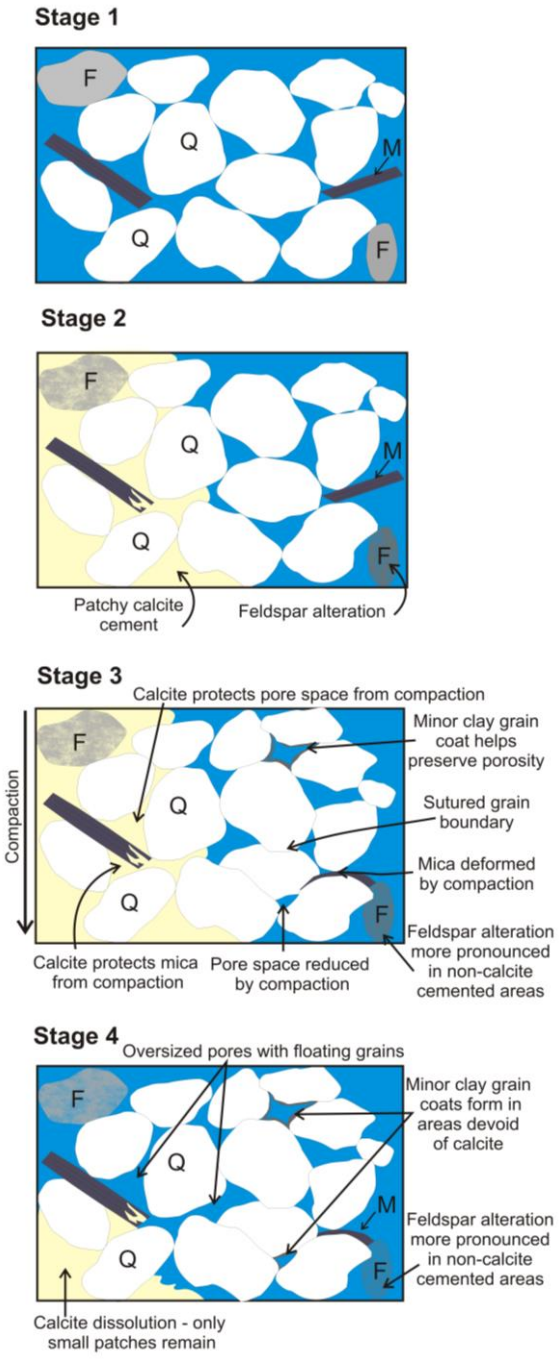

Figure 7.7: Simplified paragenetic sequence for the Group 6 samples.

7.4 Relating paragenetic mineralogy to temperature

The simplified paragenetic sequences for each of the sample groups are discussed in detail above. Using cross cutting relationships within the samples palagonite was found to be the earliest phase, whereas chlorite and calcite were the final phases to form. The formation of each phase can now be tentatively linked to the temperature range in which it formed (summarised in Figure 7.8).

The maximum reported temperature of palagonite formation is ~150 °C, with fibro-palagonite only found above ~90 °C (Gifkins et al., 2005). The rate of palagonitisation is dependent on temperature and time. Hekinian and Hoffert (1975) calculated that 3 µm of palagonite would develop in 1000 years, but at increased temperatures (100 °C) the rate of palagonitisation increases to 2.8 µm per year and doubles for every 12 °C increase in temperature (Jakobsson and Moore, 1986). However, within this study, the thickness of the palagonite varies extensively (up to 3 mm) from clast to clast, even within individual samples, indicating that the relationship between palagonite formation and temperature is not clearly defined. Several authors suggest that the time a clast is exposed to fluid is more influential than temperature (e.g. Staudigel et al., 1981; Jercinovic et al., 1990; Stroncik and Schmincke 2001). This study has found that palagonite coatings tend to be thicker in glassy scoria clasts, than in crystalline lava clasts, implying that palagonitisation starts earlier on the labile glass clasts.

Smectite typically forms below 150 °C, whereas saponite can reach higher temperatures of ~200 °C (Gifkins et al., 2005). The first appearance of corrensite occurs at temperatures as low as ~60 °C but it is more typically found from ~100 °C to 250 °C (Chang et al. 1986; Gaines et al., 1997). Corrensite alters to chlorite, and corrensite disappears at ~250 °C (Kristmannsdóttir, 1975, 1979; Evarts and Schiffman, 1983). Although no definitive link between chlorite platelet size and temperature of formation exists (Walker, 1993; de Caritat et al., 1993; Hillier, 1994; Shanvas Sathar pers.comm.), large platelets (thought to be of the most stable form of chlorite), form at sub-metamorphic temperatures, up to ~300 °C (Hayes, 1970, Weaver et al., 1984, Gifkins et al., 2005), and at a maximum of 3-4 km depth (Karpova, 1969). All chlorite in the samples is Fe-rich potentially indicating its "hot" formation, as Fe rich chlorites typically form at the highest temperatures (above 150° C) (de Caritart et al., 1993).

Calcite forms at a wide range of temperatures, up to and exceeding 300 °C (Gifkins et al., 2005), and therefore, it is not surprising that several phases of calcite are found throughout the samples. Analcime typically forms at temperatures between ~50 - 120 °C (Gifkins et al., 2005); however, analcime has been formed in the lab at temperatures as high as 250 °C (Höller and Wirsching, 1978). Jørgensen (2006) suggests that analcime forms in a wide range of temperatures from 65 °C to as high as 300 °C and claimed that different volcanic glass compositions caused the temperature of formation of zeolites to increase by up to 100 °C. This highlights the inherent difficulties with using zeolites as paleo-indicator minerals. Albitisation can begin at temperatures as low as 25 °C if sea water is present, but more commonly starts at ~100 °C (Gifkins et al., 2005; Ramseyer et al., 2006). Alkali feldspar alteration typically forms below 100 °C (Gifkins et al., 2005); however, K-metasomatism can occur at much higher temperatures (>200 °C). The temperature dependence of this process is poorly understood, meaning that the presence of K-metasomatism cannot be used as an accurate geothermometer.

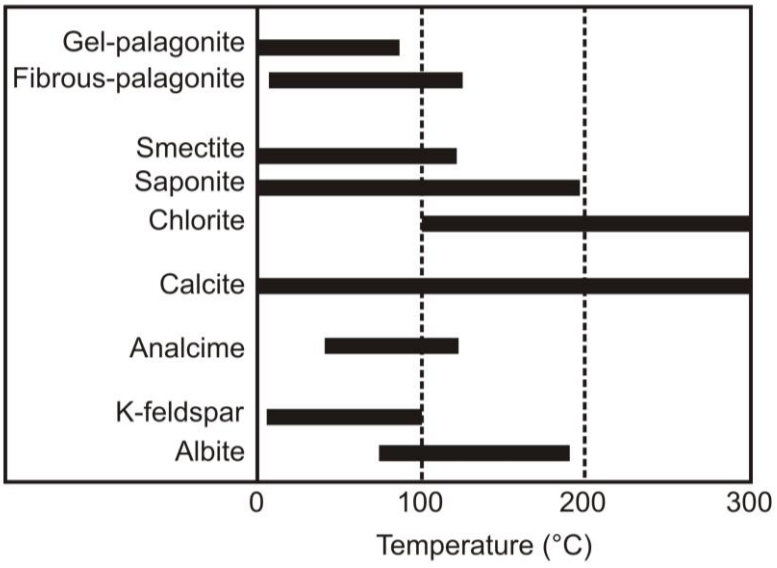

Figure 7.8: Estimated temperature range of diagenetic mineral growth for the key minerals found within this study (edited from Gifkins et al., 2005 and references therein).

7.5 Regional diagenetic paragenesis in the Staffa Formation rocks

It is estimated that approximately 1.6 km of rock has been eroded from the Staffa section (Holford et al, 2010). Even with an elevated geothermal gradient due to the Ross of Mull Granite, burial temperatures would be unlikely to reach the high temperatures responsible for the large chlorite platelets to develop. This chlorite may be linked to late stage hydrothermal fluid circulating through the limited remaining pore network. Isotopic data in this study support this conclusion, and Williamson and Bell (2012) also attribute calcite and zeolite formation to hydrothermal waters.

Walker (1971), note the presence of several late stage zeolites filling vesicles and fractures in the Staffa Formation lavas in this study. Figure 7.9 (Walker, 1971) shows the proposed zeolite zones for the Mull Central Complex. The samples from this study are all on the outermost fringes of the aureole, within the mesolite zone and locally, the laumontite zone. Walker (1971) proposes depths for the Mull lavas of greater than 1500 m; however, only analcime was discovered within this study. Laumontite is a Ca-rich zeolite commonly formed at high temperatures of 110°C–140°C, whereas mesolite is a Na-rich zeolite found in geothermal areas and typically forms between 70 °C- 90°C (Kristmannsdóttir and Tómasson, 1978). Fission track results agree with Walker's interpretation and estimate palaeo-temperatures (for the areas within this study) of a maximum of 150 °C within the Central Complex (Holford et al, 2010).

The presence of analcime within the samples rather than mesolite or laumontite indicates similar temperatures of formation, but implies pore waters that were enriched in Na relative to Ca. The isotopic data also indicate some influence from geothermal waters, suggesting that the Staffa samples may have been affected by heat from the Mull Central Complex.

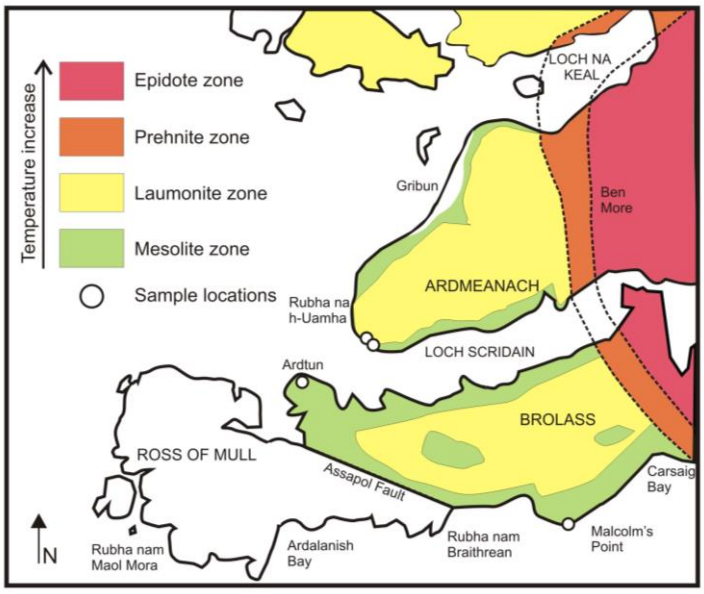

Figure 7.9: Zeolite zone map, showing the sample locations from this study within the mesolite and laumontite zones (redrawn and edited from Walker, 1971).

7.6 Regional diagenetic paragenesis in the Rosebank rocks

Heat flow and burial histories have been estimated in the Faeroe-Shetland Basin, with an average present day geothermal gradient of 34.6 °C/km estimated using temperature data from wells in the south of the basin (Gatliff et al., 1996). As the Rosebank rocks are currently at ~2500 m depth this would imply maximum temperatures of around 90 °C. However, the wells used within the Gatliff study have not extensively been affected by Palaeogene volcanism, and wells that underlie the flood basalts were not included in the study. This suggests that the geothermal gradient within the Rosebank rocks may be higher. Fluid inclusions found within Upper Vaila Sandstone samples (the Vaila Formation underlies the Flett Formation) have temperatures as high as 200 °C, which Parenell et al. (1999) linked to volcanism during the Eocene. Fluid inclusion studies in the Rosebank discovery well estimate temperatures of up to 127 °C at depths of ~3510 m approximately 1000 m below the Rosebank reservoir rocks hinting the geothermal gradient might be ~36°C/km. Zeolites have been used to estimate the paleo-geothermal gradient on the Faroe Islands, with Jørgensen (2006) estimating an average geothermal gradient of 60°C/km, which was regionally constant across the Faeroe-Shetland basin. This is much higher than the present day geothermal gradient.

Using a combination of rifting / volcanic subsidence history and maturation, the burial history of the southern Faeroe-Shetland Basin was estimated (Carr and Scotchman, 2003). The Flett Formation was rapidly buried to ~ 1 km within the early Palaeogene. Subsidence stopped and minor uplift occurred due to volcanism associated with the Icelandic plume (Clift, 1999). This was followed by a second phase of subsidence after the volcanism ceased (Jones et al., 2001). A compressional event in the Oligo-Miocene (Doré and Lundin, 1996) led to uplift and erosion. In the 205/22-1 well to the south of Rosebank, late stage uplift occurred in the Neogene, followed by subsidence. Together, this led to a final depth for the Flett Formation of ~2500 m.

This burial history is for the area to the south and south west of the Rosebank Field and must only be used as an estimate; however, the complex history could in part explain the paragenesis seen within the Rosebank rocks. The rapid subsidence could result in samples experiencing elevated temperatures earlier in the diagenetic history. This could explain the greater quantities of zeolite found in the Rosebank rocks, as higher temperatures would promote zeolite formation.

The uplift phases could correspond to differences in pore waters, potentially leading to the multiple phases of calcite precipitation and dissolution. Isotopic data indicate the presence of hot geothermal waters. Samples located close to lava contacts did not have markedly different isotopic signatures indicating that meteoric water temperatures at the surface were not elevated by lavas. Instead, meteoric waters more likely mixed with relatively large hydrothermal cells that developed around large scale intrusions (Gifkins et al., 2005).

7.7 Model for predicting diagenetic evolution of volcaniclastic rocks

Figure 7.10 provides a simplified flow chart showing the typical diagenetic phases identified within this study and their net effect on the reservoir quality of the rock. Timing of the diagenetic phases is extremely important. Many of the early stage events such as the development of smectite or chlorite grain coats and the precipitation and subsequent dissolution of calcite cements, protects pores from compaction. The dissolution of mineral phases such as volcanic glass, feldspar and pyroxene leads to production of secondary, often intragranular and moldic, porosity. In the majority of currently producing volcaniclastic reservoirs worldwide, these processes have preserved

reservoir quality (Zou et al., 2013). The main difference between this study and previous examples is that clay formation has not stopped at the grain coating phase and has continued to fill much of the porosity. This may be due to rapid burial promoting clay development or simply reflect the abundance of volcanic clasts that react with pore waters.

The main conclusion from this study is that the diagenetic mineral paragenesis is highly dependent on localised mineralogy and can vary considerably throughout individual samples. This ultimately makes predicting reservoir quality significantly more challenging than in a typical sandstone reservoir that may be affected by basin wide changes in pore water. The rapid burial, combined with a highly reactive mineralogy and potentially increased temperatures due to geothermal effects, results in the destruction of the pore network at relatively shallow depths, early in the diagenetic history. As a result, fluid pathways through the rocks become limited and the rock behaves as a closed system. Lava flows above and below the reservoir rocks, as well as intrusions, compartmentalise the reservoir, further reducing fluid pathways. This results in a feedback mechanism, as small amounts of pore waters become trapped within the pores. These waters cannot exchange with an outside source and become enriched in elements such as Na, which in turn accelerates alteration, causing more authigenic minerals to be formed and further reducing the fluid pathways available. This feedback also causes more pronounced isotopic fractionation.

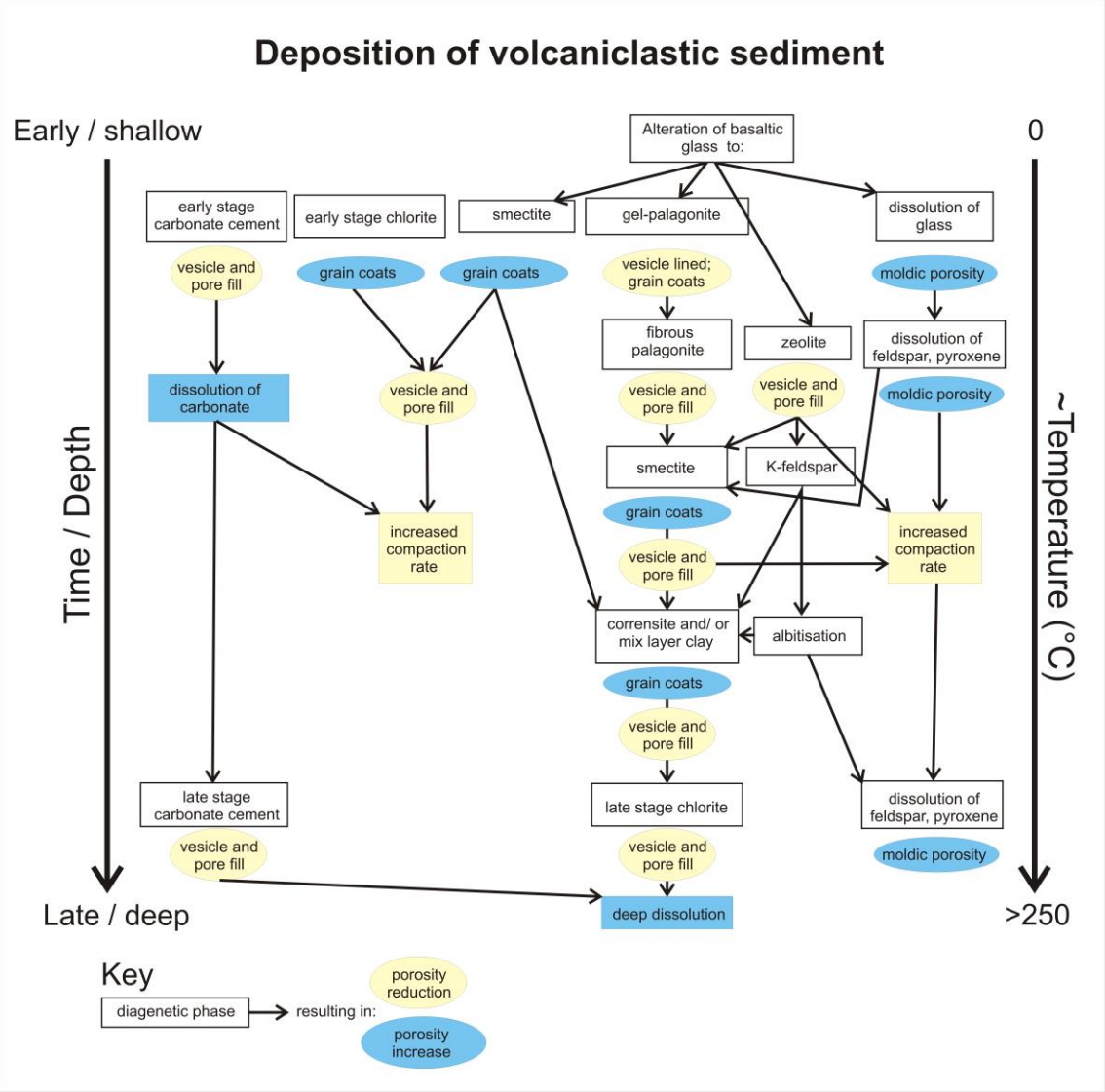

Figure 7.10: Diagenetic flow chart highlighting the simplified diagenetic reactions that occur when a basaltic volcaniclastic sediment is buried in a non-marine environment. Boxes represent the diagenetic phase. Ovals represent the consequence to porosity. Blue is a net porosity increase. Yellow is a net porosity decrease.

Figure 7.11 uses data gathered within this study to provide a porosity/permeability "risk" chart, in order to de-risk future exploration in basaltic volcaniclastic rocks. Red on the colour chart indicates rocks that are likely to have poor reservoir qualities (< 5 % porosity and < 5 mD permeability), whereas green indicates rocks that are likely to have good reservoir qualities (>20% porosity and > 100 mD permeability). .

This study found that vent proximal rocks (within 250 m of the vent) were likely to have a significantly greater reduction in porosity and permeability during diagenesis than rocks located at more distal locations (>1 km). A threshold of 10% volcanic clasts was identified using point counting data, whereby those above the threshold are likely to have lower resultant macro porosity and permeability. The volcanic clast type was found to influence diagenetic paragenesis, with pyroclasts and ash having a greater (and earlier) effect on the pore network than crystalline lava clasts. The overall heterogeneity of the samples was also found to be an important factor (e.g. Group 2 rocks have the most complex paragenesis due to their highly variable original mineralogy). As with all rock types, grain size and sorting also influence the subsequent reservoir quality of rock during burial.

A combination of all the above factors, together with changes in pore water chemistry and temperature, ultimately control the final reservoir quality of the rock. Therefore, the risk chart can only be used a guide in predicting the likely of reservoir quality. For example, a rock found at a vent distal location with abundant lava clasts should have higher reservoir quality than a rock from a vent distal location that comprises abundant pyroclasts.

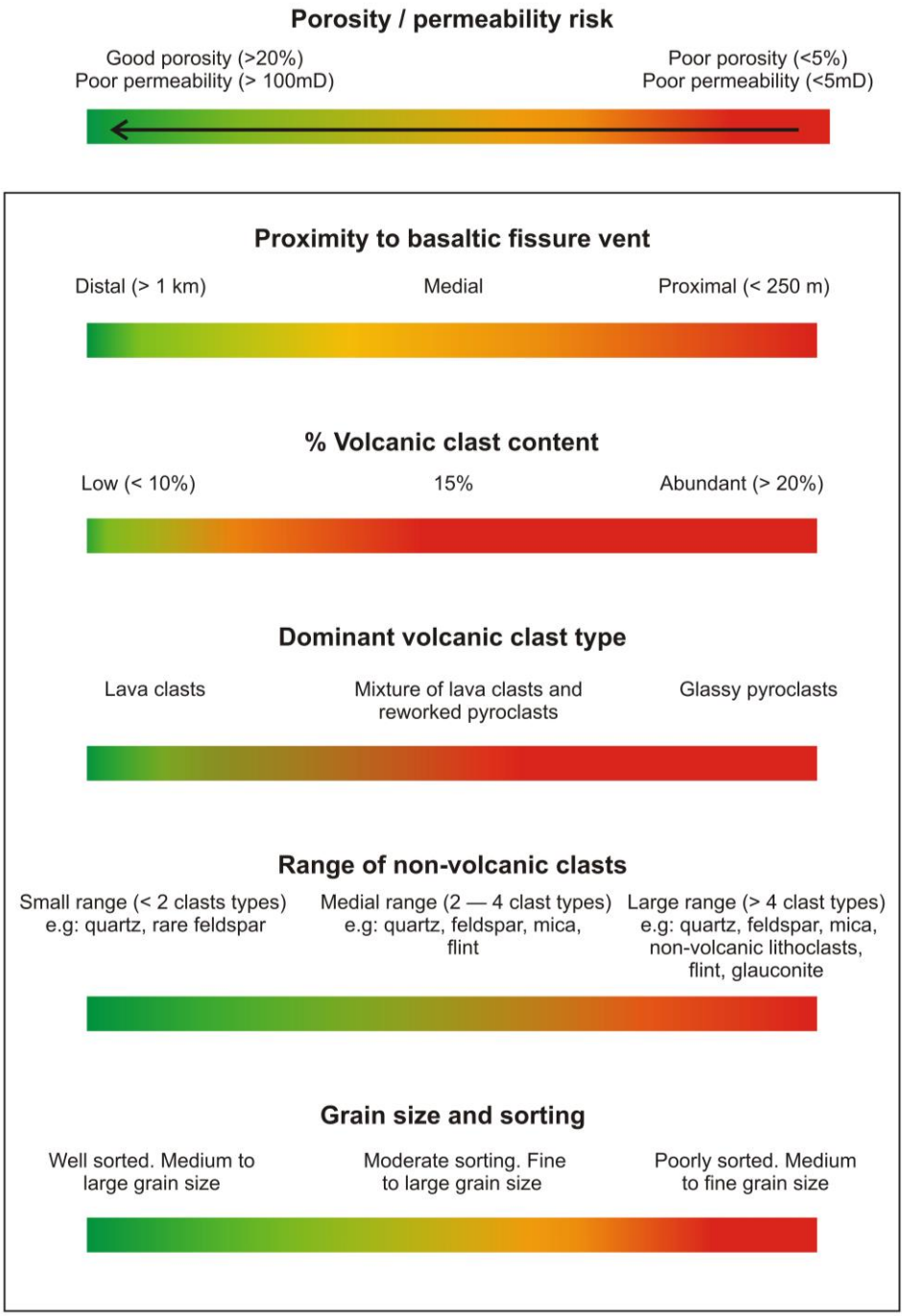

Figure 7.11: Porosity / permeability risk chart. The colour scales ranges from red (poor reservoir quality) to green (good reservoir quality).

8 Conclusions

This thesis provides an insight into the complex diagenetic paragenesis of volcaniclastic rocks and their relationship with visible porosity. Volcaniclastic rocks are characterised and their reservoir potential quantitatively assessed, and compared with siliciclastic sandstone reservoir rocks. This is achieved by describing and classifying the volcaniclastic rocks found offshore in core from the Rosebank Field and onshore from the Staffa Formation, Mull. The nature of contacts between the igneous and sedimentary rocks was also described and classified, and diagenetic and alteration effects considered. Outputs of the study include: 1) a flow chart conceptual model that predicts how volcanic clasts react during burial; and 2) a risk chart that forecasts the reservoir quality of volcaniclastic samples. Together, these outputs will aid the assessment of potential plays in the Faroe-Shetland Basin and other volcanic rifted margins.

In the introduction to the thesis a number of questions regarding diagenesis and potential reservoir quality of volcaniclastic rocks were posed. These questions are addressed below.

8.1 How do basaltic clasts react during burial?

Basaltic clasts are highly reactive during burial. The alteration process begins at the surface, where basaltic glass alters to a wide range of diagenetic minerals such as gel- and fibro- palagonite, smectite and zeolites. The alteration products produced depend on pore water chemistry, temperature and the time the clasts are in contact with the pore fluid. Crystalline clasts similarly alter but are less reactive than there glassy counterparts. Alteration therefore, was more prevalent in basaltic glass than in basaltic lava clasts.

8.2 What physical and chemical changes do basaltic clasts in clastic rocks undergo during diagenesis?

Basaltic glasses were diagenetically flattened resulting in greater levels of compaction and an associated reduction in porosity. The basaltic glass found in this study alters

firstly to gel-palagonite, early after burial. With increasing pressure and temperature the gel-palagonite alters to fibro-palagonite and then to smectite, which forms grain coats and locally reduces porosity. The smectite underwent chloritisation, resulting in the production of corrensite and late stage chlorite pore fill, which significantly reduced porosity and reservoir quality. The formation of zeolites (analcime) from volcanic glass also locally reduced porosity in some samples.

8.3 What factors control diagenetic history (e.g. particle size, clast type, abundance)?

Clast type is an important control on diagenetic history. Vesiculated pyroclasts and glass fragments underwent higher amounts of diagenetic flattening than crystalline lava clasts. Compaction was greatest in the samples that contained pyroclasts, with localised porosity severely reduced. Crystalline lava clasts retained their structure better, preserving the surrounding porosity. Glass-rich clasts were the most severely altered due to the reactive nature of the glass, which in turn altered to pore-filling clays.

The greater the abundance of volcanic clasts within a sample, the lower the porosity. Particle size can also influence diagenesis. For example, small ash sized basaltic particles were typically the most altered.

8.4 What effect does volcanic material have on reservoir quality (e.g. porosity and permeability)?

Dissolution of glass and feldspar leads to the formation of moldic secondary porosity; though this is not commonly interconnected. While early grain coating smectite can help to preserve net porosity, localised pore space is reduced and pore throats are impeded. In this study the smectite grain coats acted as a precursor to corrensite and chlorite, which filled pores, reducing porosity. Zeolite and calcite cements produced as a by-product of volcanic glass and clay alteration also reduced the net porosity of the samples.

8.5 Does the distance from volcanic source have an impact on subsequent reservoir quality?

Within the Staffa Formation sample set, distance from the volcanic source affected diagenetic paragenesis. Vent proximal samples had a higher percentage of glass-rich pyroclasts and therefore, lower visible porosity. Rocks at vent medial and distal locations (>250 m from the postulated vent) show a reduction in porosity; however, volcanic clast type and abundance have more influence on resulting porosity in these locations.

8.6 How much volcaniclastic material do you need before reservoir quality is degraded?

In this study, all samples that contained more than 10% volcanic clasts, regardless of clast type, had less than 10% resultant porosity. Pittman and Larese, (1991) state the economic minimum visible porosity is 12%. However, this study has also highlighted the heterogeneity of volcaniclastic samples and the complex result this has on the paragentic sequence. Therefore, although the 10% threshold can be applied to the rocks in this study, caution must be applied when applying the threshold elsewhere. Although abundance of volcanic clasts is important, other factors such as clast type, timing, pore water composition and location within the volcanic terrain must all be considered when evaluating the reservoir quality of volcaniclastic rocks.

8.7 What are the diagenetic effects of lavas at sediment/lava interfaces?

A range of igneous-sediment contacts were identified in the Rosebank and Staffa Formation rocks, and demonstrate complex interaction between the igneous and sedimentary components and considerable variation over small distances (cm scale). The contact types identified were; 1) Straight; 2) loaded; 3) Irregular; 4) Fluidal; 5) peperitic and 6) passive. The type of contact produced depends on a number of factors including: 1) the nature of the igneous body; 2) the rate and angle at which the igneous body intrudes/invades; 3) the composition, porosity, permeability and rigidity of the

sediment; and 4) water content. Previous studies (e.g. Girard et al., 1989; Merino et al., 1997; Doyle, 2001; Mckinley, 2001; Iima and De Ros, 2002; Bernet and Gaupp 2005; Jerram, and Stollhofen, 2002; Grove, 2013) have found contact diagenetic and metamorphic effects surrounding intrusions and at the base of lava flows; however, no obvious contact effects (e.g. induration, magmatically derived calcite, or thermal effects, such as melting of feldspars), other than the formation of thin chilled margins and localised fluidisation of the sediment, was identified in this study. In many examples in the Staffa Formation a small organic-rich siltstone layer underlies the lava, which may provide enough thermal insulation to protect the underlying sediment. In other cases poor initial porosity would force any magmatically derived fluids along the base and up into the igneous body rather than percolating down into the sediment. As a result, contact effects may be focussed towards the sill tip or lava lobe toe. Isotopic results from samples close to an igneous contact were not markedly different to those several meters from the contact, indicating that the lavas did not significantly alter the pore waters in which the authentic clay mineral phases formed.

8.8 What is the paragenetic sequence of the Rosebank Field and Staffa Formation, and can this be linked to basin wide evolution?

The paragenetic sequence within the volcaniclastic rocks both on and offshore varies considerably on a centimetre scale due to heterogeneity in mineralogy and as a result only tentative links can be made to basin wide pore waters. A simplified model of paragenesis was presented within Chapter 7.

8.8.1 Staffa Formation- vent proximal rocks (Group 1)

The paragenetic sequence observed in the vent proximal rocks is controlled by the alteration of glassy pyroclasts. The lack of more chemically inert phases such as quartz, results in greater levels of alteration, earlier (and therefore shallower) in the diagenetic history. This in turn leads to earlier porosity reduction. Basaltic volcanic glass alters to palagonite and then to smectite, that coats grains. This smectite then undergoes chloritisation that leads to the development of pore filling corrensite and chlorite. Hydrothermal waters associated with emplacement of the Mull Central Complex are

likely to be responsible for elevated pore water temperatures and therefore, the extensive authigenic clay development.

8.8.2 Staffa Formation – volcanic clast-rich rocks (Group 2)

The paragenetic sequence in these rocks is much more complex due to their heterogeneity. The rocks comprise a mixture of pyroclasts, crystalline lava, quartz, flint, and mica. During burial each mineral reacts differently, resulting in a complex paragenesis. As the pore network is impeded by the development of smectite grain coats and pore-filling zeolite, corrensite and chlorite (due to the alteration of volcanic clasts), the water-rock ratio is low. As a result the rock acts as a closed system, with pore waters becoming more enriched in certain ions as alteration proceeds. This in turn accelerates the dissolution of remaining glass and the alteration of clays.

8.8.3 Staffa Formation – volcanic clast-poor rocks (Group 3)

Paragenesis in these rocks is highly dependent on the type of volcanic clast present. Alteration is more pronounced in rocks that contain glassy pyroclasts than crystalline lava clasts. The paragenetic sequence is very similar to the Group 2 samples; however, clay formation and therefore, porosity reduction, is focused in pores surrounding volcanic clasts. Consequently, porosity is only limited in areas surrounding volcanic clasts and overall net porosity may be retained. In Group 3 from Ardtun, porosity is eliminated by a late stage calcite cement.

8.8.4 Staffa Formation – siliciclastic samples (Group 4)

Group 4 samples have a much simpler paragenetic sequence as they are dominated by relatively inert minerals such as quartz. Sutured grain contacts show some compaction has occurred, reducing porosity. Minor clay coats are locally present; however, porosity is not extensively affected. A patchy silica cement locally occludes porosity.

8.8.5 Rosebank – volcaniclastic rocks (Group 5)

Volcanic clasts within these samples are extensively altered to gel- and fibro-palagonite. This palagonite altered to smectite, which formed extensive grain coats that reduced porosity and clogged pore throats. Alteration of the volcanic glass also formed analcime, which further reduced porosity. Chloritisation of smectite led to the growth of mix layer smectite / chlorite and corrensite that filled much of the remaining pore space. Albitisation of plagioclase released Ca into pore waters resulting in the development of a localised calcite cement. Isotopic data demonstrate that magmatic water from intrusions is likely to have mixed with meteoric waters and led to elevated temperatures at shallower depths, promoting and accelerating clay growth. Seawater may also have mixed with meteoric and hydrothermal waters, elevating deuterium values in some samples.

8.8.6 Rosebank – siliciclastic rocks (Group 6)

These samples have good porosity and, in places, have large oversized pores or floating grains. Evidence of compaction includes minor sutured quartz grain contacts and the deformation of mica and mud lithoclasts around framework grains. The remnants of an early patchy calcite cement, which helped protect the rocks from compaction, is found within some samples. Much of this calcite was dissolved creating the large oversized pores and floating grains. Minor late stage illite and kaolinite clays coat the grains and help to prevent nucleation of late stage quartz cements.

Compartmentalisation of these reservoir rocks due to the lava flows and potential intrusions could impede the circulation of large-scale basin-wide pore fluids, protecting the rocks from late stage silica precipitation.

8.9 Is the Staffa Formation a viable onshore analogue?

Although differences between the Staffa Formation and the Rosebank Field exist (e.g. detrital mineralogy, scale and age), the paragenetic sequence found in both sample sets is remarkably similar. In both settings, volcanic clasts behaved in a similar way during

burial, with the extensive production of palagonite and subsequent alteration to smectite, corrensite and chlorite. Alteration textures such as Ti-banding formed during glass alteration, moldic porosity created from the dissolution of feldspars, albitisation, K-metasomatism, and the concentration of metal oxides into anastomosing, axiolitic texture, all occurred in both sample sets. Therefore, the Staffa Formation provides a viable analogue for the Rosebank Field.

8.10 Further work

This thesis highlights the complex diagenetic paragenesis that volcaniclastic samples undergo during burial. However, the following studies could be undertaken in order to better understand the influence of volcanic material within sedimentary basins.

Further work could be undertaken to correlate the lithofacies seen within the Rosebank cores across the full Rosebank field area. A new ocean bottom detection seismic data set has been recently acquired that will provide further precision in the mapping of lithofacies (e.g. identifying fluvial channel directions). FMI data could also be better linked to wireline and core data, using the method outlined in Watton (2013), in order to better interpret the relationship between the volcanic and siliciclastic rocks. Other wells that drilled volcanic sequences within the Faeroe-Shetland Basin could also be examined and there reservoir qualities examined.

Microprobe analysis may help to improve the chemical data set, providing a better understanding of elemental movement. Clay separation and fluid inclusion work could help to better constrain temperature and pore water chemistry, and if compositional data were known for individual clay phases then more accurate fractionation factors could be developed to improve further isotopic analysis. Isotopic analysis of calcite phases may also help to define pore water evolution.

Mercury injection methods (e.g. Pittman, 1992; Tang et al., 2008) may provide more accurate data on the permeability of the onshore samples; however, it is anticipated that all volcaniclastic and pyroclastic samples would have poor permeability (<5 millidarcies) similar to their offshore equivalents.

References

A

Argyll, Duke of. (1851). On Tertiary Leaf-Beds in the Isle of Mull. With a note on the vegetable remains from Ardtun by E. Forbes. Quarterly Journal of the Geological Society, 7, 89-103.

B

Bailey, E. B. and Anderson, E. M. (1925). The Geology of Staffa, Iona and western Mull. Memoir of the Geological Survey of Great Britain, HMSO, Edinburgh.

Bailey, E. B., Clough, C. T., Wright, W. B., Richey, J. E. and Wilson, G. V. (1924). Tertiary and Post-Tertiary Geology of Mull, Loch Aline and Oban. Memoir of the Geological Survey of Great Britain, HMSO, Edinburgh.

Bailey, N. J. L., Burwood, R., and Harriman, G. E. (1990). Application of pyrolysate carbon isotope and biomarker technology to organofacies definition and oil correlation problems in North Sea basins. Organic Geochemistry, 16(4), 1157-1172.

Bailey, N. J. L., Walko, P., and Sauer, M. J. (1987). Geochemistry and source rock potential of the west of Shetlands. Petroleum Geology of North West Europe. Graham and Trotman, London, 711-721.

Banfield, J. F., Jones, B. F., and Veblen, D. R. (1991). An AEM-TEM study of weathering and diagenesis, Abert Lake, Oregon: I. Weathering reactions in the volcanics. Geochimica et Cosmochimica Acta, 55(10), 2781-2793.

Beaufort, D., Baronnet, A., Lanson, B., and Meunier, A. (1997). Corrensite: A single phase or a mixed-layer phyllosilicate in the saponite-to-chlorite conversion series? A case study of Sancerre-Couy deep drill hole (France). American Mineralogist, 82(1), 109-124.

Beckinsale, R. D., Pankhurst, R. J., Skelhorn, R. R. and Walsh, J. N. (1978). Geochemistry and Petrogenesis of the Early Tertiary Lava Pile of the Isle of Mull, Scotland. Contributions to Mineralogy and Petrology 66, 415-27.

Bell, B. (2008). Lithostratigraphy well reports for wells 205/1-1, 213/26-1, 213/26-1z and 213/27-1. In-house report Chevron Upstream Europe.

Bell, B. R., and Williamson, I. T. (2002). Tertiary igneous activity. The Geology of Scotland, 371-407.

Berger, A., Gier, S., and Krois, P. (2009). Porosity-preserving chlorite cements in shallow-marine volcaniclastic sandstones: Evidence from Cretaceous sandstones of the Sawan gas field, Pakistan. AAPG bulletin, 93(5), 595-615.

Berner, E. K., and Berner, R. A. (2012). Global environment: water, air, and geochemical cycles. Princeton University Press.

Bernet, M., and Gaupp, R. (2005). Diagenetic history of Triassic sandstone from the Beacon Supergroup in central Victoria Land, Antarctica. New Zealand Journal of Geology and Geophysics, 48(3), 447-458.

Bhattacharya, A. (1997). On the origin of non-tidal flaser bedding in point bar deposits of the river Ajay, Bihar and West Bengal, NE India. Sedimentology,44(6), 973-975.

Biron. A., Sotak, J., and Bebej, J. U. R. A. J. (1999). Diagenetic trioctahedral phyllosilicates from sediments of the Sambron Zone (eastern Slovakia): XRD, SEM and EMPA study. Geologica carpathica-Bratislava-, 50, 257-272.

Bjorlykke, K. (1984). Formation of secondary porosity: how important is it. Clastic diagenesis: AAPG Memoir, 37, 277-286.

Bjørlykke, K., and Gran, K. (1994). Salinity variations in North Sea formation waters: implications for large-scale fluid movements. Marine and petroleum geology, 11(1), 5-9.

Blatt, H. (1979). Diagenetic processes in sandstones. The Society of Economic Paleontologists and Mineralogists (SEPM), SPEM Special Publication, 26 (141-157) (March).

Bloch, S., Lander, R. H., and Bonnell, L. (2002). Anomalously high porosity and permeability in deeply buried sandstone reservoirs: Origin and predictability. AAPG bulletin, 86(2), 301-328.

Bohor, B. F., and Triplehorn, D. M. (1993). Tonsteins: altered volcanic ash layers in coal-bearing sequences (Vol. 285). Geological Society of America.

Boldreel, L. O., and Andersen, M. S. (1994). Tertiary development of the Faeroe-Rockall Plateau based on reflection seismic data. Bulletin of the Geological Society of Denmark, 41(2), 162-180.

Boles, J. R., and Coombs, D. S. (1977). Zeolite facies alteration of sandstones in the Southland Syncline, New Zealand. American journal of science, 277(8), 982-1012.

Bonatti, E. (1965). Palagonite, hyaloclastites and alteration of volcanic glass in the ocean. Bulletin Volcanologique, 28(1), 257-269.

Boulter, M. C. and Kvacek, Z. (1989). The Palaeocene flora of the Isle of Mull. Special Papers in Palaeontology 42, The Palaeontological Association. 149 pages.

Branney, M. J., and Sparks, R. S. J. (1990). Fiamme formed by diagenesis and burial-compaction in soils and subaqeuous sediments. Journal of the Geological Society, 147(6), 919-922.

Brayshaw, A. and Hogg, A. (1992). Lithofacies. Internal BP report.

Brey, G., and Schmincke, H. U. (1980). Origin and diagenesis of the Roque Nublo breccia, Gran Canaria (Canary Islands)—Petrology of roque nublo volcanics, II. Bulletin Volcanologique, 43(1), 15-33.

Brigatti, M. F., and Poppi, L. (1984). Crystal chemistry of corrensite: A review. Clays clay miner. Clays Clay Miner., 32(5), 391.

Brimhall, G. H., and Dietrich, W. E. (1987). Constitutive mass balance relations between chemical composition, volume, density, porosity, and strain in metasomatic

hydrochemical systems: results on weathering and pedogenesis. Geochimica et Cosmochimica Acta, 51(3), 567-587.

Brooks, J. R. V., Stoker, S. J., and Cameron, T. D. J. (2001). Hydrocarbon exploration opportunities in the twenty-first century in the United Kingdom.

Brown, R. (2012) The Interplay of volcanism, tectonism and sedimentation in the Columbia River Basalt Province, WA, USA. VMRC Fieldtrip Guidebook.

Brown, D. J., and Bell, B. R. (2007). Debris flow deposits within the Palaeogene lava fields of NW Scotland: evidence for mass wasting of the volcanic landscape during emplacement of the Ardnamurchan Central Complex. Bulletin of Volcanology, 69(8), 847-868.

Brown, D. J., Holohan, E. P., and Bell, B. R. (2009). Sedimentary and volcano-tectonic processes in the British Paleocene Igneous Province: a review. Geological Magazine, 146(3), 326.

Bryant, S., and Blunt, M. (1992). Prediction of relative permeability in simple porous media. Physical Review A, 46(4), 2004.

Burley, S, D, and Worden R,H. (2003), Sandstone Diagenesis: Recent and Ancient: Blackwell Publishing

Busby-Spera, C. J., and White, J. D. (1987). Variation in peperite textures associated with differing host-sediment properties. Bulletin of Volcanology,49(6), 765-776.

Büyükutku, A. G. (2006). Diagenesis of Upper Eocene volcaniclastic rocks and its relevance to hydrocarbon exploration in the Thrace Basin, Turkey. Energy Sources, Part A, 28(11), 1039-1049.

C

Calanchi, N., Gasparotto, G., and Romagnoli, C. (1994). Glass chemistry in volcaniclastic sediments of ODP Leg 107, Site 650, sedimentary sequence: provenance and chronological implications. Journal of volcanology and geothermal research, 60(1), 59-85.

Carr, A. D., and Scotchman, I. C. (2003). Thermal history modelling in the southern Faroe Shetland Basin. Petroleum Geoscience, 9(4), 333-345.

Carroll, D. (1970). Clay minerals: a guide to their X-ray identification (Vol. 126). Geological Society of America.

Cas, R. A., and Wright, J. V. (1987). Volcanic successions, modern and ancient: A geological approach to processes, products, and successions. Allen and Unwin.

Chambers, L. M., and Pringle, M. S. (2001). Age and duration of activity at the Isle of Mull Tertiary igneous centre, Scotland, and confirmation of the existence of subchrons during Anomaly 26r. Earth and Planetary Science Letters, 193(3), 333-345.

Chan, M, A. (1985). Correlations of diagenesis with sedimentary facies in Eocene sandstones, western Oregon: Journal of Sedimentary Petrology 55 (323-333).

Chang, H. K., Mackenzie, F. T., and Schoonmaker, J. (1986). Comparisons between the diagenesis of dioctahedral and trioctahedral smectite, Brazilian offshore basins. Clays and Clay Minerals, 34(4), 407-423.

Chapin, C. E., and Lindley, J. I., (1985). Potassium metasomatism of volcanic and sedimentary rocks in rift basins, calderas, and detachment terranes. Paper presented to the Conference on Heat and Detachment in Crustal Extension on Continents and Planets, 10-12 October 1985, Sedona, AZ Houston, TX: Lunar and Planetary Institute, 25-31.

Clark, S., Campbell, E. (2011). Longmorn Peer Assist. In-house report Chevron Upstream Europe.

Cleal, C. J., Thomas, B. A., Batten, D. J. and Collinson, M. E. (2001). Mesozoic and Tertiary Palaeobotany of Great Britain. Geological Conservation Review Series, 22, Joint Nature Conservation Committee, Peterborough.

Clift, P. D. (1999). The thermal impact of Paleocene magmatic underplating in the Faeroe. Petroleum Geology, 5, 585-593.

Cockell, C. S., Olsson-Francis, K., Herrera, A., and Meunier, A. (2009). Alteration textures in terrestrial volcanic glass and the associated bacterial community. Geobiology, 7(1), 50-65.

Cole, D. R., and Ripley, E. M. (1999). Oxygen isotope fractionation between chlorite and water from 170 to 350 C: A preliminary assessment based on partial exchange and fluid/rock experiments. Geochimica et Cosmochimica Acta, 63(3), 449-457.

Crovisier, J. L., Honnorez, J., Fritz, B., and Petit, J. C. (1992). Dissolution of subglacial volcanic glasses from Iceland: laboratory study and modelling. Applied geochemistry, 7, 55 81.

Cukur, D., Horozal, S., Kim, D.C., Lee, G.H., Han, H.C. and Kang, M.H. (2010). The distribution and characteristics of the igneous complexes in the northern East China Sea Shelf Basin and their implications for hydrocarbon potential. Marine Geophysical Research, 31, 299-313.

D

Davidson, P. J. (1989). "Stevensite, a smectite-group mineral from Corstorphine Hill, Edinburgh." Scottish Journal of Geology 25.1: 63-67.

Davies D. K., Ethridge F. G. (1975) Sandstone composition and depositional environment. Bulletin of the American Association of Petroleum Geologists 59:239–264.

Davis, J. S., and Keller, H. M. (1983). Dissolved Loads in Streams and Rivers-Discharged and Seasonally Related Variations.

de Caritat, P., Hutcheon, I., and Walshe, J. L. (1993). Chlorite geothermometry; a review. Clays and Clay Minerals, 41(2), 219-239.

Dean, K., Mclachlan, K. and Chambers, A. (1999). Rifting and the Development of the Faeroe-Shetland Basin. In Petroleum Geology of Northwest Europe: Proceedings of the 5th Conference (edited by A.J. Fleet and S.A.R. Boldy). The Geological Society of London, 533-544.

Deer, W. A., Howie, R. A., and Zussman, J. (1992). An introduction to the rock-forming minerals (Vol. 2). Hong Kong: Longman Scientific and Technical.

de'Gennaro, M., Cappelletti, P., Langella, A., Perrotta, A., and Scarpati, C. (2000). Genesis of zeolites in the Neapolitan Yellow Tuff: geological, volcanological and mineralogical evidence. Contributions to Mineralogy and Petrology, 139(1), 17-35.

Delgado, A., Reyes, E. (1996). Oxygen and hydrogen isotope compositions in clay minerals: A potential single-mineral geothermometer. Geochimica et Cosmochimica Acta, Volume 60, Issue 21, November 1996, Pages 4285-4289.

Dimroth, E., and Lichtblau, A. P. (1979). Metamorphic evolution of Archean hyaloclastites, Noranda area, Quebec, Canada. Part I: Comparison of Archean and Cenozoic sea-floor metamorphism. Canadian Journal of Earth Sciences, 16(7), 1315-1340.

Dobson, P. F., Kneafsey, T. J., Hulen, J., and Simmons, A. (2003). Porosity, permeability, and fluid flow in the Yellowstone geothermal system, Wyoming. Journal of Volcanology and Geothermal Research, 123(3), 313-324.

Donaire, T., Sáez, R., Pascual, E., (2002). Rhyolitic globular peperites from the Aznalcollar mining district (Iberian Pyrite belt, Spain): physical and chemical controls. In: Skilling, I. P., White, J. D. L. and McPhie, J. (Eds.), Peperite: Processes and Products of Magma–Sediment Mingling. J. Volcanol. Geotherm. Res. 114, 119–128.

Donnelly, T., Waldron, S., Tait, A., Dougans, J., Bearhop, S. (2001) Hydrogen isotope analysis of natural abundance and deuterium-enriched waters by reduction over chromium on-line to a dynamic dual inlet isotope-ratio mass spectrometer. Rapid Communications In Mass Spectrometry, 15, 1297-1303.

Doré, A. G., and Lundin, E. R. (1996). Cenozoic compressional structures on the NE Atlantic margin; nature, origin and potential significance for hydrocarbon exploration. Petroleum Geoscience, 2(4), 299-311.

dos Anjos, S. M., De Ros, L. F., de Souza, R. S., de Assis Silva, C. M., and Sombra, C. L. (2000). Depositional and diagenetic controls on the reservoir quality of Lower Cretaceous Pendencia sandstones, Potiguar rift basin, Brazil. AAPG bulletin, 84(11), 1719-1742.

Doyen, P. M. (1988). Permeability, conductivity, and pore geometry of sandstone. Journal of Geophysical Research: Solid Earth (1978–2012), 93(B7), 7729-7740.

Doyle, M. G. (2000). Clast shape and textural associations in peperite as a guide to hydromagmatic interactions: Upper Permian basaltic and basaltic andesite examples from Kiama, Australia. Australian Journal of Earth Sciences, 47(1), 167-177.

Doyle, M. G. (2001). Volcanic influences on hydrothermal and diagenetic alteration: evidence from Highway-Reward, Mount Windsor Subprovince, Australia. Economic Geology, 96(5), 1133-1148.

Duncan L., Helland-Hansen, D., and Dennehy, C. (2009). The Rosebank Discovery: A new play type in intra basalt reservoirs of the North Atlantic volcanic province. Devex Conference 13/05/2009 Aberdeen Exhibition and Conference Centre (AECC).

E

Eggleton, R. A., and Keller, J. (1982). The palagonitization of limburgite glass–a TEM study. Neues. Jahrb. Mineral, 7, 321-336.

Ehrenberg, S. N., (1990), Relationship between diagenesis and reservoir quality in sandstones of the Garn Formation, Haltenbanken, mid-Norwegian continental shelf: AAPG Bulletin, v. 74, p. 1538-1558.

Eldholm, O., and Grue, K. (1994). North Atlantic volcanic margins: dimensions and production rates. Journal of Geophysical Research: Solid Earth (1978–2012), 99(B2), 2955-2968.

Ellis, D., Bell, B. R., Jolley, D. W., and O'Callaghan, M. (2002). The stratigraphy, environment of eruption and age of the Faroes Lava Group, NE Atlantic Ocean.Geological Society, London, Special Publications, 197(1), 253-269.

Ellis, D., Jolley, D. W., Passey, S. R. and Bell, B. R. (2009). Transfer zones: The application of new geological information from the Faroe Islands applied to the offshore exploration of intra basalt and sub-basalt strata. In: Faroe Islands Exploration Conference: Proceedings of the 2nd Conference (edited by H. Ziska and T. Varming). Annales Societatis Scientarum Faroensis, Supplement 50, 205-226.

Ely, L. L., Brossy, C. C., House, P. K., Safran, E. B., O'Connor, J. E., Champion, D. E., and Turrin, B. D. (2012). Owyhee River intracanyon lava flows: Does the river give a dam? Geological Society of America Bulletin, 124(11-12), 1667-1687.

Emeleus, C. H., and Gyopari, M. C. (1992). British Tertiary volcanic province. London: Chapman and Hall.

Escande, M. A. (1983) Echangeabilité et fractionnement isotopique de l'oxygène des smectites magnésiennes de synthèse. Etablissement d'un géothermomètre, Thèse Doctorat Univ. Paris Sud, 150 p.

Eslinger, E., and Pevear, D. R. (1988). Clay minerals for petroleum geologists and engineers. Society of Economic Paleontologists and Mineralogists.

Evans, J., Cade, C., and Bryant, S. (1997). A geological approach to permeability prediction in clastic reservoirs. In Kupecz, J.A., Gluyas, J., and Bloch, S., eds., Reservoir quality prediction in sandstones and carbonates: AAPG Memoir 69, p.91-101.

Evarts, R. C., and Schiffman, P. (1983). Submarine hydrothermal metamorphism of the Del Puerto ophiolite, California. American journal of science, 283(4), 289-340.

F

Fielding, K. D., Burnett, D., Crabtree, N. J., Ladegaard, H., and Lawton, L. C. (2014). Exploration and appraisal of a 120 km2 four-way dip closure: what could possibly go wrong? Geological Society, London, Special Publications, 397(1), 145-162.

Fisher, R. V. (1961). Proposed classification of volcaniclastic sediments and rocks. Geological Society of America Bulletin, 72(9), 1409-1414.

Fisher, R. V., and Schmincke, H. U. (1984). Pyroclastic Rocks and Tectonic Environment (pp. 383-409). Springer Berlin Heidelberg.

Fletcher, R., Kusznir, N., Roberts, A., and Hunsdale, R. (2013). The formation of a failed continental breakup basin: The Cenozoic development of the Faroe-Shetland Basin. Basin Research.

Frostick, L. E., and Jones, S. J. (2002). Impact of periodicity on sediment flux in alluvial systems: grain to basin scale. Geological Society, London, Special Publications, 191(1), 81-95.

Furnes, H. (1975). Experimental palagonitization of basaltic glasses of varied composition. Contributions to Mineralogy and Petrology, 50(2), 105-113.

Furnes, H. (1984), Chemical-changes during progressive subaerial palagonitization of a subglacial olivine tholeiite hyaloclastite — A microprobe study, Chem. Geol., 43(3–4), 271 285.

G

Gaines, R. V., Skinner, H. C, Foord, E. E., Mason, B., and Rosenzweig, A. (1997). Dana's new mineralogy: The system of mineralogy of James Dwight Dana and Edward Salisbury Dana, Eighth Edition. New York: Wiley.

Gallagher, J. W. and Dromgoole, P. W. (2008). Seeing below the basalt – offshore Faroes. Geophysical Prospecting, 56, 33-45.

García-Romero, E., Vegas, J., Baldonedo, J. L., and Marfil, R. (2005). Clay minerals as alteration products in basaltic volcaniclastic deposits of La Palma (Canary Islands, Spain). Sedimentary Geology, 174(3), 237-253.

Gardner, J. S. (1887). On the Leaf-beds and Gravels of Ardtun, Carsaig, andc., in Mull. With notes by Grenville A.J. Cole. Quarterly Journal of Geological Society of London 43, 270-300.

Gatliff, R. W., Hitchen, K., Ritchie, J. D. and Smythe, D. K. (1984). Internal structure of the Erlend Tertiary volcanic complex, north of Shetland, revealed by seismic reflection Journal of the Geological Society, London, 141, 555-562.

Geikie, A. (1888). The History of Volcanic Action during the Tertiary Period in the British Isles. Transactions of the Royal Society of Edinburgh 35, 21-184.

Gieskes, J. M., and Lawrence, J. R. (1981). Alteration of volcanic matter in deep sea sediments: evidence from the chemical composition of interstitial waters from deep sea drilling cores. Geochimica et Cosmochimica Acta, 45(10), 1687-1703.

Gifkins, C. C., Herrmann, W., and Large, R. R. (2005). Altered volcanic rocks: A guide to description and interpretation (Published by CODES, Centre for Ore Deposit Research, University of Tasmania).

Giles, M. R., Stevenson, S., Martin, S. V., Cannon, S. J. C., Hamilton, P. J., Marshall, J. D., and Samways, G. M. (1992). The reservoir properties and diagenesis of the Brent Group: a regional perspective. Geological Society, London, Special Publications, 61(1), 289-327.

Gilg, H. A., Girard, J. P., and Sheppard, S. M. (2004). Conventional and less conventional techniques for hydrogen and oxygen isotope analysis of clays, associated minerals and pore waters in sediments and soils. Handbook of stable isotope analytical techniques, 1, 38-61.

Girard, J. P., Deynoux, M., and Nahon, D. (1989). Diagenesis of the upper Proterozoic siliciclastic sediments of the Taoudeni Basin (West Africa) and relation to diabase emplacement. Journal of Sedimentary Research, 59(2).

Gislason, S. R., and Oelkers, E. H. (2003). Mechanism, rates, and consequences of basaltic glass dissolution: II. An experimental study of the dissolution rates of basaltic glass as a function of pH and temperature. Geochimica et Cosmochimica Acta, 67(20), 3817-3832.

Gislason, S. R., and Arnórsson, S. (1993). Dissolution of primary basaltic minerals in natural waters: saturation state and kinetics. Chemical Geology, 105(1), 117-135.

Gislason, S. R., and Eugster, H. P. (1987). Meteoric water-basalt interactions. II: A field study in NE Iceland. Geochimica et Cosmochimica Acta, 51(10), 2841-2855.

Glennie, K. W. (2002). Permian and Triassic. The geology of Scotland, 4th ed.: Geological Society (London), 301-321.

Gluyas, J., Clark S. J. and Boyce, A. (2012) Direct and indirect diagenetic effects in igneous affected basins - Constraining diagenetic timings, processes and reservoir quality. NERC in Kind Grant.

Graham, C. M., Atkinson, J. and Harmon, R.S. (1984b). Hydrogen isotope fractionation in the system chlorite-water. NERC 6th Progress Report of Research 1981-1984, NERC Publication Series D, No. 25, p. 139.

Grossenbacher, K. A., and McDuffie, S. M. (1995). Conductive cooling of lava: columnar joint diameter and stria width as functions of cooling rate and thermal gradient. Journal of volcanology and geothermal research, 69(1), 95-103.

Grove, C. (2014) Direct and indirect effects of flood basalt volcanism on reservoir quality sandstone. (Doctoral dissertation, Durham University).

Grove, C and Jerram D. A, (2011). jPOR: An ImageJ macro to quantify total optical porosity from blue-stained thin sections, Computers and Geosciences, Volume 37, Issue 11, November, Pages 1850-1859

H

Hardwick, A. J., Whittaker, J., and Woodburn, N. (2012, June). Combining Bandwidth Extension Techniques and Pre-stack Q Inversion for Enhanced Imaging of Intra-basalt Plays. In 74th EAGE Conference and Exhibition.

Hawlader, H. M. (1990). Diagenesis and reservoir potential of volcanogenic sandstones—Cretaceous of the Surat Basin, Australia. Sedimentary Geology, 66(3), 181-195.

Hay, R, L. (1978). Geologic occurance of zeolites, in Sand, L,B, and Mumpton, F,A, Natural Zeolites: Occurance, Properties, Use: Oxford, Pergamon Press, P 135-143

Hay, R. L. (1966). Zeolites and zeolitic reactions in sedimentary rocks (Vol. 85). Geological Society of America.

Hay, R. L. (1978). Geologic occurrence of zeolites. Natural zeolites: occurrence, properties, use, 135-143.

Hay, R. L., and Iijima, A. (1968). Nature and origin of palagonite tuffs of the Honolulu Group on Oahu, Hawaii. Geological Society of America Memoirs, 116, 331-376.

Hayes, J. B. (1970). Polytypism of chlorite in sedimentary rocks. Clays and Clay minerals, 18, 285-306.

Head III, J. W., and Wilson, L. (1989). Basaltic pyroclastic eruptions: influence of gas-release patterns and volume fluxes on fountain structure, and the formation of cinder cones, spatter cones, rootless flows, lava ponds and lava flows.Journal of Volcanology and Geothermal Research, 37(3), 261-271.

Hein, J. R., and Scholl, D. W. (1978). Diagenesis and distribution of late Cenozoic volcanic sediment in the southern Bering Sea. Geological Society of America Bulletin, 89(2), 197-210.

Hekinian, R., and Hoffert, M. (1975). Rate of palagonitization and manganese coating on basaltic rocks from the Rift Valley in the Atlantic Ocean near 36 50′ N. Marine Geology, 19(2), 91-109.

Helland-Hansen, D. (2009). Rosebank – challenges to development from a subsurface perspective. In: Varming, T. and Ziska, H. (eds): Faroe Islands Annales Societatis Scientarium Faeroensis, Supplementum 50, 241–245.

Hillier S. (1999) Use of an air-brush to spray dry samples for X-ray powder diffraction. Clay Miner. 34, 127-135.

Hillier S. (2002) Spray drying for X-ray powder diffraction specimen preparation. IUCR Commission on Powder Diffraction Newsletter No. 27. June 2002. www.iucr.org/iucr-top/comm/cpd/Newsletters/no27jul2002/index.html

Hillier S. (2011) Spray drying kit for the preparation of random powder samples for x-ray powder diffraction operation and instruction manual. Version 1.4. The James Hutton Institute, Aberdeen.

Hillier, S., (1994). Pore-Lining Chlorites in Siliciclastic Reservoir Sandstones - Electron-Microprobe, Sem and Xrd Data, and Implications for Their Origin. Clay Minerals, 29(4): 665-679.

Hitchen, K., and Ritchie, J. D. (1987). Geological review of the West Shetland area. Petroleum Geology of North West Europe, 2, 737-749.

Hogg, A. J., Mitchell, A. W., and Young, S. (1996). Predicting well productivity from grain size analysis and logging while drilling. Petroleum Geoscience, 2(1), 1-15.

Holdsworth, R. E., Harris, A. L., and Roberts, A. M. (1987). The stratigraphy, structure and regional significance of the Moine rocks of Mull, Argyllshire, W. Scotland. Geological Journal, 22(2), 83-107.

Hole, M., Jolley, D., Hartley, A., Leleu, S., John, N., and Ball, M. (2013). Lava–sediment interactions in an Old Red Sandstone basin, NE Scotland. Journal of the Geological Society, 170(4), 641-655.

Holford, S. P., Green, P. F., Hillis, R. R., Underhill, J. R., Stoker, M. S., and Duddy, I. R. (2010). Multiple post-Caledonian exhumation episodes across NW Scotland revealed by apatite fission-track analysis. Journal of the Geological Society, 167(4), 675-694.

Holler, H., and Wirsching, U. (1978). Experiments on the formation of zeolites by hydrothermal alteration of volcanic glasses (pp. 329-336). Pergamon Press, Oxford.

Holmes, A. J., Griffith, C. E., and Scotchman, I. C. (1999, January). The Jurassic petroleum system of the West of Britain Atlantic margin–an integration of tectonics, geochemistry and basin modelling. In Geological Society, London, Petroleum Geology Conference series (Vol. 5, pp. 1351-1365). Geological Society of London.

Holz, M., Soares, A. P., and Soares, P. C. (2008). Preservation of aeolian dunes by pahoehoe lava: An example from the Botucatu Formation (Early Cretaceous) in Mato Grosso do Sul state (Brazil), western margin of the Paraná Basin in South America. Journal of South American Earth Sciences, 25(3), 398-404.

Honnorez, J. (1978), Generation of phillipsites by palagonitization of basaltic glass in sea water and the origin of K-rich deep-sea deposits, in Natural Zeolites, Occurrence, Properties, Use, edited by L. B. Sand and F. A. Mumpton, pp. 245– 258, Elsevier, New York.

Huppert, H. E., and Sparks, R. S. J. (1989). Chilled margins in igneous rocks.Earth and Planetary Science Letters, 92(3), 397-405.

I

Iijima, A. (1978). Geological occurrences of zeolite in marine environments. Natural zeolites, 175-198.

Iijima, A. (2001). Zeolites in petroleum and natural gas reservoirs. Reviews in mineralogy and geochemistry, 45(1), 347-402.

Iliffe, J. E., Robertson, A. G., Ward, G. H. F., Wynn, C., Pead, S. D. M., and Cameron, N. (1999, January). The importance of fluid pressures and migration to the hydrocarbon prospectivity of the Faeroe–Shetland White Zone. In Geological Society, London, Petroleum Geology Conference series (Vol. 5, pp. 601-611). Geological Society of London.

Imam, M. B. (1986). Post depositional changes in the miocene-pliocene sandstones of Bangladesh. Journal of Bangladesh Academy of Sciences, 10(2).

Inoue, A. (1987). Conversion of smectite to chlorite by hydrothermal and diagenetic alterations, Hokuroku Kuroko mineralization area, northeast Japan. In Proceedings of the International Clay Conference, Denver 1985 (pp. 158-164). The Clay Minerals Society, Bloomington, Indiana.

Inoue, A., Uuoa, M. (1991). Smectite-to-chlorite transformation in thermally metamorphosed yolcanoclastic rocks in the Kamikita area, northern Honshu, Japan Arsuyuxr lNour.

J

Jackson, M. L., and Barak, P. (2005). Soil chemical analysis: advanced course. UW-Madison Libraries Parallel Press.

Jakobsson, S. P., and Moore, J. G. (1986). Hydrothermal minerals and alteration rates at Surtsey volcano, Iceland. Geological Society of America Bulletin, 97(5), 648-659.

Jercinovic, M. J., Keil, K., Smith, M. R., and Schmitt, R. A. (1990). Alteration of basaltic glasses from north-central British Columbia, Canada. Geochimica et Cosmochimica Acta, 54(10), 2679-2696.

Jerram, D. A., and Stollhofen, H. (2002). Lava–sediment interaction in desert settings; are all peperite-like textures the result of magma–water interaction?. Journal of Volcanology and Geothermal Research, 114(1), 231-249.

Jerram, D. A., and Stollhofen, H. (2002). Lava–sediment interaction in desert settings; are all peperite-like textures the result of magma–water interaction?. Journal of Volcanology and Geothermal Research, 114(1), 231-249.

Jerram, D. A., and Widdowson, M. (2005). The anatomy of Continental Flood Basalt Provinces: geological constraints on the processes and products of flood volcanism. Lithos, 79(3), 385-405.

Jolley, D. W. (2007). Biostratigraphy and ecology internal reports. Chevron Upstream Europe.

Jolley, D. W., and Bell, B. R. (2002). The evolution of the North Atlantic Igneous Province and the opening of the NE Atlantic rift. Geological Society, London, Special Publications, 197(1), 1-13.

Jolley, D. W., Bell, B. R., Williamson, I. T., and Prince, I. (2009). Syn-eruption vegetation dynamics, paleosurfaces and structural controls on lava field vegetation: An

example from the Palaeogene Staffa Formation, Mull Lava Field, Scotland. Review of Palaeobotany and Palynology, 153(1), 19-33.

Jolley, D. W., Morton, A.C. and Prince, I. (2005). Volcanogenic impact on phytogeography and sediment dispersal patterns in the NE Atlantic. In: Petroleum Geology of Northwest Europe: Proceedings of the 6th Conference (edited by A.G. Dore and B.A. Vining). The Geological Society of London, 969-975.

Jones, S. M., White, N., Clarke, B. J., Rowley, E., and Gallagher, K. (2002). Present and past influence of the Iceland Plume on sedimentation. Geological Society, London, Special Publications, 196(1), 13-25.

Jørgensen, O. (2006). The regional distribution of zeolites in the basalts of the Faroe Islands and the significance of zeolites as palaeotemperature indicators. Geological Survey of Denmark and Greenland Bulletin, 9, 123-156.

K

Karpova, G. V. (1969). Clay mineral post-sedimentary ranks in terrigenous rocks. Sedimentology, 13(1-2), 5-20.

Kawano, M., and Tomita, K. (1997). Experimental Study on the Formation of Zeolites from Obsidian by Interaction with NaOH and KOH Solutions at 150 and 200 C. Clays and Clay Minerals, 45, 365-377.

Kawano, M., Tomita, K., and Shinohara, Y. (1997). Analytical electron microscopic study of the non-crystalline products formed at early weathering stages of volcanic glass. Clays and Clay Minerals, 45(3), 440-447.

Kerr, A. C. (1995a). The geochemical stratigraphy, field relations and temporal variation of the Mull-Morvern Tertiary lava succession, NW Scotland. Transactions of the Royal Society of Edinburgh: Earth Sciences 86, 35-47.

Kerr, A. C. (1995b). The geochemistry of the Mull-Morvern Tertiary lava succession, NW Scotland: an assessment of mantle sources during plume-related volcanism. Chemical Geology 122, 43-58.

Kerr, A. C. (1997). The geochemistry and significance of plugs intruding the Tertiary Mull– Morvern lava succession, NW Scotland. Scottish Journal of Geology 33, 157-67.

Kerr, A. C. (1998). On the nature of the parental magma of the Palaeogene Staffa Magma subtype, Isle of Mull, Scotland. Transactions of the Royal Society of Edinburgh: Earth Sciences 89, 87-93.

Kerr, A. C., Kent, R.W. Thomson, B.A., Seedhouse, J.K. and Donaldson, C.H. (1999). Geochemical evolution of the Tertiary Mull Volcano, Western Scotland. Journal of Petrology 40, 873-908.

Khalaf, E. E. D. A. H. (2013). Diagenetic evolution of the volcaniclastic deposits: an example from Neoproterozoic Dokhan Volcanics in Wadi Queih basin, central Eastern Desert, Egypt. Arabian Journal of Geosciences, 1-22.

Kiørboe, L. (1999, January). Stratigraphic relationships of the Lower Tertiary of the Faeroe basalt plateau and the Faeroe–Shetland Basin. In Geological Society, London, Petroleum Geology Conference series (Vol. 5, pp. 559-571). Geological Society of London.

Knox, R. O. B., and Morton, A. C. (1988). The record of early Tertiary N Atlantic volcanism in sediments of the North Sea Basin. Geological Society, London, Special Publications, 39(1), 407-419.

Kokelaar, B. P. (1982). Fluidization of wet sediments during the emplacement and cooling of various igneous bodies. Journal of the Geological Society,139(1), 21-33.

Kristmannsdottir, H. (1975, May). Hydrothermal alteration of basaltic rocks in Icelandic geothermal areas. In Proceedings of the 2nd UN Symposium on the Development and Uses of Geothermal Resources, US Govt Printing Office, Washington, DC (pp. 441-445).

Kristmannsdóttir, H. (1979). Alteration of Basaltic Rocks by Hydrothermal-Activity at 100-300° C. Developments in sedimentology, 27, 359-367.

Kristmannsdóttir, H. and Tómasson, J. (1978). Zeolite zones in geothermal areas in Iceland. In Natural Zeolites, Occurrence, Properties, Use, Pergamon Press, Oxford., 277-284.

Kuno, H., Ishikawa, T., Katsui, Y., Yagi, K., Yamasaki, M., and Taneda, S. (1964). Sorting of pumice and lithic fragments as a key to eruptive and emplacement mechanism. Jpn. J. Geol. Geogr, 35, 223-238.

L

Lamers, E., and Carmichael, S. M. M. (1999, January). The Paleocene deepwater sandstone play West of Shetland. In Geological Society, London, Petroleum Geology Conference series (Vol. 5, pp. 645-659). Geological Society of London.

Larsen, M., Rasmussen, T., and Hjelm, L. (2010, January). Cretaceous revisited: exploring the syn-rift play of the Faroe–Shetland Basin. In Geological Society, London, Petroleum Geology Conference series (Vol. 7, pp. 953-962). Geological Society of London.

Leder, F., and Park, W. C. (1986). Porosity reduction in sandstone by quartz overgrowth. Am. Assoc. Pet. Geol., Bull.;(United States), 70(11).

Lenhardt, N., and Götz, A. E. (2011). Volcanic settings and their reservoir potential: An outcrop analog study on the Miocene Tepoztlán Formation, Central Mexico. Journal of Volcanology and Geothermal Research, 204(1), 66-75.

Lima, R. D., and De Ros, L. F. (2002). The role of depositional setting and diagenesis on the reservoir quality of Devonian sandstones from the Solimoes Basin, Brazilian Amazonia. Marine and petroleum geology, 19(9), 1047-1071.

Lirer, L.,Vinci, A., Alberico I, Gifuni, T., Bellucci, F., Petrosino, P and Tinterri, R. (2001). Occurrence of inter-eruption debris flow and hyperconcentrated flood-flow deposits on Versuvio volcano, Italy. Sedimentary Geology 139, 151-67.

M

Maresh, J., White, R. S., Hobbs, R. W., and Smallwood, J. R. (2006). Seismic attenuation of Atlantic margin basalts: Observations and modeling. Geophysics, 71(6), B211-B221.

Martin, A. J. (2000). Flaser and wavy bedding in ephemeral streams: a modern and an ancient example. Sedimentary Geology, 136(1), 1-5.

Mathisen, M. E and McPherson, J.G. (1991). Volcaniclastic deposits implications for hydrocarbon exploration. Sedimentation in Volcanic Settings. SEPM Special Publication No 45. SEPM Society for Sedimentary Geology.

Mathisen, M. E. (1984). Diagenesis of Plio-Pleistocene Nonmarine Sandstones, Cagayan Basin, Philippines: Early Development of Secondary Porosity in Volcanic Sandstones: Part 2. Aspects of Porosity Modification.

Mathisen, M. E. (1991). Volcaniclastic deposits: implications for hydrocarbon exploration.

McBride, E. F. (1989). Quartz cement in sandstones: a review. Earth-Science Reviews, 26(1), 69-112.

McKerrow, W. S., Mac Niocaill, C., and Dewey, J. F. (2000). The Caledonian orogeny redefined. Journal of the Geological society, 157(6), 1149-1154.

McKinley, J. M., Worden, R. H., and Ruffell, A. H. (2001). Contact diagenesis: the effect of an intrusion on reservoir quality in the Triassic Sherwood Sandstone Group, Northern Ireland. Journal of Sedimentary Research, 71(3), 484-495.

McKinley, J. M., Worden, R. H., and Ruffell, A. H. (2003). Smectite in sandstones: a review of the controls on occurrence and behaviour during diagenesis. Worden RH,

Morad S. Clay mineral cements in sandstones, International Association of Sedimentolo gists Special Publication, 34, 109-128.

McPhie, J., Doyle, M., Allen, R., and Allen, R. L. (1993). Volcanic textures: a guide to the interpretation of textures in volcanic rocks. CODES-University of Tasmania.

Merino, E., Girard, J. P., May, M. T., and Ranganathan, V. (1997). Diagenetic mineralogy, geochemistry, and dynamics of Mesozoic arkoses, Hartford rift basin, Connecticut, USA. Journal of Sedimentary Research, 67(1).

Moore, D. and R. C. Reynolds, Jr. (1997). X-Ray Diffraction and the Identification and Analysis of Clay Minerals, 2nd ed.: Oxford University Press, New York

Morad, S., Worden, R. H., and Ketzer, J. M. (2003). Oxygen and hydrogen isotopic composition of diagenetic clay minerals in sandstones: a review of the data and

controls. Clay Mineral Cements in Sandstones:(Special Publication 34 of the IAS), 34(34), 63-91.

Morrison, M. A., Thompson, R. N. and Dickin, A. P. (1985). Geochemical evidence for complex magmatic plumbing during development of a continental volcanic centre. Geology 13, 581-4.

Morrison, M. A., Thompson, R. N., Gibson, I. L. and Mariner, G. F. (1980). Lateral chemical heterogeneity in the Palaeocene upper mantle beneath the Scottish Hebrides. Philosophical Transactions of the Royal Society of London, Series A297, 229-44.

Morton, A. C., and Knox, R. O. B. (1990). Geochemistry of late Palaeocene and early Eocene tephras from the North Sea Basin. Journal of the Geological Society, 147(3), 425-437.

Moy, D. J. and Imber, J. (2009). A critical analysis of the structure and tectonic significance of rift-oblique lineaments ('transfer zones') in the Mesozoic-Cenozoic succession of the Faroe -Shetland Basin, NE Atlantic margin. Journal of the Geological Society, 166, 831-844.

Mudge, D., Spencer, S., Mander, D., Gall, M., Penman, C., Holdoway, K (2009) Regional Play Fairway Evaluation of the UK Atlantic Margin. Ternan Ltd, Senergy.

N

Nadeau, P. H., and Reynolds, R. C. (1981). Volcanic components in pelitic sediments. Nature 294, 72-4

Naylor, D., and Shannon, P. M. (2005, January). The structural framework of the Irish Atlantic Margin. In Geological Society, London, Petroleum Geology Conference series (Vol. 6, pp. 1009-1021). Geological Society of London.

Naylor, P. H., Bell, B. R., Jolley, D. W., Durnall, P., and Fredsted, R. (1999, January). Palaeogene magmatism in the Faeroe–Shetland Basin: influences on uplift history and sedimentation. In Geological Society, London, Petroleum Geology Conference series (Vol. 5, pp. 545-558). Geological Society of London.

Nelson, C. E., Jerram, D. A., and Hobbs, R. W. (2009). Flood basalt facies from borehole data: implications for prospectivity and volcanology in volcanic rifted margins. Petroleum Geoscience, 15(4), 313-324.

Nelson, C. E., Jerram, D. A., Single, R. T., and Hobbs, R. W. (2009). Understanding the facies architecture of flood basalts and volcanic rifted margins and its effect on geophysical properties. In Faroe Islands Exploration Conference: Proceedings of the 2nd Conference. Annales Societatis Scientarium Faroensis.

Noh, J. H., and Boles, J. R. (1989). Diagenetic alteration of perlite in the Guryongpo area, Republic of Korea. Clays and Clay Minerals, 37(1), 47-58.

O

Oliver, G. J. H. (2002). Chronology and terrane assembly, new and old controversies. The Geology of Scotland, 201-211.

Omotoso, O., McCarty, D. K., Hillier, S., and Kleeberg, R. (2006). Some successful approaches to quantitative mineral analysis as revealed by the 3rd Reynolds Cup contest. Clays and Clay Minerals, 54(6), 748-760.

Oxtoby, N. H. and Grant, S. M. (1992). How can I predict porosity? Internal BP report.

P

Parnell, J., Carey, P. F., Green, P., and Duncan, W. (1999, January). Hydrocarbon migration history, West of Shetland: integrated fluid inclusion and fission track studies. In Geological Society, London, Petroleum Geology Conference series (Vol. 5, pp. 613-625). Geological Society of London.

Parra, M., Delmont, P., Dumon, J. C., Ferragne, A., and Pons, J. C. (1987). Mineralogy and origin of Tertiary interbasaltic clays from the Faeroe Islands, northeastern Atlantic. Clay Miner, 22, 63-82.

Passey, S. R. (2004). The volcanic and sedimentary evolution of the Faeroe plateau lava group, Faeroe Islands and Faeroe-Shetland Basin, NE Atlantic (Doctoral dissertation, University of Glasgow).

Passey, S. R., and Bell, B. R. (2007). Morphologies and emplacement mechanisms of the lava flows of the Faroe Islands Basalt Group, Faroe Islands, NE Atlantic Ocean. Bulletin of Volcanology, 70(2), 139-156.

Passey, S. R., and Hitchen, K. (2011). Cenozoic (igneous). Geology of the Faroe-Shetland Basin and adjacent areas, 209-228.

Passey, S. R., and Jolley, D.W. (2009) A revised lithostratigraphic nomenclature for the Palaeogene Faroe Islands Basalt Group, NE Atlantic Ocean. Earth Environ. Sci.Trans. Roy. Soc. Edinburgh, 99,127-158.

Passey, S. R., and Varming, T. (2010). Surface interpolation within a continental flood basalt province: An example from the Palaeogene Faroe Islands Basalt Group. Journal of Structural Geology, 32(5), 709-723.

Peacock, M. A. (1926), The petrology of Iceland, Part 1, The basic tuffs, R. Soc. Edinburgh, Trans., 55, 53–76.

Peters, K. E., Moldowan, J. M., Driscole, A. R., and Demaison, G. J. (1989). Origin of Beatrice oil by co-sourcing from Devonian and Middle Jurassic source rocks, inner Moray Firth, United Kingdom. AAPG Bulletin, 73(4), 454-471.

Petersen, U. K., Brown, R. J., and Andersen, M. S. (2013). P-wave velocity distribution in basalt flows of the Enni Formation in the Faroe Islands from refraction seismic analysis. Geophysical Prospecting, 61(1), 168-186.

Petry, K., Jerram, D. A., de Almeida, D. D. P. M., and Zerfass, H. (2007). Volcanic-sedimentary features in the Serra Geral Fm., Paraná Basin, southern Brazil: Examples of dynamic lava-sediment interactions in an arid setting. Journal of Volcanology and Geothermal Research, 159(4), 313-325.

Pettijohn, F,J, Potter, P,E and Siever, R. (1987). Sand and Sandstone. Published by Springer

Pittman, E. D. (1972). Diagenesis of quartz in sandstones as revealed by scanning electron microscopy. Journal of Sedimentary Research, 42(3), 507-519.

Pittman, E. D. (1992). Relationship of porosity and permeability to various parameters derived from mercury injection-capillary pressure curves for sandstone (1). AAPG Bulletin, 76(2), 191-198.

Pittman, E. D. (1979). Recent advances in sandstone diagenesis. Ann. Rev. Earth Planet Sci. 7 (39-62)

Pittman, E. D., and Larese, R. E. (1991). Compaction of Lithic Sands: Experimental results and applications (1). AAPG Bulletin, 75(8), 1279-1299.

Potts, G.J., Hunter, R. H., Harris, A. L., and Fraser, F. M. (1995). Late-orogenic extensional tectonics at the NW margin of the Caledonides in Scotland. Journal of the Geological Society, London, 152, 907–910.

Preston, R. J., Bell, B. R. and Rogers, G. (1998). The Loch Scridain Xenolithic Sill Complex, Isle of Mull, Scotland: Fractional Crystallization, Assimilation, Magma-Mixing and Crustal Anatexis in Subvolcanic Conduits. Journal of Petrology, 39, 519-50.

Q

Quinn, M., Varming, T., and Ólavsdottir, J. (2011). Petroleum geology. Geology of the Faroe-Shetland Basin and adjacent areas: British Geological Survey Research Report RR/11/01, Jarðfeingi Research Report RR/11/01.

R

Ramseyer, K., Boles, J. R., and Lichtner, P. C. (1992). Mechanism of plagioclase albitization. Journal of Sedimentary Research, 62(3).

Rasmussen, J. and Noe-Nygaard, A. (1970). English edition: Geology of the Faeroe Islands (Pre-Quaternary). Trans: Henderson, G., Geological Survey of Denmark, Copenhagen, 1/25, p 142. (Original publication: (1969). Beskrivelse til Geologisk Kort over Færøerne. Danmarks geol. Unders. (1), 24, 370 pp).

Rateau, R., Schofield, N., and Smith, M. (2013). The potential role of igneous intrusions on hydrocarbon migration, West of Shetland. Petroleum Geoscience,19(3), 259-272.

Rawlings, D. J. (1993). Mafic peperite from the Gold Creek Volcanics in the Middle Proterozoic McArthur Basin, Northern Territory. Australian Journal of Earth Sciences, 40(2), 109-113.

Remy, R. R. (1994). Porosity reduction and major controls on diagenesis of Cretaceous Paleocene volcaniclastic and arkosic sandstone, Middle Park Basin, Colorado. Journal of Sedimentary Research, 64(4).

Revil, A., Hermitte, D., Spangenberg, E., and Cochémé, J. J. (2002). Electrical properties of zeolitized volcaniclastic materials. Journal of Geophysical Research: Solid Earth (1978–2012), 107(B8), ECV-3.

Reynolds, R. C. Jr (1980) Interstratified clay minerals. In: Brindley GW, Brown G (eds) Crystal structures of clay minerals and their X-ray identification. Mineralogical Society, London, pp 249-303

Ritchie, D., and Ziska, H. (2011). Introduction. Geology of the Faroe-Shetland Basin and adjacent areas: British Geological Survey Research Report RR/11/01, Jarðfeingi Research Report RR/11/01.

Ritchie, D., Ziska, H., Kimbell, G., Quinn, M., and Chadwick, A. (2011). Petroleum geology. Geology of the Faroe-Shetland Basin and adjacent areas: British Geological Survey Research Report RR/11/01, Jarðfeingi Research Report RR/11/01.

Ritchie, J. D., Gatliff, R. W., and Richards, P. C. (1999, January). Early Tertiary magmatism in the offshore NW UK margin and surrounds. In Geological Society, London, Petroleum Geology Conference series (Vol. 5, pp. 573-584). Geological Society of London.

Ritchie, J. D. and Hitchen, K. (1996) Early Palaeogene onshore igneous activity to the northwest of the UK and its relationship to the North Atlantic Igneous Province. In: Correlation of the Early Palaeogene in Northwest Europe (Ed. by R. W. O'. B. Knox, R. M. Corfield and R. E. Dunay), Geol. Soc. Spec. Publ., 101,63-78.

Ritchie, J. D., Gatliff, R.W., Richards, P.C., Fleet, A.J. and Boldy, S.A.R. (1999) Early Tertiary magmatism in the onshore NW UK margin and surrounds. In: Petroleum Geology of Northwest Europe: Proceedings of the 5th Conference (Ed. by A. J. Fleet and S. A. R. Boldy), Geol. Soc. London, 573-584.

Roberson, R. E. (1988) Random mixed-layer chlorite-smectite: Does it exist? (abs). Clay Minerals Society, 25th Annual General Meeting.

Roberts, D. G., Thompson, M., Mitchener, B., Hossack, J., Carmichael, S., and Bjørnseth, H. M. (1999, January). Palaeozoic to Tertiary rift and basin dynamics: mid-Norway to the Bay of Biscay–a new context for hydrocarbon prospectivity in the deep water frontier. In Geological Society, London, Petroleum Geology Conference series (Vol. 5, pp. 7-40). Geological Society of London.

Robinson, D. T., and Bevins, R. E. (1994). Mafic phyllosilicates in low-grade metabasites. Characterization using deconvolution analysis. Clay Minerals, 29(2), 223-238.

Rohrman, M. (2007). Prospectivity of volcanic basins: Trap delineation and acreage derisking. American Association of Petroleum Geologists Bulletin, 91 (6), 915-939.

Rosebank Team (2009). 213/27-Y Subsurface Peer Assist. In-house report Chevron Upstream Europe.

S

Sabine, P. A. (1971). Bentonitic beidellite-mudstone from the Faeroe Islands. Clay Miner, 9, 97-106.

Saunders, A. D., Fitton, J. G., Kerr, A. C., Norry, M. J., and Kent, R. W. (1997). The north Atlantic igneous province. Large igneous provinces: Continental, oceanic, and planetary flood volcanism, 45-93.

Savin, S. M., and Lee, M. L. (1988). Isotopic studies of phyllosilicates. Reviews in Mineralogy and Geochemistry, 19(1), 189-223.

Schmidt, V., and McDonald, D. A. (1979). Secondary reservoir porosity in the course of sandstone diagenesis.

Schofield, N., and Jolley, D. W. (2013). Development of intra-basaltic lava-field drainage systems within the Faroe–Shetland Basin. Petroleum Geoscience,19(3), 273-288.

Schofield, N., Heaton, L., Holford, S.P., Archer, S.G., Jackson, C.A.-L. and Jolley, D.W. (2012). Seismic imaging of 'broken bridges': linking seismic to outcrop-scale investigations of intrusive magma lobes. Journal of the Geological Society of London, 169, 421-426.

Schofield, N., Stevenson, C., and Reston, T. (2010). Magma fingers and host rock fluidization in the emplacement of sills. Geology, 38(1), 63-66.

Schultz, L. G. (1963) Clay minerals in the Triassic rocks of the Colorado Plateau. U.S. Geological Survey Bulletin, 1147-C, 1-71.

Schutter, S. R. (2003). Occurrences of hydrocarbons in and around igneous rocks. Geological Society, London, Special Publications, 214(1), 35-68.

Scotchman, I. C., and Thomas, J. R. W. (1995). Maturity and hydrocarbon generation in the Slyne Trough, northwest Ireland. Geological Society, London, Special Publications, 93(1), 385-411.

Scotchman, I. C., Carr, A. D., and Parnell, J. (2006). Hydrocarbon generation modelling in a multiple rifted and volcanic basin: a case study in the Foinaven Sub-basin, Faroe–Shetland Basin, UK Atlantic margin. Scottish Journal of Geology, 42(1), 1-19.

Seemann, U., and Scherer, M. (1984). Volcaniclastics as potential hydrocarbon reservoirs. Clay Minerals, 19(9), 457-470.

Self, S., Keszthelyi, L., and Thordarson, T. (1998). The importance of pahoehoe. Annual Review of Earth and Planetary Sciences, 26(1), 81-110.

Self, S., Thordarson, T., Keszthelyi, L., Walker, G. P. L., Hon, K., Murphy, M. T., and Finnemore, S. (1996). A new model for the emplacement of Columbia River basalts as large, inflated pahoehoe lava flow fields. Geophysical Research Letters, 23(19), 2689-2692.

Selley, R. C. (1978). Porosity gradients in North Sea oil-bearing sandstones.Journal of the Geological Society, 135(1), 119-132.

Sharp, Z. D. (1990). A laser-based microanalytical method for the in situ determination of oxygen isotope ratios in silicates and oxides: Geochimica Cosmochimica Acta, v. 54, 1353-1357.

Shau, Y. H., Peacor, D. R., and Essene, E. J. (1990). Corrensite and mixed-layer chlorite/corrensite in metabasalt from northern Taiwan: TEM/AEM, EMPA, XRD, and optical studies. Contributions to Mineralogy and Petrology, 105(2), 123-142.

Shaw, F., Worthington, M. H., White, R. S., Andersen, M. S., and Petersen, U. K. (2008). Seismic attenuation in Faroe Islands basalts. Geophysical Prospecting, 56(1), 5-20.

Sheppard S. M. F. (1986) Characterization and isotopic variations in natural waters. Reviews in Mineralogy and Geochemistry, January, v. 16, p. 165-183

Sheppard, S. M. F., and Gilg, H. A. (1996). Stable isotope geochemistry of clay minerals. Clay Minerals, 31(1), 1-24.

Siebert, R. M., Moncure, G. K., and Lahann, R. W. (1984). A theory of framework grain dissolution in sandstones: Part 2. aspects of porosity modification.

Siever, R. (1962). Silica solubility, 0-200 C., and the diagenesis of siliceous sediments. The Journal of Geology, 127-150.

Siggerud, E. I. H. (2008). Facies analysis, depositional model a tentative sequence stratigraphy for the Paleocene Rosebank Discovery. In-house report Chevron Upstream Europe.

Skilling, I. P., White, J. D. L., and McPhie, J. (2002). Peperite: a review of magma–sediment mingling. Journal of Volcanology and Geothermal Research,114(1), 1-17.

Smallwood, J. R., and Maresh, J. (2002). The properties, morphology and distribution of igneous sills: modelling, borehole data and 3D seismic from the Faroe-Shetland area. Geological Society, London, Special Publications, 197(1), 271-306.

Smallwood, J. R. and Kirk, W. J. (2005). Paleocene exploration in the Faroe–Shetland Channel: disappointments and discoveries. In: Petroleum Geology: North-West Europe and Global Perspectives: Proceedings of the 6th Conference (edited by A. G. Dore and B.A. Vining). The Geological Society of London, 977–991.

Smith, W. W. (1960). Some interstratified clay minerals from basic igneous rocks. Clay Miner Bull, 4, 182-190.

Smykatz-Kloss, W. (1974). Smectites and Vermiculites: The Distinction between Di- and Tri-Octahedral Minerals and Grain Size Determination. In Differential Thermal Analysis (pp. 128-130). Springer Berlin Heidelberg.

Sohn, Y. K., Rhee, C. W., and Kim, B. C. (1999). Debris flow and hyperconcentrated flood-flow deposits in an alluvial fan, northwestern part of the Cretaceous Yongdong basin, central Korea. The Journal of Geology, 107(1), 111-132.

Soper, N. J., and Woodcock, N. H. (2003). The lost Lower Old Red Sandstone of England and Wales: a record of post-Iapetan flexure or Early Devonian transtension?. Geological Magazine, 140(6), 627-647.

Sørensen, A.B. (2003). Cenozoic basin development and stratigraphy of the Faroes area. Petroleum Geoscience, 9, 189-207.

Spitzer, R., White, R. S., and Christie, P. A. (2008). Seismic characterization of basalt flows from the Faroes margin and the Faroe-Shetland basin. Geophysical Prospecting, 56(1), 21-31.

Spitzer, R., White, R.S. and iSIMM Team (2005). Advances in seismic imaging through basalts: a case study from the Faroe–Shetland Basin. Petroleum Geoscience, 11, 147 156.

Sruoga, P., and Rubinstein, N. (2007). Processes controlling porosity and permeability in volcanic reservoirs from the Austral and Neuquen basins, Argentina. AAPG bulletin, 91(1), 115-129.

Sruoga, P., Rubinstein, N., and Hinterwimmer, G. (2004). Porosity and permeability in volcanic rocks: a case study on the Serie Tobífera, South Patagonia, Argentina. Journal of Volcanology and Geothermal Research, 132(1), 31-43.

Staudigel, H., and Hart, S. R. (1983). Alteration of basaltic glass: Mechanisms and significance for the oceanic crust-seawater budget. Geochimica et Cosmochimica Acta, 47(3), 337-350.

Staudigel, H., Muehlenbachs, K., Richardson, S. H., and Hart, S. R. (1981). Agents of low temperature ocean crust alteration. Contributions to Mineralogy and Petrology, 77(2), 150 157.

Steefel, C. I., and Lasaga, A. C. (1994). A coupled model for transport of multiple chemical species and kinetic precipitation/dissolution reactions with application to reactive flow in single phase hydrothermal systems. American Journal of Science, 294(5), 529-592.

Stewart, R. J, and McCulloch, T. H. (1977). Widespread Occurrence of Laumontite in Late Mesozoic and Tertiary Basins of Pacific Margin. AAPG Bulletin, V 61.

Stoker, M. S., and Varming, T. (2011). Cenozoic (sedimentary). Geology of the Faroe-Shetland Basin and adjacent areas: British Geological Survey Research Report RR/11/01, Jarðfeingi Research Report RR/11/01.

Stoker, M. S., and Ziska, H. (2011). Cretaceous. Geology of the Faroe-Shetland Basin and adjacent areas: British Geological Survey Research Report RR/11/01, Jarðfeingi Research Report RR/11/01.

Stoker, M. S., Hitchen, K. and Graham, C.C. (1993). United Kingdom Offshore Regional Report: The geology of the Hebrides and West Shetland shelves, and adjacent deep-water areas. British Geological Survey, pp. 149.

Stollhofen, H. and Stanistreet, I.G. (1994). Interaction between bimodal volcanism, fluvial sedimentation and basin development in the Permo-Carboniferous Saar–Nahe Basin (south-west Germany). Basin Research, 6, 245–267.

Strachan, R. A., Smith, M., Harris, A. L., and Fettes, D. J. (2002). The northern Highland and Grampian terranes. The Geology of Scotland, 81-147.

Stroncik, N. A., and Schmincke, H. U. (2001). Evolution of palagonite: Crystallization, chemical changes, and element budget. Geochemistry, Geophysics, Geosystems, 2(7).

Stroncik, N. A., and Schmincke, H. U. (2002). Palagonite–a review. International Journal of Earth Sciences, 91(4), 680-697.

Surdam R, C, and Boles, J, R. (1979). Diagenesis of volcanic sandstones, in Scholle, P. A and Schluger, P. R, Aspects of Diagenesis: SEPM, Special Publication 26 (227-242).

Surdam, R. C. (1977). Zeolites in closed hydrologic systems. Mineralogy and Geology of Natural Zeolites, edited by J. Boles et al, 65-92.

Surdam, R. C., Boese, S. W., and Crossey, L. J. (1984). The chemistry of secondary porosity. Clastic diagenesis. Am. Ass. Petrol. Geol. Mem, 37, 127-149.

T

Tang, H, Pang, Y and Bian, W. (2008). Quantitative analysis on reservoirs in volcanic edifice of Early Cretaceous Yingcheng Formation in Songliao Basin. Acta Petrolei Sinica, 29(6): 841-845.

Tang, Z., Parnell, J., Alastair, H. R. (1994). Deposition and diagenesis of the lacustrine fluvial Cangfanggou Group (uppermost Permian to Lower Triassic), southern Junggar Basin, NW China: a contribution from sequence stratigraphy. Journal of Paleolimnology. 11 (67-90).

Thompson, R. N., Morrison, M. A., Dickin, A. P., Gibson, I. L. and Harmon, R. S. (1986). Two contrasting styles of interaction between basic magmas and continental crust in the Tertiary Volcanic Province. Journal of Geophysical Research 91, 5985-97.

Thorez, J., and Thorez, J. (1976). Practical identification of clay minerals: a handbook for teachers and students in clay mineralogy (p. 90). Lelotte.

Thorseth, I. H., Furnes, H., and Tumyr, O. (1991). A textural and chemical study of Icelandic palagonite of varied composition and its bearing on the mechanism of the glass-palagonite transformation. Geochimica et Cosmochimica Acta, 55(3), 731-749.

Trabucho-Alexandre, J. (2007) Climatic Origin of Sedimentary Colour Cycles in the Ain el Beida Section (Atlantic Morocco). MSc Thesis under the supervision of Dr. FJ Hilgen. Institute of Paleoenvironments and Paleoclimate Utrecht, The Netherlands.

U

Utada, M. (1970). Occurrence and distribution of authigenic zeolites in the Neogene pyroclastic rocks in Japan. Sci. Papo Coll. Gen. Educ. Univ. Tokio, 20, 191-262.

V

Valentine, G. A., and Gregg, T. K. P. (2008). Continental basaltic volcanoes—processes and problems. Journal of Volcanology and Geothermal Research,177(4), 857-873.

Van der Neut, M. and Eriksson, P. G (2009). Paleohydrological parameters of a braided fluvial system. In Fluvial Sedimentology VI: (Special Publication 28 of the IAS) (vol. 26) by Smith, N. D., and Rodgers, J. John Wiley and Sons.

Vernik, L. (1990). A New Type of Reservoir Rock in Volcaniclastic Sequences (1). AAPG Bulletin, 74(6), 830-836.

Verstraete, J., Khouchaf, L., Bulteel, D., Garcia-Diaz, E., Flank, A. M., and Tuilier, M. H. (2004). Amorphisation mechanism of a flint aggregate during the alkali–silica reaction: X-ray diffraction and X-ray absorption XANES contributions. Cement and concrete research, 34(4), 581-586.

Viereck, L. G., Griffin, B. J., Schmincke, H. U., and Pritchard, R. G. (1982). Volcaniclastic rocks of the Reydarfjordur drill hole, eastern Iceland: 2. Alteration. Journal of Geophysical Research: Solid Earth (1978–2012), 87(B8), 6459-6476.

Vosgerau, H., Guarnieri, P., Weibel, R., Larsen, M., Dennehy, C., Sørensen, E. V., and Knudsen, C. (2010). Study of a Palaeogene intrabasaltic sedimentary unit in southern East Greenland: from 3-D photogeology to micropetrography. Geological Survey of Denmark and Greenland Bulletin, 20, 75-78.

W

Waagstein, R. (1988). Structure, composition and age of the Faeroe basalt plateau. Geological Society, London, Special Publications, 39(1), 225-238.

Waichel, B. L., de Lima, E. F., Sommer, C. A., and Lubachesky, R. (2007). Peperite formed by lava flows over sediments: An example from the central Paraná Continental Flood Basalts, Brazil. Journal of volcanology and geothermal research, 159(4), 343-354.

Waichel, B. L., Scherer, C., and Frank, H. T. (2008). Basaltic lava flows covering active aeolian dunes in the Paraná Basin in southern Brazil: Features and emplacement aspects. Journal of Volcanology and Geothermal Research, 171(1), 59-72.

Walker J.R. (1993) Chlorite polytype geothermometry. Clays Clay Miner. 41,260-267.

Walker, G. P. (1991). Structure, and origin by injection of lava under surface crust, of tumuli,“lava rises”,“lava-rise pits”, and “lava-inflation clefts” in Hawaii. Bulletin of Volcanology, 53(7), 546-558.

Walker, G. P. L. (1971). The distribution of amygdale minerals in Mull and Morvern (Western Scotland). In Murty, T. V. V. G. R. K. and Rao, S. S. (eds) Studies in Earth Sciences, West Commemoration Volume. University of Saugar, India, 181–194.

Walker, R. G. (1963). Distinctive types of ripple-drift cross-lamination. Sedimentology, 2(3), 173-188.

Walker, R. J., Holdsworth, R. E., Imber, J., and Ellis, D. (2012). Fault-zone evolution in layered basalt sequences: A case study from the Faroe Islands, NE Atlantic margin. Geological Society of America Bulletin, 124(7-8), 1382-1393.

Walton, A. W., and Schiffman, P. (2003). Alteration of hyaloclastites in the HSDP 2 Phase 1 Drill Core 1. Description and paragenesis. Geochemistry, Geophysics, Geosystems, 4(5).

Watton, T. (2013). A multidisciplinary assessment of hyaloclastite deposits in petroleum systems using field studies, drill core, borehole image and wire-line log datasets (Doctoral dissertation, Durham University).

Welton, J. E. (1984). SEM Petrology Atlas. AAPG Methods in Exploration Series, 4, 237.

White, J. D. L., and Houghton, B. F. (2006). Primary volcaniclastic rocks. Geology, 34(8), 677-680.

White, J. D., McPhie, J., and Skilling, I. (2000). Peperite: a useful genetic term. Bulletin of Volcanology, 62(1), 65-66.

White, N., and Lovell, B. (1997). Measuring the pulse of a plume with the sedimentary record. Nature, 387(6636), 888-891.

White, R., and McKenzie, D. (1989). Magmatism at rift zones: the generation of volcanic continental margins and flood basalts. Journal of Geophysical Research: Solid Earth (1978–2012), 94(B6), 7685-7729.

Whitney, G., and Northrop, H. R. (1986). Vanadium chlorite from a sandstone-hosted vanadium uranium deposit, Henry basin, Utah. Clays and Clay Minerals, 34(4), 488-495.

Williamson, I. T., and Bell, B. R. (2012). The Staffa Lava Formation: graben-related volcanism, associated sedimentation and landscape character during the early development of the Palaeogene Mull Lava Field, NW Scotland. Scottish Journal of Geology, 48(1), 1-46.

Willumsen, P., and Schiller, D. M. (1994). High quality volcaniclastic sandstone reservoirs in East Java, Indonesia.

Worden, R. H., and Morad, S. (2003). Clay minerals in sandstones: controls on formation, distribution and evolution (pp. 1-41). Blackwell Publishing Ltd.

Wright, K. (2013). Seismic Stratigraphy and Geomorphology of Palaeocene Volcanic Rocks, Faroe-Shetland Basin (Doctoral dissertation, Durham University).

Wu, C., Gu, L., Zhang, Z., Ren, Z., Chen, Z., and Li, W. (2006). Formation mechanisms of hydrocarbon reservoirs associated with volcanic and subvolcanic intrusive rocks: Examples in MesozoicCenozoic basins of eastern China. AAPG bulletin, 90(1), 137 147.

Y

Yamagishi, H. (1985). Growth of pillow lobes—Evidence from pillow lavas of Hokkaido, Japan, and North Island, New Zealand. Geology, 13(7), 499-502.

Yeh, H. (1980). D/H ratios and late-stage dehydration of shales during burial. Geochim. Cosmochim. Acta 44, pp. 341-352.

Z

Zheng, Y. F. (1993a). Calculation of oxygen isotope fractionation in anyhydrous silicate minerals. Geochim. Cosmochim. Acta, 57, 1079-1091

Zheng, Y. F. (1993b). Calculation of oxygen isotope fractionation in hydroxyl- bearing silicates minerals. Earth Planet. Sci. Lett., 120, 247-263.

Zhou, L., and Friis, H. (2013, April). Quartz cementation mechanisms between adjacent sandstone and shale in Middle Cambrian, West Lithuania. In EGU General Assembly Conference Abstracts (Vol. 15, p. 8168).

Zhou, Z., and Fyfe, W. S. (1989). Palagonitization of basaltic glass from DSDP Site 335, Leg 37: Textures, chemical composition, and mechanism of formation. American Mineralogist, 74(9), 1045-1053.

Ziolkowski, A., Hanssen, P., Gatliff, R., Jakubowicz, H., Dobson, A., Hampson, G., Li, X-Y. and Liu, E. (2003). Use of low frequencies for sub-basalt imaging. Geophysical Prospecting, 51, 169-182.

Zou, C. N., Zhao, W. Z., Jia, C. Z., Zhu, R. K., Zhang, G. Y., Zhao, X., and Yuan, X. J. (2008). Formation and distribution of volcanic hydrocarbon reservoirs in sedimentary basins of China. Petroleum Exploration and Development, 35(3), 257-271.

Zou, C., Zhang, G., Zhu, R., Yuan, X., Zhoa, X., Hou, L., Wen, B., and Wu, X. (2012). Volcanic reservoirs in petroleum exploration. Research Institute of Petroleum Exploration and Develop.